INFORMATION TO USERS

This manuscript has been reproduced from the microfilm master. UMI films the text directly from the original or copy submitted. Thus, some thesis and dissertation copies are in typewriter face, while others may be from any type of computer printer.

The quality of this reproduction is dependent upon the quality of the copy submitted. Broken or indistinct print, colored or poor quality illustrations and photographs, print bleedthrough, substandard margins, and improper alignment can adversely affect reproduction.

In the unlikely event that the author did not send UMI a complete manuscript and there are missing pages, these will be noted. Also, if unauthorized copyright material had to be removed, a note will indicate the deletion.

Oversize materials (e.g., maps, drawings, charts) are reproduced by sectioning the original, beginning at the upper left-hand corner and continuing from left to right in equal sections with small overlaps. Each original is also photographed in one exposure and is included in reduced form at the back of the book.

Photographs included in the original manuscript have been reproduced xerographically in this copy. Higher quality 6" x 9" black and white photographic prints are available for any photographs or illustrations appearing in this copy for an additional charge. Contact UMI directly to order.

UMI®

Bell & Howell Information and Learning
300 North Zeeb Road, Ann Arbor, MI 48106-1346 USA
800-521-0600

Structural Analysis of Amylin and Its Analogs by NMR Spectroscopy

Zhihong Liu

A Dissertation submitted in partial fulfillment
of the requirements for the degree of

Doctor of Philosophy

University of Washington

1999

Program Authorized to Offer Degree: Department of Chemistry

In presenting this dissertation in partial fulfillment of the requirements for the Doctoral degree at the University of Washington, I agree that the Library shall make its copies freely available for inspection. I further agree that extensive copying of this dissertation is allowable only for scholarly purposes, consistent with "fair use" as prescribed in the U.S. Copyright Law. Requests for copying or reproduction of this dissertation may be referred to University Microfilms, 1490 Eisenhower Place, P.O. Box 975, Ann Arbor, MI 48106, to whom the author has granted "the right to reproduce and sell (a) copies of the manuscript in microform and/or (b) printed copies of the manuscript made from microform."

Signature Zhihong Liu

Date May 17, 1999

University of Washington
Graduate School

This is to certify that I have examined this copy of a doctoral dissertation by

Zhihong Liu

and have found that it is complete and satisfactory in all respects,
and that any and all revisions required by the final
examining committee have been made.

Chair of Supervisory Committee:

Niels H. Andersen

Reading Committee:

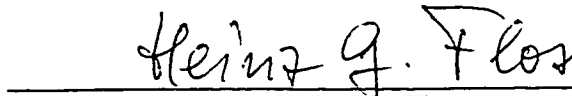

Heinz G. Floss

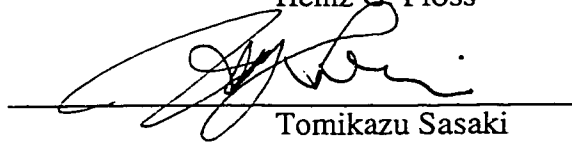

Tomikazu Sasaki

Date: May 17, 1999

University of Washington

Abstract

Structural Analysis of Amylin and Its Analogs by NMR Spectroscopy

Zhihong Liu

Chairperson of the Supervisory Committee:
Professor Niels H. Andersen
Department of Chemistry

Amylin is a 37 residue peptide hormone, which is believed to be involved in metabolic diseases, such as diabetes. The studies presented in this dissertation were initially carried out on rat and human amylin, and later concentrated on pramlintide, an agonist of human amylin. The conformational preferences of these peptdes in various solvent systems were determined mainly from chemical shift deviation (CSD) and nuclear Overhauser effect (NOE). An α-helix from residue 5 $\rightarrow$ 17 was present under all conditions examined. The Cys^2 - Cys^7 disulfide loop appeared to be constrained and underwent slow exchange. The C-terminal portion of the peptide was very flexible. The solution structure of pramlintide in 25-35% of HFIP was also determined by XPLOR dynamics simulated annealing.

The helical domain of amylin was further investigated, including the C-capping, disulfide nucleation, and specific site mutation effects. Ten amylin helix related peptides with various mutations were studied by both NMR and CD, and their helical propensity and stability were evaluated. Finally, a comparison study of amylin, calcitonin and calcitonin gene related peptide fragments is presented, and the similarities and differences among these biologically closely related peptides is discussed.

Table of Contents

List of Figures iv

List of Tables x

Chapter 1: Pancreatic Amylin – Background Materials 1

1.1 Amyloidogenicity 1

1.2 Biological Functions 2

1.3 Role in Diabetes 3

1.3.1 About Diabetes 3

1.3.2 Role of Amylin in Diabetes 4

1.4 Amylin, Calcitonin and CGRP 6

1.5 About This Thesis Research 7

Chapter 2: Conformational Analysis of Polypeptide 13

2.1 Polypeptide Structure and Dynamics 13

2.1.1 Regular Secondary Structure Motifs 13

2.1.2 Conformational Averaging and Flexibility 15

2.2 Structural Information from NMR Spectroscopy 16

2.2.1 Nuclear Overhauser Effect 16

2.2.2 Chemical Shifts and Secondary Structure 19

2.2.3 Other Structural Insights in NMR Data 21

2.3 Constrained Molecular Dynamics 22

2.4 Circular Dichroism, Secondary Structure Signatures 25

Chapter 3: Materials And Methods 40

3.1 Peptides 40

3.2 NMR Spectroscopy 40

3.2.1 General Methods 40

3.2.2 Important Multi-Dimentional NMR Experiments 43

3.2.2.1 2D Homonuclear Experiments 43

3.2.2.2 2D and 3D Heteronuclear Experiments 44

3.3 Resonance Assignment, CSD and NOE Ratios Histogram 46

3.4 Structure Ensemble Calculation 48

3.4.1 Constraint Extraction 48

3.4.2 Simulated Annealing 49

3.5 CD Experiments 51

Chapter 4: Structure and Dynamics of Amylins and Pramlintide..... 62
4.1 Rat and Human Amylin in the DMSO Solution State..... 62
4.1.1 Resonance Assignment..... 62
4.1.2 Proline Cis/Trans Isomerization..... 64
4.1.3 Comparison of Rat and Human Amylin..... 65
4.2 Pramlintide Assignment..... 65
4.2.1 Resonance Assignment in Aqueous Buffer..... 65
4.2.2 Resonance Assignment in 25-35% HFIP Aqueous Media..... 66
4.3 Structural and Dynamical Features of Pramlintide..... 69
4.3.1 Initial Structural Assessment..... 69
4.3.1.1 Pramlintide in Buffer and in 35% HFIP..... 69
4.3.1.2 Comparisons with Human and Rat Amylin..... 70
4.3.2 Further Investigation of Leu^{12} Conformation..... 71
4.3.3 Indications of Helix Curvature..... 73
4.3.4 Cosolvent and Temperature Induced Helix Dynamics..... 74
4.3.5 Evidence of Slow and Rapid Conformer Interconversions..... 76
4.4 Structural Details from NOE-based Refinement..... 77
4.4.1 Constraints..... 77
4.4.2 Restrained MD and Structural Details..... 79
4.5 Discussions and Conclusions..... 81
Chapter 5: Factors Governing Amylin Helicity.....142
5.1 C-Capping Effects.....143
5.2 Disulfide Nucleation Effect.....145
5.3 Aib Stabilization Effect.....146
5.4 The Arg/His^{18} Mutation.....148
5.5 Helical Propensity and Stability of Amylin-Related Peptides as Determined by Circular Dichroism.....149
5.6 An Aside -- Cold Denaturation of Amylin-Related Peptides.....153
5.7 Conclusions.....155
Chapter 6: Comparison Study of Calcitonin, CGRP and Amylin Fragments.....223
6.1 CD Studies.....223
6.2 Resonance Assignments of sCT(1-20)G and hCGRP(1-21).....225
6.2.1 Assignments of sCT(1-20)G.....225

6.2.2 Assignments of hCGRP(1-21) 227
6.3 sCT, hCGRP and Amylin Fragments: Structural Insights 229
6.4 Amylin/hCGRP Hybrids 232
6.5 Conclusions 233
References **286**
Appendix A NMR Pulse Programs and Transformation Macros **305**
Appendix B Final Constrain Tables and Molecular Dynamic Protocols **325**

List of Figures

Number		Page
1.1	Sequence Comparison for Amylins, Calcitonin, and CGRP	9
1.2	Biological Functions of Amylin	10
1.3	Insulin Responses to Intravenous Administration of Glucose	11
1.4	Pramlintide Lowers Glucose Levels in IDDM	12
2.1	Cis/Trans Peptide Bond Isomers	31
2.2	Peptide Backbone Nomenclature Conventions	32
2.3	α Helix and β Strand	33
2.4	γ and β Turns	34
2.5	Two Different Arrangements of a Three-spin System	35
2.6	The Relation between the $d_{N\alpha}/d_{\alpha N}$ Ratio and the Major Secondary Structure Regions	36
2.7	Dependence of α - ^1H shift on ϕ and φ in a Dipeptide Model	37
2.8	CD Spectra of Regular Peptide Secondary Structures	38
2.9	Far UV CD Spectra of Disordered Aromatic Side Chain Chromophores	39
3.1	WATERGATE Pulse Scheme	56
3.2	Pulse Schemes of Common Homonuclear 2D Experiments	57
3.3	Pulse Sequence of HMQC	58
3.4	Pulse Sequence of RELAY-HMQC	59
3.5	Pulse Sequence of NOESY-HMQC	60
3.6	Information used for stereospecific assignment of β-methylene protons	61
4.1	αN Region of the COSY Spectrum of rAM in 'DMSO'	94
4.2	NH Portion of the TOCSY Spectrum of rAM in 'DMSO'	95
4.3	αN Region of the NOESY Spectrum of rAM in 'DMSO'	96
4.4	NN Region of the NOESY Spectrum of rAM in 'DMSO'	97
4.5	NH Portion of the TOCSY Spectrum of hAM in 'DMSO'	98
4.6	Portion of NOESY Spectrum of hAM in 'DMSO'	99
4.7	αH and NH Chemical Shift Deviation Comparisons of Human and Rat Amylin in 'DMSO'	100
4.8	ROESY Spectrum of Pramlintide in Aqueous Buffer (αN Region)	101
4.9	1D Spectrum of Pramlintide in Aqueous Buffer	102
4.10	Portions of COSY Spectrum of Pramlintide in Aqueous D_2O Buffer	105
4.11	1D Spectrum of Pramlintide in Aqueous 35 vol% HFIP (NH Region)	106

4.12 TOCSY Correlations for Pramlintide in Aqueous HFIP (α/β Region)..... 107
4.13 TOCSY Correlations for Pramlintide in Aqueous HFIP (α/γδ Region)..... 108
4.14 αN Region of the NOESY Spectrum of Pramlintide in 35 Vol% HFIP Aqueous Media..... 109
4.15 NOESY Spectrum of Pramlintide (NN Region)..... 110
4.16 ^{13}C 1D Spectrum of ^{13}C-L-pram in 35 vol% HFIP Aqueous Media..... 111
4.17 ^{13}C-Leu RELAY-HMQC Correlation for Pramlintide in 35% HFIP..... 112
4.18 An αH-CSD Comparison for Pramlintide in Aqueous Buffer and in 35% Aqueous HFIP..... 113
4.19 Comparison of Dipolar Coupling (Through-Space) Correlations for Pramlintide with and without HFIP Addition..... 114
4.20 Summary of Key NOEs for Pramlintide in 25-35% HFIP..... 115
4.21 An αH-CSD Comparison of Pramlintide in Aqueous Buffer and Amylins in DMSO..... 116
4.22 The αH-CSD Histograms of hAM, Pramlintide and rAM in 25% Aqueous HFIP..... 117
4.23 An NH-CSD Comparison for Pramlintide (in Aqueous Buffer and in 35% HFIP) and hAM (in 35% HFIP)..... 118
4.24 Inter/Intra-Residue Hα/HN NOE Ratios of Pramlintide in 35% HFIP..... 119
4.25 Hα and Hβ Chemical Shift Differences of Pramlintide in 35% HFIP and in Buffer..... 120
4.26 An αH-CSD Comparison of Pramlintide and D-Leu^{12}-Pram in 25% HFIP..121
4.27 Plot of Amide ^{1}H and ^{15}N CSDs of Pramlintide in 35% HFIP at 285K..... 122
4.28 Correlation Between Amide ^{1}H and Amide ^{15}N Chemical Shifts of Pramlintide in 35% HFIP at 285K..... 123
4.29 The αH-CSD Profile of Pramlintide under Various Conditions..... 124
4.30 Correlation Between NH Temperature Gradient and Chemical Shift Deviation for Pramlintide in 35% HFIP Media and in Aqueous Buffer..... 126
4.31 NOESY Spectrum (αN Region) of Pramlintide Collected on a DMX750MHz NMR Spectrometer at 275K..... 127
4.32 ^{15}N-HMQC Temperature Gradient Study of ^{15}N-pram in 35 vol% HFIP..... 128
4.33 Two Cys-Cys Loop Conformations Encountered During the Early Stage of hAM Structure Refinement..... 129
4.34 NOESY Spectrum (NN Region) of Pramlintide Collected on

the 750MHz NMR Spectrometer 130
4.35 NOESY Spectrum (αβ Region) of Pramlintide Acetate Recorded on 750MHz NMR Spectrometer 131
4.36 Comparison of 2D and 3D NOESY Spectra of Pramlintide in 35% Aqueous HFIP (16, 26, 27 N) 132
4.37 Selected Planes of the 3D ^{15}N - Edited NOESY Spectrum (8 and 9N) 133
4.38 Selected Planes of the 3D ^{15}N - Edited NOESY Spectrum (15, 18, 19, and 20 N) 134
4.39 αN Portion of the NOESY Spectrum of Amylin Fragment c21Y in 16% TFE Aqueous Medium 135
4.40 55ms Mixing Time TOCSY Spectrum of Pramlintide in D_2O at 295K 136
4.41 The ϕ and φ Plots for Two NMR Structure Ensembles Derived for Pramlintide in 25-35% HFIP 137
4.42 Overview of Pramlintide Structure Ensemble of Pramlintide in 25-35% HFIP (Residue 8-24) 138
4.43 The Ramachandran Plot for the Pramlintide Structure Ensemble 139
4.44 The Hydrophobic and Polar Faces of Pramlintide Helix in 25-35% HFIP ... 140
4.45 Comparison of Pramlintide Side Chain Shifts with and without HFIP Addition 141
5.1 αN Region of the TOCSY Spectrum of [hAM(1-22)G] in Buffer 166
5.2 αN Region of the TOCSY Spectrum of [hAM(1-22)G] in 25% HFIP 167
5.3 NN Region of the NOESY Spectrum of [hAM(1-22)G] in 25% HFIP 168
5.4 αN Region of the NOESY Spectrum of [hAM(1-22)GY] in 25% HFIP 169
5.5 α/βγδ Region of the TOCSY Spectrum of [hAM(1-22)GY] in 25% HFIP ... 170
5.6 α/βγδ Region of the TOCSY Spectrum of [hAM(1-20)G] in Buffer 171
5.7 α/βγδ Region of the TOCSY Spectrum of [hAM(1-20)G] in 25% HFIP 172
5.8 αN Region of the TOCSY Spectrum of [hAM(1-20)G] in Buffer 173
5.9 αβ Region of the NOESY Spectrum of [hAM(1-20)G] in 25% HFIP 174
5.10 αN Region of the NOESY Spectrum of [hAM(1-20)GY] in 25% HFIP 175
5.11 αβ Region of the NOESY Spectrum of [hAM(1-20)GY] in 25% HFIP 176
5.12 NN Region of the NOESY Spectrum of [hAM(1-20)GY] in 25% HFIP 177
5.13 αH-CSD and NH-CSD Histograms for [hAM(1-20)GY], [hAM(1-22)GY] and Pramlintide in Buffer 178
5.14 αH-CSD and NH-CSD Histograms for [hAM(1-20)GY],

[hAM(1-22)GY] and Pramlintide in 25% HFIP 179
5.15 αH-CSD Comparisons of Fragments with and without NN C-capping Unit in 25% HFIP 180
5.16 αH-CSD and NH-CSD Comparisons of Fragments with and without NN C-capping Unit in Buffer 181
5.17 αN Region of the TOCSY Spectrum of [S2,7-hAM(1-20)G] in Buffer 182
5.18 αN Region of the TOCSY Spectrum of [A2,7-hAM(1-20)G] in Buffer 183
5.19 α/βγδ Region of the TOCSY Spectrum of [A2,7-hAM(1-20)G] in Buffer ... 184
5.20 αN Region of the NOESY Spectrum of [A2,7-hAM(1-20)G] in 25% HFIP 185
5.21 NN Region of the NOESY Spectrum of [A2,7-hAM(1-20)G] in 25% HFIP 186
5.22 α/βγδ Region of the NOESY Spectrum of [A2,7-hAM(1-20)G] in 25% HFIP 187
5.23 αH-CSD and NH-CSD Comparisons of Fragments with and without Disulfide Closure in Buffer at 285K 188
5.24 αH-CSD and NH-CSD Comparisons of Fragments with and without Disulfide Closure in Aqueous HFIP 189
5.25 αN Region of the TOCSY Spectrum of [S2U7-hAM(1-20)G] in Buffer 190
5.26 α/βγδ Region of the TOCSY Spectrum of [S2U7-hAM(1-20)G] in Buffer .. 191
5.27 αN Region of the NOESY Spectrum of [S2U7-hAM(1-20)G] in Buffer 192
5.28 NN Region of the NOESY Spectrum of [S2U7-hAM(1-20)G] in Buffer 193
5.29 αH-CSD and NH-CSD Comparisons of [S2U7-hAM(1-20)G] with a Cyclic and an Acyclic Fragment in Buffer 194
5.30 αN Region of the NOESY Spectrum of [S2U7-hAM(1-20)G] in 25% HFIP 195
5.31 NN Region of the NOESY Spectrum of [S2U7-hAM(1-20)G] in 25% HFIP 196
5.32 α/βδγ Region of the TOCSY Spectrum of [S2U7-hAM(1-20)GY] in 25% HFIP 197
5.33 αH-CSD and NH-CSD Comparisons of [S2U7-hAM(1-20)G] with a Cyclic and an Acyclic Fragment in 25% HFIP 198
5.34 αN Region of the TOCSY Spectrum of [R18-hAM(1-20)GY] in Buffer 199
5.35 α/βγδ Region of the TOCSY Spectrum of [R18-hAM(1-20)GY] in Buffer .. 200

5.36 αN Region of the NOESY Spectrum of [R18-hAM(1-20)GY] in Buffer.....201
5.37 The NH/CH Region of the NOESY Spectrum of [R18-hAM(1-20)GY] in 25% HFIP 202
5.38 NN Region of the NOESY Spectrum of [R18-hAM(1-20)GY] in 25% HFIP.....203
5.39 α/βγδ Region of the NOESY Spectrum of [R18-hAM(1-20)GY] in 25% HFIP.....204
5.40 αH-CSD and NH-CSD Histograms of [R18-hAM(1-20)GY] and [hAM(1-20)GY] in Buffer.....205
5.41 αH-CSD and NH-CSD Histograms of [R18-hAM(1-20)GY] and [hAM(1-20)GY] in 25% HFIP.....206
5.42 HFIP Titration of hAM(1-20)GY at 25 °C.....207
5.43 TFE Titration of hAM(1-20)GY at 25 °C.....208
5.44 CD Thermal Study of hAM(1-22)G in 25% HFIP.....209
5.45 CD Thermal Study of A2,7-hAM(1-20)G in Buffer.....210
5.46 CD Thermal Study of hAM(1-20)GY in Buffer.....211
5.47 Thermal and Titration Difference Spectra of hAM(1-22)GY.....212
5.48 Titration Curves of Amylin-Related Peptides.....213
5.49 CD Thermal Study of S2U7-hAM(1-20)G in 8% HFIP.....214
5.50 CD Thermal Study of sCT(1-20)G in 5% HFIP 215
5. 51 Temperature Dependence of [θ] for [R18-hAM(1-20)GY] in 7% HFIP, Monitored at 191, 208, and 221nm 216
5.52 CD Thermal Study of S2U7-hAM(1-20)GY in 16% TFE.....217
5.53 Temperature Dependence of $[\theta]_{221}$ for [CGRP(1-21)] at Different levels of HFIP.....218
5.54 CD Thermal Study of D-Leu^{12}-pramlintide in 9% HFIP.....219
5.55 Thermal Difference CD Spectra of hAM(1-22)GY in 8% HFIP 220
5.56 [S2U7-hAM(1-20)G] in 8% HFIP: Temperature Dependence of αH-CSDs 221
5.57 Temperature Dependence of $[\theta]_{221}$ for [S2U7-hAM(1-20)G] at Different levels of HFIP.....222
6.1 CD Comparison of sCT(1-20)G, hAM(1-20)G and hCGRP(1-21) in Buffer.....238
6.2 Thermal CD Study of hCGRP(1-21) in Aqueous Buffer 239

6.3 CD Comparison of sCT(1-20)G, hAM(1-20)G and hCGRP(1-21) in 25% HFIP....240
6.4 1D Spectrum of sCT(1-20)G in Buffer (NH Region)....241
6.5 N/αβγδ Region of the TOCSY Spectrum of sCT(1-20)G in Buffer....242
6.6 α/βγδ Region of the TOCSY Spectrum of sCT(1-20)G in Buffer....243
6.7 αN Region of the TOCSY and NOESY Spectra of sCT(1-20)G in Buffer...244
6.8 N/αβγδ Region of the TOCSY Spectrum of sCT(1-20)G in 25% HFIP....245
6.9 1D Spectrum of sCT(1-20)G in 25% HFIP (NH Region)....246
6.10 α/βγδ Region of the TOCSY Spectrum of sCT(1-20)G in 25% HFIP....247
6.11 αN Region of the NOESY Spectrum of sCT(1-20)G in 25% HFIP....248
6.12 Aliphatic-NH Region of the NOESY Spectrum of sCT(1-20)G in 25% HFIP....249
6.13 NN Region of the NOESY Spectrum of sCT(1-20)G in 25% HFIP....250
6.14 α/βγδ Region of the NOESY Spectrum of sCT(1-20)G in 25% HFIP....251
6.15 1D Spectrum of hCGRP(1-21) in Buffer (NH Region)....252
6.16 N/αβγδ Region of the TOCSY Spectrum of hCGRP(1-21) in Buffer....253
6.17 α/βγδ TOCSY Spectrum of hCGRP(1-21) in Buffer....254
6.18 αN Region of the NOESY Spectrum of hCGRP(1-21) in Buffer....255
6.19 1D Spectrum of hCGRP(1-21) in 25% HFIP (NH Region)....256
6.20 N/αβγδ Region of the TOCSY Spectrum of hCGRP(1-21) in 25% HFIP...257
6.21 N/αβγδ Region of the NOESY Spectrum of hCGRP(1-21) in 25% HFIP...258
6.22 α/βγδ Region of the TOCSY Spectrum of hCGRP(1-21) in 25% HFIP....259
6.23 NN Region of the NOESY Spectrum of hCGRP(1-21) in 25% HFIP....260
6.24 α/βγδ Region of the NOESY Spectrum of hCGRP(1-21) in 25% HFIP....261
6.25 αH-CSD and NH-CSD Histograms of sCT(1-20)G, hCGRP(1-21) and hAM(1-20)G in Buffer....262
6.26 Alpha-CSD of hCGRP(1-21) in Buffer at Different Temperatures....263
6.27 αH-CSD and NH-CSD Histograms of sCT(1-20)G, hCGRP(1-21) and hAM(1-20)G in 25% HFIP....264
6.28 Sequential and Medium Range NOEs of sCT(1-20)G in 25% HFIP....265
6.29 αH-CSD Comparisons of sCT in 90% MeOH or TFE Aqueous Media and sCT(1-20)G in 25% HFIP....266
6.30 αH-CSD and NOE Ratios Histograms of sCT(8-32) in 25% HFIP....267
6.31 Sequential and Medium Range NOEs of hCGRP(1-21) in 25% HFIP....268

6.32 αH-CSD Comparisons of hCGRP-1 in 50% TFE and hCGRP(1-21) in 25% HFIP....269
6.33 CD Comparison of hAM(1-20)GY and hAM/hCGRP Fragment Hybrids in Aqueous Buffer....270
6.34 Thermal CD Study of V8S9-hAM(1-20)GY in Aqueous Buffer....271
6.35 N/αβγδ Region of the TOCSY Spectrum of V8-hAM(1-20)GY in Buffer...272
6.36 α/βγδ Region of the TOCSY Spectrum of V8-hAM(1-20)GY in Buffer....273
6.37 αN Region of the NOESY Spectrum of V8-hAM(1-20)GY in 25% HFIP...274
6.38 NN Region of the NOESY Spectrum of V8-hAM(1-20)GY in 25% HFIP....275
6.39 α/βγδ Region of the NOESY Spectrum of V8-hAM(1-20)GY in 25% HFIP....276
6.40 N/αβγδ Region of the TOCSY Spectrum of V8S9-hAM(1-20)GY in Buffer....277
6.41 α/βγδ Region of the TOCSY Spectrum of V8S9-hAM(1-20)GY in Buffer....278
6.42 N/αβγδ Region of the TOCSY Spectrum of V8S9-hAM(1-20)GY in 25% HFIP....279
6.43 α/βγδ Region of the TOCSY Spectrum of V8S9-hAM(1-20)GY in 25% HFIP....280
6.44 αN Region of the NOESY Spectrum of V8S9-hAM(1-20)GY in 25% HFIP....281
6.45 NN Region of the NOESY Spectrum of V8S9-hAM(1-20)GY in 25% HFIP....282
6.46 α/βγδ Region of the NOESY Spectrum of V8S9-hAM(1-20)GY in 25% HFIP....283
6.47 αH-CSD Comparisons of V8S9-hAM(1-20)GY, V8-hAM(1-20)GY, and hAM(1-20)GY....284
6.48 αH-CSD Comparisons of hCGRP(1-21), V8S9-hAM(1-20)GY, and hAM(1-20)GY....285

List of Tables

Number		Page
1.1	Effects of Amylin, Calcitonin (CT) and Calcitonin Gene-related peptide (CGRP)	8
2.1	Parameters for Regular Peptide Secondary Motifs	28
2.2	Typical Interproton Distances in Regular Peptide Secondary Structures	29
2.3	Correlations between CSDs and Secondary Structure in Peptides/Proteins	30
3.1	Peptides Investigated in This Project	53
3.2	Random Coil Reference Values	55
4.1	The Backbone Proton Chemical Shifts of Human and Rat Amylin in DMSO	86
4.2	The ^{1}H Chemical Shifts of Pramlintide in Aqueous Buffer	87
4.3	The ^{1}H Chemical Shifts of Pramlintide and Its C-terminal Free Acid in 35 Vol% HFIP	88
4.4	The Amide ^{15}N and ^{1}H Chemical Shifts of Pramlintide in 35% HFIP at Different Temperatures	90
4.5	^{13}C Chemical Shifts for Leucines in Pramlintide in 35% HFIP	91
4.6	NH Temperature Gradient and Chemical Shift Deviation (at 285K) of Pramlintide in 35% HFIP and in Buffer	92
4.7	Statistical Evaluation of Pramlintide Structure Ensembles	93
5.1	Backbone Proton Chemical Shifts of [hAM(1-22)GY] and [hAM(1-22)G] in Buffer and in 25% HFIP at 285K	157
5.2	Backbone Proton Chemical Shifts of [hAM(1-20)GY] and [hAM(1-20)G] in Buffer and in 25% HFIP at 285K	158
5.3	Backbone Proton Chemical Shifts of [S2,7-hAM(1-20)G] and [A2,7-hAM(1-20)G] in Buffer and in 25% HFIP at 285K, and [Ac-hAM(5-20)G] in 30% HFIP at 295K	159
5.4	Backbone Proton Chemical Shifts of [S2U7-hAM(1-20)GY], [S2U7-hAM(1-20)G] and [R18-hAM(1-20)GY] in Buffer and in 25% HFIP at 285K	160
5.5	CD Data for Amylin-Related Peptides	161
5.6	Helicities of Amylin-Related Peptides (Derived from the Combined Analysis of NMR and CD Data)	163
5.7	CD Data for Cold Denaturation Studies of Amylin-Related Peptides	164

6.1 Backbone Proton Chemical Shifts of sCT(1-20)G and hCGRP(1-21) in Buffer and in 25% HFIP at 285K.....235
6.2 CD Data Comparison for sCT, hCGRP and Amylin-Related Peptides.....236
6.3 Backbone Proton Chemical Shifts of V8Y and V8S9Y in Buffer and in 25% HFIP at 285K.....237

Acknowledgments

The author wishes to thank Professor Niels H. Andersen, whose enthusiasm toward science has always encouraged me, for his guidance and support throughout this doctoral program. Special thanks to Dr. Tom K. Pratum, without whose assistance, many critical NMR experiments would not have been accomplished. Especial thanks also to my supervisory committee members, Professor Heinz Floss, Professor Michael Heinekey, Professor Terry Lybrand and Professor Tomikazu Sasaki, who have challenged me and supported my development as a scientist. Thanks to Dr. Jeff Godden for his special friendship, encouragement and assistance in the final stage of preparation of this dissertation. Thanks also to members of the Andersen research group: John Cort, Greg Lee, John Tomaszewski, Yong Li, Hui Tong, Jonathan Neidigh, Matthew Fesinmeyer, and former members Bolong Cao, Chinpan Chen, Scott Harris and Rob Palmer. Particular to John Cort, who helped to complete final structure ensemble analysis.

I also wish to thank Amylin Pharmaceutics, Inc., for their financial support of this project.

Lastly and most importantly, I am grateful to my family members, far away across the Pacific Ocean, for their profound love and sacrifices during the pursuit of my doctoral degree.

Chapter 1

Pancreatic Amylin - Background Materials

Amylin is a 37 amino acid peptide hormone synthesized in pancreatic beta-cells and cosecreted with insulin (Butler et al., 1990; Sanke et al., 1991) in response to physiological stimuli. Amylin was initially isolated, purified, and correctly characterized chemically as the major component of amyloid deposits from human type II diabetic subjects (Cooper et al., 1987). Deposition of amyloid plaque in pancreatic islets is a common feature of type-II (non-insulin-dependent) diabetes mellitus (NIDDM). Amylin is structurally similar to calcitonin (CT) and calcitonin gene-related peptide (CGRP), and they exhibit overlapping bioactivities through cross reacting with separate receptors (Muff et al, 1995). During the last ten years, extensive studies have been carried out on amylin and many of these studies suggest that one of the major biological functions of amylin is to regulate fuel metabolism; consequently, it may play an important role in metabolic diseases, such as diabetes (Cooper et al., 1989; Rink et al., 1993; Castillo et al., 1995; Sacks 1996; Ludvik et al., 1997).

1.1 *Amyloidogenicity*

Amyloid deposits are found in pancreatic islets of over 90% of patient with NIDDM and some elderly nondiabetic subjects. "Amyloid" refers to a mass of fibrils that can be visualized with light microscopy, after staining with amyloid-specific dyes (Oosterwijk et al., 1995). Amyloid fibrils have been assumed to have a pleated β-sheet conformation held together by hydrogen bonding, and there is some evidence for this in the case of pancreatic islet amyloid (Ashburn et al., 1992, 1993; Cort et al. 1994). It has been reported that fibril formation, instead of peptide aggregation, is necessary for amylin toxicity to insulin-producing islet cells, while soluble amylin is not toxic (Lorenzo & Yankner, 1996).

The causes for fibrillogenesis of amylin are not clear (Clark et al., 1993; Oosterwijk et al., 1995; Clark et al., 1996). Amyloid fibrils formed from a large number of different proteins and peptides are often associated with genetic abnormalities. However, the amino acid sequence of the normally occurring amylin is identical to the one isolated from islet amyloid (Mosselman et al., 1989); therefore, amyloid formation in NIDDM patient is not due to mutation of the primary sequence of

the hormone. The properties of the physiological agent itself and its environment must be sufficient for the formation of amyloid.

Islet amyloid only occurs in certain mammalian species. Humans, monkeys and cats develop islet amyloid in conjunction with type II diabetes; dogs and most rodents, such as rat, do not (Betsholtz et al., 1989, 1990, 1993). The sequence divergence may provide an explanation for the differences in amyloidogenicity for different species. A comparison of amylin sequence from various mammalian species (Figure 1.1) reveals that the two biologically important post-translational modifications, the N-terminal Cys-Cys disulfide loop and the amidated C-terminal, are well conserved; while, the sequence 20→29, especially 25 → 29, that is reported to be important of amyloid formation (Nishi et al., 1989; Westermark et al., 1990) is less well conserved. Unlike human amylin (hAM), rat amylin, with three proline substituents at 25, 28 and 29, is known not to form amyloid fibrils either in vitro and in vivo (Betsholtz et al., 1990b).

However, the amino acid sequence of amylin cannot be the only determining factor for amyloidogenesis. Other prerequisites for amyloid formation may include elevated local concentration and high glucose levels (Clark et al., 1996).

1.2 *Biological Functions*

The biological actions of amylin are still under active investigation, with some functions not found at physiological concentrations. There are conflicting reports concerning the lower concentration limits to induce the different actions. The putative biofunctions of amylin are summarized in Figure 1.2 (Castillo et al., 1995). Amylin evokes biological effects in different tissues including skeletal muscle, liver, pancreas, bone, gastrointestinal tract, the central nervous system and the cardiovascular system; and may influence different metabolic processes, such as fuel, particularly carbohydrate, and calcium metabolism.

Amylin clearly has effects on carbohydrate metabolism. Traditionally, greater attention has been focused on insulin and the mechanisms that regulate glucose disposal rather than on the absorption of glucose. Amylin, in contrast, appears to affect both the absorption and disposition of glucose (Young et al., 1995). Amylin's regulatory effects on carbohydrate metabolism can be direct or indirect. Direct actions are induced by amylin by acting directly on target cells. Alternatively, or additionally, amylin may also act by effecting changes in plasma levels of other hormones or metabolites that, in turn, influence metabolic processes in different cells. Amylin has been proposed to be an

endocrine partner of insulin; it not only increases blood glucose levels, but also plasma lactate levels (Young et al., 1991). In skeletal muscle, amylin, antagonizing the effects of insulin, opposes glycogen synthesis by inhibiting muscle glycogen synthase, enhances glycogenolysis (increasing intracellular glucose-6-phosphate content) and glycolysis (increasing lactate production) by activating glycogen phosphorylase. Consequently, amylin enhances lactate output by muscle and increases the plasma lactate concentration (Deems et al., 1991; Young et al., 1992). In liver, amylin also increases glucose production, which may be mediated by changes in the amount of gluconeogenic substrates, such as lactate, delivered to the liver; in addition, amylin may also have direct glycogenolytic actions on the liver, enhancing glucose production (Ciaraldi et al, 1992; Young et al., 1993). In the pancreas, amylin can elicit effects on glucose metabolism by influencing insulin secretion from islet β cells. Some studies have suggested that amylin inhibits insulin biosynthesis and secretion, mostly at pharmacological concentrations (Ohsawa et al., 1989; Silvestre et al. 1990).

Many functions of amylin unrelated to glucose metabolism have also been reported. For instance, amylin stimulates pancreatic exocrine secretion and plasma gastrin levels (Funakoshi et al., 1992) and delays gastric emptying (Brown et al., 1994; Young et al., 1996); suppresses the hyperphagic effect of insulin (Cooper, 1994) and influences memory through actions on the central nervous system (Flood, 1992); inhibits bone resorption, displays a calcitonin-like decrease in serum calcium concentrations (Cooper, 1994); and increases blood flow, with temporary drops in blood pressure, and smooth muscle relaxation (Young et al., 1993).

1.3 *Role in Diabetes*

1.3.1 *About Diabetes*

Diabetes mellitus, the most common endocrine disease, is estimated to afflict 16 million people in the US, about 8% of the total population (Cefalu, 1996; US Department of Health and Human Services 1995). Diabetes mellitus is characterized by chronic hyperglycemia and is often strongly associated with obesity, hypertension and hyperlipidemia. It can lead to long-term complications, including a high rate of cardiovascular disease and amputation, as well as the typical complications of diabetes such as retinopathy, nephropathy, and neuropathy. The economic burden created by diabetes and its complications has been estimated at over $92 billion annually in the United States, almost 15% of US annual health care expenditures (Sacks and Mcdonald,

1996). There are two major forms of diabetes mellitus: type I or Insulin-dependent diabetes mellitus (IDDM), and Type-II or Non-insulin-dependent diabetes mellitus (NIDDM). IDDM is characterized by profound insulin deficiency due to a selective, immune-mediated destruction of pancreatic β-cells. Approximately 90% of diabetic patients are NIDDM, and it typically onsets in middle-aged to elderly individuals, 80% of those are obese. NIDDM is a polygenic and heterogeneous disease with genetic and environmental factors. An individual with type II diabetes may have multiple genetic defects contributing to it; while not all population with NIDDM have the same genetic factors (Kahn et al., 1996).

Insulin is the major circulating hormone capable of promoting the utilization of nutrients by peripheral tissues and lowering blood glucose levels, counteracting the effects of hyperglycemic hormones such as amylin and glucagon. Blood glucose levels of a non-diabetic subject are maintained in a very narrow range (80-130mg/dl), despite considerable variations in glucose availability. NIDDM subjects suffer from chronic hyperglycemia as a result of β-cells dysfunction and insulin resistance (Poitout, V. 1996). β-cell dysfunction in type II diabetes is characterized by a specific lack of first-phase glucose-induced insulin secretion (Figure 1.3), and is often referred to as glucose desensitization (reversible) or glucose toxicity (irreversible). Insulin resistance, a major abnormality in NIDDM, has two aspects: decreased sensitivity, more hormone is needed to produce the same effect, a shift in the dose-response curve; and decreased responsiveness, a decrease in maximal response. Decreased sensitivity implies a change in insulin receptor number or affinity, while decreased responsiveness implies a change in a rate-limiting step (Pillay and Makgoba, 1991).

1.3.2 *Role of Amylin in Diabetes*

Amylin has been widely studied in diabetes mellitus, but its significance in the disease is still open to debate. However, a large body of evidence supports its involvement (Cooper, 1994; Castillo et al. 1995; Cooper & Tse, 1996): firstly, islet amyloid formation is a common feature of NIDDM patients; secondly, amylin basal serum concentration is abnormal in both type I and type II diabetes mellitus; thirdly, recent clinical trials show that amylin agonist or antagonist therapy is beneficial to diabetes patients.

Amyloid deposits are a common finding in the vast majority of patients with NIDDM, on the contrary, only few nondiabetic subjects show minor islet amyloid

depositions (Turner et al., 1992; Yki-Järvinen, 1994). Amylin fibrils have been shown to be toxic to the beta cells of the pancreas (Lorenzo et al., 1994). Although some researchers suggested that amyloid deposits may be the result of NIDDM, many others believe that amyloid deposite formation may contribute to the progression of NIDDM by impairing beta-cell function, and that this may be initiated by locally elevated amylin concentrations, induced by insulin-resistance-associated beta-cell hyperactivity (Betsholtz et al., 1993; Oosterwijk et al., 1995).

Although cosynthesized with insulin, amylin secretion is only 2-5% of the amount of insulin released, resulting in very low basal serum concentrations. The normal basal levels of amylin range from 1 to 10 pM, rising to 15-20 pM after meals or oral glucose loads (Kanatsuka et al., 1989). Either deficiency or excess may cause metabolic disorder. Amylin is deficient or even absent in type-I (autoimmune) diabetes mellitus, and is commonly elevated in hyperinsulinaemic states such as insulin resistance, mild glucose intolerance and hypertension, known as a pre-diabetic (Type II) state (Huang et al., 1992; Koda et al., 1992; Pieber et al., 1993). Amylin has been reported to cause insulin resistance and glucose intolerance (Molina et al., 1990); and it has been hypothesized that this may be responsible for the insulin resistance seen in NIDDM (Oosterwijk et al., 1995; Tokuyama T. 1997).

Clinical trials show that the administration of an amylin mimic can help diabetic patients achieve better blood glucose control. Recent evidence indicates that intravenous infusion of an amylin analog, pramlintide -- (a fully active agonist), reduces postprandial hyperglycemia in patients with IDDM (Figure 1.4); and that this may be predominantly mediated via slowing of gastric emptying (Kolterman et al., 1995; Fran, 1996; Kolterman et al., 1996; Schmitz et al., 1997; Thompson et al., 1997). It has also been reported that pramlintide reduces blood glucose spiking in type II diabetes patients. Furthermore, amylin blockade therapy is also under investigation for treating metabolic disorders, such as insulin resistance syndrome, with its associated hypertension, obesity, and hyperinsulinemia. (Amylin Pharmaceuticals 1996).

Taken together, the potential role of amylin in the pathogenesis of diabetes has not been established, but a substantial body of data supports its involvement. Additional studies are required to elucidate the molecular mechanisms of amylin function and its potential role in diabetes mullitus.

1.4 Amylin, Calcitonin, and CGRP

Amylin, calcitonin (CT) and calcitonin gene-related peptide (CGRP) are closely related structurally; and they exhibit overlapping biological actions (Wimalawansa, 1997). Calcitonin is a peptide hormone of 32 residues synthesized in and secreted from, parafollicular or C-cells of the thyroid gland. It plays a central role in calcium-phosphorus metabolism, and has been postulated to be a neuromodulator and/or neurotransmitter (Fischer & Born, 1985). CGRP is a minor product of thyroid C-cells, containing 37 amino acid residues and is a widely distributed neuropeptide and potent vasodilator (O'Halloran & Bloom. 1991).

The primary sequences of human amylin (hAM), CT and CGRP are shown in Figure 1.1. Amylin and CGRP have almost 50% sequence identity; they also have some structural homology to the calcitonins. All three peptides have a Cys-Cys disulfide loop at the N-terminus and an amidated C-terminus; both of these two post-translational modifications are essential for the full biological activity of amylin (Cooper et al., 1988). Experimental studies showed that both calcitonin and CGRP have an α-helix domain (Motta et al., 1989; Breeze et al., 1991), while secondary structure prediction and tertiary structure model-building had suggested that amylin and CGRP have a similar α-helix/β-strand motif (Saldanha & Mahadevan, 1991).

Amylin, CT and CGRP produce qualitatively similar biological effects in many tissues but with different potencies. For example, amylin, much like CT and CGRP but with a higher potency, inhibits glucose transportation into the skeletal musculature and gluconeogenesis (Leighton & Cooper, 1988); CGRP is the most potent vasodilator, but shares this effect with CT and amylin, acting by enhancing blood flow through relaxation of resistance vessels (Drain, 1990). CT lowers blood calcium levels through inhibition of osteoclastic bone resorption and stimulation of the urinary calcium excretion (Alam et al., 1993). Many other similarities (Cooper, 1994; Muff et al., 1995) have been reported, and these are summarized in Table 1.1.

The biological similarities among Amylin, CGRP, and CT likely result due to their structural similarities and cross-reactivity between the different receptors (Zhu et al., 1991; Muff et al., 1995). For instance, it was proposed that biological effects of amylin in bone may be mediated, at least in part, through binding of amylin to calcitonin receptors on bone cells (Cooper, 1994). Another example, is that it appears the N-terminally truncated CGRP is a competitive antagonist of the metabolic actions of amylin (Wang et al., 1991). So far, only the structures of the calcitonin receptor and subtypes

have been identified. The majority of the receptors remain unknown. It does, however, appear that all of the receptors belong to the family of G-protein-coupled receptors (Force et al., 1992).

1.5 *About This Thesis Research*

Although the importance of amylin's biological functions, such as carbohydrate metabolism has been recognized, the significance of amylin in the onset and progression of islet dysfunction and insulin resistance is not fully understood. Because of its insolubility and aggregation phenomena, the structure of amylin monomer has not been determined. Early amylin structural models of the constituent cross-β fibril are only based on the low-resolution technique of X-ray fiber diffraction. More recently, electron microscopy (EM), Fourier-transform infrared spectroscopy (FTIR), and empirical molecular modeling were used to explore the structure of amylin (Saldanha & Mahadevan, 1991; Ashburn, 1992; Ashburn & Lansbury, 1993). However, none of these techniques can provide detailed structural information about amylin. It is of great importance to further investigate the structure of amylin and determine the conformational basis of amyloidogenicity which may lead to the design of drugs to disaggregate amyloid in the NIDDM pancreas and inhibit amylin's action by blocking its receptors.

This dissertation presents structural and dynamics information obtained for amylin and its analogues. To the best of our knowledge, this study is the most comprehensive, systematic structural study of amylin to date. The next chapter presents general features of peptide structure and dynamics, along with the techniques used to study these questions. Chapter 3 describes specific experimental procedures used in the present study. Chapter 4 presents the results for human and rat amylin , and for a fully active amylin agonist, pramlintide. A detailed structural study of amylin fragments is presented in Chapter 5, revealing the factors stabilizing secondary structure in these peptides. Chapter 6 is a comparison study of amylin, salmon calcitonin and CGRP fragments, which reveals the structure similarities and differences among these peptides.

Table 1.1 Effects of Amylin, Calcitonin (CT) and Calcitonin Gene-related peptide (CGRP). (Muff et al. 1995)

	Amylin	CT	CGRP
Bone Resorption	↓	↓↓	↓
Pain Perception	ND	↓	↑
Gastrointestinal			
Acid output	ND	↓	↓
Food intake	↓	↓	↓
Cardiovascular			
Vasodilatation	↑	↑	↑↑
Arterial pressure	↓	→	↓
Chronotropic action	↑	→	↑
Contractility heart	ND	→	↑
Renal			
Blood flow	ND	→	↑
Glomerular filtration rate	ND	→	↑
Renin secretion	↑	↑	↑
Gluconeogenesis in the Skeletal			
Musculature	↓	↓	↓

Symbols: ND not done; → No influence; ↑ Stimulate; ↓ Suppress.

```
human Amylin   KCNTATCATQRLANFLVHSSNNFGAILSSTNVGSNTY NH2
   Monkey AM   -----------------R------T---------D-- -
      Cat AM   ----------------IR----L-----P-------- -
      Dog AM   ----------------RT---L-----P-------- -
      Rat AM   ----------------R----L-PV-PP-------- -
    Mouse AM   ----------------R----L-PV-PP-------- -
  Hamster AM   ------------------N--L-PV--P-------- -
Ginea pig AM   -----------T----R--H-L--A-LP-D------ -
     Degu AM   -----------T----R--H-L--A-PP-K------ -
   Rabbit AM   ----------------I---------F-PPS------ -
     Hare AM   ----------------I---------F-PPN------ -

        hCT    CG-LS--MLGTYTQDFNKFHT      FPQ-AI-VGAP -
  salmon CT    CS-LS--VLGK-SQE-HKLQT      YPR--T--G-P -
    hCGRP-I    A-D----V-H---GL-SR-GGVVKNNFVP-----KAF -
   hCGRP-II    A------V-H---GL-SR-GGMVKSNFVP-----KAF -
```

Figure 1.1 Sequence Comparison for Amylins, Calcitonin, and CGRP (Meadows et al., 1991; Steiner et al., 1991; Cooper, 1994; Muff et al. 1995).

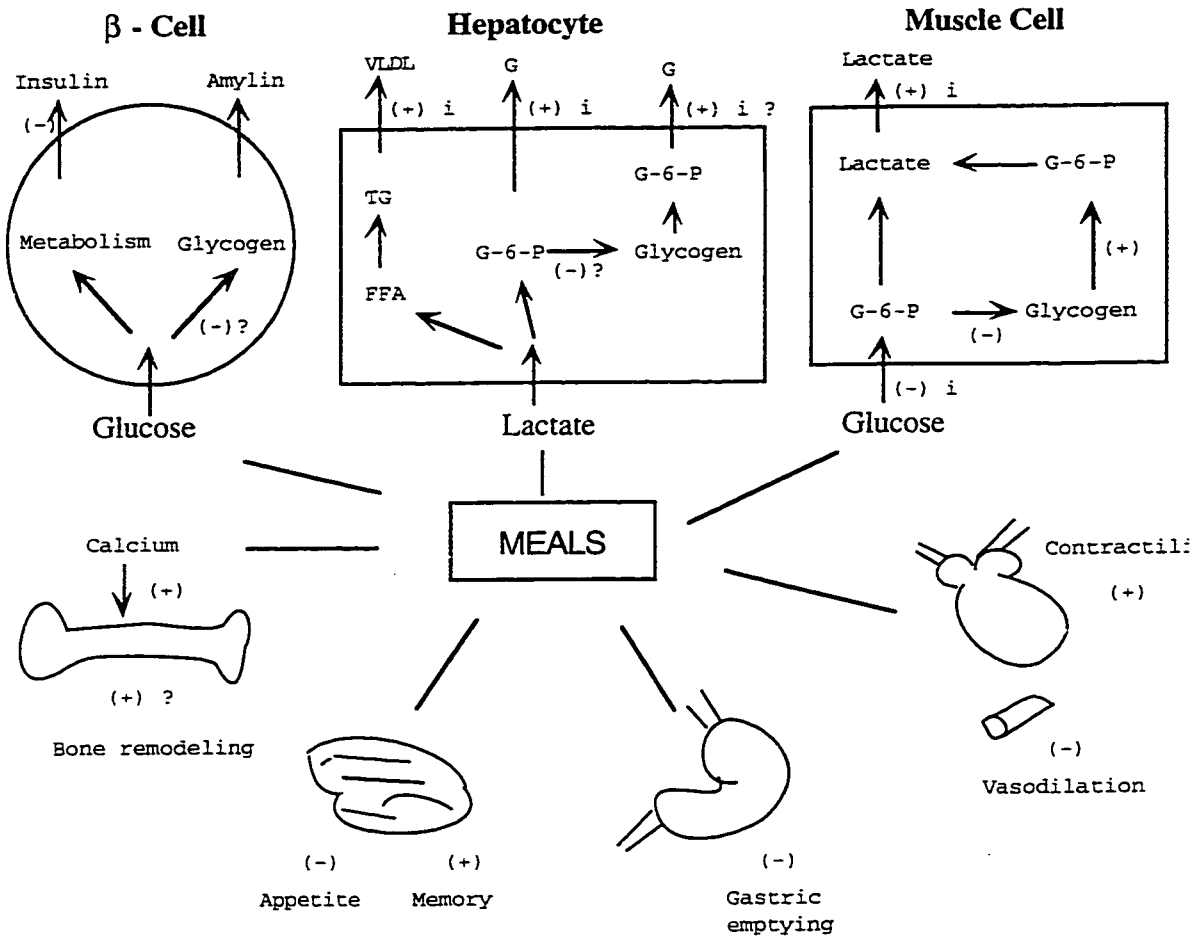

Figure 1.2 Biological Functions of Amylin (Castillo et al. 1995)
Symbols: (+) stimulatory, (-) inhibitory, i indirect effect, ? suspected actions

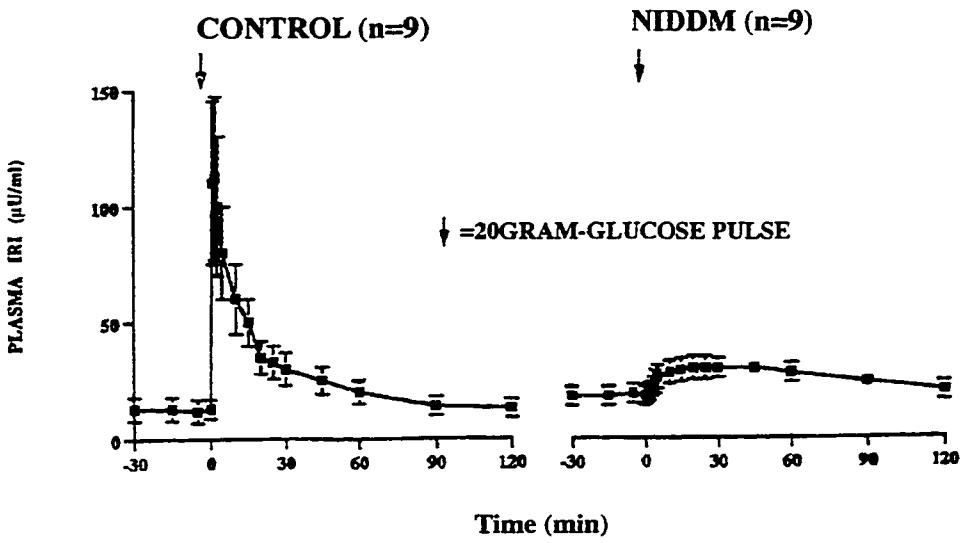

Figure 1.3 Insulin Responses to Intravenous Administration of Glucose. (Pfeifer et al., 1981)

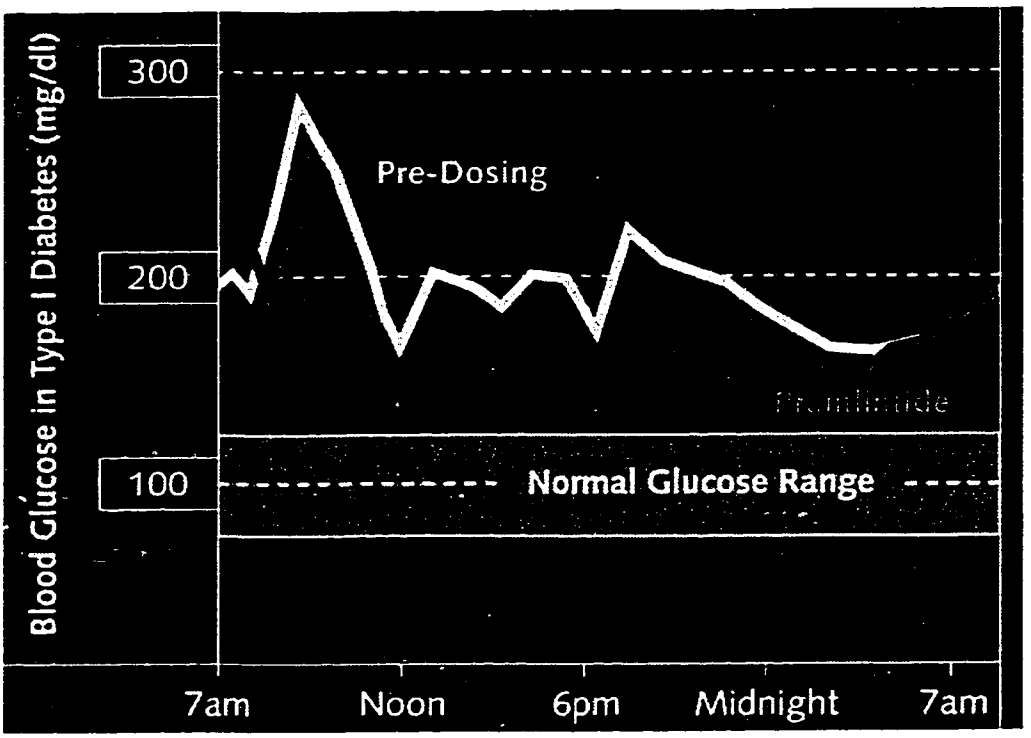

Figure 1.4 Pramlintide Lowers Glucose Levels in IDDM (Amylin Annual Report, 1995; Kolterman et al., 1996). (Pre-dosing curve: Average glucose for 38 patients before dosing; Pramlintide curve: Average glucose for 38 patients after 28-day injection of 30 μg pramlintide at meals.)

Chapter 2

Conformational Analysis of Polypeptides

2.1 *Polypeptide Structure and Dynamics*

2.1.1 *Regular Secondary Structure Motifs*

A polypeptide is a string of amino acids linked by peptide bonds. The peptide bond torsion angle (ω) is usually planar, owning to the partial double bond. Normally, the trans form of the peptide bond (ω=180°) is favored 10^3 fold over the cis form (ω=0°), due to the side chain repulsion. In the case of proline, a secondary amide is involved, the trans form is only slightly favored by about 4 fold (Figure 2.1) (Creighton 1993).

A model of peptide unit is shown in Figure 2.2. The peptide backbone consists of a repeated sequence of three atoms: the amide N, the alpha C ($C\alpha$), and the carbonyl C (C'). The dihedral angle about the N–C_α bond is called ϕ, and that about the C_α–C' bond is called φ. Since the peptide group is rigid and planar, the conformation of the backbone is completely defined by these dihedral angles. The side chain conformation is defined by torsions χ^1, χ^2,..., etc. There are geometrical restraints on possible ϕ and φ values, only certain combinations of backbone dihedral angle are allowed, which usually presented in a Ramachandran plot -- a two-dimensional map of the ϕ - φ plane with the indication of permitted values of ϕ and φ (Ramachandran & Sasisekharan 1968). Peptide backbone can fold into regular repeating structures, and the following are the most common ones.

The right-handed α helix (Figure 2.3 left panel) is the best-known and most prominent of the regular secondary structures (Richardson, 1981). It was first deduced by Pauling and Corey (Pauling & Corey, 1951), and proven to be correct six years later by x-ray crystallography. It has 3.6 residues per turn with a translation of 5.41Å. The tightly coiled backbone forms the inner part of the helix, and the side chains extend outward in a helical array. The α helix is stabilized by hydrogen bonds between the backbone carbonyl oxygen and the amide proton of the fourth residue along the chain. These hydrogen bonds are nearly parallel to the helix axis and this aligns the carbonyls resulting in a large helix dipole. In peptides, helices usually loosen up at both ends, termed "end fraying", due to the lack of H-bond partners. The averaged ϕ and φ backbone dihedral values of an α helix are -57° and -47°, respectively (Barlow &

Thornton 1988; Creightton 1993). It has been reported that systematic variation of ϕ and φ value can produce bent helices (Blundell et al., 1983).

The *3_{10} helix* is a tighter helix compared to α helix. It contains 3 residues per turn, and one less residue per hydrogen bond. This type of helix is usually short, only one or two turns. In proteins, it is also observed at the ends of α helices. However, it is more common in peptides, especially in Aib (amino-isobutyric acid) rich sequences (Karle & Balaram, 1990; Andersen et al., 1996b).

Pro I and Pro II 'helices'. As the only naturally occurring tertiary amide in polypeptides, proline is not compatible with either α helix or β sheet. Homopolymers of proline have some unusual conformation, known as Pro I and Pro II helices. Pro I contains all *cis* peptide bonds, and is a right-handed helix with 3.3 residues per turn; Pro II has all *trans* peptide bonds, and is a left-handed helix with 3.0 residues per turn (Creighton, 1993). The Pro II conformation represents a relatively deep energy well in the β-region of the Ramachandran chart (Woody, 1994). This conformation is quite extended with a 3.12 Å translation per residue.

β strand (Figure 2.3 right panel) is another periodic secondary structure found in proteins, which has not been well defined in monomeric peptides due to the tendency of β-peptides to aggregate. In a β strand conformation, the polypeptide chain is nearly fully extended. The axial distance between adjacent amino acids is 3.5Å. The extended conformation is a significant contributor to the disordered state of peptides. In proteins, β strands aggregate side by side forming β sheets.

Reversing Turns (β and γ) (Figure 2.4). Polypeptide chains reverse direction sharply in only a limited number of ways. These turns occur over 3 (γ turns) or 4 (β turns) residue-spans and often include a hydrogen bond between the carbonyl oxygen of residue *i* and the amide proton of residue *i+2*, or *i+3*. γ turns are relatively rare in proteins (Richardson, 1981). All of these turns are characterized by distinct ϕ and φ values for the residues at the corners of the turn. β turns can be divided into sub-types: type III turns resemble a single turn of a 3_{10} helix, while type I and II are the most common reverse turn in globular proteins. Types I' and II' have also been identified, with the prime indicating an approximate 180° rotation of the peptide group of the *i+1* residue.

Table 2.1 summarizes the parameters for above common polypeptide conformations.

2.1.2 *Conformational Averaging and Flexibility*

Unlike proteins, peptides have no tertiary structure, some even have little secondary structure. Small linear peptides, usually sample a large number of conformations which are in rapid equilibrium. This is the so called "random coil" or disordered conformation. The random coil is not really random; in fact, Ramachandran and co-workers concluded that for single amino acids larger than alanine only 23% of the ϕ/φ conformational space was allowed (Ramachandran & Sasisekharan, 1968). Although not truly "random", these are conformationally averaged systems; and the "structural" analysis of peptides with more than a few conformations is not possible by any available experimental method. As the size of the peptide increases, more secondary structural elements emerge. Some may have a few conformers under slow exchange; while others may have only one major conformer in equilibrium with decreasing amounts of the "random coil" state.

There are many structural factors that influence the conformational preference of peptides. Some specific sequences or amino acids can stabilize helices (Vijayakumar & Balaram 1983; Imperiali et al., 1992). For example, α, α-di-methyl amino acids are well known to stabilize helices. Covalent linkage, such as cyclic amides, disulfide bridge and lactone structures can dramatically reduce the flexibility of a peptide or small protein (Ösapay & Taylor, 1992; Luo et al., 1994). Previous work from our group (Andersen et al., 1993, 1992a) and from other researchers, have shown that medium sized peptides with covalent cross links, may only adopt limited number of backbone conformations (often only one) (Kessler, 1982). Hevein (Andersen et al., 1993), a 43-residue protein with 4 disulfide linkages, and endothelin (Andersen et al., 1992a), a 21-residue medium sized peptide with 2 disulfide bridge, both have single predominant conformer which can be deduced by NMR.

Peptide conformation is greatly influenced by the conditions under which the system exists. Peptides are temperature sensitive: usually, as the temperature decreases, more secondary structure can be detected; however, there are cases in which, as the temperature goes down, the peptide becomes more disordered; this is known as "cold denaturation" (Doty & Yang, 1956; Calvin et al., 1959; Privalov, 1990; Andersen et al., 1996a; Lacassie et al., 1996). Peptides are also more sensitive to the solvent than proteins, since they have a larger ratio of surface area to volume than proteins. It has been reported that some solvents, such as flouroalchohols (Tamburro

et al., 1968; Parrish & Blout 1972; Dealba et al., 1996) or cryomixtures (Temussi et al., 1992), can induce structure. Other factors, like pH, and ionic strength can also have a large influence on peptide conformation.

2.2 *Structural Information from NMR Spectroscopy*

Nuclear Magnetic Resonance (NMR) spectroscopy has been one of the most powerful tools for structure elucidation in the past twenty years. The development of 2D NMR began in the seventies (Aue et al. 1976). In the eighties, many 2D NMR techniques emerged (Bax & Lerner, 1986; Ernst et al., 1987), followed by the development in heteronuclear 3D, and, 4D methodologies in the nineties which makes it possible to study the structure and dynamics of proteins in the 20 - 40 kDa range (Clore & Gronenborn 1993). The importance of NMR has continued to increase; the Chemistry Nobel Prize in 1991 was awarded to the Swiss physical chemist Richard R. Ernst for his outstanding contributions to the development of experimental NMR techniques.

In this dissertation, the author does not intend to review the details of the NMR theory or its application to peptide or protein research. The NMR theory or a review of such applications can be found in numerous articles and text books (Wüthrich, 1986; Derome, 1987; Neuhaus & Williamson, 1989; Sanders & Hunter 1993; Clore & Gronenborn 1993; Croasmun & Carlson 1994; Günther, 1995). Nonetheless, important concepts and experiments critical to this dissertation, will be briefly introduced in the following sections.

2.2.1 *Nuclear Overhauser Effect (NOE)*

An NMR-based assignment, secondary structure characterization, and structure ensemble calculation strategy for polypeptides was established some time ago. (Wüthrich, 1986; Dyson, 1991). The Nuclear Overhauser Effect is the key to all aspects.

Nuclear Overhauser Effect (NOE). A nuclear Overhauser effect is a change in the intensity of an NMR resonance when the transitions of another one are perturbed. It is the major mechanism of z magnetization relaxation. It does not depend on the presence of scalar coupling, instead, it is a through space dipolar coupling interaction, the magnitude of which is related to internuclear distances and molecular motion. It is well known that the magnetization transfer (or cross-relaxation) rate (which is

proportaional to r^{-6}) corresponds to the initial growth rate of the NOE, thus the interproton distances (d_{ij}) can be calculated from the intensity (S) of the NOE cross peaks using following equation, assuming that all NOE cross peaks are still in their linear growth phase:

$$d_{ij} = r_{ref}\left(\frac{S_{ref}}{S_{ij}}\right)^{1/6}$$

where S_{ref} is the intensity of the cross peak representing an interaction with a known distance, r_{ref}.

Obtaining accurate distance constraints is critical for the success of structure elucidation. Many factors can influence NOE intensities. Insufficient relaxation delay and magnetization leakage are the major problems with small molecules, since magnetization in small molecules at individual spin sites decays slowly, largely by leakage rather than transfer to other sites. For macromolecules, such as peptides and proteins, spin diffusion is one of the major obstacles for obtaining accurate distance constraints. In macromolecules, NOE cross-peaks cannot be viewed as a series of isolated two spin system; rather, intensities depends in a more complex way on all of the distances. Magnetization can be transfered indirectly from protons other than the pair of proton under consideration. NOEs observed in NOESY spectra with sufficient long mixing time can be secondary -- transfered from more remote pair interactions, as illustrated in Figure 2.5. Therefore, observation of an NOE between two protons does not, on its own, provide sufficient evidence that they are 'close'. Thus, for macromolecules, it is important to used short mixing time NOESY spectra to derive distance constraints for structure emsemble calculation.

Another difficulty of NOE based structure elucidation of medium-sized peptide is that, as previously mentioned, such peptides are conformationally averaged systems. The measured NOE growth rate is the population weighted average over all conformations of the peptide. However, the observation of a direct NOE between a pair of protons does indicate the presence of at least a threshold population of conformers in which the distance between these protons is relatively short.

Another problem frequently encounted is that medium to small sized peptides are of a size or have segmental motions that quite often place the effective correlation

time at the point where NOEs are near zero. The magnetization cross transfer rate between spin i and j, σ_{ij}, can be expressed as following:

$$\sigma_{ij} = \frac{K\tau_c}{r_{ij}^6}\left(1 - \frac{6}{1+4\omega_0^2\tau_c^2}\right)$$

where ω_0 is the Larmor frequency, r_{ij} is the interproton distance, τ_c is the correlation time, and K is 5.7×10^{10} for proton systems, when the units of ω_0, r_{ij}, τ_c are rad/s, Å, s, respectively. When $(\omega_0\tau_c)^2 \rightarrow 1.25$, $\sigma_{ij} \rightarrow 0$; thus, the NOE $\rightarrow 0$. One way out of this is to either change field strengths or change correlation time (τ_c) of the molecule by changing solvent or temperature. Another solution to this problem is using Rotating frame Overhauser Effect (ROE) spectroscopy. ROEs are due to cross relaxation of transverse magnetization and have a similar intensity to distance relationship as NOEs. In contrast to NOEs, ROEs are always positive; however, they are more difficult for quantitative, since the spin-lock field introduces intensity variations into the spectrum.

Characteristic NOEs in Regular Secondary Motifs. Usually, an NOE is observed for nuclei within 4 Å, sometimes detectable to 5 - 5.5 Å, but may be secondary. The characteristic NOE observations for an α-helix include: a series of relatively strong $d_{NN}(i, i+1)$ NOE connectivities, accompanied by a diminished magnitude of the $d_{\alpha N}(i, i+1)$ NOE, along with medium-range $d_{\alpha N}(i, i+3)$, $d_{NN}(i, i+2)$, $d_{\alpha\beta}(i, i+3)$, and $d_{\alpha N}(i, i+4)$ NOEs. In contrast, strong $d_{\alpha N}(i, i+1)$ NOE connectivities and the absence of observable $d_{NN}(i, i+1)$ NOEs are the characteristic NOE pattern of a β strand or disorder states which include extended backbone conformations; long range ^1H-^1H contacts between neighboring strands in β-sheets can also be observed. The accepted criteria for turn formation includes: $d_{NN}(i, i+1)$ NOE connectivities between residues 3 and 4 of the turn, a $d_{\alpha N}(2, 4)$ NOE connectivity, and medium-range $(i, i+2)$ NOE connectivity which unambiguously establishes the bend of the polypeptide chain at this site. Table 2.2 summarizes short sequential and medium-range inter-residue ^1H distances in polypeptide secondary structures, which are expected to give rise NOEs. Generally, inter proton distances extracted from NOE intensities are used to set experimental constraints for Molecular Dynamic (MD) calculations.

NOE Ratios. More recently, a novel method has been used for deducing the conformational preferences of peptides based on the relative intensities of NOEs. This NOE ratio method was first suggested by Bradley et al (Bradley et al., 1990), followed by other research groups (Jimenez et al., 1993; Waltho et al., 1993; Gagné et al.,

1994). Figure 2.6 shows, for instance, that the $I_{Ni\alpha i}/I_{\alpha i-1Ni}$ NOE ratio (where I is the intensity of the NOE) is smaller than 1 for β-strands, and larger than 1 for right-handed α-helices. Since the variation of amide exchange rates for different residues is one of the main causes of inaccuracy in NOE quantitation, utilizing NOE ratios, which are independent of amide exchange, (as the two NOEs employed are measured at the same amide HN frequency), can be seen as a distinct advantage. Another example is the use of relative magnitudes of the medium-range $d_{\alpha\beta}$ (i, i+3) NOE connectivities as an indicator of helical population distribution. Local NOE ratios reflect specific residue ϕ/φ values, and thus provide a more dependable quantitative estimate for the fractional helicity at each residue. In this research group, we extended these approaches to make use of additional NOE ratios and established a method to quantitate sequence specific fractional helicity (Lee et al., 1994; Andersen et al., 1995a).

2.2.2 Chemical Shifts and Secondary Structure

Nowadays, NOE based structure elucidation has nearly become routine for relatively rigid small protein systems; however, determining the solution conformations of medium to small sized linear peptides remains a difficult task due to conformational averaging. As previously mentioned, one of the problems in using NOE-based methods is that, in many cases, medium to small sized peptides are of a size or have segmental motions that place the effective correlation times where NOEs are near zero. Furthermore, even if NOEs are detected and quantifiable, quantitative interpretation is almost impossible since the observed NOEs result from population-weighted magnetization transfer rates. On the other hand, chemical shifts are the most accessible quantities in NMR spectroscopy, and for conformational mixtures the chemical shifts are direct population weighted averages. Can chemical shifts provide structural information for peptide/protein structure elucidation?

Because chemical shifts can be easily measured with high accuracy, it has long been believed that they could eventually be the richest source of structural information for peptides and proteins. Many attempts to explore this tremendous source of information have appeared since 1960 (Markley, et al., 1967; Tigelaar & Flygare 1972; Clayden & Williams, 1982); however, all met with little succeed owing to a lack of chemical shift data. Not until the late 80s and early 90s, with the rapid growth of the chemical shift database to over 100 proteins, was the significance of chemical shift for peptide/protein secondary structure determination statistically verifiable. Many research

groups pioneered the use of chemical shifts for peptide structure elucidation (Jiménez et al., 1987; Szilágyi & Jardetzky, 1989; Bruix et al., 1990; Pastore & Sauder, 1990; Williamson, 1990; Wishart et al., 1991), among which the most comprehensive survey is due to Wishart et al. (1991). The analysis of about 5000 backbone and 14,000 side-chain ^1H chemical shifts and secondary structure designations from over 70 proteins revealed very strong relationships between ^1H NMR chemical shifts and protein secondary structure. It was found that the α-^1H chemical shift of all naturally occurring amino acids is upfield by an average of 0.39 ppm from the random coil value when the residue is in a helical configuration; while it is downfield by an average of 0.37 ppm when it is in a β-strand. Similar analyses and theoretical calculations of chemical shifts for other nuclei also revealed correlations between chemical shifts and secondary structure, which are summarized in Table 2.3. A novel method using Chemical Shift Indices (CSIs) (Wishart et al., 1992; Wishart & Sykes, 1994), has been put into use based on these relationships. Since then, many groups, including our research group, have further advanced this methodology and demonstrated that Chemical Shift Deviations from random coil values ($CSD = \delta_{obs} - \delta_{ref}$) are useful for rapidly and quantitatively determining the identity, location, and extent of secondary structural elements (Andersen et al., 1992b; Jiménez et al. 1993; Case et al., 1994; Andersen et al., 1995a), especially for conformationally averaged peptides.

Some caution is required when using the CSD method. It is absolutely critical to the success of CSD-based structure elucidation to choose or calibrate the chemical shift standards carefully. In the past, many chemical shift references have been used under various conditions without proper calibration, which led to widespread distrust of the method within the biochemical NMR community. A comparison of different chemical shift standards has been done by Wishart & Sykes (1994), which reveals that many references are sensitive to pH, temperature, and cosolvents. It was estimated that there are systematic errors of between 0.05-0.15 ppm for ^1H, approximately 2.0 ppm for ^{13}C, and at least 2.0 ppm for ^{15}N chemical shift data, due to calibration and referencing problems. These 'random errors' in the chemical shift data can defeat CSD based analyses. It was recommended to use DSS as the 0.000 ppm reference in aqueous media, since its shift is not pH or temperature dependent. TSP is equally good at low pHs, however, it is pH dependent.

Another equally important aspect of CSD analysis is the use of appropriate random coil values, which should represent the intrinsic shift of each amino acid

primarily determined by the chemical properties of the side chain of the residue. Many investigators have attempted to derive random coil reference values. As early as 1975, Wüthrich and coworkers published random coil values for all naturally occurring amino acids (except Pro) in DMSO (Bundi et al., 1975). As the CSD method is now widely accepted, there are several sets of the random coil values (determined either experimentally or statistically) published (Braun et al., 1994; Wishart et al., 1994; 1995a; Merutka et al., 1995). Our research group has put lot of effort in improving the random coil values. By combining published data and data from this laboratory, a set of coil value for α-^{1}H and amide ^{1}H was derived, with corrections for terminal end effects, nearest-neighbor interactions, and cosolvent effect (Andersen et al., 1995b, 1996b, 1997). It will be described in detail in the next chapter.

As the CSD method has become more and more popular, there have been efforts to discover the origins of structure-dependent chemical shifts. Chemical shifts are governed by local magnetic fields arising from anisotropies of distant functional groups; and local electric fields created by distant dipoles or charges. Peptide groups, ring current, and electrostatic charges can be represented empirically, and chemical shifts are usually calculated using semiempirical or *ab initio* quantum calculations. Calculation of structural shifts for the α-proton in a dipeptide as a function of the ϕ and φ dihedral angles revealed that the principal variation arises from ϕ (See Figure 2.7, Ösapay & Case 1991). More recently, amide ^{1}H, ^{15}N, ^{13}C shifts prediction also become available (Oldfield, 1995; Asakura et al., 1995; Ösapay & Case 1994; De Dios et al., 1993; Herranz et al., 1992). Amide ^{1}H and ^{15}N shifts largely depend on H-bond length. ^{13}C shifts mainly depend on ϕ and φ torsion angles. Chemical shift prediction and experimental shift data can be used for structure refinement in conjunction with NOE based molecular dynamic calculation.

In conclusion, CSD analysis has become an important supplement for more traditional NOE-based structure elucidation. It is an even more important tool for the evaluation of conformationally averaged system (Case et al., 1994; Andersen et al., 1995a).

2.2.3 Other Structural Information from NMR Data

Spin-spin coupling constants have also proven to be very useful in structure determination. Coupling constants can give direct information on dihedral angles and stereospecific assignments of prochiral groups (Case et al., 1994; Smith et al. 1991).

For example, $^3J_{HN\alpha}$ is commonly related to the dihedral angle ϕ according to a Karplus equation (Bystrov 1976):

$$^3J_{HN\alpha} = A \cos^2 \theta - B \cos \theta + C$$

Where $\theta = \phi - 60°$, and the estimated coefficients A, B, and C are 6.4, -1.4, and 1.9. $^3J_{HN\alpha}$ is large (8-10 Hz) when the residue is in β conformation ; while it is small (4-5.6 Hz) when the residue is in a helix. Another useful coupling constant is $^3J_{\alpha\beta}$, which can be related to the side chain dihedral angle χ_1 through a Karplus equation. Extreme values (>10 or < 5 Hz) of $^3J_{\alpha\beta}$ indicate that one rotamer is predominantly populated (this will be illustrated in more detail later). In the case of conformationally averaged system, J coupling is also averaged.

The resonance linewidth can also provide structural insights. The linewidth is related to a relaxation time constant, T_2*:

$$\Delta\upsilon_{1/2} = 1/T_2^* \pi$$

where $\Delta\upsilon_{1/2}$ is the width at half the height of the peak, and T_2* is the transverse relaxation time constant, which can act as an indicator of molecular motion.

The temperature coefficients of amide NH chemical shifts can provide valuable information on the interaction of the amide proton with hydrogen-bond-accepting solvent molecules (Llinás & Klein, 1975); also it can be used as an indicator of conformational transitions (Liu et al., 1994). In rigid structures, the temperature gradient reflects solvent exposure, typically it is assumed that gradients more positive than -4 ppb/°C indicate H-bonding (-7.6 ppb/°C is for the random coil value) (Andersen et al., 1997). However, in conformational averaged systems, the observed temperature gradient will reflect changes in conformer population in addition to the interaction with the bulk solvent, and it correlates better with NH CSD than exchange protection. As a result, it can provide measurements for both ΔG and the degree of cooperativity in a peptide structure $\leftrightarrow$ coil transition (Andersen et al., 1997).

2.3 *Constrained Molecular Dynamics*

From the advent of two-dimensional NMR techniques (Wüthrich 1986), and now with a whole array of 3- or 4-dimensional heteronuclear NMR techniques (Clore 1994), it has become possible to obtain virtually complete resonance assignments and a large number of distance constraints for polypeptide structures. A number of computational methods have been developed to use the distance constraints extracted

from NMR experiments to generate 3D structures of proteins. To date, there are essentially two general classes of methods: distance space methods, which are generally referred to as metric matrix distance geometry; and real space methods, including restrained least squares minimization in torsion angle space, restrained molecular dynamics and dynamics simulated annealing (Brünger 1987, Clore & Gronenborn 1989; Gronenborn & Clore 1991; Brünger & Nilges 1993). Among various of simulation methods, molecular dynamics, especially restrained molecular dynamics simulated annealing, based on the XPLOR program (Brünger 1987), is one of the most powerful and widely used methods for deriving the 3D protein structures from experimental NMR data. It was employed in this project.

Molecular dynamics simulations involve solving Newton's equation of motion (shown below) for all atoms of the system simultaneously.

$$m_i \frac{\partial^2 r_i}{\partial t^2} = -\nabla_i E^{pot}$$

In the case of determination and refinement of three-dimensional structures of proteins from NMR data using restrained molecular dynamics, the experimental information is incorporated into the simulation by using a hybrid potential energy function as the target function, for which the global minimum region is searched (Nilges 1988a; Brünger & Karplus 1991).

$$E_{pot} = E_{chemical} + \omega E_{expt}$$

Where $E_{chemical}$ is an empirical energy function which provides information about equilibrium covalent bonding geometry, hydrogen-bonded interactions, and nonbonded interactions (Brooks 1983). E_{expt} reflects experimental constraints derived from NMR data, usually represented by the square-well potentials for the NOE distance and torsion angle restraints (shown below). And ω is the relative weight of E_{expt}.

$$E_{NOE} = \begin{cases} k_{NOE}(r_{ij} - r_{ij}^{u})^2 & \text{if} \quad r_{ij} > r_{ij}^{u} \\ 0 & \text{if} \quad r_{ij}^{l} \le r_{ij} \le r_{ij}^{u} \\ k_{NOE}(r_{ij} - r_{ij}^{l})^2 & \text{if} \quad r_{ij} < r_{ij}^{l} \end{cases}$$

where r_{ij}^{u} and r_{ij}^{l} are the upper and lower limits of the target distances, and k_{noe} is the NOE force constant.

$$E_{tor} = \begin{cases} k_{tor}(\psi_i - \psi_i^u)^2 & \text{if} \quad \psi_i > \psi_i^u \\ 0 & \text{if} \quad \psi_i^l \le \psi_i \le \psi_i^u \\ k_{tor}(\psi_i - \psi_i^l)^2 & \text{if} \quad \psi_i < \psi_i^l \end{cases}$$

where ψ_i^u and ψ_i^l are the upper and lower limits of the target range of a particular torsion angle, and ψ_i is its calculated value.

Dynamics simulated annealing is different from conventional molecular dynamics, such as gradient descent or least-squares optimization. The basis of dynamics simulated annealing involves raising the temperature of the system followed by slow cooling in order to overcome local minima and locate the global minimum region of the target function. It achieves more optimal solutions than only searching energetically downhill (Kirkpatrick 1983). The likelihood of going uphill is controlled by temperature which is directly proportional to the kinetic energy of the system. Because fast cooling might trap the system in a meta-stable state, the temperature is decreased at a rate slow enough to ensure that the system reaches equilibrium at each stage of the annealing procedure. In dynamics simulated annealing, all non-bonded interaction terms (except hydrogen bonding potentials) of the empirical energy function are usually simplified: instead of using standard Lennard-Jones van der Waals function, a van der Waals repulsion term E_{rep} is used in the initial stages of refinement.

$$E_{repel} = \begin{cases} 0 & \text{if} \quad r \ge s.r_{min} \\ k_{rep}(s^2 r_{min}^2 - r^2)^2 & \text{if} \quad r < s.r_{min} \end{cases}$$

The values of r_{min} are the standard values of the van der Waals radii as represented by the Lennard-Jones potential used in the CHARMM empirical energy function (Brooks 1983); s is a van der Waals radii scale factor, which is initially small to facilitate sampling conformational space, and k_{rep} is the van der Waals repulsion force constant.

A set of strategies based on the principle of dynamics simulated annealing for protein structure determination by NMR have been developed using a modified version of XPLOR. In one approach, dynamical simulated annealing is initiated with an extended strand (Nigles et al., 1988a) or randomly generated structures. Another approach is a hybrid distance-space/real-space method (Nilges et al., 1988b). Still another, is a new real space method based on the principles of dynamical simulated annealing, circumventing problems associated with folding entirely (Nilges et al., 1988c).

The success of such protein structure refinement protocols is largely dependent on occurrence of regular secondary structure motifs *and* long-range NOEs which reflects sequence remote contacts associated with tertiary structure (Borgias & James 1988; Andersen et al., 1990). Small physiologically active peptide systems would not meet these requirements since they lack tertiary structure. Moreover, as already mentioned, small peptides are more likely to retain regions of segmental motion which complicates NOESY analysis and precludes the use of coupling constants as added constraints (which greatly improves the resolution in protein NMR structures). Therefore, other methods must be applied to conformationally versatile small or medium-sized peptides.

2.4 *Circular Dichroism, Secondary Structural Signatures*

Another widely used technique to investigate the structure of peptides and proteins is circular dichroism (CD) (Yang et al., 1986; Johnson 1992; Woody 1992; Towell & Manning 1994). Plane polarized light contains equal portions of left- and right- handed circularly polarized light (Fresnel 1824). When the circularly polarized light passes through a optically active sample, the sample absorbs left- and right-handed circularly polarized light differentially; and the difference in extinction coefficient $\Delta\varepsilon = \varepsilon_L - \varepsilon_R$ results in circular dichroism (CD). When differential absorption occurs, the resulting light is no longer linearly polarized, instead is elliptically polarized; thus, the elllipticity of the resulting light, θ_λ, which is proportional to $\Delta\varepsilon$, is commonly used as a measurement of CD (Adler et al., 1973).

CD spectroscopy is not only sensitive to the local chirality of the peptide unit; more importantly, it also reflects global chirality, that is, the way the chiral units are arranged in space. Therefore, CD can provide both qualitative and quantitative information concerning secondary and tertiary structure in peptides and proteins. There are two spectral regions are of interest for peptide/protein structure studies: the far UV (175-250 nm) region and the near UV (240-320 nm) region. Far UV absorptions are mainly due to the peptide backbone, more specifically, amide bonds; and typically reflect the secondary structure. Side chain chromophores, such as aromatic side chains (Tyr, Trp, and Phe), and disulfides are the only contributors in the near UV regions, they also have absorptions in the far UV region. Usually, near UV bands are much weaker than far UV bands; and the changes in near UV region reflects changes in tertiary structure.

Figure 2.8 shows the reference CD spectra for four main classes of polypeptide secondary structures: α helix, β strand, β turn and random coil, either derived in our laboratory or from other publications.

The CD signature of an α helix is characterized by an intense double minimum (bands near 221nm and 208nm), and a strong positive band near 192nm. The exact position and the intensity of the double minimum depends on the length of the helix, the exact ϕ and ψ angles, and the solvent. The ellipticity at 221nm corresponding to 100% helicity in the literature ranges from 32,000-42,500 deg cm^2/amide-dmol; and the positive band is typically a bit more than twice the ellipticity value at 221nm (Chen et al., 1974; Gans et al., 1991; Manning & Woody 1991). These bands are associated with the amide chromophore: the 222 nm band is the $n \rightarrow \pi^*$ transition, 208 nm and 192 nm bands are parallel-polarized $\pi \rightarrow \pi_{\parallel}^*$ exciton transition and perpendicular-polarized $\pi \rightarrow \pi_{\perp}^*$ exciton transition, respectively (Holzwarth & Doty 1965).

The CD spectra of other helixes, such as poly(Pro)II, 3_{10} helix, ω, π, and α_{II} helix, are much less well defined. For instance, many attempts have been made to distinguish 3_{10} helix from α helix by CD, however, the results are still controversial (Millhauser 1995; Andersen et al., 1996b; Toniolo et al., 1996).

The CD spectra of β sheet containing structures display a single negative band near 217 nm, although the position can vary by up to 5 nm. The chiral absorption becomes positive at about 205nm, followed by a positive band around 195nm. Due to the lack of well-defined model compounds, the reference spectrum for the β state is much less well defined than for an α helix. The peptide-derived β strand reference spectrum from our laboratory (Cort et al., 1994) is illustrated in Figure 2.8. Another challenge is to distinguish parallel from antiparallel β strand (Perczel et al., 1992), which is still an ongoing question.

CD spectra of β turns are similar to those of β strands, but with red-shifted extrema. The difficulty of characterizing the CD of β turns is, once again, the lack of well-characterized model compounds, plus the variation of backbone dihedral angles in different β turns. Many attempts to derive the CD signature for β turn have been based on theoretical predictions or deconvolution analysis (Woody 1974; Perczel & Fasman 1992).

The CD of denatured proteins or small peptides, namely random coil structure, displays one dominant feature: a strong negative band near 198 nm and the intensity can reach -40,000 deg cm^2/amide dmol. Sometimes, a weak positive band near 215-226

nm may be observed depending on the particular system or conditions. It has been proposed that this reflects the contribution of the poly(Pro)II conformation to the "disordered" equilibrium, particularly at low temperatures (Tiffany & Krimm 1968a,b; Woody 1992).

Figure 2.9 shows the far UV CD spectra of a few aromatic side chains in disordered coil state (Harris 1993). In addition, near UV bands occur near the ^1L_b absorption maxima (280 - 290 nm for Trp, near 275-280 nm for Tyr, and around 250 - 260 nm for Phe). They are much less intense than the far UV backbone spectra, but they are good indicators of tertiary structure changes, since the CD of aromatic side chain depends on the local environment. For instance, they were used to successfully probe the aggregation of human amylin (Cort et al., 1994).

Compared to the aromatic chromophores, the CD spectra of disulfides in peptides or proteins has received little attention, owning to the fact that the absorbance is very weak, the nature of the transition is poorly understood and little data is available.

Generally, based on a knowledge of the CD signatures of polypeptide secondary structure, one can obtain qualitative information about peptide structure. Unlike NMR method, which can provide structural information at an atomic level, CD is the sum of the chiral UV spectra over each chromophore in each species present. CD and NMR signal detection have widely different time scales. Experimentally, CD is less time-consuming than NMR and can be accomplished with smaller samples. In this dissertation, CD was employed to probe helix/coil transitions, thermal denaturation, or other structural changes induced by cosolvent additions, in a timely fashion.

Table 2.1 Parameters for Regular Polypeptide Conformations (Creighton 1993)

	Bond Angles (°)			Residues Per turn	Translation Per residue (Å)
	ϕ	φ	ω		
Right-handed α-helix	-57	-47	180	3.6	1.50
3_{10}-helix	-49	-26	180	3.0	2.00
π-helix	-57	-70	180	4.4	1.15
Antiparallel β-sheet	-139	+135	-178	2.0	3.4
Parallel β-sheet	-119	+113	180	2.0	3.2
Polyproline I	-83	+158	0	3.33	1.9
Polyproline II	-78	+149	180	3.00	3.12

Turn type	Dihedral Angles of Central Residues (°)			
	ϕ_{i+1}	φ_{i+1}	ϕ_{i+2}	φ_{i+2}
γ classical	70 to 85	-60 to –70		
γ inverse	-70 to -85	60 to 70		
β Type I	-60	-30	-90	0
β Type I'	60	30	90	0
β Type II	-60	120	80	0
β Type II'	60	-120	-80	0
β Type III	-60	-30	-60	-30
β Type III'	60	30	60	30

Table 2.2 Typical Interproton Distances (Å) in Polypeptide Secondary Structures (Wüthrich 1986).

	α-helix	310 helix	β_A	β_p	Turn I	Turn II
αiNi+1	3.5	3.4	2.2	2.2	3.4	2.2
					3.2	3.2
αiNi+2	4.4	3.8			3.6	3.3
αiNi+3	3.4	3.3			3.1-4.2	3.8-4.7
αiNi+4	4.2					
NiNi±1	2.8	2.6	4.3	4.2	2.6	4.5
					2.4	2.4
NiNi+2	4.2	4.1			3.8	4.3
βiNi+1	2.5-4.1	2.9-4.4	3.2-4.5	3.7-4.7	2.9-4.4	3.6-4.6
					3.6-4.6	3.6-4.6
αiβi+3	2.5-4.4	3.1-5.1				

Table 2.3 Correlations between CSDs and Secondary Structure in Peptides/Proteins

	α helix	β sheet	Other related comments
α^1H	Upfield	Downfield	The backbone dihedral angle psi [ϕ] of the preceding [i-1] peptide group is the most important determinant. It can also be used to probe peptide flexibility. The relationship between shift periodicity and peptide amphipathic character is discussed [b, d]. Aromatic residues considerably distort the periodicity of the helix shifts [b].
amide ^1H	Upfield[a, c] Both [b, d]	Downfield	The effect of helix dipole on amide helix shift is noted, N-terminal residue shifts are more downfield. H-bond energy and Δδ correlation is noted. The discrimination of α-helix and β-sheet is not very clear, overlap 1ppm. The amide ^1H has largest helix shift, but less-sharply defined periodic [b]. Upfield shift originates in residues i-2 and i-3[c]. Correlation between HN and H-bond length is noted[c, d, e]. It is highly sensitive to local sequence variations and probably also to solution conditions [f].
β^1H	Downfield	Upfield	The difference in helix and sheet is about 0.1ppm; consequently there is overlap. Helix periodicity has been noted [b].
$^{13}C{=}O$	Downfield	Upfield	Provides a rather sensitive measure: Δδ of α-helix versus random coil is 2.9 ppm.
$^{13}C_\alpha$	Downfield	Upfield	Provides a rather sensitive measurement. Φ and φ torsion angles contribute the dominant shielding for C_α [g, h].
$^{13}C_\beta$	Upfield[f]	Downfield[f]	Φ and φ torsion angles dominate shielding for C_β.
^{15}N	Upfield	Downfield	Essential to make nearest neighbor corrections [i]. Correlates with amide ^1H. Not as informative due to overlap (3ppm) between helix and sheet. Both torsion and H-bond effects are important [h]. Side chain torsion is also important [g].

(a) Wishart et al., 1991; comments not noted all from a. (b) JIMÉNEZ et al., 1992. (c) Asakura et al., 1995. (d) Blanco et al., 1992. (e) Zhou et al., 1992. (f) Merutka et al., 1995. (g) De Dios et al., 1993. (h)Oldfield 1995. (i) Braun et al., 1994.

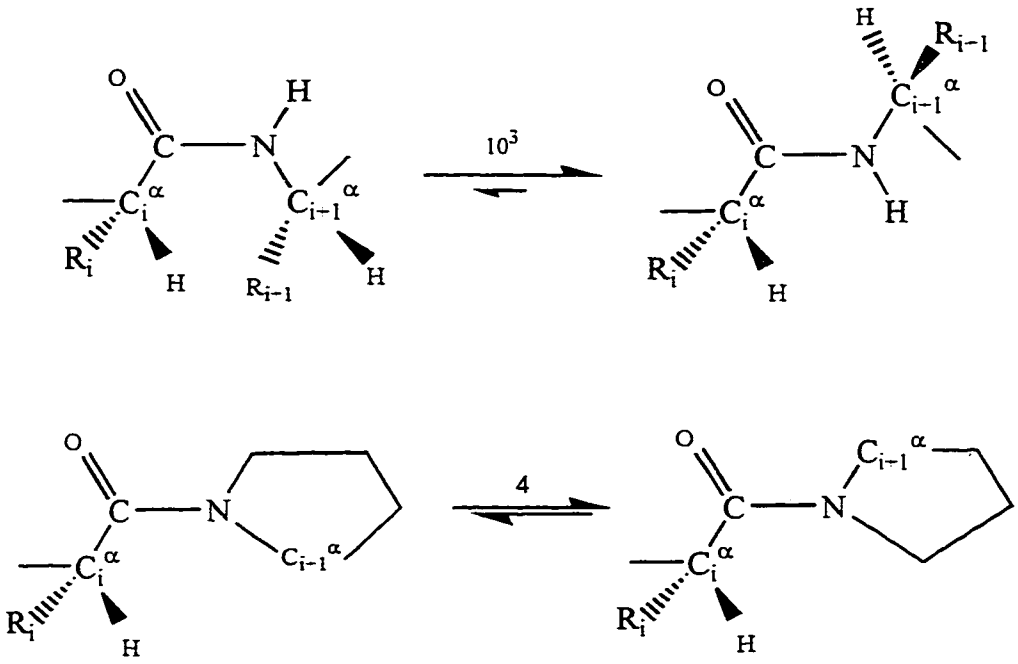

Cis Trans

Figure 2.1 Cis/Trans Peptide Bond Isomers

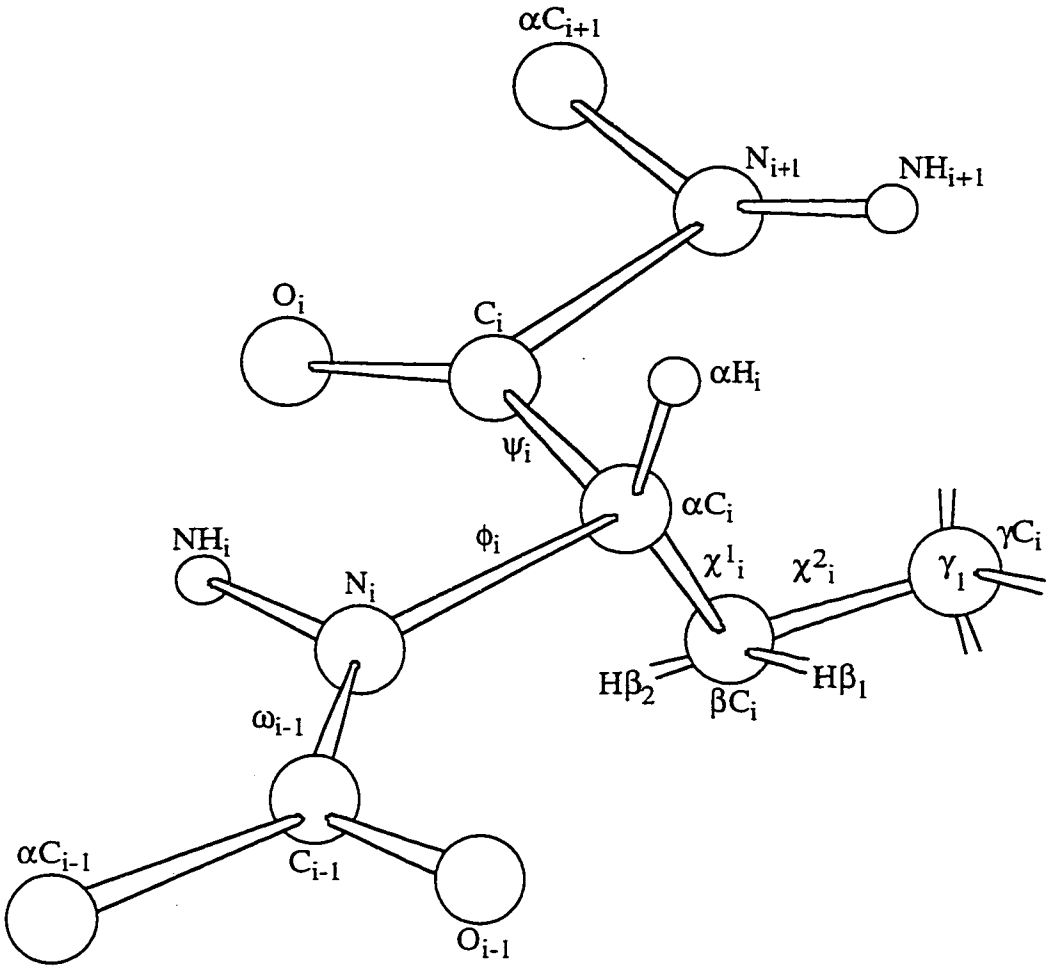

Figure 2.2 Peptide Backbone Nomenclature Conventions

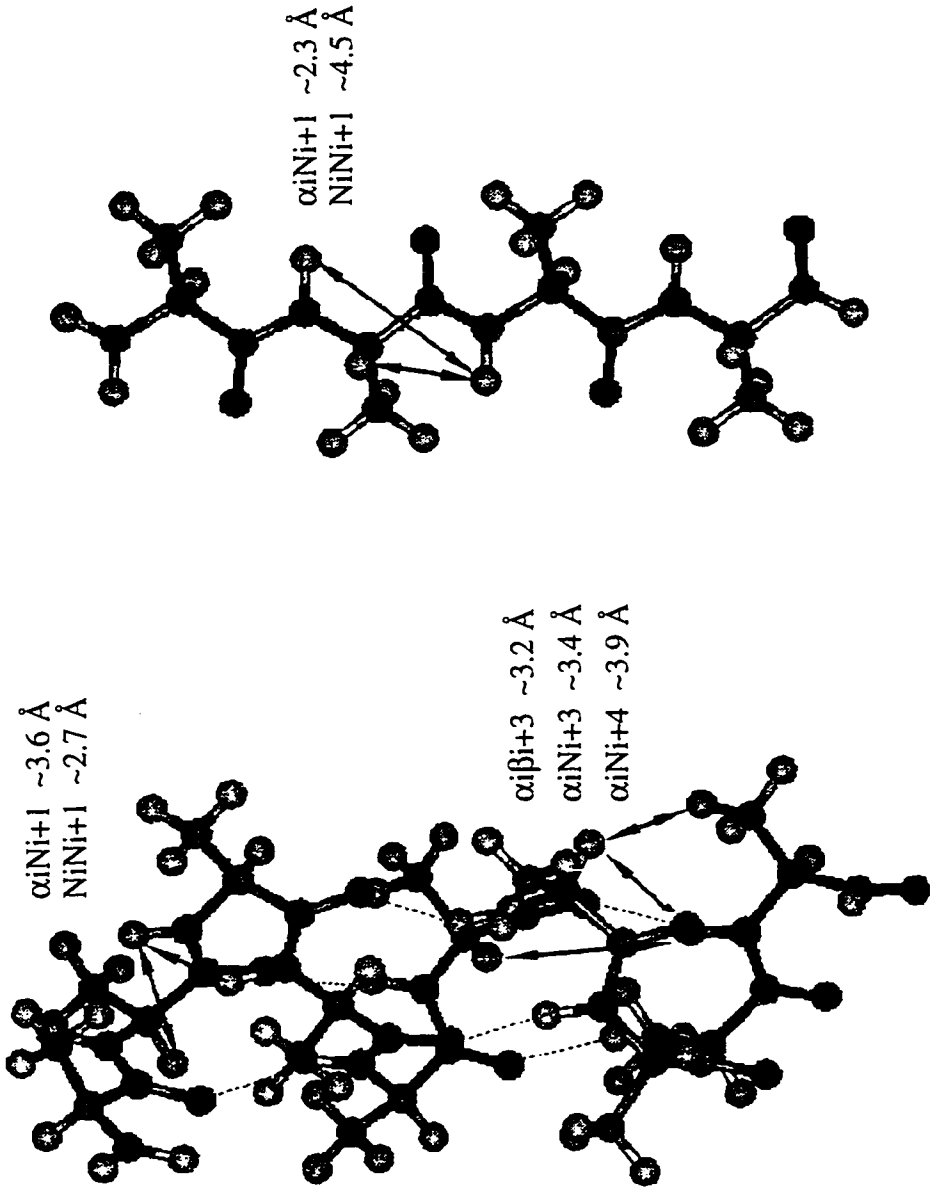

Figure 2.3 α Helix and β Strand

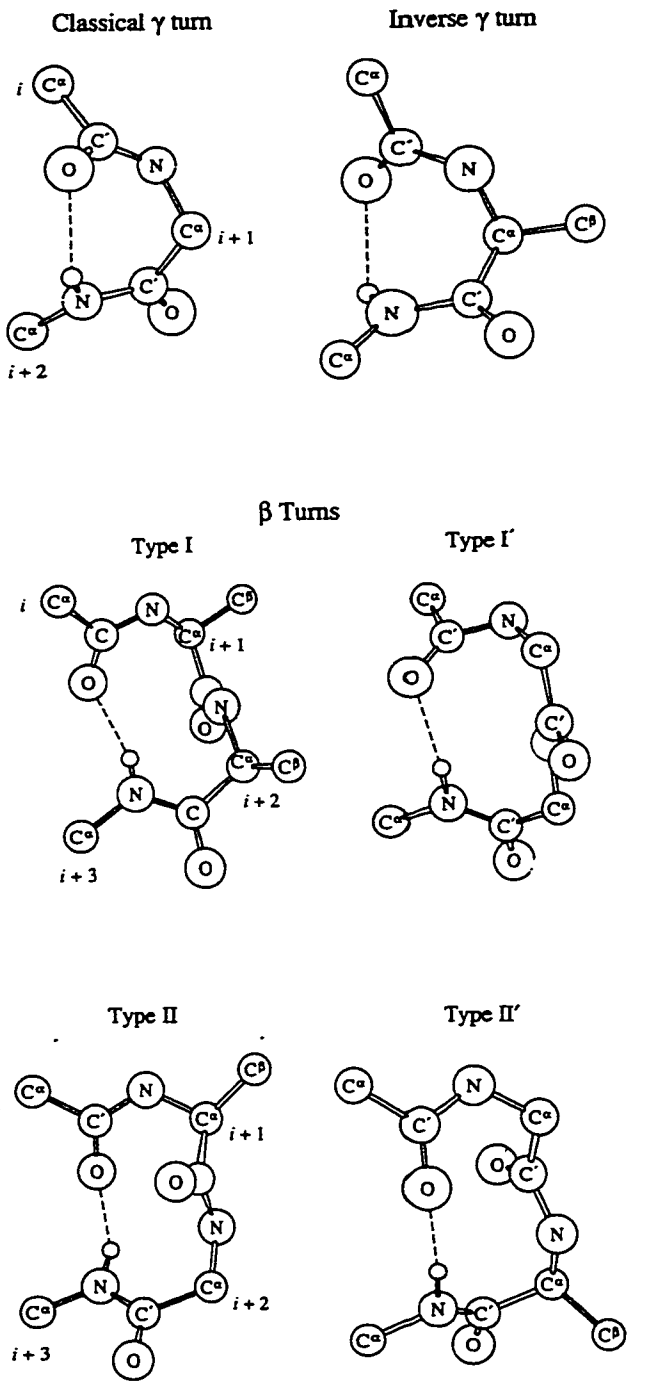

Figure 2.4 Common γ and β Turns (Rose et al., 1985).

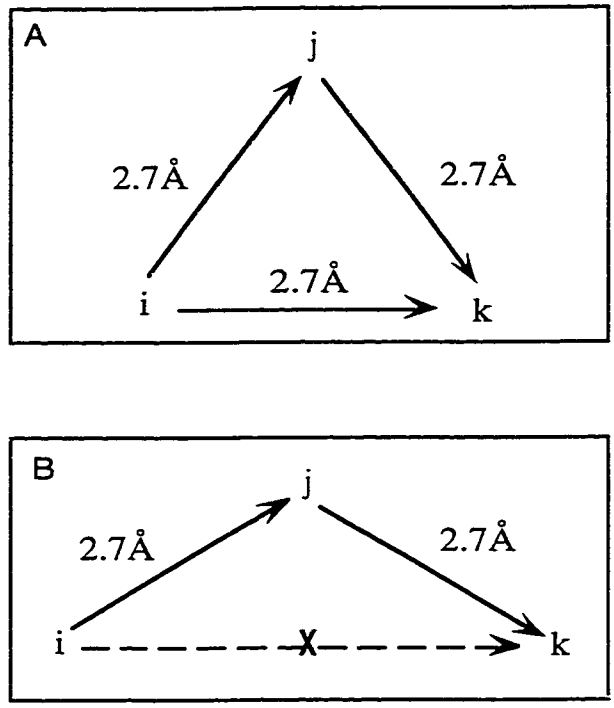

Figure 2.5 Two Different Arrangements of a Three-spin System.
(In panel A, magnetization transfers from spin i to j or k are equally sufficient; while in panel B, magnetization transfer from spin i to k is insufficient due to long inter-nuclei distance. Magnetization transfer is most likely transfer from spin i to j, then to k; the observed NOE is secondary.)

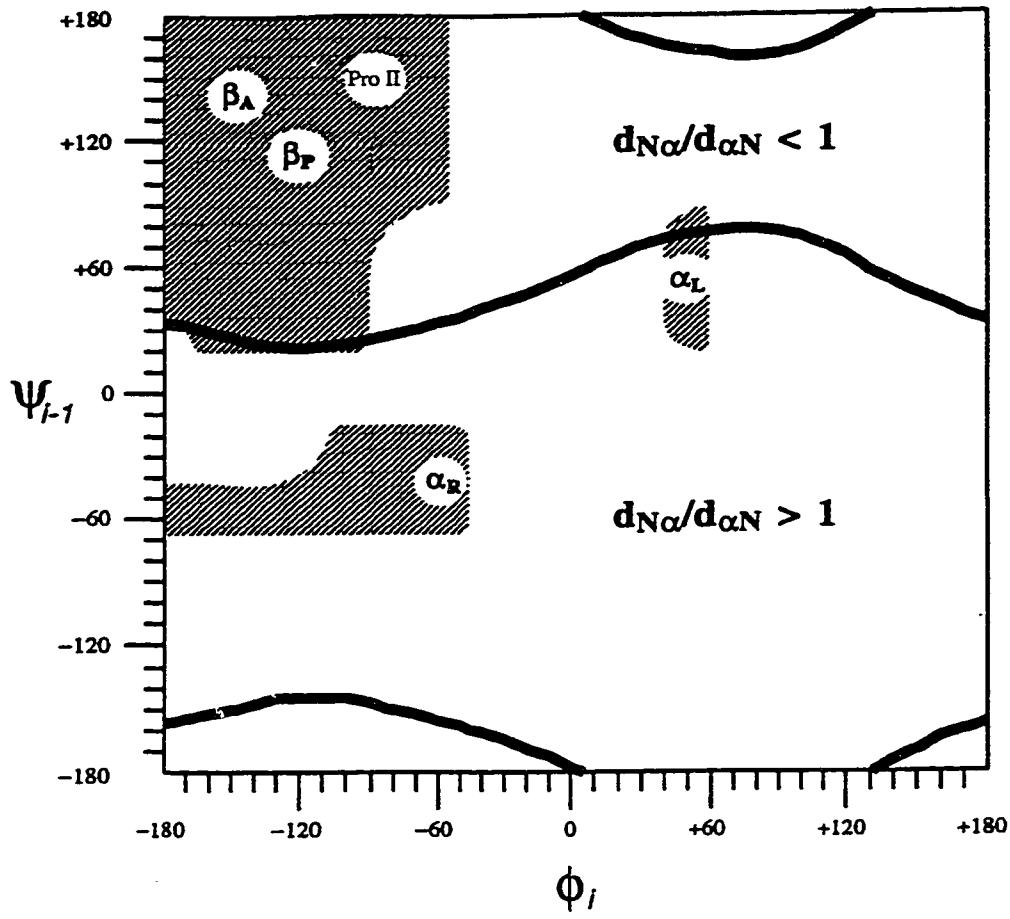

Figure 2.6 The Relation between the $d_{N\alpha}/d_{\alpha N}$ Ratio and the Major Secondary Structure Regions (where $d_{N\alpha}$ and $d_{\alpha N}$ are the interproton distances of Niαi and αi-1Ni). In this Ramachandran plot, the shaded areas represent the energy-favored ϕ_i/φ_{i-1} regions for 2 residues in a protein. β_A, β_p, α_r, α_l and ProII represent ideal ϕ/ φ angles for antiparallel β-sheet, parallel β-sheet, right-handed α-helix, left-handed α-helix and PolyProII, respectively (Gagné et al., 1994).

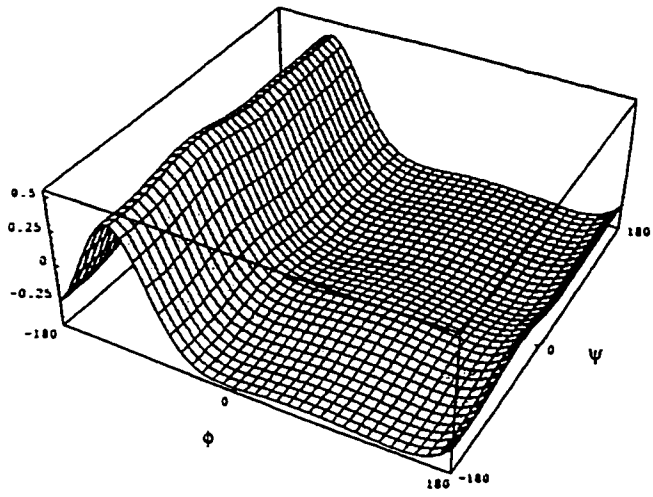

Figure 2.7 Dependence of α - ^{1}H Shift on φ and φ in a Dipeptide Model (Ösapay & Case 1991).

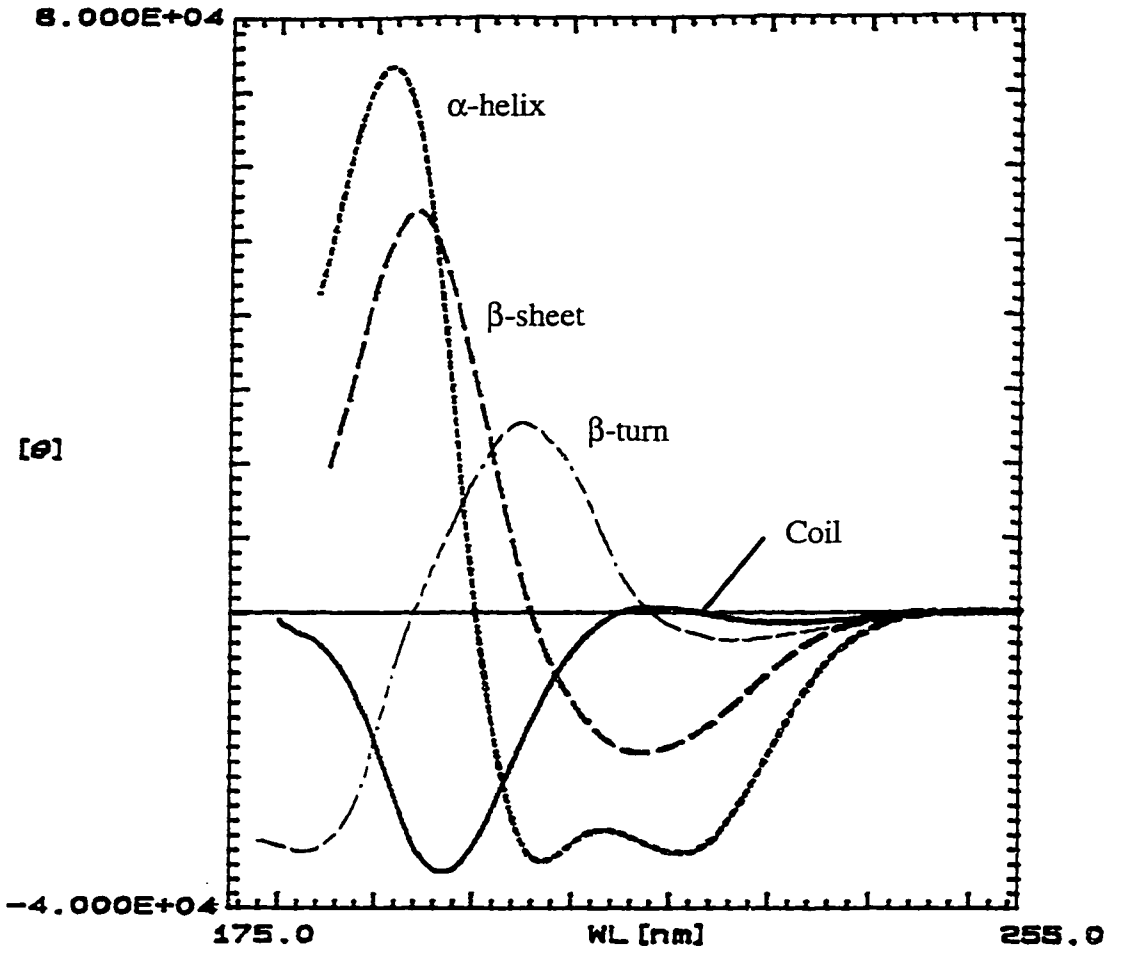

Figure 2.8 CD Spectra of Regular Peptide Secondary Structures.
α-helix (Yang et al., 1986), β-sheet (Cort 1994), Beta turn (Harris 1993), and Coil (Schurke 1996)

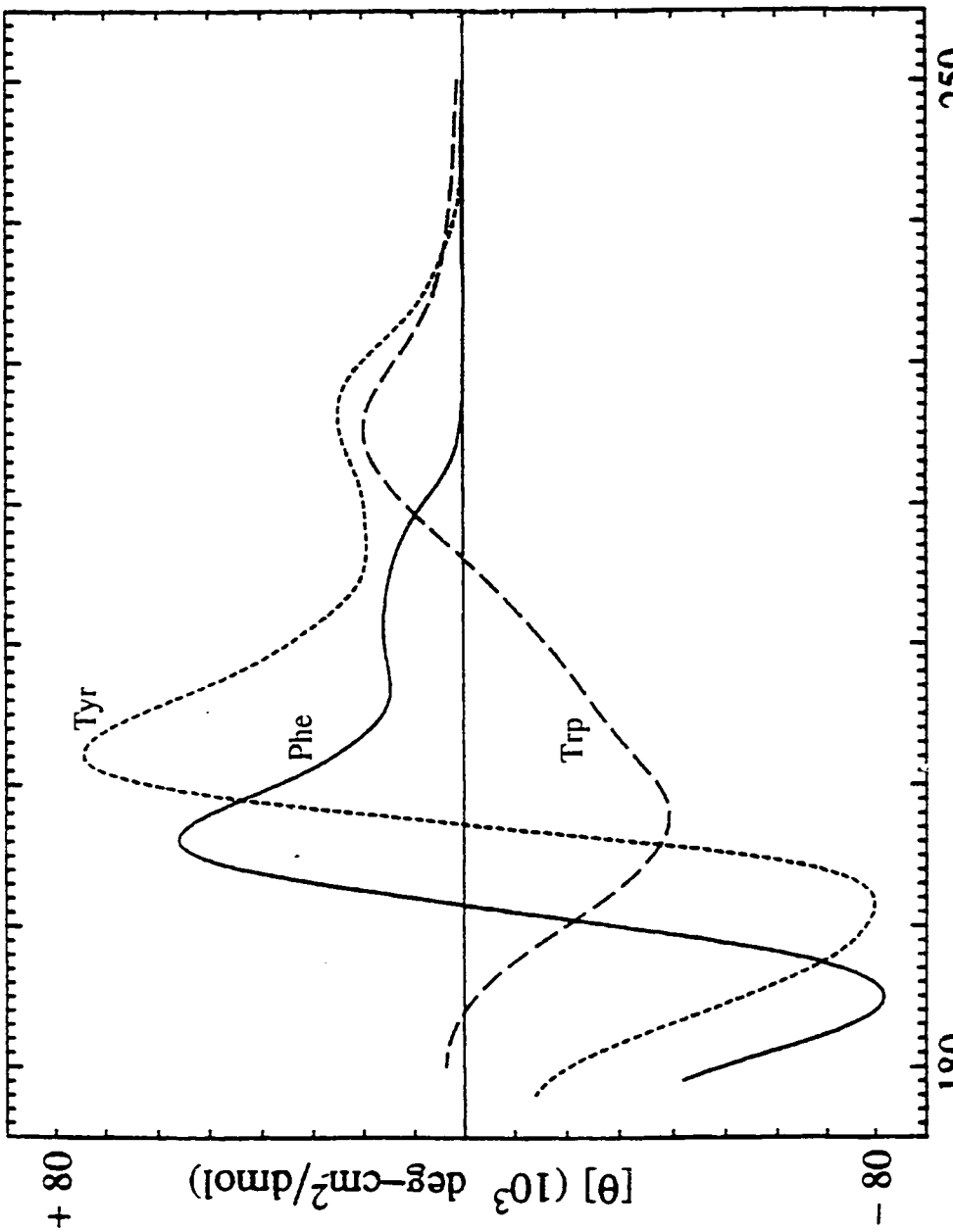

Figure 2.9 Far UV CD Spectra of Disordered Aromatic Side Chain Chromophores (Harris 1993).

Chapter 3

Material and Methods

3.1 *Peptides*

Table 3.1 listed the abbreviations, sequences, likely salt form, molecular weight, and AC# used by Amylin Pharmaceuticals for the peptides studied in this dissertation. These peptides were supplied by Amylin Pharmaceuticals, Inc. and used without further purification. All peptides, except [U-^{15}N]-pram, were synthesized by automated solid phase synthesis using standard FMOC protocols and purified by reverse phase HPLC with acetonitrile/0.1% aqueous trifluoroacetic acid gradient. Several different lots of pramlintide were examined: pramlintide TFA salt contained the expected equivalents of trifluoroacetate and circa 10% of water by weight; pramlintide acetate salt was obtained by further purification from pramlintide TFA salt. The master reference pramlintide sample employed for the definitive NMR studies was 85.5% peptide by amino acid analysis, 8% water by weight and contained 4.8 equivalents of acetate. The acetate content and peptide purity were confirmed by NMR studies at U.W. [U-^{15}N]-pramlintide was expressed as a fusion protein in *E. coli* in a ^{15}N labeled minimal medium. [U-^{15}N]-pramlintide was 98% pure with 93% ^{15}N incorporation based on electrospray ionization MS data. For all peptides, amino acid content and sequence was confirmed by fast atom bombardment mass spectrometry (FAB-MS) and by the 2D NMR experiments detailed herein.

3.2 *NMR Spectroscopy*

3.2.1 *General Methods*

Sample preparation. Weighted amounts of peptides, normally 6-10 mg for amylin analogs or 3-5 mg for fragments, were directly dissolved in freshly prepared media ranging from DMSO to 20 mM acetic acid/formic acid/ Milli Q water buffer (pH = 2.5), to buffer/fluoroalcohol mixture, resulting the final peptide concentration of 2-4 mmol and pH circa 3.2. This pH was chosen in aqeous media both because it maximises the solubility of the peptide, and because it minimizes backbone amide proton exchange rate. Fluoroalcohol mixtures were prepared with high precision gas tight microliter syringes to minimize evaporation. Fluoroalcohol content is given as vol-% of the final solution. There was usually 8-15% of D_2O in H_2O samples to

provide a lock signal. Samples in D_2O media were prepared by repeated lyophilization and addition of 99.99% D_2O. Deuterated DMSO (containing 0.03% TMS), HFIP, TFE and 99.96+% D_2O were purchased from Cambridge Isotope Laboratories. Sodium 3-trimethlsilyl-propionate (TSP) was used as an internal reference in all aqueous samples. After preparation, NMR samples were transferred to 5 mm sample tubes. Regular sample tubes require a minimum of 400 µl of sample, while, microtubes purchased from Shigemi, Inc. require only 200 - 250 µl of sample.

NMR Experiments. Unless specifically labeled in the figure legend, all spectra presented in this dissertation were collected on a Bruker AM-500 equipped with an Aspect 3000 computer for FID signal accumulations and data storage. Several critical experiments, such as a short mixing time NOESY, ^{15}N HMQC and the ^{15}N HMQC-NOESY were recorded on Bruker DMX-750 equipped with a SGI workstation and UXNMR based software for data collection and processing. The temperature control range, without additional equipment, was 275-330 K or 268-330 K on AM-500 and DMX-750, respectively. Prior to recording any spectra, the NMR samples were always equilibrated at the desired temperature for at least half an hour, then the probe was carefully tuned and matched; the magnet was shimmed on either the lock signal or using the FID.

A ^1H 1D control spectrum was always recorded (16K or 32K data points), prior to any other experiments. 2K (or 4K) 1D spectra were also recorded to match 2D experiments. For ^1H spectra, the spectral width was normally in the range of 10 -11 ppm, the preparatory delay was 1.0-1.2s, typically 64 scans were accumulated at each t_1. Two dummy scans were inserted prior to FID accumulation for protic media. The 90° pulse width and power lever depends on the condition of the instrument, and was measured each time. In the case of pramlintide with universally ^{13}C labeled Leu ([U-^{13}C-Leu]-pram), ^{13}C 1D spectra were recorded with ^1H decoupling and a preparatory delay of 2s, line broadening (5 Hz) was used prior to Fourier transformation to improve the signal to noise ratios.

Key pulse sequences for 2D or 3D experiments are discussed in next section. Pulse programs used in this project are gathered in Appendix A. Generally, homonuclear 2D data sets were 2K (or 4K) by 512^+ t_1's, with 16n (n=2 to 8) scans for each t_1 increment depending on instrument time availability and the quality requirement of the spectrum. All spectra were collected using the phase sensitive TPPI (Time Proportional Phase Incrementation) method.

All data were transferred to and processed on Silicon Graphics Personal Iris 4D/25TG or Indigo workstation using Felix2.3 or Felix95.0. During 2D data processing, the first t_1 increment of multi-D experiments was multiplied by 0.5 to attenuate t_1 ridges in all spectra (Otting et al., 1986). A sine bell apodization shifted by 10°, 25° or 60° was applied to COSY, TOCSY, and NOESY & ROESY data, respectively, for both dimensions prior to Fourier transformation. The t_1 dimension was zero filled to 2K(or 4K) complex to increase the apparent resolution. Cubic spline baseline corrections were applied to some regions of the NOESY spectra recorded on AM-500 spectrometer. Macros used for typical 2D, 3D transformations, and a macro for cubic spline correction are also gathered in Appendix A.

Water Suppression. For protic media, different methods of water suppression were used on different spectrometers. On the Bruker AM-500, water suppression was achieved by irradiation of the water signal during the preparatory delay (and mixing time in the case of NOESY spectra) with the decoupler cycled through 22 offsets (usually 7-8 Hz) at a low power level (Zagorski 1990a). This method suppresses the water resonance much more completely and also gives less baseline distortion than irradiating at a single offset. On the DMX-750, the WATERGATE (WATER suppression by GrAdient-Tailored Excitation) sequence (Piotto et al., 1992) could easily be applied. In this gradient echo sequence (Figure 3.1), two shaped magnetic field gradients and two selective 90° pulses with the opposite direction of rotation are symmetrically added to the traditional none-selective 180° spin-echo radiofrequency pulse. This combination achieves highly selective and effective water suppression, provides a perfectly flat baseline and is suitable for single-scan acquisition.

Shift Referencing. Spectra recorded in DMSO media were referenced using TMS as 0.000 ppm. For all spectra collected in aqueous media, TSP was used as an internal reference. ^{13}C, ^{15}N spectra referencing was done using Ξ ratios method which was first described by Live et al. (1984), and highly recommended by Wishart et al. recently (1995b). This method allows the indirect referencing of ^{13}C and ^{15}N chemical shifts through direct referencing to a single, well-determined ^{1}H standard. And it is independent of both the spectrometer design and the sample geometry. The Ξ ratio for ^{13}C was defined as the ratio of the ^{13}C frequency of the methyl resonance of TSP divided by the ^{1}H frequency of the methyl resonance of TSP; the Ξ ratio for ^{15}N was defined as the ratio of the ^{15}N frequency of external anhydrous liquid NH_3 divided by

the ^{1}H frequency of the methyl resonance of TSP. The ratios adopted in this project for ^{13}C and ^{15}N were 0.251449530 and 0.101329144, respectively.

3.2.2 *Important Multi-Dimensional NMR Experiments*

3.2.2.1 2D Homonuclear Experiments

The pulse sequence of all 2D NMR experiments can be generally represented as following:

Preparation-Evolution (t_1)-Mixing-Detection (t_2)

Figure 3.2 shows the pulse sequences of some common homonuclear 2D experiments, which are very useful for peptide and protein studies.

COSY (COrrelation SpectroscopY) spectra were used to correlate the chemical shifts of ^{1}H nuclei which are J-coupled to one another (Marion & Wüthrich 1983). In the COSY pulse sequence (in Figure 3.2), the first 90° pulse, the preparation pulse, creates transverse magnetization components, followed by the evolution time t_1 during which the various magnetization components are labeled with their characteristic precession including both chemical shifts and homonuclear J-coupling. Then the mixing pulse, the second 90° pulse, transfers magnetization components among all transitions that belong to the same coupled spin pair, and the final distribution of labeled magnetization components is detected during t_2. Since the spin systems of many amino acids are unique, in theory, they can be distinguished easily in COSY spectra.

TOCSY (Total Correlation SpectroscopY), also called HOHAHA (HOmonuclear HArtmann-HAhn Experiments), provides another means to identify spin systems. In TOCSY, cross peaks are generated not only for neighboring nuclei, but for all members of the coupled systems; and they are in-phase multiplets, thus much better resolved than COSY peaks. TOCSY Pulse sequence shown in Figure 3.2 (Bax 1985; Griesinger et al., 1988; Bax 1989) contains a MLEV-17 multiple-pulse spin-lock sequence followed by a 2.5 ms trim pulse, replacing the second 90° mixing pulse in COSY. The length of the spin-lock period and the series of coupling constants involved determine how 'far' the spin network will be probed. Usually, a mixing time of 65 ms was used to probe whole spin system of the amino acids for the peptides studied herein; 55ms mixing time TOCSY spectra in D_2O media were recorded to provide anti/gauche assignments for $\alpha/\beta\beta'$ and similar interactions (Driscoll et al., 1989). All TOCSY spectra were performed using inverse detection (using the decoupler as transmitter).

NOESY (Nuclear Overhauser Effect SpectroscopY) spectra were collected for

sequential assignments, and more importantly, for distance constraint extraction. In NOESY, direct dipolar couplings are the primary means of cross-relaxation, thus cross peaks for spins close to each other are generated (Bodenhausen et al., 1984). The basic NOESY sequence (in Figure 3.2) consists of three 90° pulse. Transverse magnetization is created by the preparatory pulse (first 90° pulse), and precesses during the evolution time t_1. The second 90° pulse returns the frequency modulated transverse magnetization component to longitudinal magnetization. During the mixing time (τ_m), longitudinal magnetization is exchanged and relaxes. The third 90° pulse brings back the remaining longitudinal magnetization to the transverse plane for detection. Mixing times ranging from 90 ms to 300 ms were used under different conditions and for different purposes.

ROESY (Rotating-frame Overhauser Effect SpectroscopY), also called CAMELSPIN, measures dipolar coupling effects under spin-locked conditions (Bothner-By et al., 1984; Hwang & Shaka 1992). It is very useful for studies of molecules in which magnetic dipolar relaxation of the nuclei is in neither the extreme narrowing or large molecule limit. Under these condition the laboratory-frame NOE can be close to zero, however, the rotating-frame NOE (ROE) is always positive. In a ROESY experiment, a spin lock is applied during mixing time (in Figure 3.2), during which spin exchange occurs among spin-locked magnetization components of different nuclei. For pramlintide acetate in aqueous buffer, a ROESY was collected to confirm sequential assignments. To minimize TOCSY cross peaks, the spin-lock employed was a train of small flip angle pulses followed by a 180° pulse, (Kessler et al., 1987; Zagorsky 1990b). The spin lock field was 12.5 kHz, and the mixing time was 250ms.

3.2.2.2 2D or 3D Heteronuclear Experiments

Heteronuclear experiments were done on universally ^{15}N labeled pramlintide free acid ([U-^{15}N]-pram) and [U-^{13}C-Leu]- pram.

HMQC (Heteronuclear Multiple Quantum Correlation spectroscopy) is an inverse-detected chemical shift correlation experiment, giving cross peaks for ^1H-X connections (where X can be ^{13}C or ^{15}N, etc.). Indirect ^1H detection improves the sensitivity relatively to a directly detected XHCORR, due to differences in magnetogyric ratios and the faster relaxation of protons. The HMQC pulse sequence (Figure 3.3) employed here incorporated a WATERGATE sequence (Piotto et al., 1992; Sklenar et al., 1993) into a basic HMQC (Bax et al., 1983; Bendell et al., 1983; Bax & Subramanian 1986). The first ^1H 90° pulse creates transverse magnetization,

some of which evolved into anti-phase magnetization at the end of the first delay ($1/2J_{XH}$) and is converted into zero- and double-quantum coherence by the X 90° pulse. The zero- and double-quantum coherence evolve during t_1 and are exchanged by the ^1H 180° pulse so that single-quantum X frequencies can be observed in F1. The final X 90° pulse converts multiple-quantum coherence into observable ^1H transverse magnetization, followed by a $1/2J_{XH}$ delay which brings ^1H magnetization components back in phase when the acquisition with X-decoupled starts. The WATERGATE sequence prior to the acquisition suppresses ^1H signals, including the water signal, which are not coupled to ^{15}N nuclei. [U-^{15}N]-pram HMQC spectra were recorded at five different temperatures (268K, 275K, 285K, 300K and 315K) consecutively. The sweep width was 11 ppm for ^1H dimension, and 26 ppm for ^{15}N dimension. Data sets were 4K x 256 t1 complex points. No window function was applied in data processing.

"RELAY-HMQC" was done on [U-^{13}C-Leu]-pram in the 35% HFIP medium to provide ^{13}C shift assignments and differentiation of the β, β' and γ proton resonances for all three leucines. The RELAY-HMQC experiment was based on an inverse-detected ^{13}C-INADEQUATE pulse sequence (Pratum & Moore 1993), and it provides cross peaks with ^1H in f_2 at ^{13}C frequencies in f_1, which are either directly or indirectly attached to the protons. The RELAY-HMQC pulse sequence and phase cycling are shown in Figure 3.4. In this sequence, the first INEPT sequence is used to polarize ^{13}C from directly attached ^1H, and thus creates heteronuclear multiple-quantum coherence. A homonuclear dephasing period follows (second INEPT sequence), during which polarization is transferred from directly attached ^{13}C to indirectly attached ones. ^{13}C chemical shifts precess during t_1, followed by a rephasing period and the polarization goes back to directly attached ^{13}C sites (third INEPT sequence), then returns to ^1H magnetization for detection. The RELAY-HMQC spectrum was recorded on the Bruker AM500, with a 10 ppm sweep width for ^1H dimension and 180 ppm for ^{13}C dimension. J_{CC} is the homonuclear carbon-carbon coupling constant and J_{CH} is the heteronuclear carbon-proton coupling constant. $1/2J_{CC}$ and $1/2J_{CH}$ were set to 5ms and 3.5 ms respectively. 2K x 606 t_1 data set was collected, 5Hz line broadening in ^{13}C dimension and a 90° shifted sine bell window function was used prior to FT.

3D NOESY-HMQC. Any 3D experiments can be generally represent as follows:

Preparation-Evolution(t_1)-Mixing - Evolution (t_2) - Mixing -Detection(t_3)

3D NOESY-HMQC (also called ^{15}N-edited NOESY) is just like a stack of 2D homonuclear NOESY spectra with each plane at a different ^{15}N chemical shift, and only the residue(s) whose amide nitrogen is at that shift will appear on that plane. The pulse sequence employed to record NOESY-HMQC spectrum for [U-^{15}N]-pramlintide free acid in 35% HFIP is shown in Figure 3.5. Similar to the 2D NOESY experiment, the first 90° pulse excites the ^{1}H magnetization, which is chemical-shift labeled during t_1, returned by the second 90° pulse back to longitudinal magnetization, and transferred during mixing time τ_m to all spins in close spatial proximity. The 180° pulse applied on ^{15}N during t_1 removes heteronuclear scalar couplings. The sequence that follows the mixing period is similar to the regular ^{1}H-X HMQC scheme described earlier. The new gradient-tailored excitation scheme (Piotto et al., 1992; Sklenar et al., 1993) described in previous section was incorporated into the basic NOESY-HMQC sequence (Marion et al., 1989; Kay et al., 1989) for efficient water suppression. Since only the z component of magnetization exchanged during the mixing time would be detected, the ^{1}H carrier can be easily switched to the center of the amide region for the HMQC step, which maximizes the digital resolution in the acquisition domain. The data set of the NOESY-HMQC for [U-^{15}N]-pramlintide was collected on Bruker DMX750, at 295 K, with 2K x 256 x 64 complex points, corresponding to 3.5x10x26.3 ppm. 15872 t_1's were collected resulting 62 data points in the ^{15}N dimension. Eight scans were accumulated for each t_1. The mixing time was 110ms and $1/4J_{XH}$ was set to 3ms, corresponding to ^{15}N and ^{1}H heteronuclear coupling constant about 80 Hz. During data processing, the matrix was set to 1024x256x64. The second ^{1}H dimension (F1) was zero filled to 512 points and ^{15}N dimension (F2) was linear predicted to 128. A 90° shifted sine bell window function was applied to both F1 and F2 dimensions.

3.3 *Resonance Assignment, CSD and NOE Ratios Histogram*

Assignment. All spectra used for assignments were from Bruker AM-500 data, unless specifically stated to the contrary. After gathering necessary NMR spectra for each peptide sample, the assignments for ^{1}H resonance were achieved using the standard sequence-specific resonance assignment strategy (Wüthrich, 1986). COSY and TOCSY spectra were employed to identify the spin system, and NOESY or ROESY spectra were used for sequential assignment. Detailed assignment procedures for peptide sequences are illustrated in the following chapters.

The ^{15}N and ^{13}C resonance assignments were achieved by correlation to the known proton shifts.

CSD (chemical shift deviations) are defined as:

$$CSD = \delta_{obs} - \delta_{ref}$$

And are presented as a CSD vs residue histograms. The "coil reference values" for alpha methine and amide ^{1}H in both aqueous and DMSO media are listed in Table 3.2, along with the values needed to calculate amide ^{15}N coil reference in aqueous media (Braun et al., 1994).

The reference values for alpha methine and amide ^{1}H sites in aqueous media are the mean of our previously published set (Andersen et al., 1995b) and others reported in the literature (Merutka et al., 1995; Wishart et al., 1995a), and was published recently (Andersen et al., 1996b, 1997a). The correction of Hα reference values for the effect of a following Pro residue (Xaa-Pro effect): for all Xaa, are +0.29, except for Gly, is +0.17. The corrections for fluoroalcohol content of the medium were: 25-35 vol-% HFIP, +0.075; 12.5-16 vol-% HFIP (and 50 vol-% TFE), +0.05; 25-30 vol-% TFE (and 10 vol-% HFIP), +0.035; and 10-15 vol-% TFE and 4-6 vol-% HFIP, +0.015 ppm. Reference values for amide protons were corrected to the temperature of the experimental values using a coil gradient of -7.6ppb/°C prior to H_N CSD calculation.

Reference values for DMSO media are from Bundi's published data (Bundi et al., 1975), with the exception of Pro (4.36 no previous value), Val (4.19 versus 4.26), and Ile (4.22 versus 4.25 ppm) and include the corrections for the random coil reference values of Hα of Xaa in Xaa-Pro which are used in aqueous medium. For a $^{+}H_3N$- terminated peptide in DMSO, the correction for the Hα of the first residue is -. 0.4, and the '2'-effect (+0.54) and '3'-effect (+0.26) are assumed for NH reference values (Andersen et al., 1995b).

^{15}N reference values for the NH between residues Y and X, which is a part of the X residue, are defined as:

$$\delta_{rc}^{YX} = \delta_{rc}^{GX} + \Delta\delta^{Y}$$

where δ_{rc}^{YX} is the sequence-corrected 'random coil' reference value for Xaa following Yaa, δ_{rc}^{GX} is the reference value for Xaa preceded by Gly, and $\Delta\delta^{Y}$ is an increment accounting for the influence of replacing Gly by Yaa in the position preceding the residue considered (Braun et al., 1994).

NOE Ratio Histograms. Inter/intra-Residue Hα/HN NOE ratios are presented as Δncl vs residue histograms (Lee et al., 1994). The Δncl value is the difference in the number of contour levels observed for inter- vs intra-residue peaks using a contour level multiplier of 1.4. The values thus correspond to $\log_{1.4}$ [inter-NOE/intra-NOE] with positive values indicating the increasing contribution of extended chain conformations at that site. For each residue, the Δncl value from the HN line (NOE to α_{i-1} vs α_i, predominantly reflecting φ_{i-1}) and the measure at the H_α line (NOE to N_{i+1} vs. N_i, reflecting φ_i) are shown. The values expected for a fully disordered and a 100% helical segment are +1.6 and -4.5±0.6, respectively; the distances in a fully extended β-strand would yield a value of +4.3.

3.4 *Structure Ensemble Calculation*

3.4.1 *Constraint Extraction*

Distance Constraints. Relative NOE intensities were taken from NOESY spectra contour plots with a 1.4 contour level multiplier. The observed NOE intensities, recorded as number of contour levels, were corrected for relative peak width in the directly detected dimension and for peaks involving amide protons according to the H/D ratio in the media. The intensity scale was calibrated using the following reference distances (in Å):

α_iN_{i+1} (smallest) = 3.55±0.25; α_iN_{i+1} (largest) = 2.2±0.20;

N_iN_{i+1}(largest in a helical segment) =2.45-2.90; $< \alpha_iN_i > = 2.8$

Both the high and low distance bounds derived from NOEs due to methyl groups were increased by a factor of 1.2. This procedure results in relatively tight distance constraints, $r_{ij} = (d_{ij}\text{-}d_-)\rightarrow(d_{ij}+d_+)$, rather than a conservative four class grouping: L (1.8-2.7), M (2.0 - 3.5), S (2.5 - 4.0), and VS (2.7-5.0). When inter-residue NOEs that would be diagnostic for a particular secondary structure were completely absent, low-bound-only (LBOs) constraints, also known as 'Anti Distance Constraints'(ADCs) (Brushweiler et al., 1991) were employed. An alternative 'loose bounds set' was created by increasing each upper bound by 4% and setting the low bound to the larger of $0.8*(d_{ij}\text{-}d_-)$, $(d_{ij}$- 1Å) or 1.9Å; these changes also serve to eliminate the influence of low-bound-only constraints and correspond (approximately) to a "conservative" treatment of NOE intensities.

Dihedral Angle Constraints. A limited number of backbone dihedral constraints were derived either from chemical shift indices and local NOE ratios (Andersen et al., 1995a), or the $^3J_{HN\alpha}$ coupling constant measured from 1D spectra in aqueous buffer.

Hydrogen Bond Constraints for an $N_iH_i \leftarrow O{=}C_j$ interaction supported by NH exchange protection and spatial proximity in 80% of the structures in an ensemble calculated without H-bond constraints took the form:

$$r(H_iO_j) = 1.71\text{-}2.21 \text{ and } r(N_iO_j) = 2.65\text{-}3.25 \text{ Å}$$
$$\text{or } r(H_iO_j) = 1.71\text{-}2.01 \text{ and } r(N_iO_j) = 2.78\text{-}3.03 \text{ Å}$$

depending on the NH exchange protection factor observed.

Stereospecific Assignments for prochiral β methylenes were derived as follows:

1) Early stage structures were generated using only the shorter of the NOE distances to any other spin with r^{-6} averaging.

2) Anti/gauche assignments were made from the 55 ms mixing time TOCSY spectra recorded in d_2-HFIP/D_2O, since the shape of the cross peaks in TOCSY reflects the $^3J_{\alpha\beta}$ coupling constant (Driscoll et al., 1989). The assignments were then confirmed by the αβ/ αβ' NOE ratios observed in the short mixing time NOESY. Figure 3.6 is a summary of information used to achieve stereospecific assignments of β-methylene protons based on $^3J_{\alpha\beta}$ coupling constant (or TOCSY cross peak shape), and NOEs.

3) The α/ββ' anti/gauche relationships were expressed as distance constraints 2.8-3.15/2.2-2.7Å, respectively, and both possible assignments were examined for these and all β_iN_{i+1}/ β_iN_i/ $\beta_i\alpha_{i-3}$ constraints. If one assignment produced lower E_{NOE} values for a large majority of the structures in the ensemble, that stereospecific version of the constraints was used in the next round of the refinement.

A similar procedure was used for Gly-α α', Val-γγ', and Leu-δδ' assignments.

NOE distance constraints were placed in three categories which were assigned different weights during the protocol. The heavily weighted category contained those intermediate range constraints that were fully confirmed and relatively strong. In the terminal portion of the cool-down and subsequent minimization of the final stage the NOE force constants were 32, 14, and 7 kcal·Å^{-2}/mol respectively for the three categories. A fourth 'trial' category with even lower weighting which employed soft-square, rather than a biexponential energy function, was used for distances derived from NOEs that could be predominantly secondary and for alternate attributions of NOE peaks that had two or more potential assignments. During the course of the refinement, those 'trial' distances due to the unambiguously determined distance constraints that

could be satisfied without increasing the E_{NOE} term were incorporated into the other categories.

The final set of constraint tables for pramlintide in 25-35% HFIP are given in Appendix B.

3.4.2 *Simulated Annealing*

Ensemble Calculation. The structure ensemble for pramlintide in 25-35% HFIP was obtained by constrained dynamics simulated annealing using XPLOR 3.1 (Brünger et al., 1992); and the structures were visualized and compared using INSIGHT (Biosym Technologies Inc.). All computations and visualizations were performed on Silicon Graphics Personal Iris 4D/25TG or Indigo workstations.

A three-stage simulated annealing (SA) protocol essentially the same as previously described (Kraulis et al., 1989; Andersen et al., 1993) was employed with a few exceptions:

1) The constraints involving rotation symmetry equivalent aromatic hydrogens were equated with $[\Sigma r_{ij}^{-6}]^{-1/6}$ rather than with the r^{-6} average (Constantine et al., 1995),

2) A limited number of backbone dihedral constraints were included in the first high temperature dynamics of each stage; these were given an ineffectively small weighting in the subsequent dynamics and during minimization.

3) During the cool-down dynamics and Powell minimization of stage three the E_{repel} function was replaced by a standard Lennard-Jones van der Waals function.

The starting structures were randomly generated by XPLOR. The three stages of SA were: 1st stage - predisposing acyclic structures for disulfide closure; 2nd stage - high-temperature constrained dynamics of cyclized structures; and 3rd stage - further SA with added low-bound-only constraints. In each stage, the temperature was brought to 1000K during the high temperature dynamics with a step size of 2.0 fs; then slowly cooled down to 300K in 258 steps each of 100-fs duration and then subjected to a brief Powell mininization. Exaggerated bond length, angle and improper torsional potentials were employed in order to maintain standard geometry. The 3rd stage XPLOR protocol is included in Appendix B.

Structure assessment. The standard output from XPLOR was used to select the best-fitting low energy structures from the complete set. E_{impr} and E_{vdw} were used as a measurement of strain and conflict between NOEs and low energy conformations; and E_{NOE} was used as the initial measure of fit. Typically 60-80% of the structures had

values of all three energy terms that were within 15 kcal/mol of the lowest values observed in that set of structures for each energy term; these constitute the 'accepted structures' that were used to derive the ensemble statistics report. Consensus conformations for segments which have a defined structure were derived by eliminating a few outliers based on ϕ/ φ versus residue plots of 'accepted structures'. Backbone rmsd measures of convergence are pairwise over the consensus conformation or ensemble; the carbonyl oxygen is included in the definition of backbone for rmsd measures.

3.5 *CD Experiments*

Sample Preparation and Quantitation. CD stock solutions were prepared by dissolving weighted amounts (typically 1.00-3.00 mg) of peptides directly in a 20 mM acetic acid/formic acid/ Milli Q water buffer (pH ~ 2-3), with typical concentrations of 300-600 μM. For peptides without a Tyr residue, the concentrations were estimated by weight, assuming the sample was 90% peptide salt by weight. When a Tyr is present, the concentrations of the stock solutions were determined by UV, assuming the extinction coefficient $\varepsilon_{274} - \varepsilon_{310} = 1405$ cm^2/mmol for systems lacking a disulfide linkage and 1530 cm^2/mmol when a disulfide is present (Milhalyi 1968). The stock solution was diluted 10 - 15 fold using appropriate amounts of buffer, TFE, or HFIP, etc, to the final volume-% fluoroalcohol required. All volume measurements and transfers were accomplished with high precision gas tight microliter syringes. The final CD sample concentrations were typically 30-60 μM.

Spectra Recording. CD spectra were recorded using a JASCO model J720 spectropolarimeter, which was frequently calibrated using the (+)-10-camphorsulfonic acid (CSA) sample provided by JASCO and assuming that the CSA has a minimum $[\theta]_{192.5}$=-15,600 (Yang et al., 1986; Johnson, 1990). The spectropolarimeter was always stabilized for at least 30 min with a nitrogen flow rate of 5 L/min before any spectra were recorded. The temperatures were controlled by a thermal bath using 50% aqueous ethylene glycol as the cryogen which was pumped through the metal block holding the CD cells. A minimum of 20 minutes was allowed for thermal equilibration prior to recording spectra at different temperatures; and the temperatures, ranging from –3 to 80°C for thermal unfolding studies, were read from a calibrated thermometer inserted in the cell block. Typically, 1 mm CD cells were used with the peptide concentrations in the range of 30-60 μM. The CD cells were always carefully rinsed

and dried to eliminate the adsorption of the analyte to the surface of the cells. The averaged spectra were recorded between 185-270 nm with scan rate 100 nm/min, a step resolution of 0.2 nm, by the accumulation of 16-24 scans.

Data Processing. After subtracting the solvent baseline, the CD spectra were trimmed at a photomultiplier voltage of 650 V. Then, the data was smoothed using the reverse Fourier transform procedure in the JASCO software, followed by zeroing to the value less than 10^{-7} at 260nm. All subsequent CD spectral values for peptides are expressed in units of mean residue molar ellipticity (deg·cm^2/residue dmol); solvent composition as volume % values, with the volume designation deleted, and temperatures are reported in Kelvin.

Data Assessment. CD data for melting studies are presented as a formula that will reproduce the observed value over the 0 - 30°C, $[\theta]_\lambda=[\theta]_0+(\Delta\theta/\Delta T)(^\circ C)$. Several means were used to assess the helicity of peptides from CD data. R1 and R2 value (Bruch et al. 1991; Munoz et al. 1995), defined as $[\theta]_{191}:[\theta]_{min}$ and $[\theta]_{221}:[\theta]_{min}$, respectively, were used to reflect helicity. $[\theta]_{191}$ is the ellipticity at 191nm or the maxima between 185-195nm; $[\theta]_{min}$ is the minima ellipticity between 196-208nm; and $[\theta]_{221}$ is the ellipticity at 221nm or the minima between 220-223nm. Another more commonly used measure was the fractional helicity $\langle f_H\rangle_{CD}$ over the helical domain, which was calculated from following equation:

$$\langle f_H\rangle_{CD} = (N\text{-}1/n\text{-}1)*(-[\theta]_{221}+[\theta]_{coil})/37600$$

where N is the total number of amide units in the peptide, n is the number of the residue in helical domain determined by NMR, and 37600° corresponding to the mid-point of literature value (32000 to 42500°) of $(-[\theta]_{221}+[\theta]_{coil})$ for 100% helicity. $[\theta]_{coil}$ values at 0°C were calculated as described by Andersen and Tong (1997b).

Table 3.1 Peptides Investigated in This Project

Amylins:			
abbreviation	primary sequence or specification	MW(g/mol)	AC#
hAM (human amylin)	KCNTATCATQRLANFLV**H**SSNN**FGAIL**S**S**TNVGSNTY·4TFA	4,355.89	001
rAM (rat amylin)	**R L PV PP** ·4TFA	4,377.00	0128
Pramlintide	**P PP** ·4TFA	4,401.89	0137
	·4OAc	4,185.89	MSAAC137
Pramlintide free acid*	·4TFA	4,402.89	2616
D-L^{12}-pram	pramlintide with a D-Leu^{12}·4TFA	4,401.89	2401
[U-^{13}C-Leu]- pram	pramlintide with universally ^{13}C labelled Leu·4TFA	4,423.60	2681
[U-^{15}N]- pram*	universally ^{15}N labelled pramlintide free acid ·4TFA* (93% ^{15}N)	4,408.45	2616

*All peptides listed here are C-terminal amidated, except the ones with * are free acid.

Table 3.1 Continue

Fragments:			
abbreviation	primary sequence	MW(g/mol)	AC#
c23Y [hAM(1-22)GY]	KCNTATCATQRLANFLVHSSNN**GY**·4TFA	3,068.90	2747
c23 [hAM(1-22)G]	KCNTATCATQRLANFLVHSSNN**G**·4TFA	2,902.70	2604
c21Y [hAM(1-20)GY]	KCNTATCATQRLANFLVHSS**GY**·4TFA	2,840.70	2739
c21 [hAM(1-20)G]	KCNTATCATQRLANFLVHSS**G**·4TFA	2,675.50	2421
17mer [Ac-hAM(5-20)G]	Ac-AT**S**ATQRLANFLVHSS**G**·2TFA	2027.99	2376
A2,7 [$A^{2,7}$-hAM(1-20)G]	K**A**NTAT**A**ATQRLANFLVHSS**G**·4TFA	2,613.42	2680
S2,7 [$S^{2,7}$-hAM(1-20)G]	K**S**NTAT**S**ATQRLANFLVHSS**G**·4TFA	2,644.42	2375
S2U7Y [S^{2},U^{7}-hAM(1-20)GY]	K**S**NTAT**U**ATQRLANFLVHSS**GY**·4TFA	2,806.60	2871
S2U7 [S^{2},U^{7}-hAM(1-20)G]	K**S**NTAT**U**ATQRLANFLVHSS**G**·4TFA	2,643.44	2738
R18Y [R^{18}-hAM(1-20)GY]	KCNTATCATQRLANFLV**R**SS**GY**·4TFA	2,857.76	2844
sCT [sCT(1-20)G]	CSNLSTCVLGKLSQELHKLQ**G**·4TFA	2,713.66	2756
hCGRP [hCGRP(1-21)]	ACNTATCVTHRLAGLLSRSGG·4TFA	2,543.42	2741
V8Y [V^{8}- hAM(1-20)GY]	KCNTATC**V**TQRLANFLVHSS**GY**·4TFA	2,866.70	2903
V8S9Y [$V^{8}S^{9}$- hAM(1-20)GY]	KCNTATC**VS**QRLANFLVHSS**GY**·4TFA	2,852.70	2902

Table 3.2 Random Coil Reference Values (in ppm).

residue	Hα	HN	Hα	HN	$^{15}N\ \delta^{GX}/\Delta\delta^{Y}$
	H_2O, 25°, pH 3–5 [a]		DMSO, 25° [b]		aq. pH ~2 [c]
Gly	3.96	8.28	3.76	8.15	108.7/0.0
Val	4.10	8.08	4.18	7.88	119.1/4.2
Ile	4.15	8.08	4.21	8.26	119.8/4.5
Leu	4.32	8.17	4.37	7.95	121.8/1.5
Ala	4.32	8.21	4.34	8.04	123.7/-0.2
Glu^-	4.32	8.37	4.34	8.05	120.8/1.8
Lys	4.32	8.19	4.29	8.06	121.1/2.1
Arg	4.34	8.24	4.38	8.07	120.7/2.3
Glu^0/Gln	4.34	8.27	4.32	8.06	119,8/2.0/119.9/2.1
Thr	4.37	8.15	4.22	7.83	113.9/3.2
Pro	4.43	–	4.36	–	133.9/0.6
Met	4.48	8.25	4.41	8.07	119.9/2.1
Ser	4.47	8.26	4.34	7.98	115.6/2.0
Tyr	4.56	8.13	4.46	8.04	120.0/2.3
Phe	4.61	8.25	4.56	8.14	119.9/2.3
His^+	4.70	8.35	4.66	8.31	118.1/2.8
Trp	4.65	8.05	4.58	8.09	120.7/2.3
$(Cys)_2$	4.69	8.34	4.64	8.29	118.1/2.0
Asp^0/Asn	4.72	8.40	4.61	8.14	118.8/0.8/118.5/0.7
Asp^-	4.65	8.29	4.63	8.21	120.4/0.3
Aib	–	8.08			

[a] These values were published by Andersen et al., 1996b, 1997a; and were the average of the values published by Andersen et al., 1995b, Merutka et al., 1995, and Wishart et al., 1995a.

[b] There values were published by Bundi et al., 1975, except the value for Pro, Val, and Ile which were adjusted in our research group.

[c] These values were published by Braun et al. (1994).

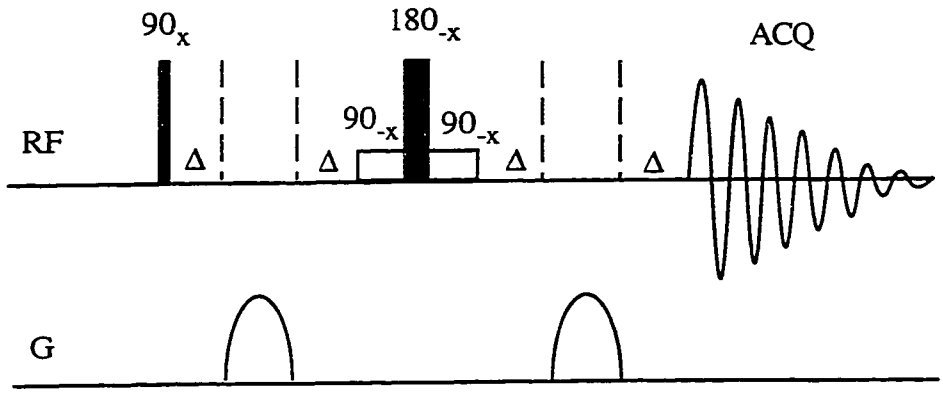

Figure 3.1 The WATERGATE Pulse Scheme (Piotto et al., 1992).

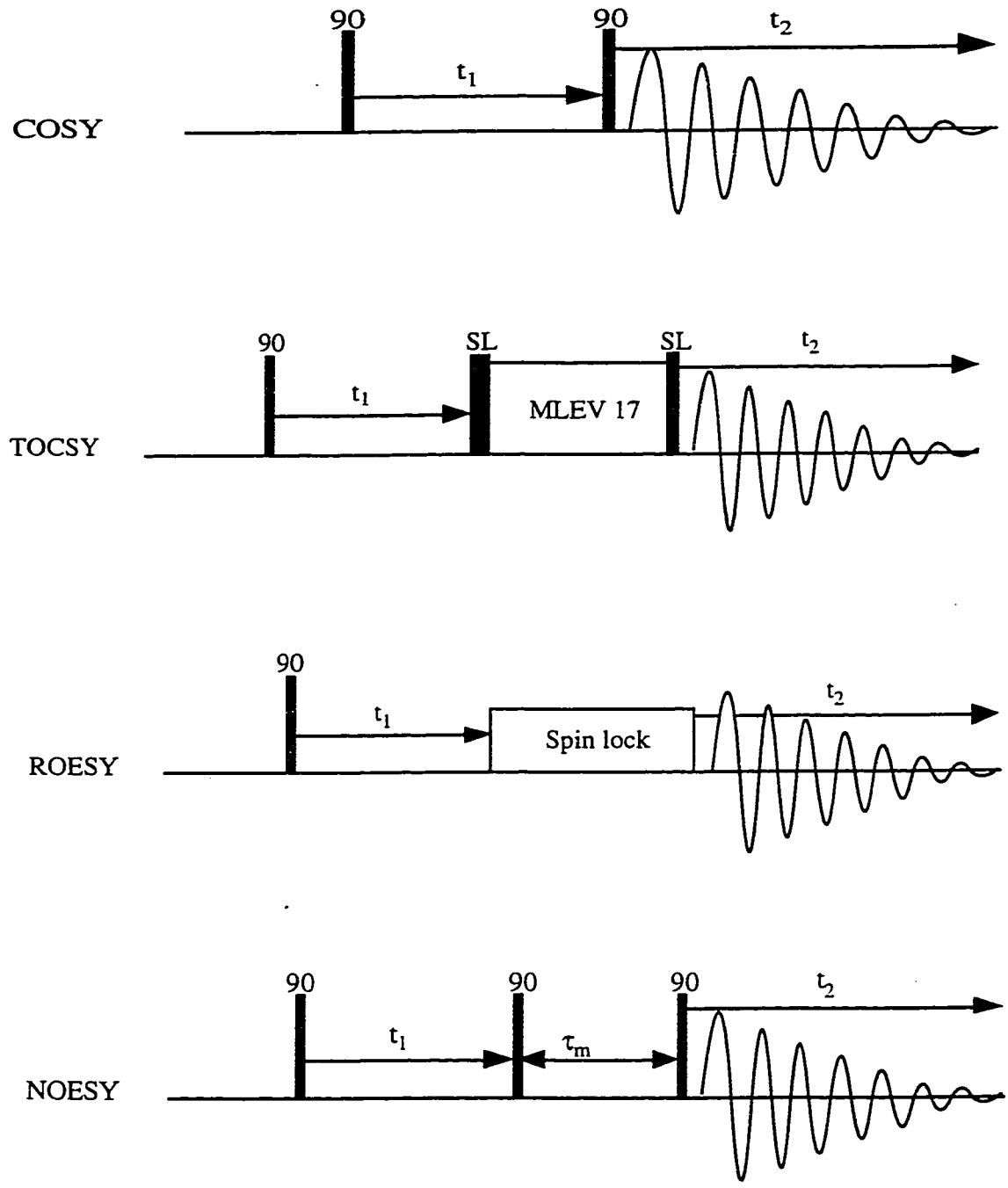

Figure 3.2 Pulse Schemes of Common Homonuclear 2D Experiments.

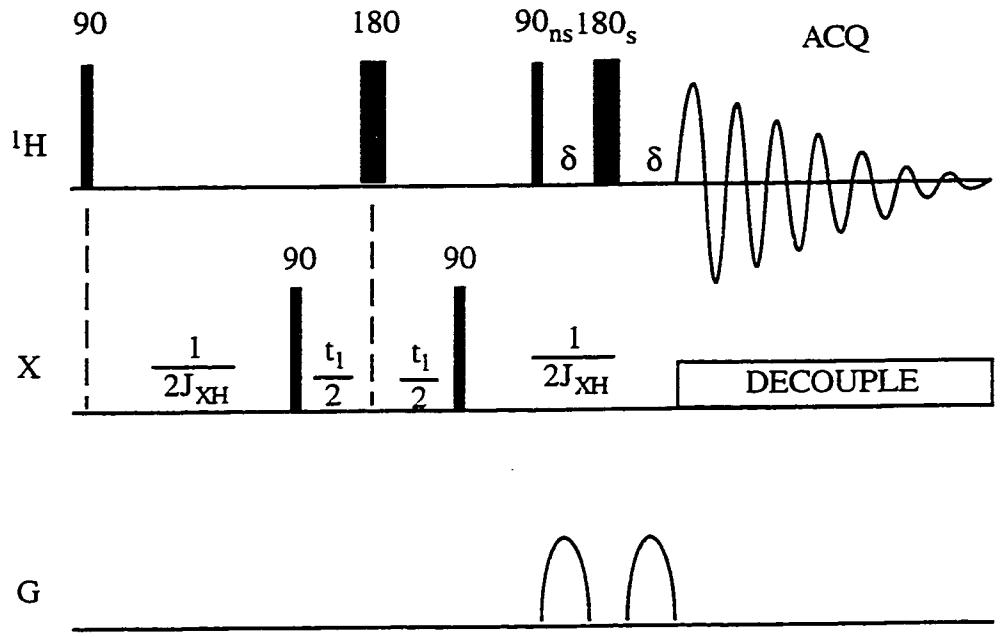

Figure 3.3 The Pulse Sequence for HMQC Spectra.

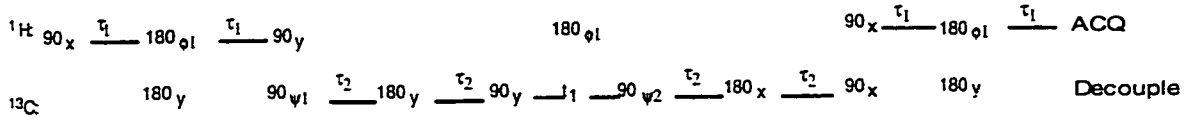

$\phi 1$: y, y, -y, -y

$\psi 1$: x, -x

$\psi 2$: y, y, y, y, y, y, y, y, -y, -y, -y, -y, -y, -y, -y, -y

$\tau_1 = 1/4J_{CH}$

$\tau_2 = 1/8J_{CC}$

Figure 3.4 The Pulse Sequence for the RELAY-HMQC Experiment.

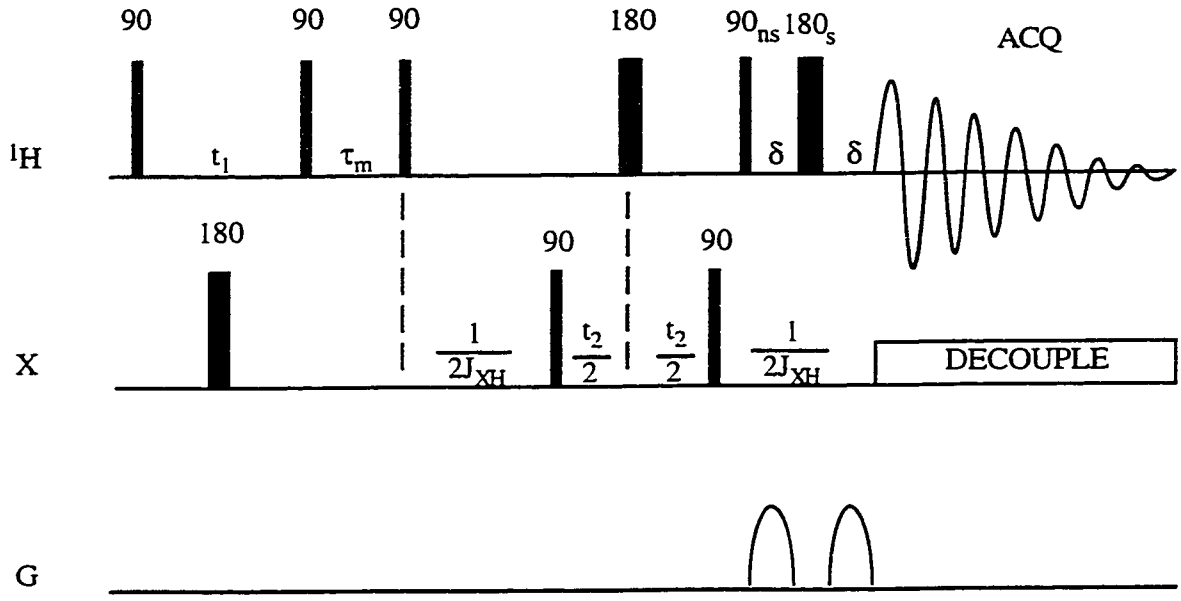

Figure 3.5 The Pulse Sequence for the NOESY-HMQC Experiment.

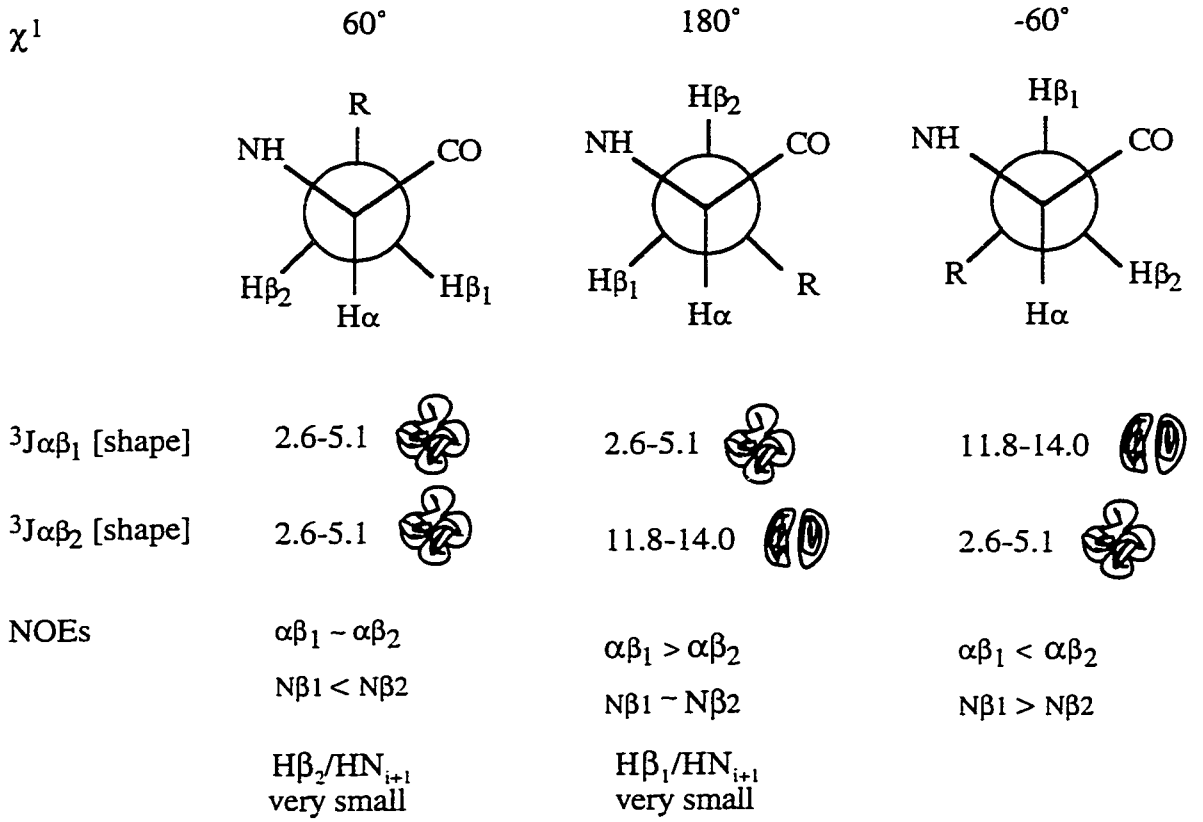

Figure 3.6 Information used for stereospecific assignment of β-methylene protons. ($^3J_{\alpha\beta}$ are adapted from Basus V. J. (1989), and they are in Hz; 'shape' refers to the shape of the corresponding peak in 55 ms mixing time D_2O media TOCSY.)

Chapter 4

Structure and Dynamics of Amylins and Pramlintide

The first section of this chapter presents the early stage of this research project. Due to the fact that the hAM aggregates in aqueous buffer at NMR concentrations, an initial comparison of rat and human amylin was carried out in DMSO. Later, the project concentrated on Pramlintide -- a human and rat amylin hybrid, specifically the $Pro^{25,28,29}$ substituted form of human amylin; both because of its biological activity (as described in Chapter 1) and its improved solubility and suitability for NMR studies. The preliminary result of pramlintide study was presented at 38th Experimental NMR Conference (Liu et al. 1997).

4.1 *Rat and Human Amylin in the DMSO-Solution State*

4.1.1 *Resonance Assignment*

All spectra presented in section 4.1.1 were recorded in an 88/11/1 vol/vol mixture of d_6-DMSO/CD_3CO_2D/H_2O, a presumably denaturing medium. Thoughout, this medium will be designated as 'DMSO'.

Rat amylin rAM in DMSO was the first assignment effort in this project; therefore, no analogies were available. Although the 'DMSO' spectra did display a wide range of HN shifts (8.9 - 7.3 ppm for the backbone amides) the region around 8.0 ± 0.14 ppm was particularly crowded. A complete self-consistent sequential assignment was not achieved until a considerable effort was made.

The standard sequence-specific resonance assignment strategy (Wüthrich, 1986) was employed. COSY and TOCSY spectra were used to define spin systems; and NOESY spectra were used for sequential assignments. Initially, it is very helpful to examine the peptide sequence, classify residues into groups and define the spin systems. rAM has 1 Lys, Glu, Phe, Tyr; 2 Cys, Arg, Gly; three Ala, Val, Ser, Pro; 4 Leu; 5 Thr; and 6 Asn, for a total of 37 residues to be distinguished. Of these, the unique Glu, Phe and Tyr residues should serve as starting points.

Figure 4.1 is the annotated $\alpha_i N_i$ region of a COSY spectrum of rAM in DMSO recorded at 310K. Lower panel is the enlarged version of the crowded region in the upper panel. Residues, except prolines and the first residue, have cross peak(s) in this region. Prolines lacking of amide proton do not show up in this region; and first residue

Lys did not show up due to the fact that its amide proton was in fast exchange with the solvent. Some residues, such as Gly^{24}, were assigned to more than one set of peak(s), and this was attributed to Xaa-Pro isomers. There are extra peaks not assigned in Figure 4.1, which are most likely also due to minor isomers.

TOCSY spectra provided critical information about sidechains. For instance in Figure 4.2, six sets of $\beta_i N_i$ peaks from 6 Asn are distinguished; peaks around 3 ppm are most likely $\beta_i N_i$ peaks of Cys, Phe, and Tyr; those relatively broad, very intense peaks at about 1.3 ppm are very good indications of methyl containing residues, such as Ala. 'Doublets' between 1.5-2.0ppm are $\beta_i N_i$ peaks for long side chain residues, like valine. Comparing COSY and TOCSY spectra, Thr Hα can be easily distinguished from Hβ, although they can have very similar chemical shifts.

After having fairly complete definition of spin systems from COSY and TOCSY spectra, a NOESY spectrum collected under similar condition (305K) was used for sequential assignments. In DMSO, there were very few medium ranged NOE connectivities in $\alpha\beta$ region, thus sequential assignments were mainly based on $\alpha_i N_{i+1}$ and $N_i N_{i+1}$ connectivities, shown in Figure 4.3 and 4.4 respectively. The most downfield COSY peak in αN region was assumed to be due to residue #2, which was supported by two $\beta_i N_i$ NOE peaks and an $\alpha_i N_{i+1}$ peak (due to Lys^1) which did not have a correlated $\alpha_i N_i$ NOESY or COSY peak. Other evidence supporting this assumption were the clear unambiguous $\alpha_i N_{i+1}$ connectivity string from residue 1 to 8 (Figure 4.3) and an $N_i N_i$ connectivity string from residue 3 to 11 (Figure 4.4). Assignment of residue Asn^3 and Cys^7 were further supported by $\beta_i N_i$ NOE, while assignment of residue Thr^4, Ala^5, Thr^6, Ala^8, and Thr^9 were supported by their methyl/NH NOE peaks, and the residue Glu^{10}, Arg^{11} assignments are confirmed by their relatively long sidechains. Another break through in assignment was at the unique Phe^{15}. The aromatic Hδ gave NOE connectivities to the corresponding Hα and Hβ resonances, which were thus distinguished unambiguously. A $\alpha_i N_{i+1}$ string connectivities then spanned from Phe^{15} through Arg^{18}. These two strings were broken most likely by the near NN shift coincidence of residue 12,13, and 14. Another string spanned Thr^{30} to Thr^{36} which displayed an unambiguous string of $N_i N_{i+1}$ connectivities show in Figure 4.4.

To distinguish repetitive residues, for instance six Asn, especially Asn^{21} and Asn^{22}, was a difficult task. The identification was achieved first by analyzing $\alpha_i \beta_i$

COSY peaks and $\beta_i N_i$ NOE peaks, then confirmed by sequential assignment. The strong sidechain HδHβ NOE peaks also served to distinguish six asparagines.

Shift coincidences also complicated the assignment. For example, Ser^{19} still remained uncertain. Its NH was most likely shift coincident with the NH shift of Ser^{20}, and its Hα happened to be at α_{18} position. Leu^{12} and Leu^{23} could also have very similar chemical shifts, and they were buried in the very crowed region labeled in Figure 4.1.

The assignment process was also complicated by Xaa-Pro cis/trans isomers, which resulted in the appearance of multiple peaks for Gly^{24} and Pro^{25}. In Figure 4.1, Gly^{24} has two sets of $\alpha_i N_i$ peaks, which were assigned using $\alpha_{24}\delta_{25}$ connectivities in NOESY spectrum. The set with the larger αH chemical shift difference, and reduced intensity, was attribute to the cis isomer.

Despite of all the difficulties, a self consistent assignment of rat amylin in DMSO was achieved; the backbone chemical shifts are tabulated in Table 4.1.

With one completed assignment, the next (hAM) was a relatively easy task, since hAM and rAM are only different by 6 residues. Also, there were no complications due to the cis/trans isomerization in hAM. A set of COSY, TOCSY, and NOESY spectra were collected at 308K for assignment purpose. Figure 4.5 is the NH region of a TOCSY spectrum of hAM in DMSO. All residues were clearly evident, as annotated. Single letter designations for the amino acids are used in front of residue numbers, indicating the six residues which are different in hAM. Figure 4.6 is a portion of NOESY spectrum, corresponding to the crowed region in Figure 4.5. Sequential $\alpha_i N_{i+1}$ NOE peaks are indicated by arrows; while $\alpha_i N_i$ COSY peaks are indicated by crosses. The complete hAM backbone chemical shifts assignment in DMSO is tabulated in Table 4.1, along with the shifts of rAM.

4.1.2 *Proline Cis/Trans Isomerization*

Cis/trans isomerization was observed in proline containing rAM, not in hAM. Proline is well known by its unique ability to form cis peptide bonds and undergo cis-trans isomerization (Creighton 1993). It was also observed for pramlintide in aqueous buffer and 25 vol% HFIP aqueous medium, later in the project. The clearest case, for which assignment was fully confirmed, was for the amide bond between Gly^{24}-Pro^{25} in DMSO. The analysis of the NOESY spectrum indicated that the conformer interconversion rate is in excess of 20/min, somewhat faster than the usual amide bond cis/trans interconversion rate at 305K. Although this aspect was not the major concern

of this project and no further investigation carried out, it is worth noting that cis/trans isomerization of salmon calcitonin, which shares structural and biological similarity with amylin, has been studied in detail in many different solvent systems (Amodeo et al., 1994; Meadows et al., 1991; Motta et al., 1989).

4.1.3 *Comparison of Rat and Human Amylin*

Preliminary efforts to derive a structure of rAM from NOESY data for DMSO solutions using NOE distance constrained dynamics did not yield converged structures suggesting conformational averaging is extensive. Therefore, chemical shift deviations were used to compare rat and human amylin in DMSO. αH and NH CSD histograms appear in Figure 4.7. The high degree of similarity between rAM and hAM over all regions except the immediate vicinity of the Pro substitutions can be seen in this comparison of the backbone hydrogen chemical shifts. Based on Figure 4.7, the only substantially structured region is the disulfide loop, which displays shift deviations as large as 0.6 ppm from the coil values. The amyloidogenic species, hAM, displays only a few weakly positive Hα shift deviations in the amyloidogenic span. With the exception of Leu^{12}, a string of negative Hα values is observed from Thr^{9} to Val^{17}. In aqueous medium this would be evidence for a partially helical region (Wishart et al., 1992). NOE-based structure calculation for rAM in DMSO also agreed with these observation: a converged disulfide loop conformation followed by a less well-defined helix. The exceptional behavior of Leu^{12} was later observed in 25% HFIP, a medium which favors helix formation (*vide infra*); and was investigated in more detail in the later medium.

4.2 *Pramlintide Assignment*

4.2.1 *Resonance Assignment in Aqueous Buffer*

Unlike human amylin which aggregates in aqueous buffers, pramlintide (the $Pro^{25, 28, 29}$ – substituted hAM) is readily soluble (up to 10mg/mL) at neutral to acidic pH in aqueous buffers, which provides the possibility for NMR studies under these conditions. After the assignment effort of rAM and hAM in DMSO described in previous section, to recognize the spin pattern for each amino acid (using TOCSY and COSY spectra) in other solvent system became relatively straightforward. A sample of 2.3mM pramlintide in aqueous buffer (deuterated 11mM acetate, 9mM formate, 6mM trifluoroacetate) was used to record the ROESY spectrum (Figure 4.8), which was the

key to the sequential assignment. In Figure 4.8, the αN fingerprint region of the ROESY spectrum is fully annotated, with vertical lines (or crosses) indicating COSY peaks (through bond connections) and horizontal arrows indicating ROESY peaks (through space connections). Since i/i+3 and N_iN_{i+1} connectivities are either absent or present at barely detectable levels in the ROESY spectrum, the sequential assignment were mainly based on α_iN_{i+1} connectivities. Some (but not complete) β_iN_{i+1}, γ_iN_{i+1} connectivities (not shown) also served to confirm the assignment. The chemical shift pattern of Cys-Cys disulfide loop was somewhat similar to the one seen in DMSO, thus the assignment from 1→8 was easily determined. The assignment of other spans, such as 14→18, 23→24, 26→27, and 29→37 were also relatively straightforward as there were very clear α_iN_{i+1} connectivities supporting the assignment. However the appearance of proline residues did make the assignment more difficult because they broke the string of α_iN_{i+1} connectivities. Assignments in the residue 9 to 13 span were complicated by αH and/or NH chemical shifts coincidence. At this point, sidechain information became crucial. Residue Thr^9 was located by the unique pair of peaks -- Hα and Hβ to HN (in TOCSY spectrum), and confirmed by a γ_8N_9 connectivity in upfield ROESY spectrum (not shown). Residue 10 and 11 were basically located by their long side chain; also, $\alpha_{11}N_{12}$ and $\alpha_{12}N_{13}$ peaks in Figure 4.8 confirmed the assignment in this span. The assignment of the double repeats, $Ser^{19}Ser^{20}$ and $Asn^{21}Asn^{22}$, were also difficult. The final assignments were supported by, and are consistent with, other evidence -- either of pramlintide in different solvent system or the assignment of fragments in later chapters.

Figure 4.9a→c is the 16K complex points 1D control spectrum corresponding to the ROESY, recorded at the same temperature (290K) with sample spinning. Figure 4.9a (NH region) is fully annotated. This high resolution 1D spectrum provided α_iN_i coupling constants for those NH doublets that are well-resolved. Figure 4.10 shows portions of a COSY spectrum of pramlintide recorded under the same condition, but in D_2O media. The COSY spectrum provided accurate chemical shifts for upfield protons, especially methyl groups.

The complete assignment of pramlintide in aqueous buffer appears in Table 4.2.

4.2.2 *Resonance Assignment in 25-35% HFIP Aqueous Media*

Pramlintide has been studied with a wide range of co-solvents, which will be presented in the later section. Both pramlintide and hAM, however, showed maximum

structural content with the addition of ≥16 vol% HFIP to aqueous medium by CD spectroscopy. And hAM displayed better solubility in 25-35 vol% of HFIP. In order to compare pramlintide with hAM easily, 25 and 35 vol% HFIP media were chosen for the assignment, and later for NOE based structure ensemble calculations.

The assignment in high HFIP media was completed by using spectra recorded on Bruker AM-500, although there were additional studies done on a modern Bruker DMX750 spectrometer later in the project.

^1H Assignment. Figure 4.11 shows the NH region of a 16K 1D control spectrum of pramlintide in aqueous 35 vol% HFIP at 295K. The sample was difficult to shim with high d_2-HFIP content, which interferes with the D_2O lock signal. As a result, the NH peaks are not sharp doublets (as they were in aqueous buffer, see Figure 4.9), instead, they became much broader singlets, which did not provide any $J_{\alpha N}$ coupling constants. However, the 2D spectra recorded under this condition were very informative. Due to increased NH and αH dispersion (versus the DMSO and aqueous buffer spectra), all of the assignments were relatively straightforward.

Annotated regions of the TOCSY spectrum of pramlintide in the 25% HFIP medium recorded at 305K appear in Figure 4.12 (α/β region) and 4.13 (α/γδ region); these provided a clear picture of the spin systems of pramlintide. Peaks from the minor isomer were labeled as the residue number followed by a prime, for instance: 30', 26', etc.

Figure 4.14 and 4.15 are portions of one of the representative NOESY spectra of pramlintide in 35% HFIP medium recorded at 295K. Starting with the two most downfield αHs, which were tentatively assigned as Cys^2 and Asn^3 based on their spin patterns; and from other NOESY spectra where the NHs were not coincident, they could be seen to be next to each other from the appearance of $H\alpha_i$, $H\beta_i$ to HN_{i+1} peaks. The NH pattern in the loop was quite similar to what had been seen in aqueous buffer (and DMSO). Another entry was the very sharp pair of peaks on the 7.44 ppm line (3.2-3.4 ppm in the other dimension), and they were assigned as the aromatic Hδ of unique residue His^{18} to its own ββ'. Then the 18 NH was located easily, and a string of N_iN_{i+1} connectivities extended through residues 12 and 20, as labeled in Figure 4.15. In the upfield NH region (Figure 4.14), α_iN_{i+1} and/or β_iN_{i+1} connectivities were also complete in this span. In addition, many α_iN_{i+3} and α_iN_{i+4} peaks were observed, among which the two most downfield NHs (16N and 17N) were the clearest cases. In between the disulfide loop (2→7) and the 12→20 span, the assignment was complicated by the NH

shifts coincidence of 8&9, and 11&12. Arg^{11} was initially identified by the unique side chain δ (3.26 ppm)/NH_e(7.175 ppm) cross peak; then residue 9 and 10 were located by $H\beta_i$ or $H\gamma_i$ to HN_{i+1} connectivities and Ala^8 were confirmed by 7 $H\beta\beta'$ to HN_8 peaks. An entry point for the C-terminal portion assignment was the COSY peaks at about 4.0/8.3 ppm. Since there were no other side chain peaks appearing on this NH line, they were assigned to Gly^{33}, and was confirmed by the clear string in NN region 30→36. Although $\alpha_i N_{i+1}$ connectivities were discontinuous at residue 31 and 35 in this NOESY spectrum, due to the bleaching from water suppression close to their Hα frequency, it was not very difficult to locate their Hα by comparing with the TOCSY spectrum. Between residue 21 and 29, the assignment was complicated both by the $N^{21}N^{22}$ repeat, and by three prolines lacking of NHs. Pro^{25} and Pro^{29}, on the other hand, had very clear $\alpha_i N_{i+1}$ peaks. After the Thr^{30} NH line was assigned, Pro^{29} was automatically assigned, followed by Pro^{25} and Ile^{26}. Gly^{24} was assigned by elimination, after Gly^{33} was confirmed. So was Phe^{23}, since there were clear $H\alpha_{23}$, $H\beta\beta'_{23}$ to HN_{24} connectivities. The initial assignment for Asn^{21} and Asn^{22} were tentative, with the possibility that the assignment was switched. However, they were later confirmed by $\alpha_{18}\beta_{21}$ and $\alpha_{19}\beta_{22}$ peaks. In fact, all the assignments of residue 5→22 were confirmed by the $\alpha_i\beta_{i+3}$ connectivities observed from either a NOESY spectrum collected in 35% HFIP D_2O media (not shown), or from the NOESY spectrum recorded on 750MHz spectrometer (vide infra). After considering all the cross peaks observed in NOESY spectra comprehensively, a self consistent assignment was achieved. A COSY spectrum (not shown) was used to obtain side chain chemical shifts. The complete proton chemical shift assignment of pramlintide in 35% HFIP aqueous media is reported in Table 4.3.

A NOESY spectrum of pramlintide free acid in 35% HFIP was taken and assigned. Pramlintide free acid gave essentially the same spectra as its carboxamide forms. With the exception of only three residues, including the C-terminal Tyr, the NH shifts of the remaining residues are essentially within experimental error -- $\langle d_{amide} - d_{acid} \rangle$ = +0.007±0.007 ppm. All of the differences can rationalized assuming a ±0.005 ppm calibration error and a 1°C difference in the actual temperatures of the experiments.

^{15}N Resonances Assignment. A HMQC spectrum of [U-^{15}N]-pram (universally ^{15}N labeled pramlintide free acid) in 35% HFIP was initially recorded at 285K on 500MHz NMR; and ^{15}N resonances were assigned by using the known amide ^{1}H shifts, and the assignment was further confirmed by a 3D NOESY-HMQC spectrum. Later, a

series of HMQC spectra of [U-^{15}N]-pram in the same solvent composition were recorded consecutively at five different temperatures on a Bruker DMX750 spectrometer; and the assignments were made by analogy. Since the published ^{15}N chemical shift data are still quite limited (compare to ^{1}H shifts), the amide ^{15}N shifts, as well as the corresponding amide ^{1}H shifts are tabulated in Table 4.4 at all five temperatures.

^{13}C Resonances Assignment. Pramlintide incorporating U-^{13}C-Leu ([U-^{13}C-Leu]-pram) was available. Figure 4.16 is the ^{13}C 1D spectrum of [U-^{13}C-Leu]-pram in 35% HFIP D_2O at 290K. The complete ^{13}C assignment was achieved using the RELAY-HMQC spectrum (Figure 4.17) recorded at 295K on the same sample. In RELAY-HMQC spectrum, the directly detected dimension was ^{1}H, and ^{13}C frequency was the indirectly detected dimension. The cross peaks from directly attached ^{1}H-^{13}C are positive; while the relay peaks are negative. The assignment started from the well confirmed Hα shifts of the three leucines, and subsequently, all of the ^{13}C shifts were assigned. The RELAY-HMQC spectrum, in turn, provided differentiation of the β, β' and γ proton resonances for all three leucines. The complete ^{13}C resonance assignments are listed in Table 4.5 in the next section, along with their respect random coil values.

4.3 *Structural and Dynamical Features of Pramlintide*

4.3.1 *Initial Structural Assessment*

4.3.1.1 Pramlintide in Buffer and in 35% HFIP

As discussed earlier in Chapter 2, chemical shifts are the most accessible quantities in NMR spectroscopy, and have become more and more important in evaluating conformational preferences of peptides. After the completion of the pramlintide assignments in different media, Chemical Shift Deviation (CSD) analysis provided a quick assessment of pramlintide secondary structure. A comparison of Hα shift deviation histograms of pramlintide in aqueous buffer and aqueous HFIP media appears in Figure 4.18. In aqueous buffer, pramlintide has minimal structure, as most of the Hα shift deviations are within ± 0.1 ppm. The disulfide loop is the most structured part of the peptide under this condition; and it adopts a very similar conformation to that in the aqueous HFIP, indicated by very similar CSD pattern for loop region in both media. In buffer, the small but continuously negative CSDs in residue 5 - 17 span suggest a loosely formed helix. On the contrary, large CSDs are observed in this span (except Leu^{12}) of pramlintide in aqueous HFIP medium, indicating

a fully populated helix with gradually end fraying at residue 19 to 22. The C-terminal portion of the molecule has little structure in both media.

The major conformational difference of pramlintide in buffer and in HFIP is the extent of the helicity in residue 5 to 20 span. This difference can also be seen by detailed comparison of dipolar coupling correlations of pramlintide with and without HFIP addition. The αN finger print region of a ROESY spectrum in buffer (upper panel) and a NOESY (lower panel) spectrum in 35% HFIP of pramlintide shown in Figure 4.19. With HFIP addition, the i/i+3 and i/i+4 NOEs which are characteristic for helix formation were detected throughout residue 5 to 20 span. The clearest cases, as labeled in Figure 4.19 lower panel, are $\alpha_{13}N_{16}$, $\alpha_{12}N_{16}$, $\alpha_{14}N_{17}$and $\alpha_{13}N_{17}$ peaks. The key NOEs of pramlintide observed in HFIP medium are summarized in Figure 4.20, combining the information from both 2D and 3D NOESY spectra. Medium-range side chain interactions were also detected, such as $\alpha_{12}\delta_{15}$, and $\alpha_{14}\varepsilon_{His18}$ NOEs, etc. In buffer, the rich web of i/i+3 connectivities for i = 5 – 20 observed in aqueous HFIP are either absent or present at barely detectable levels (Figure 4.19 upper panel). Further more, unlike in the HFIP medium where the inter αN peaks are smaller than intra αN peaks in this span; in buffer, the inter-residue NOEs are much larger than intra-residue NOEs. For instance, $\alpha_{16}N_{17}$ is bigger than $\alpha_{17}N_{17}$, and $\alpha_{17}N_{18}$ is bigger than $\alpha_{18}N_{18}$. All these suggest that in buffer, helix formation is not complete, and the extended conformation is a significant contributor.

Despite the big difference in helicity, the N-terminal disulfide loop conformation is not much altered and the C-terminal segment remains minimally structured upon HFIP addition.

4.3.1.2 Comparisons with Human and Rat Amylin

Amylins in Non-Structure-Promoting Media. With regard to pramlintide in aqueous buffer and human/rat amylin in DMSO, the differences in αH-CSD at residue 3, 5 and 7 shown in Figure 4.21 suggested that the disulfide loop conformation is not quite the same in the two solvent systems. Nevertheless, the disulfide loop is the most structured segment of the peptide in both media. Apparently the disulfide closure prevents the loop from sampling all conformational space; and a single turn of helix (residue 5-7) is locked in by the disulfide loop conformational preference. In both DMSO and aqueous buffer, the prenucleated helix propagates out into the residue 8-17 span in some of the conformers that are present in these non-helix-stabilizing media.

This provides a rationale for the residual helicity observed by CD even in the presence of high concentrations of denaturant. Further investigation of the effect of disulfide closure on helix formation and stabilization will be presented in chapter 5.

Amylins in 25-35% HFIP. The Hα chemical shift deviation histograms for hAM, pramlintide, and rAM in 25% HFIP reveal the structural alteration that occur upon introducing the prolines into the sequence. The CSDs (Figure 4.22) are nearly identical from the N-terminus to Ser^{20} and from Thr^{30} to the C-terminus for all three peptides. The one exception to this is rAM, which has an H18R mutation. The rat amylin histogram differs from the others at Asn^{14}, Phe^{15}, and Asn^{21} reflecting the expected periodicity of an a helix about the site of the mutation. With the exception of Leu^{12}, there is a continuous string of upfield shifted Hα resonances from Ala^{5} to Ser^{20} for all three amylins, indicating a common helical span. For hAM from residue Phe^{23} to Ser^{29}, which is believed to be the amyloidgenetic sequence (Ashburn & Lansbury 1993; Ashburn et al., 1992), a second helix is suggested. Apparently, the introduction of prolines largely alters the conformational preference of this region in pramlintide and rAM. The structure of C-terminal portion of all three peptides is not well defined. The pattern of small alternating upfield and downfield shifts in the C-terminal segment does not correspond to any known regular secondary structural feature. A set of conformers with β-turns at different loci in this span could rationalize this observation, and is consistent with the observation of weak i+3 NOE connectivities at C-terminal (see Figure 4.20).

The HN chemical shift deviation histograms provided additional evidence supporting helix formation. In Figure 4.23, the HN CSDs of residue 1-20 of pramlintide and hAM in 35% HFIP are essentially identical. The HN chemical shifts of residue 16, 17 and 13 are far downfield, compared to the shifts for pramlintide in buffer. These downfield shifts are most likely due to particularly strong H-bonds in the helical segment. This is also consistent with the H/D exchange experiment performed on hAM(Cort, 1994): the NHs of residues 16, 17 and 13 had the slowest exchange rates. Exchange at the NHs of residues 12, 14, 15 in this span, was also significantly retarded. The correlation between HN-CSD and H-bond energy has also been reported previously by other scientists (Wishart et al. 1991).

4.3.2 *Further Investigation of Leu[12] Anomaly*

As noted in the previous section, the Leu[12] has a close to random coil Hα shift for all three amylin discussed. However, the medium range i/i+3, i/i+4 NOE connectivities throughout the residue 5 to 20 span (Figure 4.20) suggest one well-defined helix domain rather than two short helices. Further investigation was carried out on this issue.

A detailed examination of inter/intra-Hα/HN NOE ratios of pramlintide in 35% HFIP results in Figure 4.24. Values of –3.5 to –4.5 represent full population of helical psi values at that locus. As the NOE ratio histogram shows that Leu[12] is as helical as neighboring-residues. An examination of HFIP induced βH shift changes in this region also support this conclusion. The differences of αH and βH shifts in HFIP and in buffer appear in Figure 4.25. βH shifts are expected to be more downfield upon helix formation, which has the opposite trend of αH shifts (Wishart et al., 1991). Unlike αH of Leu[12], which has a minimal change upon HFIP addition, the βH shifts significantly downfield, indicating helix formation at Leu[12] upon HFIP addition. It is interesting to note that βH shift changes gradually increase toward the C-terminal portion of the helix. This is because the N-terminal portion of the helix is already populated in buffer due to the nucleation effect of the disulfide loop; however, the helix propagates toward the C-terminus with severe end fraying. Upon HFIP addition, the helix becomes fully populated through Ala[5] – Ser[20]; thus, it is not surprising to see larger shift changes in C-terminal portion of the helix. Also notable is that the so-called "α-helix periodicity" (the alternating minima and maxima in every three or four residues) is evident for βH shift changes in Figure 4.25, with maximum shift changes at residue 7, 11, and 15; and minimum shift changes at residue 6, 9, and 12. Similar observations have also been reported by other researchers for αH, βH and NH shifts (Jiménez et al., 1992). However, it is not evident for αH in pramlintide due to the abnormal shift of Leu[12].

Two alternative explanations for the anomalous shift of the Leu[12] Hα signal can be suggested: a kink or other local distortion of the helix at this point or a large deshielding ring current contribution associated with a specific orientation of the Phe[15] sidechain. Downfield shifts of alpha methines at both i-2 (Andersen & Tong 1997) and i-3 (Andersen et al., 1995b) locations relative to Phe/Tyr residues in helices have been noted previously.

If the anomalous shift of Leu[12] Hα is due to the specific orientation of the phenyl ring of Phe[15], the Hα of a D-amino acid at this position will be influenced

differently assuming the overall peptide retains same conformation. This prompted a study on D-Leu^{12}-Pram (pramlintide with a D-amino acid at residue 12). As we hoped, the introduction of a single D-amino acid into the sequence did not destroy the overall conformation of the peptide. In fact, the Hα–CSD histograms in Figure 4.26 suggests that the D-Leu^{12} -Pram retains a very similar conformation to pramlintide. The most significant difference in this plot is at residue 12. In D-Leu^{12}-Pram, the Hα shift deviation of D-Leu^{12} is as negative as neighboring residues, indicating a well defined continuous helix in residue 5-20 span. Other minor (but significant) differences in CSD are at residue Thr^{9}, Leu^{16} (3 or 4 residue away from D-Leu^{12}) and Arg^{11} (the preceding residue).

More direct evidence supporting the "ring current" explanation came from the experiments with universally ^{13}C labeled Leu ([U-^{13}C-Leu]-pram). The diamagnetic anisotropy contributions of the phenyl ring should be relatively smaller for ^{13}C chemical shifts. The ^{13}C shifts for the three leucines are given in Table 4.5. Both Leu^{16} and Leu^{12} display shifts for C', C_α and C_β that are fully consistent with a helical conformation. In contrast the C' and C_α shifts of Leu^{27} suggest and an extended (β) conformation. Thus it seems very unlikely that the backbone torsions at and around Leu^{12} deviate significantly from helical values.

4.3.3 *Indications of Helix Curvature*

Quite a few studies have noted that the magnitude of the helix secondary shifts is not evenly distributed along the peptide chain, rather, alternating maxima and minima appear every three or four residues, which is very similar to the α helix periodicity. This helix secondary shift periodicity has been observed experimentally and theoretically predicted for α, β, and especially for amide proton shifts (Asakura et al., 1995; Blanco et al., 1992; Jimemez et al. 1992; Zhou et al., 1992;).

In the case of pramlintide, as noted in section 4.3.2, the "periodicity" was observed for Hβ shift changes from buffer to aqueous HFIP; but not evident for Hα, which may be due to the shift distortion from the ring current of Phe^{15}. Figure 4.27 shows the CSDs of both amide ^{1}H and ^{15}N versus residue number of pramlintide in 35% aqueous HFIP at 285K. The periodicity is observed for both nuclei in the helical span, with $^{1}H_N$ having clearer maxima (at residue 9, 13, and 16/17) and minima (at residue 10, 14 and 18). The amide protons of fatty residues exhibit a large positive shift

deviation, and these residues presumably are in the center of the hydrophobic face of the helix.

It has been suggested that the cause of such periodicity is the existence of helix curvature originated by its amphipathic character; and the magnitude of helix shifts is directly related to the minor geometric distortions of helices (Jiménez et al., 1992; Kuntz et al., 1991; and Bruix et al., 1990). As observed in protein crystals, natural amphipathic helices in solution are bent so that the hydrophobic side has shorter hydrogen bonds. The differences involved in the geometries of distorted helices are extremely small, typically 0.1-0.2Å (Blanco et al., 1992). This is almost impossible to detect through conventional NOE-based structure refinements. The observation of the conformational shift periodicity in pramlintide suggested that like other amphipathic helices, a curvature exist in the helical domain of pramlintide.

Another observation from Figure 4.27 is that the periodicity of ^{1}H and ^{15}N is not quite 'in phase'. For instance, the maxima of ^{15}N deviation are at residue 12 and 15, instead of at residue 13, 16 as in ^{1}H. This seems contrary to Wishart's statement (Wishart et al. 1991) that amide ^{1}H and ^{15}N shift deviations are linearly correlated to each other. Figure 4.28 is an attempt to find a correlation between the ^{1}H and ^{15}N CSDs. Obviously, there is no general correlation between these two. However, surprisingly, an excellent correlation with R^2 of 0.997 was observed for residue Ala^5, Ala^{13}, Leu^{16} and Val^{17}; among which Ala^{13}, Leu^{16} and Val^{17} have slowest exchange rates according to the H/D exchange study performed on hAM, while the exchange rate of Ala^5 was not measurable (but could be slow) due to a shift coincident. This observation suggests that there is a correlation between ^{1}H and ^{15}N CSD only when the amide group is strongly hydrogen bonded; which is somewhat different from the conclusion of Wishart et al. (1991).

4.3.4 *Cosolvent and Temperature Induced Helix Dynamics*

To investigate the dynamics of pramlintide, fluoroalcohol titration and thermal unfolding experiments were carried out. These studies provided insights into how the helix is induced by the cosolvent; and the effects of warming (and cooling).

Both 2,2,2-trifluoroethanol (TFE) and 1,1,1,3,3,3-hexafluoroisopropanol (HFIP) are well known secondary structure promoters for peptides (Cammers-Goodwin et al., 1996; Andersen et al., 1995c; Sonnichsen et al. 1992; Nelson & Kalllenbach, 1989; Parrish & Blout 1972; Tamburro et al., 1968), and it is believed that the dominant

effect of these fluoroalcohols is caused by their significantly weaker basicity, as the pKa of TFE and HFIP are 12.4 and 9.2, respectively. They are better protonating agents; thus reducing the H-bond accepting capability of the bulk medium and hydrogen bonding of amide protons to the solvent, which strengthens intramolecular hydrogen bonds and therefore stabilizes secondary structure (Nelson & Kellenbach, 1986).

Like many other peptides, the helicity of pramlintide dramatically increased upon fluoroalcohol addition. The αH-CSD histograms of pramlintide with different percentages of fluoroalcohol as cosolvent appear in Figure 4.29. Figure 4.29a is focused on the helical domain, and it is clear that the rates of the helicity increase at different residues are not the same. Apparently, the helicity grows in faster at the residues close to disulfide loop, which is believed to be the nucleation site of the helix. With some cooling and a minimal level of TFE (10%), the helicity of the N-terminal residues of the helix almost reached their maximal values. However, the C-terminal portion of the helix did not grow in fully until fairly large amount of HFIP (25%) -- a stronger secondary structure promoting agent, were added. The most dramatical change occurred at residue His^{18}, which is the C-cap of the helix in buffer. Despite of the large helicity increasing, not all regions of the peptide become helical. TFE and HFIP only stabilize helices in regions with some α-helical propensity. As shown in Figure 4.29b, the fluoroalcohol addition had, with exception of Thr^{6}, very little effect on the N-terminal and C-terminal of pramlintide.

Temperature dependent study is another way to monitor the dynamics of a peptide. Although backbone amide NH chemical shift temperature gradient is frequently used as an indicator of H-bond formation, the gradient caused by conformational changes of the peptide is often overlooked. A novel method to correlate NH chemical shift temperature gradient and NH chemical shift deviation and to evaluate peptide conformational preferences was first reported from our laboratory (Andersen et al., 1992, 1997; Liu et al., 1994).

The correlation plots of amide NH temperature gradient ($\Delta\delta/\Delta T$) vs. chemical shift deviation of pramlintide in 35% HFIP and in buffer appear in Figure 4.30. The corresponding values are listed in Table 4.6. The plot is formatted so as to place downfield NH resonances to the left as in typical NMR spectra. The chemical shift deviations are derived from the lowest temperature included in the experiment. In HFIP aqueous medium, an excellent correlation between $\Delta\delta/\Delta T$ and CSD was observed, especially for helical residues ($R^2 = 0.824$); which suggests that the helical structure

melts with a significant degree of cooperativity (Andersen et al., 1997). The slope of the correlation plot is a measure of the decrease in the population of the structured state upon warming. The occurrence of large shift deviations and abnormal gradients are diagnostic for structuring at lower temperatures which becomes increasingly randomized on warming. It appears that essentially all of the NH shift deviation from reference values is due to the concerted formation of a single structured state on cooling. In buffer, a poor correlation is observed, with $R^2 = 0.26$, indicating pramlintide is quite random in buffer even at low temperature; and that the structure that does form is not a single domain formed in a cooperative manner.

4.3.5 *Evidence of Slow and Rapid Conformer Interconversion*

Evidences pointing to the existence of slow exchanging conformers appeared several times during the studies of pramlintide.

The first observation was on a pramlintide acetate sample in DMSO-rich media. The initial solution included only stoichiometric quantities of CH_3CO_2H, insufficient to protonate the N-terminus, and changes in the spectrum were monitored as the DMSO/H_2O solution was progressively acidified – first with acetic acid (pKa = 12.3 in DMSO), then DCO_2D, and finally TFA (pKa = 3.5). Not until acids more acidic than acetic were added, did the NHs for the loop region (particularly those of Thr^4 and Thr^6) sharpen and shift toward the characteristic chemical shift values observed in previous samples which had been of TFA salts. Protonation of the N-terminus apparently leads to either a significant conformational change or has large coulombic contributions to the chemical shifts of sequence remote NH signals. Although further studies are required to define the changes occurring, the analysis to date suggests that the two-protonation states are not in rapid equilibrium. In retrospect, this was the first evidence suggesting the existence of multiple conformations of the loop which are in slow exchange.

Another observation is that at low temperatures, several NHs in the disulfide closed loop (Cys^2-Csy^7) were absent or very broad, particularly at 17.6 Tesla. As shown in Figure 4.31 -- the αN region of a NOESY spectrum recorded on 750MHz NMR at 275K, residue Thr^4, Ala^5, Thr^6 and Cys^7 are very broad. These signals became sharp, and were not cross-saturated by presaturation of the water signal, at ambient and higher temperatures. This behavior can be attributed to the interconversion of loop conformers with ms lifetimes at the low temperature limit.

The series of gradient-enhanced ^{15}N-HMQC spectra at 268-315K (Figure 4.32) provided additional evidence of different time scales of conformational averaging in different portions of the sequence. The ^{15}N-^{1}H correlation peaks for residues 3, 4, and 5 broaden significantly on cooling and disappear from the HMQC spectra recorded at 275K or lower temperatures. Those for residues 6, 8, 9 (and probably also 7) disappear into the noise at 268K. In contrast the correlations for residues 30-37 are relative more intense at the lower temperatures. Segmental motion more rapid than molecular tumbling is suggested for the C-terminal segment. The broadening of the peaks for the loop region could represent increased lifetimes of multiple loop conformers with divergent chemical shifts. This conclusion is consistent with that two major conformers with different ϕ values at Thr^4 were observed in the early stage of hAM structure refinement (shown in Figure 4.33). The chemical shifts of the NHs of residues 3-5 would be very different in the two loop conformers. Thus, if they were relatively long-lived at the lower temperatures, they would explain the disappearance of these peaks at low temperature.

4.4 *Structural Details from NOE-based Refinement*

4.4.1 *Constraints*

Distance Constraints.

The majority of the NOE distance constraints employed for structure elucidation of pramlintide were derived from the short mixing time 2D (τ_m = 90ms, T = 275K) and 3D ^{15}N edited NOESY (τ_m = 110ms, T = 295K) spectra recorded at 750MHz. The availability of the data taken from DMX750 Bruker NMR greatly improved the accuracy of the distance constraints.

The DMX750 NMR has much higher sensitivity than the AM500, which allowed us to use a short mixing time and avoid secondary NOEs. Comparing the 90ms mixing time NOESY spectrum recorded on DMX750 (Figure 4.31, 4.34) and the 200ms long mixing time NOESY (Figure 4.14, 4.15) from AM500 reveals the differences. For instance, on 16 NH line in Figure 4.14, the i+4 peak is almost as large as i+1 peak, which is caused by the secondary NOE; while in Figure 4.31, i+4 peak is much smaller than i+1 peak. Comparing Figure 4.34 and Figure 4.15, the secondary NiNi+2 peaks (such as $N_{17}N_{15}$ peak) were eliminated in Figure 4.34. In addition, due to the high sensitivity, there were quite a few NOE peaks, which were not detected on the AM500, that were detected on the DMX750. For instance, $\alpha_{29}N_{32}$,

$\alpha_{28}N_{31}$, and $\alpha_{28}N_{30}$ peaks in Figure 4.31, and $\alpha_{18}\beta\beta'_{21}$, $\alpha_{19}\beta\beta'_{22}$ and $\alpha_{32}\beta_{35}$ peaks in Figure 4.35, were not detected in AM500 NOESY.

The availability of 3D ^{15}N edited NOESY-HMQC data resulted in many new constraints which were impossible to obtain in 2D NOESY due to NH shift coincidence. A number of NOE peaks observed in 2D NOESY corresponded to the sum of two or more interproton cross-relaxation processes; with the assistant of the 3D data, the intensity of each peak was measured on different ^{15}N layer with much higher accuracy. Figure 4.36-4.38 illustrate this situation. In Figure 4.36, panels a&c and b,d,e are portions of 2D and 3D NOESY spectra, respectively. When there was no NH overlap, 2D and 3D data were essentially identical, as 16 NH line shown in α and β. When there is a shift coincidence, for instance, NH 26 and 27 were always almost on top of each other under all conditions examined, 3D data provided many new constraints from the peaks labeled with * in d&e, since residue 26 and 27 have different ^{15}N shifts. Figure 4.37 shows residue 8 and 9 which had both NH and αH overlapping problems. Again, four new constraints emerged since in 3D data residue 8 and 9 are on different ^{15}N layer. However, the αH shift coincidence still could not be resolved. For example, α_9N_9 and α_8N_9 peak intensities could not be determined with certainty. A ^{13}C labeled sample is needed to resolve this problem. Figure 4.38 is another example, showing the overlapping of 15&19, and 18&20 NHs and the resolution available from the 3D data. Many new NOEs were measured with accuracy from the 3D data, including $N_{18}N_{19}$, and $N_{19}N_{20}$ connectivities.

NOE information obtained from amylin analogs was also helpful for determining some distance constraints for pramlintide. Since all of the backbone chemical shifts and NOE ratios are essentially identical for pramlintide and a variety of abbreviated analog over the common residue 2-19 span, we could assume that clarifications of the partitioning of some overlapped NOEs in analogs apply to pramlintide as well. One example of the use of an analog in this process is given here. In the hAM(1-20)GYNH$_2$ analog, with residues 21-36 replaced by a single glycine, Hα and Hβ of Thr^4 are shift coincident in both aqueous buffer and in 20+% aqueous HFIP. This is an unfortunate overlap since Thr^4-Hα/Hβ displays significant NOEs to a number of sites including the NHs of Ala^5 and Thr^6. This shift coincidence is broken in 16% aqueous TFE (Figure 4.39) and also in analogs with an A8V mutation. Studies of these systems revealed a constant ratio of NOEs with, for example, a very dominant

$H\beta_4/HN_6$ and a major $H\alpha_4/HN_5$ contribution. The ratios observed in the analogs are assumed to apply to pramlintide as well.

H-bond Constraints.

H-bond information was also included as distance constraints. From early stage human amylin structure refinement, the backbone carbonyl H-bonding partners for the exchange protected NHs at residues 12/13/14/16/17 were clearly the i - 4 rather than the i - 3 possibility. These were also included in pramlintide structure refinement as H-bond distance constraints, since pramlintide and hAM are essentially identical for the first 20 residues.

Combining 2D, 3D NOESY data of pramlintide, as well as the information from the analogs, resulted in a rich web of NOE distances, in excess of 450 initial distances constraints. The 404 constraints used in final stage structure refinement are listed in Appendix B.

Dihedral Angle Constraints.

A few ϕ dihedral angle constraints in the disulfide loop region were included in pramlintide structure refinement. These constraints were derived based on the $^3J_{HN\alpha}$ coupling constant measured from pramlintide 1D spectrum in aqueous buffer, as it is believed that the conformation of the loop are essentially identical either in buffer or in 35% HFIP (Figure 4.18, 4.23). As shown in Figure 4.9a (also listed Table 4.2), the $^3J_{HN\alpha}$ coupling constants are quite different in the loop region, as large as is 8.5 (Asn^3) and as small as 3.0 Hz (Ala^5). Another interesting observation in the loop region is that N_4N_5 NOE is always very small (essentially zero), even at long mixing times; while N_3N_4 and N_5N_6 NOE are always big (Figure 4.15), suggesting very distinct structure feature in the loop.

The dihedral angle constraint table is also listed in Appendix B.

Stereospecific Constraints.

The 55ms mixing time TOCSY spectrum (Figure 4.40) of pramlintide in 25% HFIP/D_2O medium was the key for anti/gauche assignments. $\beta_iN_{i+1}/\beta_iN_i/\beta_i\alpha_{i-3}$ NOEs were also used to convert anti/gauche information to stereospecific assignments (see section 3.4.1 for detailed method). Stereospecific assignments for H_βs were confirmed for residue 3, 7, 12, 14, 15, 16, 18, 19, 21, 22, 23, 25, 28, 29, and 35; for H_γs were

confirmed for residue 26; and for H_δs were confirmed for residue 28 and 29, as shown in constraints table in Appendix B.

4.4.2 *Restrained MD and Structural Details*

Over 450 NOE distance constraints were initially used in restrained molecular dynamic calculation. The distances were given rather tight bounds -- the allowed range for a zero energy penalty was typically 22% of the distance derived from the NOE data. A three stage XPLOR protocol with each stage containing several cycles of dynamics simulated annealing was employed, with the inclusion of the previously verified H-bond constraints at all stages. The third stage was repeated several times during the process of deriving stereospecific constraints and eliminating unreconcilable alternate assignments for some NOE peaks. The final run employed 404 NOE distances; of which 75 were low-bounds-only constraints. The third stage molecular dynamic protocol is also reported in Appendix B.

At this high constraint density only the major disulfide loop conformer is represented in the structures that have acceptable E_{NOE} values. Significant constraint violations were found in the disulfide loop and at the C-terminus of the residue 5 - 22 helix. The latter are attributed to C-terminal fraying and to the contributions of an alternate conformation with a C-capped helix. The relatively constant intensity of $\alpha_i\beta_{i+3}$ peaks through the rest of the helix and the loss of intensity for i = 18 and 19 is shown in Figure 4.35. The complete set of diagnostic relative NOE intensities is given here—

	α_iN_i /	α_iN_{i+1} /	α_iN_{i+3} /	$\alpha_i\beta_{i+3}$
for i = 7-14,	1.00 /	0.35±0.11 /	0.42±0.12 /	0.83±0.26;
for i = 18,	1.00 /	0.69 /	0.08 /	0.24;
for i = 19,	1.00 /	0.80 /	0.04 /	0.13;
for i = 20,	1.00 /	1.08 /	<0.04 /	<0.10.

A plot of ϕ/φ values along the sequence revealed two families of structures - one in which the helix end abruptly with Ser^{20} taking on backbone torsion values of ϕ_{20}= -112±25° and φ_{20} = +179±15°; in the other, the ϕ/φ values from Ser^{19} to Asn^{22} deviated more gradually from the helical norms. In order to obtain unstrained structures of both the short and long helical forms, the third stage of refinement was repeated with the following modification: for the long helix family, the α_iN_{i+1} distances were accorded lower weight and the low bounds for the i/i+3 constraints for i = 17-20 were relaxed; for the C-capped helix refinement, the vicinal constraints

retained high weighting and the original i/i+3 constraints for i = 17-20 were moved to the lowest weight category.

The ϕ/φ versus residue plots for the two ensembles that resulted appear in Figure 4.41. The darker thin lines represent the C-capped short helix; while gray thick lines represent the long frayed helix. Figure 4.42 is the ribbon representation of these two ensembles. Both ensembles displayed convergence of the helical domain, with backbone rmsd: -- for the long frayed helix, 0.84±0.28 Å over residues 5-21; for the C-capped conformation, 0.63±0.22 Å over residues 5-18 and 0.95±0.32 Å over residues 5-21. The C-capped helix ensemble displays marginally better fits to the NOEs; the difference, however, is not statistically significant. As shown in Figure 4.41, the N-terminal loop is converged for all structure ensemble; the proline region although not converged, however, is not fully random either. The prolines may also be the cause of the relative big E_{vdw} (~-125kcal/mol) comparing to hAM (~-150kcal/mol). The extreme C-terminus is either under-determined or conformationally averaged.

In order to evaluate the potential effects of the precision of the distance constraints, a set of the 'loose' constraints, similar to those used in most protein structure elucidation was created. The violation and structure statistics for the complete ensembles against both 'tight' and 'loose' constraints appear in Table 4.7. The 'loose' constraints violation statistics provide comparisons to more standard protocols. Although total E_{NOE} is over 50 kcal/mol with 'tight' constraints, it is exceedingly low with the 'loose' constraints; especially for category I constraints. And in fact, the inter-residue NOE violations mainly come from the C-terminal portion of the peptide, rather than the helix domain, as the %-violation are 8.3±1.8 versus 1.9±0.8 kcal/mol against 'loose' constraints for the two portion of the molecule.

A Ramachandran plot of pramlintide structure ensemble is shown in Figure 4.43. The ensemble corresponds to the energetically allowed regions.

4.5 *Discussions and Conclusions*

Any potential to form β aggregates, or enhance amyloid fibril formation from native amylin peptides, would decrease the potential of pramlintide as an amylin replacement therapy. In this study, pramlintide has been shown to be essentially unaffected by the β aggregate formation phenomena of human amylin which lead to amyloid plaque formation in type II diabetes (Cooper et al., 1987). Pramlintide is

highly soluble and appears to be a monomer in aqueous buffer, a condition similar to the one used for pramlintide administration to diabetic patients, and in which human amylin aggregates extensively. Apparently, the introduction of three prolines into the amyloidogenic sequence of hAM (residue 25-29) prevents the β aggregate formation. As indicated in the ϕ/φ plot (Figure 4.41), although the proline region failed to converge into single conformer, it obviously adopts only a limited set of conformations, which cannot be accomodated in β aggregates. The NMR spectra collected under a wide range of conditions in this dissertation have provided experimental evidence supporting IND and related filings for pramlintide as a diabetic drug candidate.

All amylins examined in our laboratory display some helicity in aqueous buffer and in highly denaturing media. Even in 7.5M GdmCl, the CD data for pramlintide is consistent with the presence of three helical residues. NMR studies in DMSO and aqueous buffer in this chapter revealed the origin of the helicity, as CSD plots (Figure 4.21) indicate that the conformational preference of the disulfide loop locks in a single turn of helix, Ala^5 -Cys^7, and that this preference propagates, in part, into the Ala^8 - Val^{17} segment in these media. The absence of measurable i/i+3 NOEs in this span suggest that this represents a nascent helix (Dyson & Wright, 1991; Dyson et al., 1988), rather than a low population of a cooperatively formed helix spanning a significant segment of the Ala^8 - Val^{17} span. Upon addition of HFIP, chemical shift deviations (Figure 4.22), inter/intra-residue αN NOE ratios (Figure 4.24), and the intensity of the i/i+3 NOEs (Figure 4.20) all indicate a fully formed helix that spans from Ala^5 to Val^{17}, and extends in a frayed form to Ser^{20} or slightly further.

In all media examined, the N-terminal disulfide loop is highly restrained; and the extreme C-terminus of the peptide is quite flexible. The ϕ/φ plot (Figure 4.41) suggests only two significantly populated turn loci (type III' at 30/31 and type III at 32/33) in the C-terminus. This is consistent with what the CSD suggested and the temperature dependence of the ^{15}N-HMQC intensities (Figure 4.32), confirming that the C-terminal segment is undergoing rapid segmental motion.

No long range NOE was detected, even in 25-35% HFIP aqueous media. Thus, it is not surprising that the constrained molecular dynamics calculation failed to define a 'tertiary' structure - the relative spatial disposition of the C-terminus to the defined structural element, for the 'structured state' of pramlintide (Figure 4.42). The lacking of tertiary structure could be an inherent feature of this peptide hormone (as will be

discussed further in the later paragraph). Another possibility is that this might reflect the nature of the solvent in which the peptide was examined. As both TFE and HFIP have been reported to act as a denaturant with respect to the tertiary and quaternary structure of proteins (Cort & Andersen 1997; Slupsky et al., 1995; Lau et al., 1984).

Pramlintide is illustrative of conformationally averaged medium-sized peptide. It seems a simple peptide, but actually is a very complex system. A careful examination of all NMR structure parameters, especially the CSD histograms and backbone NOE ratios is required for a dependable diagnosis of secondary structure preferences, especially systems that lack tertiary structure. The traditional NOE based structural refinement alone, will not serve.

CSD histograms appear to provide insights into which backbone NHs have the strongest H-bonding and loci of unfolding. The NHs of Ala^{13}, Leu^{16}, and Val^{17}, which display the largest protection factors, are far downfield. In the absence of fluoroalcohol, Ala^{8} is a locus of disorder. The NOE-derived ensemble for the state present in 25-35% HFIP fails to display disorder at this point in the sequence. However, the Hα-CSD for Ala^{8} is less negative than that of all other residues in the residue 5-11 span suggesting that some local helix unwinding occurs even at high HFIP levels. The absence of NH exchange protection at Thr^{9} is consistent with this conclusion. The Hα-CSD histogram also provides a clearer picture of the increasing extent of end-fraying that occurs from His^{18} onward. The implied residue specific fractional helicities predict the decreasing relative intensities of the $\alpha_i\beta_{i+3}$ NOEs at i = 17 to within experimental error. The NOE based refinement can not distinguish nascent helices from partially populated, cooperatively formed, helices. The chemical shift data (including NH shifts due to strong H-bonds) does provide this distinction. Also, the chemical shift data provide a means to detect minor curvature of the helices, which is impossible to detect using traditional NOE-based structure refinement.

The NOE-derived structure ensembles for the 'state' favored in aqueous HFIP do, however, provide additional insights over the loop and the helical domain. The decreasing intensity of the $\alpha_i\beta_{i+3}$ NOEs at i = 17 (see Figure 4.35) and the increasing intensities of the α_iN_{i+1} NOEs through this span indicate that the helix ends abruptly at Ser^{20} in the dominant conformer, but extends (to as far as Asn^{22}) in minor conformers. Figure 4.44 shows the hydrophobic and polar faces of a representative of both the C-capped (left-hand views) and long helix (right hand views) ensembles. In both forms, the helix is amphiphilic with a well-packed continuous patch of fatty sidechains

including those of Leu^{12}, Phe^{15}, Leu^{16}, Val^{17} and extending to include the $(CH_2)_3$ chain of Arg^{11} and methyl of Thr^9 in many of the structures in the ensembles. The structures also provide a rationale for the anomalous shift of Leu^{12}-Hα. More than 90% of the structures in both ensembles place this methine close to, and in the plane of, the phenyl group; a position that predicts a 0.3 ppm or greater upfield shift based on ring current models. The polar face of the helix displays interactions between the Asn^{14}/His^{18}/Asn^{21} sidechains but there does not appear to be a sufficient number of NOEs to generate a consensus model of the specific H-bonding network through these sidechain functions. There is additional experimental evidence for sidechain structuring; helix formation is accompanied by a large increase in the dispersion of the $CONH_2$ signals. In aqueous buffer the NHs of the seven carboxamide are all within 0.06 ppm of the coil reference values; in the helical state, the signals due to the *E* - NHs (δ_2 & ε_2) are spread over a 0.7 ppm range (Figure 4.45).

Do these structural conclusions have biological relevance? It has been suggested that the amphiphilic helices of amylins, calcitonins and CGRP are an important recognition element for these physiological signaling peptides (Cooper & Tse 1996; Breeze et al., 1991). In the case of amylin, the present study reveals a helical preference over the Ala^5 - Val^{17} span that is present in all media examined. It would appear prudent to include this element in the pharmacophore model. Such a pharmacophore model has provided a basis for rationalizing the bioactivity changes associated with residue mutations (Prickett et al., 1995) and alternative helix nucleation and stabilization strategies can restore activity to analogs showing diminished helicity. The secondary structural differences between pramlintide and hAM in the C-terminal portion provided the structural basis of the different amyloidogenic properties of the two peptides. The resistance of pramlintide to the formation of β-sheet-containing states demonstrated in this study serves as a physicochemical confirmation of the lack of amyloidogenic character in this clinical drug candidate.

It has been suggested that organic cosolvent, such as TFE or HFIP, mimics the membrane lipid-water interface in stabilizing an active conformation at the receptor. In aqueous HFIP media, this study identified the same structural element -- the highly constrained disulfide loop followed by approximate three turns of helix which is presumably the binding site of the hormone, for all three amylins; and failed to define a fixed spatial disposition with the C-terminal portion of the peptide. Both extreme termini of hAM are important for agonist activity: linearization or truncation of the N-

terminal disulfide-bonded loop and deamidation at Tyr^{37}, abolish activity (Cooper et al., 1988). However, in one case, it was reported that amylin (1-23)-NH_2 showed some bioactivity of amylin in vitro (Balasubramaniam et al., 1993). Thus, the C-terminal residues (residue 23-36) seem to be not very important to biological activity, or at least not strictly sequence specific, as it is the least conserved sequence segments in mammalian amylins (Figure 1.1). Calcitonin/amylin hybrids, which have a six-residue deletion in this span, retain significant cross-reactivity at amylin receptors. Pramlintide itself, having three proline substitutions in this span, retains the full biological function of human amylin. The lack of fixed disposition of the C-terminal portion of the peptide, and the flexibility of this region might be important for the extreme N- and C-terminal to 'conmunicate' in the active state. However, the $S^{19}SNN^{22}$ unit which is among the most conserved sequence segments in mammalian amylin, and has high compact turn-forming propensity, may be essential to place the amidated Tyr^{37} close to the N-terminal loop in biological processes.

Table 4.1 The Backbone Proton Chemical Shifts of Human and Rat Amylin in an 88/11/1 vol/vol mixture of d_6-DMSO/CD_3CO_2D/H_2O.

Rat/Human residues	Human		Rat	
	NH	αH	NH	αH
Lys[1]		4.11		4.12
Cys[2]	8.87	4.72	8.89	4.72
Asn[3]	8.68	4.67	8.69	4.68
Thr[4]	7.30	4.37	7.30	4.37
Ala[5]	8.63	4.08	8.64	4.08
Thr[6]	7.48	4.14	7.48	4.15
Cys[7]	7.83	4.28	7.85	4.28
Ala[8]	7.69	4.38	7.70	4.40
Thr[9]	8.00	4.16	8.01	4.18
Gln[10]	7.90	4.25	7.90	4.26
Arg[11]	8.08	4.26	8.09	4.27
Leu[12]	7.89	4.30	7.90	4.31
Ala[13]	7.97	4.20	7.96	4.20
Asn[14]	7.99	4.51	8.00	4.52
Phe[15]	7.95	4.47	7.94	4.47
Leu[16]	8.04	4.32	8.09	4.33
Val[17]	7.63	4.12	7.63	4.18
Arg/His[18]	8.15	4.70	7.98	4.38
Ser[19]	8.01	4.39	7.96	4.38
Ser[20]	8.09	4.37	7.96	4.32
Asn[21]	8.12	4.60	8.14	4.58
Asn[22]	8.06	4.51	8.03	4.54
Leu/Phe[23]	8.10	4.41	7.90	4.31
Gly[24]	8.14	3.73	7.93	3.90
Pro/Ala[25]	7.80	4.37		4.46
Val/Ile[26]	7.86	4.15	7.84	4.13
Leu[27]	7.90	4.39	7.81	4.60
Pro/Ser[28]	7.97	4.38		4.58
Pro/Ser[29]	7.85	4.38		4.47
Thr[30]	7.73	4.28	7.70	4.20
Asn[31]	8.05	4.65	8.05	4.64
Val[32]	7.73	4.14	7.73	4.15
Gly[33]	8.16	3.79	8.19	3.79
Ser[34]	7.87	4.35	7.88	4.36
Asn[35]	8.24	4.64	8.26	4.65
Thr[36]	7.71	4.10	7.72	4.11
Tyr[37]	7.83	4.33	7.85	4.33

Shifts are in ppm.

Table 4.2 The ^{1}H Chemical Shifts of Pramlintide (2.3mM) at pH 4.0 in Aqueous Buffer (11mM Acetate, 9mM Formate, 6mM Trifluoroacetate) at 290K.

residue	HN ($^3J_{HN\alpha}$)	Hα	Hβ	others
Lys[1]	exch	4.025	1.91	Hγ 1.43, 1.41; Hδ 1.71; Hε 3.015; ε-NH 7.60
Cys[2]	9.01 (6.5)	4.725	3.28, 3.17	
Asn[3]	8.98 (8.5)	4.985	2.89	NH's (δ2 7.64; δ1 6.905)
Thr[4]	7.66	4.54	4.55[a]	Hγ 1.275
Ala[5]	8.715 (3.0)	4.215	1.495	
Thr[6]	7.945 (7.0)	4.30	4.23	Hγ 1.20
Cys[7]	8.135	4.585	3.27, 3.115	
Ala[8]	8.21	4.315	1.445	
Thr[9]	8.14	4.31	4.235	Hγ 1.23
Gln[10]	8.29	4.28	2.08, 2.025	Hγ 2.24; NH's (ε2 7.565; ε1 6.90)
Arg[11]	8.345 (6.5)	4.28	1.84, 1.77	Hγ 1.695, 1.60; Hδ 3.185; NHε 7.23
Leu[12]	8.235	4.33	1.70[b], 1.66	Hγ ~1.63; Hδ 0.93, 0.87
Ala[13]	8.265	4.22	1.335	
Asn[14]	8.275	4.59	2.72	NH's (δ2 7.605; δ1 6.955[c])
Phe[15]	8.055 (6.0)	4.575	3.16, 3.075	δ 7.245; ε 7.35; ζ 7.31
Leu[16]	8.08 (6.0)	4.30	1.61, 1.49	Hγ ~1.63; Hδ 0.895, 0.840
Val[17]	7.995 (7.5)	4.00	2.005	Hγ 0.925, 0.855
His[18]	8.625 (7.0)	4.765	3.265, 3.18	aryl-CH (ε1 8.59; δ2 7.295)
Ser[19]	8.465	4.485	3.895, 3.83	
Ser[20]	8.53	4.475	3.895, 3.855	
Asn[21]	8.465	4.665	2.71, 2.69	NH's (δ2 7.605; δ1 6.91[c])
Asn[22]	8.30	4.65	2.71, 2.60	NH's (δ2 7.54; δ1 6.865)
Phe[23]	8.26	4.675	3.23, 3.01	δ 7.26; ε 7.36; ζ 7.31
Gly[24]	8.195	4.11[d], 4.07		
Pro[25]	--	4.445	2.25, 1.88	Hγ 1.995, 1.855[b]; Hδ 3.82
Ile[26]	8.34 (6.5)	4.13	1.815	Hγ 1.53; Hγ^1 1.17; Hδ 0.835; Hγ^2 0.87
Leu[27]	8.455	4.69	1.64-1.58	Hγ 1.65; Hδ 0.92
Pro[28]	--	4.695	2.345, 1.895	Hγ 2.06, 2.01; Hδ 3.875, 3.64
Pro[29]	--	4.505	2.305, 1.955	Hγ 2.035; Hδ 3.82, 3.65
Thr[30]	8.275	4.31	4.205	Hγ 1.21
Asn[31]	8.535	4.755	2.825, 2.765	NH's (δ2 7.65; δ1 6.93)
Val[32]	8.215	4.12	2.12	Hγ 0.94, 0.92
Gly[33]	8.565	3.98		
Ser[34]	8.27	4.445	3.88, 3.85	
Asn[35]	8.575	4.765	2.78, 2.75	NH's (δ2 7.63; δ1 6.955)
Thr[36]	8.11	4.225	4.105	Hγ 1.075
Tyr[37]	8.185	4.55	3.10, 2.935	δ 7.15; ε 6.83
C-term				CONH, 7.505, 7.14

Shifts are in ppm.

[a]) Hα and Hβ of Thr[4] are nearly coincident, the downfield placement of Hβ is tentative.

[b]) Uncertain assignment [c]) These resonances may be switched

[d]) Uncertain assignment, both Hα may be at 4.07 ppm (A COSY cross-peak at 3.53/4.04ppm could be due to Gly[24]-CH_2 in a minor Gly[24]-Pro amide conformer.)

Table 4.3 The ^{1}H Chemical Shifts of Pramlintide (3.6 mM) and Its C-terminal Free Acid (2.1 mM) in 35 Vol% HFIP/10mM DCO_2D and 6.7 mM CF_3CO_2D D_2O Buffer (pH*=3.8) at 295K#. (Shifts are in ppm)

residue	HN	Hα	Hβ	others
Lys[1]	exch	4.10	2.10	Hγ 1.52; Hδ 1.80; Hε 3.10; [a]
Cys[2]	8.935	4.935	3.22, 3.19	
free acid	8.895	4.895	~3.2	
Asn[3]	8.94	5.08	3.005, 2.925	NH's (δ2 7.56; δ1 6.795)
Thr[4]	7.635	4.61[b]	4.61[b]	Hγ 1.405
Ala[5]	8.675	4.26	1.57	
Thr[6]	8.025	4.095	4.255	Hγ 1.335
Cys[7]	7.905	4.445	3.38, 3.265	
Ala[8]	8.22	4.12	1.56	
Thr[9]	8.21	4.07	4.36	Hγ 1.395
Gln[10]	7.935	4.11	2.32, 2.215	Hγ 2.65, 2.445; NH's(ε2 6.93; ε1 6.565)
Arg[11]	8.01	4.14	2.095, 2.00	Hγ 1.95, 1.75; Hδ 3.26; NHε 7.175; [a]
Leu[12]	8.03	4.36	2.025, 1.78	Hγ 1.77; Hδ 1.06, 1.00
Ala[13]	8.73	4.13	1.58	
Asn[14]	8.16	4.51	3.085, 2.915	NH's (δ2 7.55; δ1 6.57)
Phe[15]	8.33	4.44	3.535, 3.395	δ 7.255; ε 7.335; ζ 7.305[c]
Leu[16]	9.155	3.94	2.10, 1.555	Hγ 2.05; Hδ 0.985, 0.970
Val[17]	8.885	3.70	2.105	Hγ 1.07, 0.795
His[18]	7.81	4.41	3.41, 3.23	aryl-CH (ε1 8.57; δ2 7.44)
Ser[19]	8.32	4.245	3.785, 3.65	
Ser[20]	7.813	4.385	4.02, 3.975	
Asn[21]	7.825	4.755	2.815, 2.77	NH's (δ2 7.43; δ1 6.525)
Asn[22]	8.03	4.68	2.755, 2.665	NH's (δ2 7.15; δ1 6.52)
Phe[23]	8.04	4.695	3.275, 3.09	δ 7.28; ε 7.36; ζ 7.37[c]
Gly[24]	7.76	4.145, 4.00		
Pro[25]	--	4.48	2.24, 2.04[d]	Hγ 2.05[d], 2.00; Hδ 3.66, 3.53
minor isomer		4.54		
Ile[26]	7.505	4.20	1.915	Hγ 1.57; Hγ^1 1.205; Hδ 0.91; Hγ^2 0.935
minor isomer	7.67	4.21	1.92	Hγ 1.53; Hγ^1 1.21; Hγ^2 0.93
Leu[27]	7.515	4.795	1.66, 1.565	Hγ 1.70; Hδ 0.95, 0.93
Pro[28]	--	4.63	2.345, 1.985	Hγ 2.15, 2.04; Hδ 3.92, 3.63
Pro[29]	--	4.55	2.285, 2.09	Hγ 2.09, 2.06; Hδ 3.785, 3.61
Thr[30e]	7.715	4.30	4.30	Hγ 1.26
Asn[31]	8.24	4.79	2.915, 2.825	NH's (δ2 7.365; δ1 6.64)
Val[32]	7.855	4.04	2.185	Hγ 1.03, 1.01
Gly[33]	8.305	4.045, 3.985		
Ser[34]	8.055	4.43	4.015, 3.94	
free acid	8.025	4.425		
Asn[35]	8.36	4.805	2.89	NH's (δ2 7.47; δ1 6.74)
Thr[36]	7.98	4.295	4.18	Hγ 1.16
Tyr[37]	7.925	4.59	3.165, 3.015	δ 7.195; ε 6.90; $CONH_2$ (7.295, 6.87)
free acid	7.89	4.63	3.17, 3.03	

Footnotes to Table 4.3

#) The shifts of the free acid and carboxamide forms of pramlintide are essentially the same, except those listed separatly. The limited data for a minor Xaa-Pro isomer is tentative and is derived from the additional Ile^{26} NH line in the ^{15}N-dispersed NOESY of the free acid form. Shifts are in ppm.

[a]) The remaining sidechain NH's are in rapid or intermediate exchange.

[b]) Hα and Hβ of Thr^{4} are essentially shift coincident.

[c]) The para hydrogens (ζ) of the two Phe residues are not assigned with certainty.

[c&d]) For each letter, the resonances may be switched.

[e]) The α and β resonances of Thr^{30} are essentially shift coincident in the major isomer; an additional set of TOCSY peaks was observed in 25% aqeous HFIP -- α, 4.23; H β 4.36; Hγ 1.19 ppm -- which is attributed to a minor cis Xaa-Pro isomer.

Table 4.4 The Amide ^{15}N and ^{1}H Chemical Shifts of Pramlintide in 35% HFIP at Different Temperatures.

	^{15}N					^{1}H				
residue	268K	275K	285K	300K	315K	268K	275K	285K	300K	315K
Lys[1]										
Cys[2]	120.77	120.81	120.85	120.86	120.78	9.02	8.99	8.94	8.85	8.77
Asn[3]	*	121.87	121.86	121.77	121.69	*	9.07	8.99	8.87	8.75
Thr[4]	*	*	108.66	108.98	109.70	*	*	7.74	7.63	7.64
Ala[5]	*	122.79	122.57	122.38	122.30	*	8.83	8.75	8.62	8.50
Thr[6]	*	111.76	111.20	110.30	109.40	*	8.11	8.06	7.98	7.91
Cys[7]	*	119.90	119.63	119.34	118.95	*	7.93	7.88	7.81	7.75
Ala[8]	*	122.95	122.88	122.79	122.71	*	8.30	8.25	8.18	8.11
Thr[9]	*	111.74	111.40	110.91	110.42	*	8.29	8.24	8.16	8.08
Gln[10]	120.16	119.88	119.83	119.64	119.56	7.97	7.97	7.95	7.90	7.86
Arg[11]	118.84	118.81	118.71	118.52	118.34	8.10	8.07	8.03	7.96	7.88
Leu[12]	121.79	121.65	121.46	121.06	120.68	8.10	8.08	8.06	8.01	7.95
Ala[13]	121.08	121.02	120.95	120.76	120.57	8.88	8.83	8.77	8.65	8.51
Asn[14]	112.95	112.93	112.93	112.94	112.86	8.28	8.24	8.19	8.11	8.01
Phe[15]	122.60	122.36	122.07	121.57	120.98	8.41	8.39	8.36	8.29	8.20
Leu[16]	124.12	123.78	123.39	122.80	122.10	9.33	9.28	9.21	9.06	8.87
Val[17]	119.35	119.05	118.71	118.06	117.32	9.05	9.01	8.93	8.79	8.62
His[18]	114.37	114.34	114.35	114.46	114.68	7.88	7.86	7.82	7.77	7.72
Ser[19]	114.98	114.78	114.65	114.46	114.28	8.51	8.45	8.36	8.24	8.13
Ser[20]	116.30	116.09	115.97	115.68	115.50	7.88	7.86	7.84	7.80	7.78
Asn[21]	118.54	118.53	118.51	118.52	118.54	7.74	7.77	7.81	7.85	7.86
Asn[22]	116.91	116.99	117.09	117.10	117.12	8.05	8.05	8.04	8.01	7.98
Phe[23]	118.23	118.35	118.51	118.62	118.75	8.17	8.13	8.08	8.00	7.92
Gly[24]	108.28	108.22	108.15	108.06	107.88	7.86	7.83	7.78	7.71	7.64
Pro[25]	–	–	–	–	–	–	–	–	–	–
Ile[26]	118.34	118.30	118.21	118.12	117.93	7.62	7.58	7.53	7.46	7.39
Leu[27]	125.14	124.92	124.81	124.62	124.43	7.65	7.61	7.55	7.46	7.39
Pro[28]	–	–	–	–	–	–	–	–	–	–
Pro[29]	–	–	–	–	–	–	–	–	–	–
Thr[30]	110.21	110.26	110.29	110.19	110.11	7.80	7.77	7.74	7.69	7.63
Asn[31]	119.25	119.14	119.12	119.03	118.95	8.31	8.30	8.26	8.20	8.15
Val[32]	120.43	119.90	119.71	119.50	119.14	7.97	7.94	7.88	7.82	7.75
Gly[33]	110.31	110.21	110.08	109.89	109.71	8.46	8.41	8.35	8.25	8.15
Ser[34]	114.68	114.60	114.45	114.26	114.07	8.13	8.10	8.06	7.99	7.92
Asn[35]	119.55	119.50	119.53	119.44	119.36	8.42	8.41	8.39	8.34	8.28
Thr[36]	112.95	112.88	112.82	112.73	112.55	8.06	8.04	8.00	7.95	7.88
Tyr[37]	122.40	122.28	122.17	121.87	121.69	8.01	7.97	7.93	7.85	7.77

* The ^{1}H-^{15}N cross peaks were too broad to be detected.
Shifts are in ppm.

Table 4.5 ^{13}C Chemical Shifts for Leucines in Pramlintide in 35% HFIP at 295K.

seq.#	sec. str.	C=O	C_α	C_β	C_γ	C_δ [(a)]
12	α helix	178.4	57.6	41.1	26.1	23.2, 21.5
16	α helix	180.7	58.1	40.8	25.8	23.5, (20.7)
coil ref[(b)]	Leu-Xaa	177.6	55.1			
	Leu-Pro	175.6	53.1			
27	extended	173.8	51.7	41.4	26.0	(23.5), 21.4

shifts are in ppm.

(a) The parenthetic values are not securely established.

(b) The random coil ^{13}C chemical shifts for Leu were published by Wishart et al., (1995a). Downfield shifts from these values are expected for the carbonyl and alpha carbons of leucine residues that are in α helical conformation. Upfield shifts from these values are expected for the carbonyl and alpha carbons of leucine residues that are in β sheet or extended conformation.

Table 4.6 NH Temperature Gradient and Chemical Shift Deviation at 285K of Pramlintide in in Buffer and in 35 vol% HFIP.

	Buffer		35 vol% HFIP	
residue	Δδ/ΔT	NH-CSD	Δδ/ΔT	NH-CSD
Lys^{1}				
Cys^{2}	-6.84	0.12	-5.60	0.14
Asn^{3}	-7.76	0.31	-7.93	0.39
Thr^{4}	-2.17	-0.62	0.57	-0.53
Ala^{5}	-9.06	0.44	-8.20	0.54
Thr^{6}	-7.42	-0.28	-5.00	-0.09
Cys^{7}	-5.57	-0.29	-1.90	-0.40
Ala^{8}	-6.27	-0.08	-4.90	0.05
Thr^{9}	-8.00	-0.09	-5.40	0.09
Gln^{10}	-4.65	-0.10	-2.73	-0.32
Arg^{11}	-7.33	-0.02	-4.90	-0.21
Leu^{12}	-6.00	-0.06	-3.60	-0.11
Ala^{13}	-5.49	-0.06	-8.53	0.56
Asn^{14}	-5.23	-0.24	-5.93	-0.21
Phe^{15}	-5.93	-0.29	-5.30	-0.11
Leu^{16}	-5.93	-0.19	-11.33	1.04
Val^{17}	-6.99	-0.19	-10.43	0.85
His^{18}	-7.23	0.16	-3.63	-0.52
Ser^{19}	-7.45	0.09	-7.93	0.11
Ser^{20}	-7.08	0.16	-1.93	-0.42
Asn^{21}	-5.57	-0.04	2.47	-0.59
Asn^{22}	-5.57	-0.20	-1.93	-0.36
Phe^{23}	-6.72	-0.09	-5.23	-0.17
Gly^{24}	-6.51	-0.18	-4.70	-0.49
Pro^{25}				
Ile^{26}	-9.93	0.19	-4.80	-0.54
Leu^{27}	-11.57	0.22	-5.50	-0.62
Pro^{28}				
Pro^{29}				
Thr^{30}	-8.82	0.06	-3.63	-0.41
Asn^{31}	-7.45	0.04	-3.97	-0.13
Val^{32}	-8.29	0.05	-4.60	-0.20
Gly^{33}	-7.69	0.21	-6.77	0.07
Ser^{34}	-6.63	-0.08	-4.70	-0.20
Asn^{35}	-6.48	0.09	-3.73	-0.01
Thr^{36}	-5.93	-0.14	-4.07	-0.14
Tyr^{37}	-8.00	0.40	-5.33	0.23

(Δδ/ΔT) are in ppb/°C; CSDs are in ppm.

Table 4.7 Statistical Evaluation of Pramlintide Structures Ensembles
(-- generated from 404 NOE distances and 5H-bond)

	# of structures	Dev. from ideality		Eimpr	Evdw
		bonds (Å)	angles (°)	(kcal/mol)	
"long helix" ensemble	17	0.004±0.0004	2.08±0.010	37.1±1.3	-126±7.4
"C-capped helix" ensemble	17	0.004±0.0002	2.08±0.005	37.2±0.6	-124±3.6

NOE-distance Violation Statistics

restraint type (#)	"long helix" ensemble versus tight (loose) constraints		"C-capped helix" ensemble versus tight (loose) constraints	
All (404)				
E_{noe} (kcal/mol)	54.2±6.2	(17.3±3.2)	53.2±6.9	(16.7±2.7)
rms dev. (Å)	0.139±0.007	(0.084±0.006)	0.138±0.007	(0.084±0.006)
%-viol. >0.2Å	14.2±1.0	(4.2±1.0)	14.0±1.2	(4.0±0.9)
Category I (107)				
E_{noe} (kcal/mol)	5.0±2.7	(0.49±0.83)	5.2±2.4	(0.49±0.84)
rms dev. (Å)	0.037±0.010	(0.007±0.010)	0.38±0.008	(0.007±0.010)
%-viol. >0.2Å	0.9±0.8	(0.3±0.4)	1.0±0.8	(0.2±0.4)
Category II (154)				
E_{noe} (kcal/mol)	13.4±2.5	(2.55±1.33)	13.8±4.1	(2.02±1.45)
rms dev. (Å)	0.087±0.008	(0.037±0.010)	0.090±0.013	(0.032±0.012)
%-viol. >0.2Å	9.8±1.7	(1.7±0.6)	10.6±1.8	(2.0±1.5)
Low-bounds-only (75)				
E_{noe} (kcal/mol)	0.66±0.70	(0.03±0.08)	1.16±1.11	(0.0)
Inter-residue (no methyls included) (258)				
E_{noe} (kcal/mol)	37.3±5.2	(14.0±2.7)	35.6±5.2	(12.9±1.8)
rms dev. (Å)	0.148±0.010	(0.097±0.008)	0.144±0.008	(0.095±0.005)
%-viol. >0.2Å	12.5±1.2	(4.6±0.9)	11.8±1.5	(3.9±0.7)
Inter-residue (no methyls included), residues 2-19 only (142)				
E_{noe} (kcal/mol)	12.6±1.4	(5.82±0.6)	12.3±1.5	(5.27±0.5)
rms dev. (Å)	0.129±0.005	(0.095±0.005)	0.126±0.006	(0.09±0.006)
%-viol. >0.2Å	6.4±1.0	(1.9±0.8)	6.1±1.4	(1.5±0.6)
Inter-residue (no methyls included), remaining residues (116)				
E_{noe} (kcal/mol)	24.7±4.8	(8.42±2.6)	23.1±4.5	(7.60±1.8)
rms dev. (Å)	0.167±0.017	(0.099±0.016)	0.164±0.014	(0.099±0.011)
%-viol. >0.2Å	20.0±2.6	(8.3±1.8)	18.0±2.4	(6.8±1.4)

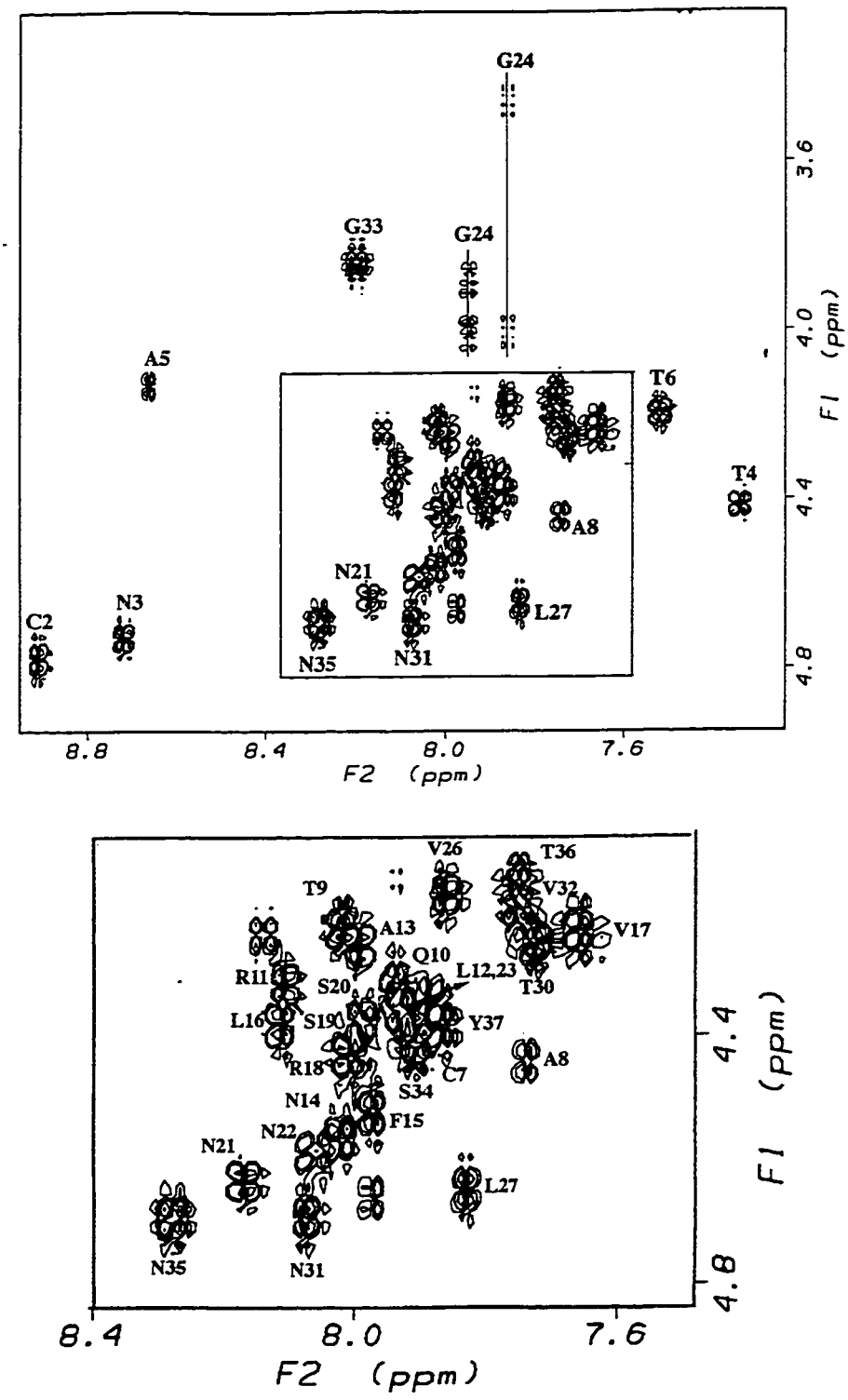

Figure 4.1 αN Region of the COSY Spectrum of rAM in an 88/11/1 vol/vol mixture of d_6-DMSO/CD_3CO_2D/H_2O. In Figure 4.1-4.6, this medium is designated as 'DMSO'.
(The lower panel is the enlarged crowded region of upper Panel. The spectrum was recorded at 310K)

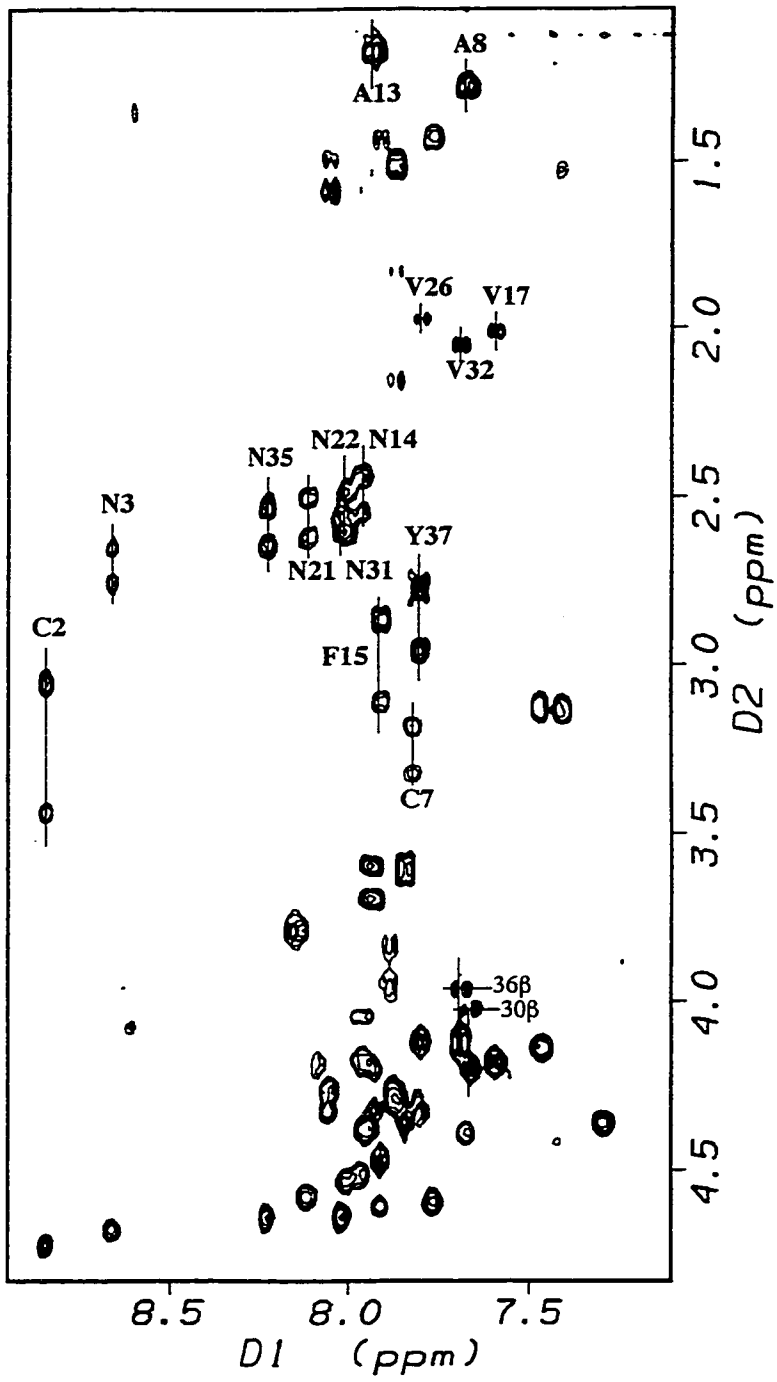

Figure 4.2 NH Portion of the TOCSY Spectrum of rAM in 'DMSO' (310K).

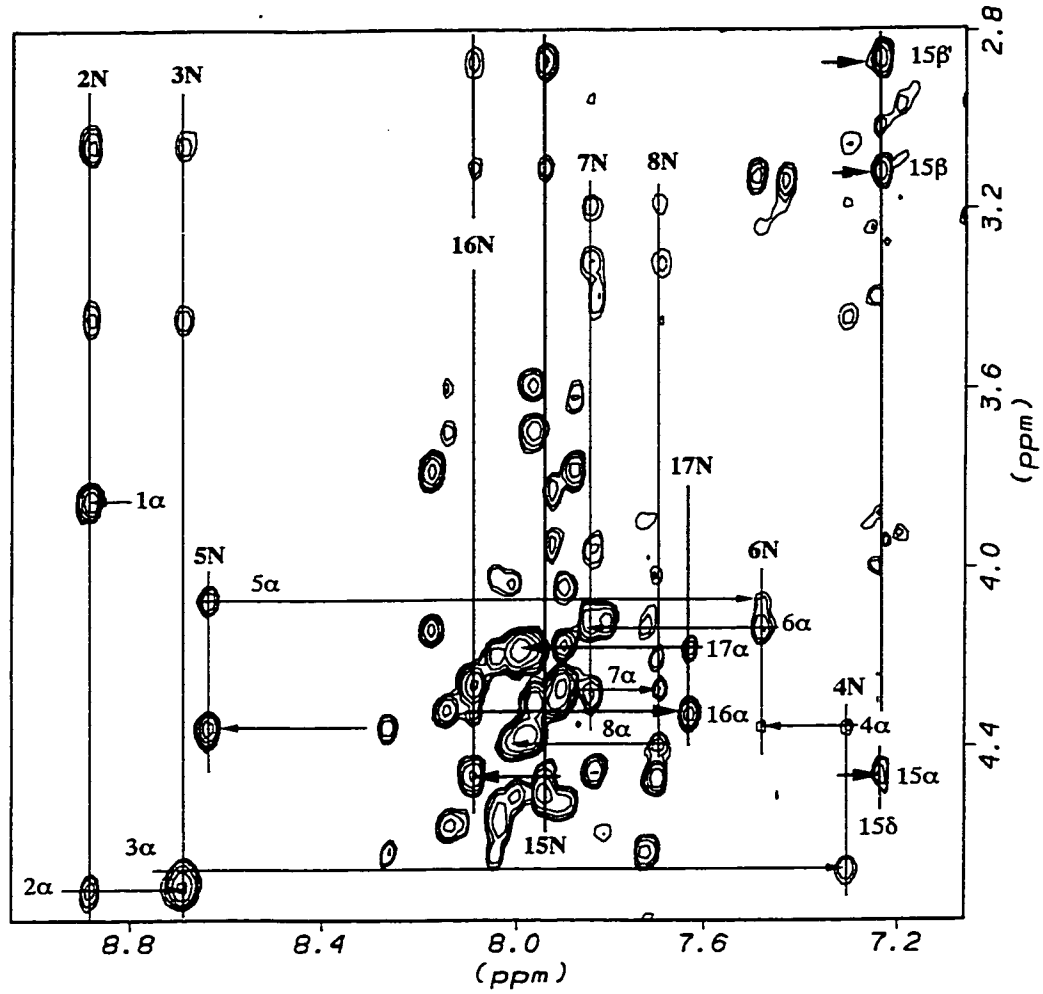

Figure 4.3 αN Region of the NOESY Spectrum of rAM in 'DMSO' (305K).

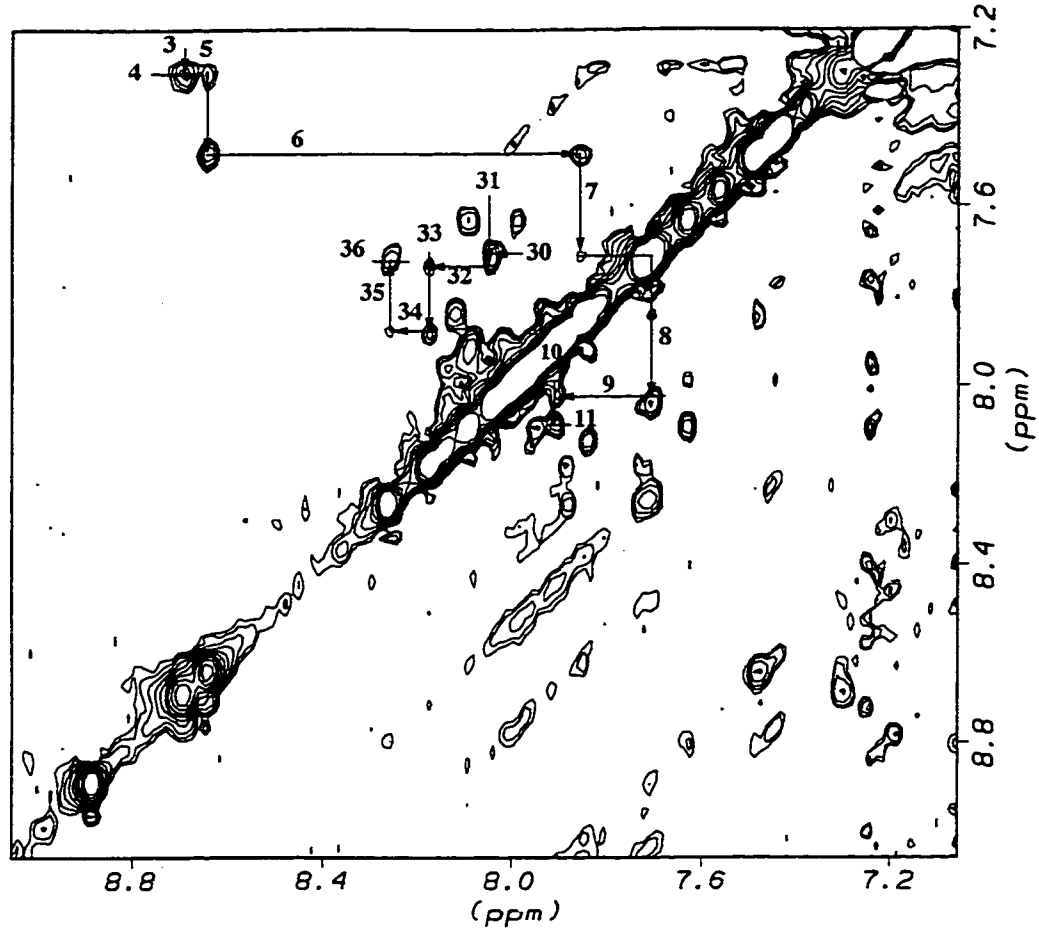

Figure 4.4 NN Region of the NOESY Spectrum of rAM in 'DMSO' (305K).

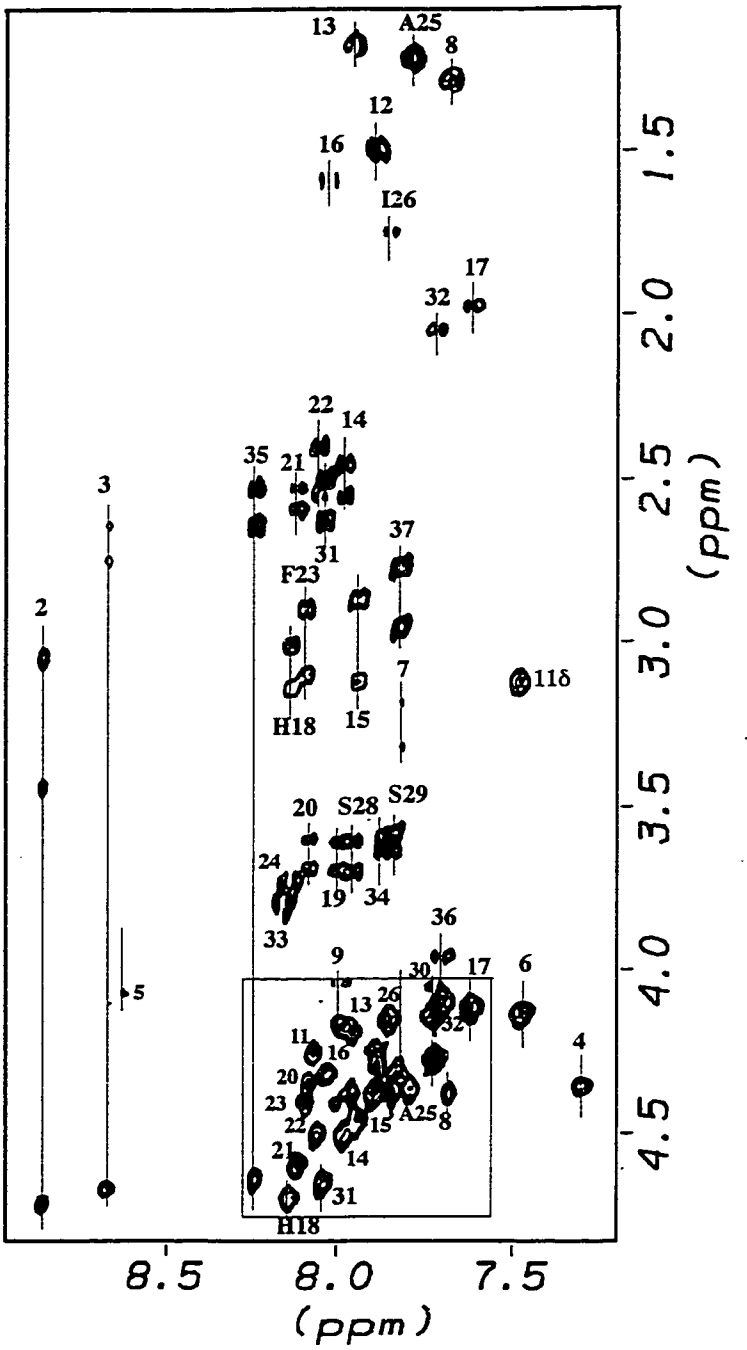

Figure 4.5 NH Portion of the TOCSY Spectrum of hAM in 'DMSO' (308K).

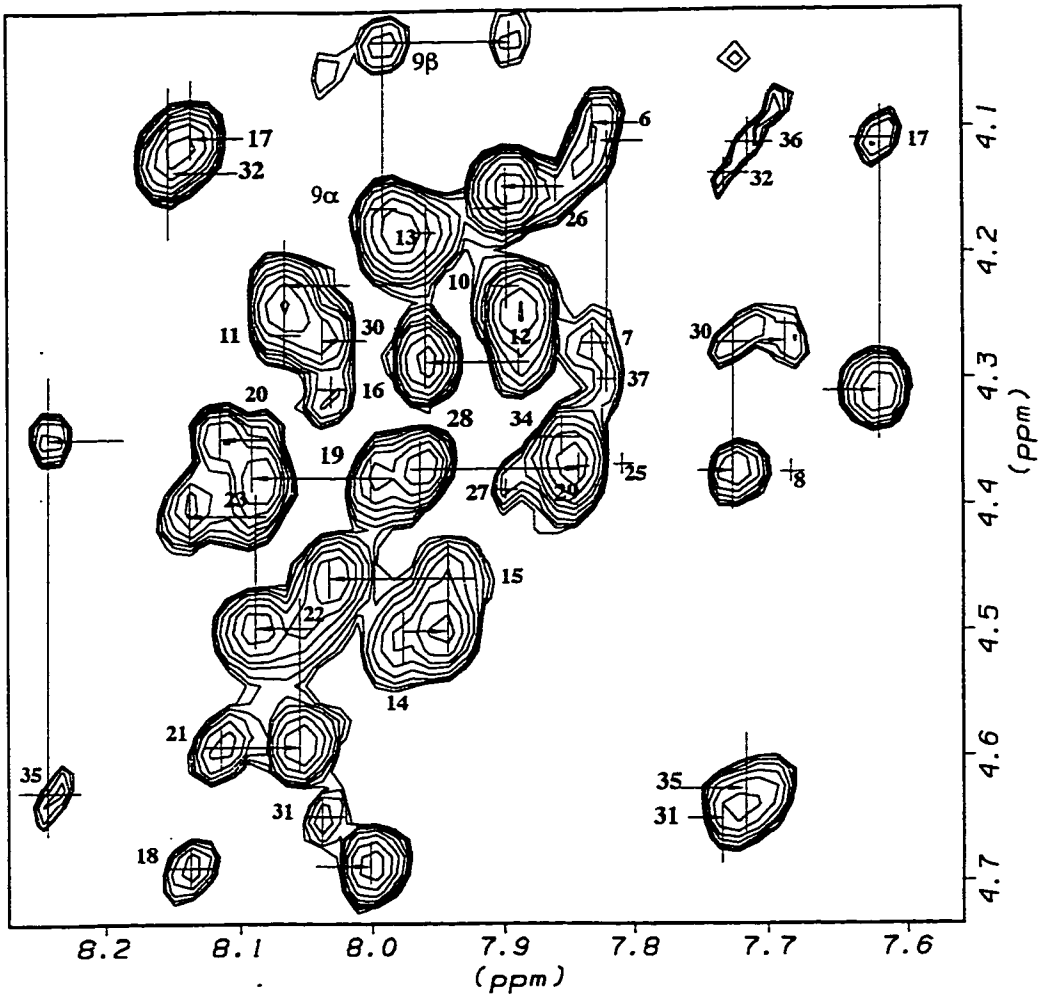

Figure 4.6 Portion of NOESY Spectrum of hAM in 'DMSO' (308K).

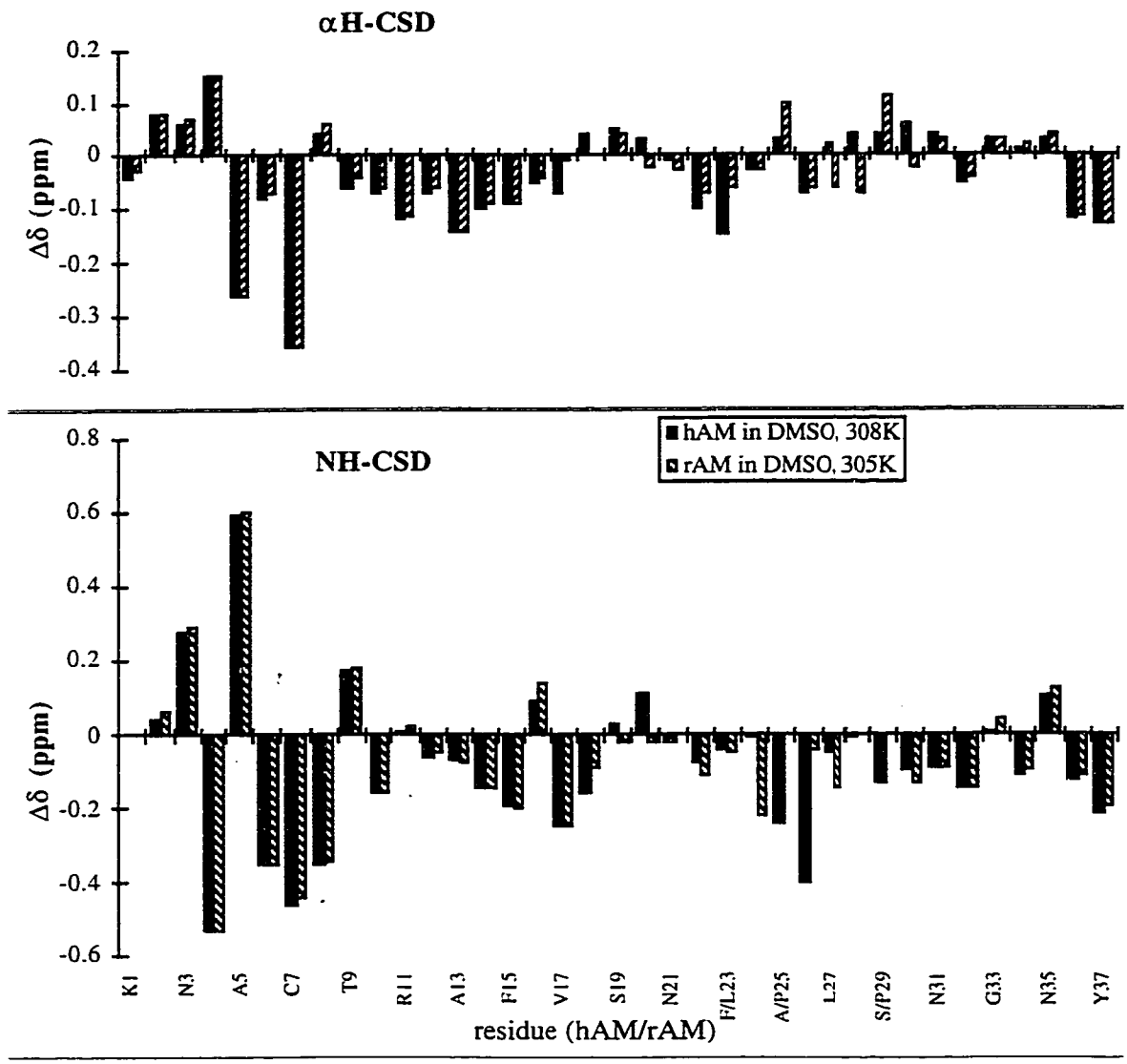

Figure 4.7 αH and NH Chemical Shift Deviation (CSD) Comparisons of Human and Rat Amylin in an 88/11/1 vol/vol mixture of d_6-DMSO/CD_3CO_2D/H_2O.

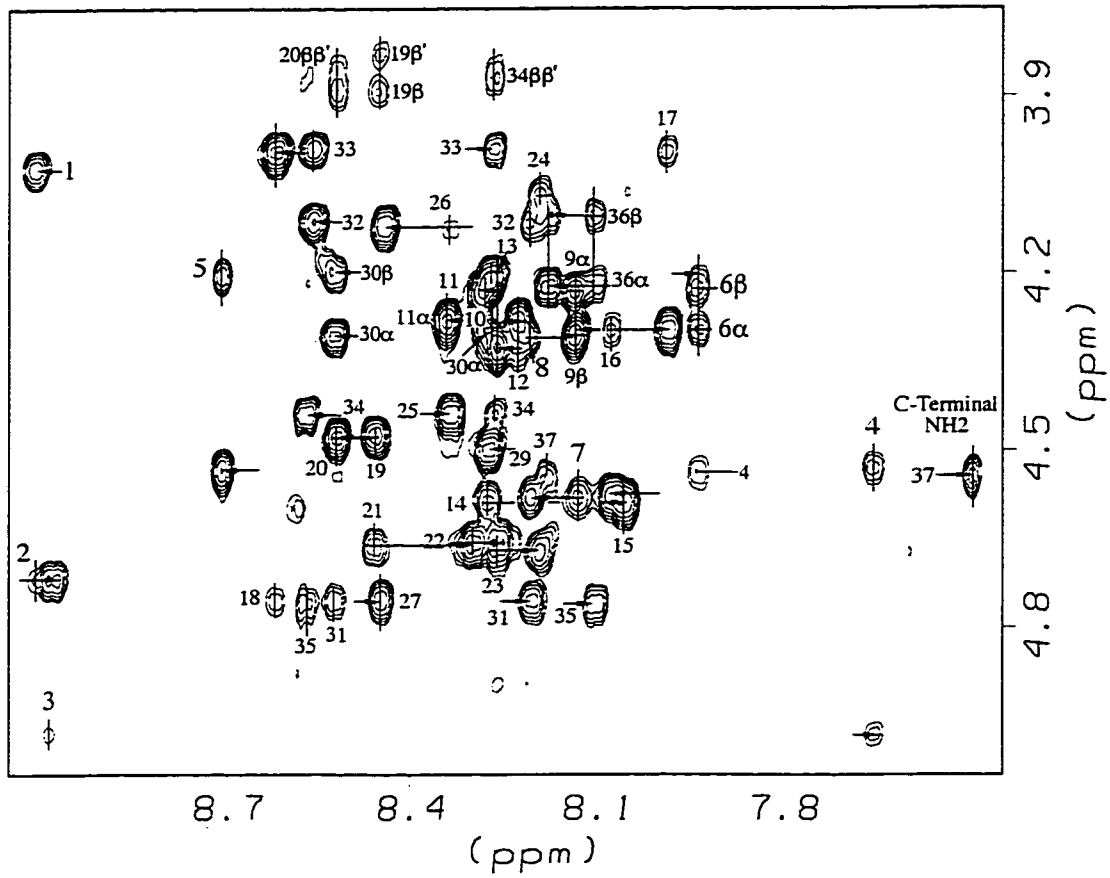

Figure 4.8 ROESY Spectrum of Pramlintide in Aqueous Buffer (αN Region).

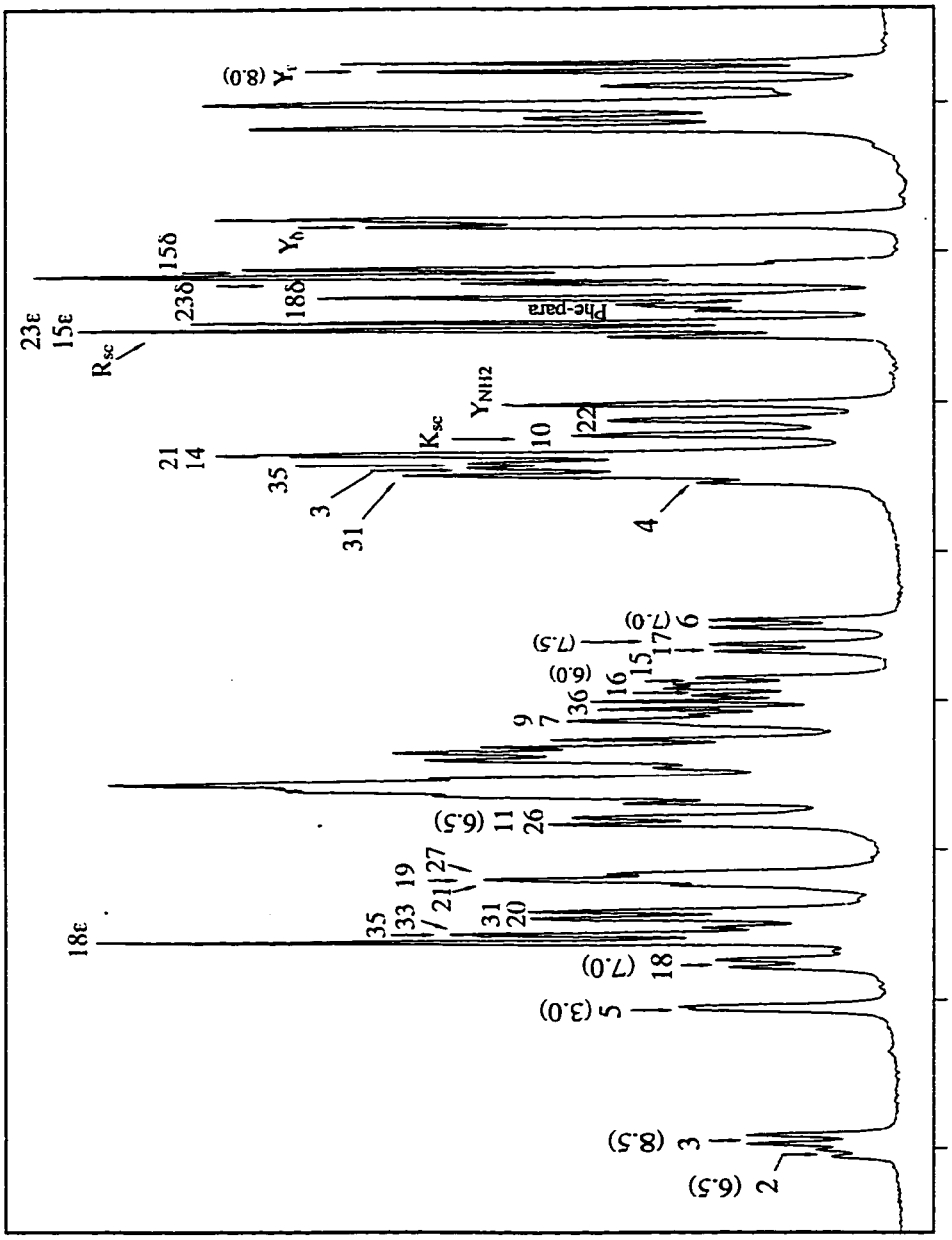

Figure 4.9a 1D Spectrum of Pramlintide in Aqueous Buffer (NH Region).

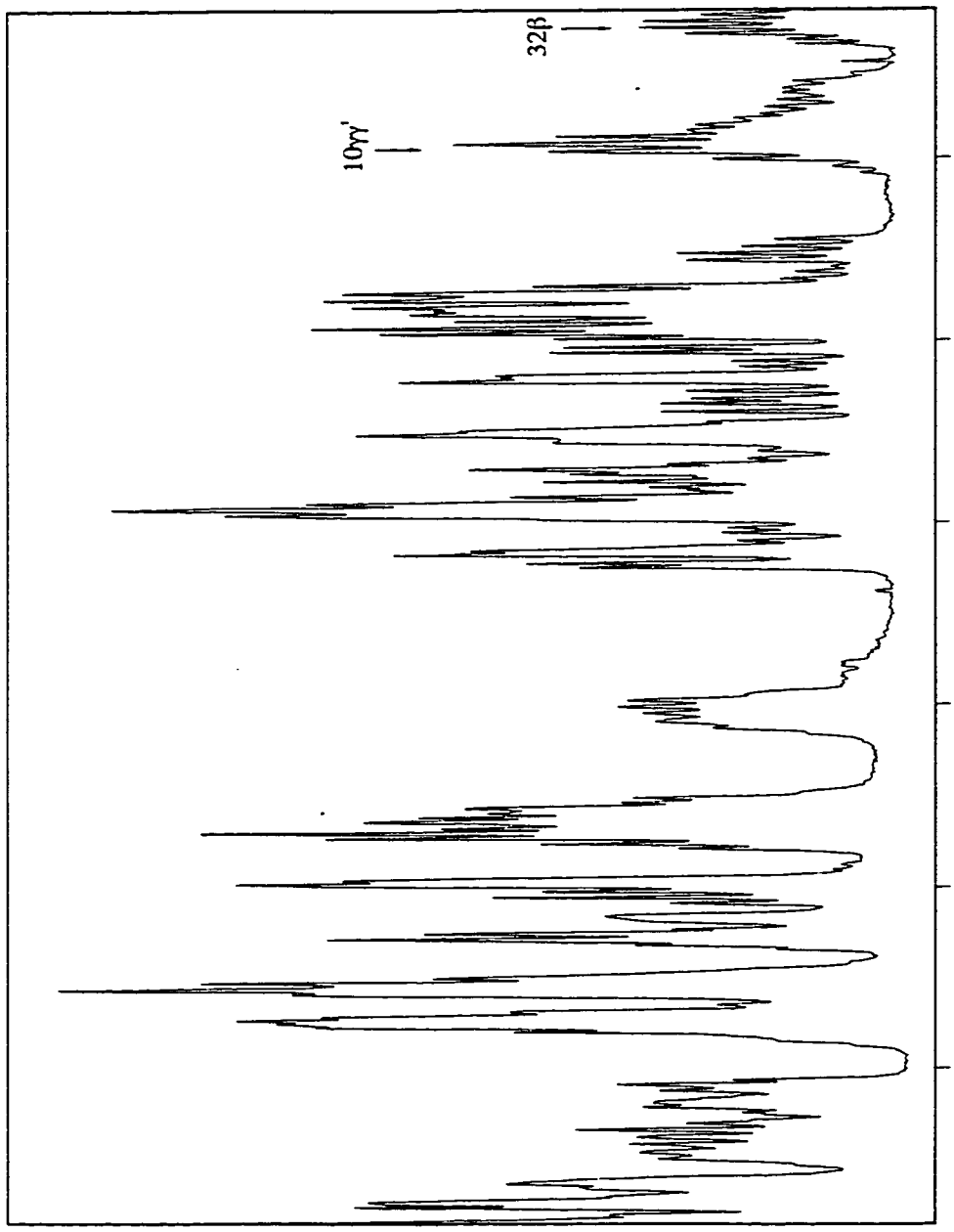

Figure 4.9b 1D Spectrum of Pramlintide in Aqueous Buffer (αβ Region).

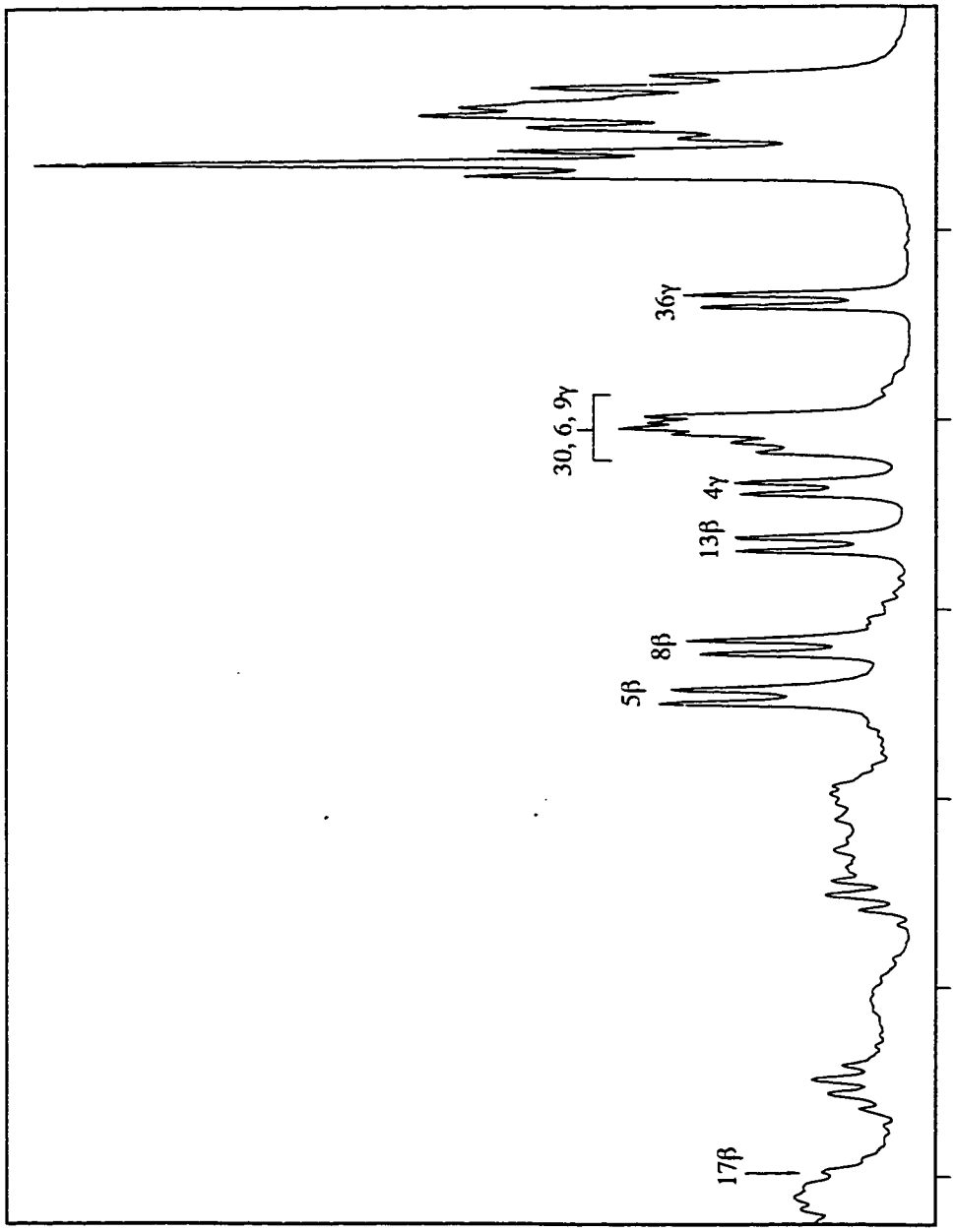

Figure 4.9c 1D Spectrum of Pramlintide in Aqueous Buffer (β, γ, Methly Region).

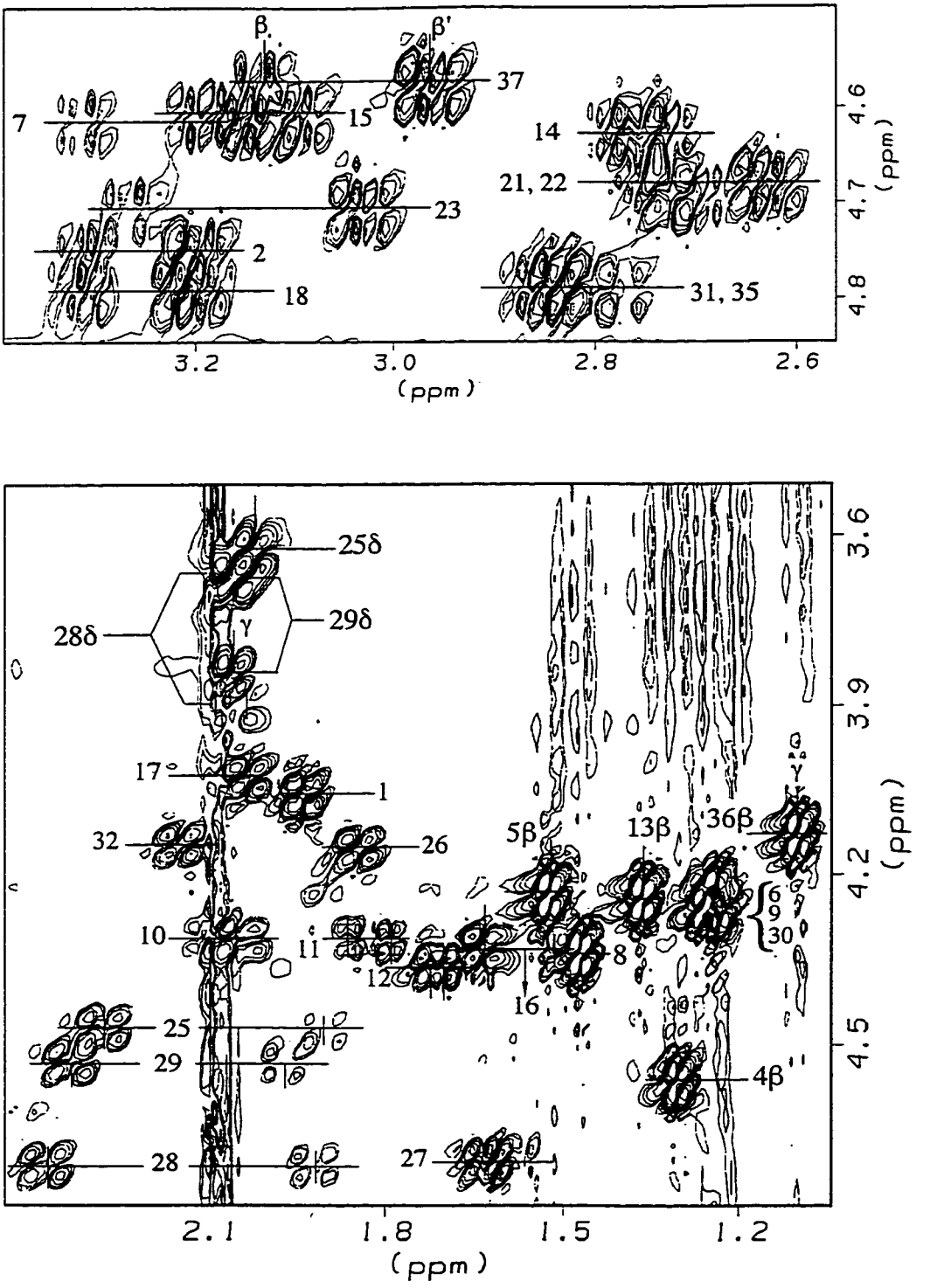

Figure 4.10 Portions of COSY Spectrum of Pramlintide in Aqueous D_2O Buffer.

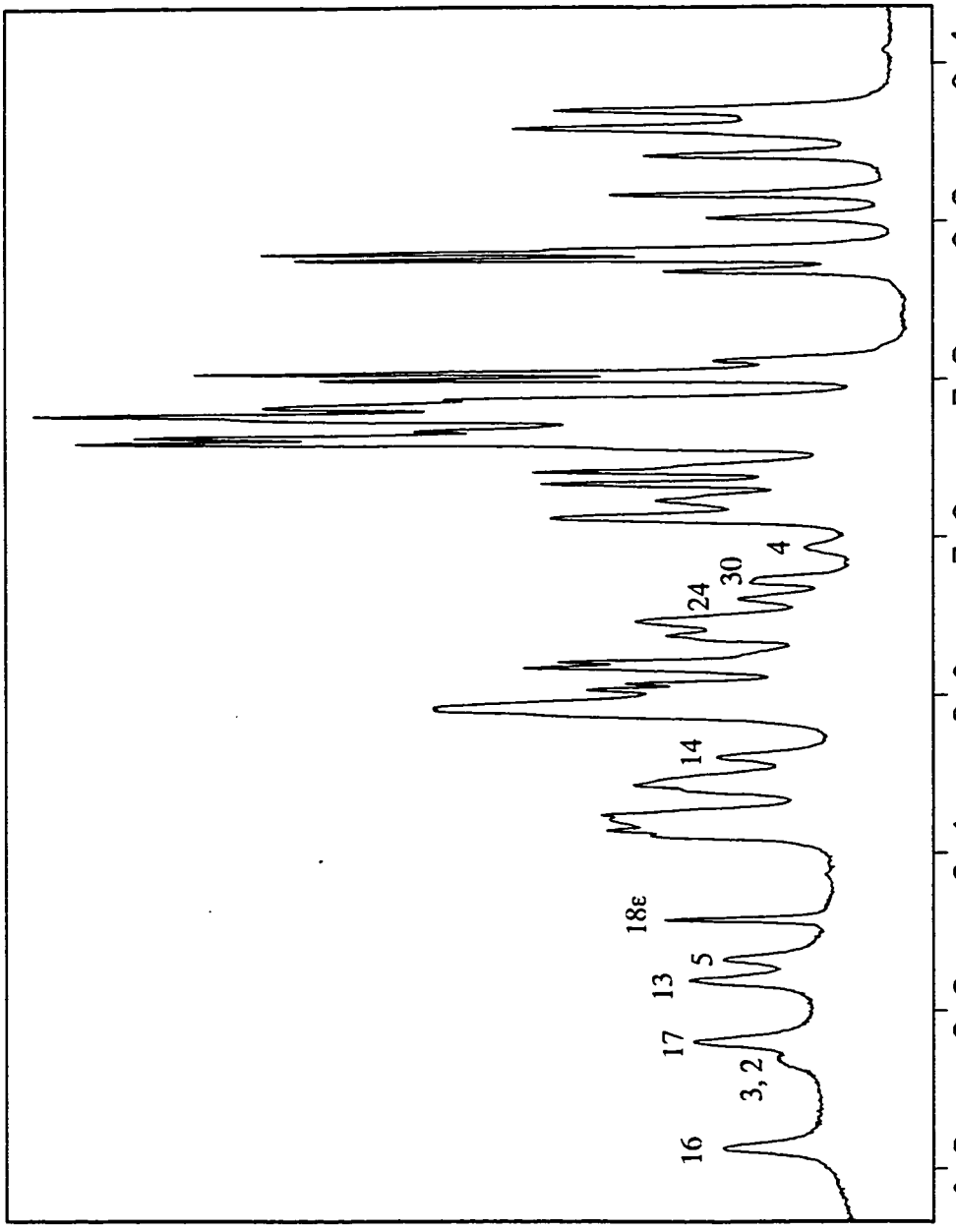

Figure 4.11 1D Spectrum of Pramlintide in Aqueous 35 vol% HFIP (NH Region).

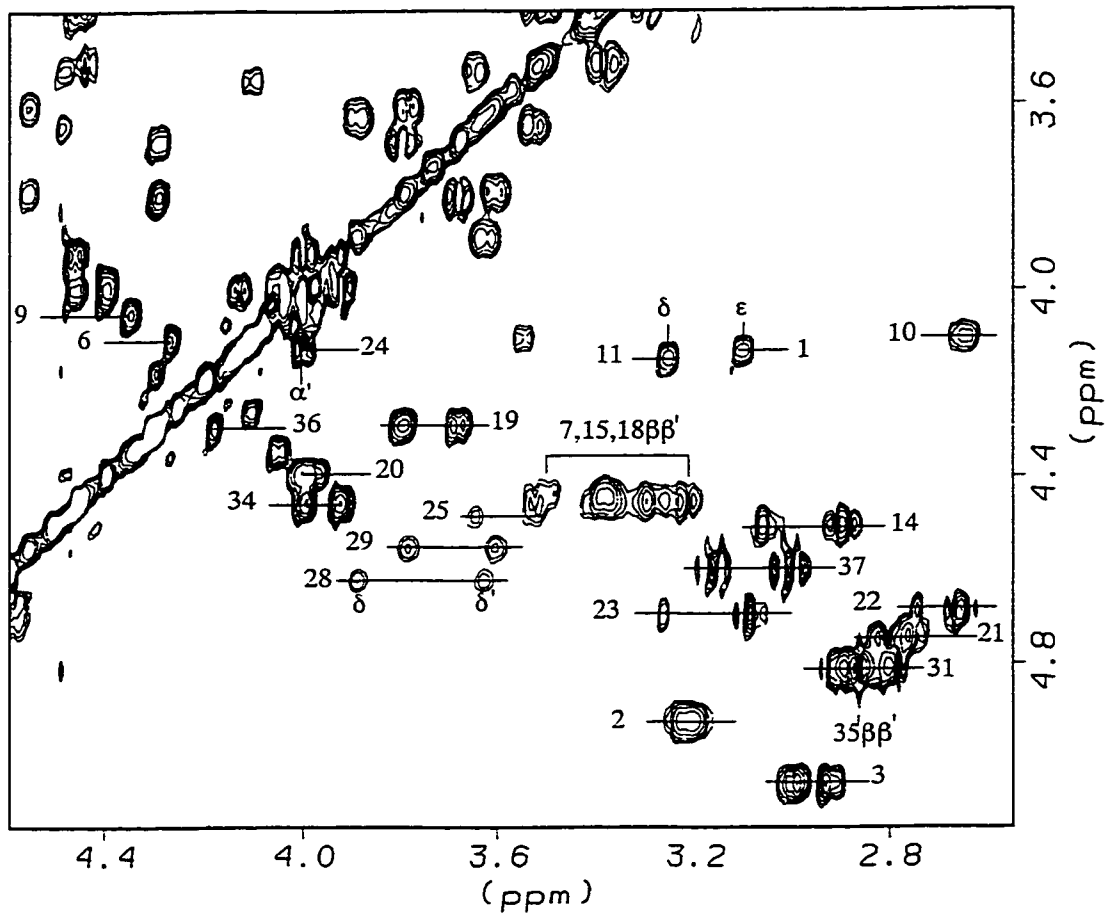

Figure 4.12 TOCSY Correlations for Pramlintide in Aqueous HFIP (α/β Region).
(25% HFIP, 305K)

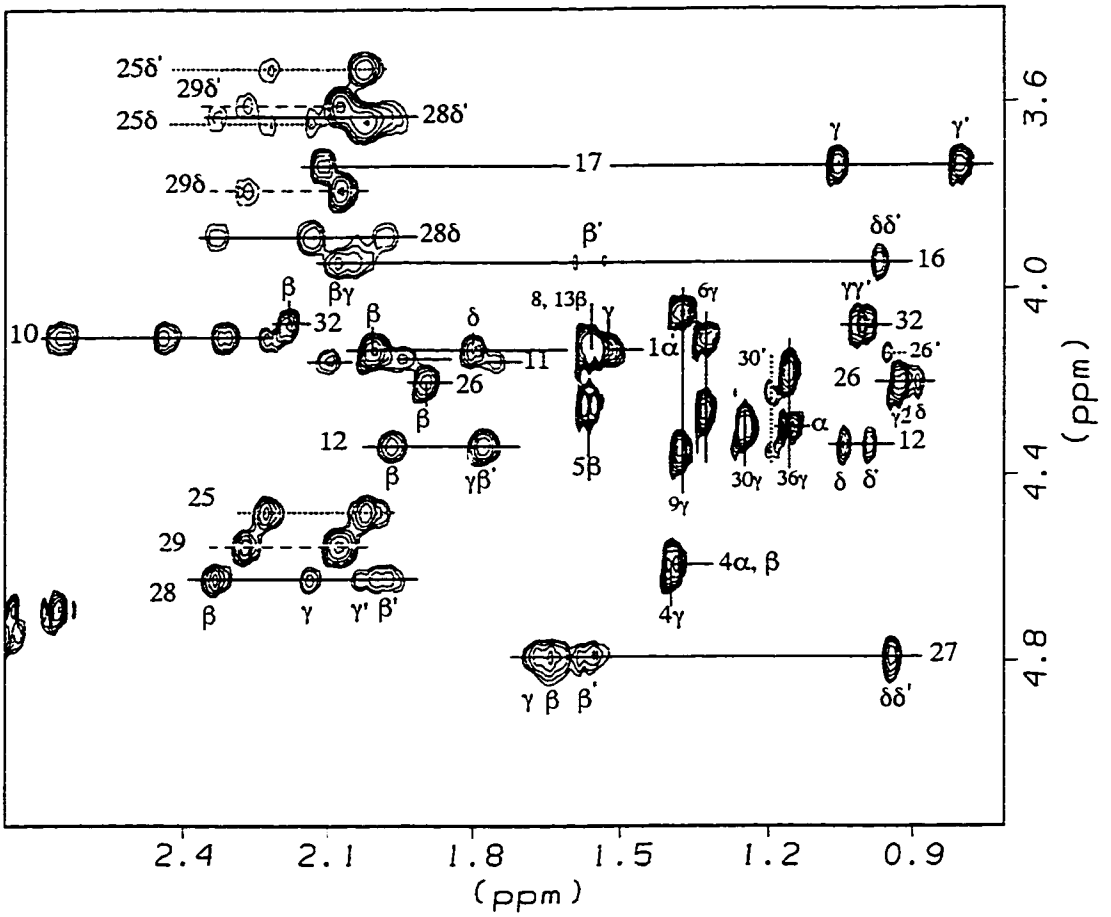

Figure 4.13 TOCSY Correlations for Pramlintide in Aqueous HFIP (α/γδ Region).
(25% HFIP, 305K)

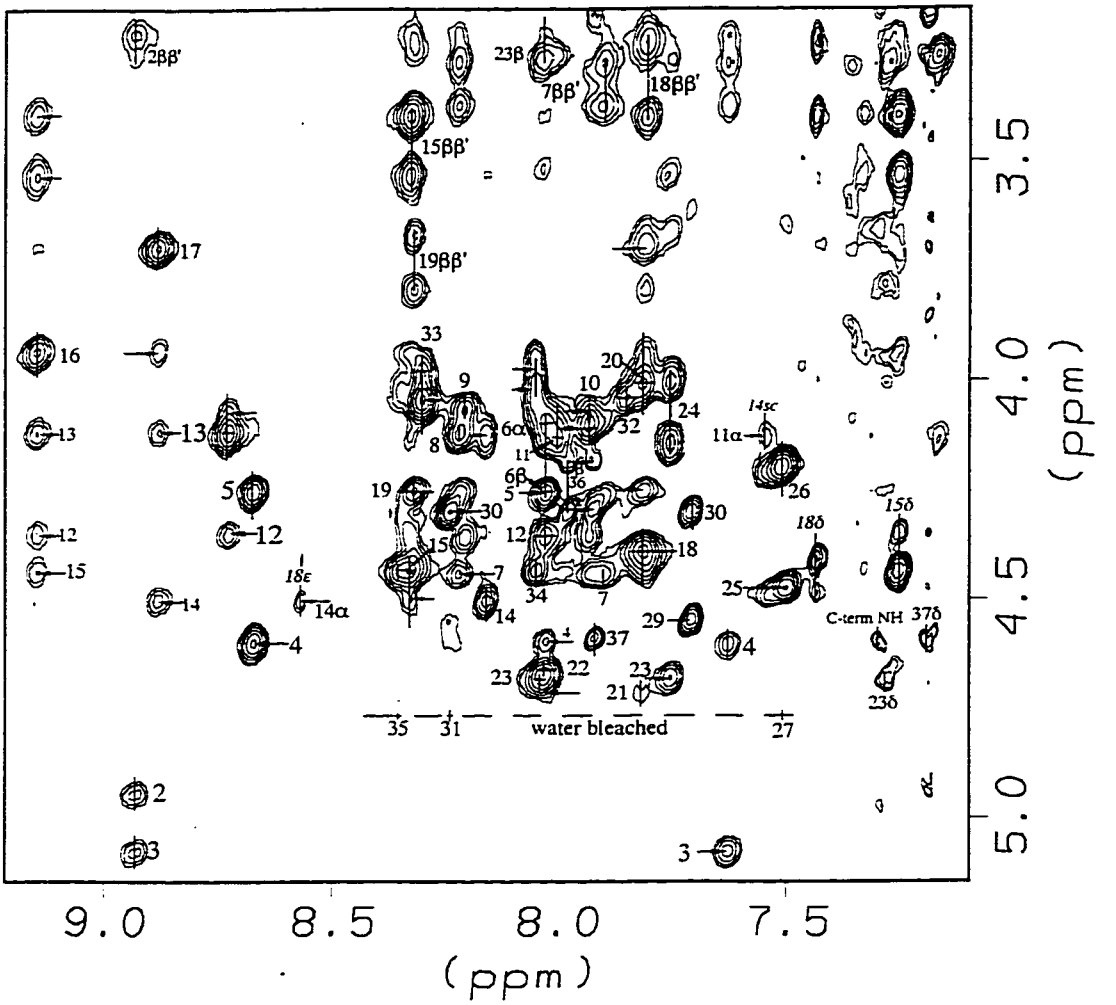

Figure 4.14 αN Region of the NOESY Spectrum of Pramlintide in 35 vol% HFIP Aqueous Media.

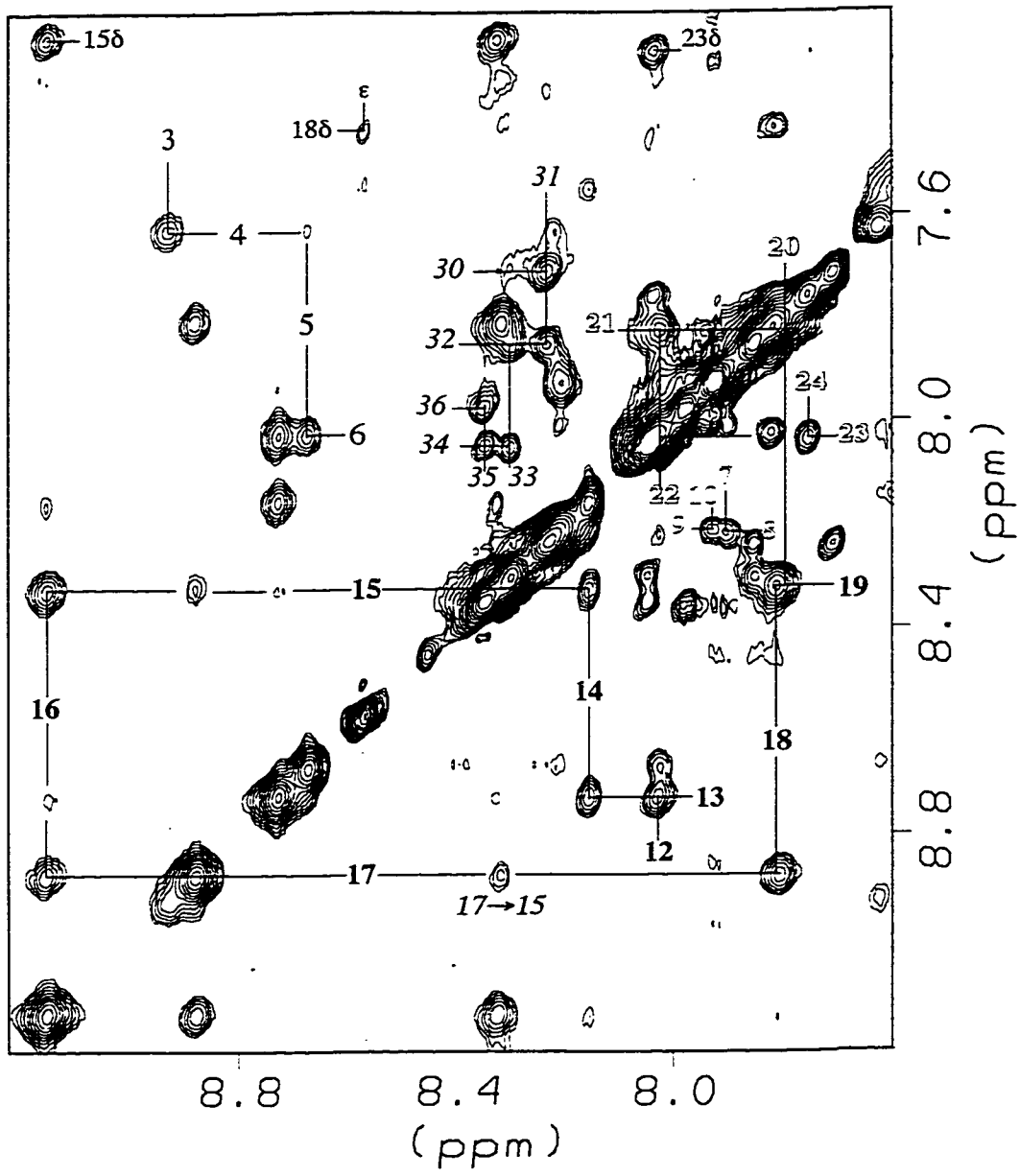

Figure 4.15 NOESY Spectrum of Pramlintide (NN Region).

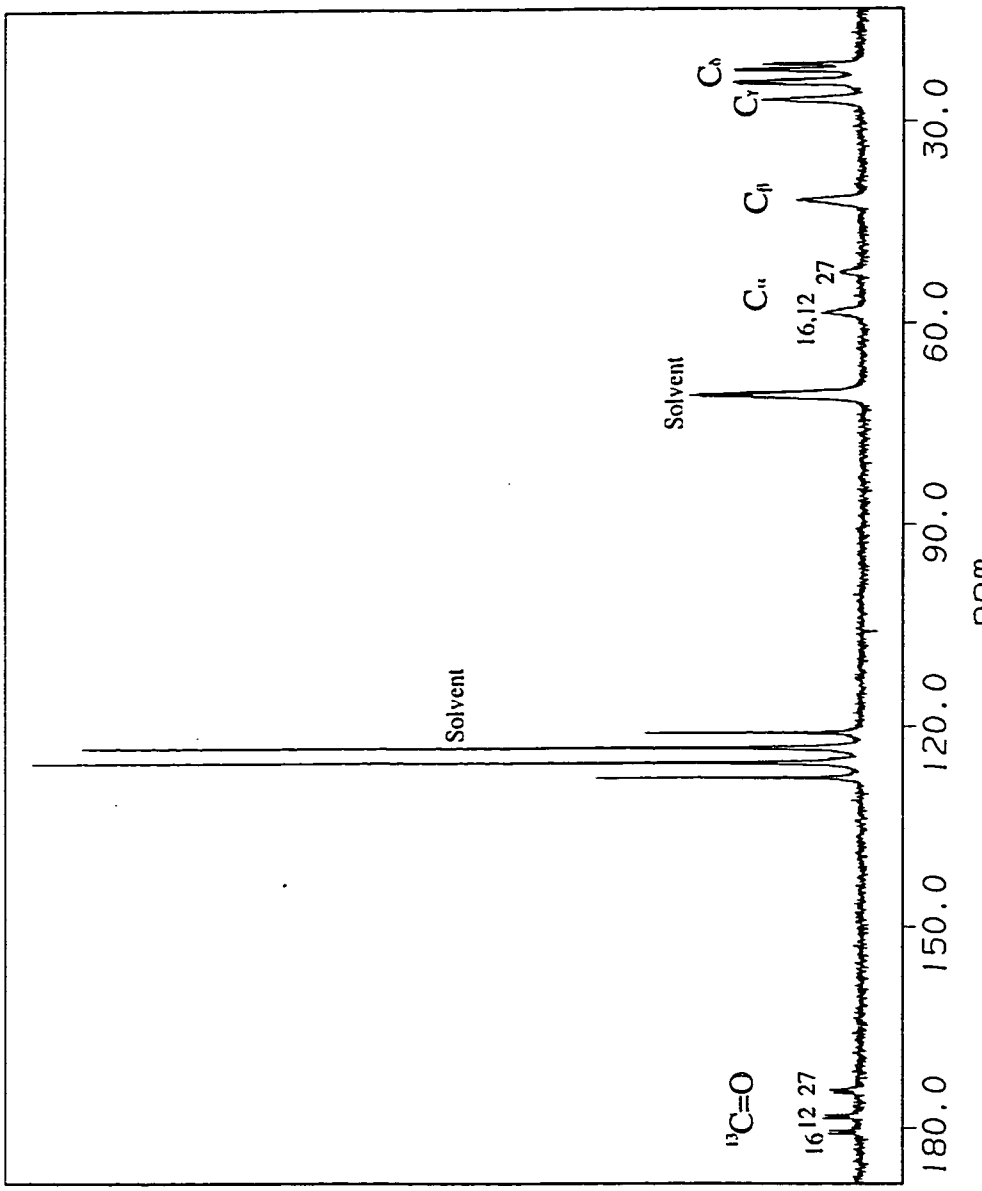

Figure 4.16 ^{13}C 1D Spectrum of ^{13}C-Leu-pramlintide in 35 vol% HFIP Aqueous Medi

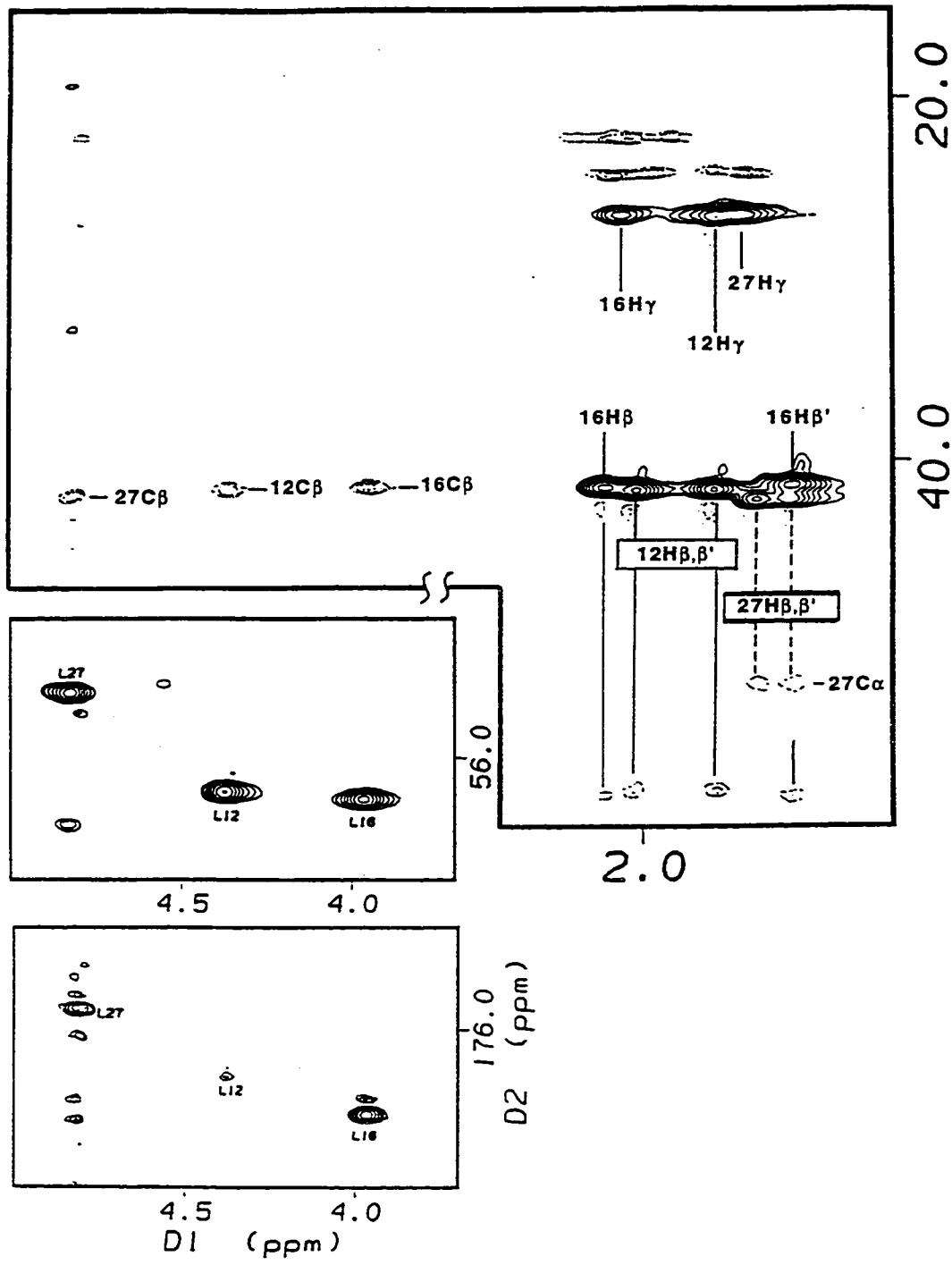

Figure 4.17 ^{13}C-Leu RELAY-HSQC Correlation for Pramlintide in 35% HFIP.
(The cross peaks from directly attached ^{1}H-^{13}C are positive; while the relay peaks are negative)

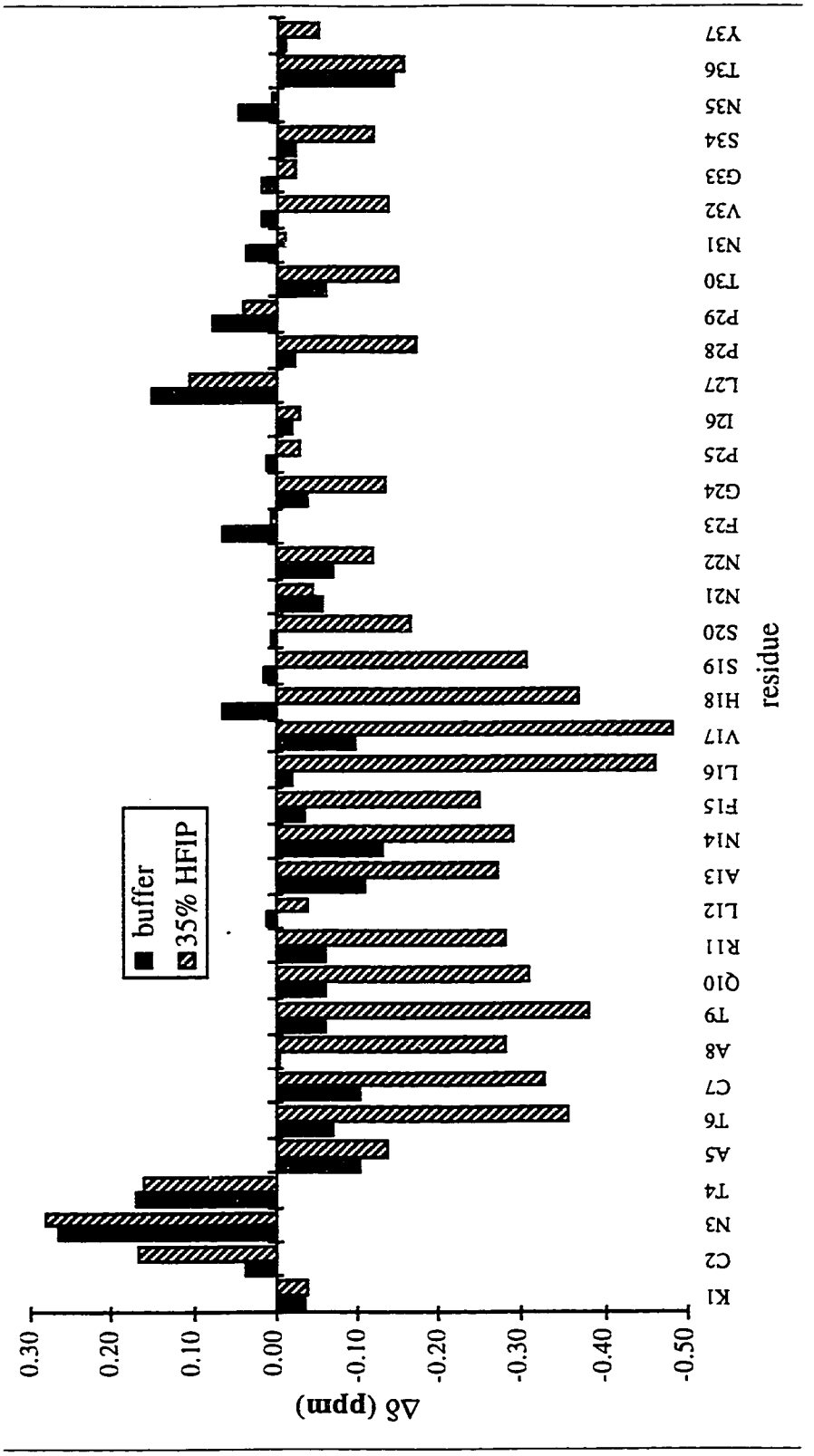

Figure 4.18 An αH-CSD Comparison for Pramlintide in Aqueous Buffer and 35% Aqueous HFIP.

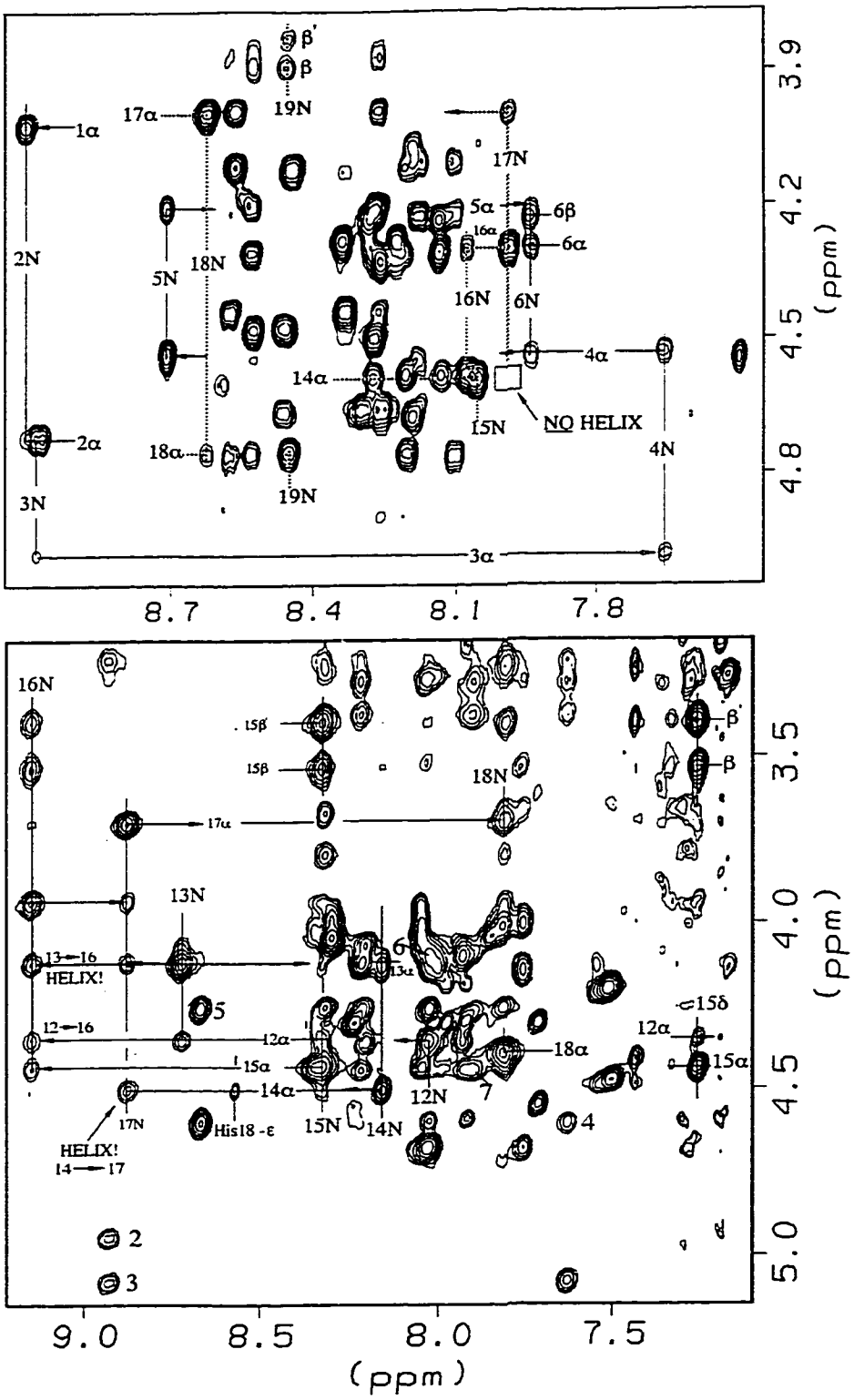

Figure 4.19 Comparison of Dipolar Coupling (Through-Space) Correlations for Pramlintide with (Lower Panel) and without (Upper Panel) HFIP Addition.

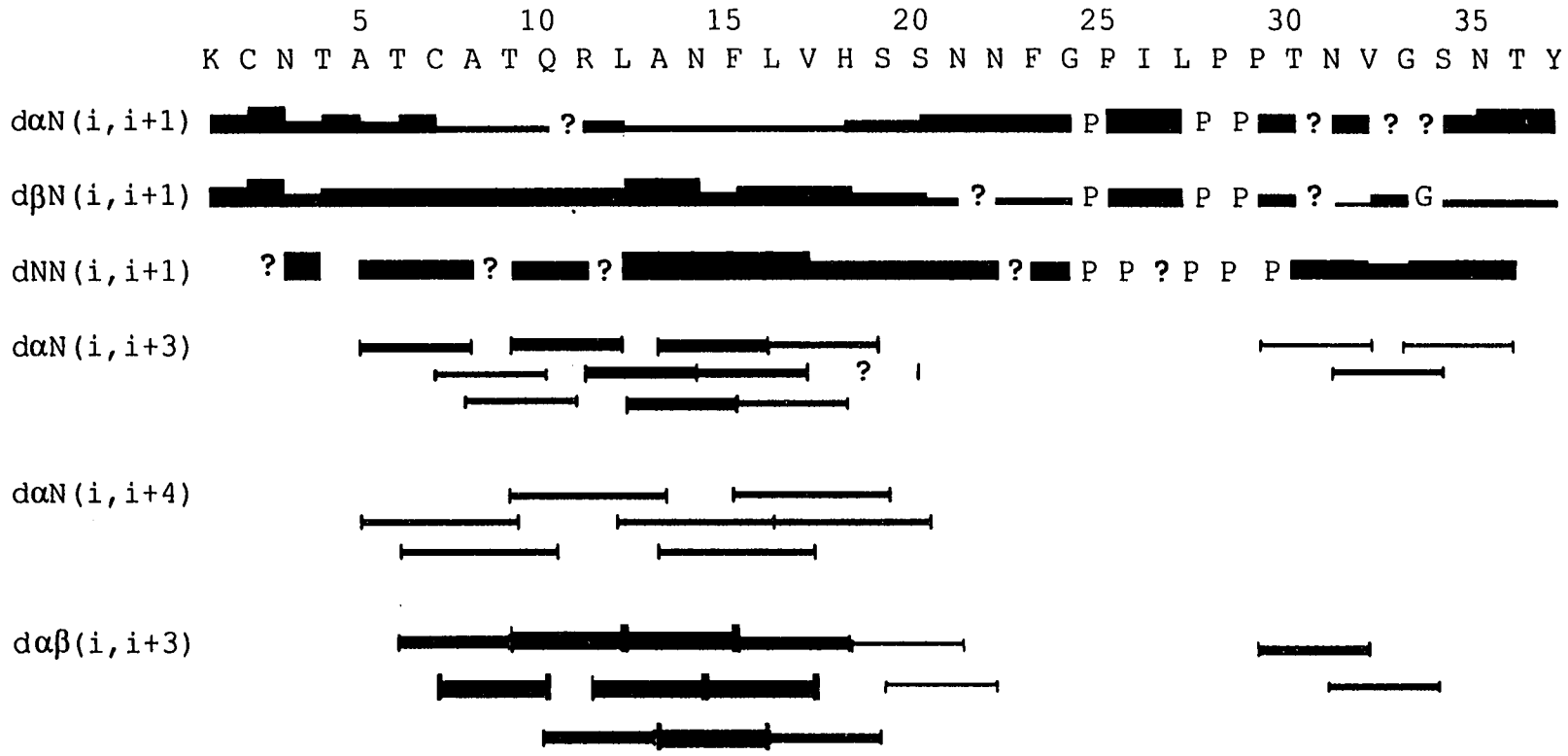

Figure 4.20 Summary of Key NOEs for Pramlintide in 25-35% HFIP.
(The thickness of the bars corresponding to the intensity of NOE peaks. Symbol: ?:ambiguity due to shift coincidence; P: no peak due to the presence of a proline; G: no peak because the presence of a glycine; blank: no detectable peak)

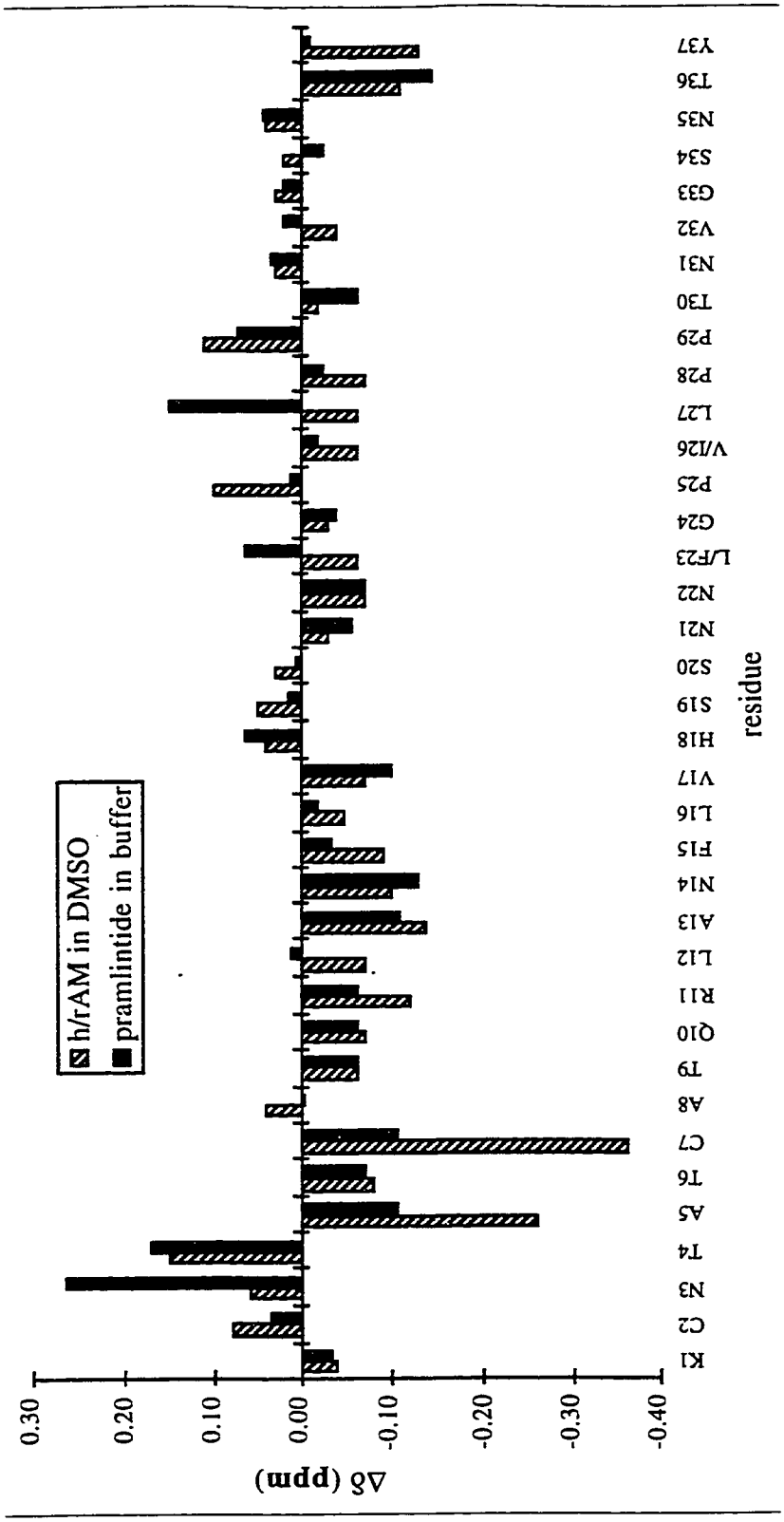

Figure 4.21 An αH-CSD Comparison of Pramlintide in Aqueous Buffer and Amylins in DMSO.

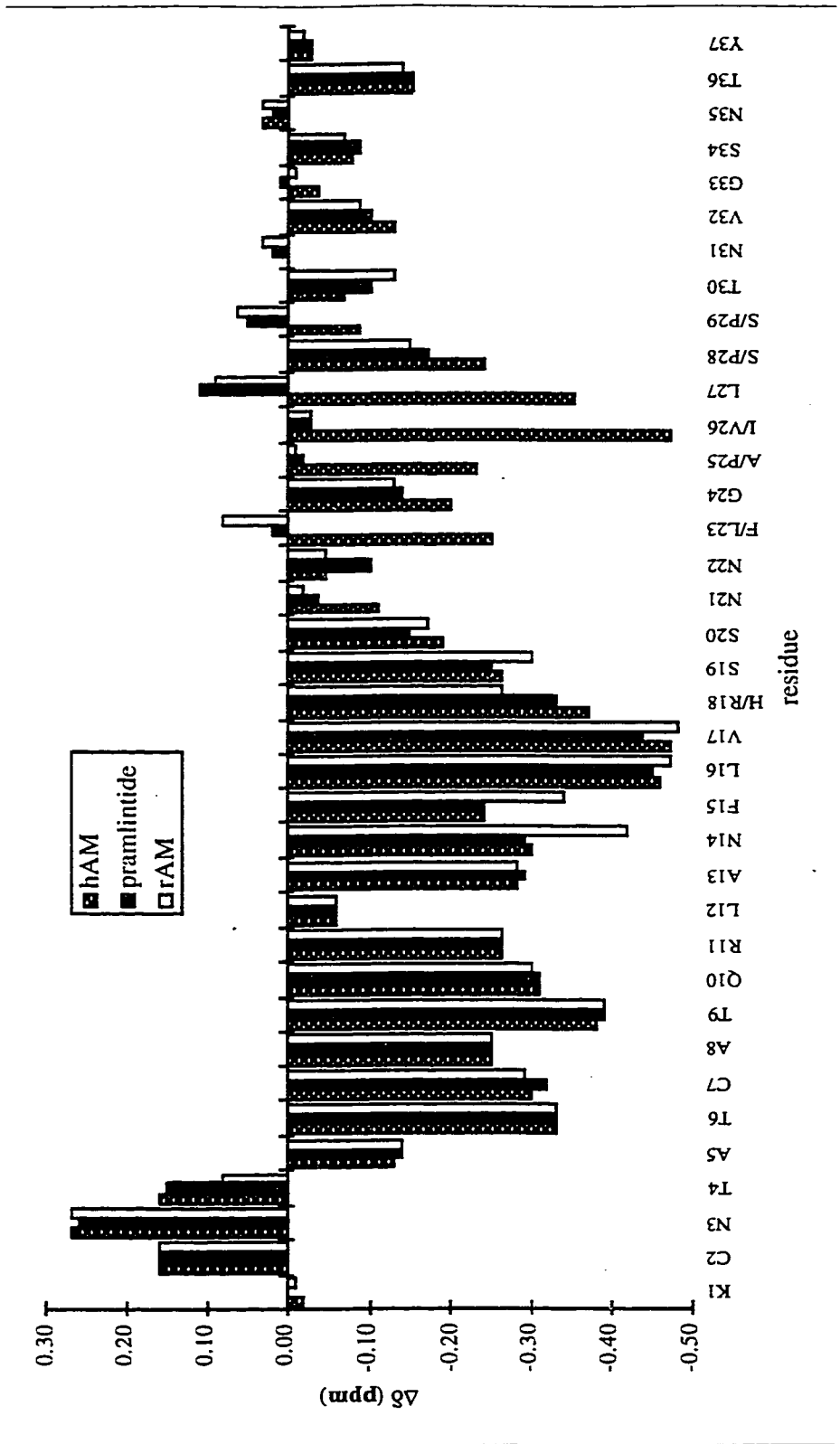

Figure 4.22 The αH-CSD Histograms of hAM, Pramlintide and rAM in 25% Aqueous HFIP.

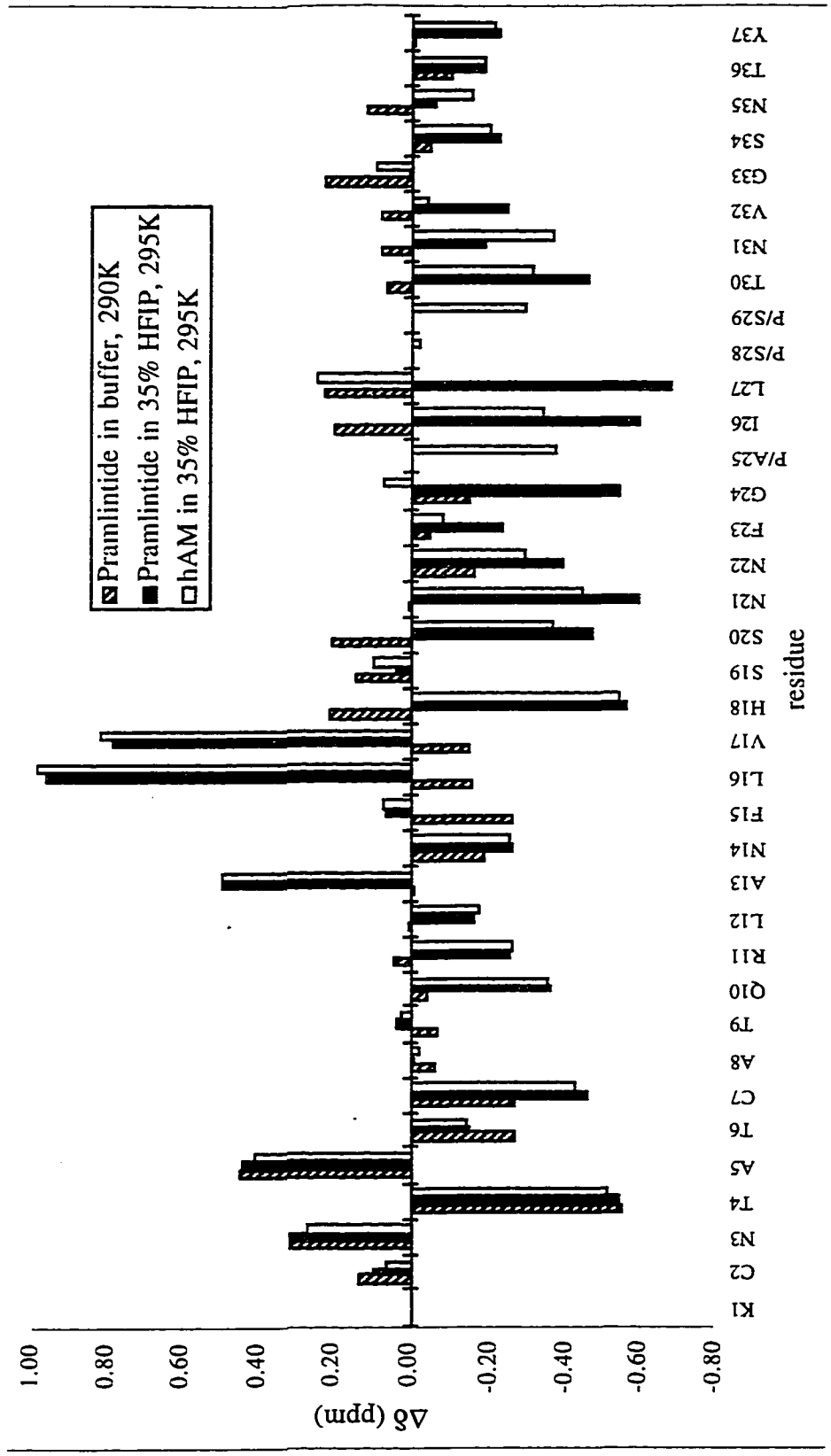

Figure 4.23 An NH-CSD Comparison for Pramlintide (in Aqueous Buffer and 35% HFIP) and hAM (in 35% HFIP).

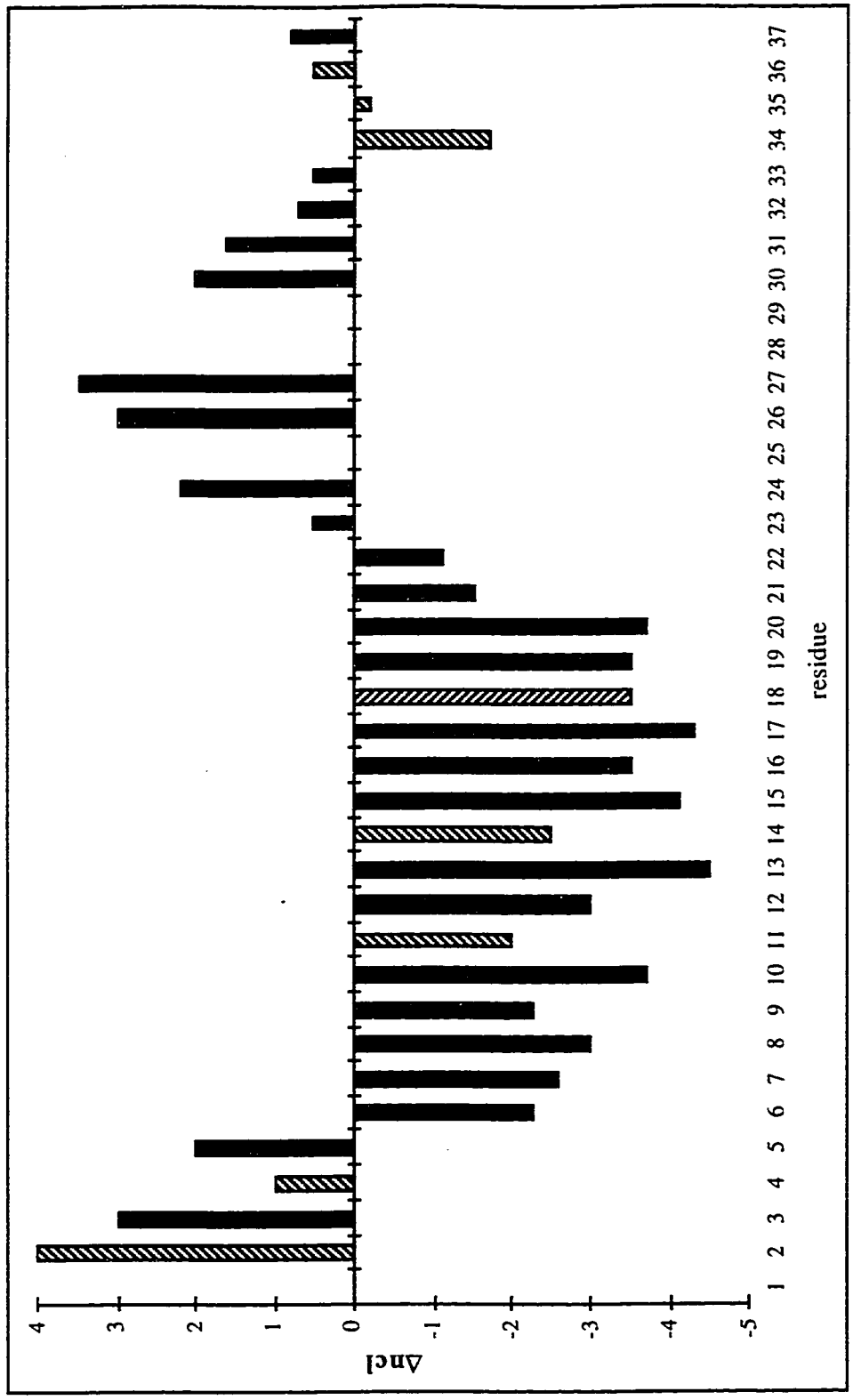

Figure 4.24 Inter/Intra-Residue Hα/HN NOE Ratios for Pramlintide in 35% HFIP

The plot corresponds to the difference in contour levels (Δncl, inter less intra) at a contour level multiplier of 1.4 using the method given in Lee et al. [FEBS Lett. 355, 140 (1994)]. Values of -3.5 to -4.5 represent full population of helical psi values at that locus: the less well-determined values are shown by hatched, rather than filled, bars.

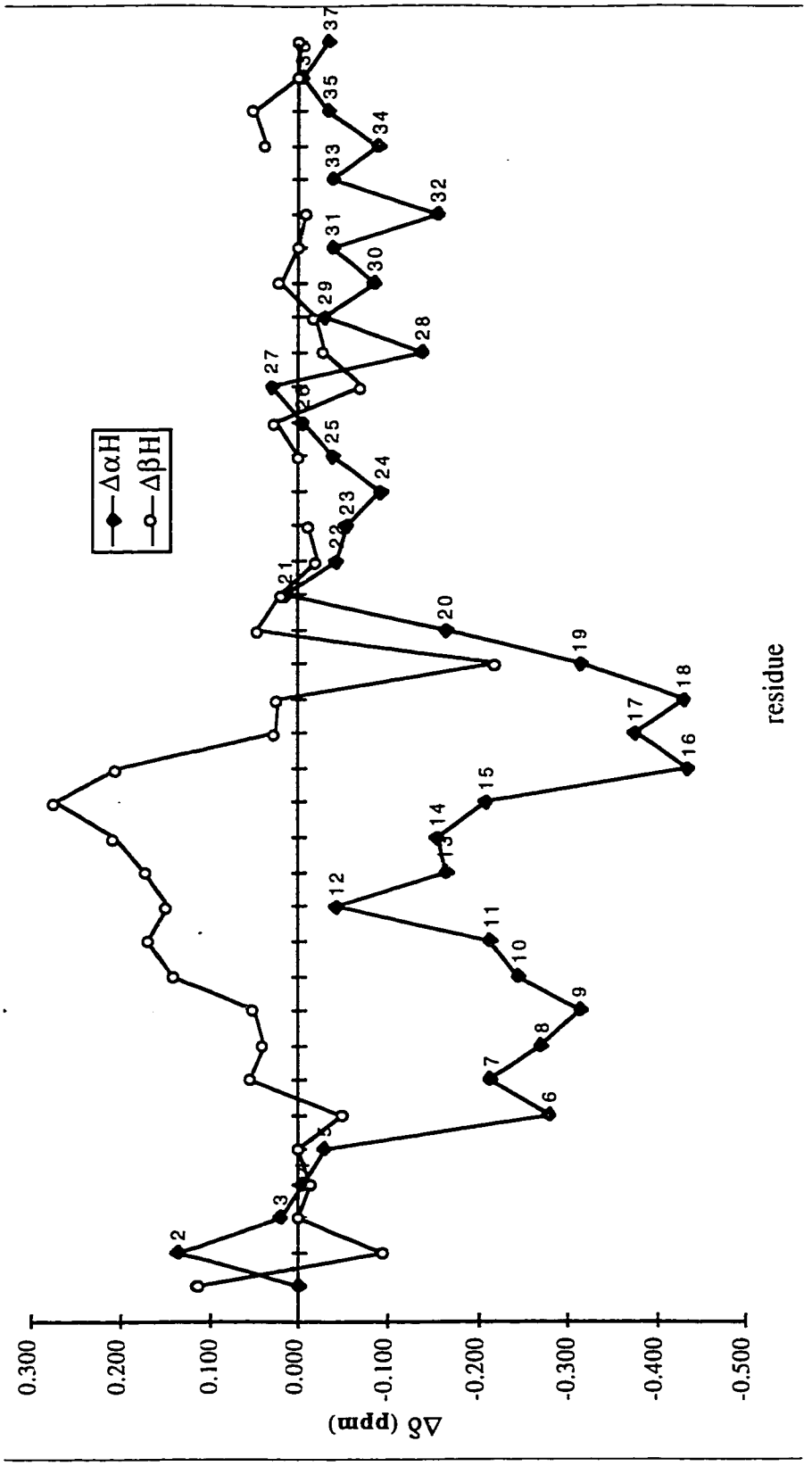

Figure 4.25 Hα and Hβ Chemical Shift Differences for Pramlintide in 35% HFIP and in Buffer (δ_{buffer} - $\delta_{35\%HFIP}$ - 0.075).
(0.075 is the correction of solvent effect. For the residues which have two βHs, the average of the two was used.)

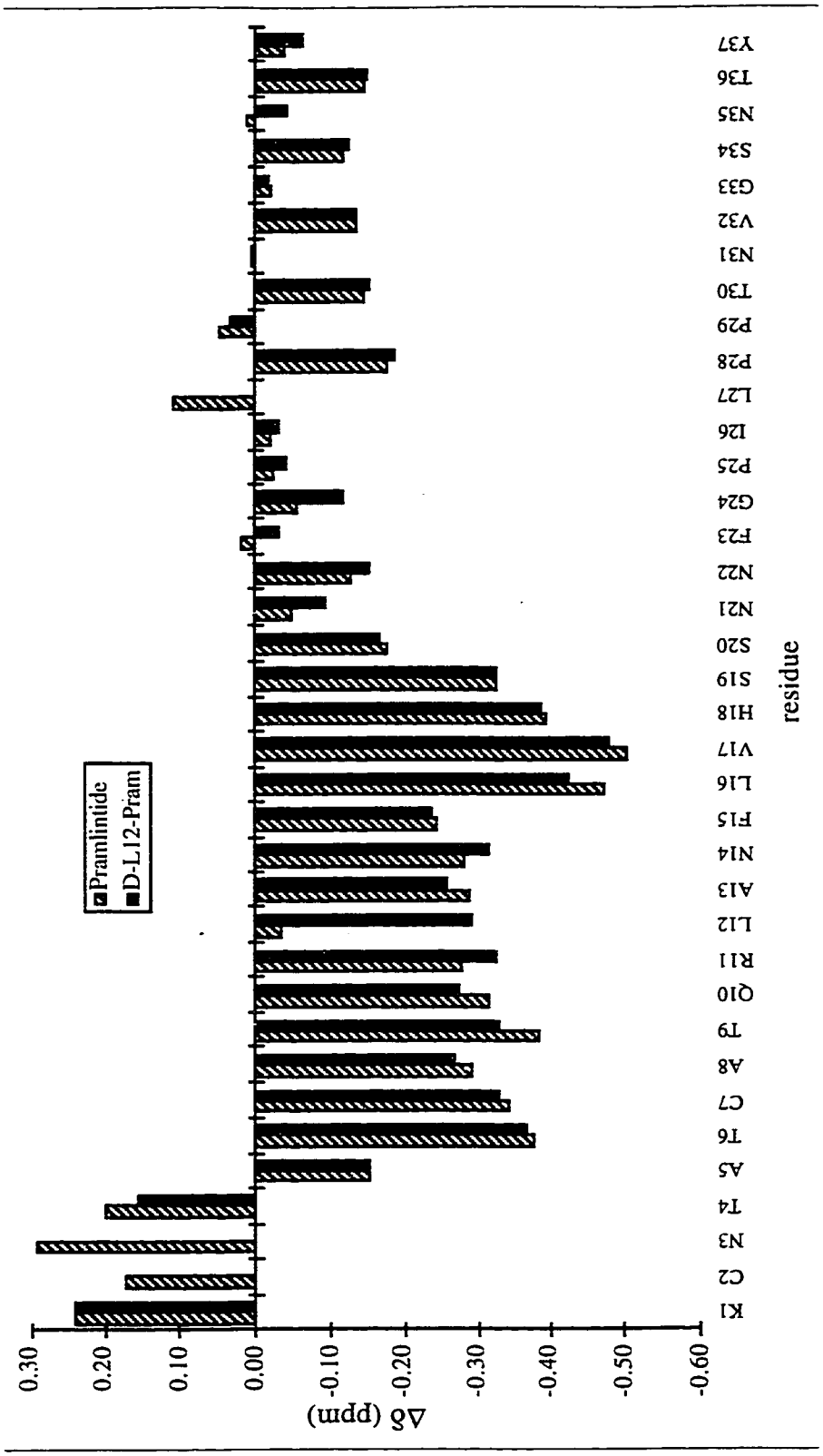

Figure 4.26 An αH-CSD Comparison of Pramlintide and D-Leu^{12}-Pram in 25% HFIP, at 285K.
(Note: missing data at residue 2,3, and 27 due to overlap with H_2O signal)

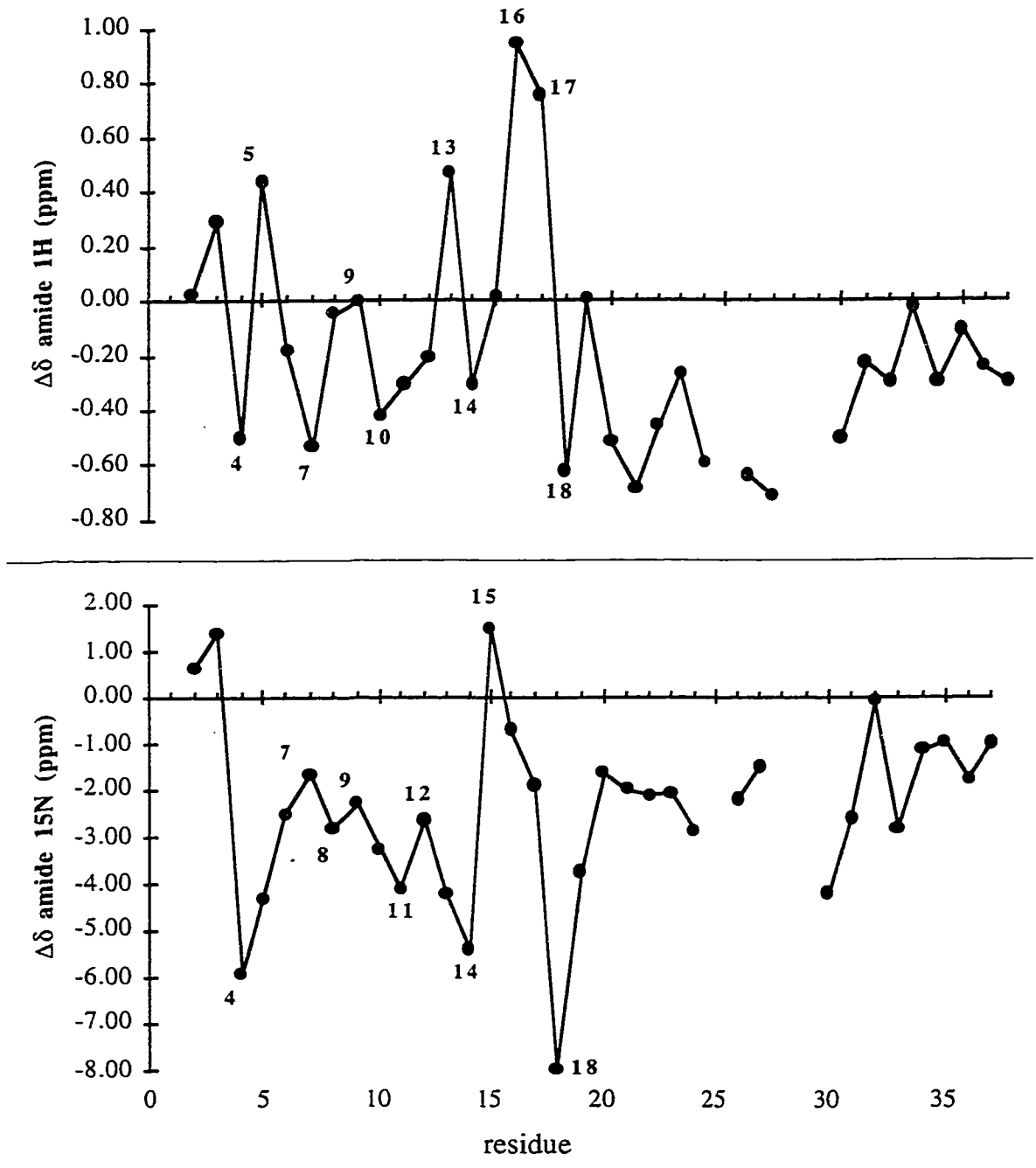

Figure 4.27 Plot of Amide ^{1}H and ^{15}N CSDs of Pramlintide in 35% HFIP at 285K.

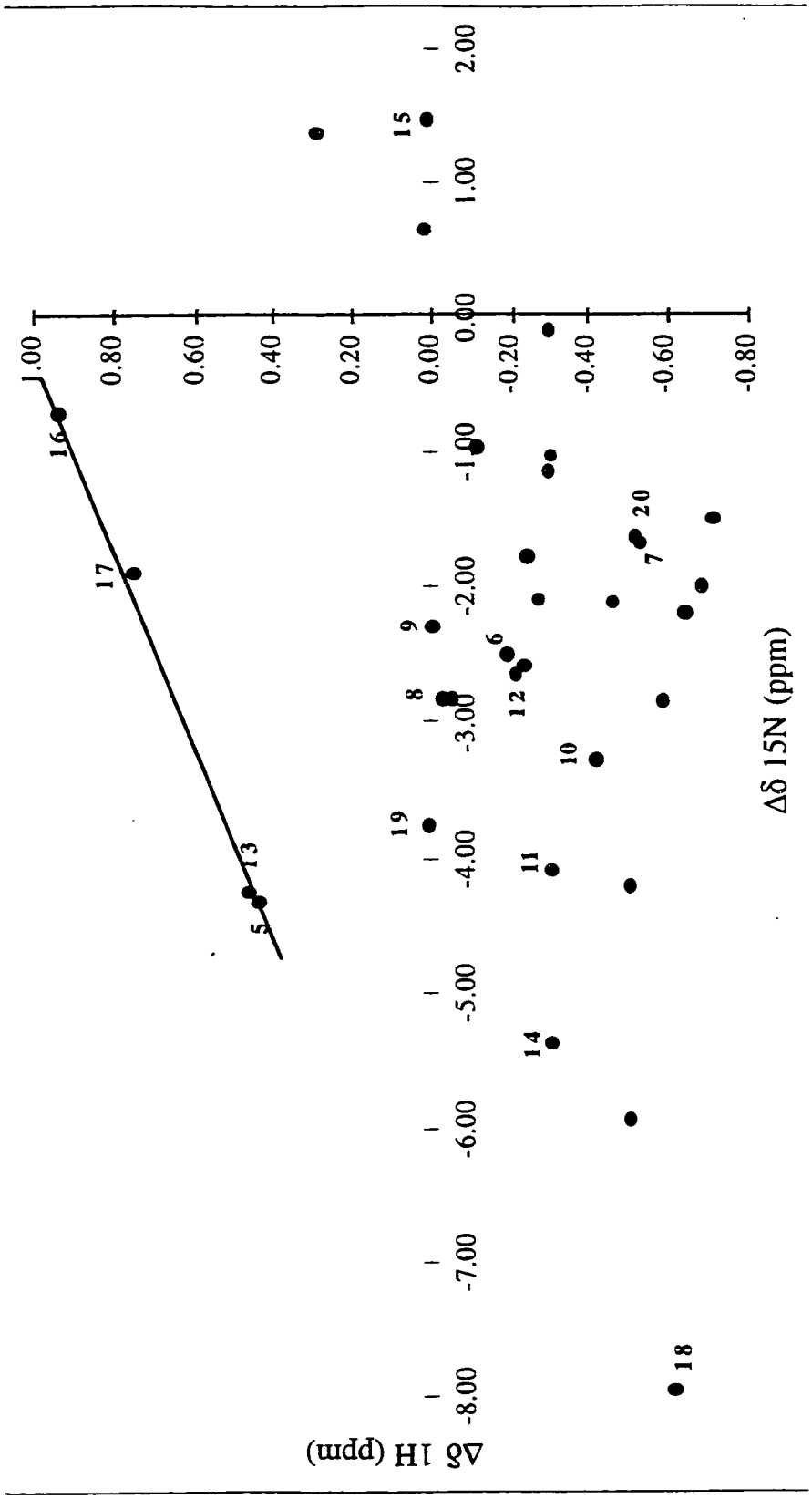

Figure 4.28 Correlation Between Amide ^{1}H and Amide ^{15}N Chemical Shifts of Pramlintide in 35% HFIP at 285K. ($R^2 = 0.997$ for the 4 ^{1}H that are shifted downfield)

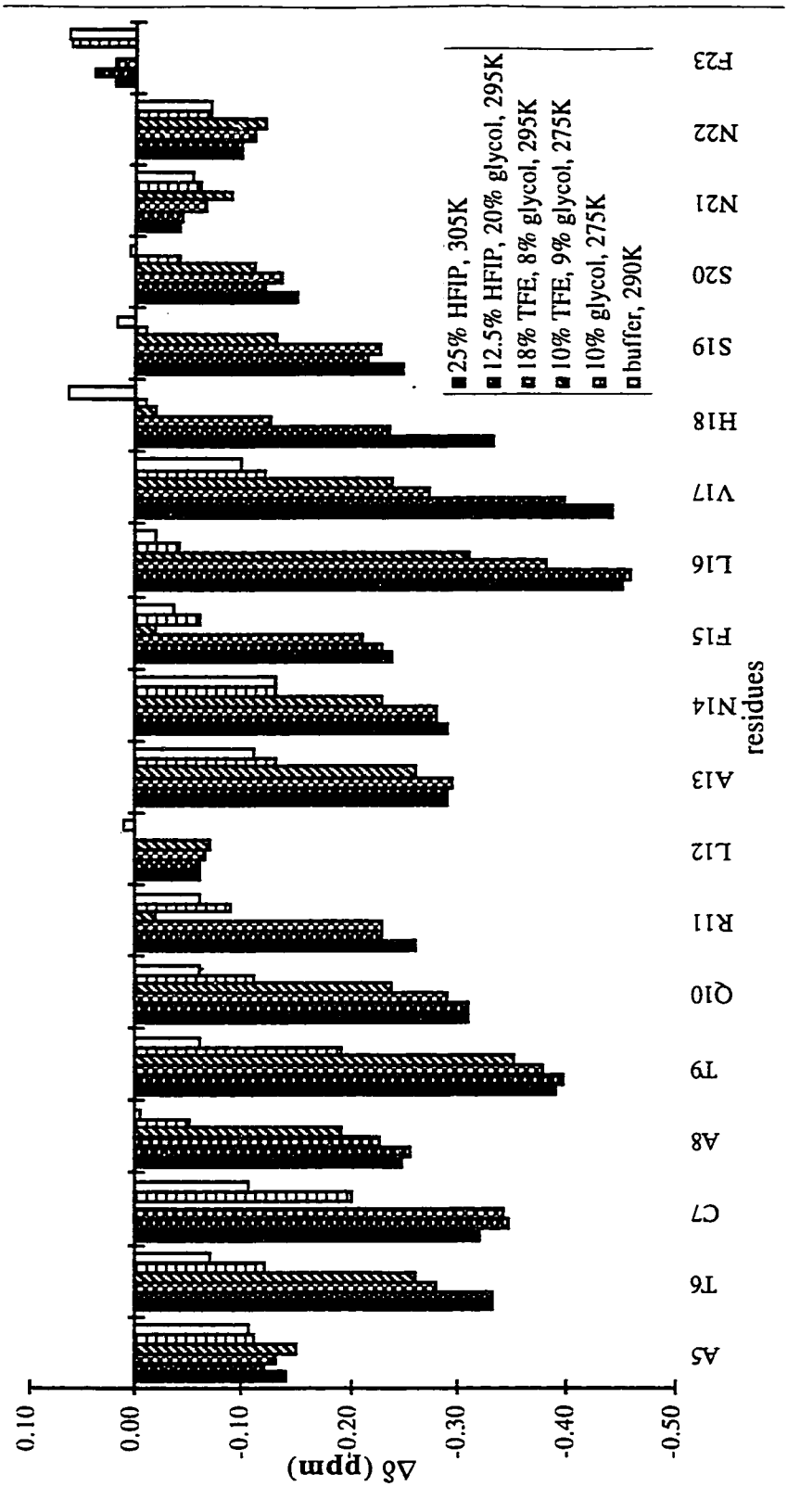

Figure 4.29a The αH-CSD Profile of Pramlintide under Various Conditions (residues 5-23).

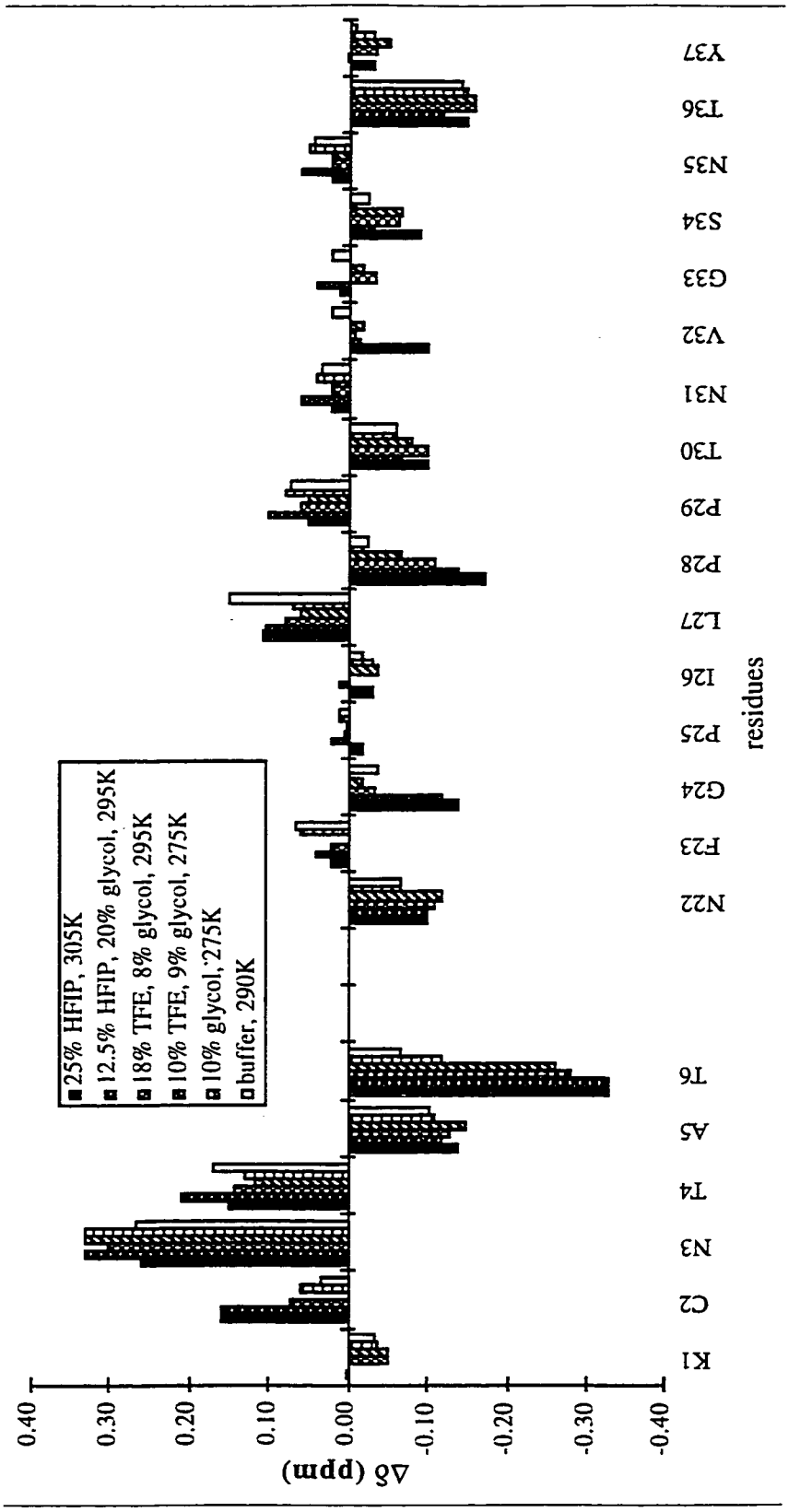

Figure 4.29b The αH-CSD Profile of Pramlintide under Various Conditions (residues 1-6, 22-37).

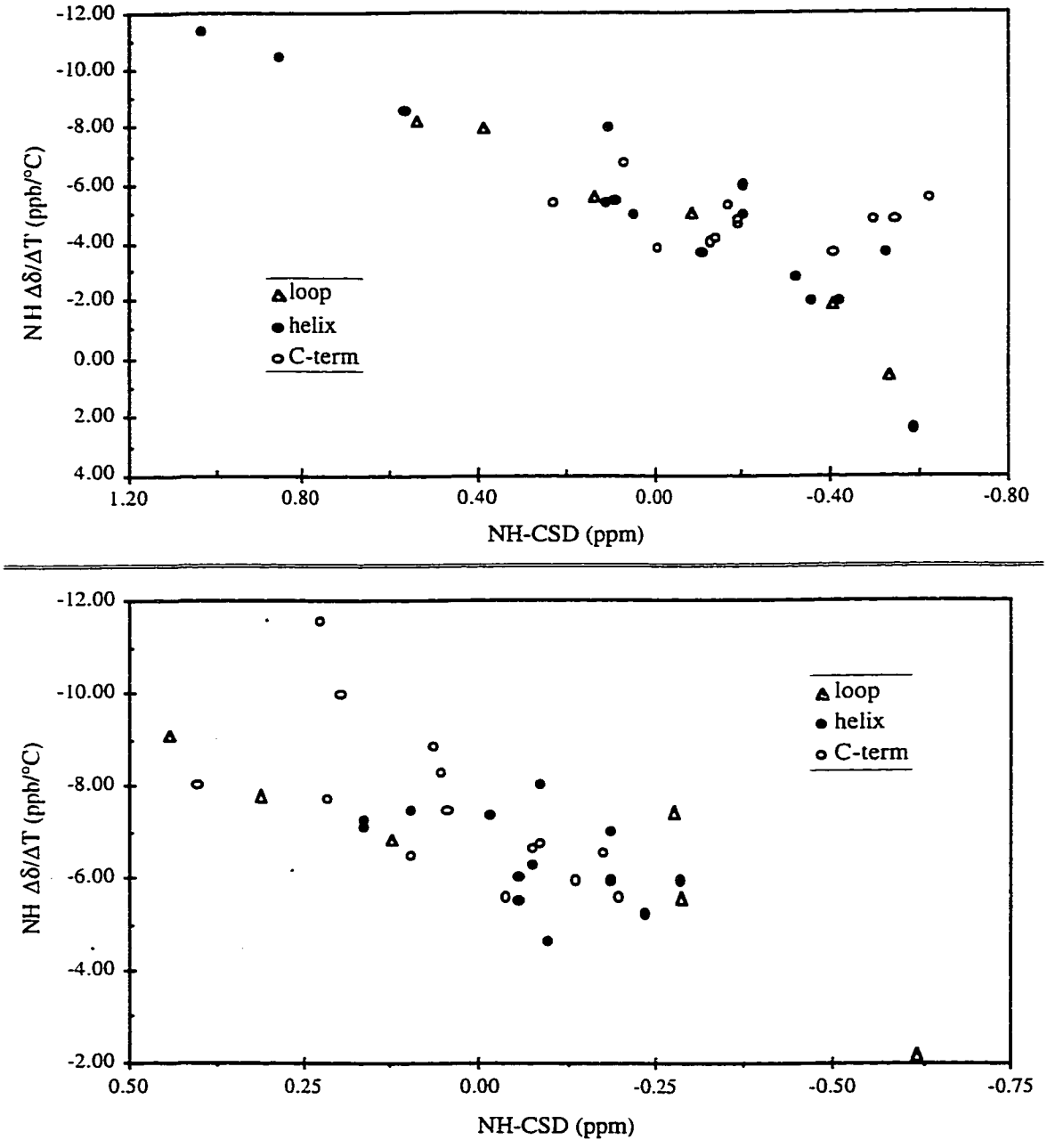

Figure 4.30 Correlation Between NH Temperature Gradient and Chemical Shift Deviation for Pramlintide in 35% HFIP Media (Upper Panel) and in Aqueous Buffer (Lower Panel).

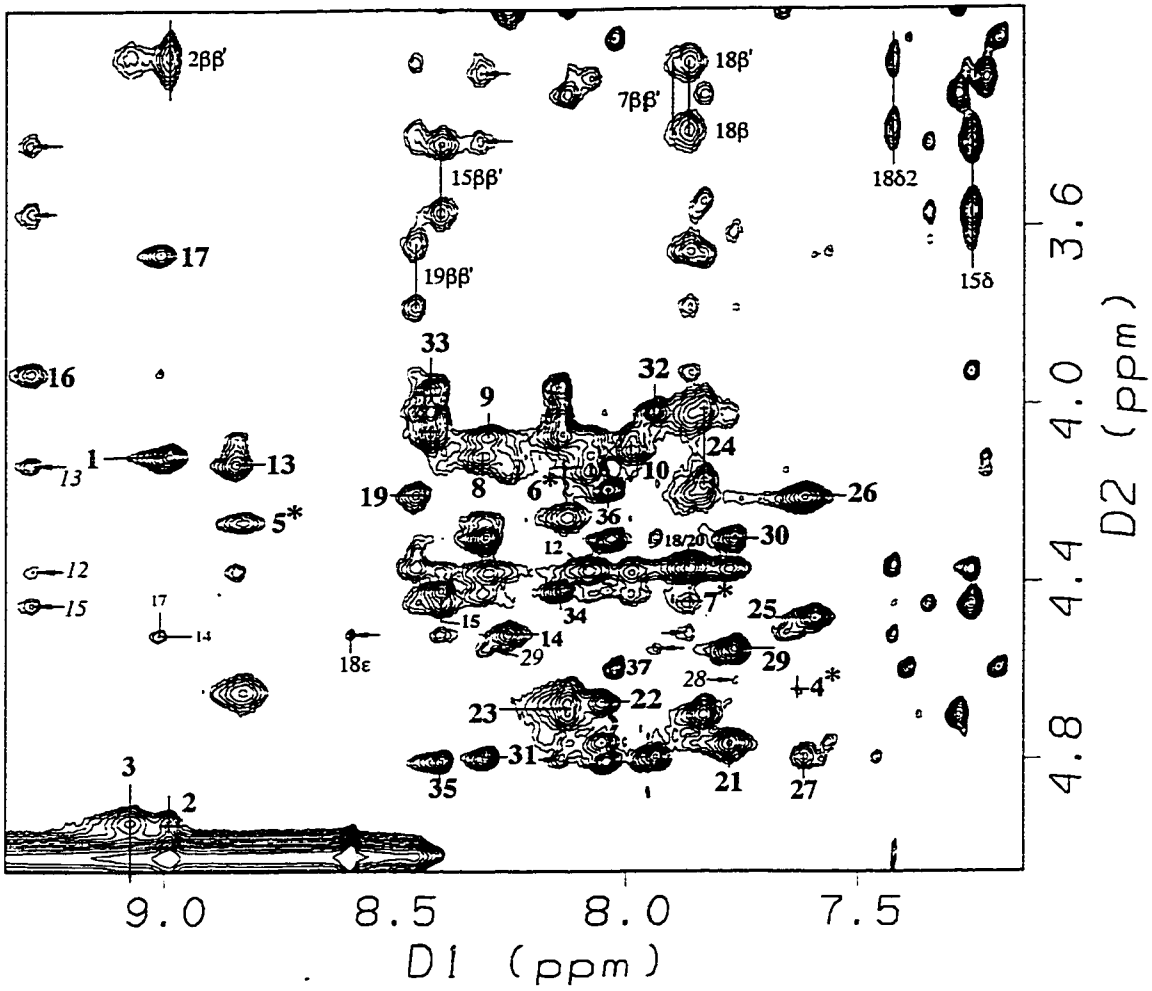

Figure 4.31 NOESY Spectrum (αN Region) of Pramlintide Collected on a DMX750MHz NMR Spectrometer at 275K.

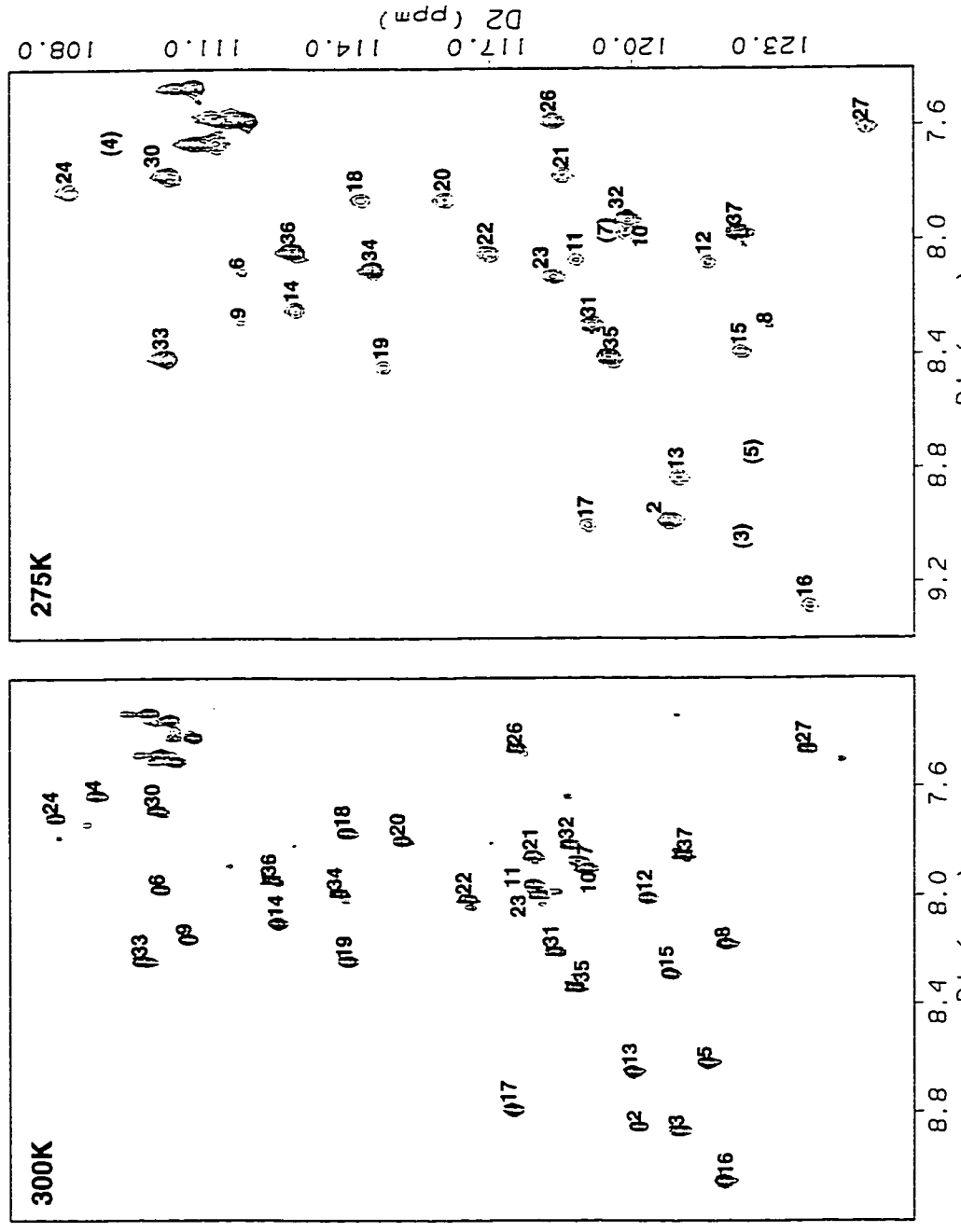

Figure 4.32 ^{15}N-HMQC Temperature Gradient Study of U-^{15}N-pram in 35% vol% HFIP.

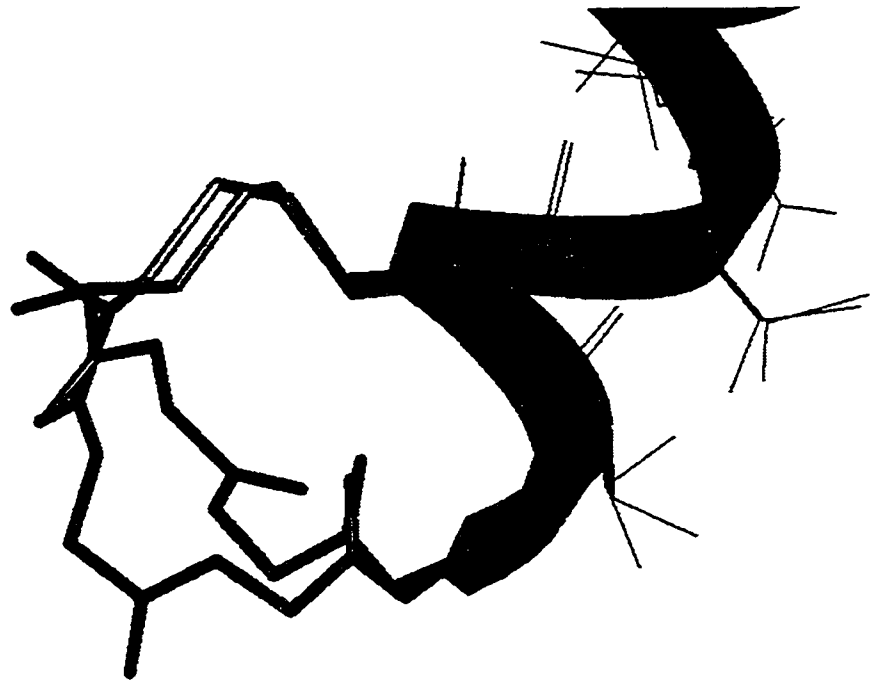

Figure 4.33 Two Cys-Cys Loop Conformations Encountered During the Early Stage of the hAM Structure Refinement (Adapted from the thesis of Cort 1997).

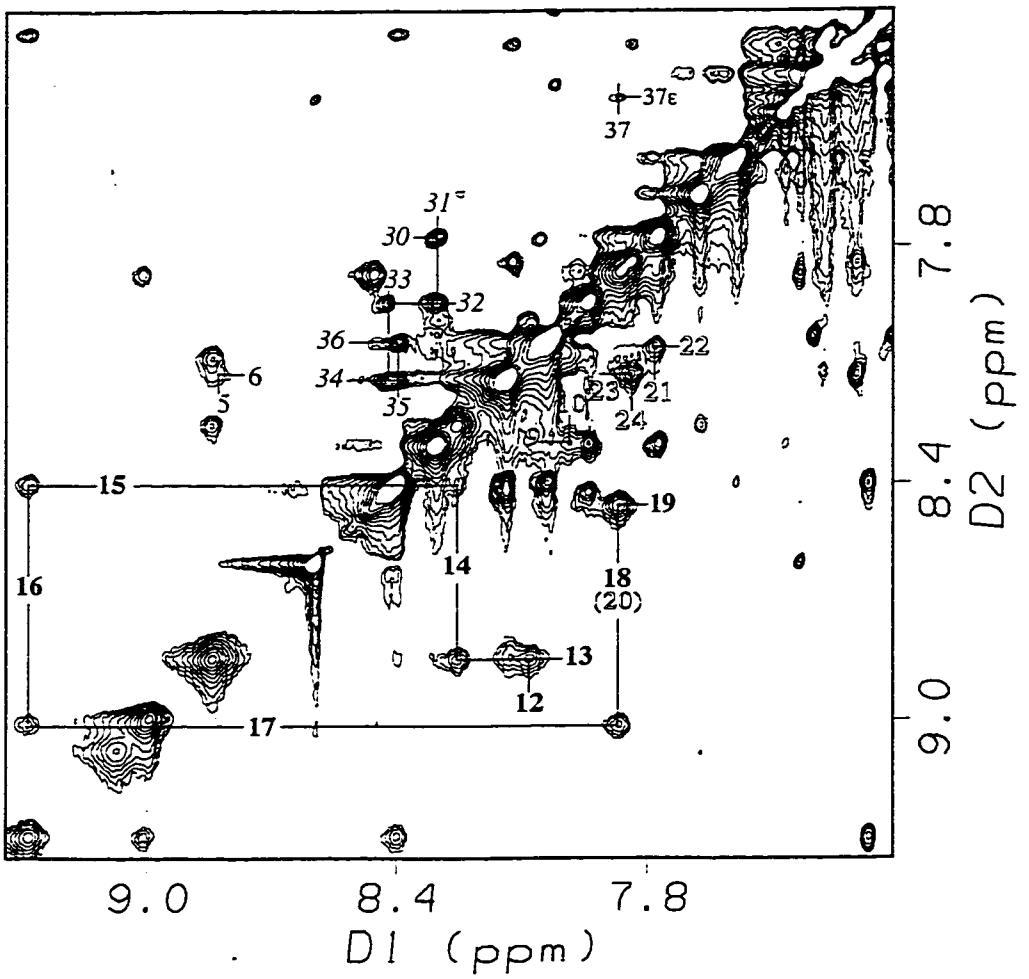

Figure 4.34 NOESY Spectrum (NN Region) of Pramlintide Collected on the DMX750MHz NMR Spectrometer.

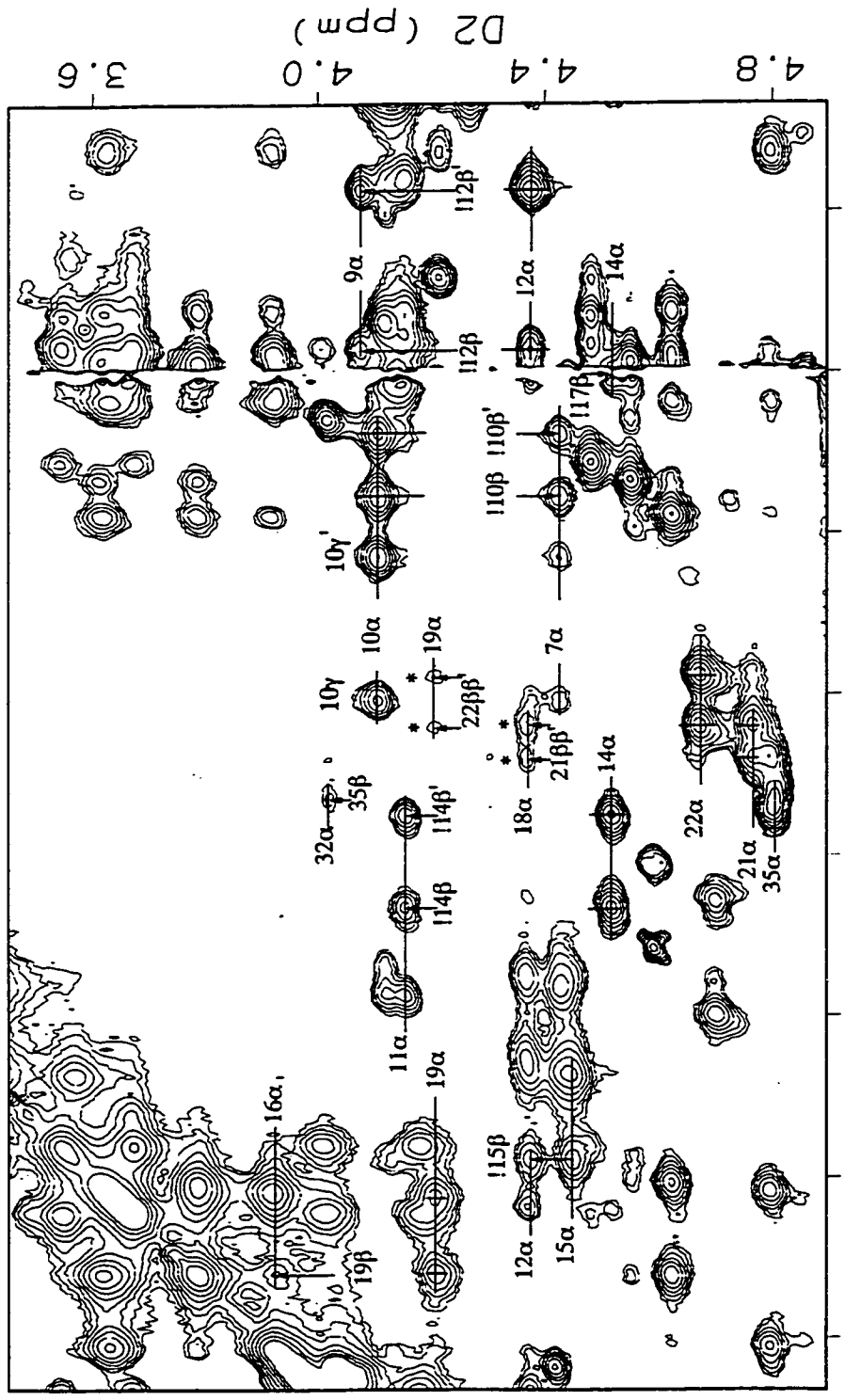

Figure 4.35 NOESY Spectrum (αβ Region) of Pramlintide Acetate Recorded on 750MHz NMR Spectrometer.

(The streak at 2.1ppm is due to $CH_3CO_2^-$)

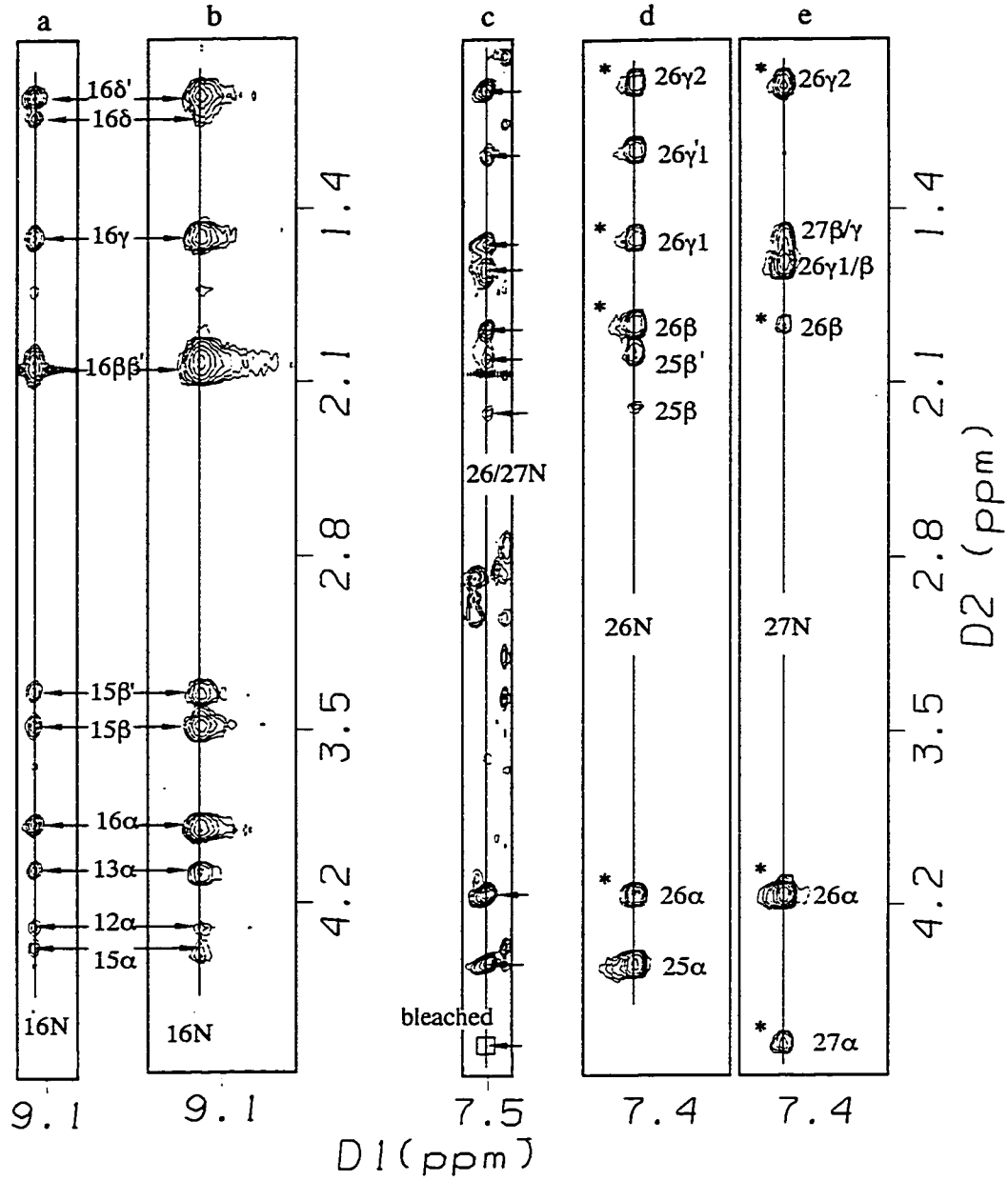

Figure 4.36 Comparison of 2D and 3D NOESY Spectra of Pramlintide in 35% Aqueous HFIP. Slices a and c are from a 2D NOESY spectra; while slices b, d,e are from the 3D NOESY. The width of all slices is 0.2ppm. The ^{15}N chemical shifts of residue 16, 26, and 27 are 122.78, 117.9, and 124.4 ppm, respectively. * indicates NOEs which are not resolved in 2D NOESY spectrum.

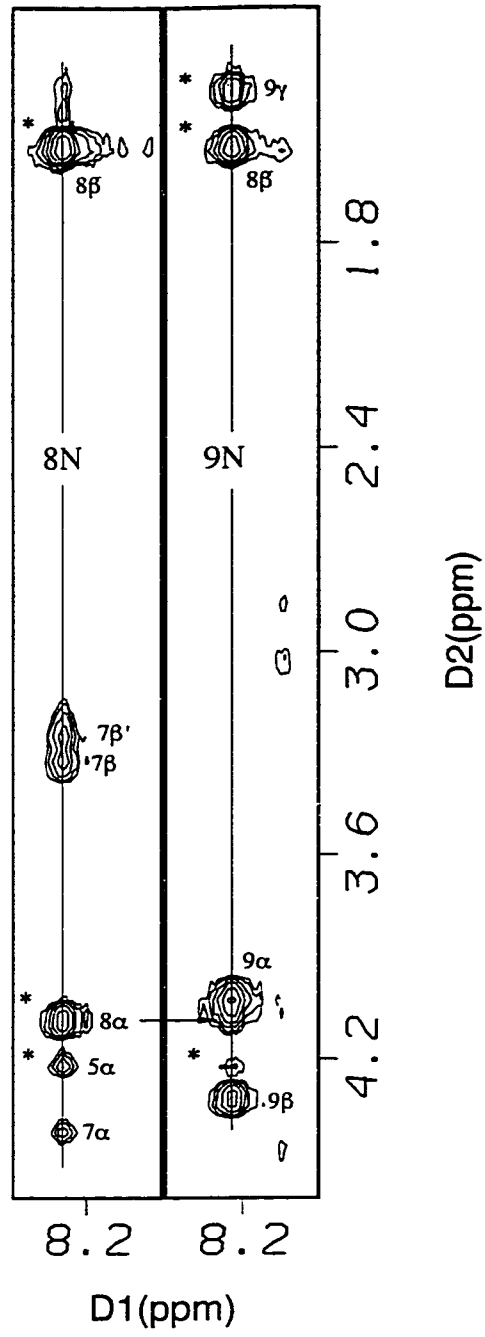

Figure 4.37 Selected Planes of the 3D N^{15}-Edited NOESY Spectrum. The ^{15}N chemical shifts of residue 8 and 9 are 122.37 and 110.86 ppm, respectively.
* indicates NOEs which are not resolved in 2D NOESY spectrum.

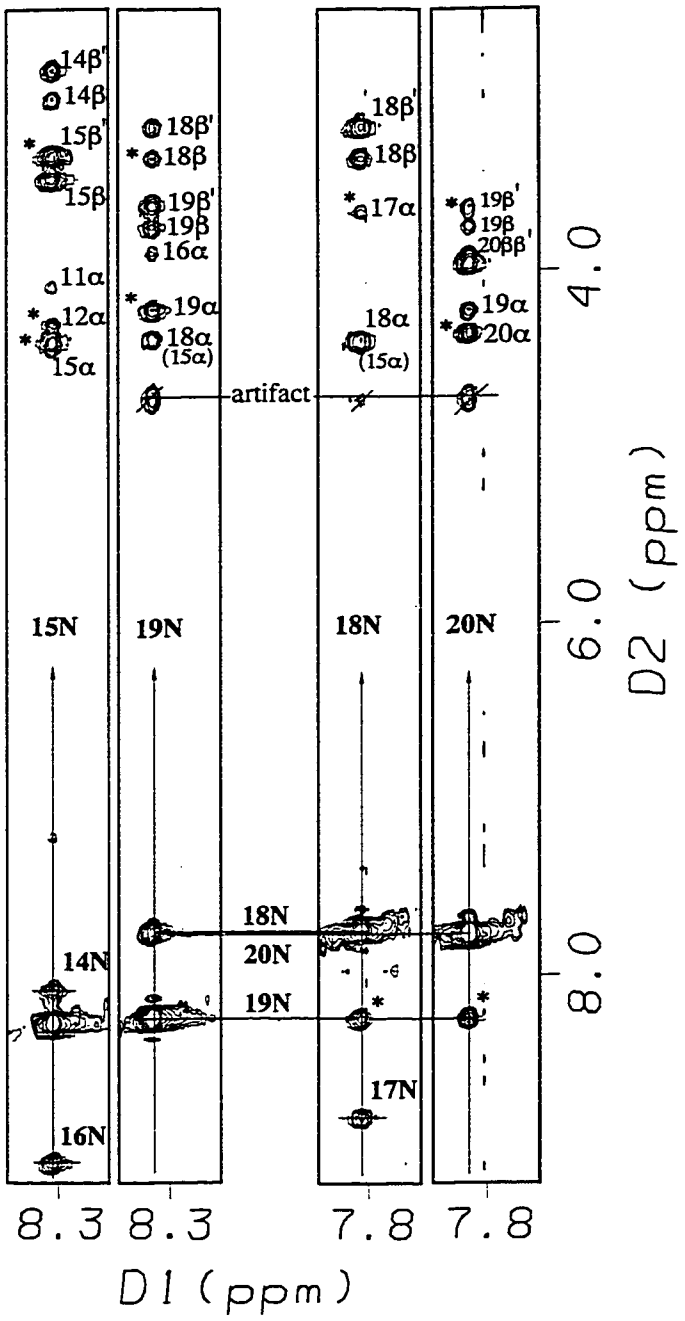

Figure 4.38 Selected Planes of the 3D ^{15}N-Edited NOESY Spectrum. The ^{15}N chemical shifts of residue 15, 18, 19, and 20 are 121.6, 114.2, 114.2, and 115.4 ppm, respectively. * indicates NOEs which are not resolved in 2D NOESY spectrum.

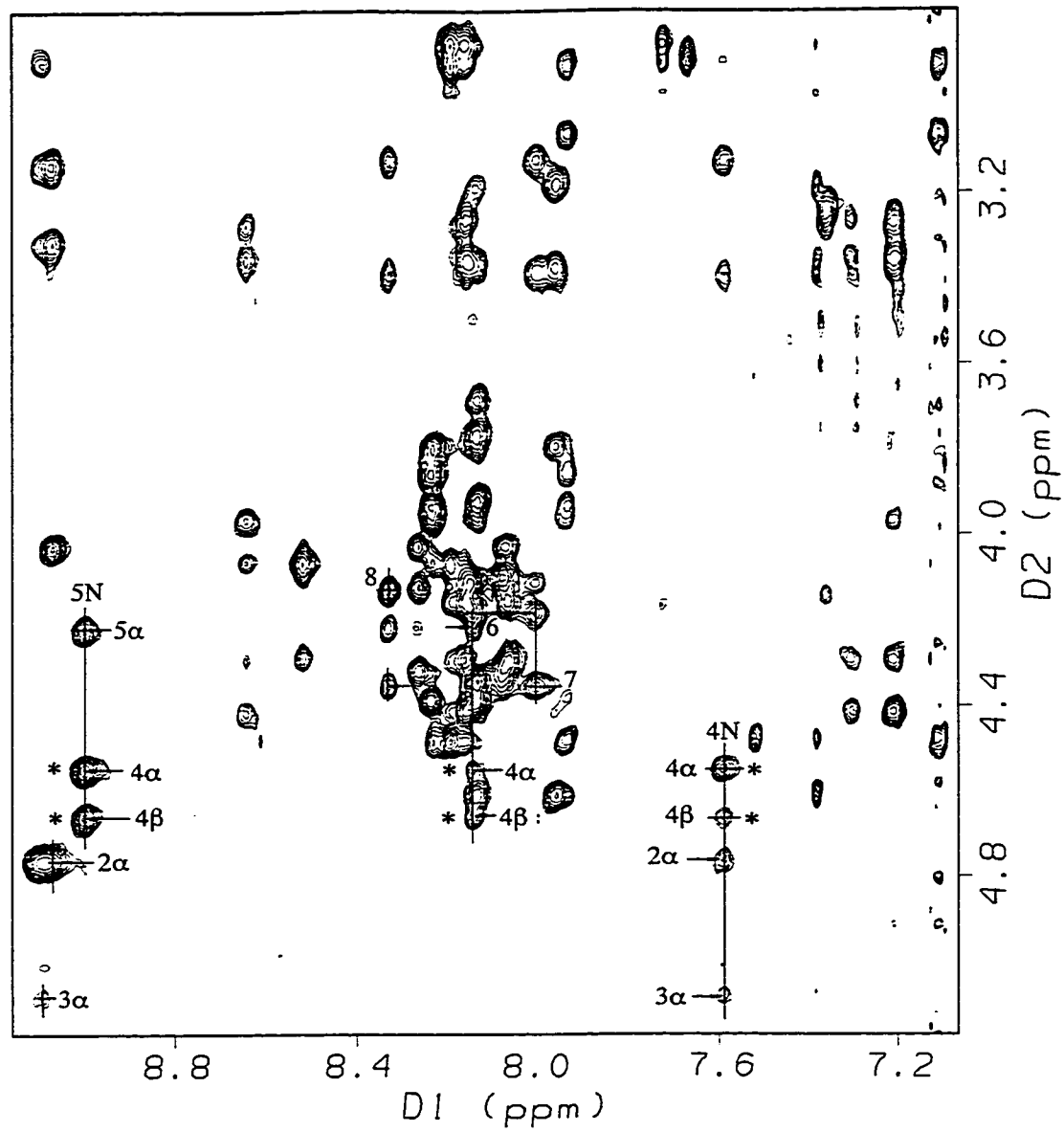

Figure 4.39 αN Portion of the NOESY Spectrum of Amylin Fragment hAM(1-20)GYNH$_2$ in 16% TFE Aqueous Medium.

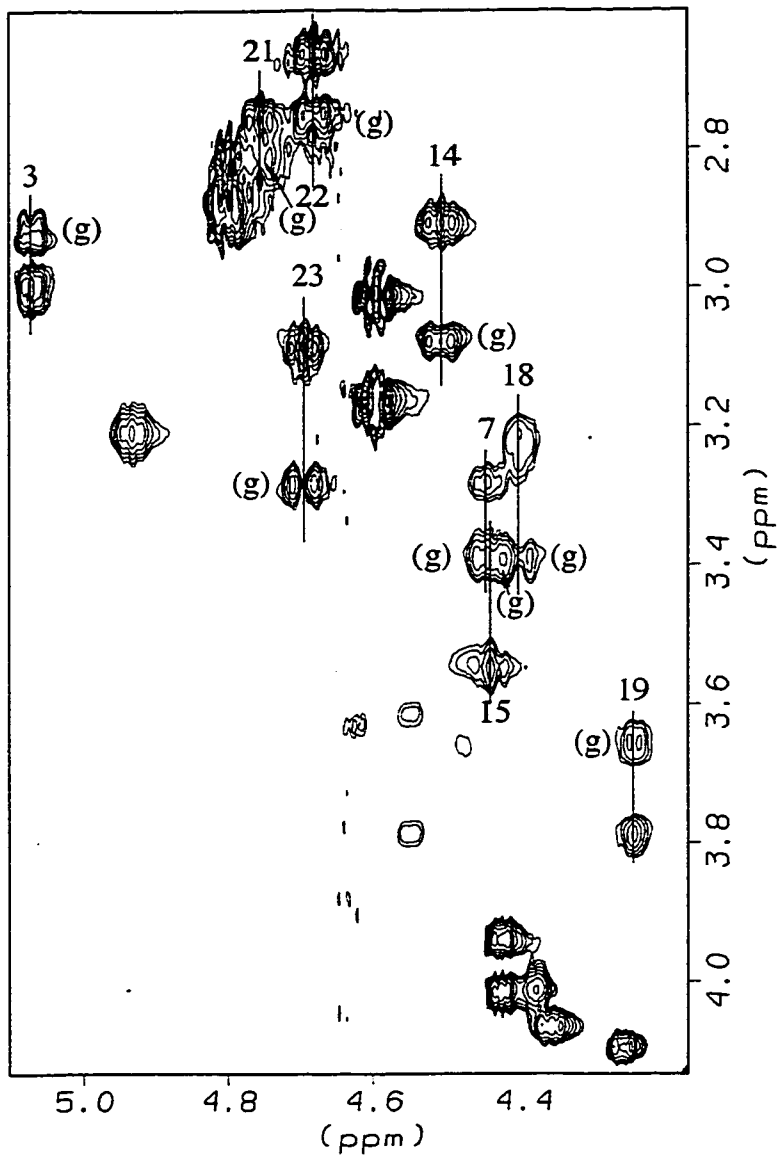

Figure 4.40 55ms Mixing Time TOCSY Spectrum of Pramlintide in D_2O at 295K.
(g) indicates that βH which is gauche to Hα; the doublet character results due to the near equivalence of the two passive couplings, $J_{\beta\beta'}$ and $J_{\alpha\beta'}$.

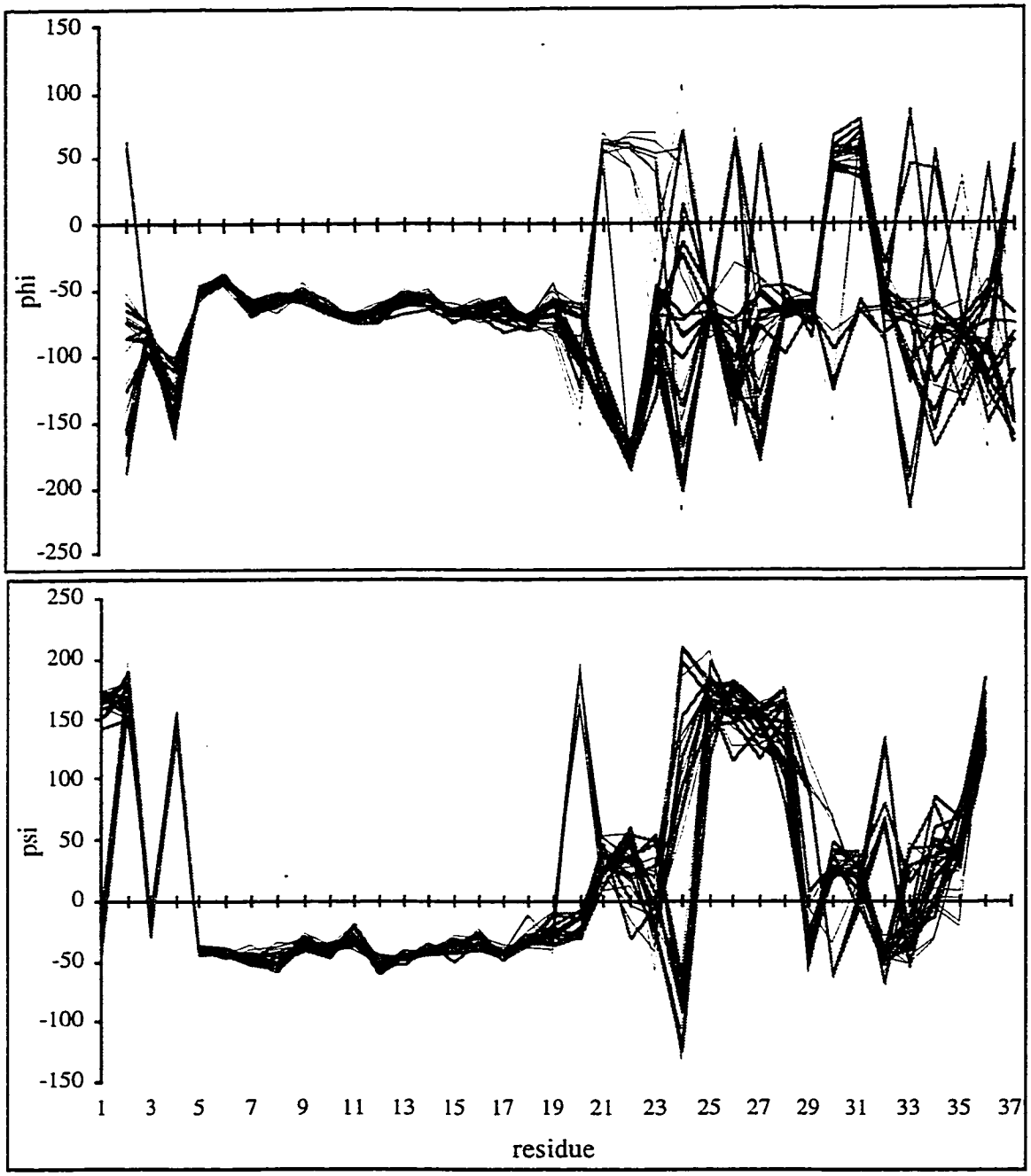

Figure 4.41 The ϕ and φ Plots for the Two NMR Structure Ensembles Derived for Pramlintide in 25-35% HFIP. (The darker thin lines represent C-capped short helicies; and the gray thicker lines represent long frayed helicies.)

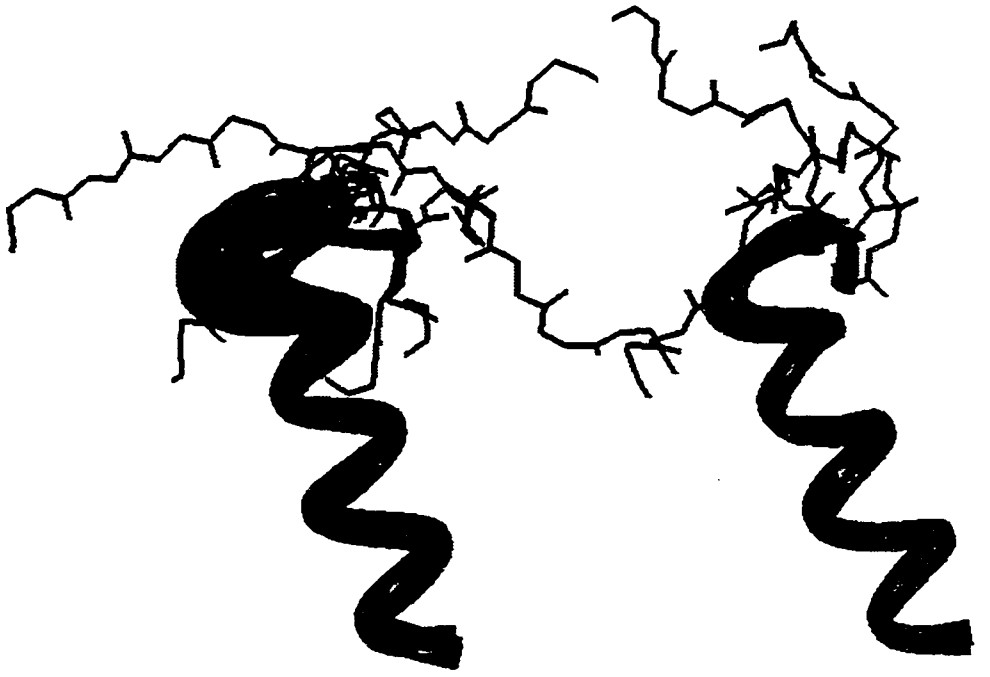

Figure 4.42 Overview of Pramlintide Structure Ensemble in 25-35% HFIP (Residue 8-24): left are capped helices, right are long helices. Residues 8-20 are shown as ribbon.

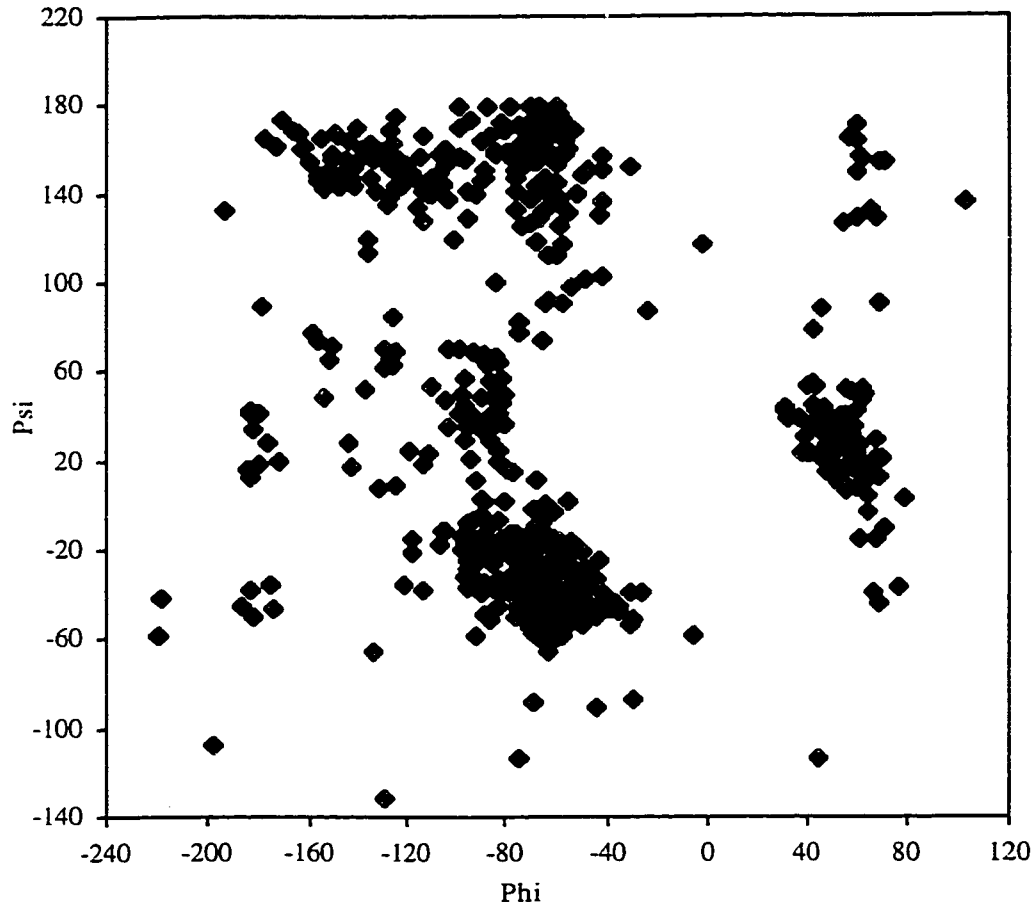

Figure 4.43 The Ramachandran Plot for the C-capped Helix Subset from the Pramlintide Structure Ensemble.

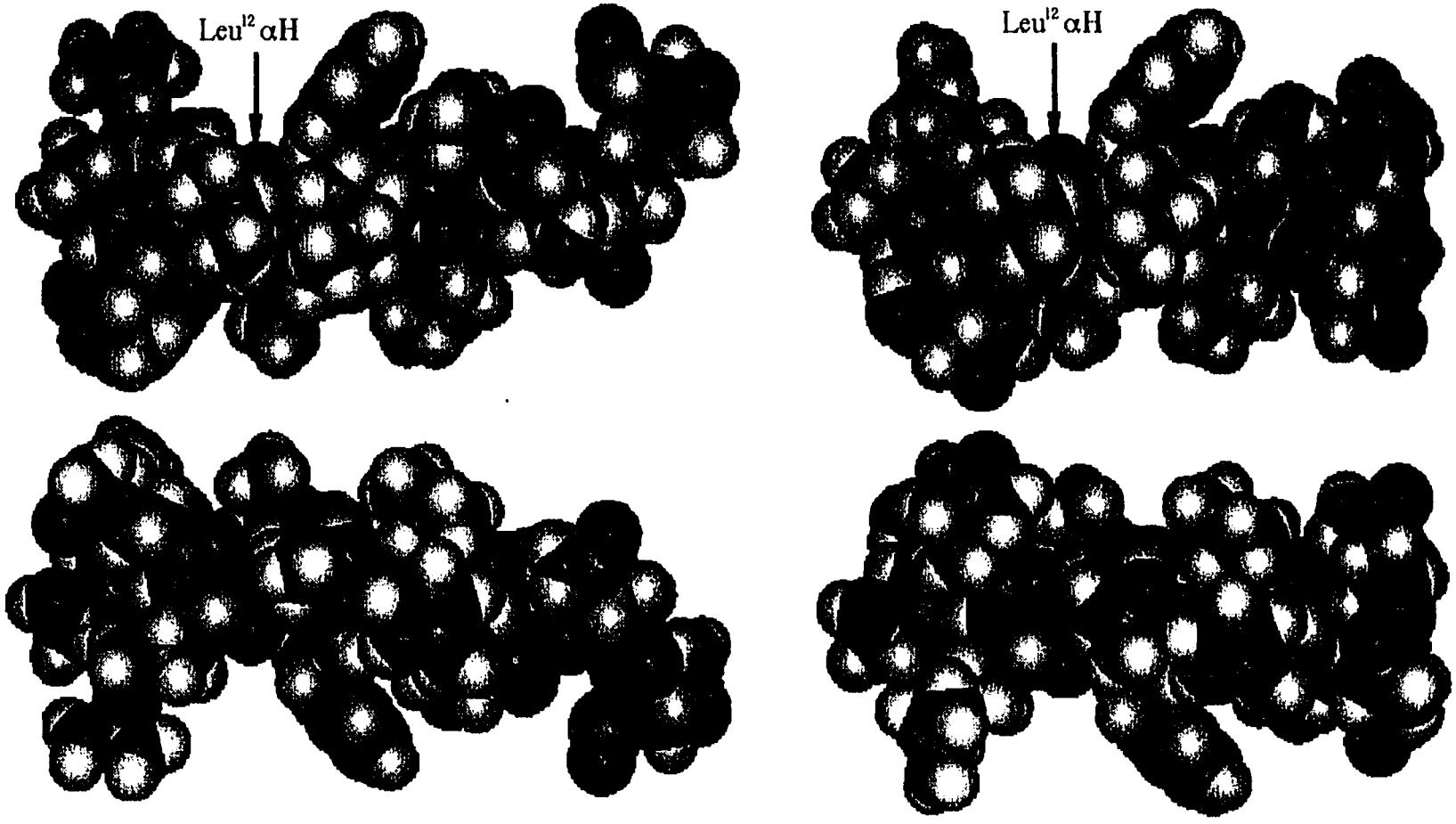

Figure 4.44 The Hydrophobic and Polar Faces of the Pramlintide Helix in 25-35% HFIP.

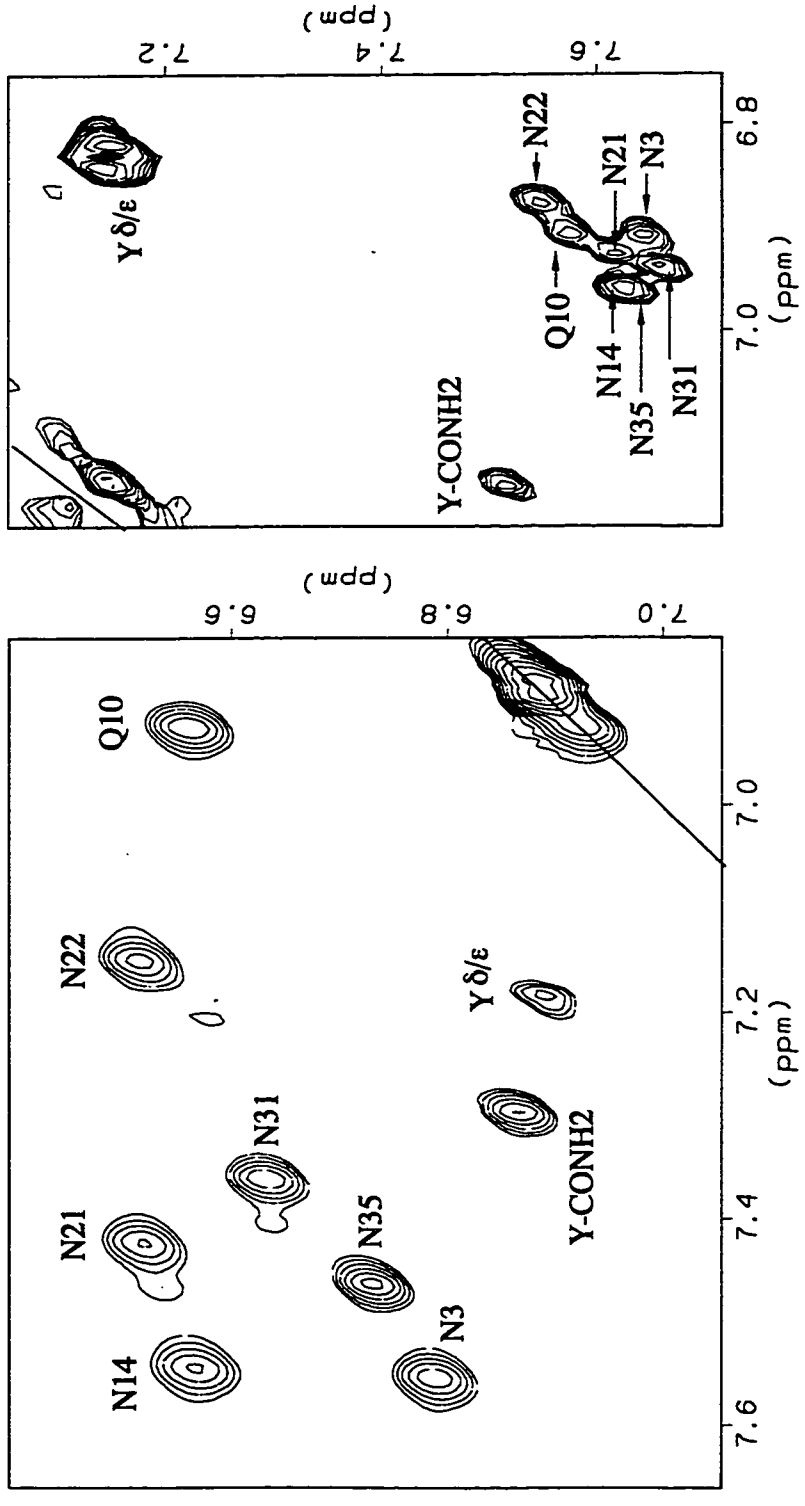

Figure 4.45 Comparison of Pramlintide Side Chain Shifts with and without HFIP Addition.

(Opposite Sides of the Diagonal Are Shown in the Two Segments)

Chapter 5

Factors Governing Amylin Helicity

The α-helix is the most abundant secondary structure in polypeptides. The general view is that native-like α-helices act as nucleation sites in the early stages of the protein folding processes (Kim & Baldwin, 1982; Wright et al., 1988; Dyson & Wright, 1991). This is consistent with the helix hypothesis of Presta & Rose (1988) which holds that short helices only occur between definable N- and C- capping motifs. Experimental studies of helix initiation, elongation and termination are thus highly pertinent to protein folding.

As discussed in Chapter 4, both human pancreatic amylin (hAM), and its biologically interesting mimic (pramlintide), have a common helical domain starting in the disulfide loop at residue 5 and extending to approximately residue 20. In hAM, after a discontinuity at $N^{21}N^{22}$, there follows another shorter and never completely populated helix between residues 23-29. The former 5-20 helix is partially populated in aqueous medium, and becomes fully populated upon fluoroalcohol addition. This chapter intends to investigate: Why do helices in both amylins terminate at NN sequence? Does this serve as a C-capping unit? What are the stabilizing effects of the disulfide closure (N-capping) on the net helicity and its distribution? How do site mutants influence the stability of the amylin helix?

The following sections present the NMR and CD studies of ten amylin-helix-related peptide fragments, designed to address these questions. In the absence of fluoroalcohol, the fragments usually failed to give reasonable NOESY spectra, which indicates relatively rapid segmental motion – however, they provided readily interpretable TOCSY spectra. NOESY (sometimes also TOCSY) spectra were collected for each fragment in aqueous HFIP. Detailed assignment procedures for each fragment will not be presented, since the spectra of the fragments are quite similar to the spectra of their parent peptide, and the assignments could usually be achieved by analogy. Chemical shift deviation and NOE techniques are adapted to assess the net helicity and where the helix starts or ends. CD studies, including HFIP titration and melting studies, served as another means to assess the helical propensity and stability of the fragments.

5.1 C-Capping Effects

Four peptides were chosen to investigate potential C-capping effect. Their sequences are shown below. The strategy for the design of c23 [hAM(1-22)G] fragment is to isolate the proposed helical region, and then examine the effect of NN C-capping on the helicity as compared to the c21 [hAM(1-20)G] in which the NN sequence is removed. Gly was introduced into each fragment as a substitute for the C-terminal portion of amylin. And Tyr was incorporated in c23Y [hAM(1-22)GY] and c21Y [hAM(1-20)GY] to assist quantitation of the peptide concentrations.

c23Y	hAM(1-22)GY	KCNTA	TCATQ	RLANF	LVHSS	NNGY-NH_2
c23	hAM(1-22)G	KCNTA	TCATQ	RLANF	LVHSS	NNG -NH_2
c21Y	hAM(1-20)GY	KCNTA	TCATQ	RLANF	LVHSS	GY-NH_2
c21	hAM(1-20)G	KCNTA	TCATQ	RLANF	LVHSS	G -NH_2

c23 was the largest amylin-related fragment examined in this project. Figure 5.1 is the αN region of the c23 TOCSY spectrum in buffer; while Figure 5.2 and 5.3 are αN and NN regions of TOCSY and NOESY spectra, respectively, for c23 in 25% aqueous HFIP. A comparison of Figure 5.1 & 2 with Figure 4.8 & 4.14, which are the spectra of pramlintide under similar conditions, shows that the spectra of c23, especially the backbone chemical shifts in this case, are essentially the same as the helical portion of amylin. The NN region NOEs of c23 (Figure 5.3) are also very similar to the NOEs of its parent peptide (Figure 4. 15). Adding a Tyr at the end of the sequence has not much influence on the peptide conformation. As shown in Figure 5.4 and 5.5, portions of NOESY and TOCSY spectra of c23Y in 25% aqueous HFIP are nearly identical to the spectra of c23 and the pramlintide helical segment (Figure 4.12-4.14).

However, significant differences were observed for c21, the fragment differing from c23 by deletion of $N^{21}N^{22}$. Figure 5.6 and 5.7 are the α/βγδ region of c21 in buffer and 25% aqueous HFIP, respectively. The biggest difference noticed here is at Val^{17} with a significant downfield αH shift in both cases, compared to either pramlintide or the c23/c23Y fragments. Figure 5.8 is the αN region of the TOCSY spectrum of c21 in buffer, confirming the correct assignment of Val^{17} and showing its NH chemical shift is also shifted downfield significantly. A close examination of αβ region of NOESY spectrum reveals that despite the large chemical shift differences at Val^{17} and neighboring residues, the medium ranged NOEs shown in Figure 5.9 are basically the same as those of pramlintide. Interestingly, simply adding a Tyr at the C-terminus

(c21Y), seems to eliminate these chemical shift differences. Figure 5.10 – 5.12 are important regions of a NOESY spectrum of c21Y in 25% aqueous HFIP, showing the backbone proton assignments and sequential and medium ranged NOEs.

Backbone proton chemical shifts for these four fragments, (both in buffer and 25% aqueous HFIP), were extracted and are listed in Table 5.1 and 5.2. The chemical shift deviations (CSDs) provide a clearer picture of the secondary structure information (Wishart 1992).

Figure 5.13 shows comparisons of c21Y and pramlintide in buffer, and Figure 5.14 shows comparisons of c21Y, c23Y and pramlintide in 25% HFIP. Similar to their parent peptides, the α chemical shift deviations of c21Y from reference values are relatively small in buffer. However, there are small, but continuously negative α-CSDs from residues 5 to 17, indicating some tendency to form an α - helix. Under these conditions, the C-terminus of the helix is less well-defined and it certainly does not extend beyond Val^{17}; and His^{18}, having a positive CSD, may serve as a helix cap. The NH-CSDs of c21Y, in the lower panel of Figure 5.13, resemble the CSD histogram of the pramlintide helical domain. In the presence of 25% HFIP, again like the parent peptide, the helix is highly populated indicated by large negative α-CSDs starting from Ala^5, passing His^{18} and extending to at least Ser^{20}, with some end fraying at the C-terminus (Figure 5.14 upper panel). Large positive NH-CSDs were observed at residues 16 and 17 for both fragments (Figure 5.14 lower panel) indicating the formation of strong H-bonds. The anomaly at Leu^{12} is also observed for the fragments in this medium as it was observed for amylins. As discussed in chapter 4, this is attributed to a deshielding by the Phe^{15} phenyl ring.

The comparisons of pramlintide, c21Y and c23Y reveal that the C-terminal portion of pramlintide (and by inference, hAM) has only a minor influence on the helical segment. There is a slight increase in helicity at Val^{17} – Ser^{19} when the asparagines are added and another minor increase when the remainder of the structure is included; these differences appear only when HFIP is added.

A significant difference, as already noticed during the initial spectra inspection, (whose origin is as yet unknown), the Val^{17} α chemical shift of c21 is significantly less upfield in 25% HFIP media (Figure 5.15). Further, it is even more distinguishable in the absence of fluoroalcohol when the chemical shift differences include the neighboring residues Leu^{16} and His^{18}, as shown in the upper panel of Figure 5.16. The differences around Val^{17} can also be found in the NH chemical shifts in Figure 5.16. The deletion

of the NN sequence would not provide a sufficient explanation for these differences, since they are not observed in c21Y or any other fragments examined. since there is no significant differences between c23 and c23Y, there is no obvious reason why adding a Tyr to c21 would be expected to restore chemical shifts that are similar to those of intact pramlintide. In conclusion, removing residue 23 and onward from amylin does not alter the conformation of their helical domains either in aqueous buffer or in HFIP; however, there is slight influence on helicity of the C-terminal residues in aqueous HFIP. The NN capping effect is not essential for helix formation, but will be discussed in a more quantitative manner in the later section. Due to the unexplained chemical shift differences observed in c21, we have come to the conclusion that instead of choosing c21 as an amylin reference, c21Y would be more suitable for the remaining comparisons (vide infra) with mutant fragments and other related peptides (presented in Chapter 6).

5.2 Disulfide Nucleation Effect

The effect of the disulfide closure on the helicity was evaluated by comparing fragments S2,7 [S2,7-hAM(1-20)G] and A2,7 [A2,7-hAM(1-20)G] with fragment hAM(1-20)GY. S2,7 and A2,7 are the non-cyclized versions with Cys to Ser or Ala substitutions, respectively. A 17mer, Ac-hAM(5-20)G, corresponding solely to the proposed helical region, was also examined. Their sequences are shown below:

S2,7	S2,7-hAM(1-20)G	KSNTATSATQRLANFLVHSSG-NH_2
A2,7	A2,7-hAM(1-20)G	KANTATAATQRLANFLVHSSG-NH_2
17mer	Ac-hAM(5-20)G	Ac-ATSATQRLANFLVHSSG-NH_2

The spectra of S2,7 and A2,7 are very similar to each other in both buffer and 25% HFIP. Figures 5.17 and 5.18 are αN portions of TOCSY spectra of the two fragments in buffer. Under these conditions, the αHs are near their random coil values (Wishart et al., 1991; Andersen et al., 1996b, 1997a). This can be seen more clearly in the α/βγδ region of A2,7 in buffer (figure 5.19). As the figure shows, NHs are very close to one other, and the distinct NH loop pattern seen in cyclic species is not observed here. In the presence of 25% HFIP the NHs are more spread out, the αHs go upfield, and many i/i+3 NOEs are observed; suggesting that the helical conformation is highly populated (see Figure 5.20, the αN region of A2,7). The N_iN_{i+1} NOE connectivities were also detected through most of the sequence, as illustrated in Figure

5.21. However, the extreme upfield location of the Thr^4 amide ^1H shift observed in cyclic fragments is not seen for these two fragments lacking the disulfide loop closure.

Without the disulfide loop restraint, it can be clearly seen that when the helix becomes fully populated, the αH shifts of amino acids are shifted upfield to greater extent toward the C-terminus. This is particularly obvious in the 25% HFIP TOCSY spectrum of A2,7 with five alanines and three threonines in the sequence (Figure 5.22). It was reported by Wishart et al. (1991) that amide protons at the N-terminus of helices tend to be shifted downfield as compared to those found at the C-terminus in proteins, which was attributed to a helix dipole effect. Does what is observed in Figure 5.22 reflect a helix dipole effect on αH chemical? Perhaps, but more likely it is a manifestation of C-terminal end fraying – residues in the middle of the helix are more helical than the ones at the termini (and thus have greater upfield shifts) and efficient N-capping.

The backbone chemical shifts of S2,7 and A2,7 with and without HFIP addition are tabulated in Table 5.3. None of the spectra of the 17mer are included in this thesis, but the backbone shifts are also listed in Table 5.3.

Figure 5.23 and 5.24 present comparisons of the αH-CSD and NH-CSD for the non-cyclic fragments and c21Y in buffer and 25% HFIP, respectively. One distinguishing difference among these peptides occurs at residue Thr^4: the non-cyclic S2,7 and A2,7 have a negative αH chemical shift deviation in both media, (indicating a near zero or positive φ value is adopted at this position), while c21Y, and all other cyclic peptides presented thus far, have a positive αH - CSI, (presumably the disulfide loop forces the peptides to adopt a β like configuration at this site). There is essentially no helicity through residues 5 → 8 for S2,7 and A2,7 in the absence of HFIP. In contrast, the cyclic ones form one turn of a helix in this region as indicated by continuous negative αH - CSDs. The explanation for this is that the disulfide loop helps to trap some helicity in this region. Another noticeable difference is, for the 17mer, although the C-terminal portion of the peptide is as helical as the other three peptides in 25% HFIP, the residues at the N-terminus do show more end fraying as compared to peptides without the residue 1 to 4 deletion.

5.3 *Aib Stabilization Effect*

As previously discussed, the disulfide loop of amylin-related peptides locks in one turn of helix (residues 5 → 8), but without the disulfide loop closure, these peptides

have very limited helicity in buffer. It is well known that α, α - dimethyl alanine (abbreviated as Aib or U) stabilizes helices (Vijayakumar & Balaram, 1983; Karle & Balaram, 1984, 1990; Karle et al., 1994). Here, we introduce an Aib into amylin at the Cys^7 locus to investigate whether it has a similar effect on helicity as disulfide loop closure. Two peptides, differing by a Tyr at the C-terminus, were studied to better understand this effect. Cys^2 and Cys^7 in the amylin sequence were substituted with Ser^2 and Aib^7. Their abbreviation, full name and sequence are shown below.

S2U7 S2U7-hAM(1-20)G KSNTATUATQRLANFLVHSSG $-NH_2$
S2U7Y S2U7-hAM(1-20)GY KSNTATUATQRLANFLVHSSGY$-NH_2$

The assignments of these two peptides were not as straight forward as the other fragments. Since Aib lacks an α proton, and consequently it does not have an intra-residue cross peak in the αN fingerprint region of spectra. Nonetheless, an assignment could be completed and the backbone shifts are tabulated in Table 5.4, along with the shifts of R18-hAM(1-20)GY which will be discussed in the next section.

Figures 5.25 and 5.26 are regions of S2U7 TOCSY spectra in aqueous buffer, with assignments labeled. As we can see, similar to other fragments in buffer, the amide protons are not well separated and αH shifts are close to their random coil values. However, unlike other fragments studied, which usually fail to give reasonable NOESY spectrum in buffer due to relatively rapid segmental motion, S2U7 gave a fairly good NOESY spectrum, particularly in the NN region, under these conditions. The NOESY spectrum not only allowed sequential assignment, but also provided information about the conformational preference. In αN region (Figure 5.27), the inter-residue NOEs are generally bigger than the intra-residue NOEs; which indicates the peptide still samples extended conformations. However, a string of $N_iN_{i\pm1}$ connectivities was also observed through residues 3 → 18 (Figure 5.28), including a relatively large N_4N_5 NOE peak, which had never been seen for any other species in this medium. The observation of $N_iN_{i\pm1}$ NOEs suggests that at least a threshold population of peptides is helical. The absent of an N_4N_5 NOE peak for cyclic amylin-related peptides are consistent with the conclusion that the disulfide loop prevents residue 4 from adopting a helical conformation, even in 25% HFIP; whereas the non-cyclic fragments are simply not sufficiently helical in buffer for a peak to be observed.

The CSD histograms give a more detailed comparison of S2U7 versus the non-cyclic S2,7 and the cyclic c21Y (Figure 5.29). The αH-CSD shows that the

substitution of Aib at residue 7 significantly increased the helicity of the segment from residue 4 to 9. Although S2U7 has a positive αH-CSD at residue 5, $H\alpha_5$ has a more down-field shift than the non-cyclic fragment. At the same time the residues (Thr^6 and Ala^8) immediately next to Aib^7 are more helical in S2U7 than in c21Y, to even a greater degree when compared to S2,7. Ala^8 is a flexible site in the parent peptides; however, in S2U7, the presence of two geminal methyl groups at the C_α at position 7 dramatically limits the range of accessible backbone conformations which forces Ala^8 into a helical conformation. It is interesting to note that the NH-CSDs of residues 7 to 10 are significantly changed, but not for the NHs of residues 4 to 6, when one compares S2U7 with S2,7. This could be a result of H-bond formation at residues 7-10 upon helix formation, while the NHs of the first 3 residues of the helix are not usually H-bonded due to lack of H-bonding partners.

Like many other peptides studied in 25% HFIP aqueous medium, both S2U7 and S2U7Y gave high quality NOESY spectra. They are nearly identical to each other, thus only one set of data is included here. Figures 5.30 and 5.31 are regions of the NOESY spectrum of S2U7. A close examination of the well separated αN inter- intra-residue NOEs reveals the conformation at each residue. α_2N_2/α_3N_2 and $\alpha_3N_3/\alpha_2N_3 << 1$, indicates the extended form; while $\alpha_{13}N_{13}/\alpha_{12}N_{13}$, $\alpha_{16}N_{16}/\alpha_{15}N_{16}$, and $\alpha_{17}N_{17}/\alpha_{16}N_{17} >> 1$, suggests the helical conformation is highly populated. A string of $N_iN_{i\pm1}$ NOEs starting from residue 3 and continuing to the C-terminus is consistent with this conclusion, and the ones 'missing' are most likely due to NH shifts coincidence. Figure 5.32 is the $\alpha/\beta\gamma\delta$ region of a TOCSY spectrum of S2U7Y in 25% HFIP. The αH shifts of repeated amino acid, such as Ala [5,8,13] and Thr [4,6,9], are not shifted as they appeared in the A2,7 fragment. Presumably, this is due to Aib^7 forcing its neighboring residues (Thr^6 and Ala^8) into a more helical conformation. This can be seen more clearly on the αH-CSD histogram (Figure 5.33), the α–CSDs of residues 6 and 8 in S2U7Y are even more negative than for the cyclic c21Y. The changes of CSD observed for residues 4 and 10 are also fairly dramatic when compared to other two peptides. Perhaps this is due to being one turn away from Aib^7. Overall, an Aib at position 7 is at least as effective as disulfide closure in nucleating the helix.

5.4 *The Arg/His[18] Mutation*

The helical domain of rat amylin differs from hAM and pramlintide by one residue: Arg^{18} versus His^{18}. This section of this thesis is focussed on the influence of

an H18R substitution. R18Y, the isolated rat amylin helical domain with a Tyr at C-terminus, (sequence shown below) was studied in both aqueous buffer and in 25% HFIP.

R18Y R18-hAM(1-20)GY KCNTATCATQRLANFLVRSSGY-NH_2

Figures 5.34 and 5.35 are portions of a TOCSY spectrum of R18Y in aqueous buffer, with assignments labeled. This is a good quality TOCSY, as all spin systems of the amino acids in the sequence show up very well, including the long side chain of R^{18}. Figure 5.36 is the αN portion of NOESY spectrum under the same conditions, providing proof of the sequential assignments. Figures 5.37-39 are portions of the NOESY spectrum for R18Y in 25% HFIP. The presence of a well-formed helix under these conditions is supported by an αN inter/intra NOE ratios << 1 starting from residue 5 onward, the nearly complete N_iN_{i+1} NOEs, and many $\alpha_i\beta_{i+3}$ medium ranged NOEs.

The CSD histograms provide a more straightforward comparison of H18R substitution effect. In buffer, the H18R mutation has a very localized effect, as the chemical shift changes are at nearby residues, mostly at Val^{17} (Figure 5.40). In 25% HFIP media, both R18Y and c21Y are observed to reach their maximum helicity. The substitution of His^{18} with Arg^{18}, (a residue with greater helix propensity), stabilizes the last turn of the helix as can be seen on αH-CSD histogram (Figure 5.41). A significant difference in α-CSD occurred at residues 14 – 18, with a maximum at residue 14 which is approximately one turn away from the mutation. These differences closely resemble what have been observed for human amylin, pramlintide and rat amylin under same conditions (Figure 4.22).

5.5 *Helical Propensity and Stability of Amylin-Related Peptides as Determined by Circular Dichroism*

Circular dichroism is another method that was adapted to evaluate the helicity of these amylin-related fragments. Fluoroalcohol titration and melting studies were performed on each peptide.

Figure 5.42 shows CD traces of c21Y with different levels of added HFIP. This illustrates the typical behavior of a linear peptide with helical propensities that can be titrated from a minimal to a high degree of helicity (from approximately 20% to 85% in the case of c21Y) by addition of the fluoroalcohol. All the CD traces come close to displaying single isodichroic point, which indicates a two-state transition during the HFIP titration. At 12% HFIP, the helicity has already almost reached its maximal, since

the CD trace in 25% HFIP (dotted line) is only slightly more negative than the one in 12% at 221nm. TFE is generally less effective than HFIP, as shown in Figure 5.43, where the helicity induced in 16% TFE is less than in 8% HFIP.

Thermal CD studies can serve as a means to evaluate the stability of secondary structure. Figure 5.44 shows the CD spectra of a typical melting study (c21 in 25% HFIP). At this high level of HFIP content, as the temperature goes up, the helix melts in a cooperate fashion, and the peptide goes through a helix/coil two-state transition indicated by an isodichroic point. In aqueous buffer, $-[\theta]_{221}$ decreases as the temperature goes down for some peptides. This is a result of a higher proportion of Poly ProII conformation at lower temperatures. Some peptides display non-linear behavior in aqueous buffer; the value of $-[\theta]_{221}$ first decreases on warming, then increases at higher temperatures. These effects are illustrated in Figures 5.45 and 5.46. Thermal CD studies at high concentrations of denaturing agent can provide essential information about the stability of the helicies, which will be presented later in this section. The unusual melting behavior that these peptides display at a intermediate HFIP concentrations will be discussed in the next section.

The difference spectra can give insights of the changes that the peptides undergo during titration and melting studies. The normalized thermal and titration difference spectra of c23Y are shown in Figure 5.47. The effect of both cooling and HFIP addition are very similar, as revealed by both difference spectra which closely resemble a typical helix CD spectrum. The small differences in the shape of the ΔCD traces may indicate the differences in the length of the helices present. Shorter helices appear to display a larger $[\theta]_{221}/[\theta]_{208}$ ration (Bruch et al., 1991; Andersen et al., 1996b). Thus, in the case of c23Y, the effect of titration from 6% to 25% of HFIP is larger than cooling from 65 to 1 °C since the helices in ensemble display increased length in the fluoroalcohol rich medium.

It is a general observation that HFIP induces helicity in these amylin-related peptides. However, the response to certain levels of HFIP for each peptide is different. Figure 5.48 is the CD titration curve of a few representative peptides, showing the percent of helicity at various HFIP level (relative to the helicity observed at 25% HFIP). For this analysis, it is assumed that $[\theta]_{221}$ is directly proportional to %-helicity. In the absence of HFIP, pramlintide appears to be more helical than the fragments; which may due to interactions with residues after residue 22. At 12% HFIP. with the exception of S2,7, all four peptides have virtually reached their maximum helicity. The percentage of

HFIP required to push the peptides to a certain level of helicity is different for each peptide. At 9% HFIP, c23, which has both the N- and C-cap, has the highest percentage of helicity among the fragments. In contrast, the 17mer with neither of the capping units has much lower (less than 40%) helicity under these conditions. Nonetheless, it is rapidly pushed into approximately the same amount of helicity as other fragments upon addition of another 3% HFIP. In the case of S2,7, polar residues S2, N3, and S7 may serve as the N-caps for helical segments leading to a helix-coil transition which appears at lower HFIP concentration than for 17mer. In order to provide more accurate estimates of helicity for the fragments that have been studied, the temperature dependence of the CD spectra of a selection of peptides under denaturing conditions (≥ 6.5M GdmCl) was determined. In addition, equations which can be used to calculate the expectation $[\theta]_{221}$ values for the coil state were developed. For the tyrosine terminated species, the expected value of $[\theta]_{221}$ at 273K is +1600±150°; for amylins containing only a Phe residue, +750±100°. Fully disordered coil states display increasingly negative ellipticities upon warming: $\Delta[\theta]_{221}/\Delta T$ = -62±6°/°C. For this series, peptides which are partially helical over their entire span, gradients of +230±30°/°C are observed in aqueous media. In 25% HFIP, the rate of thermal fraying is diminished due to the increased stability of helices – typically to +135±30°/°C.

The key CD observations used to assess helicity are: 1) the $[\theta]_{221}$ value and temperature gradient in aqueous buffer, 2) R_1 ($[\theta]_{191}/[\theta]_{min}$) and R_2 ($([\theta]_{221}/[\theta]_{min}$) value in buffer at 273 or 298 K, and 3) the vol-% of HFIP required to achieve 50% of the helicity observed for the most helical fragment of the same size at 25 vol-% HFIP. These appear in Table 5.5 for the fragments discussed in this chapter and the parent peptides. The thermal dependence of $[\theta]_{221}$ under denaturing conditions and $[\theta]_{221}$, R1 & R2 in 25% HFIP are also listed when available. In most cases the $[\theta]_{221}$ values are well approximated by a linear equation: $[\theta]_{221} = [\theta]_0 + (\Delta\theta/\Delta T)T$, and T is in °C.

The ellipticities observed in 25% HFIP are unlikely to be a reliable measure of helical propensity under less forcing conditions. All of the fragments and the hAM analogs appear to display the maximal span of helix allowed by the sequence, with no more fraying than would be anticipated for spans of that length. However, the midpoint of the HFIP titration may be a useful measure of how readily helicity can be induced.

Temperature gradients of CD ellipticities can be used as a measure of helicity. As is clear from data in the first column of Table 5.5, under denaturing conditions, most of the fragments display gradients that approach –50°/°C, which is nearly the

expectation value for a fully disordered random coil (-62±6°/°C). The exceptions are the species with the $Cys^{2,7}$ linkage, whose loop geometry results in a single turn of helix, (Ala^5 – Cys^7), which cannot be denatured. This is consistent with the conclusion from the NMR study. Those portions of the sequence that are not ordered upon fluoroalcohol addition may be presumed to continue to contribute to the gradient at a –50 → -65°/°C rate per residue. Thus, more positive gradients in aqueous buffer indicate that a significant fraction of the residues are structured. This is particularly obvious for the Aib-nucleated helix.

The R1 and R2 values are very important facts reflecting the helicity of peptides. The consensus value for the random coil state R1 = +0.7±0.15, R2 = -0.06±0.08; for 100% helicity R1 = -2.4±0.2, R2 = +1.05±0.05 (Bruch et al. 1991). It is found that R1 value correlates with %-helicity much better than R2 value, and can be expressed as a non-linear least-squares fit to the following third degree polynomial (Munoz et al. 1995):

$$y = 1.092x^3 + 11.989x^2 - 6.974x + 11.887$$

The dependence of R1 upon the portion of the sequence that can become helical can be seen in entries that appear for the full-length amylins versus fragments in the 25% HFIP column of Table 5.5. The full-length amylins display R1 values less negative than –2.0. This reflects the C-terminal portions of these sequences that never achieve any degree of helicity. Human amylin having a larger R1 than both pramlintide and $D\text{-}L^{12}$-Pram thus shows the presence of its additional helical segment in C-terminal portion of the peptide. Although the correlation of helix population with the R2 value is not as good as it is with R1 quantitatively (Munoz et al. 1995), the R2 value does reflect the helicity of the peptides quanlitatively. The general trend remains that the more helical the peptide is, the larger R2 is. R2 is close to unity in 25% HFIP, and the cyclic species have larger R2 than the non-cyclic ones. For most of the cases, R2 is larger at 273K than at 298K in both aqueous buffer and for the 25% HFIP column, indicating higher helicity at the lower temperature.

The other commonly used measure is the fractional helicity. The equation used for the calculation has been discussed in Chapter 3 in the CD section. The calculated fractional helicities for the species discussed in this chapter are collected in Table 5.6, providing a very straight-forward numerical comparison among the fragments. These are, in all cases, for aqueous buffer at circa pH 4. The ellipticity temperature gradients were converted to a measure of the fraction of the sequence that is helical (some residues

that are only partially helical were also counted as helical residues). The helical span (the caps are not included in the listing) was estimated from the Hα–CSD histograms.

5.6 An Aside – Cold Denaturation of Amylin Related Peptide

Cold denaturation has been known for molten globule states of protein (Kuroda et al., 1992; Nishii et al., 1994; Carra et al, 1994) and for helical peptide oligomers (Kitakuni et al., 1994; Hagihara et al., 1994). However, it has never been well characterized for a monomeric helical peptide (Beals, et al., 1991; Woody, 1992; Forood et al., 1993; Shalongo et al., 1994). During thermal CD studies of amylin-related peptides in water containing intermediate levels of HFIP, cold-denaturation -- peptide unfolding upon cooling, for monomeric peptide helices was first observed for the first time. This observation was first presented at the 36th Experimental NMR Conference (Liu & Andersen 1995), and later published as a J. Am. Chem. Soc. communication (Andersen et al., 1996a). Cold denaturation at intermediate levels ("4%-10%") of HFIP was generally observed for all peptides studied in our laboratory. This section summarizes previously unpublished data for the investigation of the cold denaturation phenomenon done on amylin-related fragments, and will include the data on peptides which will be presented in chapter 6.

The CD spectra at three temperatures – the low- and high- temperature extreme and at the temperature which displays maximal helicity for S2U7 in 8% HFIP and sCT(1-20)G in 5% HFIP are shown in Figures 5.49 and 5.50. These represent typical thermal behavior observed for monomeric peptides at an intermediate level of HFIP: unfolding upon cooling and melting upon warming. Moreover, this effect was seen to lack concentration dependence. Cold denaturation can be detected at different wavelength as shown in Figure 5.51. Generally, the helix is more sensitive to cooling than warming (as shown in Figure 5.49-50); which is consistent with some early reports of inverted transitions in organic media (Doty & Yang, 1956; Calvin et al., 1959). Unlike typical thermal unfolding in high HFIP media, the CD traces do not go through a single isodichroic, as the 'isodichroic' for cold denaturation is red shifted relative to melting. To date, cold denaturation for monomeric peptides has only been observed in 4-10 vol% HFIP, and not observed at the corresponding degree of helix induction with TFE, as illustrated in Figure 5.52. The extent of cold denaturation differs for a peptide at different concentrations of HFIP. Figure 5.53 shows a thermal study of hCGRP(1-21) in different levels of HFIP. In 0% and 25% HFIP, $[\theta]_{221}$ almost shows a linear

dependence on temperature; while at both 6% and 8% HFIP, cold denaturation was observed, (to larger extent at 8% HFIP). Also, the temperature at which maximum helicity is reached is lower in 8% HFIP than the one in 6%.

Among different peptides, the HFIP-level for maximum cold denaturation is also distinct. For instance, the cold denaturation is more pronounced for sCT(1-20)G in 5% HFIP than S2U7 in 8% HFIP (compare Figures 5.49 and 5.50); it is even more dramatic for the D-Leu^{12}-pram in 9% HFIP (as shown in Figure 5.54). All three peptides reached their maximum cold denaturation at those levels of HFIP. In addition, the temperature at which the maximum helicity was observed for each peptide is different at different levels of added HFIP.

Table 5.7 reports the thermal CD data for each peptide at intermediate levels of HFIP. $-[\theta]_{221}$ and $[\theta]_{191}$ values are recorded at key temperatures, including the lowest and highest temperatures examined and the temperature at which maximum helicity was noted. In addition, the exact location of the minimum, which shifts from 198nm (for a random coil) to 208nm (for an exclusively helical state) is listed. The corresponding values for 0% and 25% HFIP, (which facilitate the calculation of fractional changes in helicity during the thermal study at intermediate HFIP levels), are also recorded.

Thermal difference CD spectra provide experimental clues to reveal the nature of cold denaturation. The ΔCD spectra of c23Y appear in Figure 5.55. The shape of the ΔCD traces on warming and cooling are very similar; and correspond to the CD characteristics of an α-helix. This indicates a loss of α-helix in both processes, instead of other secondary structure involvement. NMR studies confirm the phenomenon suggested by the temperature dependent CD data. αH values move toward the random coil reference values both upon warming and cooling. Hα-CSD histograms of S2U7 at three temperatures in 8% HFIP appear in Figure 5.56; and the corresponding CD studies appear in Figure 5.57. Upon cooling, αH CSDs become less negative, indicating loss of helicity. This is a highly cooperative process as CSDs get smaller at each residue for the entire helical span. It is also shown in the CSD histograms that the helix is more sentitive to cooling than warming The mechanism of cold denaturation at an intermediate level of HFIP is not fully understood. It has been suggested that the cold denaturation is a solvophobic effect associated with a differential exposure of nonpolar surfaces. HFIP addition favors peptide helices by a medium effect that destabilizes the random coil state rather than stabilizing interactions between the helix and the HFIP. Measurable positive

ΔCp values are associated with the unfolding of monomeric helices; these can be as large as +140±10 JK^{-1}/helical-residue (Andersen et al. 1996a).

5.7 *Conclusions*

Ten amylin helix related peptides have been studied by both NMR and CD. All amylin fragments studied behave similarly to their parent peptide in buffer and 25% HFIP. All mutations, either deletion or substitution did not significantly alter the conformational preference of the amylin helix. These observations suggest that neither the disulfide closure nor the NN sequence is a prerequisite for such helix formation, and the intrinsic helix propensity is embedded in the sequence rather than a few specific residues.

Despite all the similarities among these amylin-related peptides, significant differences were noticed: 1) The C-terminal portion of amylin (residue 23 and onward) has some stabilizing effect on the helical domain, as in the absence of HFIP, the largest fragment (hAM(1-22)G) is slightly less helical than the pramlintide by CD. The role of the NN sequence as a C-cap is not very clear, and Asn^{21} is not an effective C-cap. However, the deletion of the $N^{21}N^{22}$ sequence does make the last turn of the helix slightly less helical in 25% HFIP. In contrast, addition of a Tyr at the end of a sequence generally stabilizes the helix as compared to the sequence without it.

2) The nucleating role of the disulfide is clearly evident. It stabilizes the helix as all fragments with the disulfide ring have significantly higher helix population in buffer than the ones without it. The disulfide traps one turn of helix in the loop even in the highly denaturating medium. However, the geometry of the loop prevents residue Thr^4 from adopting a helical conformation, as the helix in all cyclic species starts at Ala^5. In the absence of the disulfide, Asn^3 is an effective N-cap, with Thr^4 as the first helical residue both in water and aqueous HFIP. The characteristic pattern of NH shift deviations at Thr^4 and Ala^5 observed for pramlintide (and cyclic fragments) is the result of interactions within the disulfide ring.

3) The introduction of single Aib at position 7 is as at least as effective as disulfide closure in nucleating the helix. The Aib containing fragments are significantly more helical than the non-cyclic species in the absence of HFIP.

The R18H mutation resembles the differences seen between the helical domain of rat and human amylin. His^{18} serves as an effective C-cap of the helix in aqueous buffer, but the helix extends beyond this residue in aqueous HFIP. Arg^{18}, which has

higher helix propensity than His, stabilizes the one turn of helix immediately before it better than His[18].

Cold denaturation of amylin related peptides was investigated as ancillary project in this chapter. This phenomena is another manifestation of how media and temperature can greatly influence conformational preferences of monomeric peptides.

In this chapter, the results obtained from NMR and CD are complementary and reinforce each other. It has been demonstrated that the combination of the two techniques is a very powerful means of evaluating the conformational preferences of small to medium sized peptides.

Table 5.1 Backbone Proton Chemical Shifts of c23Y [hAM(1-22)GY] and c23 [hAM(1-22)G] in Buffer and in 25% HFIP at 285K

c23Y	Buffer		25% HFIP		c23	Buffer		25% HFIP	
residue	αH	NH	αH	NH	residue	αH	NH	αH	NH
Lys^{1}	–	–	4.12	–	Lys^{1}	4.03	–	4.26	–
Cys^{2}	–	–	4.92	8.99	Cys^{2}	4.72	9.03	4.96	8.98
Asn^{3}	–	–	5.10	9.06	Asn^{3}	5.00	9.00	5.08	9.05
Thr^{4}	–	–	4.65	7.61	Thr^{4}	4.54	7.68	4.67	7.56
Ala^{5}	–	–	4.26	8.87	Ala^{5}	4.21	8.73	4.25	8.86
Thr^{6}	–	–	4.07	8.12	Thr^{6}	4.24	7.96	4.05	8.07
Cys^{7}	–	–	4.42	7.88	Cys^{7}	4.59	8.15	4.42	7.81
Ala^{8}	–	–	4.12	8.30	Ala^{8}	4.32	8.23	4.11	8.31
Thr^{9}	–	–	4.06	8.28	Thr^{9}	4.24	8.17	4.05	8.28
Gln^{10}	–	–	4.10	7.96	Gln^{10}	4.29	8.31	4.10	7.91
Arg^{11}	–	–	4.15	8.04	Arg^{11}	4.29	8.36	4.16	8.06
Leu^{12}	–	–	4.36	8.08	Leu^{12}	4.34	8.25	4.35	8.12
Ala^{13}	–	–	4.13	8.81	Ala^{13}	4.22	8.28	4.13	8.79
Asn^{14}	–	–	4.51	8.22	Asn^{14}	4.61	8.30	4.52	8.23
Phe^{15}	–	–	4.45	8.38	Phe^{15}	4.59	8.08	4.45	8.40
Leu^{16}	–	–	3.93	9.24	Leu^{16}	4.31	8.10	3.92	9.24
Val^{17}	–	–	3.68	8.97	Val^{17}	4.00	8.02	3.67	8.98
His^{18}	–	–	4.42	7.88	His^{18}	4.77	8.67	4.38	7.90
Ser^{19}	–	–	4.27	8.39	Ser^{19}	4.50	8.59	4.25	8.44
Ser^{20}	–	–	4.40	7.88	Ser^{20}	4.50	8.48	4.40	7.88
Asn^{21}	–	–	4.81	7.98	Asn^{21}	4.76	8.57	4.84	7.87
Asn^{22}	–	–	4.72	8.27	Asn^{22}	4.72	8.54	4.76	8.31
Gly^{23}	–	–	3.93	8.33	Gly^{23}	3.92	8.46	3.99	8.41
Tyr^{24}	–	–	4.59	7.97					

Note: c23Y was not examined in buffer.

Table 5.2 Backbone Proton Chemical Shifts of c21Y[hAM(1-20)GY] and c21 [hAM(1-20)G] in Buffer and in 25% HFIP at 285K

c21Y	Buffer		25% HFIP		c21	Buffer		25% HFIP	
residue	αH	NH	αH	NH	residue	αH	NH	αH	NH
Lys^{1}	4.02		4.11		Lys^{1}	4.02		4.12	
Cys^{2}	4.71	9.05	4.94	9.00	Cys^{2}	4.73	9.03	4.93	8.96
Asn^{3}	5.00	9.04	5.03	9.07	Asn^{3}	5.00	9.01	5.09	9.03
Thr^{4}	4.53	7.67	4.66	7.59	Thr^{4}	4.53	7.66	4.65	7.61
Ala^{5}	4.22	8.77	4.26	8.91	Ala^{5}	4.20	8.75	4.25	8.82
Thr^{6}	4.29	8.00	4.07	8.14	Thr^{6}	4.29	7.97	4.07	8.08
Cys^{7}	4.56	8.17	4.42	7.90	Cys^{7}	4.56	8.13	4.43	7.88
Ala^{8}	4.29	8.26	4.12	8.30	Ala^{8}	4.28	8.23	4.11	8.28
Thr^{9}	4.23	8.20	4.06	8.30	Thr^{9}	4.22	8.16	4.06	8.25
Gln^{10}	4.27	8.31	4.09	7.96	Gln^{10}	4.27	8.28	4.10	7.93
Arg^{11}	4.27	8.36	4.15	8.03	Arg^{11}	4.28	8.33	4.16	8.09
Leu^{12}	4.33	8.24	4.36	8.08	Leu^{12}	4.33	8.21	4.34	8.08
Ala^{13}	4.21	8.28	4.12	8.81	Ala^{13}	4.18	8.25	4.12	8.73
Asn^{14}	4.60	8.31	4.51	8.22	Asn^{14}	4.60	8.26	4.56	8.34
Phe^{15}	4.56	8.09	4.45	8.38	Phe^{15}	4.56	8.08	4.37	8.57
Leu^{16}	4.28	8.11	3.92	9.23	Leu^{16}	4.24	8.10	3.90	9.23
Val^{17}	3.96	8.01	3.71	8.95	Val^{17}	4.16	8.26	3.78	8.61
His^{18}	4.74	8.63	4.45	7.88	His^{18}	4.68	8.46	4.34	8.34
Ser^{19}	4.48	8.49	4.28	8.40	Ser^{19}	4.48	8.51	4.15	8.32
Ser^{20}	4.46	8.61	4.36	7.87	Ser^{20}	4.51	8.61	4.44	7.72
Gly^{21}	3.89	8.48	3.96	8.00	Gly^{21}	3.94	8.51	3.98	7.93
Tyr^{22}	4.50	8.14	4.51	7.89					

Table 5.3 Backbone Proton Chemical Shifts of S2,7 [S2,7-hAM(1-20)G] and A2,7 [A2,7-hAM(1-20)G] in Buffer and in 25% Aqueous HFIP at 285K, and 17mer [Ac-hAM(5-20)G] in 30% HFIP at 295K

S2,7	buffer		25% HFIP		A2,7	buffer		25% HFIP		17mer	buffer		30% HFIP	
residue	αH	NH	αH	NH	residue	αH	NH	αH	NH	residue	αH	NH	αH	NH
Lys[1]	4.07	–	4.16	–	Lys[1]	4.01	–	4.13	–		–	–		
Ser[2]	4.53	8.89	4.65	8.90	Ala[2]	4.37	8.86	4.47	8.78		–	–		
Asn[3]	4.80	8.82	4.93	8.90	Asn[3]	4.76	8.79	4.88	8.60		–	–		
Thr[4]	4.31	8.27	4.24	8.35	Thr[4]	4.30	8.27	4.16	8.26	Ac	–	–		
Ala[5]	4.40	8.46	4.34	8.35	Ala[5]	4.40	8.49	4.33	8.23	Ala[5]	–	–	4.32	7.85
Thr[6]	4.37	8.27	4.20	8.23	Thr[6]	4.30	8.27	4.10	8.19	Thr[6]	–	–	4.35	8.07
Ser[7]	4.46	8.43	4.45	8.29	Ala[7]	4.28	8.49	4.23	8.06	Cys[7]	–	–	4.50	8.18
Ala[8]	4.34	8.53	4.17	8.53	Ala[8]	4.30	8.43	4.14	8.48	Ala[8]	–	–	4.20	8.26
Thr[9]	4.22	8.12	4.02	8.01	Thr[9]	4.24	8.13	4.05	8.07	Thr[9]	–	–	4.04	7.97
Gln[10]	4.27	8.29	4.08	8.04	Gln[10]	4.29	8.39	4.09	8.18	Gln[10]	–	–	4.11	7.94
Arg[11]	4.27	8.37	4.11	7.96	Arg[11]	4.28	8.39	4.12	8.03	Arg[11]	–	–	4.12	7.95
Leu[12]	4.32	8.25	4.34	8.14	Leu[12]	4.33	8.29	4.36	8.13	Leu[12]	–	–	4.35	8.07
Ala[13]	4.21	8.27	4.11	8.74	Ala[13]	4.21	8.32	4.13	8.82	Ala[13]	–	–	4.13	8.62
Asn[14]	4.59	8.29	4.50	8.20	Asn[14]	4.57	8.10	4.51	8.25	Asn[14]	–	–	4.51	8.16
Phe[15]	4.57	8.06	4.43	8.36	Phe[15]	4.60	8.32	4.46	8.40	Phe[15]	–	–	4.44	8.33
Leu[16]	4.29	8.09	3.91	9.21	Leu[16]	4.30	8.11	3.93	9.25	Leu[16]	–	–	3.94	9.14
Val[17]	3.99	8.00	3.68	8.94	Val[17]	4.00	8.04	3.69	8.98	Val[17]	–	–	3.72	8.89
His[18]	4.76	8.65	4.37	7.88	His[18]	4.76	8.69	4.38	7.91	His[18]	–	–	4.41	7.86
Ser[19]	4.49	8.48	4.27	8.36	Ser[19]	4.49	8.52	4.29	8.38	Ser[19]	–	–	4.31	8.32
Ser[20]	4.50	8.61	4.43	7.84	Ser[20]	4.50	8.64	4.45	7.85	Ser[20]	–	–	4.46	7.82
Gly[21]	3.94	8.50	3.97	8.01	Gly[21]	3.94	8.54	3.98	8.03	Gly[21]	–	–	3.98	7.99

Note: Ac-hAM(5-20)G was not examined in buffer.

Table 5.4 Backbone Proton Chemical Shifts of S2U7Y [S2U7-hAM(1-20)GY], S2U7 [S2U7-hAM(1-20)G] and R18Y [R18-hAM(1-20)GY] in Buffer and in 25% Aqueous HFIP at 285K

S2U7Y	buffer		25% HFIP		S2U7	buffer		25% HFIP		R18Y	buffer		25% HFIP	
residue	αH	NH	αH	NH	residue	αH	NH	αH	NH	residue	αH	NH	αH	NH
Lys[1]	–	–	4.16	–	Lys[1]	4.06	–	4.16	–	Lys[1]	4.03	/	4.11	–
Ser[2]	–	–	4.68	8.89	Ala[2]	4.53	8.92	4.68	8.90	Ala[2]	4.72	9.05	4.92	8.97
Asn[3]	–	–	4.87	8.99	Asn[3]	4.81	8.87	4.88	9.00	Asn[3]	5.01	9.03	5.08	9.04
Thr[4]	–	–	4.14	8.26	Thr[4]	4.27	8.29	4.14	8.26	Thr[4]	4.53	7.68	4.64	7.61
Ala[5]	–	–	4.31	8.16	Ala[5]	4.38	8.47	4.31	8.16	Ala[5]	4.21	8.77	4.25	8.84
Thr[6]	–	–	4.03	8.09	Thr[6]	4.27	8.23	4.03	8.09	Thr[6]	4.30	7.99	4.07	8.11
Aib[7]	–	–	–	8.16	Aib[7]	–	8.56	–	8.17	Cys[7]	4.57	8.17	4.42	7.92
Ala[8]	–	–	4.08	8.25	Ala[8]	4.21	8.01	4.09	8.25	Ala[8]	4.31	8.25	4.11	8.28
Thr[9]	–	–	4.06	8.07	Thr[9]	4.20	8.01	4.06	8.08	Thr[9]	4.23	8.19	4.06	8.27
Gln[10]	–	–	4.14	8.15	Gln[10]	4.27	8.16	4.15	8.16	Gln[10]	4.28	8.32	4.08	7.94
Arg[11]	–	–	4.12	8.11	Arg[11]	4.26	8.26	4.12	8.11	Arg[11]	4.28	8.37	4.16	8.05
Leu[12]	–	–	4.36	8.17	Leu[12]	4.31	8.22	4.36	8.18	Leu[12]	4.33	8.26	4.32	8.04
Ala[13]	–	–	4.12	8.69	Ala[13]	4.20	8.26	4.12	8.69	Ala[13]	4.21	8.29	4.10	8.73
Asn[14]	–	–	4.50	8.28	Asn[14]	4.58	8.30	4.50	8.28	Asn[14]	4.60	8.31	4.34	8.04
Phe[15]	–	–	4.45	8.38	Phe[15]	4.56	8.08	4.44	8.38	Phe[15]	4.56	8.10	4.33	8.18
Leu[16]	–	–	3.92	9.22	Leu[16]	4.28	8.11	3.92	9.23	Leu[16]	4.29	8.12	3.88	9.12
Val[17]	–	–	3.71	8.94	Val[17]	3.98	8.02	3.69	8.96	Val[17]	4.02	8.10	3.68	8.76
His[18]	–	–	4.45	7.88	His[18]	4.74	8.66	4.38	7.92	Arg[18]	4.36	8.49	4.15	8.15
Ser[19]	–	–	4.28	8.40	Ser[19]	4.48	8.50	4.28	8.37	Ser[19]	4.47	8.50	4.20	8.37
Ser[20]	–	–	4.36	7.86	Ser[20]	4.49	8.63	4.44	7.85	Ser[20]	4.45	8.47	4.34	7.81
Gly[21]	–	–	4.03	7.99	Gly[21]	3.93	8.53	3.98	8.03	Gly[21]	3.90	8.44	3.96	7.98
Tyr[22]	–	–	4.52	7.88						Tyr[22]	4.52	8.12	4.50	7.90

Note: S2U7-hAM(1-20)G was not examined in buffer.

Table 5.5 CD Data for Amylin-Related Peptides

Peptide	In GdnCL	In Buffer			$Titr_{50}$	In 25% HFIP		
	Formula (xM)	Formula	$R1_{273\|298K}$	$R2_{273\|298K}$	% HFIP	Formula	$R1_{273\|298K}$	$R2_{273\|298K}$
Ref:								
Human amylin*	N.A.	N.A.	N.A.	N.A.	N.A.	-23350+150T	-1.96 | N.A.	N.A.
Pramlintide *	-1065-40T (7.5) -2050-33T (5.0)	-3700-26T	+0.22 | N.A.	N.A.	6.3	-18300+105T	-1.56 | -1.44	N.A.
D-Leu[12]-Pramlintide	-850 -31T (7.1)	-2110-24T	0.47 | 0.44	0.12 | 0.19	9	-14300+105T	-1.57| 1.39	0.86 | 0.77
Non-cyclic:								
A2,7-hAM(1-20)G	+1050-52T (7.5) +100-42T (4.5)	-1700-14T	0.52 | 0.52	0.11 | 0.13	6.5	-24300+130T	-2.15 | -2.05	0.94 | 0.87
S2,7-hAM(1-20)G	+1020-52T (7.5)	-2400+3T*	0.46 | 0.46	0.13 | 0.14	7.6	-25800+135T	-2.11 | -2.03	0.93 | 0.87
Ac-hAM(5-20)G	N.A.	-3760+26T*	0.21 | 0.29	0.24 | 0.21	10	-26700+118T	-2.*11* | -2.12	N.A. | 0.89
S2U7-hAM(1-20)G	+620-42T (7.7) -620-30T (6.0)	-3630+26T*	0.31 | 0.29	0.23 | 0.21	5.5	-25900+144T	-2.16 | -2.07	0.96 | 0.90
S2U7-hAM(1-20)GY	N.A.	-3280+30T	N.A. | *-0.30*	N.A.| 0.21	N.A.	-24200	-2.11 | N.A.	N.A. | N.A.
Cyclic:								
hAM(1-20)G	-1000-31T (7.7)	-2710+17T*	N.A. | -0.05	N.A. | 0.29	7.5	-25200+142T	-2.08 | -2.03	N.A. | 0.91
hAM(1-20)GY	N.A.	-3400+30T*	.003 | -0.18	0.39 | 0.28	7	-22700+111T	-2.19 | -2.17	0.96 | 0.91
hAM(1-22)G	N.A.	-3110+8T*	N.A. | 0.89	N.A. | 0.28	6.5	-24500+149T	-2.04 | -2.01	0.97 | 0.90
hAM(1-22)GY	N.A.	-4200+34T*	-0.09 | 0.10	0.41 | 0.33	6.5	-22600+125T	-2.03 | -1.98	0.95 | 0.90
R18-hAM(1-20)GY#	N.A.	-3520+42T	-0.16 | -0.13	0.37 | 0.26	6.7	-23000+134T	-2.07 | -1.98	0.95 | 0.87

R18-hAM(1-20)GY was found to be impure by NMR. The reported CD values are thus suspect.

* Data adapted from the Ph.D. thesis of Cort (1997).

Footnotes to Table 5.5:

All [θ] values given are 221nm or at the minimum which appears within 2nm of that wavelength. The fragments are listed (in each category) in order of increasing helicity in aqueous medium.

Ellipticities in each column are given as a formula that will reproduce the observed values over the 0 – 30 °C range. The gradient was measured over this range when possible. A number of species display non-linear behavior in aqueous buffer; the value of $-[\theta]_{221}$ first decreases (+ve gradient) then increases on warming as illustrated in Figure 5.46 – these are indicated by *, and the gradients reflect the values observed at lower temperatures. The titration mid-point ($titr_{50}$) reported is for a HFIP titration at 298 K. All measurements were made using aqueous buffer at pH 4.2 ± 0.2 (prior to denaturant or fluoroalcohol addition).

Table 5.6 Helicities of Amylin-Related Peptides (Derived from the Combined Analysis of NMR and CD Data).

Peptide	No. of residues (From gradient)	NMR helical span	$\langle f_H \rangle_{CD}$
Pramlintide	4.6/37	$Ala^5 - Val^{17}$	0.423*
Ac-hAM(5-20)G	5.0/17	$Ala^5 - Val^{17}$	0.100
A2,7-hAM(1-20)G	3.5/21	$Thr^4 - Val^{17}$	0.100
S2,7-hAM(1-20)G	4.7/21	$Thr^4 - Val^{17}$	0.125
S2U7-hAM(1-20)G	6.3/21	$Thr^4 - Val^{17}$	0.180
S2U7-hAM(1-20)GY	6.9/22	$Thr^4 - Val^{17}$	0.200
hAM(1-20)G	5.6/21	$Ala^5 - Val^{17}$	0.148
hAM(1-20)GY	6.9/22	$Ala^5 - Val^{17}$	0.233
R18-hAM(1-20)GY *	7.8/22	$Ala^5 - Val^{17}$	0.238
hAM(1-22)G	5.5/23	$Ala^5 - Val^{17}$	0.183
hAM(1-22)GY	7.9/24	$Ala^5 - Val^{17}$	0.295

* The estimate for pramlintide is clearly an over-estimate – apparently some of the turns or other features outside of the $Ala^5 - Val^{17}$ span contribute a negative ellipticity at 221nm.

Table 5.7 CD Data of Cold Denaturation Studies of Amylin-Related Peptides

Peptide	%HFIP	T(°C)	$-[\theta]_{221}$	λ_{min} (nm)	$[\theta]_{191}$
Pramlintide	0	0	3,840	201	-4,544
		52	4,110	201.2	-3,200
	8	-1	8,385	204.6	n.a.
		28	13,410	206.6	n.a.
		70	9,548	205.8	n.a.
	25	4	17,290	207	30,500
		60	12,380	207	23,380
[D-L^{12}]-pram	0	0	2,110	199.8	-6,210
		64	3,470	200.8	-2,305
	10	1	5,025	203	2,305
		23	9,033	207	12,490
		64	6,178	205	6,590
	25	0	14,250	207.4	25,690
		76	6,200	204.6	9,085
Ac-hAM(5-20)G	0	-1	3,670	200.4	-3,220
		72	3,660	200.0	-3,180
	9	-1	7,100	202.4	5,480
		40	9,730	204.8	14,180
		77	7,250	203.8	9,970
A2,7-hAM(1-20)G	0	0	1,710	198.6	-9,170
		82	3,000	199.2	-4,130
	8	0	6,020	202.4	4,000
		25	15,010	206.6	31,200
		82	6,730	204.8	11,400
	25	0	24,200	207.2	55,200
		82	12,300	206.6	29,500
S2,7-hAM(1-20)G	0	0	2,420	199.2	-8,180
		76	3,280	199.6	-5,500
	8	-1	6,920	187.6	8,750
		25	13,440	190.0	27,030
		78	7,530	189.4	13,200
	25	1	25,920	207.2	58,870
		79	12,990	206.4	30,500
S2U7-hAM(1-20)G	0	0	3,500	200.2	-4,830
		82	3,780	200.0	-4,280
	8	0	9,460	204.4	11,820
		25	15,490	207.0	32,440
		82	8,600	205.8	16,700
	25	-1	26,000	207.6	58,000
		82	13,500	206.8	32,620

Table 5.7 Continue:

hAM(1-20)G	9	-2	13,900	207.0	26,520
		18	17,860	207.8	38,760
		80	8,350	205.8	18,530
R18-hAM(1-20)GY*	0	-3	3,630	202.0	1,630
		75	2,960	201.2	-380
	7	-2	6,530	205.0	9,350
		25	11,740	207.2	23,520
		75	6,800	206.2	13,150
	25	-2	22,980	208.0	50,530
		79	11,650	207.0	27,540
hAM(1-20)GY	0	1	3,650	202.8	1,740
		67	3,000	201.8	200
	8	-1	8,450	206.4	15,100
		25	15,740	207.8	34,940
		83	7,320	206.2	12,200
	25	1	22,660	208.0	51,560
		83	12,000	207.2	27,900
hAM(1-22)GY	0	1	4,250	201.8	900
		67	3,740	201.2	300
	8	0	9,600	206.6	14,610
		25	14,700	207.6	29,700
		65	10,240	207.2	20,000
	25	1	22,500	208.0	48,000
		65	14,00	207.4	31,300
sCT(1-20)G	0	0	2,310	200.0	-3,600
		83	4,060	201.0	1,440
	5	0	4,580	201.6	2,860
		12	7,120	203.6	830
		25	11,100	206.2	24,000
		36	12,500	207.0	28,600
		50	12,050	207.0	27,740
		82	8,850	206.0	18,050
	25	0	25,700	208.6	66,300
		82	16,630	207.8	43,300
hCGRP(1-21)	0	0	7,490	203.2	3,900
		72	4,630	200.6	-1,460
	6	-1	10,720	205.8	13,430
		10	11,080	206.0	14,470
		25	13,020	206.6	18,570
		42	13,680	206.6	21,810
		54	12,520	206.6	20,280
		72	9,780	205.6	15,150
	25	-2	26,600	208.0	51,200
		71	16,300	207.0	31,000

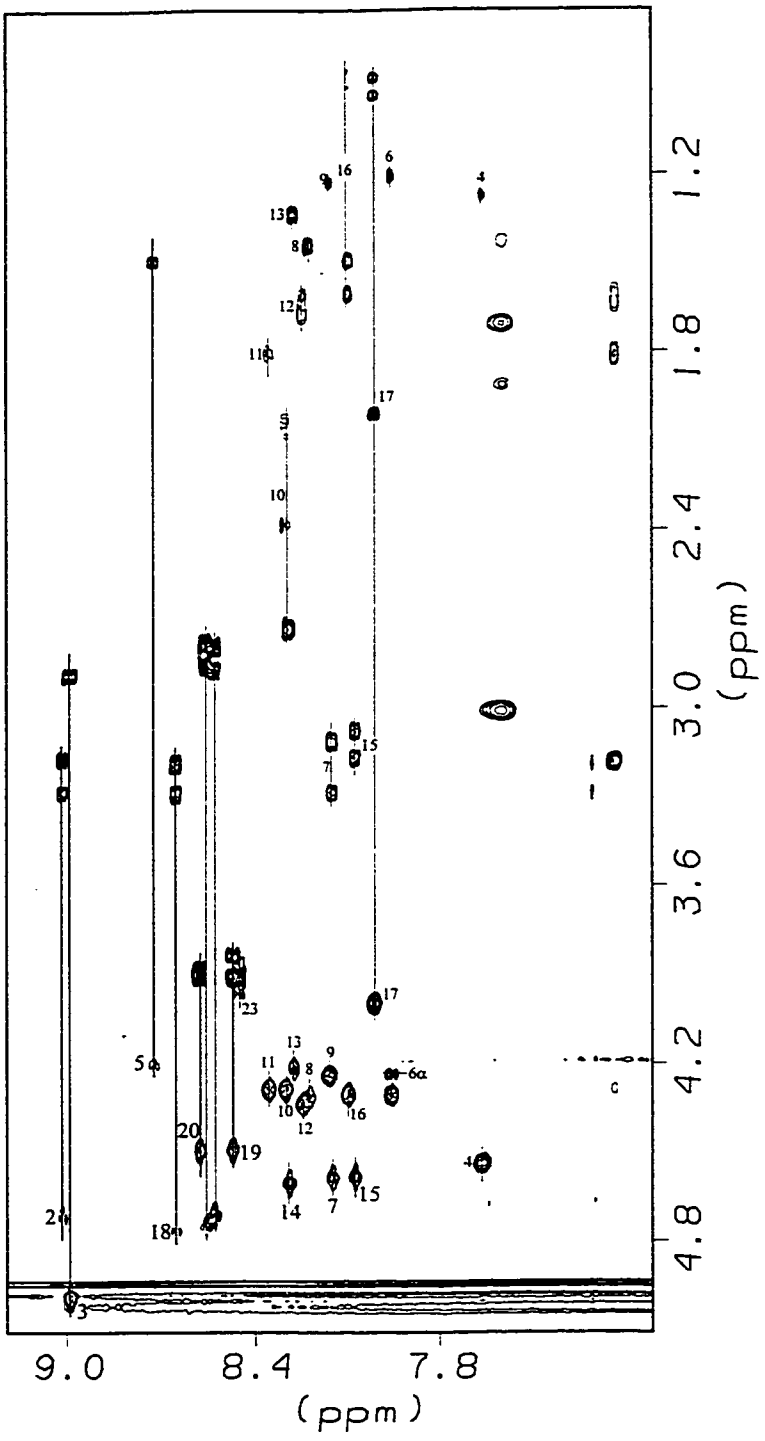

Figure 5.1 αN Region of the TOCSY Spectrum of [hAM(1-22)G] in Buffer.

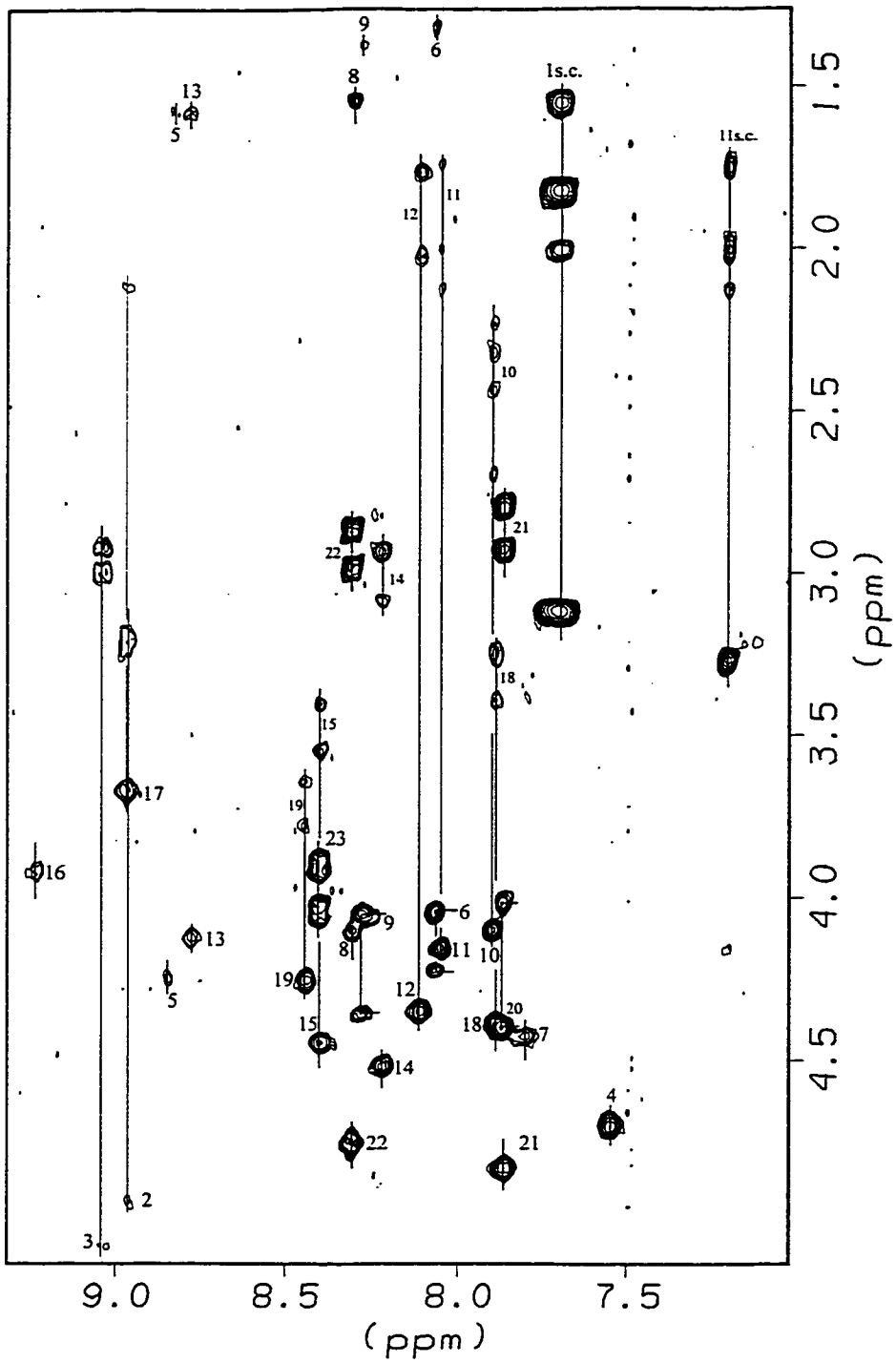

Figure 5.2 αN Region of the TOCSY Spectrum of [hAM(1-22)G] in 25% HFIP.

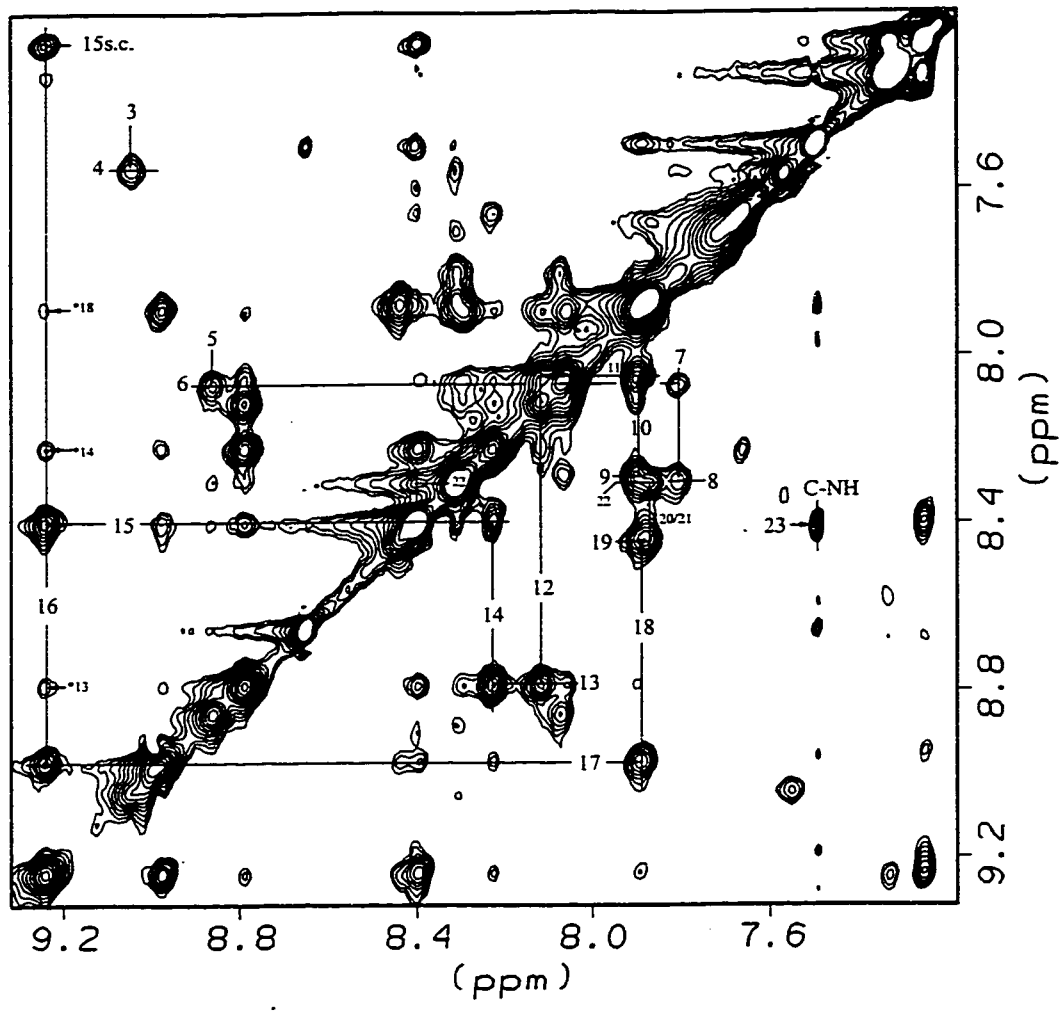

Figure 5.3 NN Region of the NOESY Spectrum of [hAM(1-22)G] in 25% HFIP.

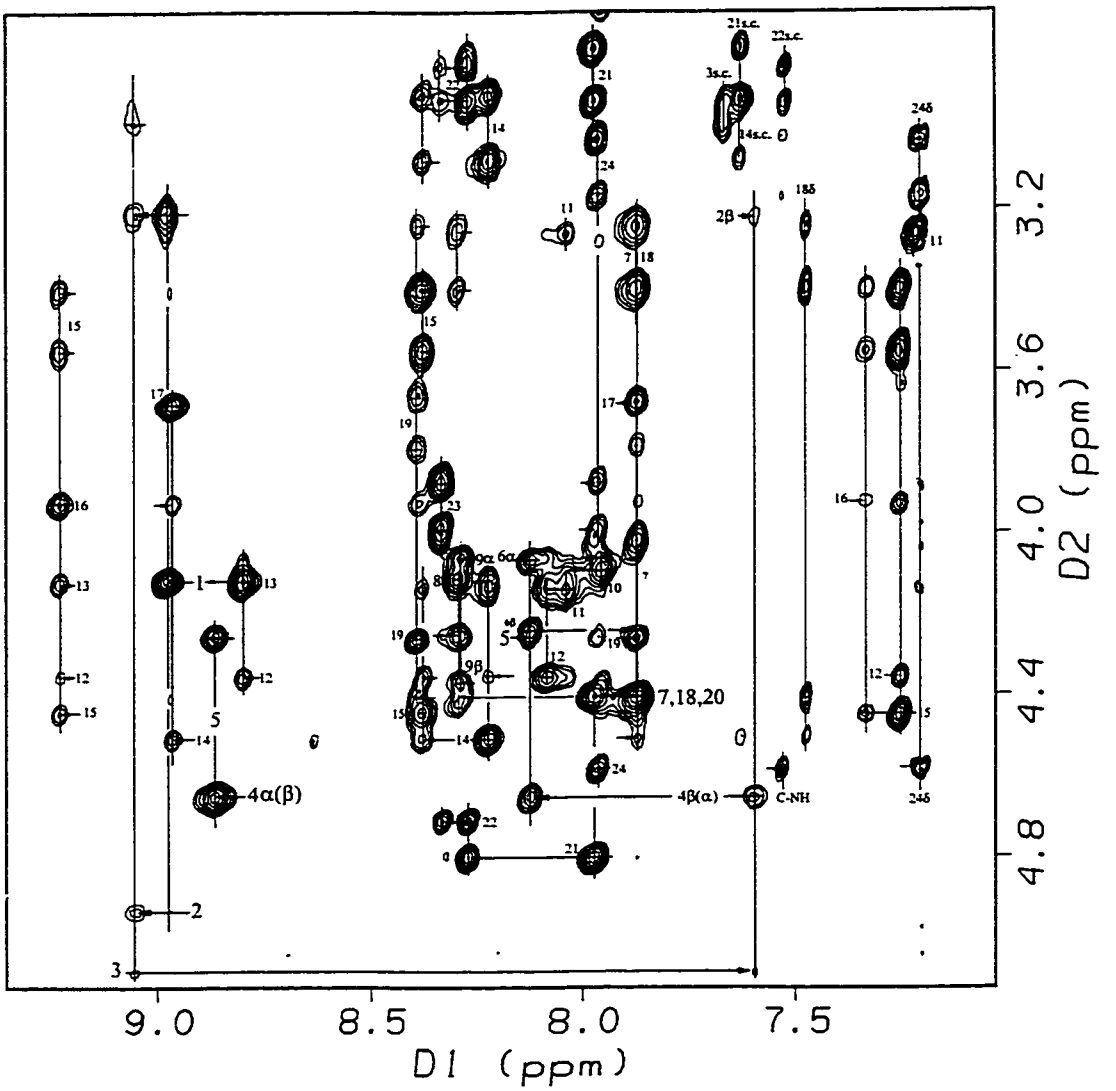

Figure 5.4 αN Region of the NOESY Spectrum of [hAM(1-22)GY] in 25% HFIP.

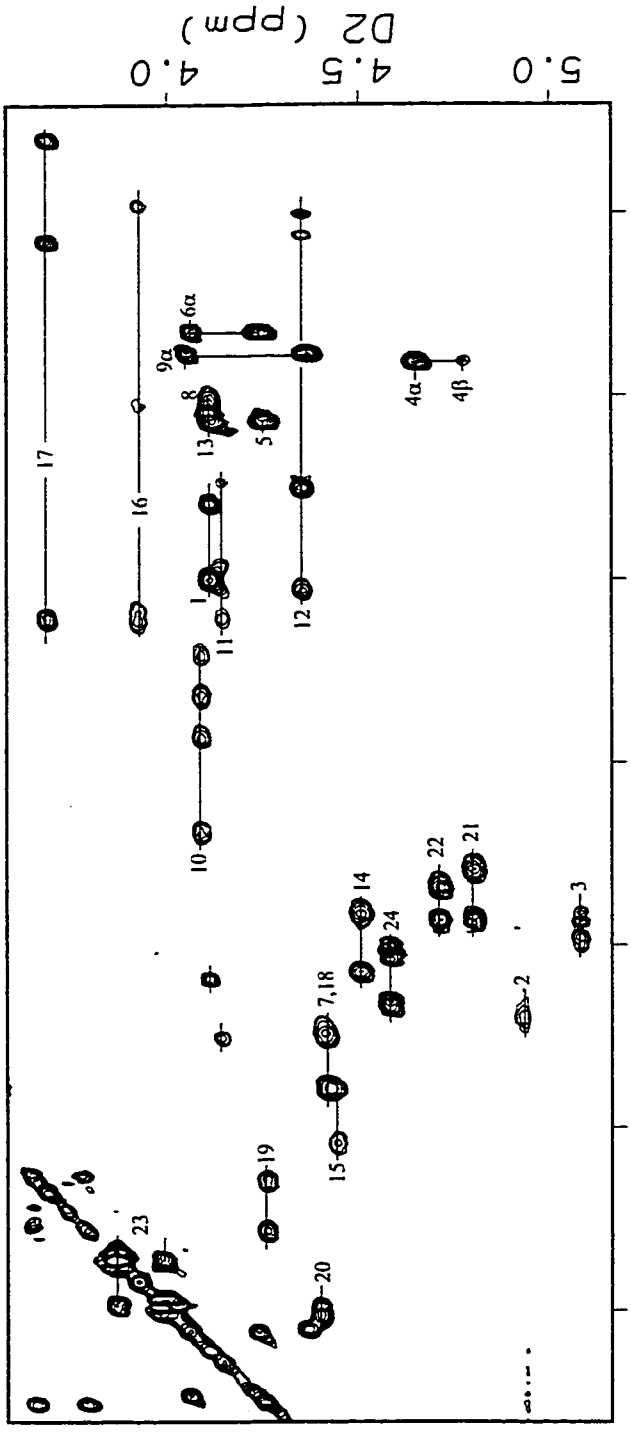

Figure 5.5 α/βγδ Region of the TOCSY Spectrum of [hAM(1-20)GY] in 25% HFIP.

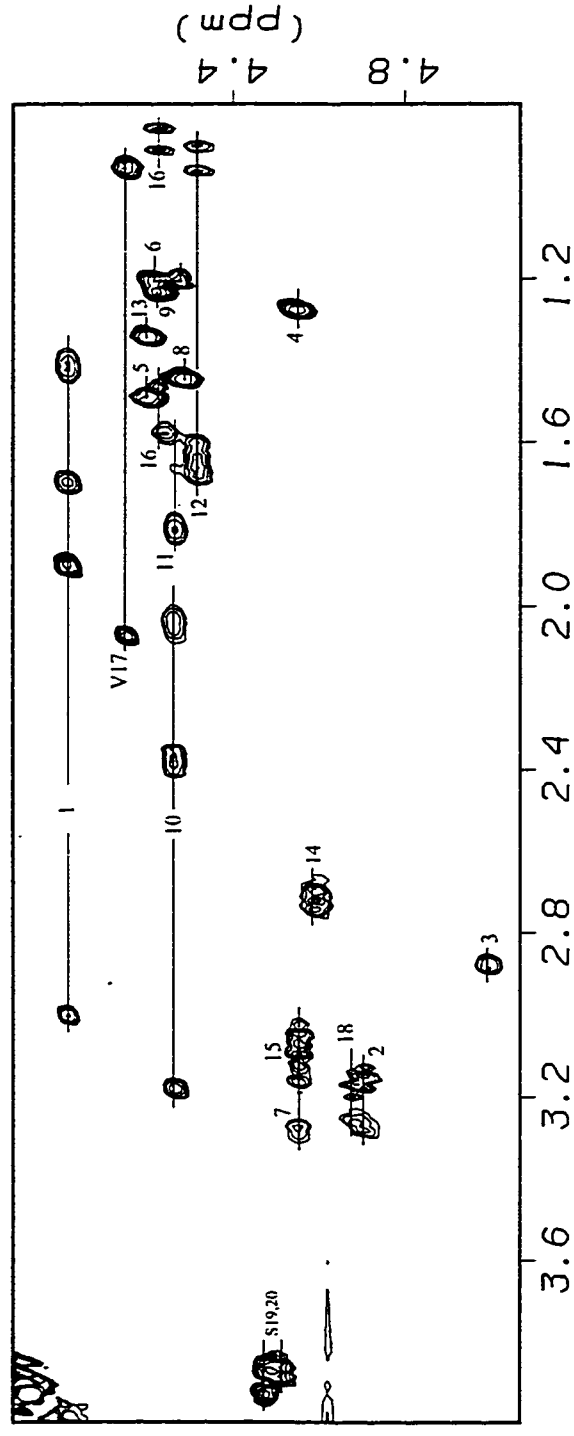

Figure 5.6 α/βγδ Region of the TOCSY Spectrum of [hAM(1-20)G] in Buffer.

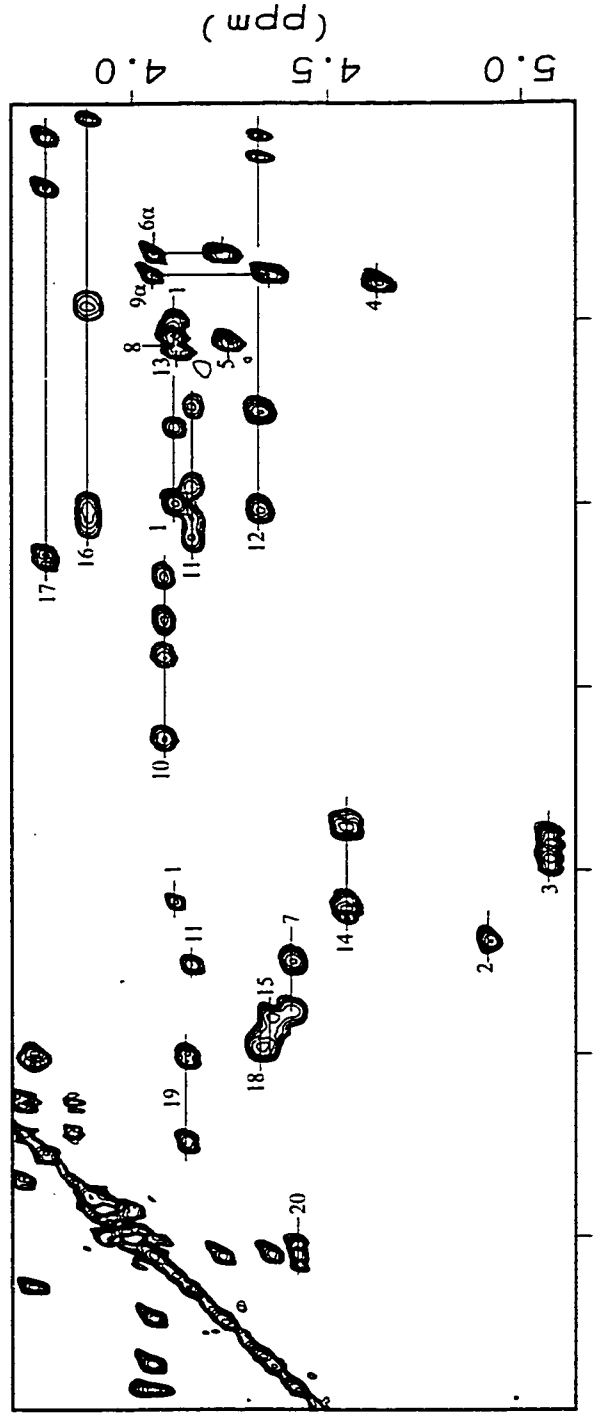

Figure 5.7 α/βγδ Region of the TOCSY Spectrum of [hAM(1-20)G] in 25% HFIP.

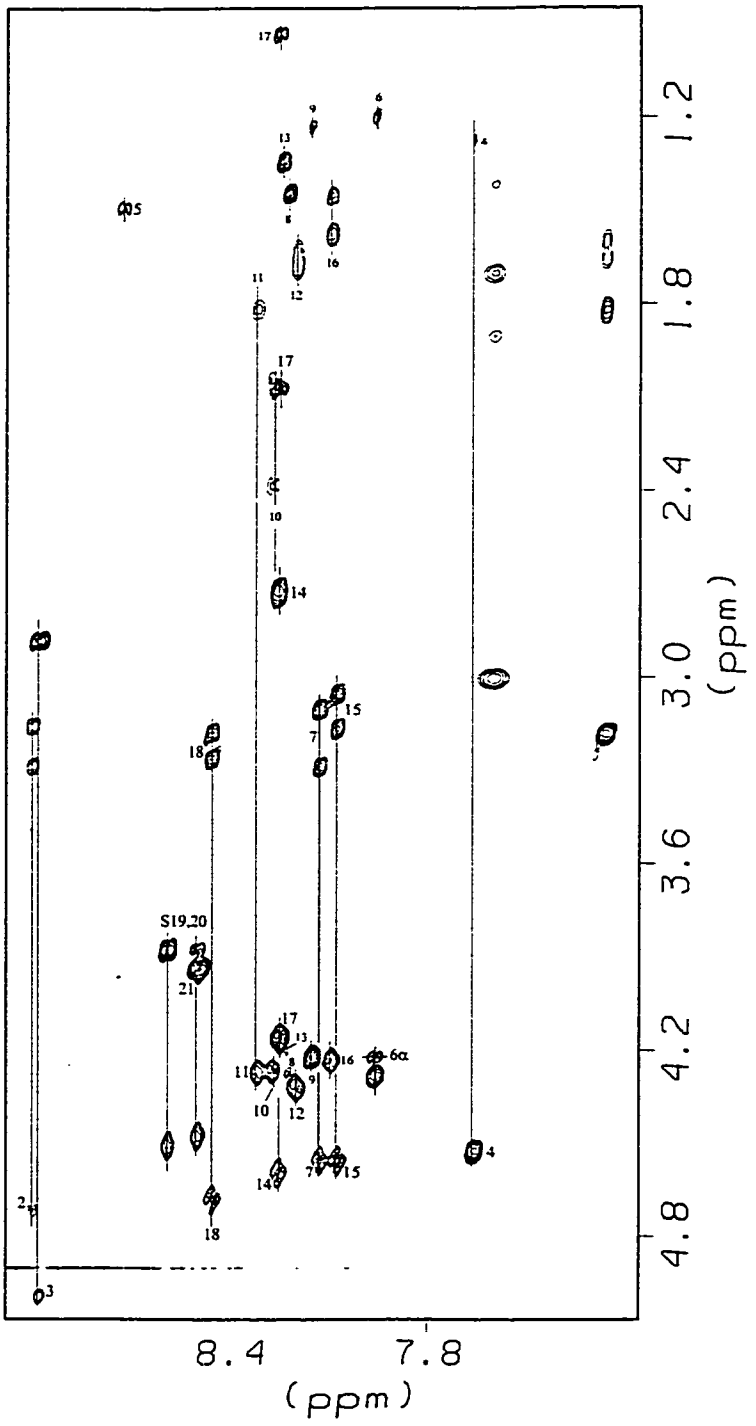

Figure 5.8 αN Region of the TOCSY Spectrum of [hAM(1-20)G] in buffer.

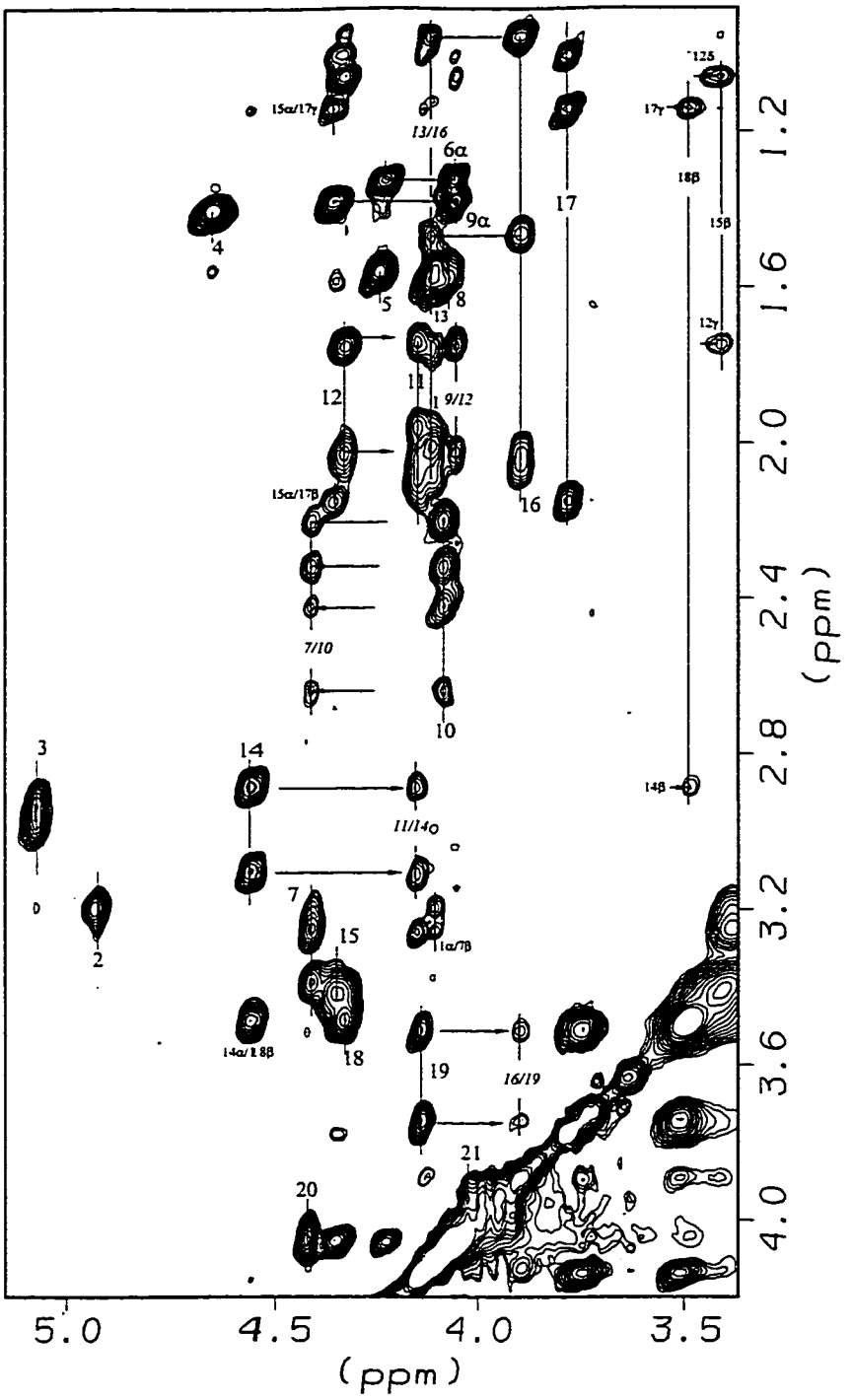

Figure 5.9 αβ Region of the NOESY Spectrum of [hAM(1-20)G] in 25% HFIP.

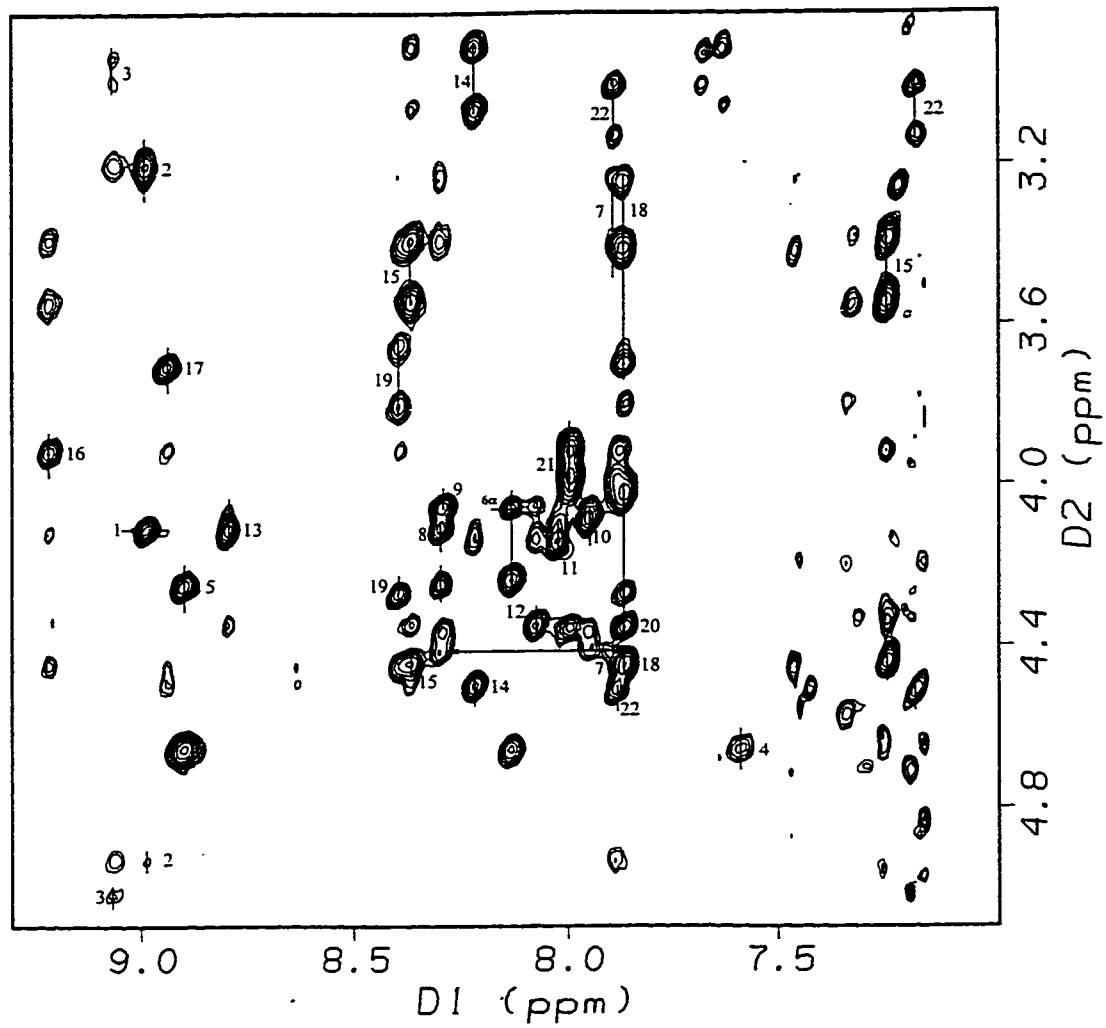

Figure 5.10 αN Region of the NOESY Spectrum of [hAM(1-20)GY] in 25% HFIP.

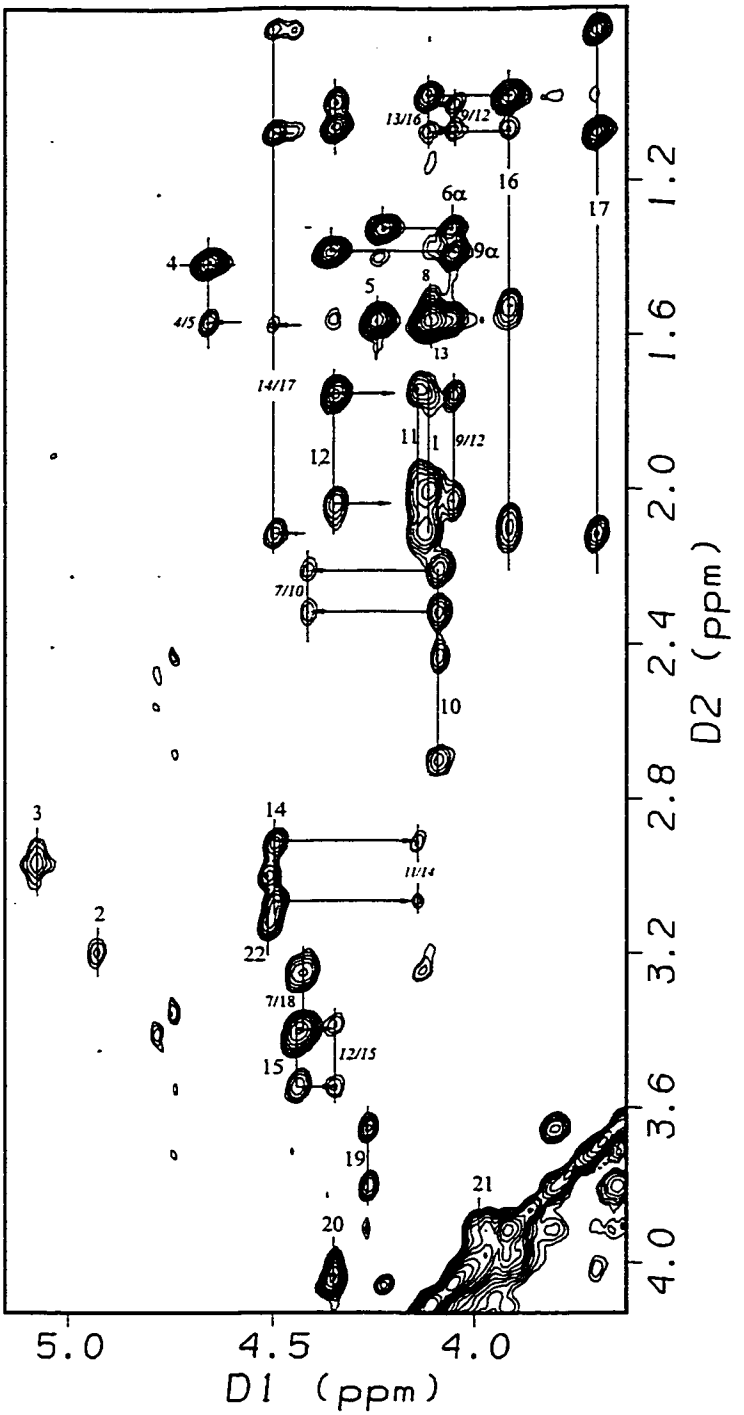

Figure 5.11 αβ Region of the NOESY Spectrum of [hAM(1-20)GY] in 25% HFIP.

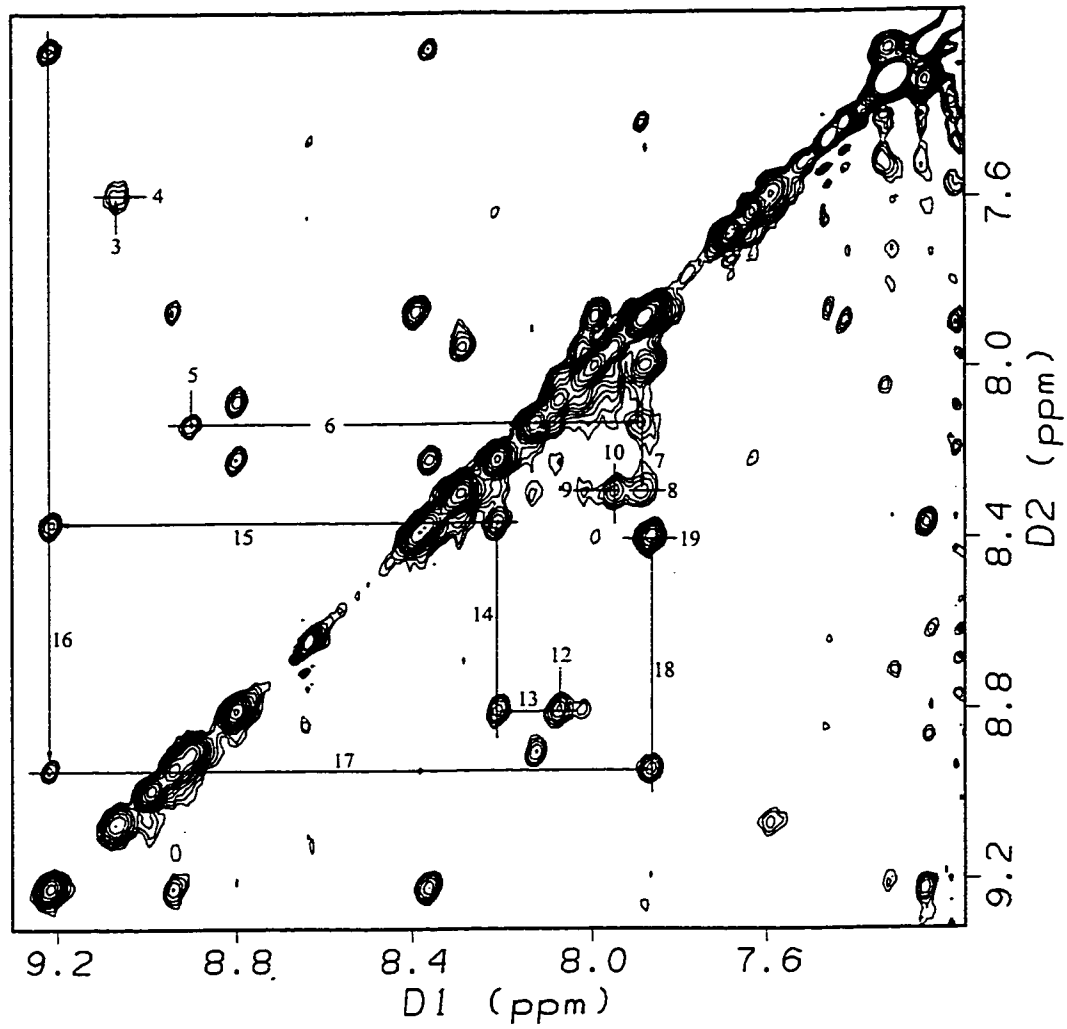

Figure 5.12 NN Region of the NOESY Spectrum of [hAM(1-20)GY] in 25% HFIP.

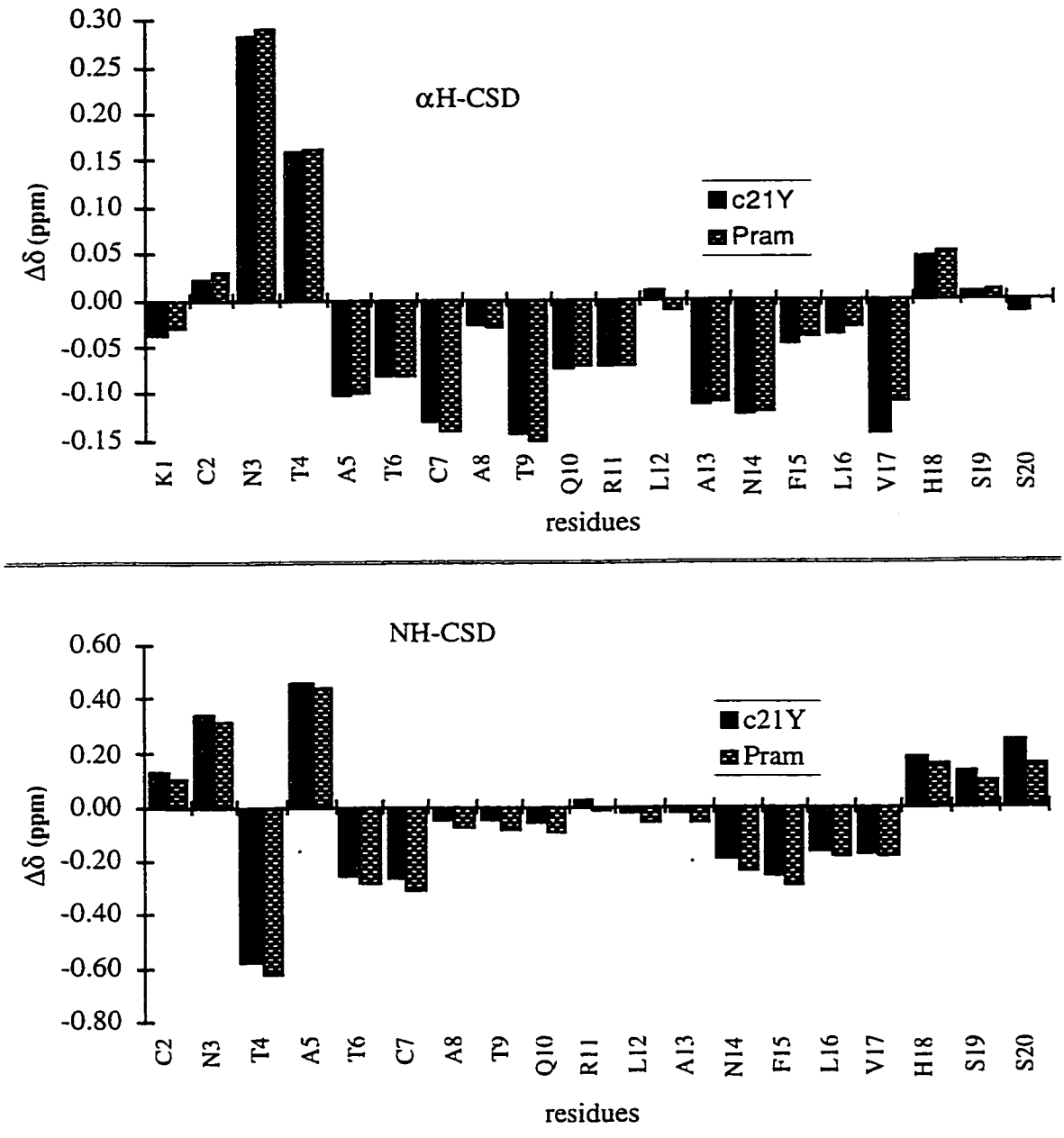

Figure 5.13 αH-CSD and NH-CSD Histograms for c21Y [hAM(1-20)GY], c23Y [hAM(1-22)GY], and Pramlintide in Buffer.

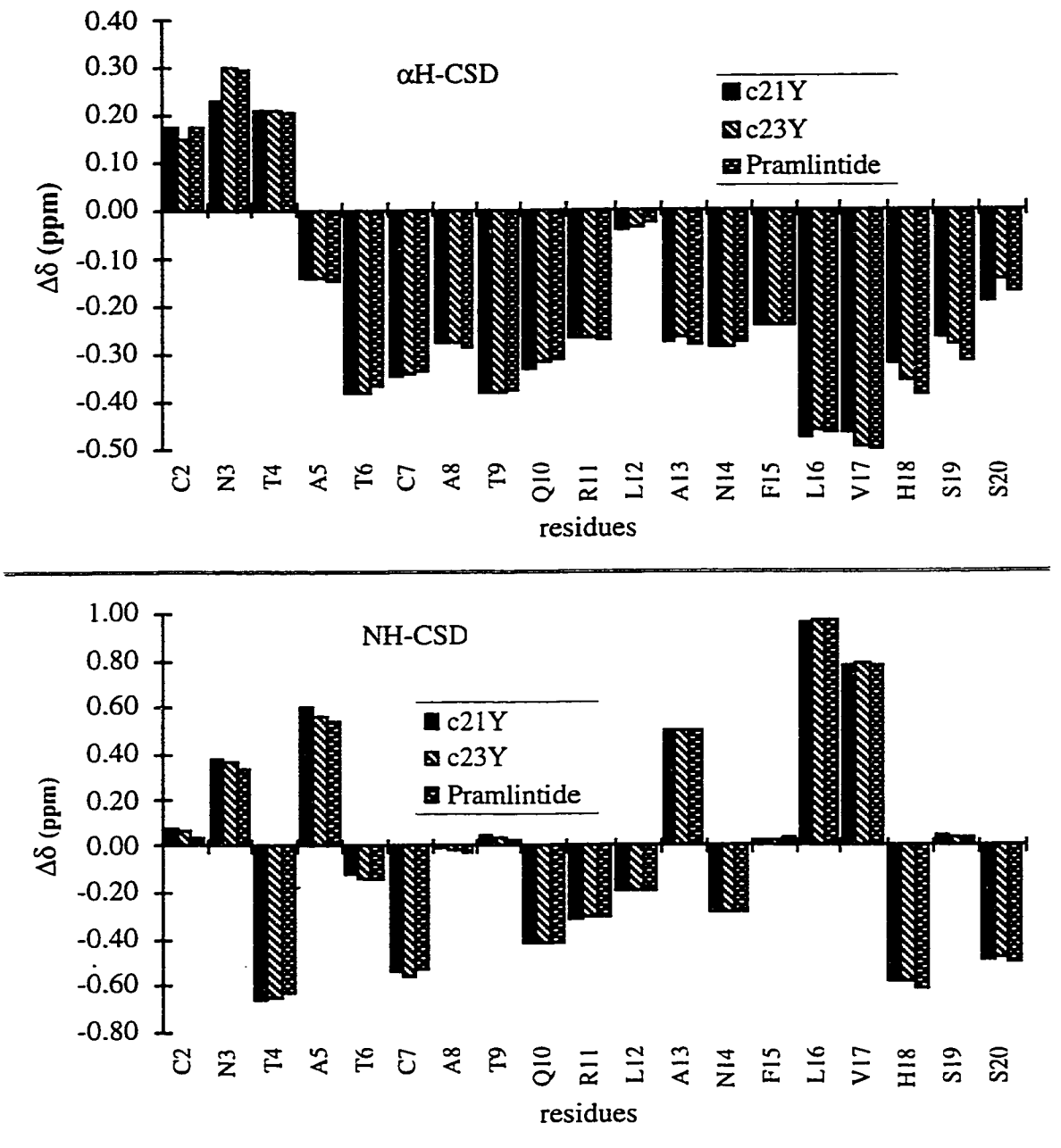

Figure 5.14 αH-CSD and NH-CSD Histograms for c21Y[hAM(1-20)GY], c23Y [hAM(1-22)GY], and Pramlintide in 25% HFIP.

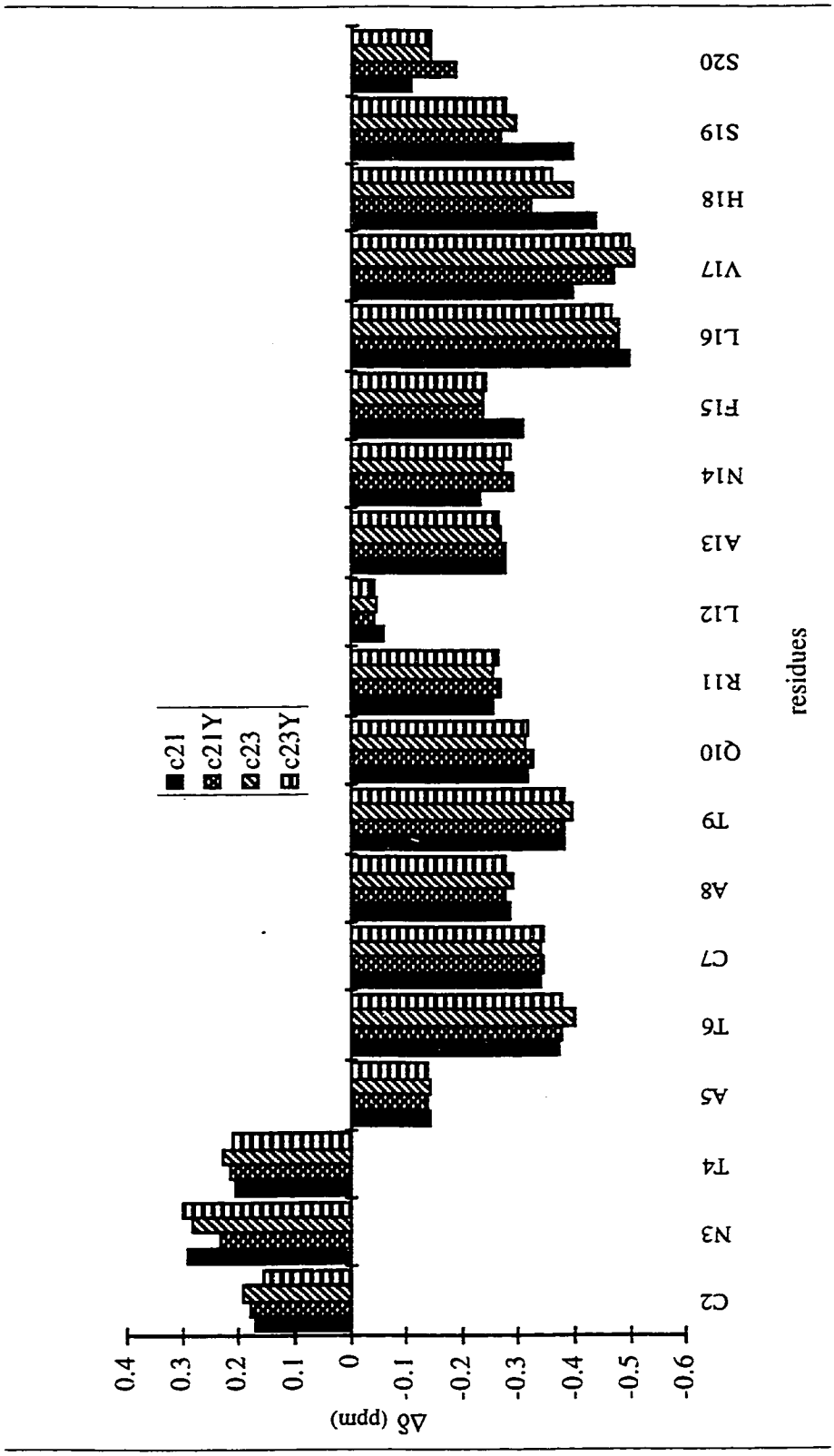

Figure 5.15 αH-CSD Comparisons of Fragments with (c23 [hAM(1-22)G], c23Y [hAM(1-22)GY] and without (c21 [hAM(1-20)G], c21Y [hAM(1-20)GY]) NN C-capping Unit in 25% HFIP.

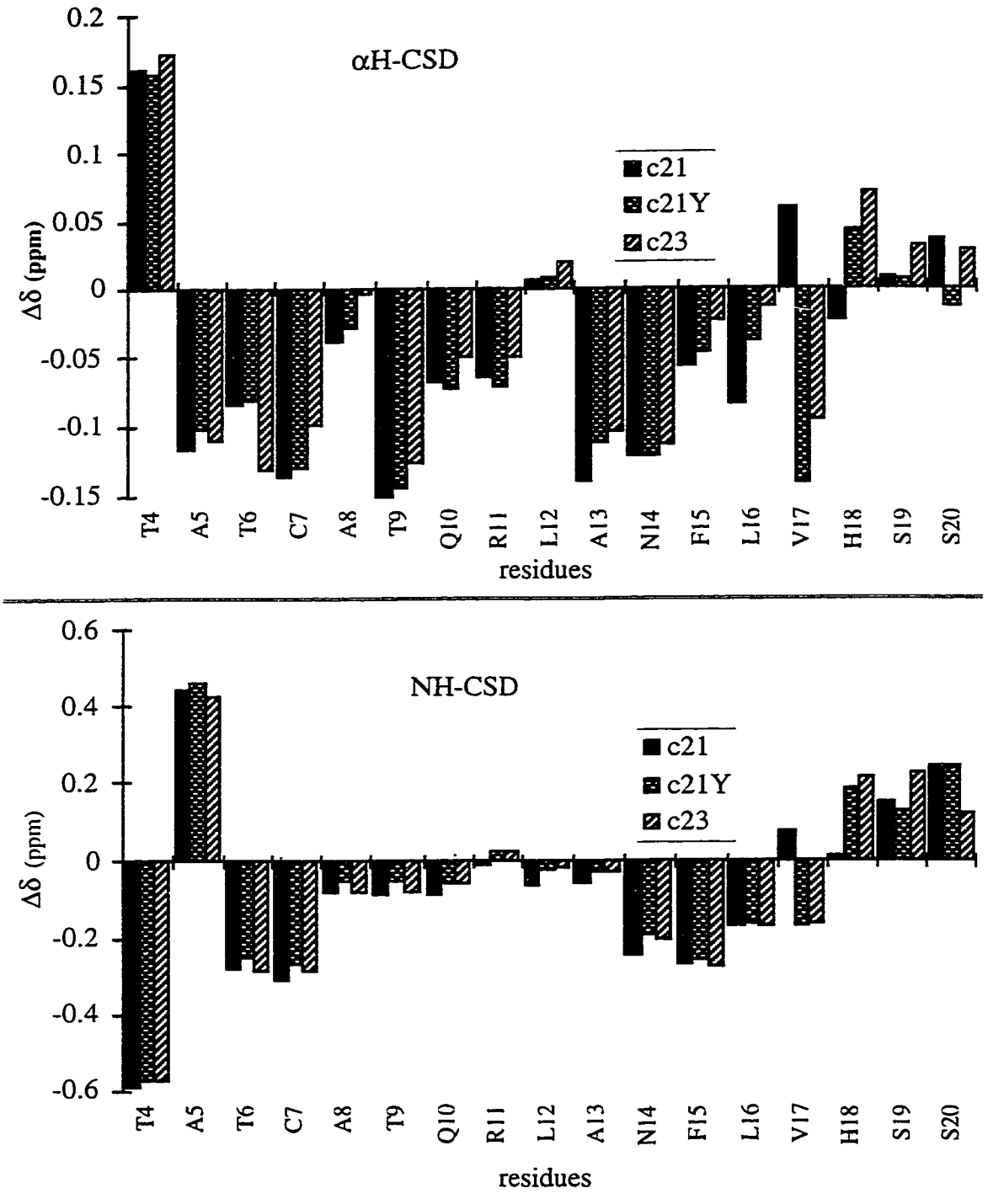

Figure 5.16 αH-CSD and NH-CSD Comparisons of Fragments with (c23 [hAM(1-22)G]) and without (c21 [hAM(1-20)G], c21Y [hAM(1-20)GY])] NN C-capping Unit in Buffer.

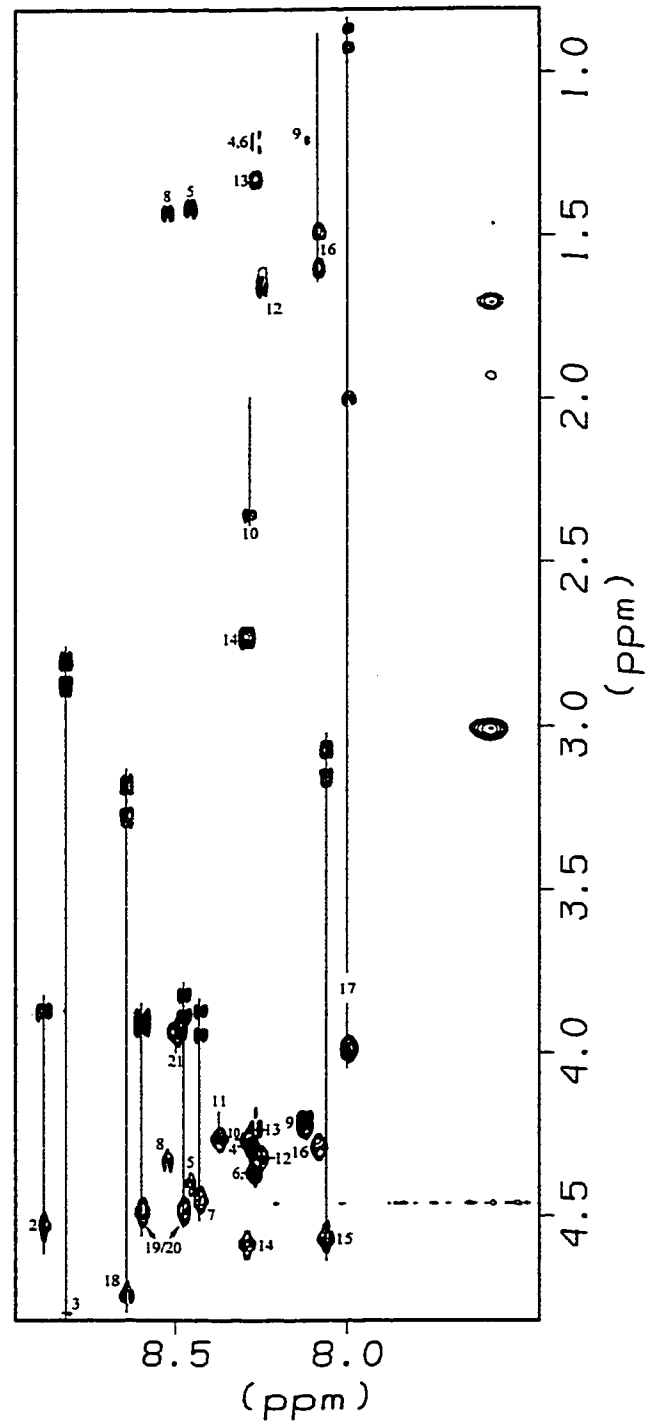

Figure 5.17 αN Region of the TOCSY Spectrum of [S2,7-hAM(1-20)G] in Buffer.

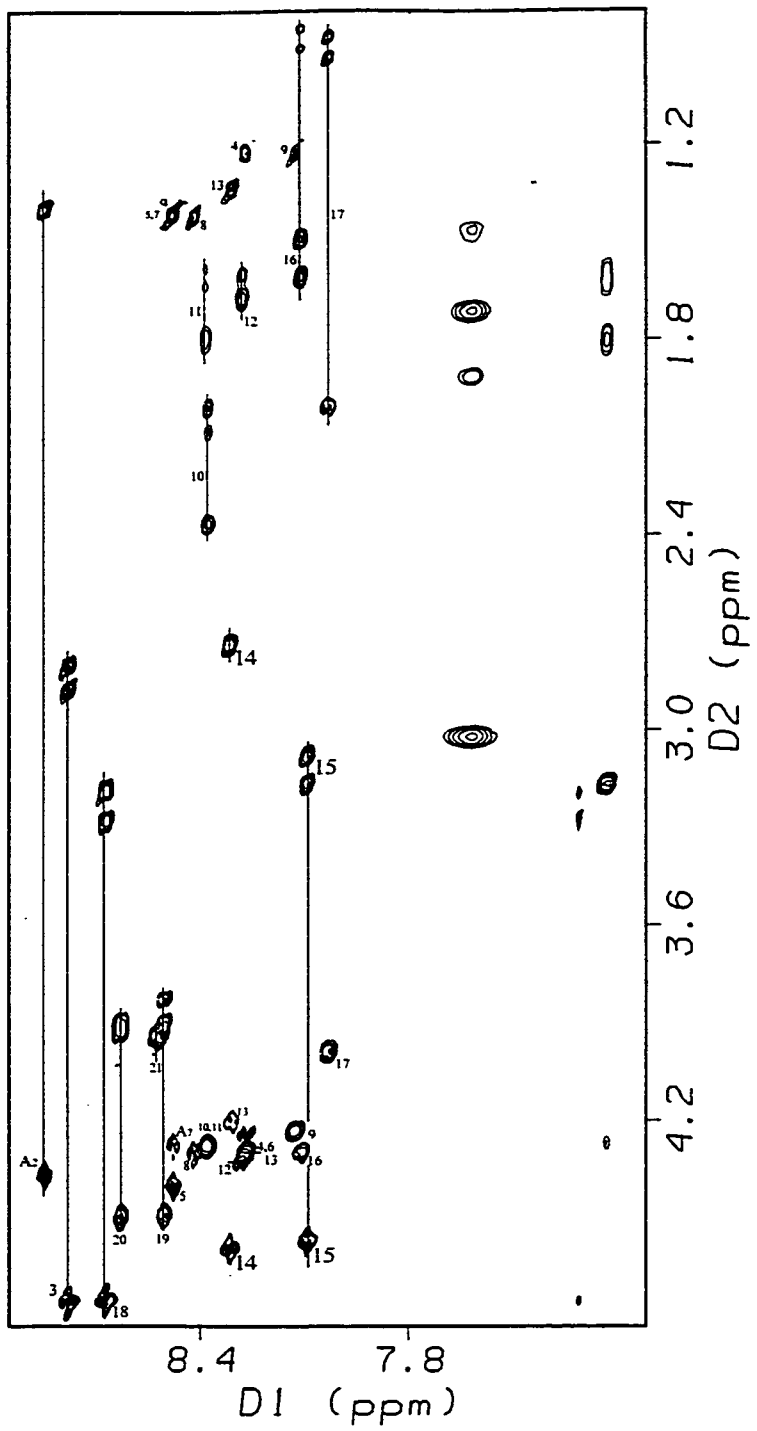

Figure 5.18 αN Region of the TOCSY Spectrum of [A2,7-hAM(1-20)G] in Buffer.

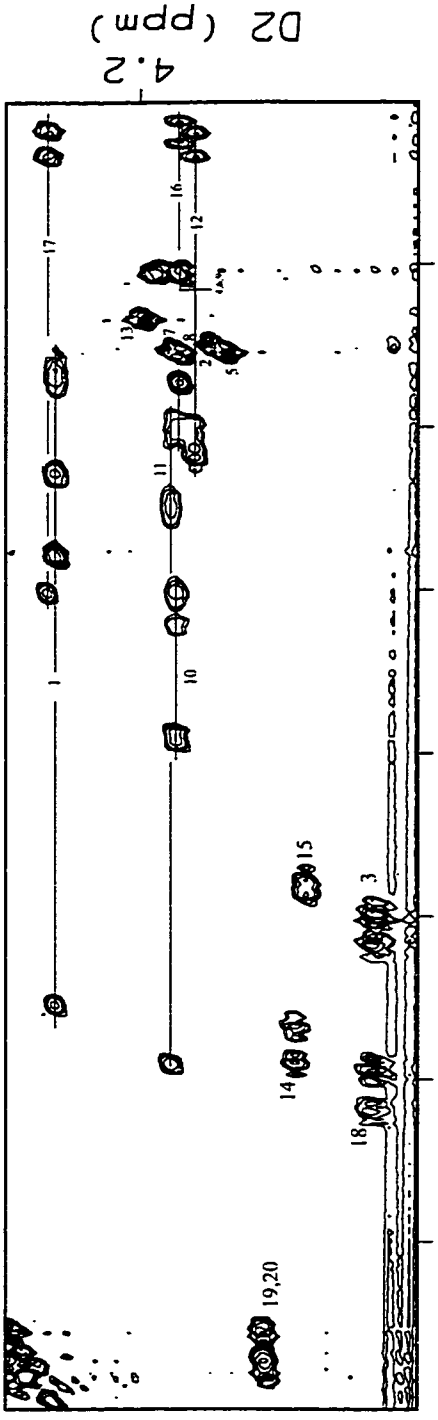

Figure 5.19 α/βγδ Region of the TOCSY Spectrum of [A2,7-hAM(1-20)G] in Buffer.

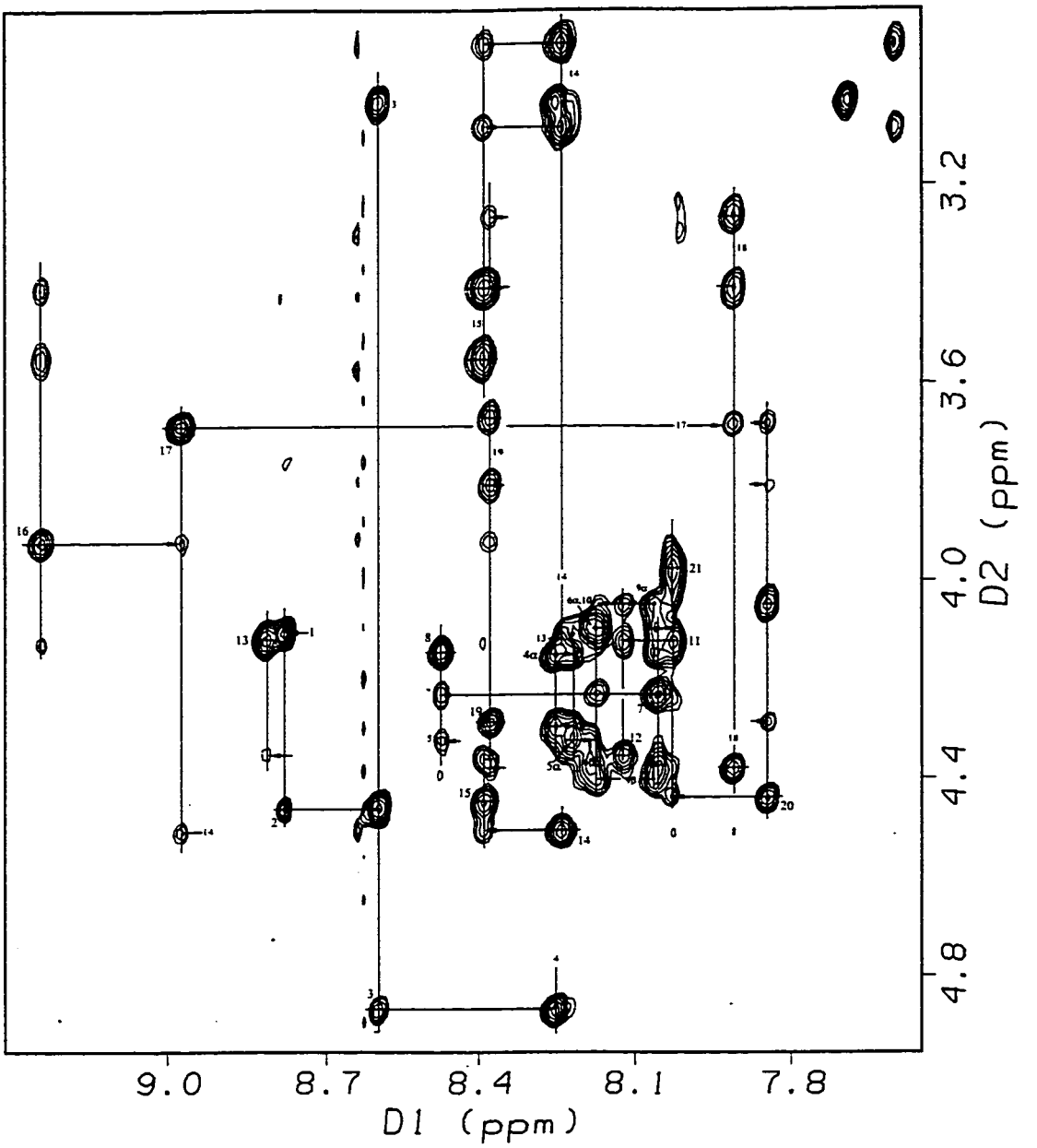

Figure 5.20 αN Region of the NOESY Spectrum of [A2,7-hAM(1-20)G] in 25% HFIP.

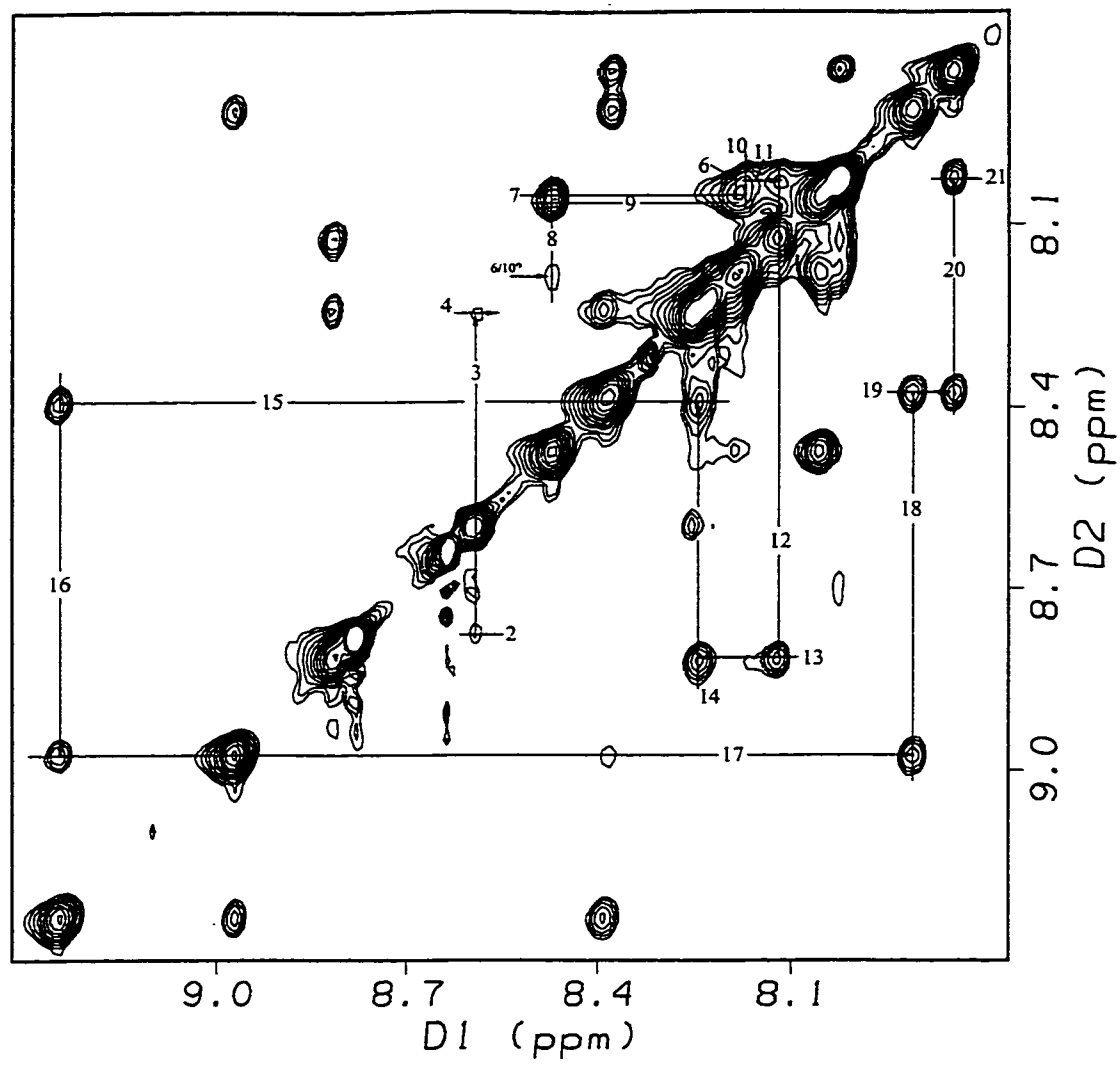

Figure 5.21 NN Region of the NOESY Spectrum of [A2,7-hAM(1-20)G] in 25% HFIP.

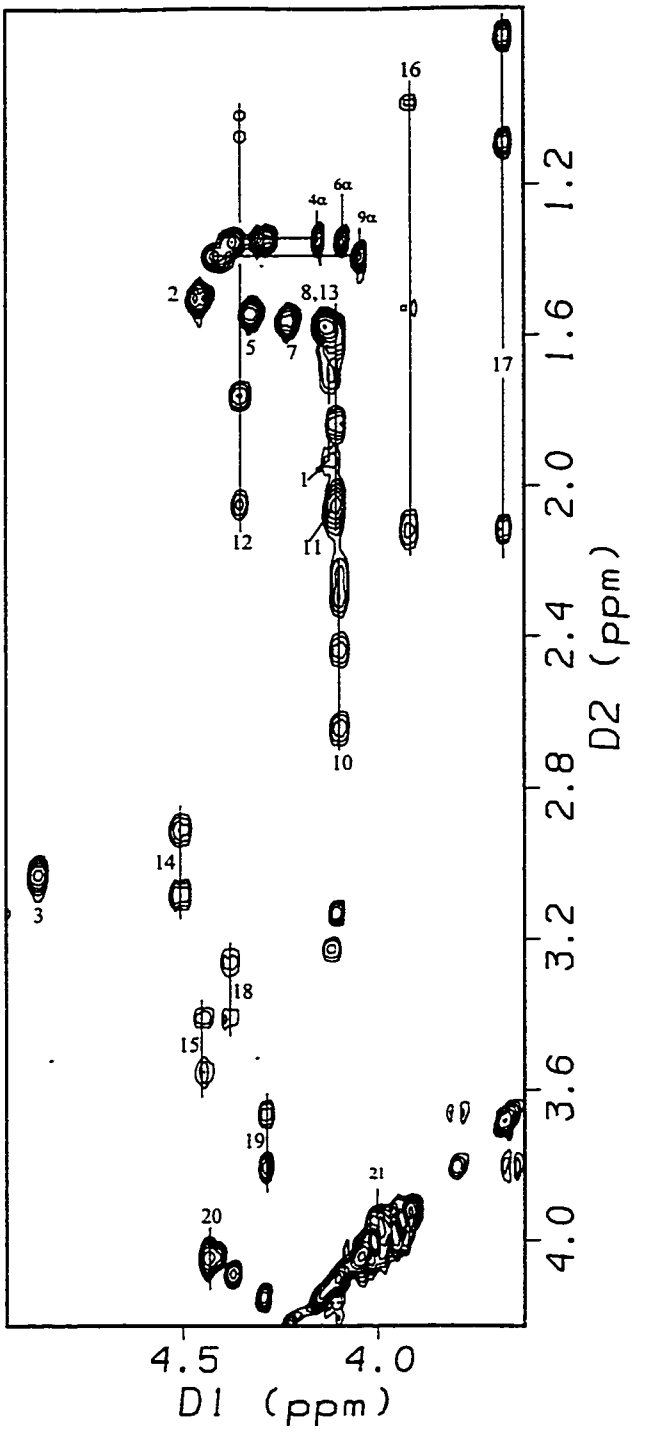

Figure 5.22 α/βγδ Region of the NOESY Spectrum of [A2,7-hAM(1-20)G] in 25% HFIP.

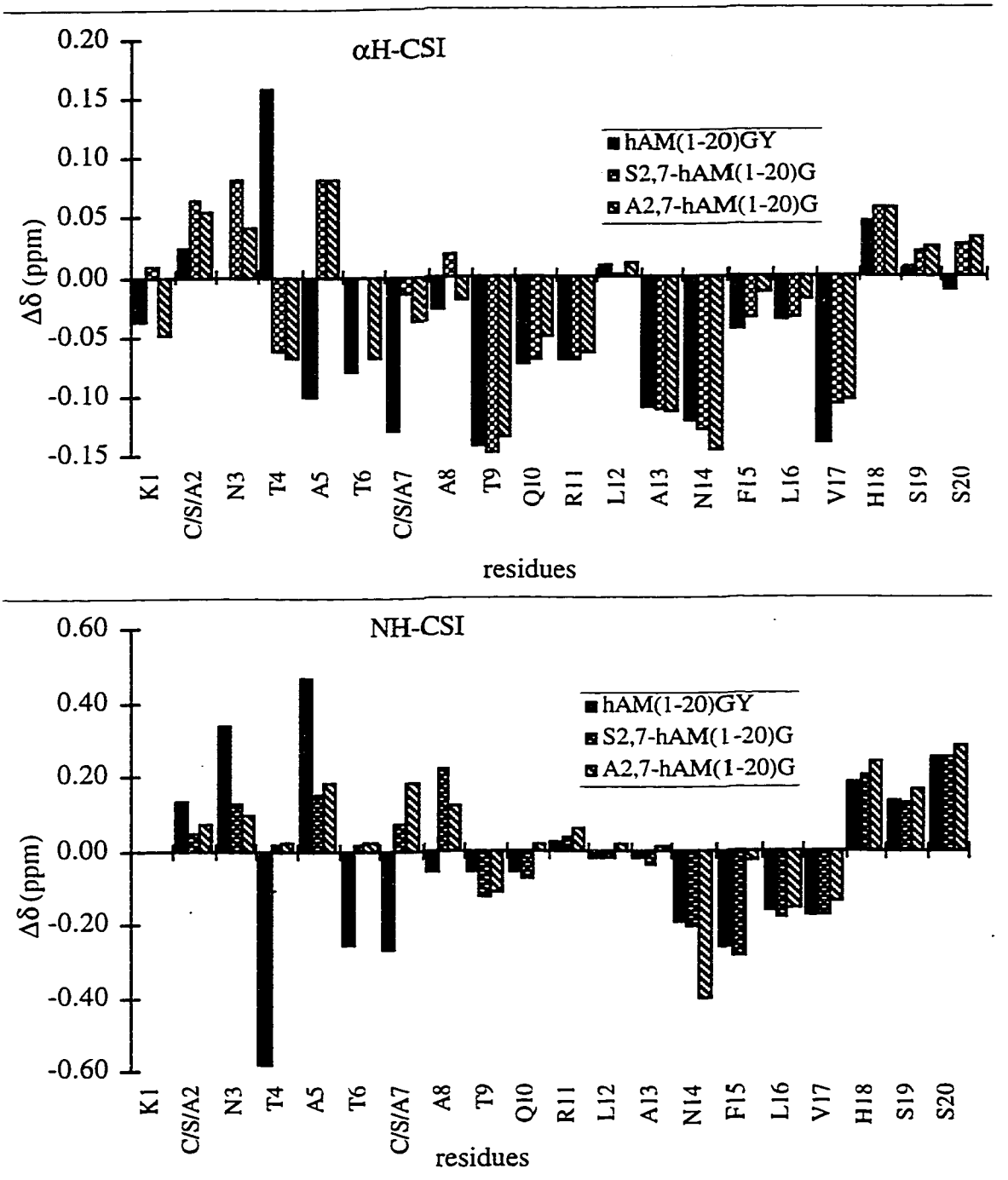

Figure 5.23 αH-CSD and NH-CSD Comparisons of Fragments with ([hAM(1-20)GY]) and without ([S2,7-hAM(1-20)G], [A2,7-hAM(1-20)G)] Disulfide Closure in Buffer at 285K.

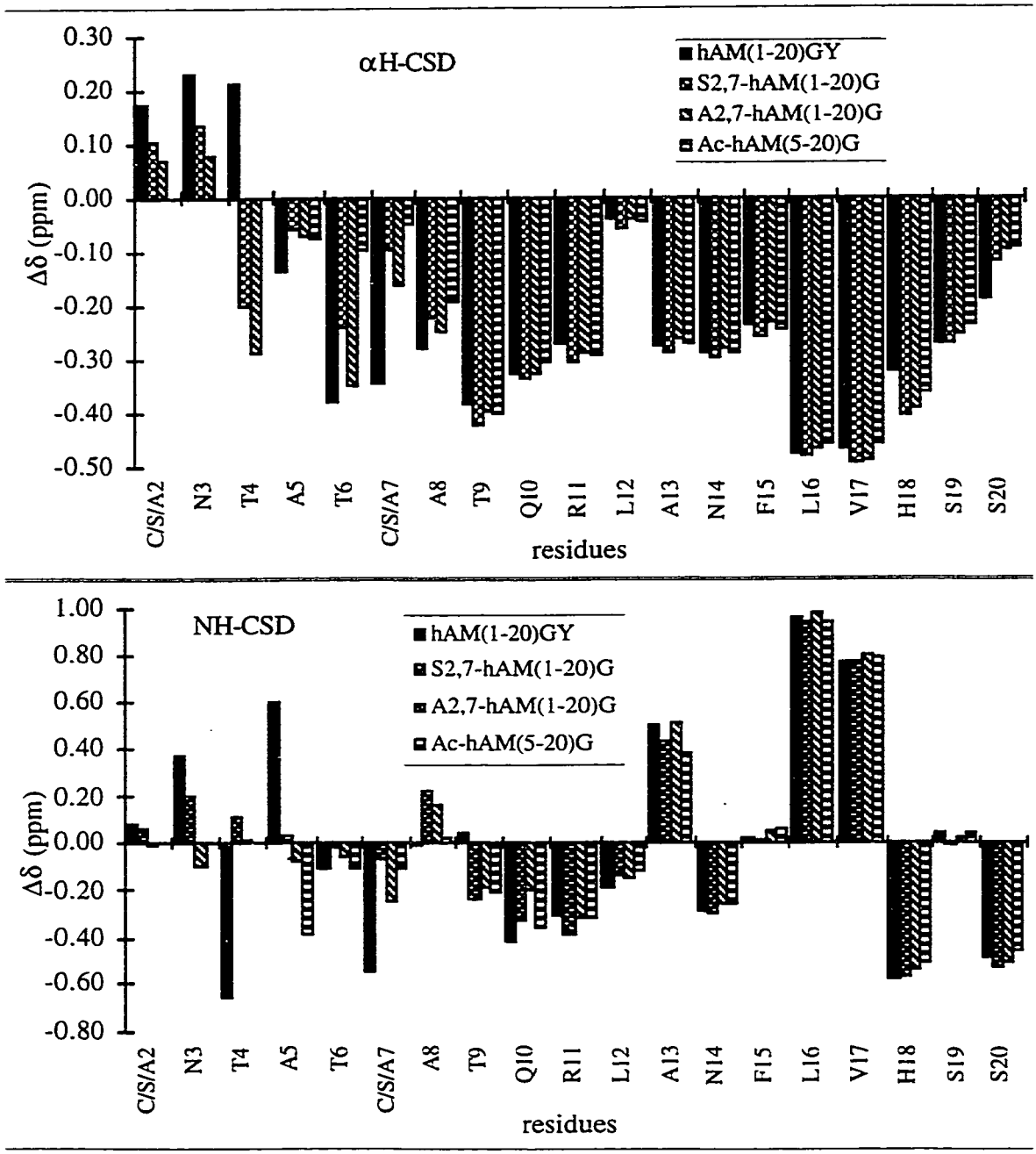

Figure 5.24 αH-CSD and NH-CSD Comparisons of Fragments with ([hAM(1-20)GY)] and without ([S2,7-hAM(1-20)G], [A2,7-hAM(1-20)G], [Ac-hAM(5-20)G)] Disulfide Closure in Aqueous HFIP. (note: Ac-hAM(5-20)G was examined in 30% HFIP at 295K, while other fragments were examined in 25% HFIP at 285K.)

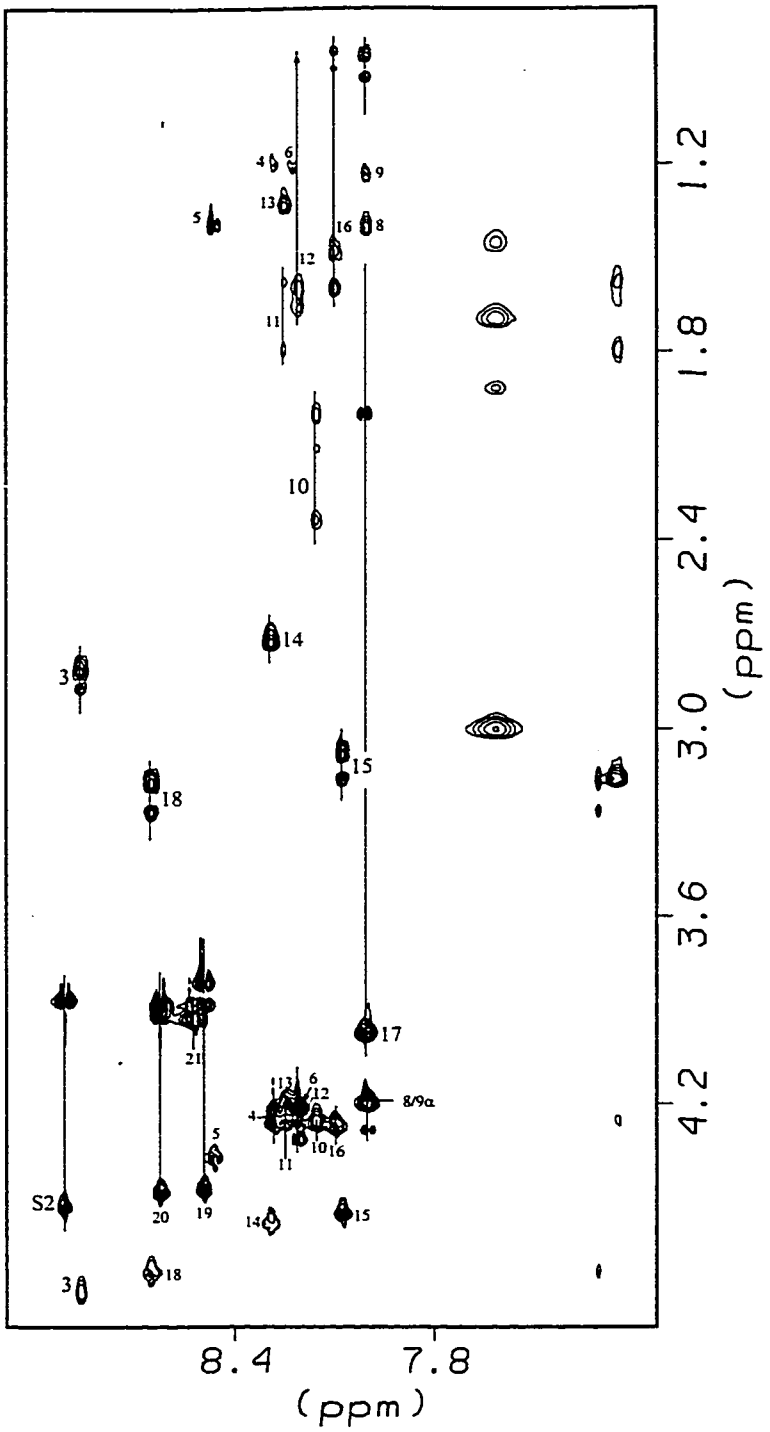

Figure 5.25 αN Region of the TOCSY Spectrum of [S2U7-hAM(1-20)G] in Buffer.

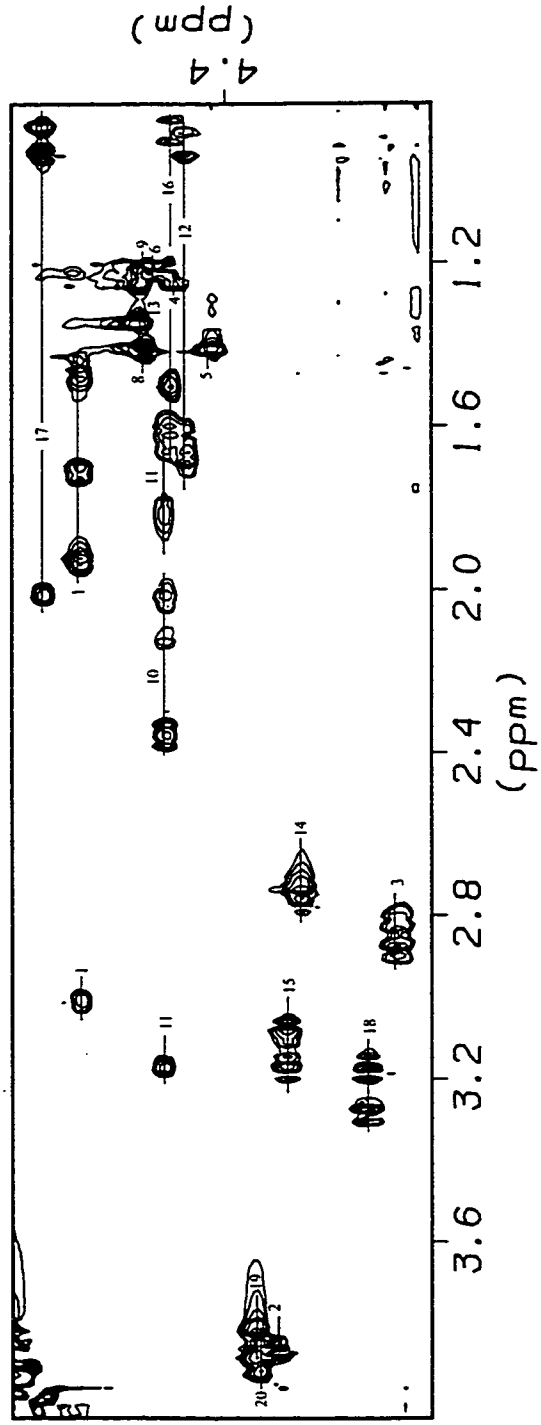

Figure 5.26 α/βγδ Region of the TOCSY Spectrum of [S2U7-hAM(1-20)G] in Buffer.

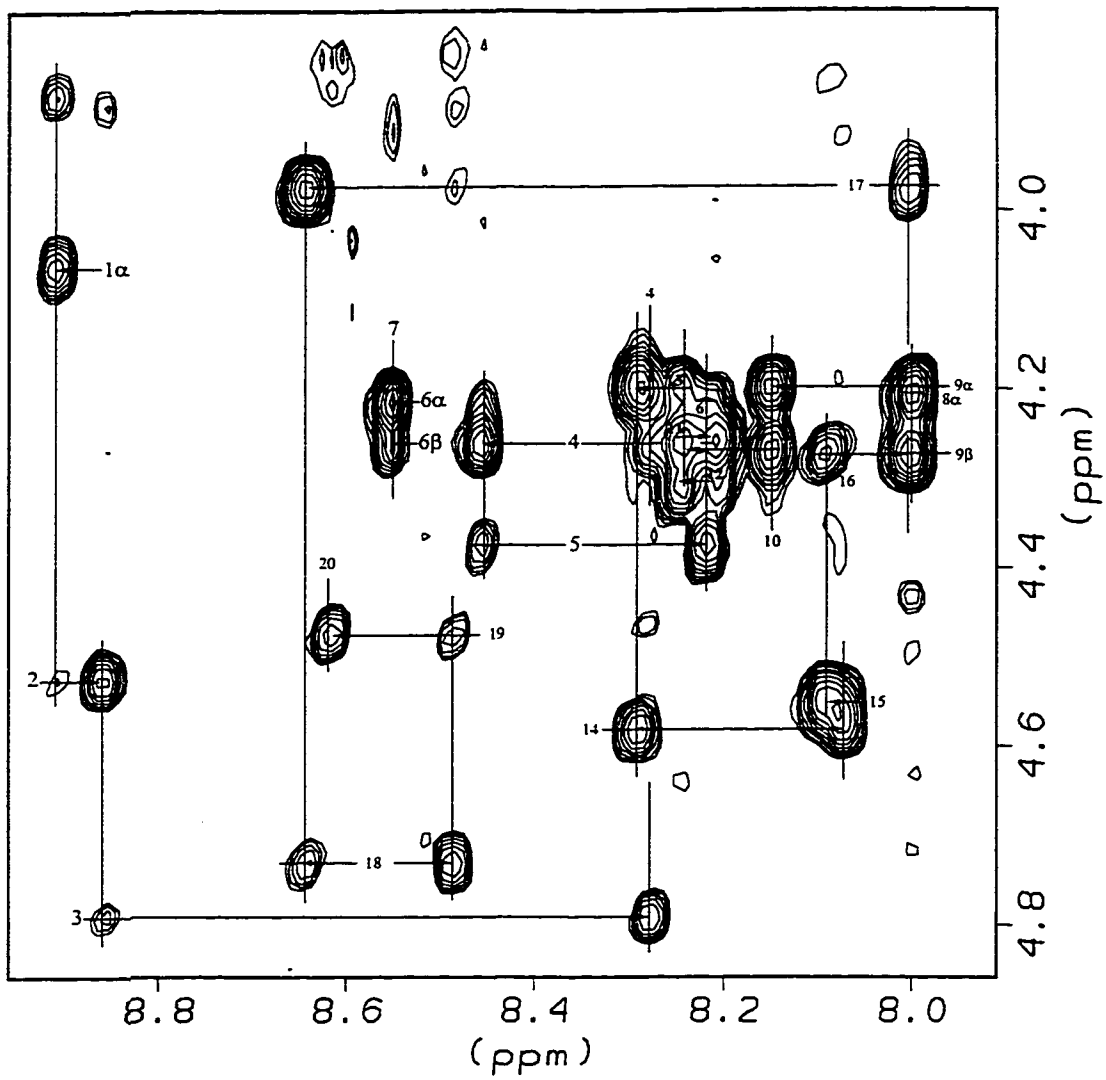

Figure 5.27 αN Region of the NOESY Spectrum of [S2U7-hAM(1-20)G] in Buffer.

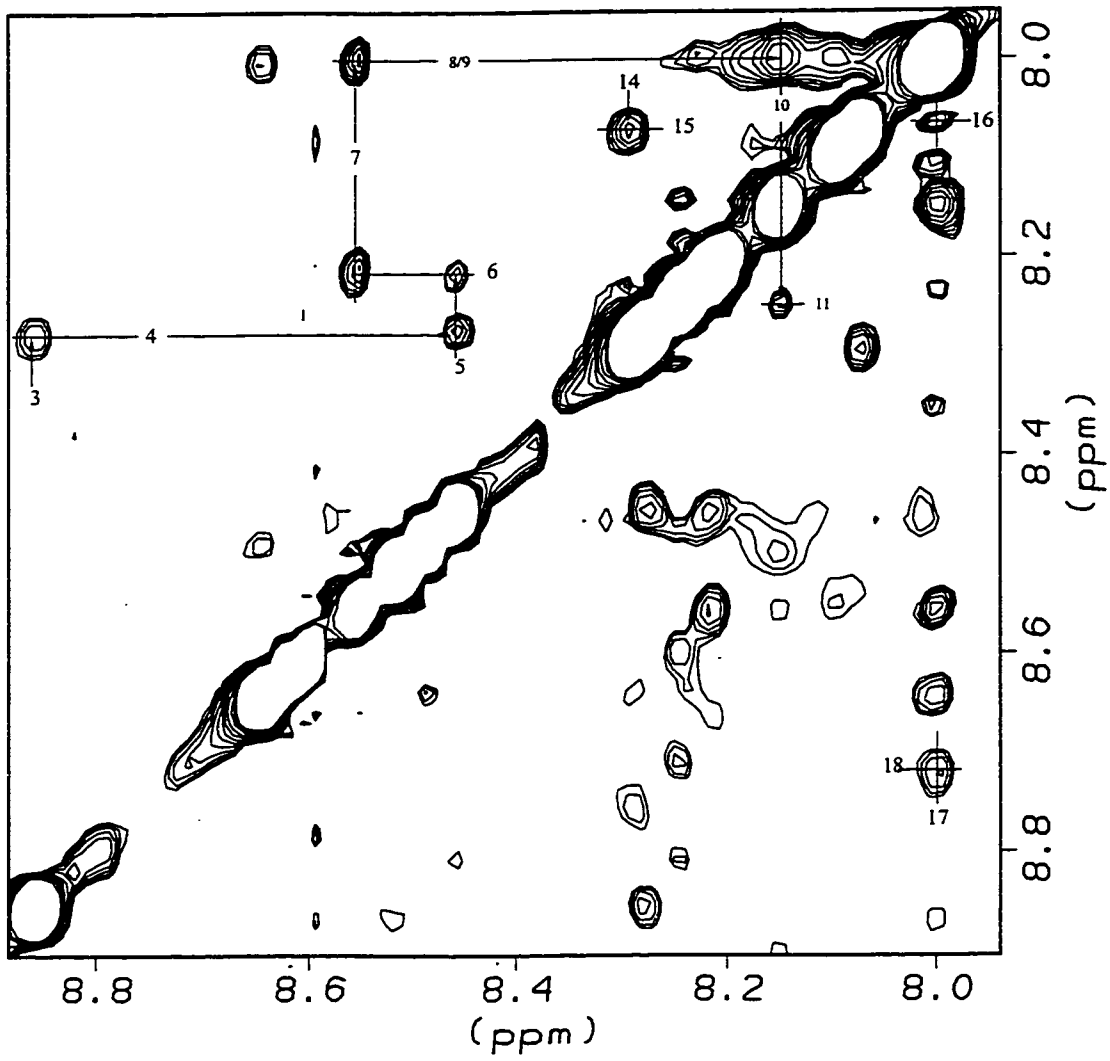

Figure 5.28 NN Region of the NOESY Spectrum of [S2U7-hAM(1-20)G] in Buffer.

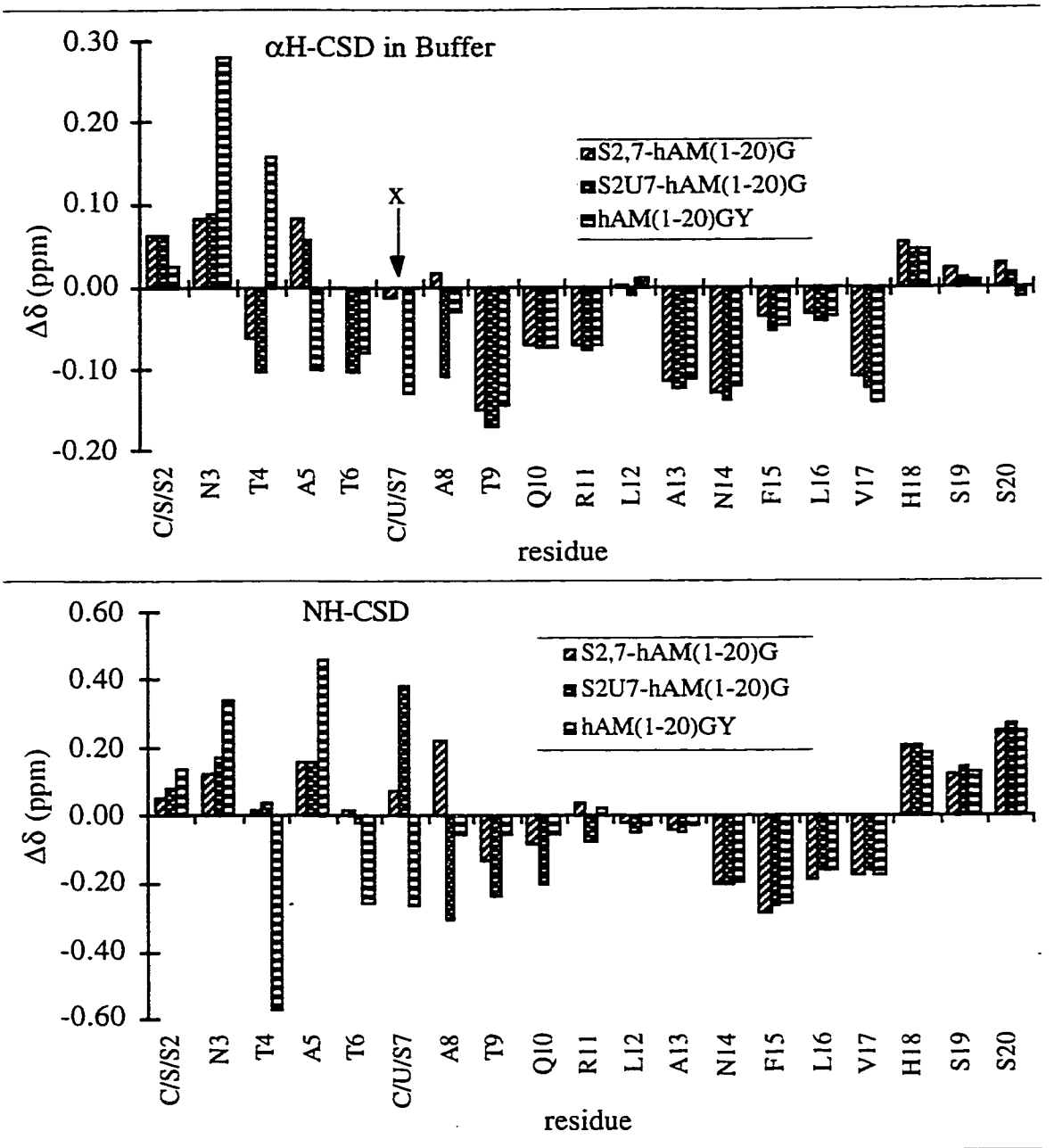

Figure 5.29 αH-CSD and NH-CSD Comparisons of [S2U7-hAM(1-20)G] with a Cyclic and An Acyclic Fragment in Buffer.
(X: Aib does not have Hα)

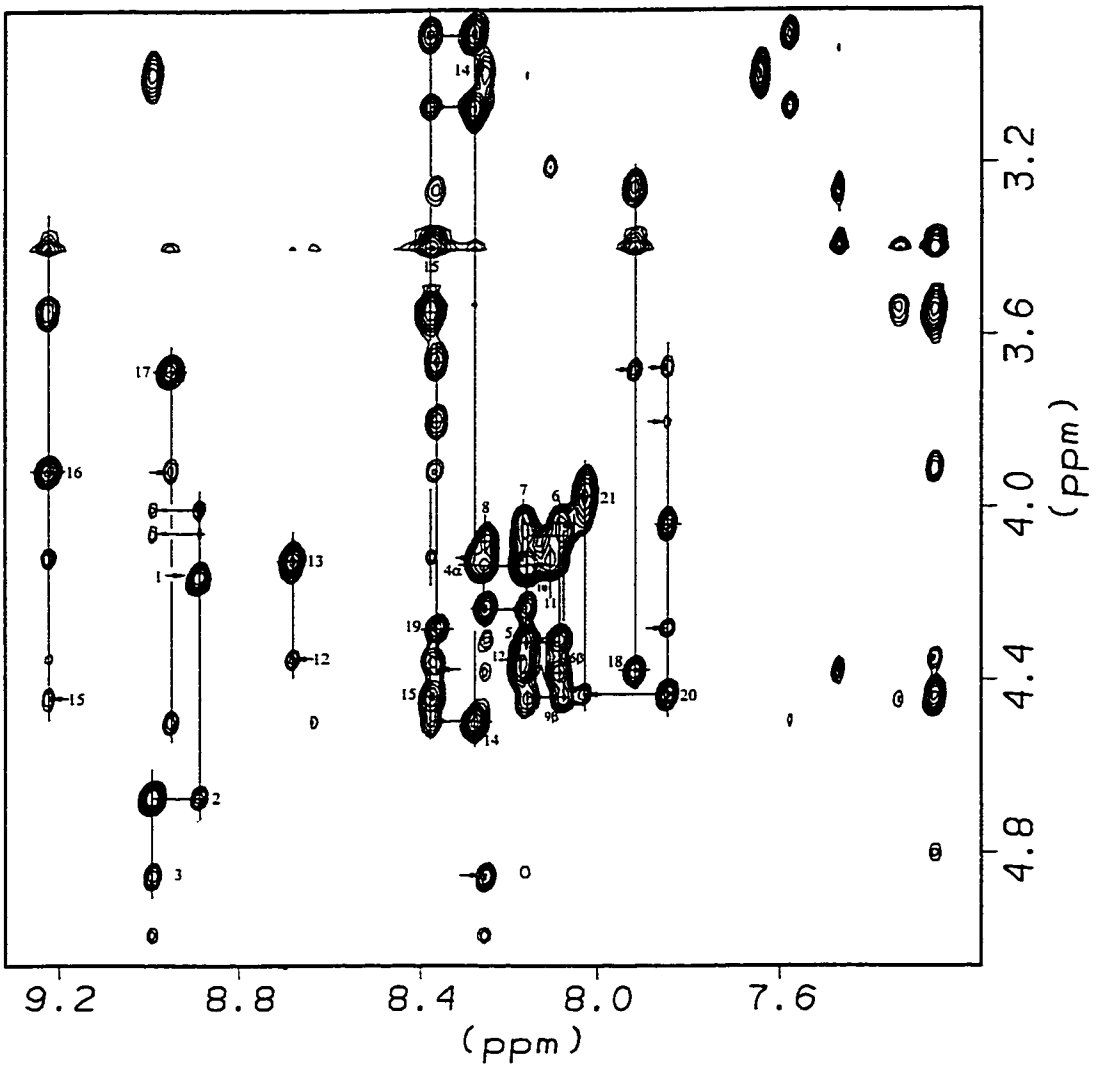

Figure 5.30 αN Region of the NOESY Spectrum of [S2U7-hAM(1-20)G] in 25% HFIP.

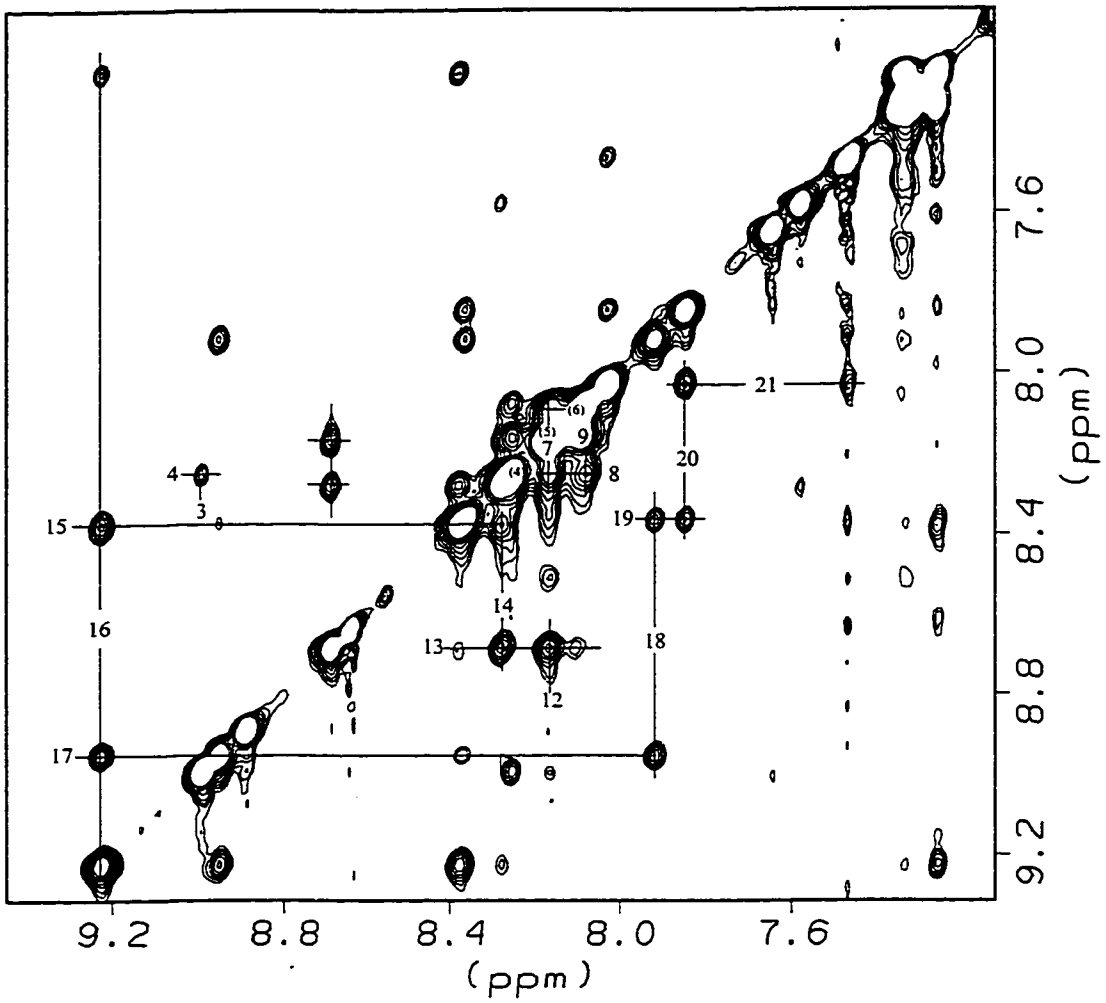

Figure 5.31 NN Region of the NOESY Spectrum of [S2U7-hAM(1-20)G] in 25% HFIP.

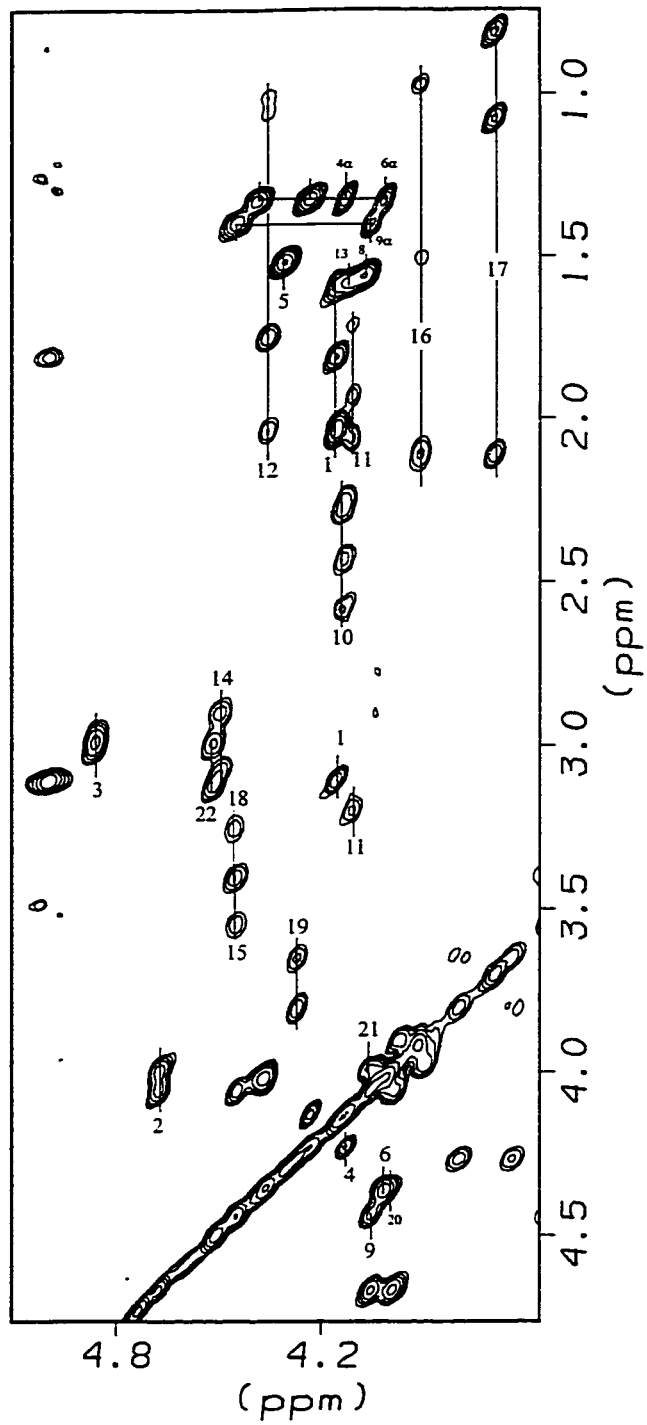

Figure 5.32 α/βδγ Region of the TOCSY Spectrum of [S2U7-hAM(1-20)GY] in 25% HFIP.

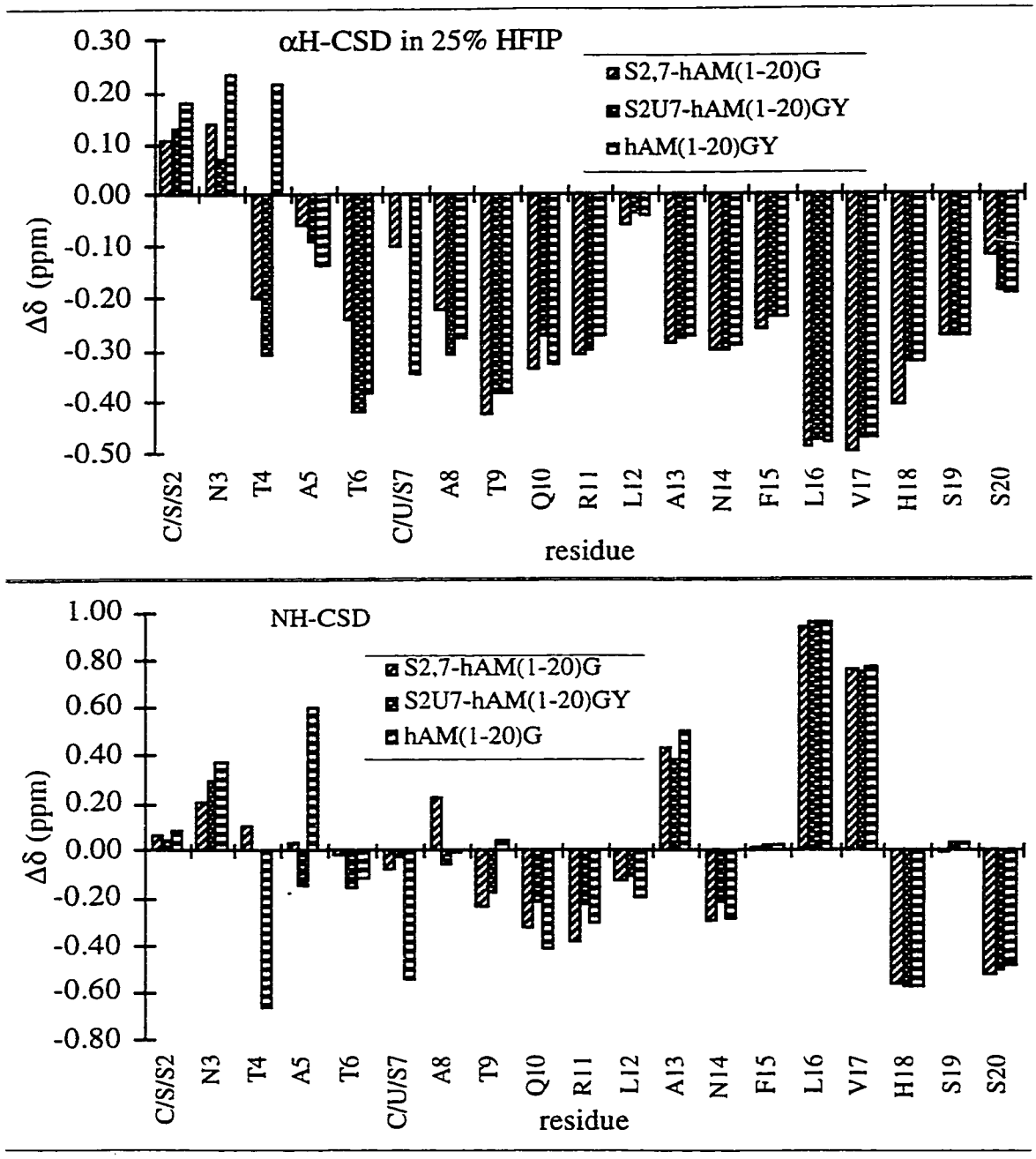

Figure 5.33 αH-CSD and NH-CSD Comparisons of [S2U7-hAM(1-20)G] with a Cyclic and An Acyclic Fragment in 25% HFIP.

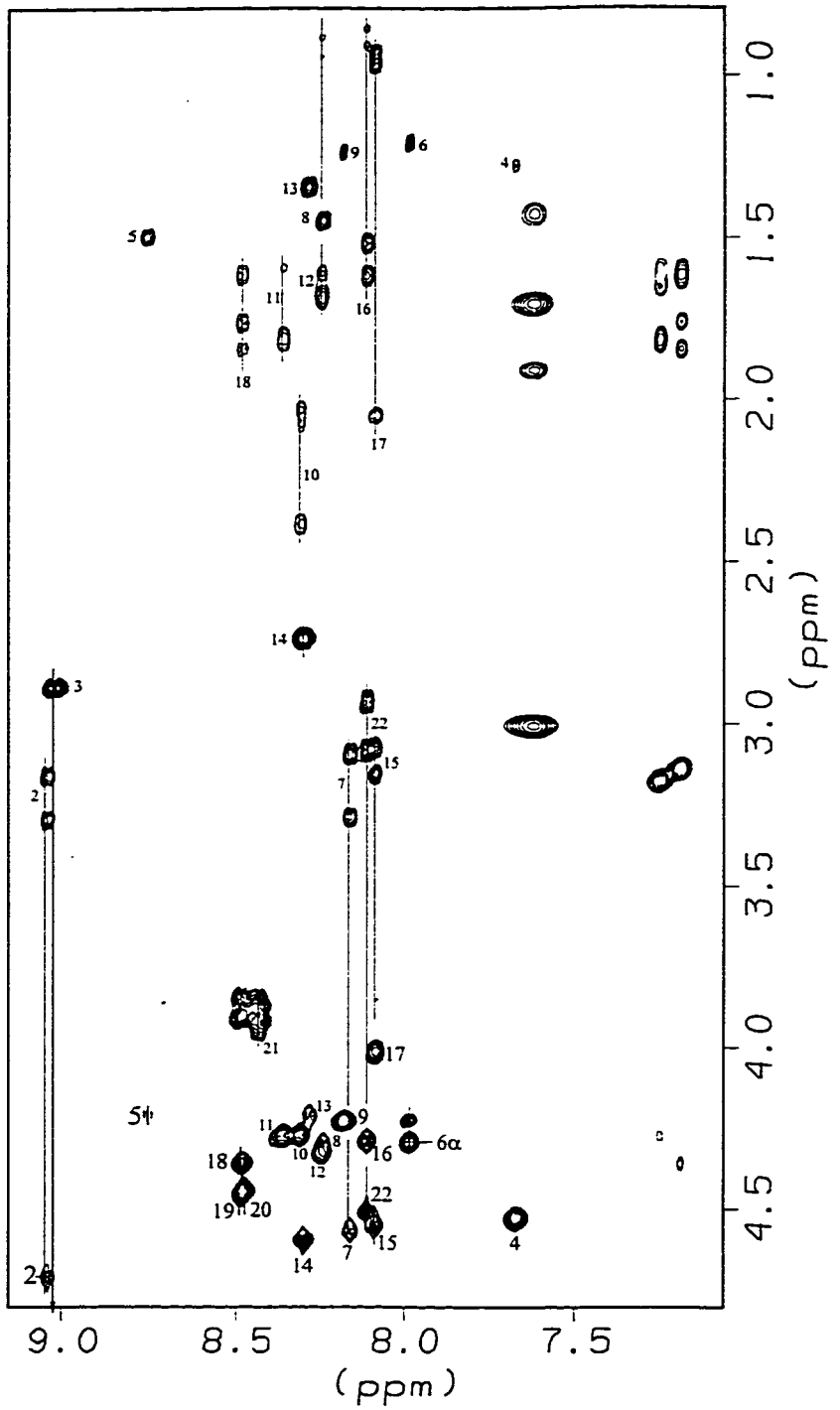

Figure 5.34 αN Region of the TOCSY Spectrum of [R18-hAM(1-20)GY] in Buffer.

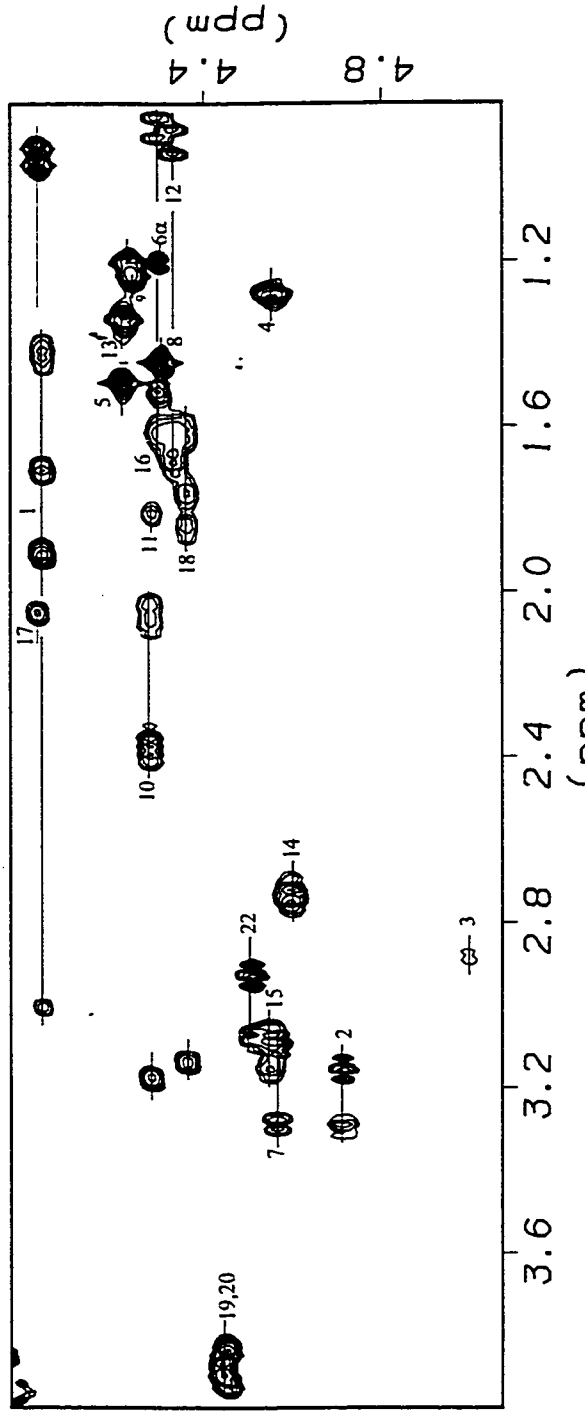

Figure 5.35 α/βγδ Region of the TOCSY Spectrum of [R18-hAM(1-20)GY] in Buffer.

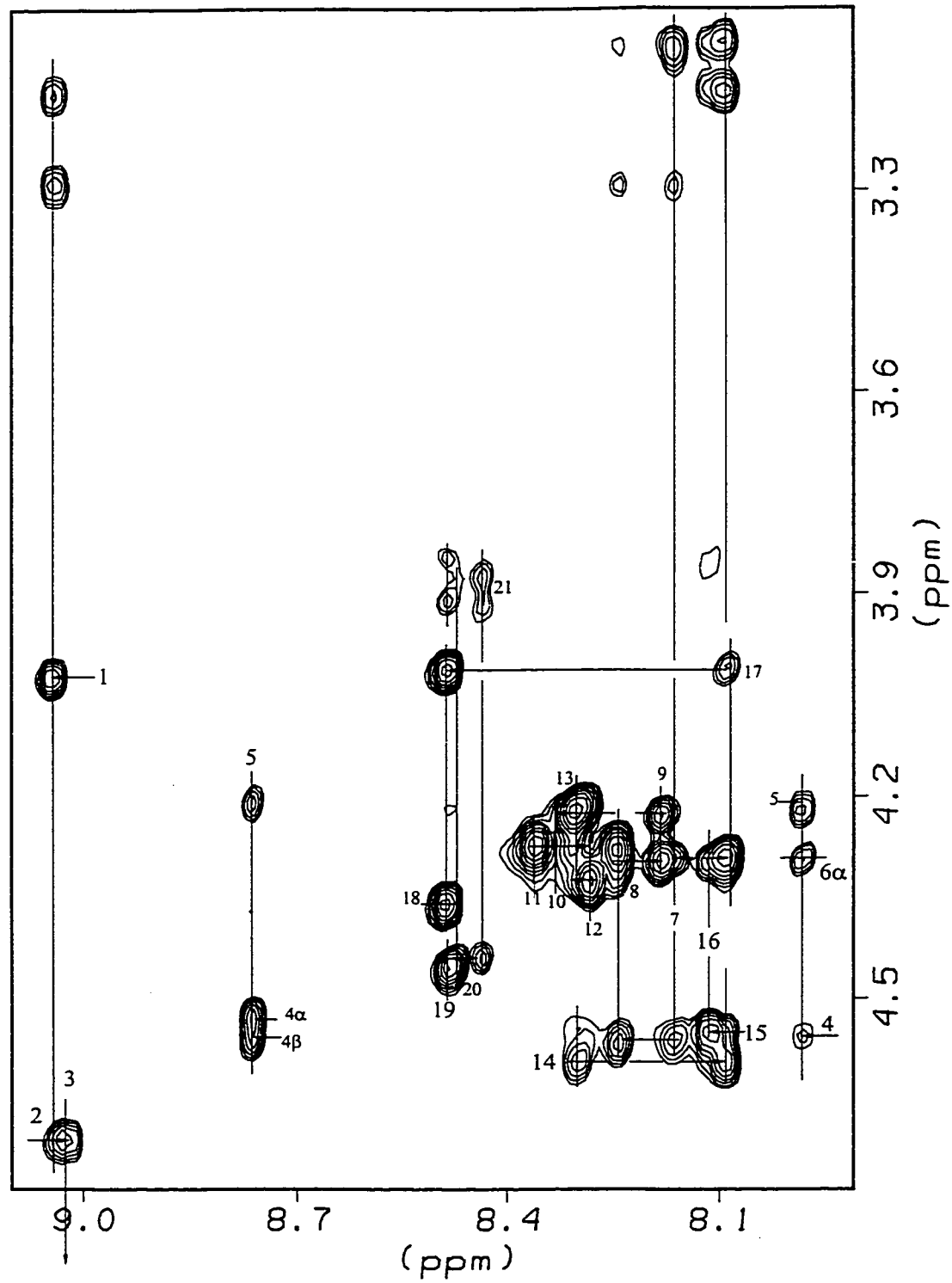

Figure 5.36 αN Region of the NOESY Spectrum of [R18-hAM(1-20)GY] in Buffer.

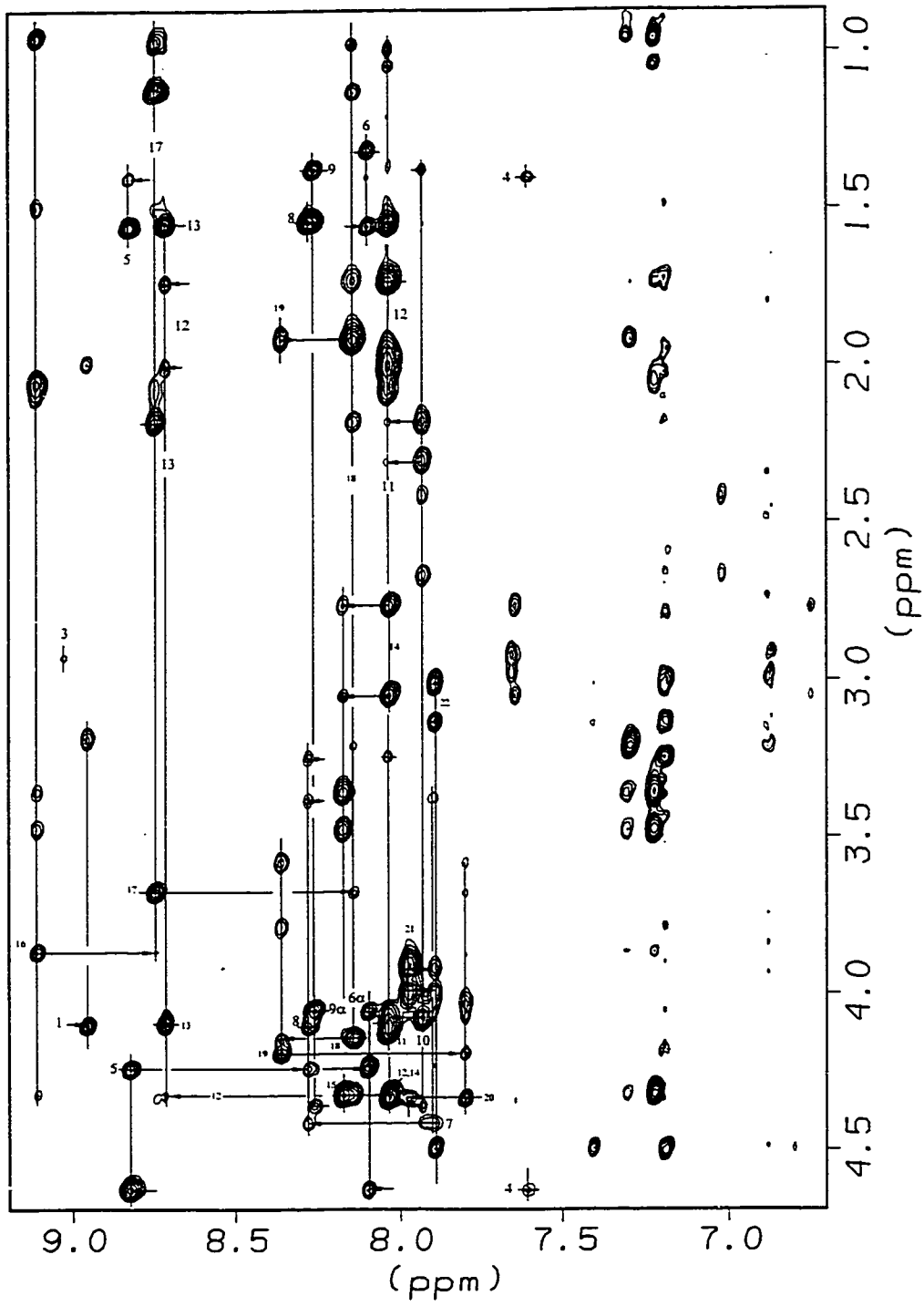

Figure 5.37 The NH/CH Region of the NOESY Spectrum of [R18-hAM(1-20)GY] in 25% HFIP.

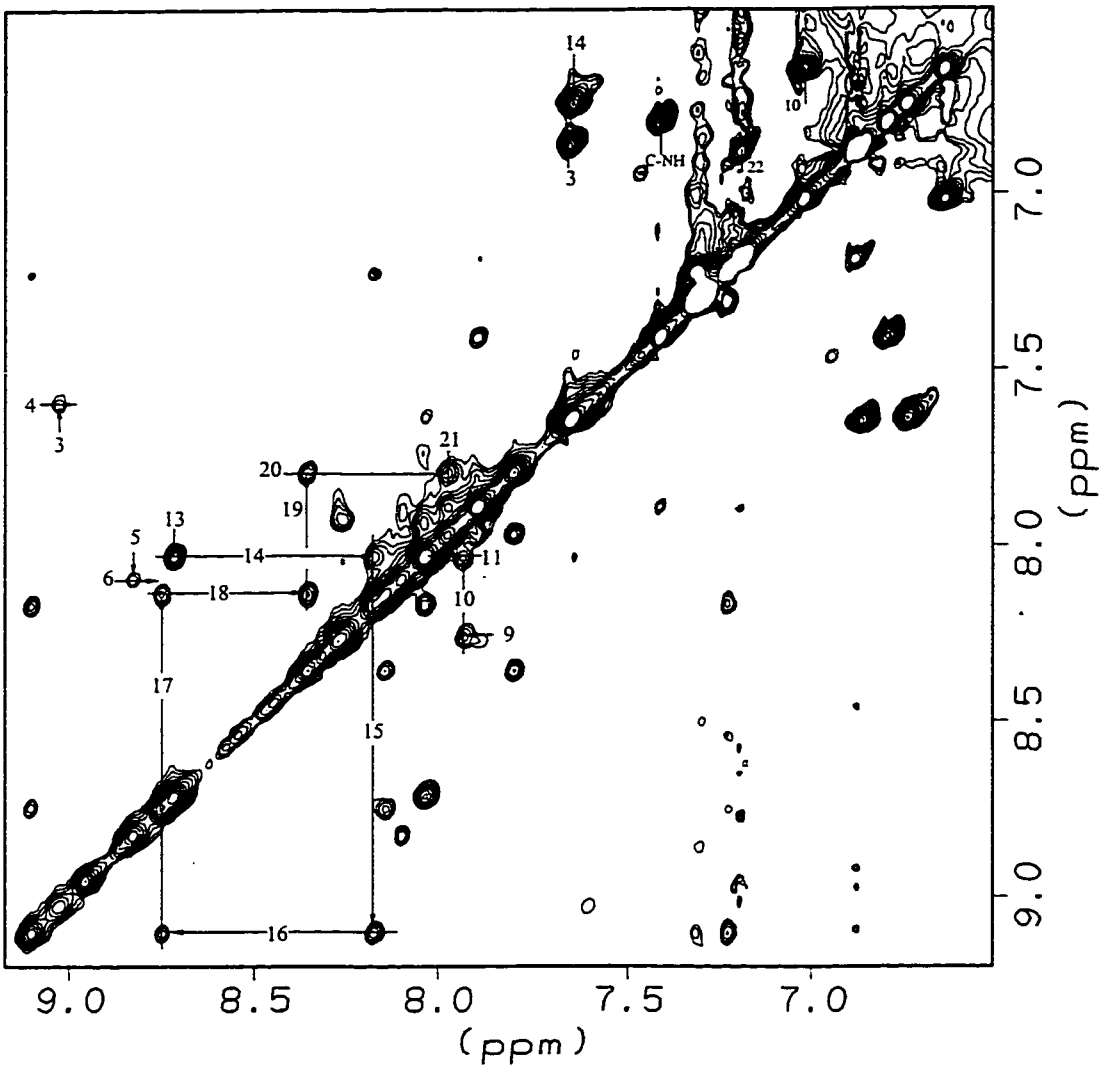

Figure 5.38 NN Region of the NOESY Spectrum of
[R18-hAM(1-20)GY] in 25% HFIP.

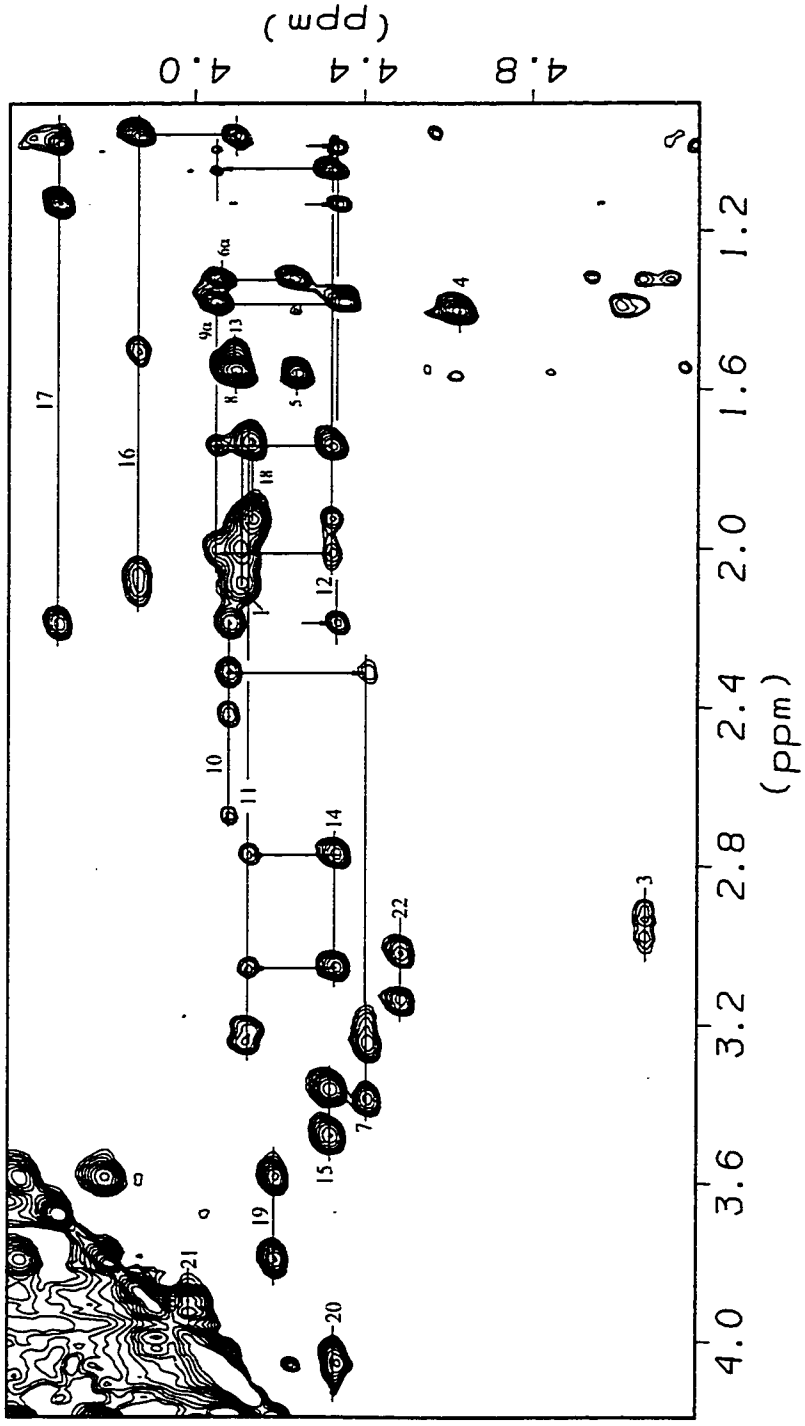

Figure 5.39 α/βγδ Region of the NOESY Spectrum of [R18-hAM(1-20)GY] in 25% HFIP.

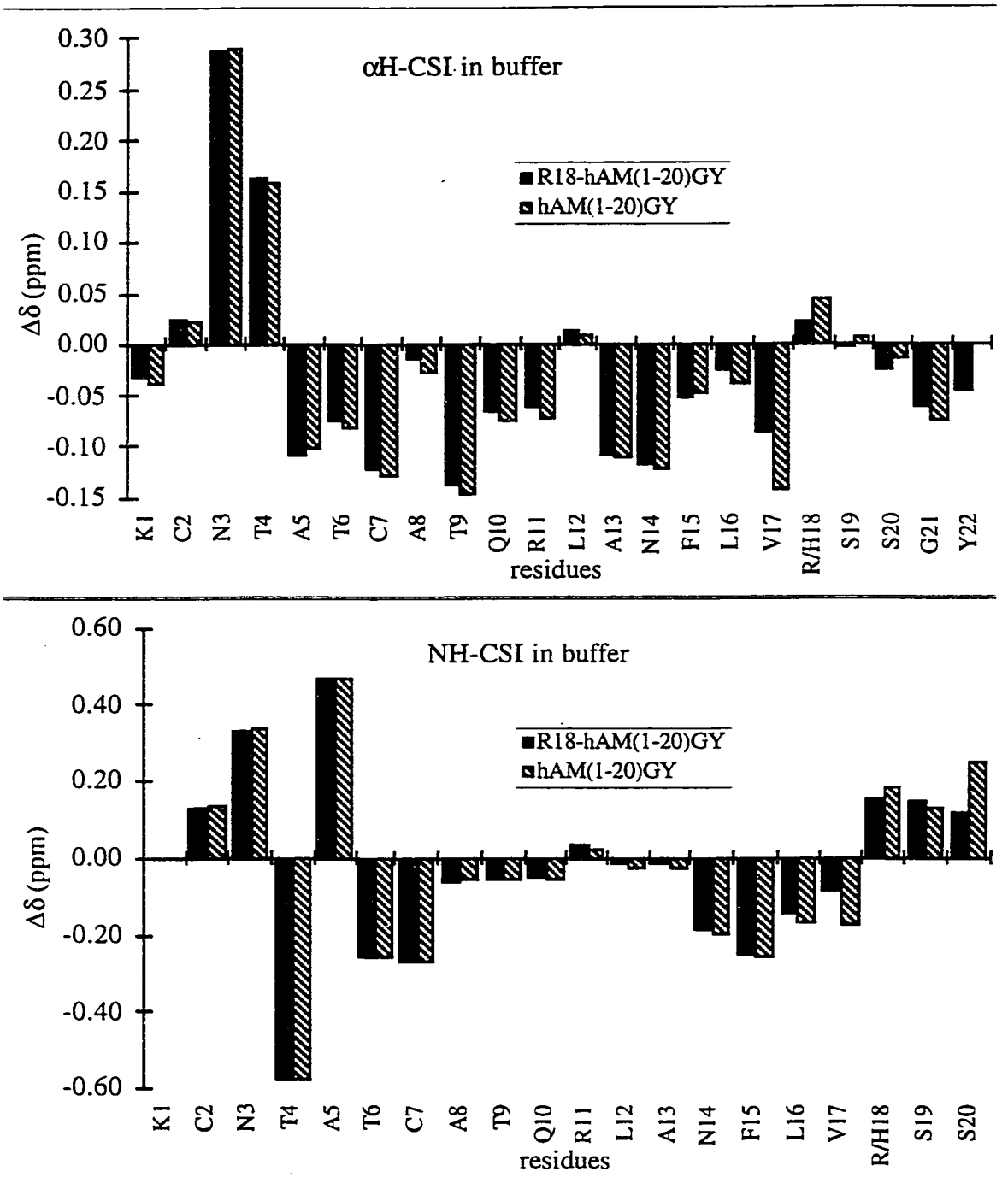

Figure 5.40 αH-CSD and NH-CSD Histograms of [R18-hAM(1-20)GY] and [hAM(1-20)GY] in Buffer.

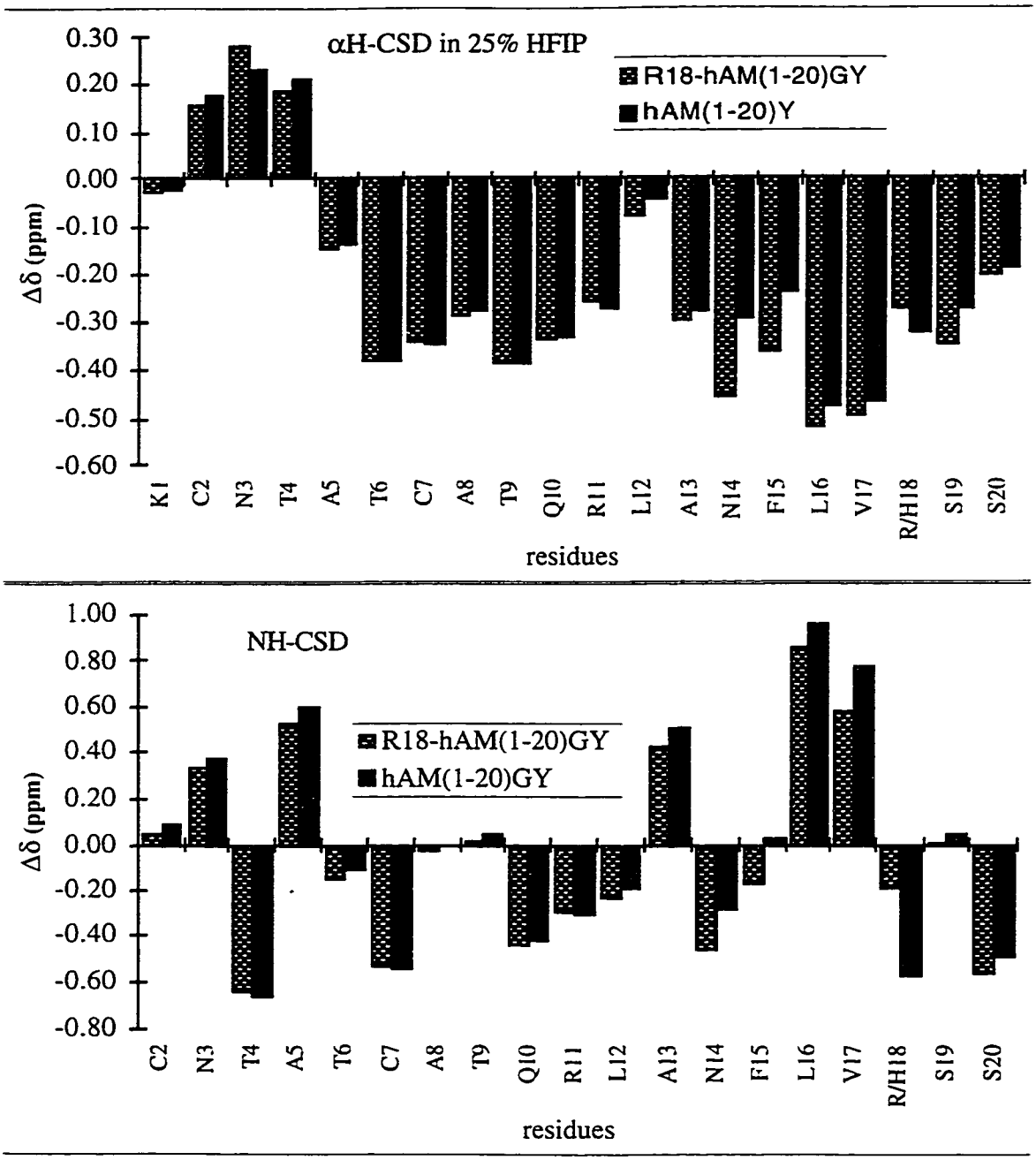

Figure 5.41 αH-CSD and NH-CSD Histograms of [R18-hAM(1-20)GY] and [hAM(1-20)GY] in 25% HFIP.

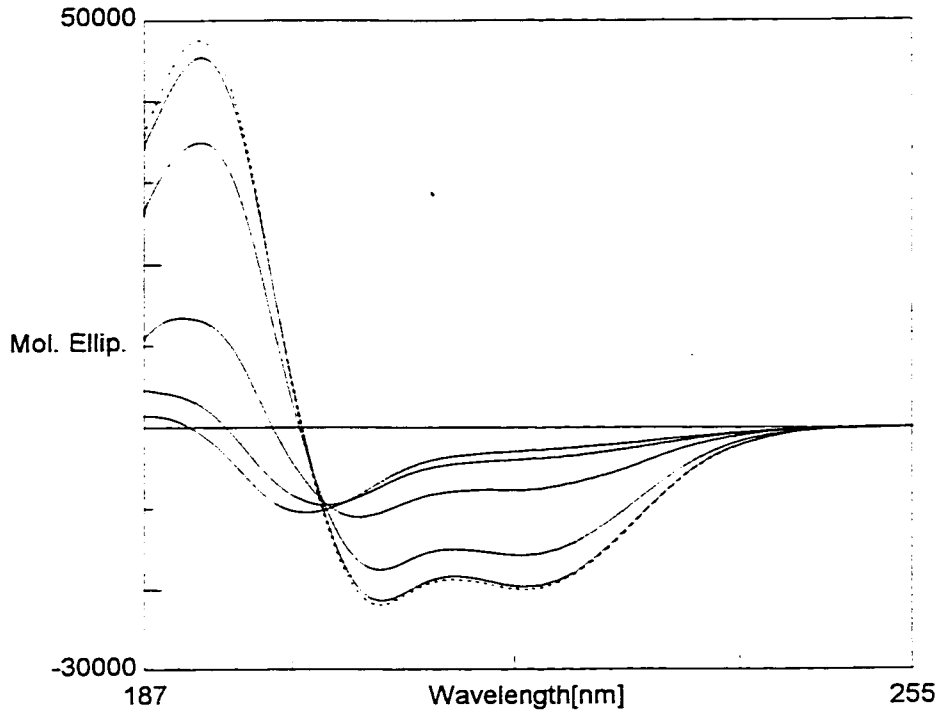

Figure 5.42 HFIP Titration of hAM(1-20)GY at 25 °C. HFIP levels, in order of increasing helicity (decreasing [θ]221): 0, 4, 6, 8, 12, 25 vol %.

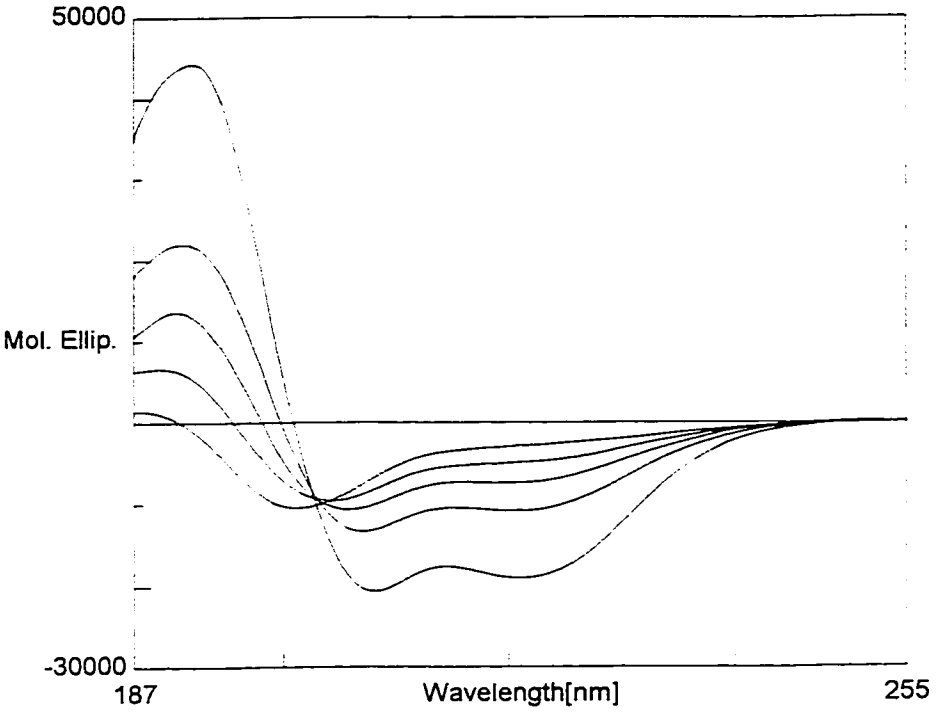

Figure 5.43 TFE Titration of hAM(1-20)GY, at 25 °C. TFE levels, in order of increasing helicity (decreasing [θ]221): 0, 10, 13, 16, 40% of TFE.

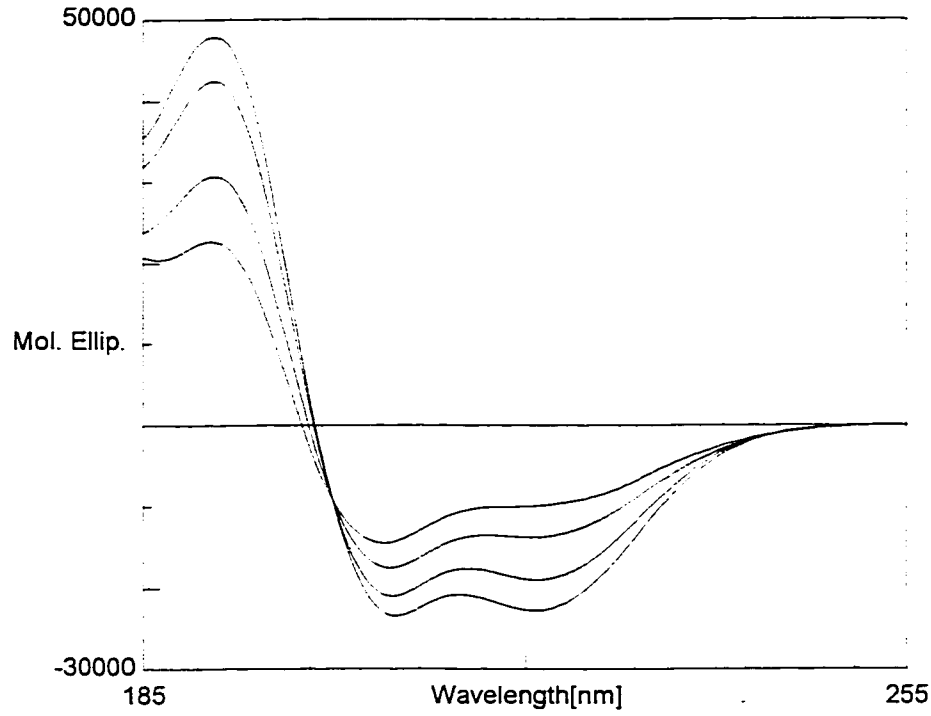

Figure 5.44 Thermal Study of hAM(1-22)G in 25% HFIP. The temperature, in order of decreasing helicity (increasing [θ]221): -3, 24, 64, 88 °C.

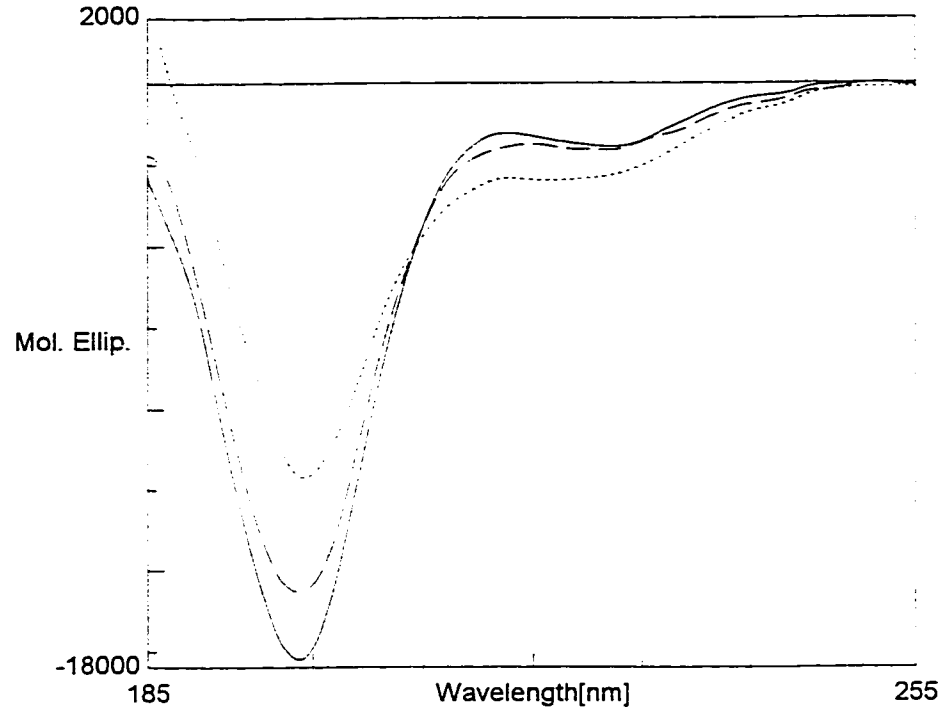

Figure 5.45 Thermal Study of A2,7-hAM(1-20)G in Buffer.
(Solid line: 0 °C; dash line: 25 °C; dotted line: 80 °C)

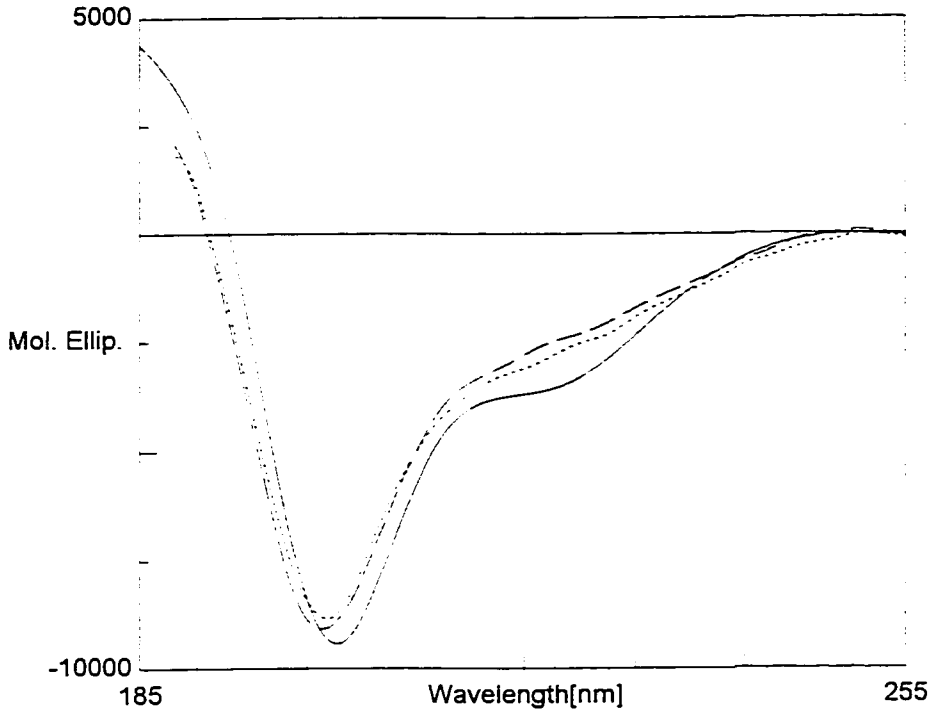

Figure 5.46 Thermal Study of hAM(1-20)GY in Buffer.
(Solid line: 1 °C; dash line: 44 °C; dotted line: 67 °C)

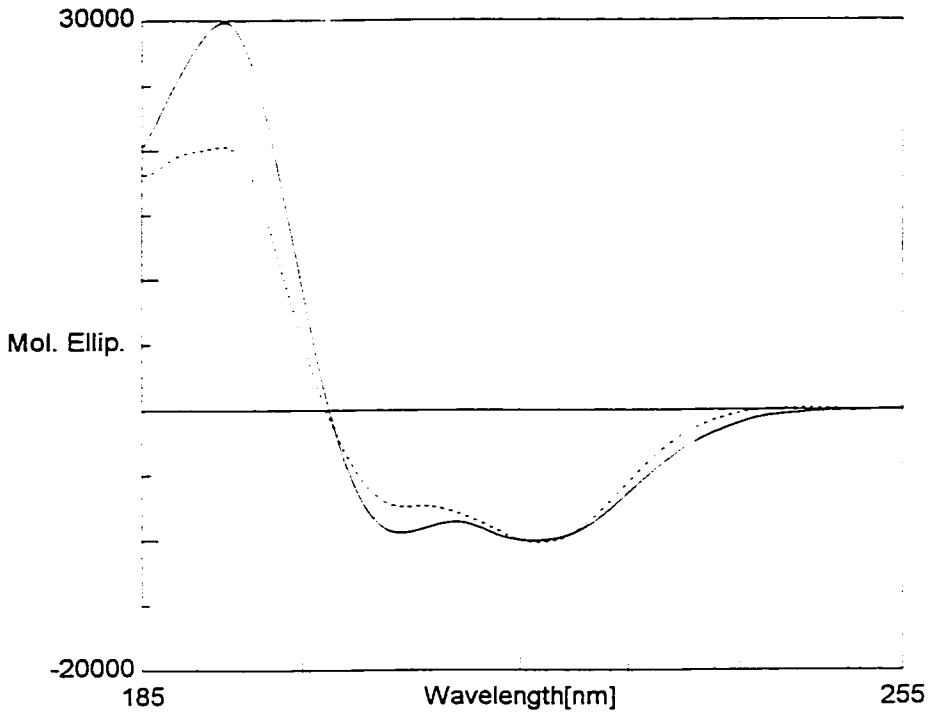

Figure 5.47 Thermal and Titration Difference Spectra of hAM(1-22)GY. Spectra are normalized at ± 10,000 at 220 nm. (dotted line: spectrum at 1°C minus spectrum at 65°C, in 25% HFIP; solid line: spectrum in 25% HFIP minus spectrum in 6% HFIP, at 25°C.) .

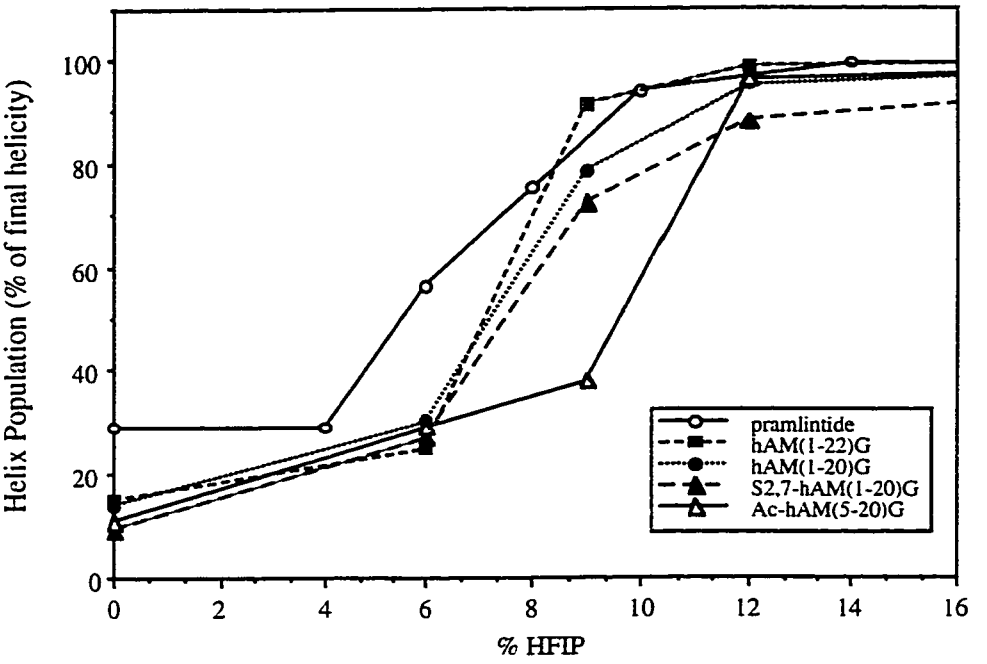

Figure 5.48 Titration Curves of Amylin-Related Peptides.

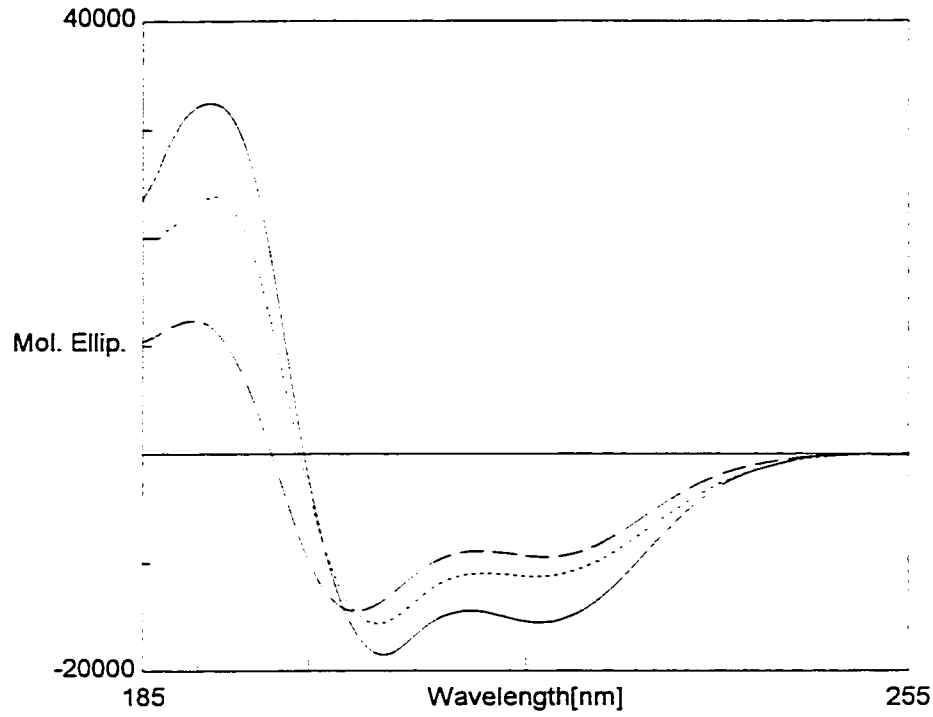

Figure 5.49 Thermal Study of S2U7-hAM(1-20)G in 8% HFIP.
(dash line: 0 °C; solid line: 25 °C; dotted line: 65 °C)

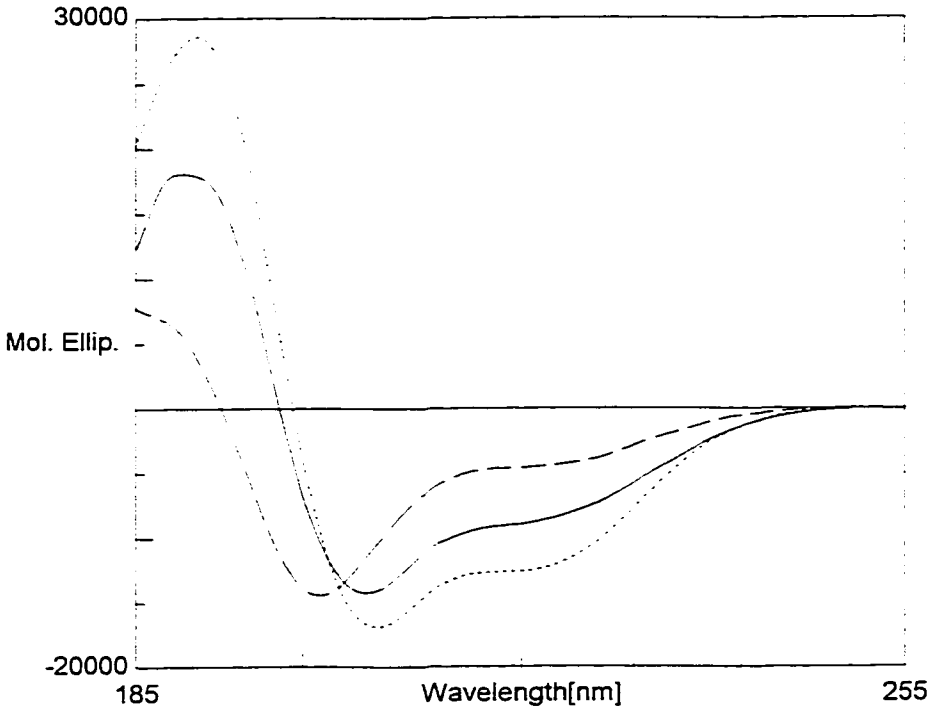

Figure 5.50 Thermal Study of sCT(1-20)G in 5% HFIP.
(dash line: 0 °C; dotted line: 36 °C; solid line: 82 °C)

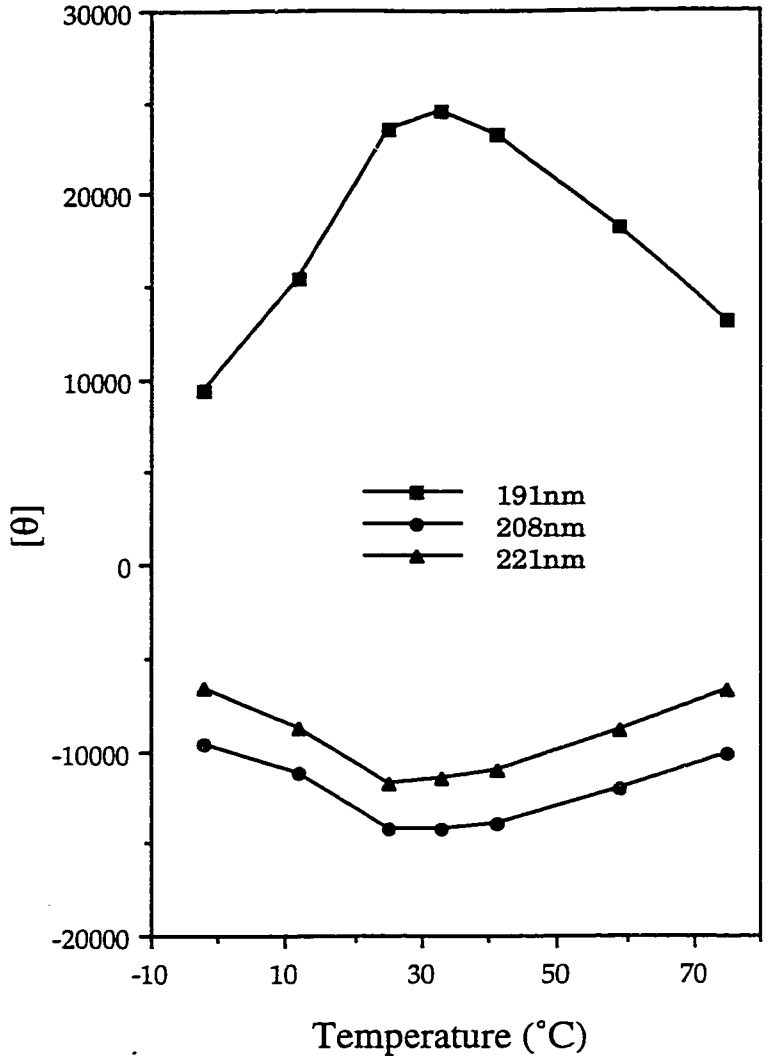

Figure 5. 51 Temperature Dependence of [θ] for [R18-hAM(1-20)GY] in 7% HFIP, Monitored at 191, 208, and 221nm.

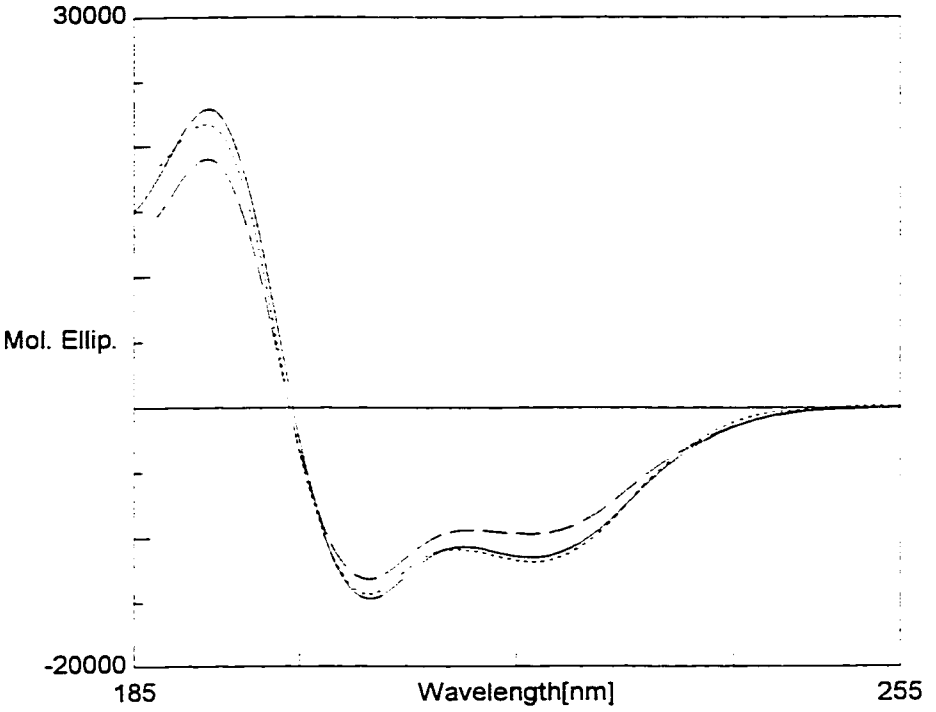

Figure 5.52 Thermal Study of S2U7-hAM(1-20)GY in 16% TFE.
(Dotted line: 0 °C; Solid line: 25 °C; dash line: 40 °C)

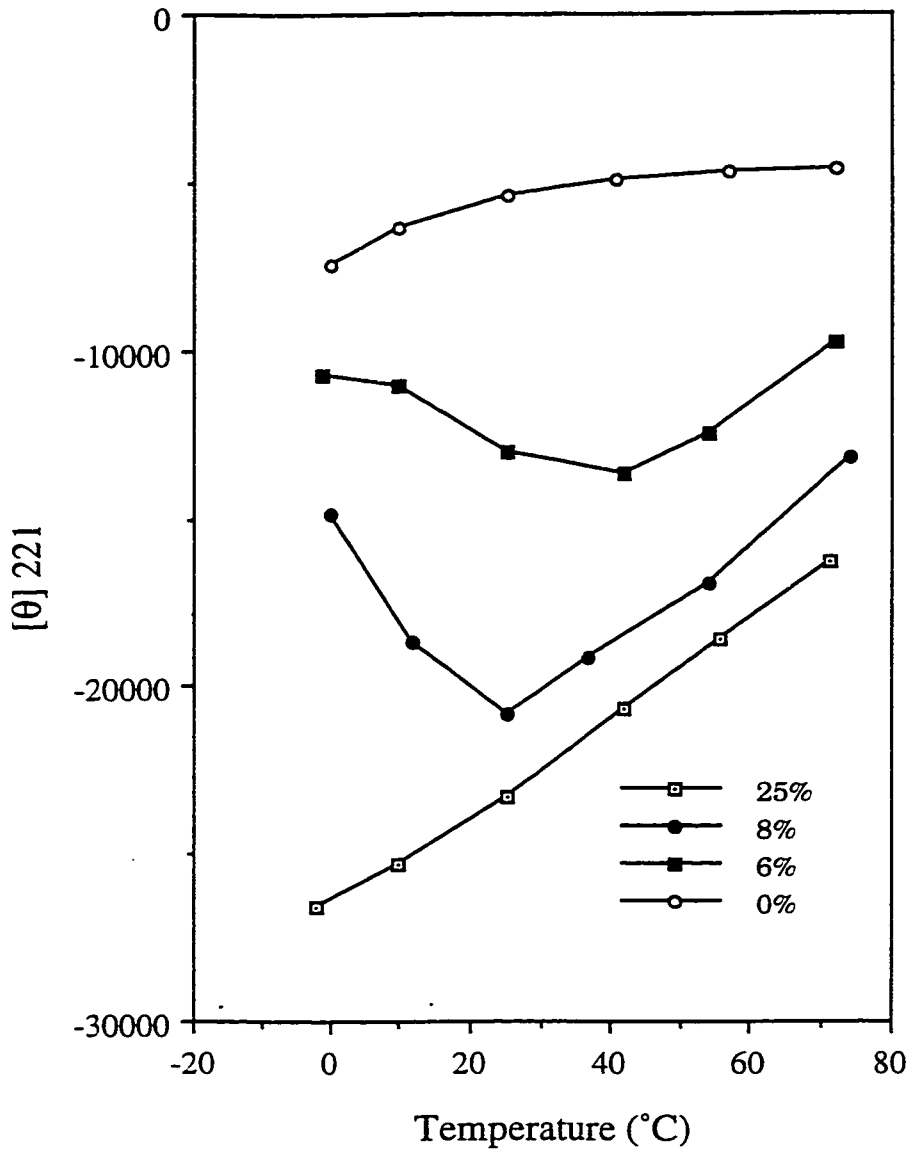

Figure 5.53 Temperature Dependence of [θ]221 for [CGRP(1-21)] at Different levels of HFIP.

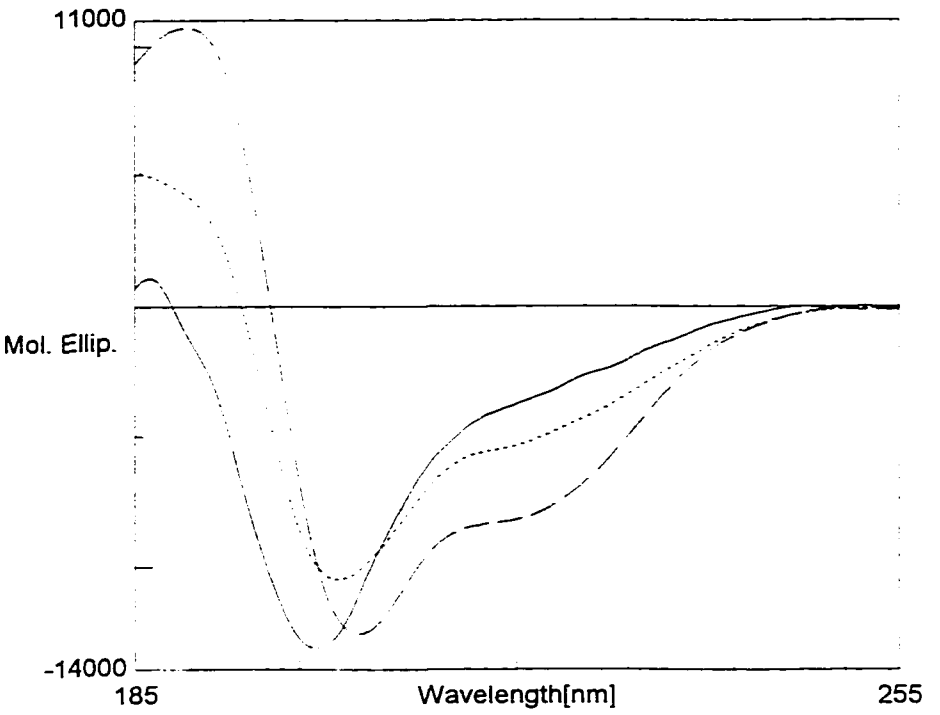

Figure 5.54 Thermal Study of D-Leu^{12}-pramlintide in 9% HFIP.
(Solid line: -2 °C; dash line: 34 °CSD; dotted line: 80 °C)

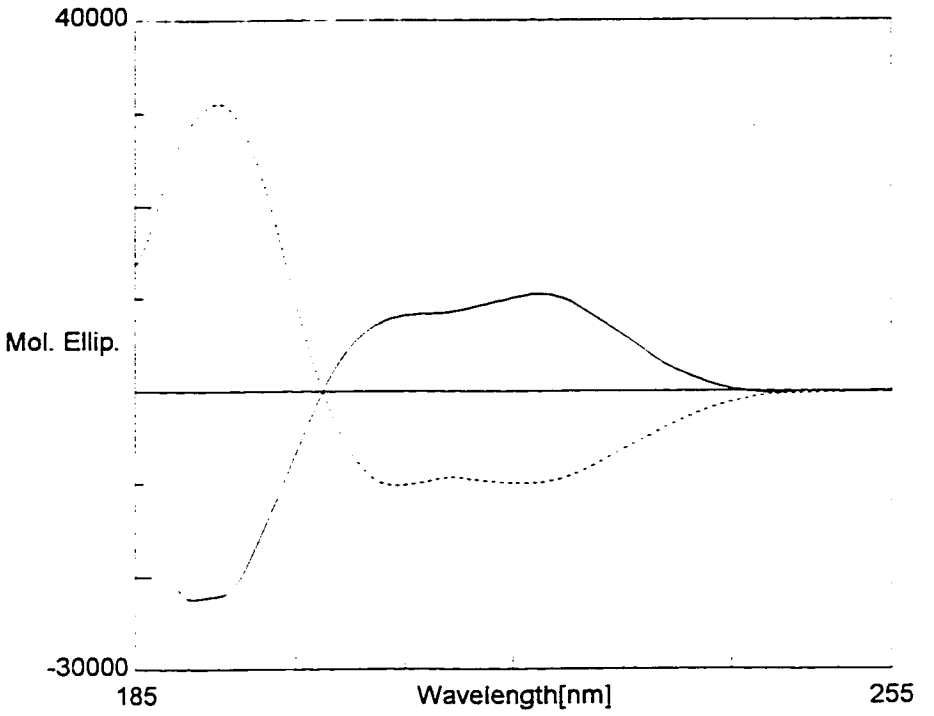

Figure 5.55 Difference Spectra for Temperature Study of hAM(1-22)GY in 8% HFIP. (dotted line: spectrum at 25 °C minus spectrum at 1 °C; solid line: spectrum at 65 °C minus spectrum at 25 °C.) Spectra are normalized at ± 10,000 at 220 nm.

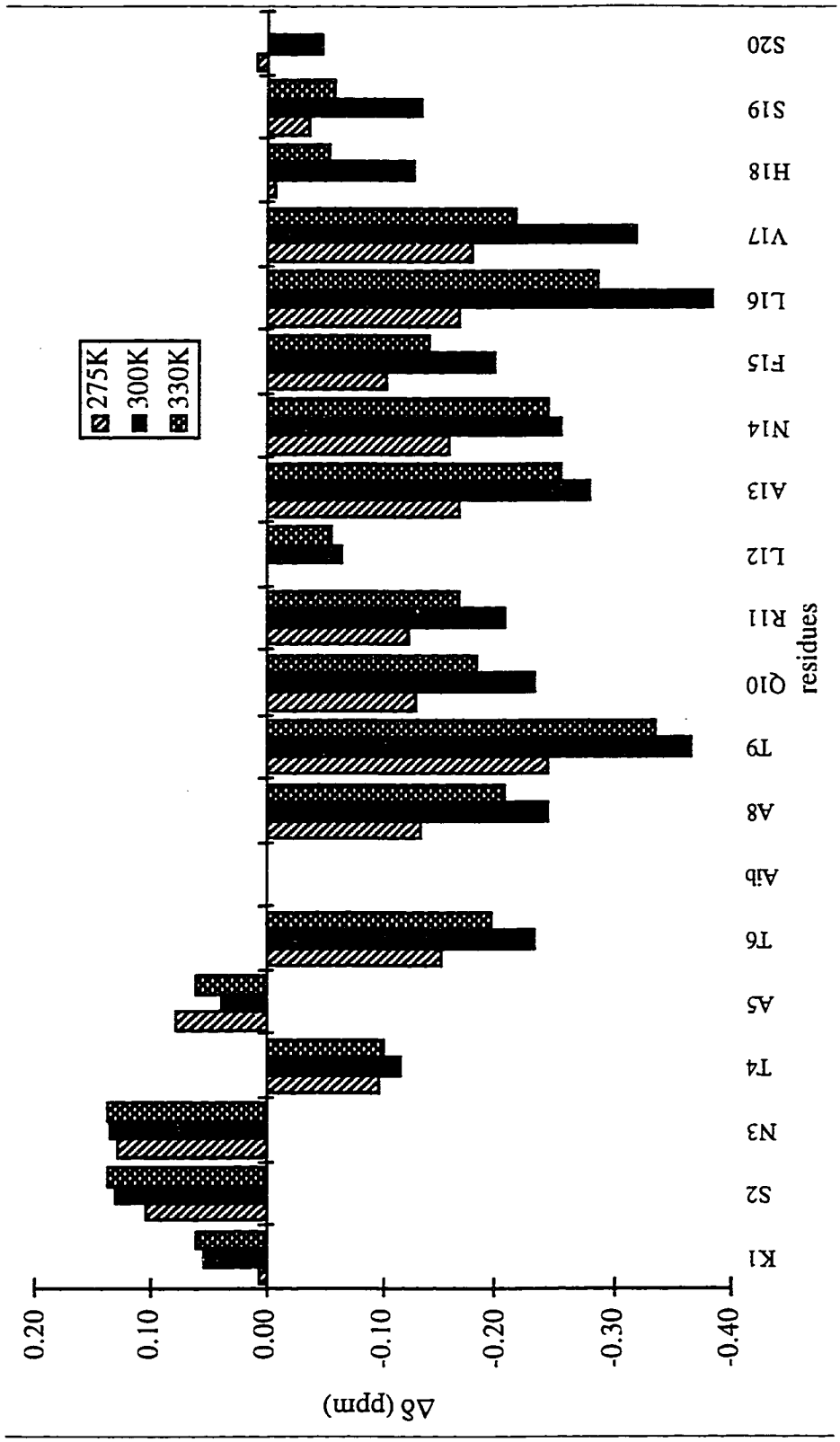

Figure 5.56 [S2U7-hAM(1-20)G] in 8% HFIP: Temperature Dependence of αH-CSDs.

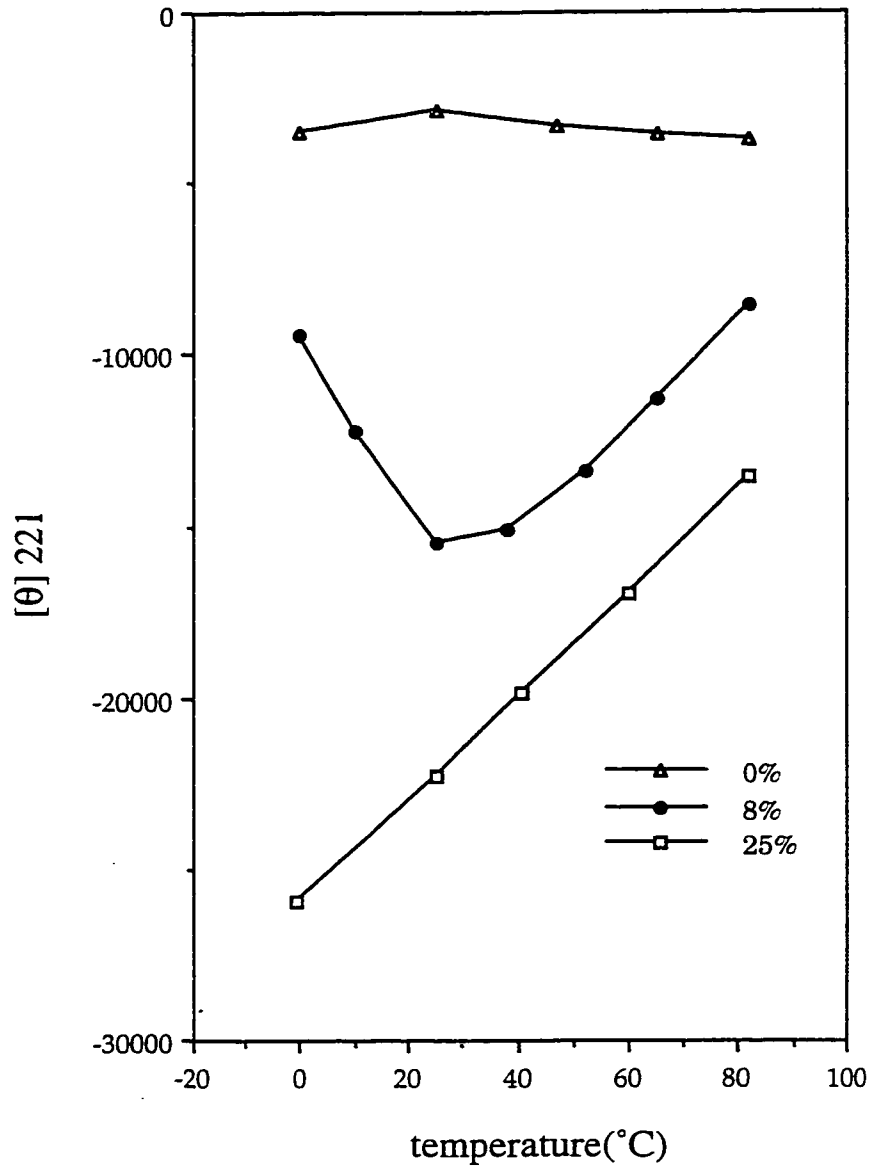

Figure 5.57 Temperature Dependence of $[\theta]_{221}$ for [S2U7-hAM(1-20)G] at Different levels of HFIP.

Chapter 6

Comparison Study of Calcitonin, CGRP and Amylin Fragments

Calcitonin (CT), calcitonin Gene-related peptide (CGRP) and amylin have an N-terminal Cys-Cys disulfide loop and a C-terminal amide, and they share some sequence homology. It has been proposed that they bind to a family of G-protein-coupled receptors (Wimalawansa, 1997). However, each of them appears to have different receptors and distinctive biological functions (Muff et al., 1995; Cooper, 1994). It was found that a salmon calcitonin C-terminal fragment was a potent inhibitor of amylin (Young et al., 1994). Furthermore, a series of amylin and salmon calcitonin hybridized peptides lacking the N-terminal disulfide loop have been found to be potent inhibitors which bind to not only amylin but also calcitonin and CGRP receptors (Prickett et al., 1995). Consequently, it may be conjectured that the N-terminal portions of these peptides are responsible for the structural specificity and unique physiological activities of these peptides.

There have been quite a few studies on solution structure of CGRP and CT (Motta et al., 1989; Breeze et al., 1991; Meadows, et al, 1991; Meyer et al, 1991; Motta et al, 1991a & b; Amodeo et al., 1994). However, these studies were all done independently of each other, and under dissimilar conditions. This is of some concern since it is well established that peptide conformation is highly sensitive to many factors, such as solvent, temperature, ionic strength and pH. For instance, it was observed that the helicity of sCT(8-32) in 16% TFE is largely depends on pH (Z. Liu unpublished data). Herein, a detailed NMR & CD comparison of N-terminal fragments under the same conditions will be presented, the aim of which is to reveal the structural basis of the specificity of calcitonin, CGRP, and amylin. The preliminary results of this study were presented at the 37th ENC (Liu & Andersen, 1996).

6.1 *CD Studies*

The initial studies concentrated on the sequences shown below. The salmon calcitonin fragment differs from the amylin/CGRP fragments in the number of residues in the N-terminal disulfide loop and all three series differ significantly in the placement of residues (Gly/Asn/His) with reduced helix propensity (Chou & Fasman, 1974)

within the residue span of 8 - 18. Gly, Asn and His also have very small helix propagation values according to Chakrabartty et al. (1994).

sCT(1-20)G CSNLS TCVLG KLSQE LHKLQ G-NH2
hCGRP(1-21) ACNTA TCVTH RLAGL LSRSG G-NH2
hAM(1-20)G KCNTA TCATQ RLANF LVHSS G-NH_2

Comparing the sequences, hCGRP(1-21) and sCT(1-20)G both have Val^8 instead of Ala^8, which has lower helix propensity. Further more, they both have Gly, which is a helix breaker, near the middle of the sequence. In sCT(1-20)G, the Gly appears earlier in the sequence, which should make helix formation even more difficult. Thus considering the peptide sequences alone, it would be expected that hAM(1-20)G would be the most helical, followed by hCGRP(1-21), leaving sCT(1-20)G as the least helical. However, this was not observed in the initial CD studies.

Figure 6.1 is a CD comparison of the three fragments in 20/20 mM AcOH/HCOOH buffer, pH~4, at 25°C. Under these conditions, all three peptides are mostly random coil, with a small fractional helicity. Unexpectedly, hCGRP(1-21) is the most helical one, followed by hAM(1-20)G. This is shown not only by a larger negative $[\theta]_{221}$, but also a red shift at the minima. More surprisingly, the thermal CD study showed that as the temperature decreases, helix content increases for hCGRP(1-21) in buffer (Figure 6.2); while hAM(1-20)G remains about the same and sCT(1-20)G increases its poly ProII content. Upon fluoroalcohol addition, all three peptides become much more helical. By the time they have reached their maximum helicity in 25% HFIP, they are all about equally helical, as shown by CD (Figure 6.3). However, significant differences in curve shape remain. The unusually large maximum at 191.2 nm of sCT(1-20)G might be an indication of higher helicity of the peptide, or that there some other factors influencing the CD curve shape.

At this stage, the questions raised are: Why does hCGRP(1-21) behave differently from other peptides in buffer? Which part of its sequence become more helical on cooling? What are the structural differences among the helices of the three peptides in high fluoroalcohol content? In order to obtain more detailed structural information directed toward these questions, NMR studies were carried out in both buffer and 25% HFIP aqueous media, and will be presented in the following sections.

6.2 *Resonance Assignments of sCT(1-20)G and hCGRP(1-21)*

6.2.1 *Assignments of sCT(1-20)G*

In any assignments of a peptide or a protein of known sequence, it is essential to keep in mind which amino acids are involved. The unique amino acids in sCT(1-20)G sequence are Asn^{3}, Thr^{6}, Val^{8}, Gln^{14}, and His^{17}. There are two each of $Cys^{1,2}$, $Gly^{10,21}$, $Glu^{15,20}$, and $Lys^{11,18}$; three $Ser^{2,5,13}$, and five $Leu^{4,9,12,16,19}$. To distinguish the five leucines might prove to be potentially difficult.

Resonance Assignments in Buffer. A 1D spectrum of sCT(1-20)G in buffer is shown in Figure 6.4. Most of the amide ^{1}H shifts are jammed into less than 0.3ppm, which greatly increases the level of assignment difficulty. As usual, a TOCSY spectrum was collected to identify spin systems, and a NOESY spectrum was used for sequential assignments.

Figure 6.5 is the NH/$\alpha\beta\gamma\delta$ region of the sCT(1-20)G TOCSY spectrum in buffer. One of the entry points is the unique Thr^{6} spin system, which is identified in Figure 6.5. The Thr^{6} spin system is characterized as having quite similar α/β chemical shifts which couple with a methyl group around 1.2 ppm. This is also seen in Figure 6.6, the $\alpha/\beta\gamma\delta$ region of the TOCSY spectrum. The Val^{8} spin system was located unambiguously, due to the unique βH shift, which couples with two methyl groups at about 1 ppm. Comparing the αN finger print region of the TOCSY and NOESY spectra recorded under the same conditions (Figure 6.7), the most down field NH line was quickly assigned to the Ser^{2} amide ^{1}H, since it sees an $\alpha_{i}N_{i+1}$ peak which does not have a correlated $\alpha_{i}N_{i}$ NOESY or TOCSY peak. Then a string from residue 1 to 9 was assigned due to $\alpha_{i}N_{i+1}$ NOESY connectivities and the spin systems identified earlier. The αHs of $Leu^{4\&9}$ were located with the assistance of $\alpha/\beta\gamma\delta$ region of the TOCSY spectrum shown in Figure 6.6.

Another entry point was His^{17} whose $\beta_{i}N_{i}$ peaks coupled with the aromatic δH. Lys^{18} was then assigned due to the $\alpha_{17}N_{18}$ NOE connectivity. Once Lys^{18} had been identified, the other Lys (residue 11) whose spin system could be identified due to coupling with side-chain NH at about 7.5 ppm, was automatically assigned. Then Gly^{10} was traced back by $\alpha_{10}N_{11}$ NOE connectivity, followed by the assignment of the other Gly (residue 21). Ser^{13} whose α/β TOCSY cross peaks can be seen very clearly in Figure 6.6, was also automatically assigned after the assignment of Ser^{2} and Ser^{5}. Gln^{14} was assigned and confirmed by $\alpha_{13}N_{14}$ and its own long side chain resonances.

At this point, two glutamines and three leucines were left. After a more careful examination of αN and NH - aliphatic regions of the NOESY spectrum, and a 'trial and error' process, a complete self-consistent assignment of sCT(1-20)G in buffer was achieved. The assigned backbone chemical shifts are tabulated in Table 6.1, together with the shifts in 25% HFIP and the backbone shifts of hCGRP(1-21) in both media.

Resonance Assignments in 25% Aqueous HFIP. The assignment of sCT(1-20)G in 25% HFIP was easier than the assignments in buffer, due to the dispersion of amide ^{1}H shifts which can be clearly seen in the NH/αβγδ region of TOCSY (Figure 6.8), or even in the 1D spectrum (Figure 6.9) taken under the same conditions. On the other hand, the αHs of some of the long side chain residues are still very close to each other as shown in Figure 6.10. As mentioned earlier, the CD data indicates that this peptide is mostly helical under these conditions. Consequently, many medium-range NOEs are detected besides the i/i+1 sequential NOEs in the finger print region of the NOESY spectrum (Figure 6.11), which can cause confusion at the beginning of the assignment process.

Initially, efforts were made to identify unique residues. The single Val^8 could be located by inspecting the TOCSY spectrum alone (Figure 6.8), but the pair of αN, βN peaks of Thr^6 were not as obvious as they were in buffer. Asn^3 was assigned due to the observation of pairs of βN and β/side-chain-NH correlations. This was also the case for Gln^{14}. The unique His^{17} was also assigned by the detection of intra-residual αH and βH NOEs with aromatic δH at about 7.4 ppm (data not shown).

After Asn and His were picked out, the only short spin system left which has βHs between 3.2-3.5 ppm was assigned as Cys^7 (Figure 6.8), because Cys^1 would not show up in this region due to fast exchange between the amide proton and the solvent. This was confirmed by α_7N_8 and γ_6N_7 connectivities. Other residues in the loop, Leu^4 and Ser^5, were easily assigned due to the observation of inter-residue NOEs. The assignment of residue Ser^2 was more difficult because of shift coincidence, however, the N_2N_3 NOE (Figure 6.13) helped to locate its NH line. And the NOEs that arise from residue Cys^1 which were not seen by its own NH further confirmed the assignment of residue 2.

Extending the assignment from Val^8 to C-terminal of the peptide, all the NHs of rest of the residues could be located by $N_iN_{i\pm1}$ connectivities, which were detectable for the entire sequence, except N_3N_4 (shown in Figure 6.13). In addition, numerous sequential NOEs were detected in the finger print and aliphatic-NH regions of the

NOESY spectrum, which allowed an unambiguously assignment of the entire sequence. For instance, the well-resolved α_8N_9, $\alpha_{10}N_{11}$, $\beta_{13}N_{14}$, and $\alpha_{17}N_{18}$ NOE peaks assisted the assignments of Leu[9], Gly[10], Ser[13] and Lys[18], respectively. Since almost half of the residues in sCT(1-20)G are long side-chain amino acids, the aliphatic-NH region was particularly important for the assignment of the peptide. The detection of $\beta_{11}N_{12}$, $\beta,\gamma_{12}/N_{13}$, $\beta,\gamma_{15}/N_{16}$, $\beta,\gamma,\delta_{16}/N_{17}$, β, γ_{19}/N_{20}, and $\beta,\gamma_{20}/N_{21}$ were crucial to confirm the assignments of Lys[11], Leu[12], Gln[15], Leu[16], Leu[19] and Gln[20], respectively (Figure 6.12).

In addition to the sequential NOEs, well resolved α_iN_{i+3}, α_iN_{i+4} and $\alpha_i\beta_{i+3}$ (Figure 6.14) connectivities served as further confirmation of these assignments.

The backbone chemical shifts of sCT(1-20)G in 25% aqueous HFIP were extracted and are listed in Table 6.1.

6.2.2 *Assignments of hCGRP(1-21)*

The unique residues in hCGRP(1-21) are Asn[3], Val[8], and His[10]. There are two each of Cys[2, 7], Arg[11, 18], Ser[17, 19] and three Ala[1, 5, 13], Thr[4, 6, 9], Leu[12, 15, 16] and Gly[14, 20, 21] in the sequence. The position and the sequence of the disulfide loop in hCGRP(1-21) is the same as in hAM.

Resonance Assignments in Buffer. Figure 6.15 is a 1D spectrum of hCGRP(1-21) in buffer, although fairly crowded in the 8.2-8.5ppm range; there are a few well separated NHs. Portions of the TOCSY spectrum are shown in Figure 6.16-17, which was used to identify the spin systems. Again, a unique Val[8] could be identified in Figure 6.16. In the α/side-chain region three very intense peaks at about 1.45 ppm in t_2 dimension were attributed to the methyls of the alanines. Among those the one that has the most upfield α shift and did not show up in Figure 6.16, was assigned to Ala[1]. Three threonine spin systems were located from the γN correlations at around 1.25ppm. Two arginines were separated from the leucines because of the correlation of side-chain CH's with εH. And the residues with characteristic βH shift around 3 ppm were grouped together. Two serines with a pair of α,β/N resonances at about 4 ppm were also located.

The quality of the NOESY spectrum in buffer was relatively poor, and only the aN region is shown in Figure 6.18. However, sequential assignment was still achievable. The detection of $\alpha,\beta_1/N_2$ and α_2N_3 NOEs allowed assignments of residue 1$\rightarrow$3. The connectivity string was lost due to the bleaching of αH of residue 3, but was picked up again by $\alpha,\beta,\gamma_4/N_5$ and β_5N_6. These were further confirmed by N_3N_4 and

N_5N_6 NOE connectivities. At this point it was noticed that the loop NH chemical shift pattern was very similar to that observed for amylin under the same conditions. However, unlike amylin, the αH and βH of Thr^4 were separated. The next string of residues, 7 → 15, was established by the observation of α_7N_8, β_8N_9, $\alpha,\beta_9/N_{10}$, $\alpha_{10}N_{11}$, $\beta_{11}N_{12}$, $\beta,\gamma_{12}/N_{13}$, $\beta_{13}N_{14}$, $\alpha_{14}N_{15}$ and N_7N_8, $N_{14}N_{15}$ sequential NOE connectivities. Subsequently, the single remaining Leu and Arg were assigned to residue 16 and 18. While the $\alpha_{18}N_{19}$ and $\alpha_{19}N_{20}$ connectivities made Ser^{17}/Ser^{19} and Gly^{20}/Gly^{21} distinguishable.

The backbone chemical shifts of hCGRP(1-21) in aqueous buffer were then extracted and are shown in Table 6.1.

Resonance Assignments in 25% Aqueous HFIP. As can be clearly seen even in the 1D spectrum, the amide ^1H of more than half of the residues were well resolved in 25% aqueous HFIP (Figure 6.19), which made the assignments relatively straight forward. The single Val^8 could be easily picked out from the TOCSY spectrum because of the unique spin pattern (Figure 6.20). His^{10} was also clear in the TOCSY spectrum,distinguished from all other amino acids due to the observation of αH to aromatic δH correlation. The αH and NH chemical shifts of His^{10} were almost coincidence with the backbone shifts of another long side chain residue, which was classified as one of the two arginines because of the detection of aliphatic/side-chain NH correlation.

In the αβγδ/N region of NOESY spectrum (figure 6.21), the unique Asn^3 was quickly identified because of the βH/side-chain-NH correlations. And the assignment of Cys^7 was established by the detection of β,β'_7N_8 NOEs. Then the only unassigned residue, which has βHs between 3.0-3.5 ppm, was assigned as Cys^2. This was confirmed by $\alpha,\beta_2/N_3$ NOE connectivities. During the water suppression, the αHs of Cys^2 and Asn^3 were bleached, however, these residues showed up in α-aliphatic region of the TOCSY spectrum (Figure 6.22). The assignments of other residues in the loop were made mainly from the NOEs detected in the NH-Methyl region, such as γ_4N_5, β_5N_6 and γ_6N_7. The NOE connectivities in the NH-aliphatic region were also crucial for the assignment of the rest of the sequence, for instance: β,γ_8N_9, γ_9N_{10}, $\beta\gamma_{11}N_{12}$, $\beta\gamma_{12}N_{13}$, $\beta_{13}N_{14}$, $\beta\gamma_{15}N_{16}$, $\beta\gamma_{16}N_{17}$, and $\beta\gamma_{18}N_{19}$. Further confirmation of the assignments came from many α_iN_{i+3} and α_iN_{i+4} correlations in the finger print region (Figure 6.21), the nearly complete string of $N_iN_{i\pm1}$ connectivities (except N_4N_5 was absent) (Figure 6.23), and some well resolved $\alpha_i\beta_{i+3}$ NOEs (Figure 6.24).

The complete backbone assignment is presented in Table 6.1.

6.3 *sCT, hCGRP and Amylin Fragments: Structural Insights*

From the inspection of the spectra, it is obvious for all three peptides, that most of the NHs are very close to each other, and the αHs are mostly near their random coil values in the absence of fluoroalcohol; apparently, the peptides have little structure under these conditions. However, one thing worth notice is that the NH chemical shifts patterns in the disulfide loop of hCGRP(1-21) and hAM(1-20)G are very similar, and distinct from that for sCT(1-20)G (See NH-CSD histograms in Figure 6.25 lower panel). hCGRP(1-21) and hAM(1-20)G have large NH chemical shift deviations in the loop region, which indicate a well defined structure; while sCT(1-20)G NH shifts are close to coil values. Furthermore, a similar pattern of N_iN_{i+1} NOE connectivities is also observed for hCGRP(1-21) and hAM(1-20)G; This pattern is different from what is seen for sCT(1-20)G . They both show strong 3/4, 5/6, and 6/7 NN connectivities, while sCT(1-20)G shows strong 2/3, 5/6, 6/7, and weak 4/5 NN connectivity. The αH-CSD comparisons (Figure 6.25 upper panel) show that sCT(1-20)G is more uniformly random in buffer; while hCGRP(1-21) and hAM(1-20)G have a partially populated helix spanning residue 5 to approximately Gly^{14} and Val^{17}, respectively, as indicated by small but continuously negative αH deviations. This is consistent with the observation from CD that hCGRP(1-21) and hAM(1-20)G are more helical than sCT(1-20)G. It is suggested that the six-residue disulfide loop in both hCGRP(1-21) and hAM(1-20)G nucleates a helix in that region, while the seven-residue loop is too flexible to produce helix nucleation.

At first, it was a little surprising that hCGRP(1-21) is more helical than hAM(1-20)G, over the residue range 6 to 9 as indicated by the αH-CSD histograms, since the helix propensity of Val is much smaller than Ala. In addition, the thermal NMR study revealed that the αH resonances of hCGRP(1-21) move upfield on cooling (Figure 6.26), an indication of increasing helicity. These changes are most dramatic at residues 7 and 8. This is consistent with what has been observed in thermal CD studies hCGRP(1-21) -- the helix freezes in as the temperature goes down. However, this was not observed for hAM(1-20)G. Therefore, it is suggested that this is due to the conformational restriction of Val^8 in hCGRP(1-21), which is replaced with the more flexible Ala^8 in hAM(1-20)G. The single turn of helix in the loop propagates more

efficiently through the less flexible Val residue. In addition, Val^8 extends a hydrophobic cluster that can be seen in Figure 4.44.

In a solution of 25 vol-% aqueous HFIP, all three peptides are judged to be mostly helical based on the αH-CSD histograms (Figure 6.27). Again, the αH and NH chemical shift deviation pattern of residues 2-5 in the loop of hCGRP(1-21) and hAM(1-20)G are quite different from the corresponding portion of sCT(1-20)G. Here, one question is raised: How does one interpret the positive a-CSD value of residue 7 in sCT(1-20)G? One explanation is that the helix does not form within the loop, and the negative α-CSD values of residues 4-6 could, instead, be an indication of a turn. An alternative interpretation is that there is a helix formed starting from residue 4 and propagating through the entire sequence and residue 7 is indeed in an α configuration; however, there are some other factors that influence its αH chemical shift. The latter is supported by NOE connectivities. Large N_iN_{i+1} connectivities were observed throughout the 4-21 span (Figure 6.13), and the $\alpha_iN_i/\alpha_iN_{i+1}$ NOE ratios available from 4-17 were also greater than 1 (Figure 6.11). Furthermore, medium-range NOEs, such as α_5N_8, α_7N_{10}, α_4N_8, α_5N_9, $\alpha_4\beta_7$ are well resolved, which are characteristic of α-helix formation (Figure 6.11, 6.14). A summary of sequential and medium-range NOEs appears in Figure 6.28. sCT(1-20)G has helical domain starting at Leu^4, and continuing nearly to the C-terminus. The helix has some flexibility at Gly^{10}, but is reinforced later in the sequence.

The structural features observed for sCT(1-20)G in this study are quite similar to the data previously reported for sCT in 90% methanol/10% H_2O (Meadows et al., 1991) and in 9 TFE/ 1 H_2O media (Meyer et al, 1991), although they both claimed that the helix does not start till Val^8. It is interesting to note that in TFE and in MeOH aqueous media, Cys^7 of sCT has a much smaller negative CSD value than neighboring residues (Figure 6.29). However, the medium-range NOE connectivities around this site reported in these literatures support that residue 7 is in the α configuration. A recently published eel calcitonin solution structure in 40% TFE aqueous media, (which has sequence identity with salmon calcitonin over the reside span 1-21), contains an amphiphilic α-helix from position Leu^4 - Gln^{20} (Ogawa et al., 1998). This is consistent with our findings. Our previous work on the sCT(8-32) fragment indicates that the helix does not start until residue Lys^{11} when the disulfide loop is absent (Liu et al., 1994; Andersen et al., 1997a), showing the end fraying effect of the linear peptide (Figure 6.30). In contrast, our current findings are quite different from what have been reported for sCT

(Motta et al., 1991) and hCT in sodium dodecyl sulfate (SDS) micelles (Motta et al., 1998).

Unlike sCT(1-20)G, the helix of hCGRP(1-21) and hAM(1-20)G starts at Ala^5. We have previously shown that disulfide loop closure prevents Thr^4 from becoming helical (Liu & Andersen, 1995; also see discussions in Chapter 5). When $Cys^{2\&7}$ are replaced with $Ser^{2\&7}$, Thr^4 adopts an α configuration in both buffer and high HFIP media. It is obvious that residues 6-8 are highly helical in hCGRP(1-21) compared to other two peptides, since all three residues have a chemical shift deviation of circa - 0.5 ppm (Figure 6.27). We attribute this to the conformational restriction associated with the six-residue disulfide loop in conjunction with Val^8. The helix becomes severely frayed from Gly^{14} onward. Some medium-range NOEs were observed within residues 5-14, and none after Gly^{14} (Figure 6.21 & 6.21). A diagram of sequential and medium-range NOEs observed for hCGRP(1-21) appears in Figure 6.31. The hCGRP(1-21) helix is much more frayed in its C-terminal section than is observed in sCT and AM fragments.

Breeze et al. (1991) concluded that the well defined helix of hCGRP in 50% TFE starts at residue 8. The comparison of αH-CSD profile (figure 6.32) suggests that the two peptides adopt very similar conformations in 50% TFE vs 25% HFIP media, with an α-helix starting at residue 5. At first glance, the αH-CSD histograms, might lead one to believe that the peptide is much more helical in 50% TFE than in 25% HFIP even at a higher temperature. However, it is suspicious that the chemical shifts seem universally shifted upfield. Since the solvent effects have already been corrected, and the residual CH resonance of TFE-d_2 (3.88ppm) was used as internal reference in the Breeze paper, the more negative CSD values are most likely due to a chemical shift referencing discrepancy. Taking this into consideration, the truncation of the C-terminal portion of the peptide does not have a large influence on the conformation of the N-terminal segment, which is similar to what has been observed for amylin.

In 25% aqueous HFIP, sCT(1-20)G, hCGRP(1-21) and hAM(1-20)G all adopt a mostly helical conformation. It is worth noting that although the helix propensity of Asn and His are small, the helix propagates well through Ans^{14} and His^{18} in hAM(1-20)G, (as well as their parent peptides), through His^{17} in sCT(1-20)G, and His^{10} in hCGRP(1-21), as supported by αH-CSDs and NOEs. However, Gly causes a weakened helix in the middle of the sCT(1-20)G sequence, and severe end fraying in hCGRP(1-21) in 25% HFIP. In aqueous buffer, the helix does not propagate through

Gly^{14} in hCGRP(1-21). It is curious that a structure-activity study (Li, et al., 1997) showed that substitution of Gly^{14} with amino acids having higher helix propensity, including Aib, does not increase the helicity of the peptide, nor have much influence on the bioactivities. This might be because that the helicity in hCGRP, at least in aqueous buffer, is mainly associated with the disulfide loop and Val^8.

6.4 *Amylin/hCGRP Fragment Hybrids*

The rationale for the surprisingly large helicity of the hCGRP fragment prompted an examination of the hCGRP/amylin hybrid structures: V8Y and V8S9Y. V8Y is hAM(1-20)GY containing an $Ala^8 \rightarrow Val^8$ mutation. V8S9Y has an additional Thr^9 to Ser^9 substitution. Serine is known to have a higher helical propensity than threonine. The sequences examined are shown below.

V8Y	V8-hAM(1-20)GY	KCNTA TCVTQ RLANF LVHSS GY-NH_2
V8S9Y	V8S9-hAM(1-20)GY	KCNTA TCVTQ RLANF LVHSS GY-NH_2

As expected, CD studies revealed, that V8Y, with the single A8V mutation, is more helical than any of the amylin fragments; and V8S9Y is more helical than V8Y. Figure 6.33 shows the CD comparison of hAM(1-20)GY, V8Y and V8S9Y in aqueous buffer. The minima are at 201.2, 201.8 and 203.0 nm for hAM(1-20)GY, V8Y and V8S9Y, respectively. A red shift of this minimum is a clear indication of increasing helicity. In addition, both V8Y and V8S9Y become more helical upon cooling in buffer, similar to what was observed for hCGRP(1-21), but to a greater extend (Comparing figure 6.34 and 6.2). As shown in Figure 6.34, at –1 °C, V8S9Y has relatively well defined helix characters, with a maximum at 189.8 nm and a double minimum at 206.6 and 221.2nm.

The CD data of the peptides discussed in this chapter are summarized in Table 6.2. It is a continuance of Table 5.5, with the same definition for each column, which as was discussed in section 5.5. In aqueous medium V8S9Y is the most helical fragment examined to date, with the largest positive temperature gradient and the largest negative R1 value. Further more, it has the smallest vol-% of HFIP requirement to achieve 50% of the maximum helicity. On the contrary, sCT(1-20)G has a negative temperature gradient and a positive R1 value in buffer, which is consistent with what has been concluded from the NMR data. However, we have no explanation for the very large negative R1 value of sCT(1-20)G in aqueous HFIP.

With regards to the NMR studies of the amylin/CGRP hybrids, the assignments of these two peptides were relatively straight forward, and chiefly made by analogy. Figure 6.35 –36 and Figure 6.37-39 are regions of the TOCSY and NOESY spectra of V8Y in aqueous buffer and HFIP. And Figure 6.40-41 and Figure 6.42-46 are regions of the labeled spectra for V8S9Y in both media. Some extra peaks were detected (as indicated in Figure 6.40), which were attributed to minor impurities. The spectra of the two peptides are nearly identical. The only obvious distinction between V8S9Y and V8Y is one pair fewer of α,β to methyl correlations from threonine (comparing Figure 6.36&41 or figure 6.39&43). The backbone chemical shifts of the two hybrids in buffer and in aqueous HFIP are tabulated in Table 6.3.

The αH-CSD comparisons of the two hybrids and hAM(1-20)GY appear in Figure 6.47, these confirm the conclusion from the CD study. The A8V mutation decreases the flexibility at the juncture between the loop and the remainder of the sequence, which allows for more efficient helix propagation. In addition, a hydrophobic cluster, particularly, Val^{8}/Leu^{12}, may also contribute to this helicity enhancement. Serine is known to have a higher helical to, propensity than threonine, however, this is probably not the cause of the effect: Figure 6.47 upper panel clearly shows that the helicity increase associated with the T9S mutation is in the loop rather than centered about the mutation site. The nearly perfect hybrid character of these analogs can be seen in Figure 6.48. In both aqueous buffer and 25% HFIP, the N-terminal of the V8S9Y resembles hCGRP(1-21), and the C-terminal of the hybrid more like hAM(1-20)GY, which makes it most helical among the peptides studied in this project.

6.5 *Conclusions*

The most instructive NMR parameters have been chemical shift deviation histograms with a few key differences in medium-range NOEs, which provide confirmation of the structural hypotheses that resulted.

The seven-residue disulfide loop is much more conformational flexible than the six-residue ring. It appears to be random in buffer, and allows residue 4 to be helical in 25% HFIP. The six-residue loop stabilizes one turn of helix (residues 5-7).

hCGRP(1-21) is more helical than hAM(1-20)G in buffer, due to the conformational restriction associated with Val^{8}. A Val^{8}/Leu^{12} hydrophobic cluster may also contribute.

Upon addition of fluoroalcohol, sCT(1-20)G may be the most helical of the three, as indicated by both CD spectra and the αH-CSD histogram.

Helices can propagate through Asn and His^+, but the more flexible Gly residue blocks helix propagation in aqueous buffer.

The amylin/hCGRP hybrids [V8-hAM(1-20)GY and V8S9-hAM(1-20)GY] present nearly perfect examples of the hybridization effect; which results in V8S9-hAM(1-20)GY being the most helical peptide studied in this present work.

Recently, more and more structure-activity studies have been published on CT, CGRP, and amylin. The disulfide loop of these peptides is of the great interest and critical for their bioactivities (Dumont et al., 1997; Howitt & Poyner, 1997; Pozvek et al., 1997; Cornish et al, 1998; Heino et al., 1998; Poyner, et al., 1998; Saha et al., 1998). The structural features uncovered in this study should help to elucidate the structure-activity relationships of this family of peptides and will lead to a greater understanding of their pathophysiological roles.

Table 6.1 Backbone Proton Chemical Shifts of sCT [sCT(1-20)G] and CGRP [CGRP(1-21)] in Buffer and in 25% Aqueous HFIP at 285K.

sCT residue	Buffer		25% HFIP		CGRP residue	Buffer		25% HFIP	
	αH	NH	αH	NH		αH	NH	αH	NH
Cys^{1}	4.38	–	4.48	–	Ala^{1}	4.07	–	4.14	–
Ser^{2}	4.59	9.03	4.73	8.80	Cys^{2}	4.72	8.96	5.03	8.97
Asn^{3}	4.66	8.40	4.74	7.95	Asn^{3}	5.01	9.04	5.03	8.88
Leu^{4}	4.32	8.31	4.08	8.56	Thr^{4}	4.49	7.65	4.73	7.47
Ser^{5}	4.43	8.40	4.18	8.07	Ala^{5}	4.20	8.81	4.18	9.09
Thr^{6}	4.40	7.92	4.23	8.23	Thr^{6}	4.21	8.03	4.00	8.24
Cys^{7}	4.76	8.28	4.81	8.70	Cys^{7}	4.45	8.08	4.23	7.79
Val^{8}	4.10	8.26	3.78	8.86	Val^{8}	3.93	8.29	3.63	8.54
Leu^{9}	4.35	8.46	4.25	8.46	Thr^{9}	4.17	8.33	4.15	8.42
Gly^{10}	3.95	8.46	3.98	8.28	His^{10}	4.65	8.39	4.36	7.85
Lys^{11}	4.30	8.28	4.30	7.83	Arg^{11}	4.27	8.37	4.22	8.33
Leu^{12}	4.35	8.46	4.20	8.96	Leu^{12}	4.30	8.40	4.23	8.63
Ser^{13}	4.36	8.36	4.18	8.71	Ala^{13}	4.27	8.26	4.10	8.45
Gln^{14}	4.32	8.43	4.20	7.90	Gly^{14}	3.95	8.29	3.89	8.05
Glu^{15}	4.29	8.32	4.28	8.32	Leu^{15}	4.31	8.08	4.25	8.12
Leu^{16}	4.35	8.40	4.20	8.94	Leu^{16}	4.37	8.30	4.12	9.02
His^{17}	4.68	8.51	4.40	8.25	Ser^{17}	4.42	8.25	4.31	8.34
Lys^{18}	4.27	8.38	4.15	8.11	Arg^{18}	4.42	8.26	4.40	7.86
Leu^{19}	4.25	8.25	4.22	8.31	Ser^{19}	4.48	8.45	4.49	8.16
Gln^{20}	4.33	8.53	4.23	8.12	Gly^{20}	4.02	8.58	4.10	8.26
Gly^{21}	3.92	8.52	3.98	7.96	Gly^{21}	3.94	8.38	3.98	8.30

Table 6.2 CD Data Comparison for sCT, hCGRP and Amylin-Related Peptides

Peptide	In GdmCl	In Buffer			$Titr_{.50}$	In 25% HFIP		
	Formula (xM)	Formula	$R1_{273\|298K}$	$R2_{273\|298K}$	% HFIP	Formula	$R1_{273\|298K}$	$R2_{273\|298K}$
sCT(1-20)G		-2310-35T	0.23 | 0.09	0.15 | 0.22	5.5	-25700+108T	-2.42 | -2.31	0.94 | 0.88
hCGRP(1-21)		-7490+88T	-0.31 | 0.04	0.58 | 0.40	5.5	-26600+124T	-1.73 | -1.63	0.89 | 0.84
hAM(1-20)G	-1000-31T (7.7)	-2710+17T*	N.A. | -0.05	N.A. | 0.29	7.5	-25200+142T	-2.08 | -2.03	N.A. | 0.91
hAM(1-20)GY		-3400+30T*	.003 | -0.18	0.39 | 0.28	7	-22700+111T	-2.19 | -2.17	0.96 | 0.91
V8-hAM(1-20)GY#	-560 – 43T (7.6)	-4620+67T	-0.35 | -0.01	0.49 | 0.33	6	-23840+112T	-2.11 | -2.03	0.94 | 0.89
V8S9-hAM(1-20)GY#	-2460-32T (7.6)	-8400+124T	-1.06 | -0.42	0.77 | 0.45	5	-24230+133T	-2.13 | -2.05	0.96 | 0.90

Peptides indicated were found to be impure by NMR. The reported CD values are thus suspect.

All [θ] values given are 221nm or at the minimum which appears within 2nm of that wavelength. The fragments are listed (in each category) in order of increasing helicity in aqueous medium.

Ellipticities in each column are given as a formula that will reproduce the observed values over the 0 – 30 °C range. The gradient was measured over this range when possible. A number of species display non-linear behavior in aqueous buffer; the value of $-[\theta]_{221}$ first decreases (+ve gradient) then increases on warming as illustrated in Figure 5.46 – these are indicated by *, and the gradients reflect the values observed at lower temperatures. The titration mid-point ($titr_{.50}$) reported is for a HFIP titration at 298 K. All measurements were made using aqueous buffer at pH 4.2 ± 0.2 (prior to denaturant or fluoroalcohol addition).

Table 6.3 Backbone Proton Chemical Shifts of V8Y [V8-hAM(1-20)GY] and V8S9Y [V8S9-hAM(1-20)GY] in Buffer and in 25% Aqueous HFIP at 285K.

V8Y	Buffer		25% HFIP		V8S9Y	Buffer		25% HFIP	
residue	αH	NH	αH	NH	residue	αH	NH	αH	NH
Lys^{1}	4.01	–	4.10	–	Lys^{1}	4.01	–	4.09	–
Cys^{2}	4.70	9.06	–	8.99	Cys^{2}	4.69	9.07	–	9.01
Asn^{3}	–	9.09	–	9.00	Asn^{3}	–	9.15	–	8.98
Thr^{4}	4.49	7.65	4.66	7.55	Thr^{4}	4.48	7.63	4.67	7.54
Ala^{5}	4.18	8.79	4.17	8.99	Ala^{5}	4.16	8.88	4.17	9.00
Thr^{6}	4.19	8.00	4.02	8.13	Thr^{6}	4.17	8.07	4.01	8.10
Cys^{7}	4.49	8.12	4.36	7.75	Cys^{7}	4.41	8.06	4.37	7.78
Val^{8}	3.95	8.26	3.63	8.18	Val^{8}	3.85	8.33	3.61	8.29
Thr^{9}	4.18	8.33	4.00	8.27	Ser^{9}	4.33	8.38	4.19	8.41
Gln^{10}	4.23	8.36	4.11	7.97	Gln^{10}	4.23	8.31	4.16	7.82
Arg^{11}	4.25	8.30	4.17	7.96	Arg^{11}	4.23	8.15	4.18	7.97
Leu^{12}	4.32	8.24	4.33	8.50	Leu^{12}	4.32	8.16	4.33	8.58
Ala^{13}	4.20	8.24	4.13	8.87	Ala^{13}	4.21	8.18	4.13	8.69
Asn^{14}	4.59	8.26	4.51	8.11	Asn^{14}	4.60	8.22	4.51	8.08
Phe^{15}	4.56	8.08	4.45	8.40	Phe^{15}	4.55	8.07	4.45	8.38
Leu^{16}	4.27	8.09	3.92	9.22	Leu^{16}	4.26	8.10	3.92	9.22
Val^{17}	3.95	7.98	3.72	8.93	Val^{17}	3.95	7.95	3.72	8.93
His^{18}	4.74	8.60	4.46	7.86	His^{18}	4.75	8.55	4.46	7.87
Ser^{19}	4.47	8.47	4.29	8.39	Ser^{19}	4.47	8.45	4.29	8.39
Ser^{20}	4.45	8.60	4.37	7.88	Ser^{20}	4.46	8.58	4.37	7.88
Gly^{21}	3.90	8.47	3.95	8.01	Gly^{21}	3.90	8.47	3.94	8.01
Tyr^{22}	4.50	8.13	4.52	7.90		4.50	8.12	4.52	7.90

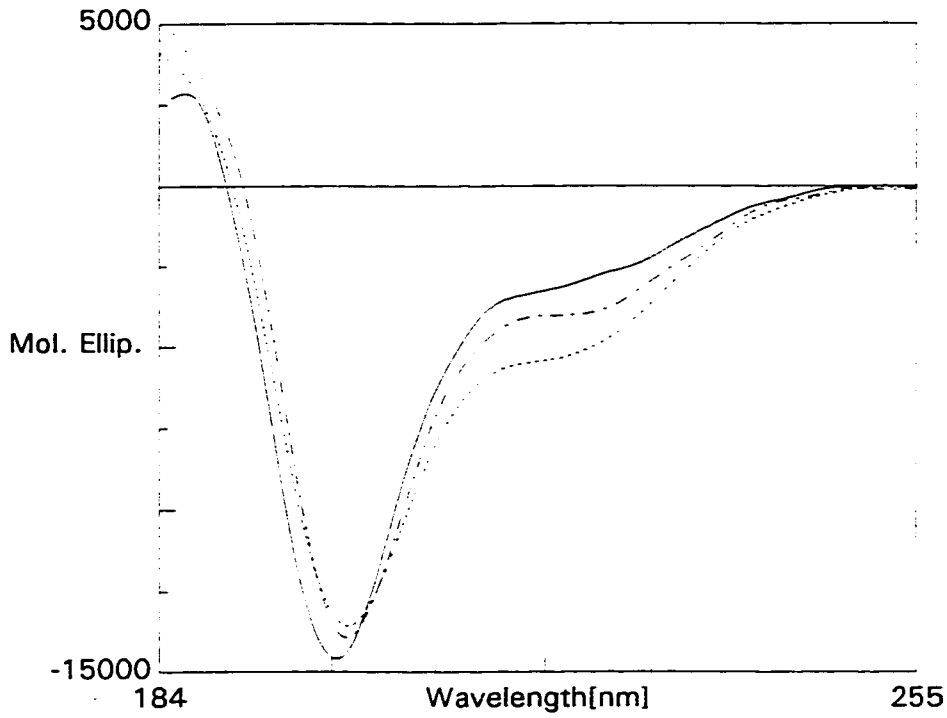

Figure 6.1 CD Comparison of sCT(1-20)G, hAM(1-20)G
and hCGRP(1-21) in Buffer (pH ~ 4, at 25 °C).
(sCT(1-20)G: solid line; hAM(1-20)G: dash line; and hCGRP(1-21): dotted line)

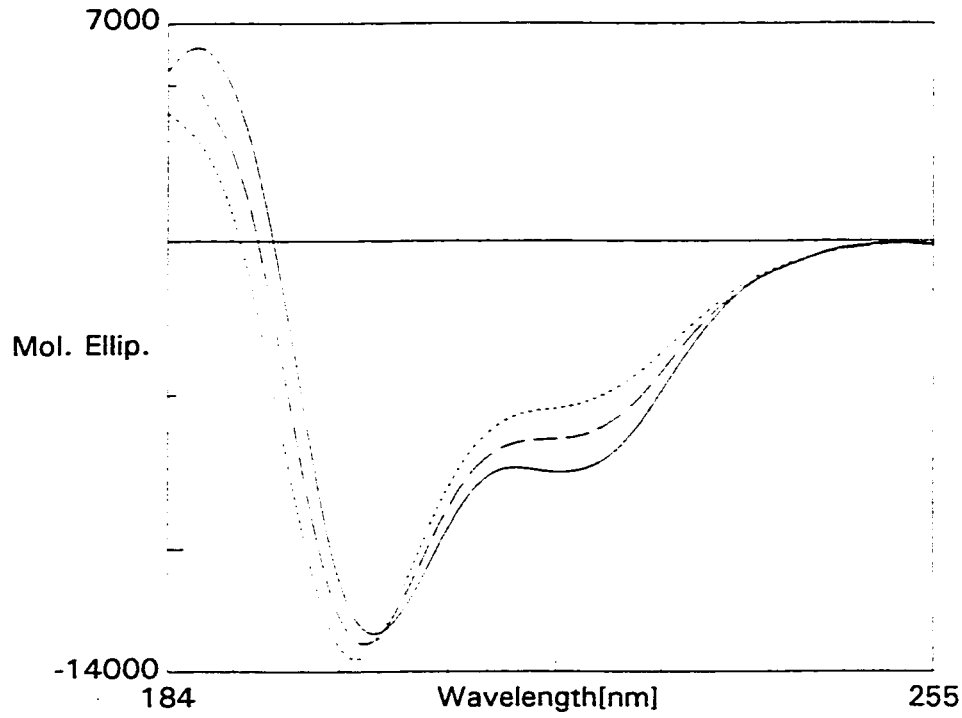

Figure 6.2 Thermal CD Study of hCGRP(1-21) in Aqueous Buffer.
(dotted line: 25 °C; dash line: 10 °C; and solid line: 0 °C)

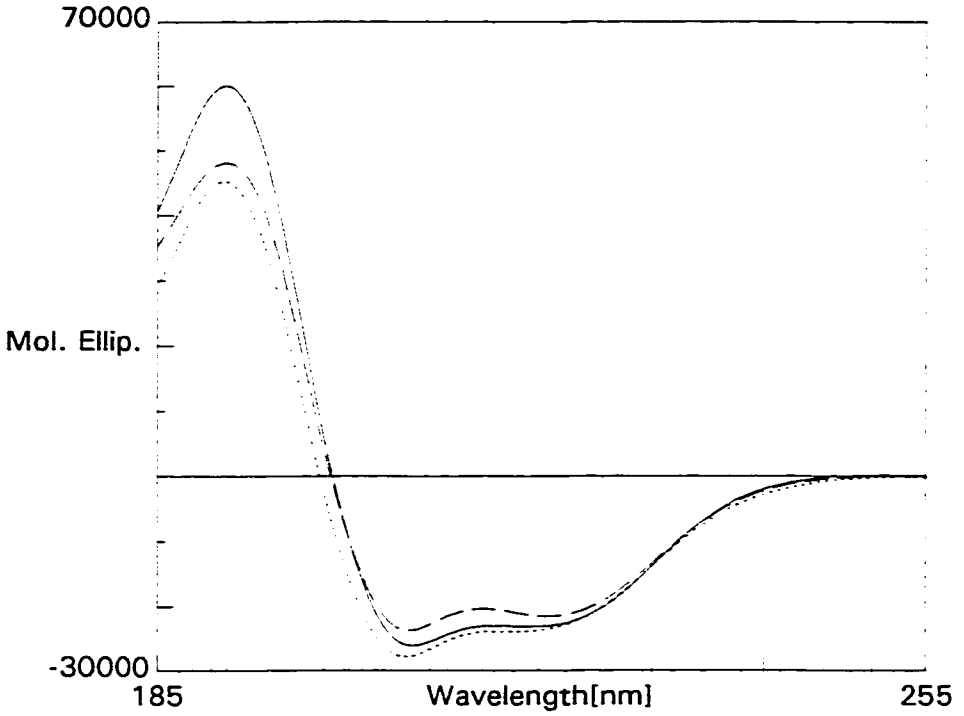

Figure 6.3 CD Comparison of sCT(1-20)G, hAM(1-20)G and hCGRP(1-21) in 25% HFIP (25 °C).
(sCT(1-20)G: solid line; hAM(1-20)G: dash line; hCGRP(1-21): dotted line)

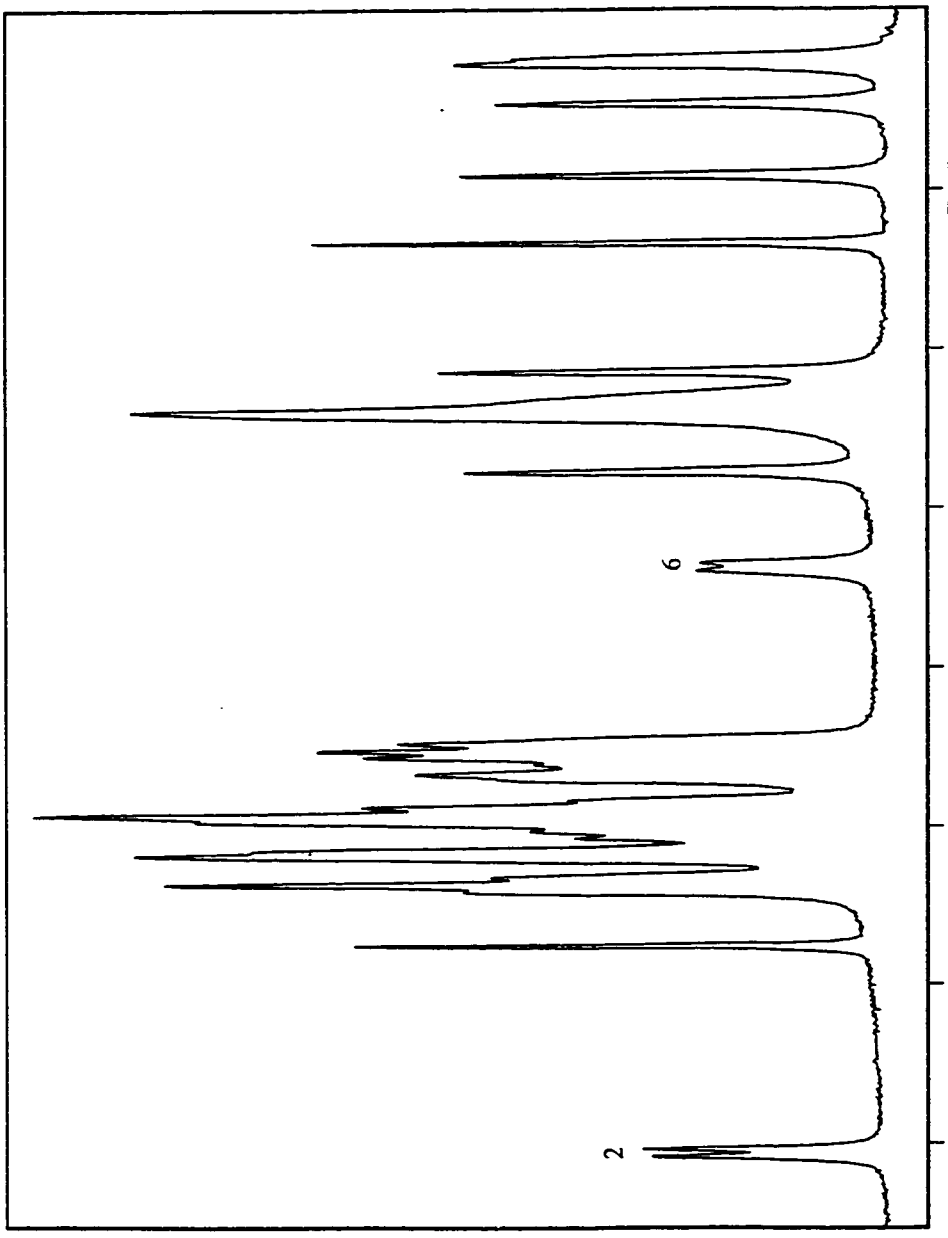

Figure 6.4 1D Spectrum of sCT(1-20)G in Buffer (NH Region).

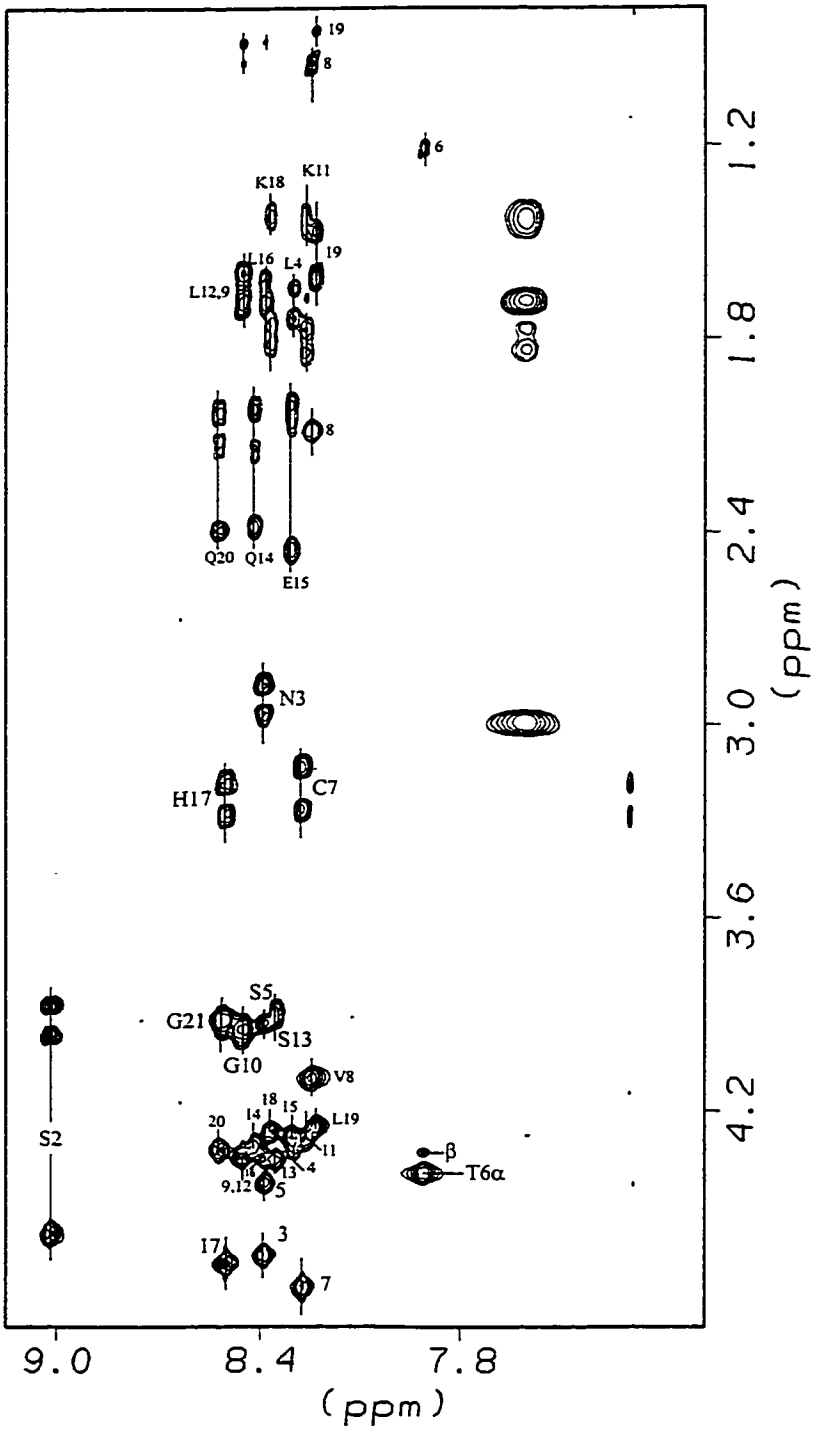

Figure 6.5 N/αβγδ Region of the TOCSY Spectrum of sCT(1-20)G in Buffer.

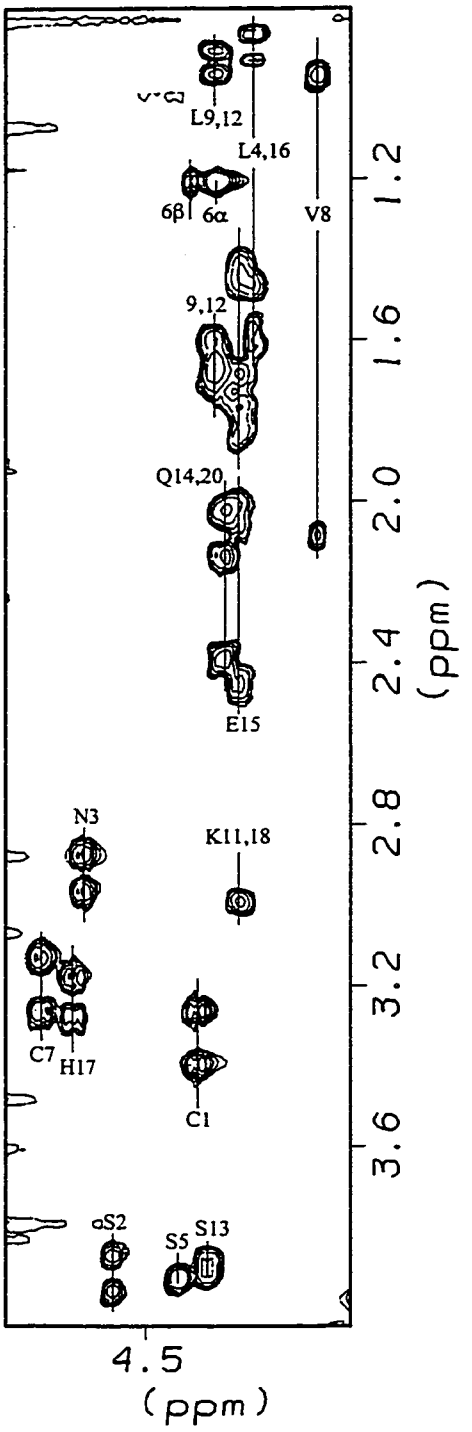

Figure 6.6 α/βγδ Region of the TOCSY Spectrum of sCT(1-20)G in Buffer.

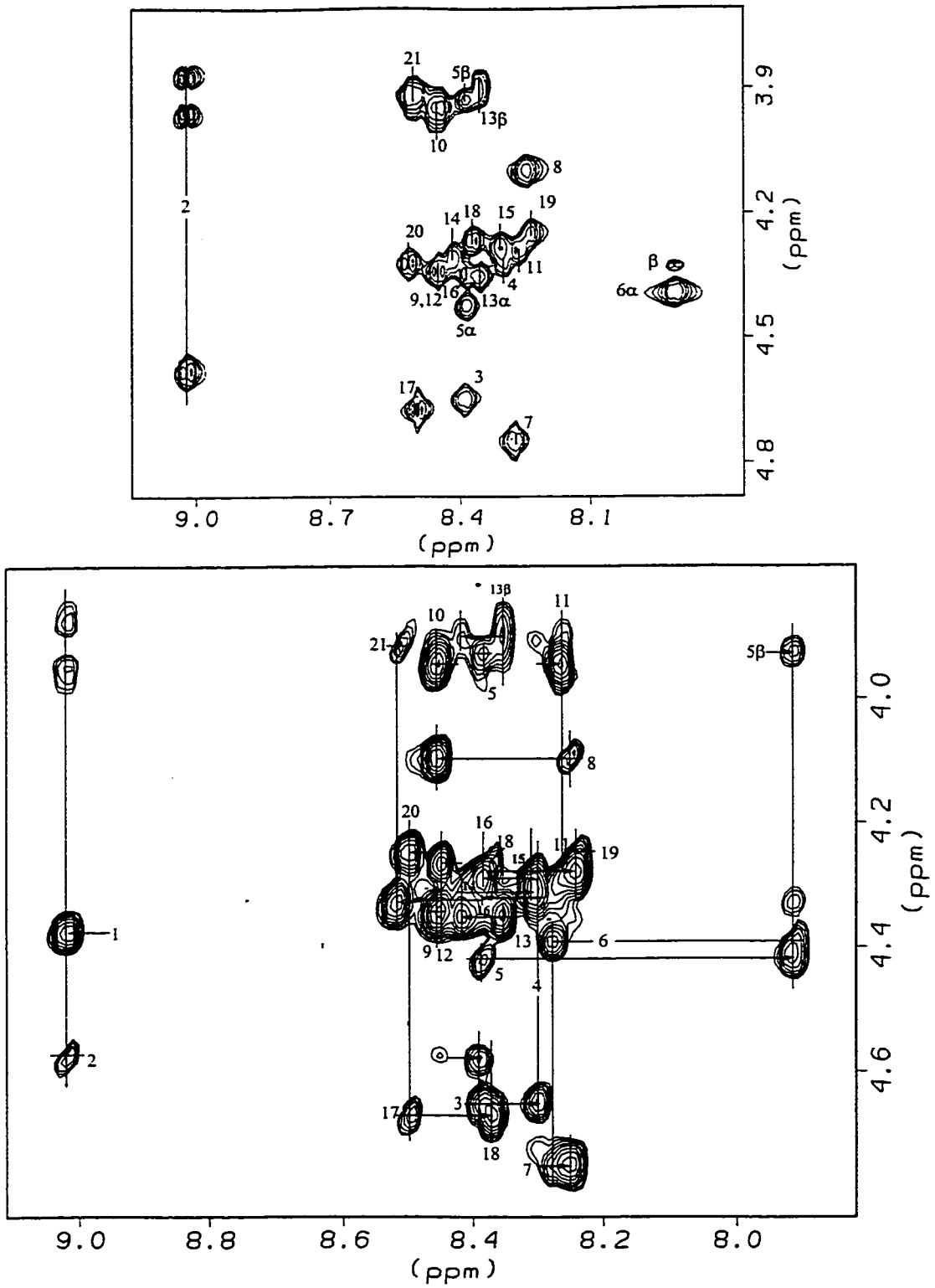

Figure 6.7 αN Region of the TOCSY (top) and NOESY (lower) Spectra of sCT(1-20)G in Buffer.

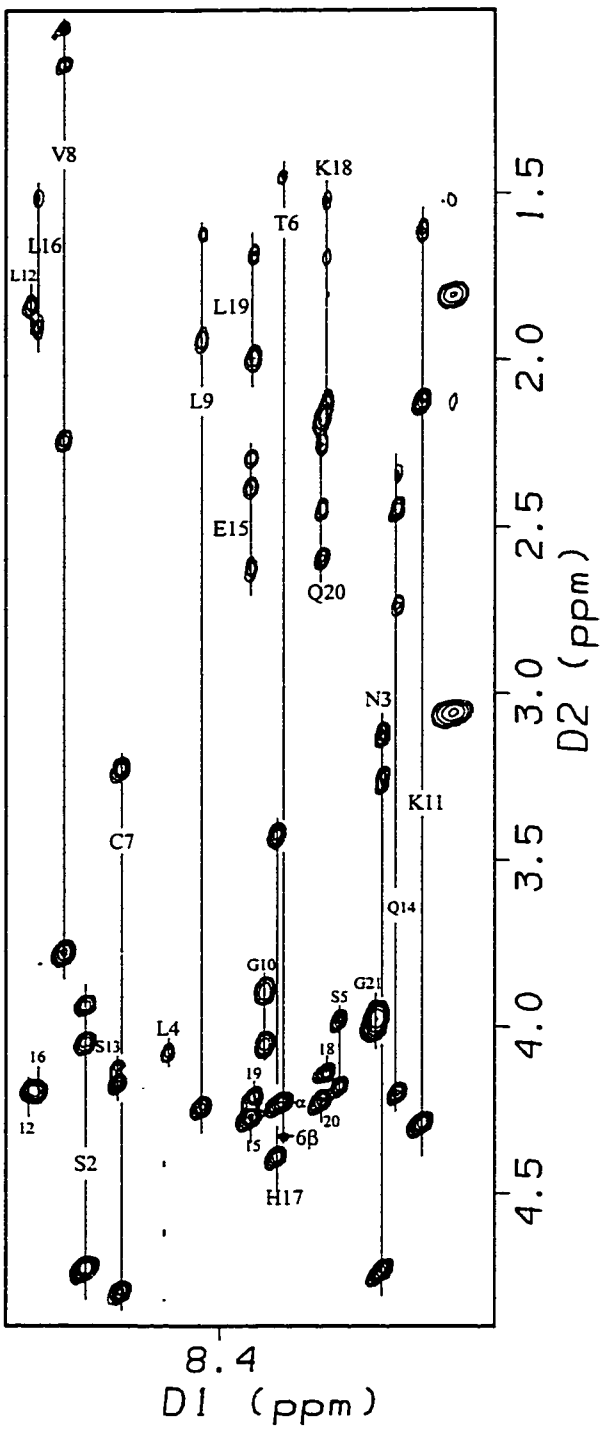

Figure 6.8 N/αβγδ Region of the TOCSY Spectrum of sCT(1-20)G in 25% HFIP.

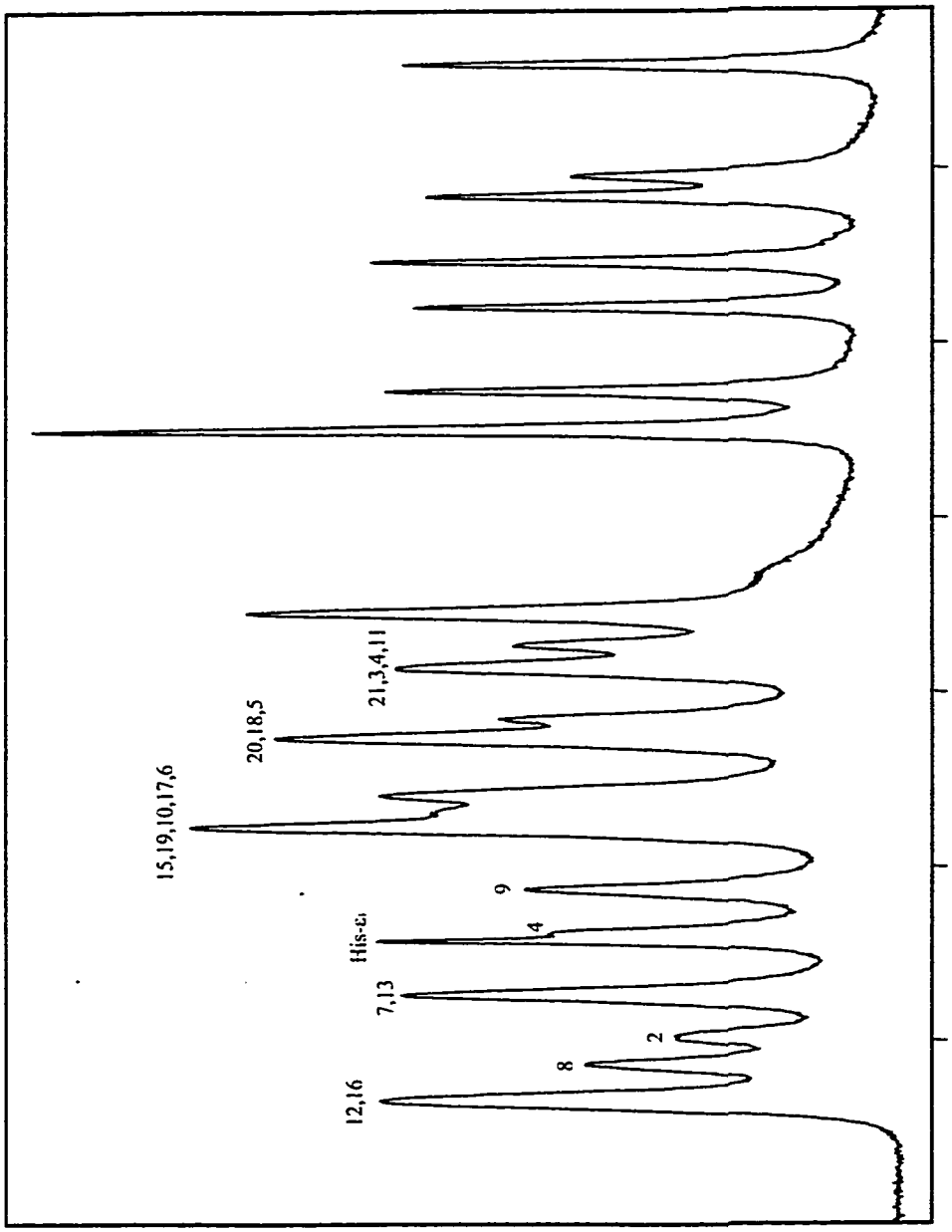

Figure 6.9 1D Spectrum of sCT(1-20)G in 25% HFIP (NH Region).

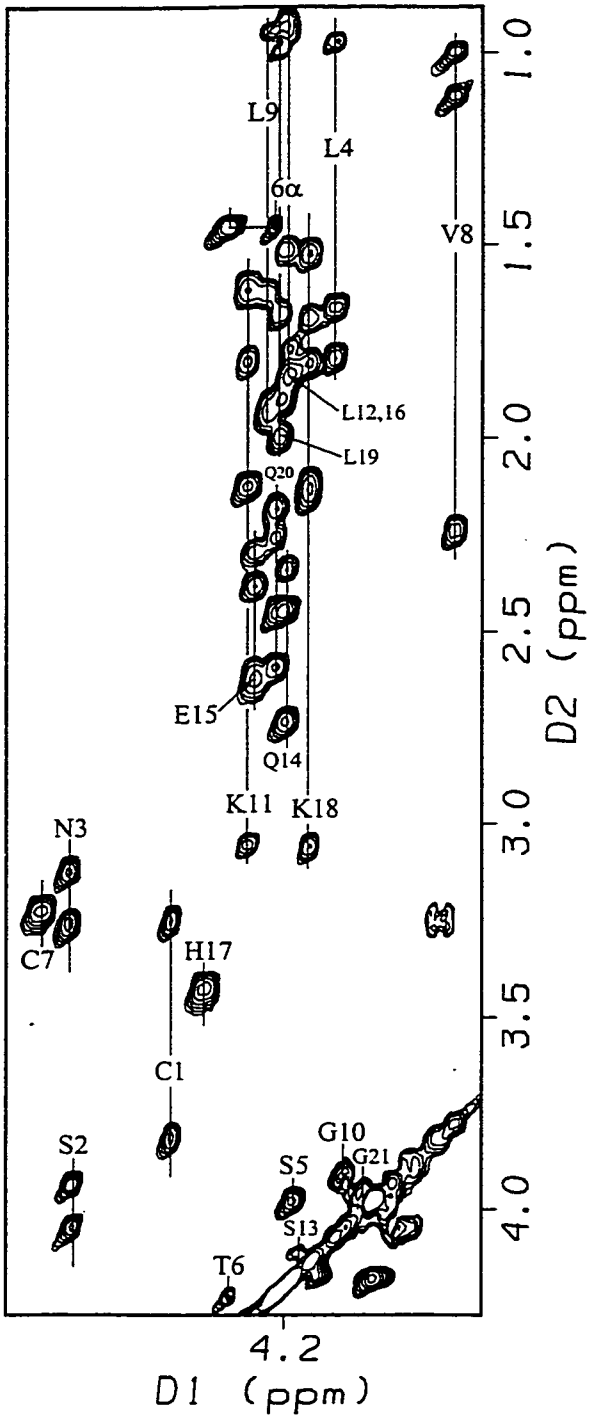

Figure 6.10 α/βγδ Region of the TOCSY Spectrum of sCT(1-20)G in 25% HFIP.

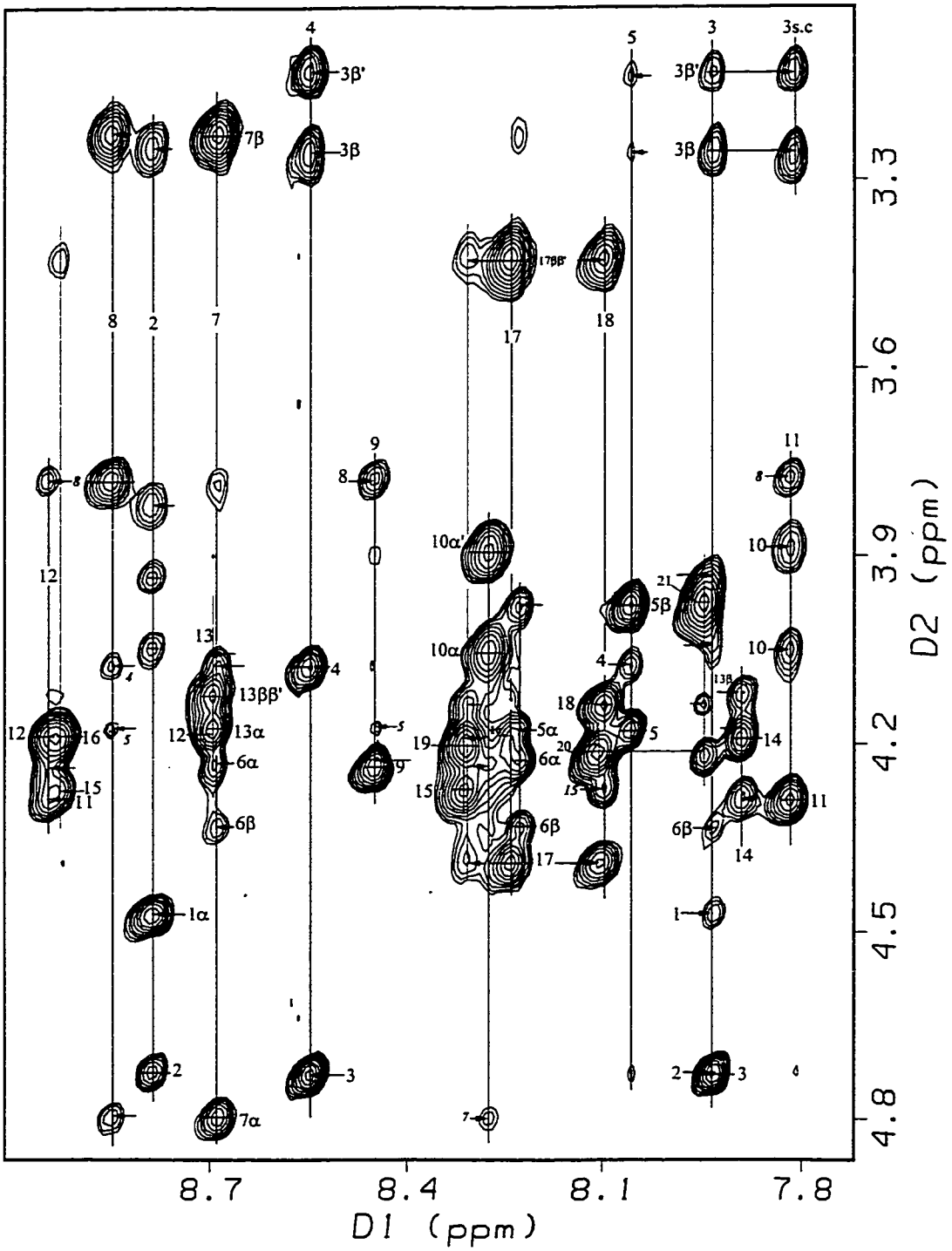

Figure 6.11 αN Region of the NOESY Spectrum of sCT(1-20)G in 25% HFIP.

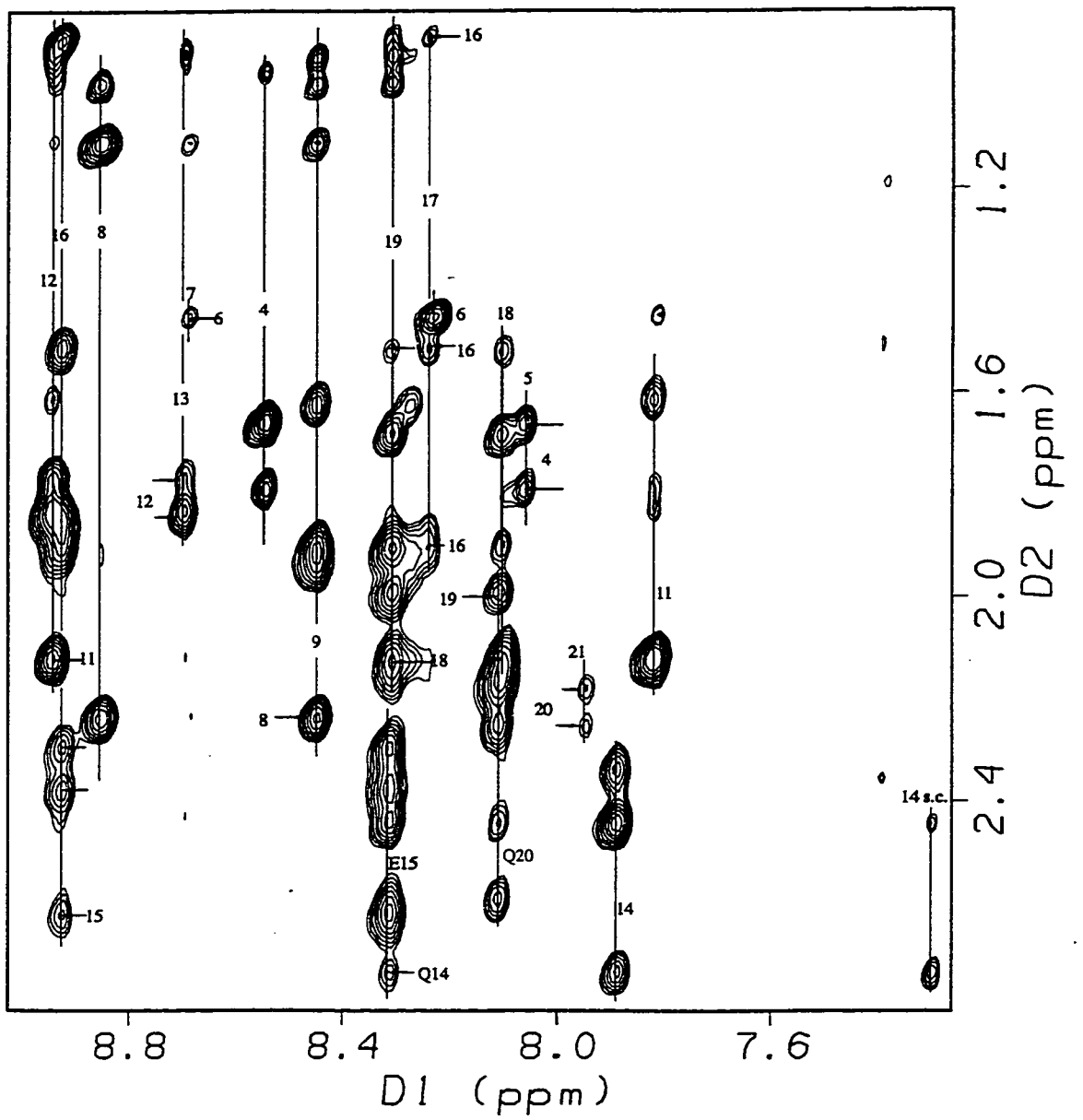

Figure 6.12 Aliphatic-NH Region of the NOESY Spectrum of sCT(1-20)G in 25% HFIP.

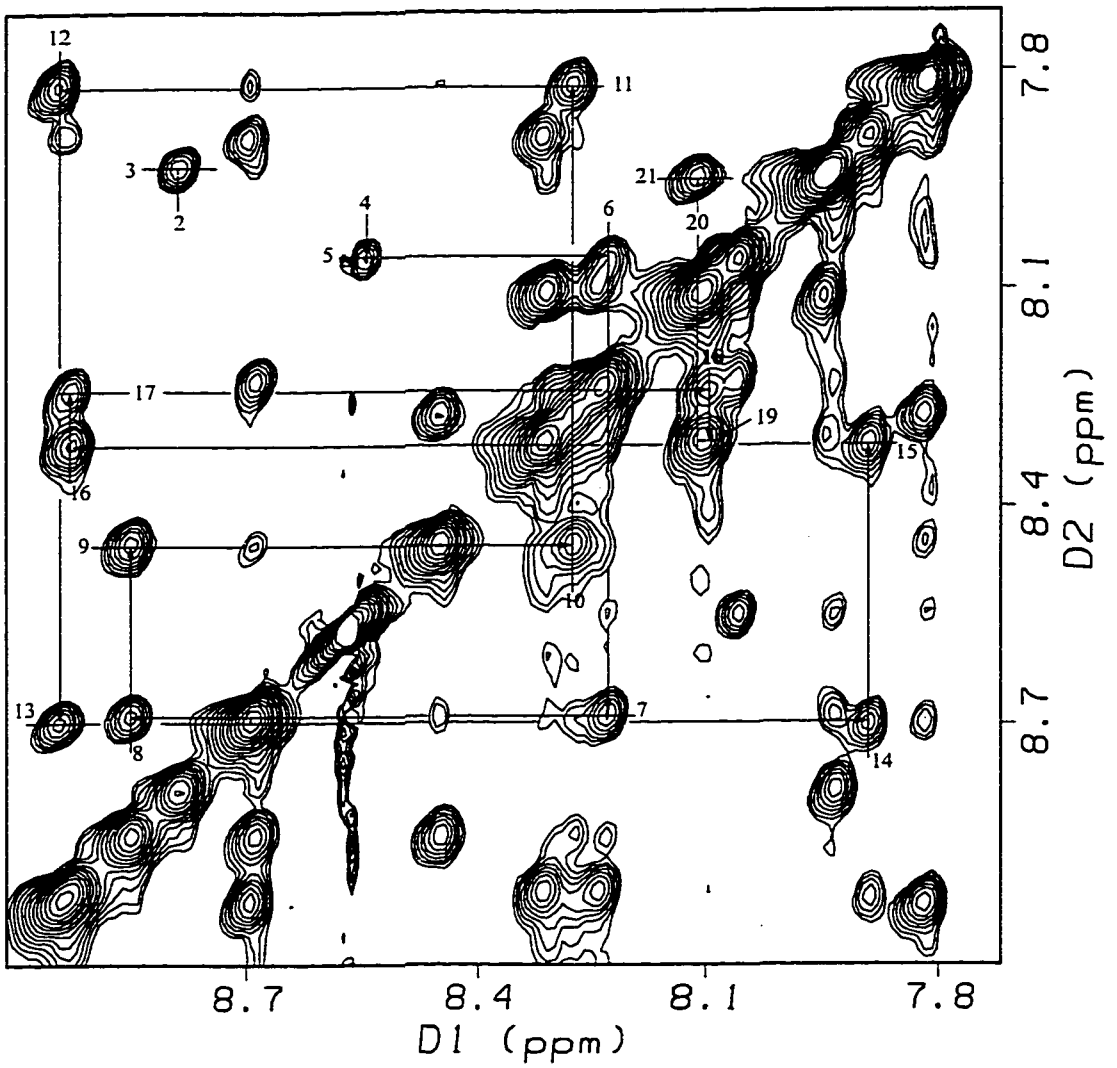

Figure 6.13 NN Region of the NOESY Spectrum of sCT(1-20)G in 25% HFIP.

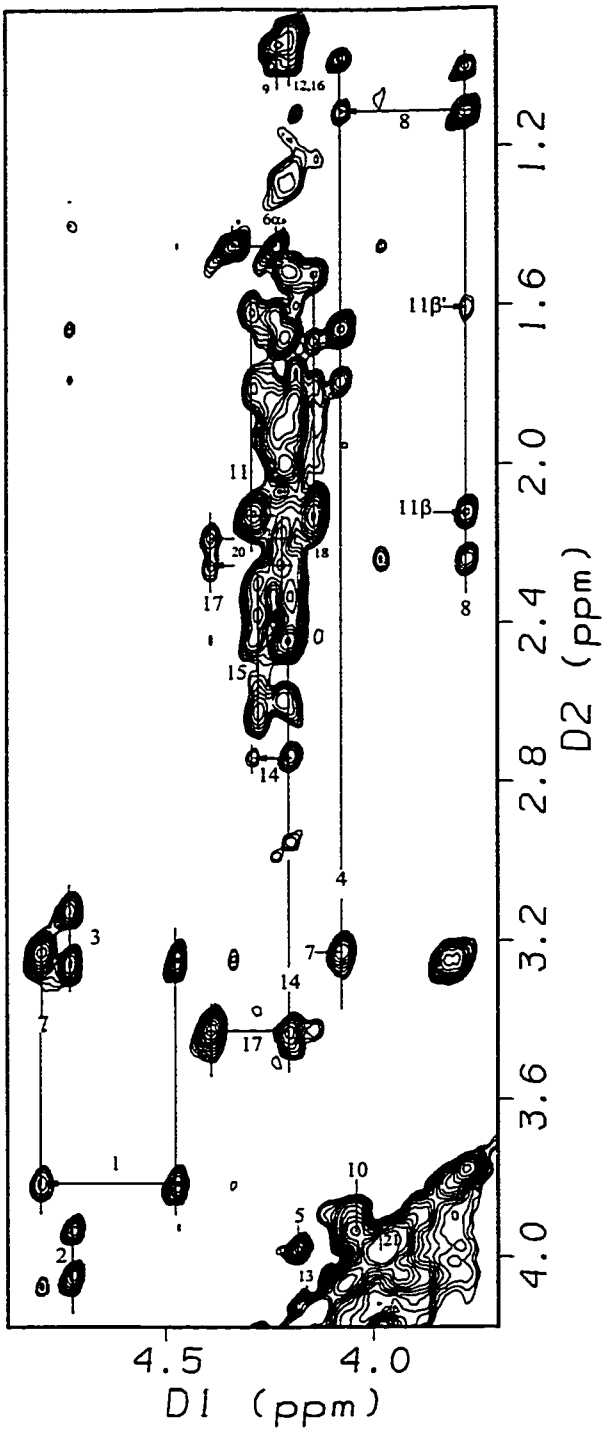

Figure 6.14 α/βγδ Region of the NOESY Spectrum of sCT(1-20)G in 25% HFIP.

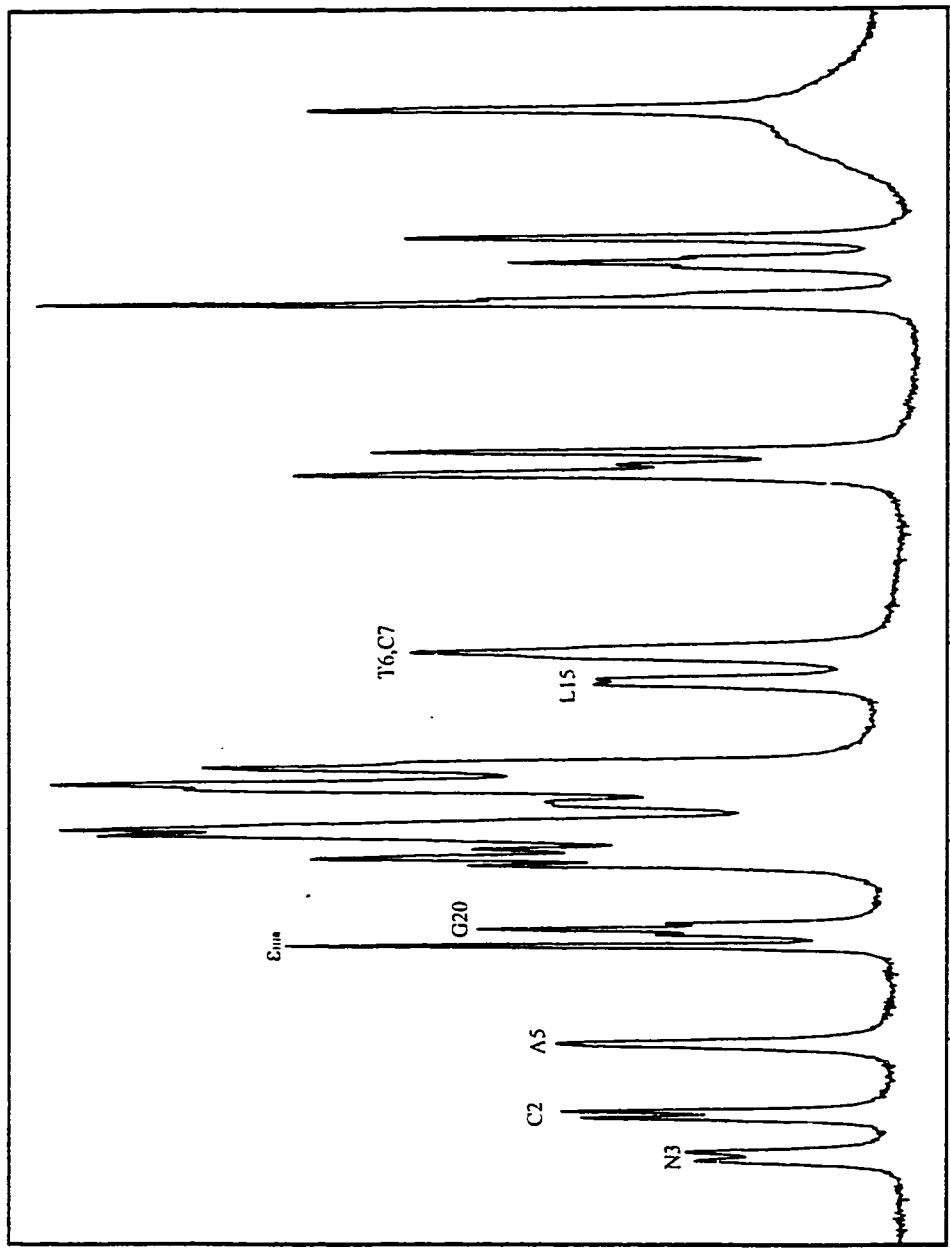

Figure 6.15 1D Spectrum of CGRP(1-21) in Buffer (NH Region).

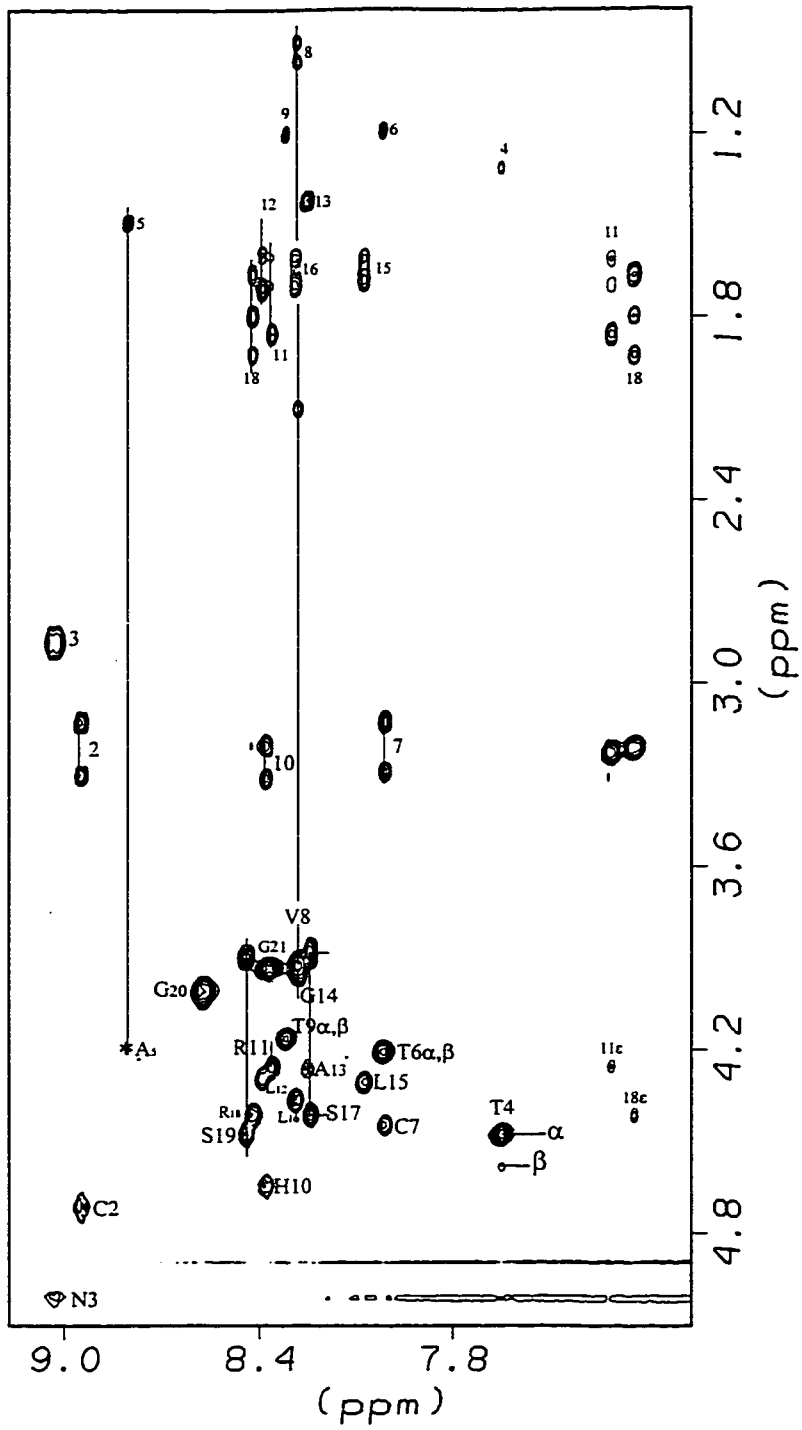

Figure 6.16 N/αβγδ Region of the TOCSY Spectrum of hCGRP(1-21) in Buffer.

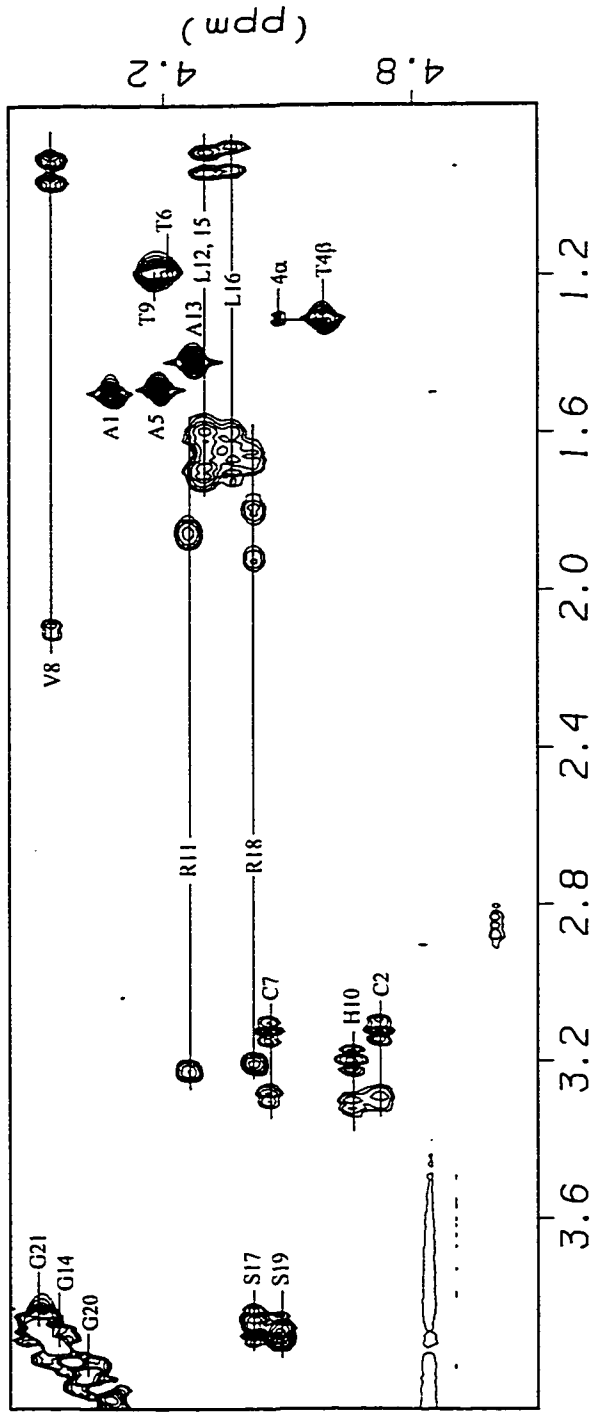

Figure 6.17 α/βγδ Region of the TOCSY Spectrum of hCGRP(1-21) in Buffer.

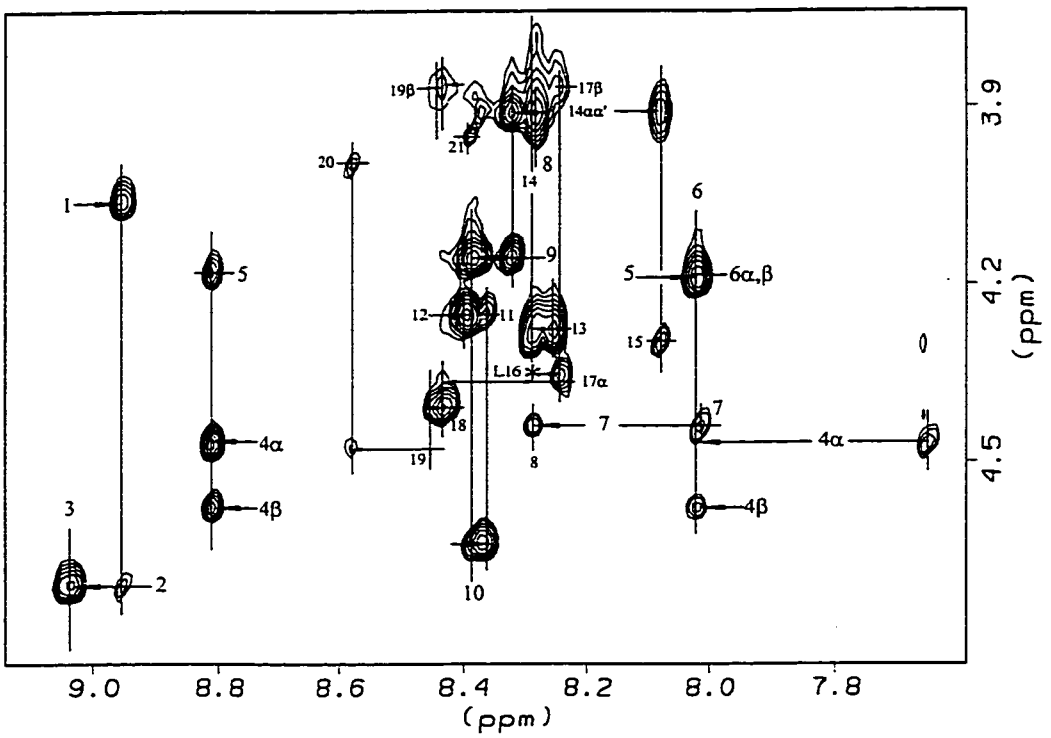

Figure 6.18 αN Region of the NOESY Spectrum of hCGRP(1-21) in Buffer.

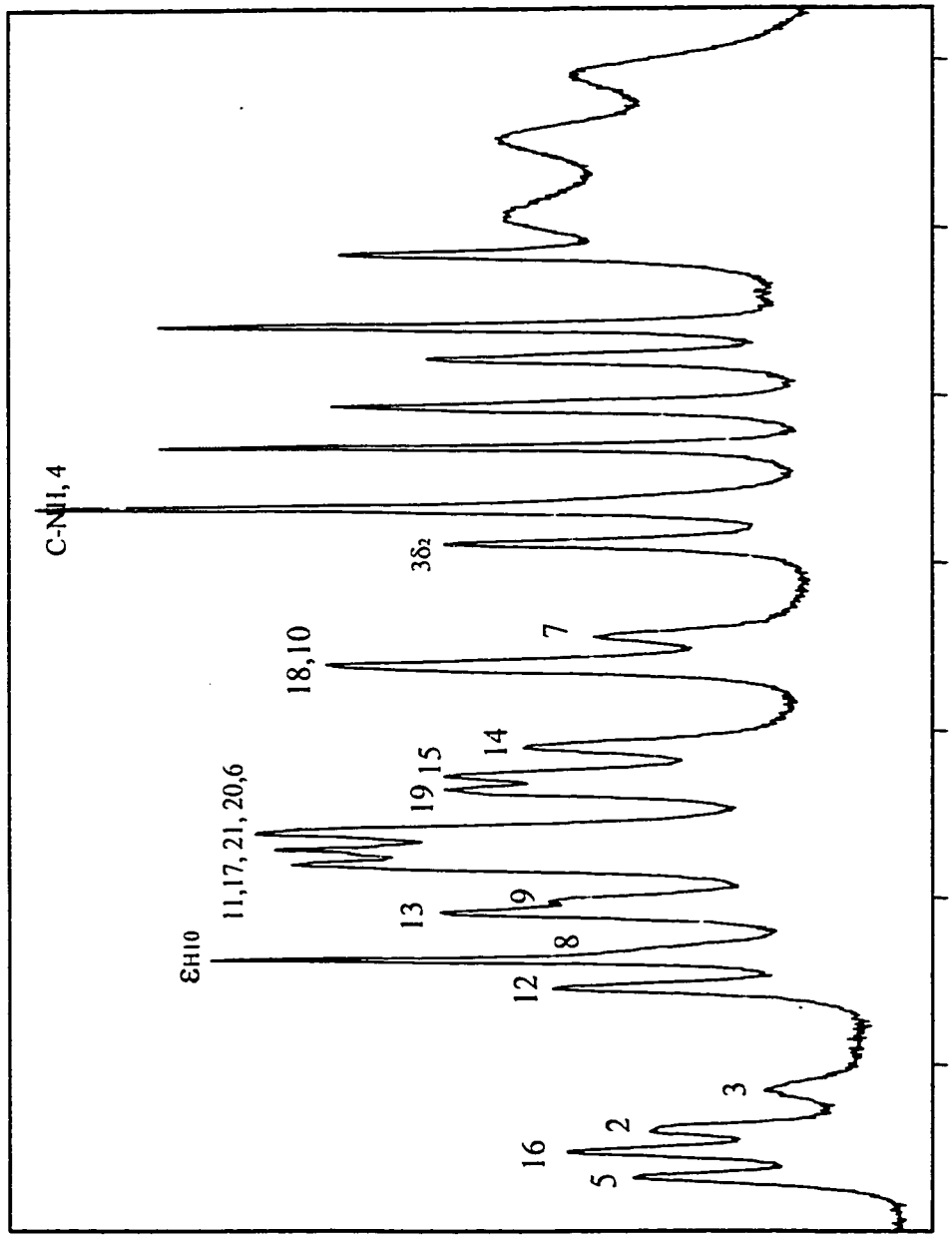

Figure 6.19 1D Spectrum of CGRP(1-21) in 25% HFIP (NH Region).

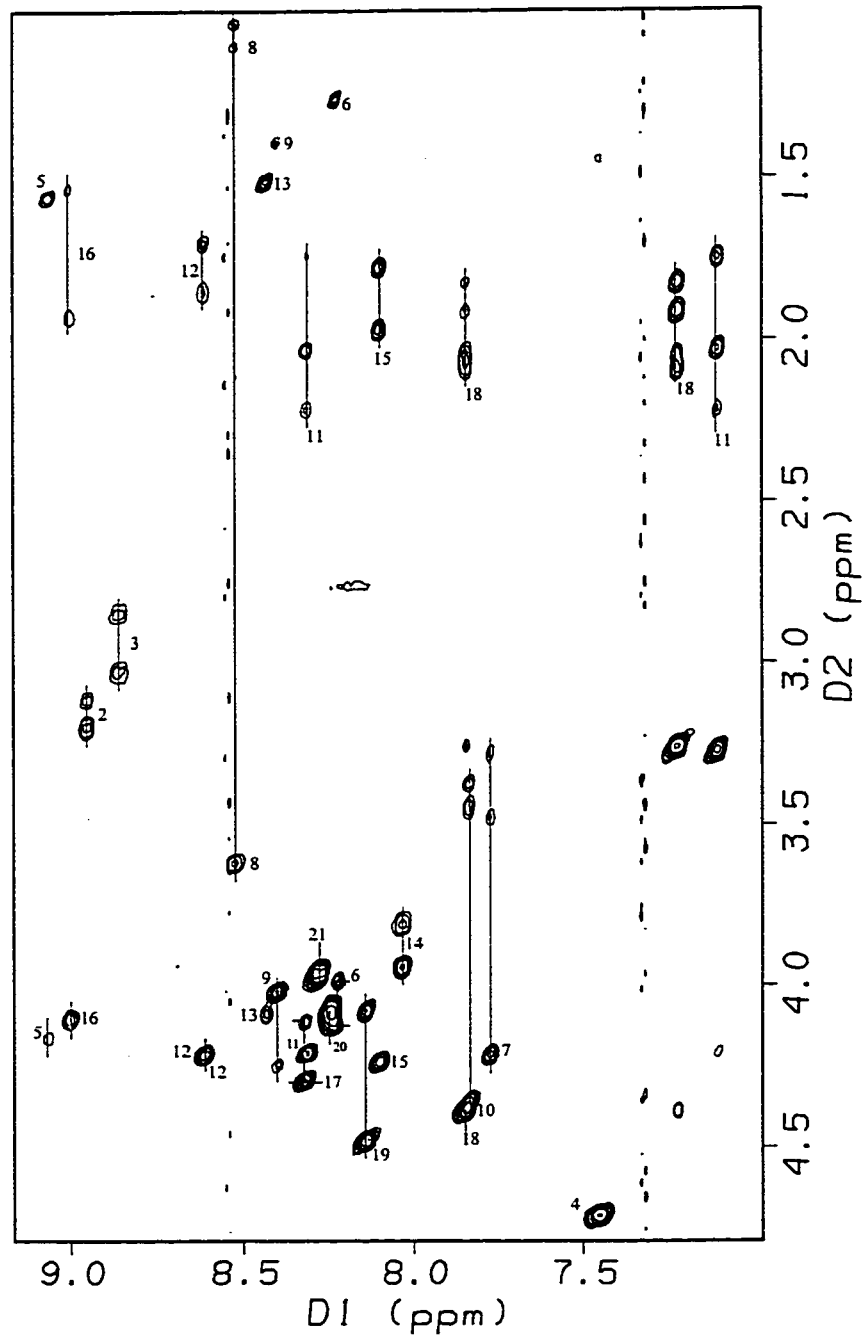

Figure 6.20 N/αβγδ Region of the TOCSY Spectrum of hCGRP(1-21) in 25% HFIP.

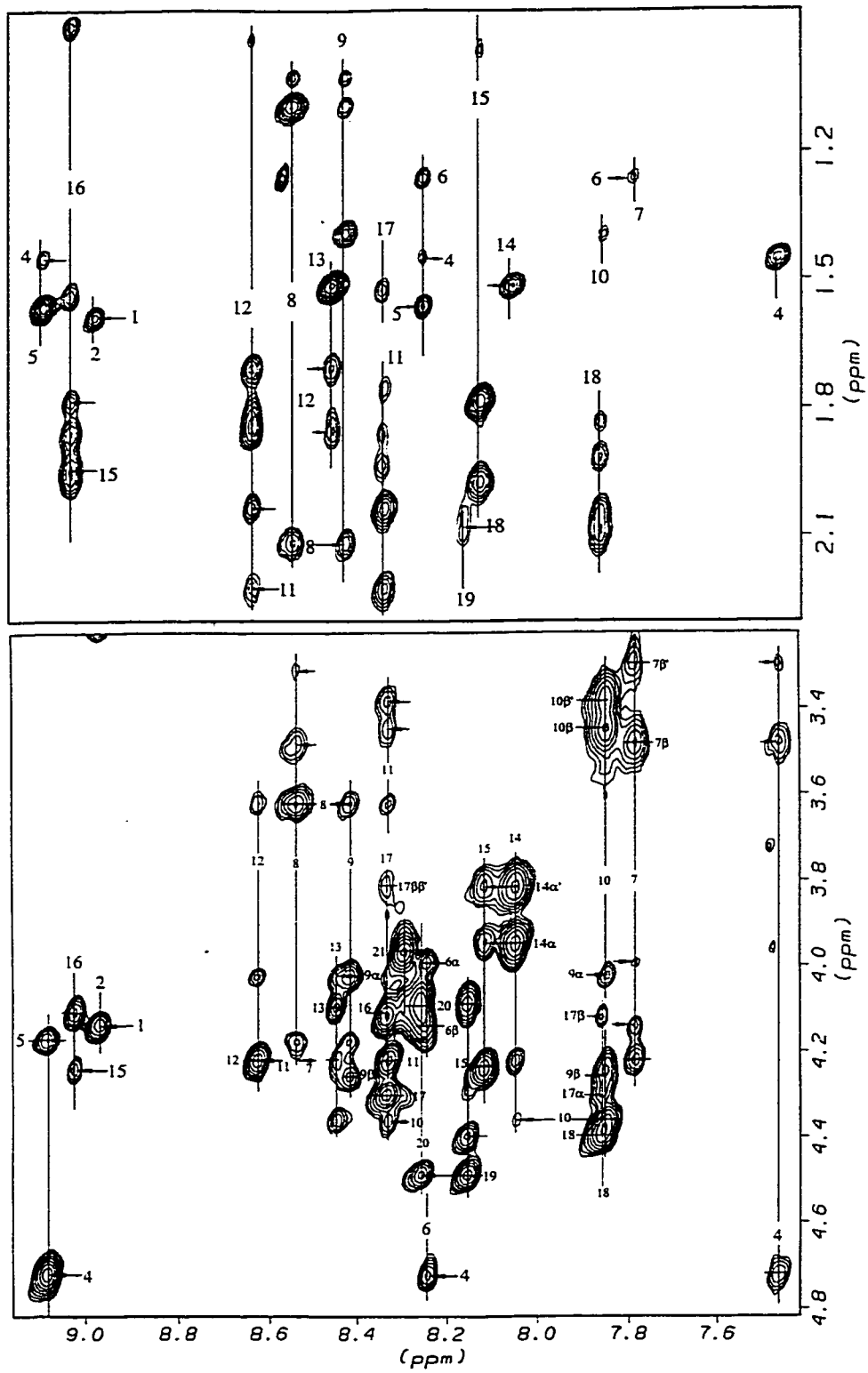

Figure 6.21 N/αβγδ Region of the NOESY Spectrum of hCGRP(1-21) in 25% HFIP.

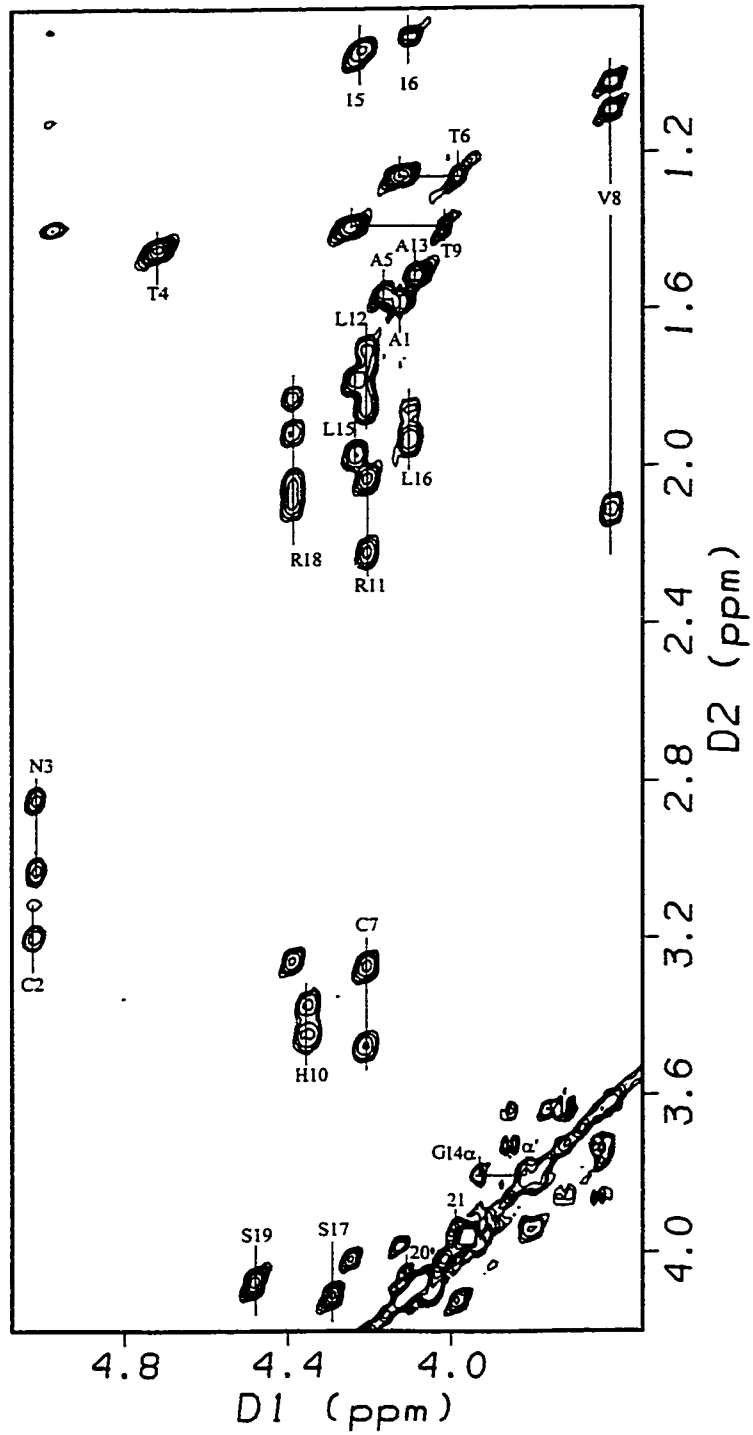

Figure 6.22 α/βγδ Region of the TOCSY Spectrum of hCGRP(1-21) in 25% HFIP.

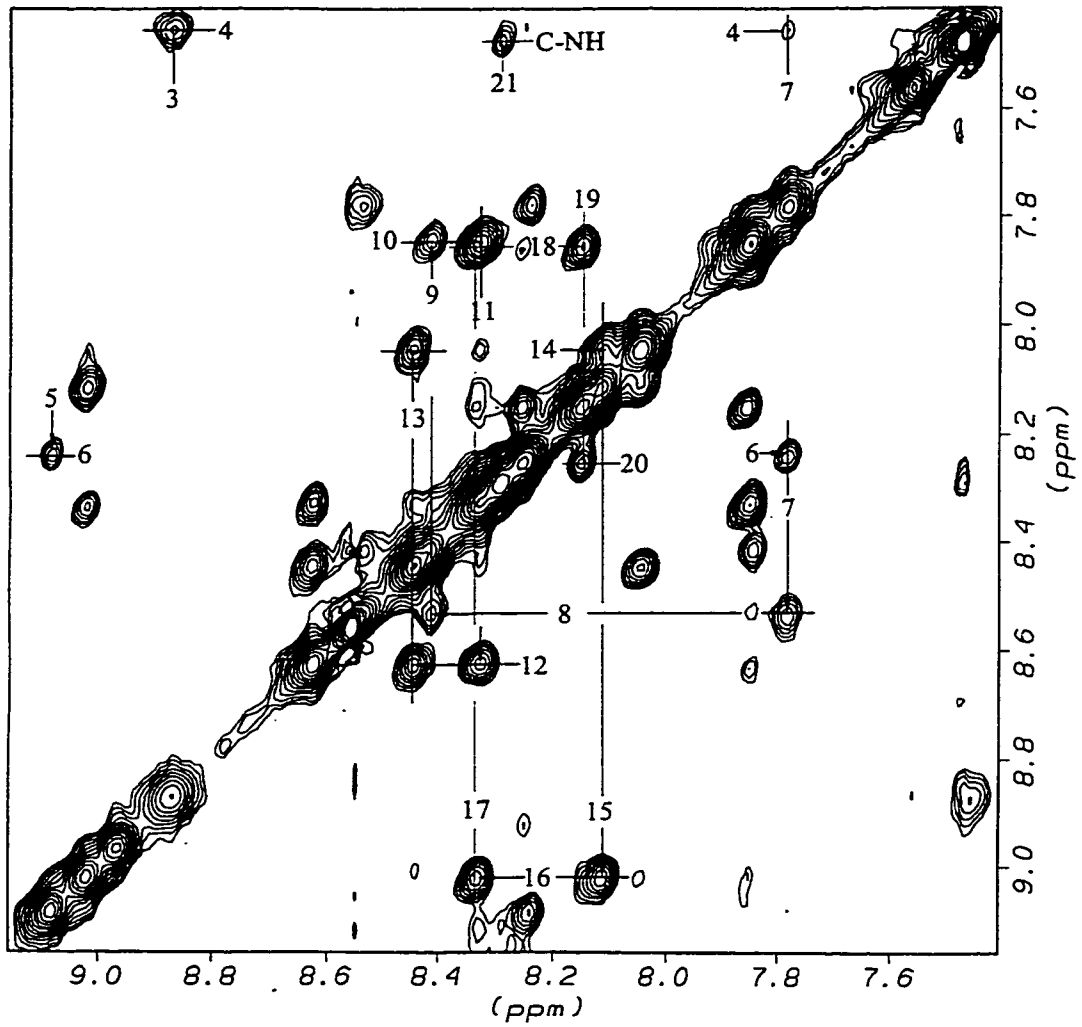

Figure 6.23 NN Region of the NOESY Spectrum of hCGRP(1-21) in 25% HFIP.

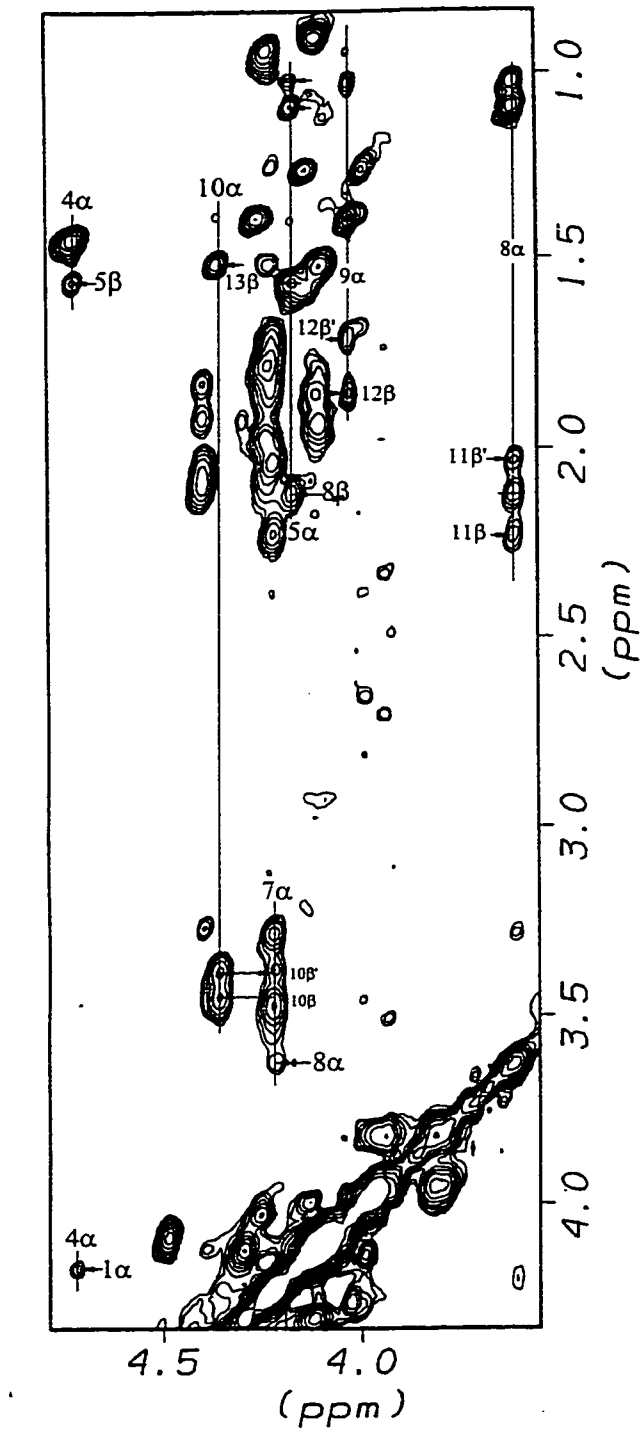

Figure 6.24 α/βγδ Region of the NOESY Spectrum of hCGRP(1-21) in 25% HFIP.

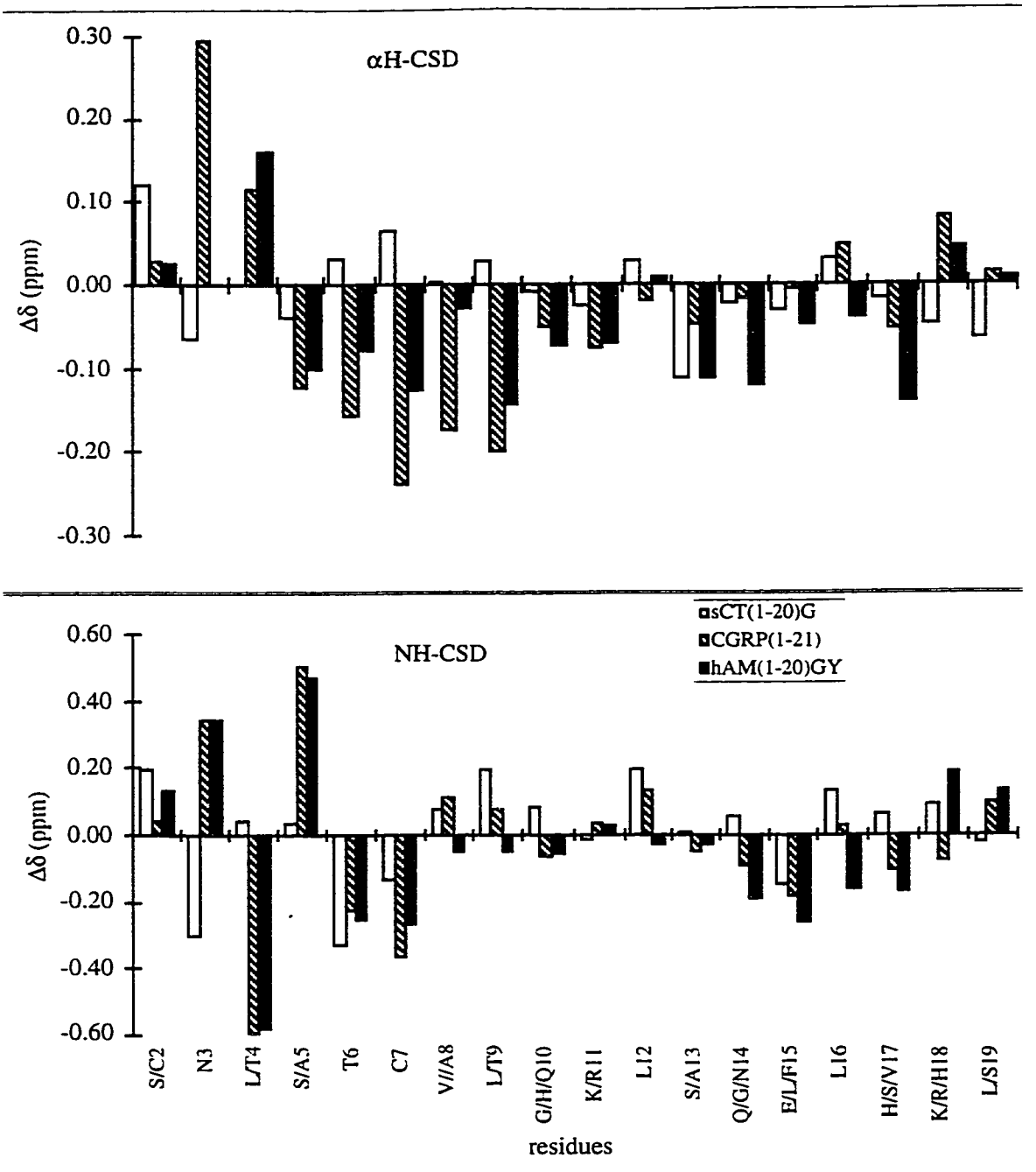

Figure 6.25 αH-CSD and NH-CSD Histograms of sCT(1-20)G, hCGRP(1-21) and hAM(1-20)G in Buffer.

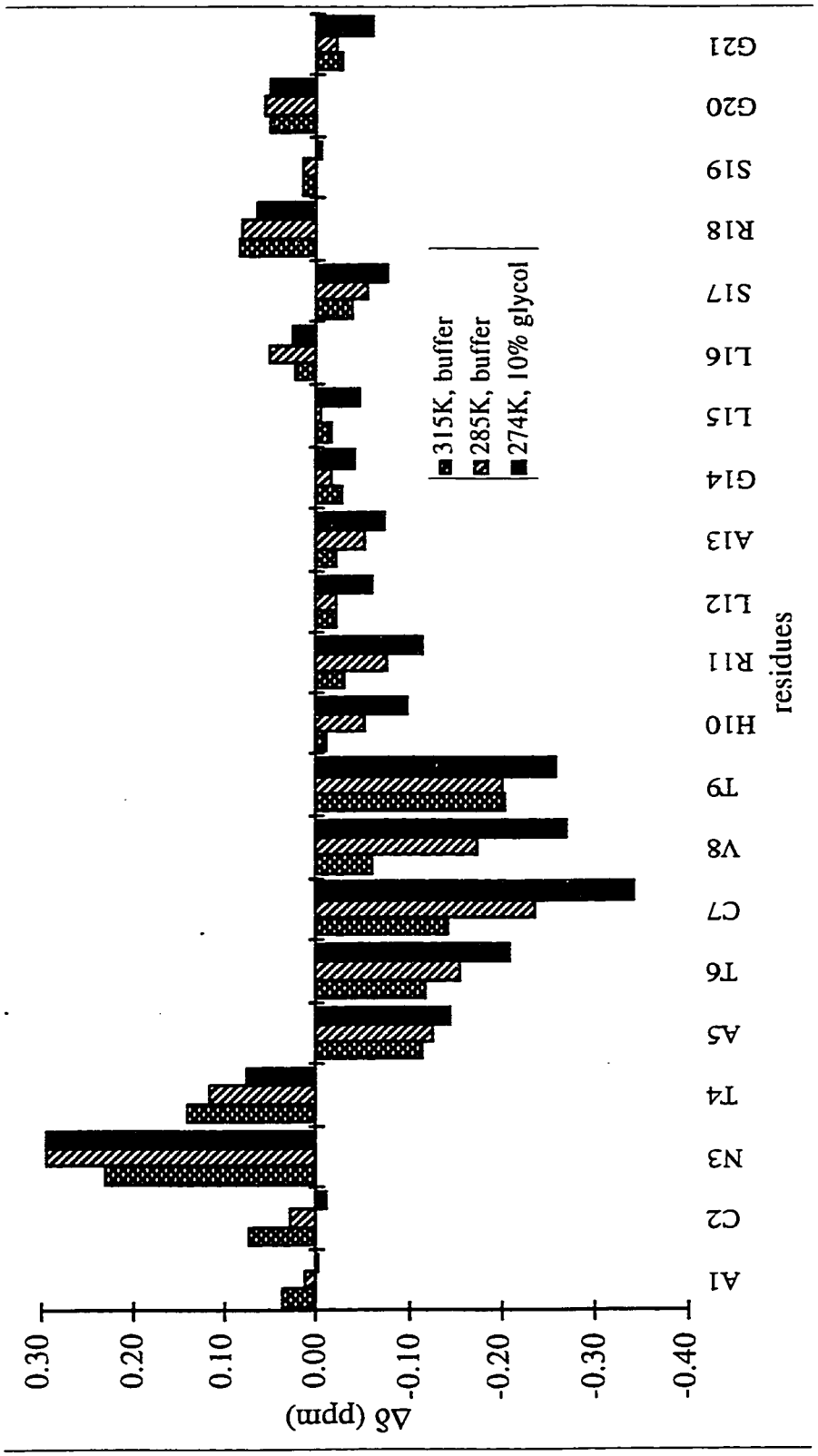

Figure 6.26 Alpha-CSD of hCGRP(1-21) in Buffer at Different Temperatures.

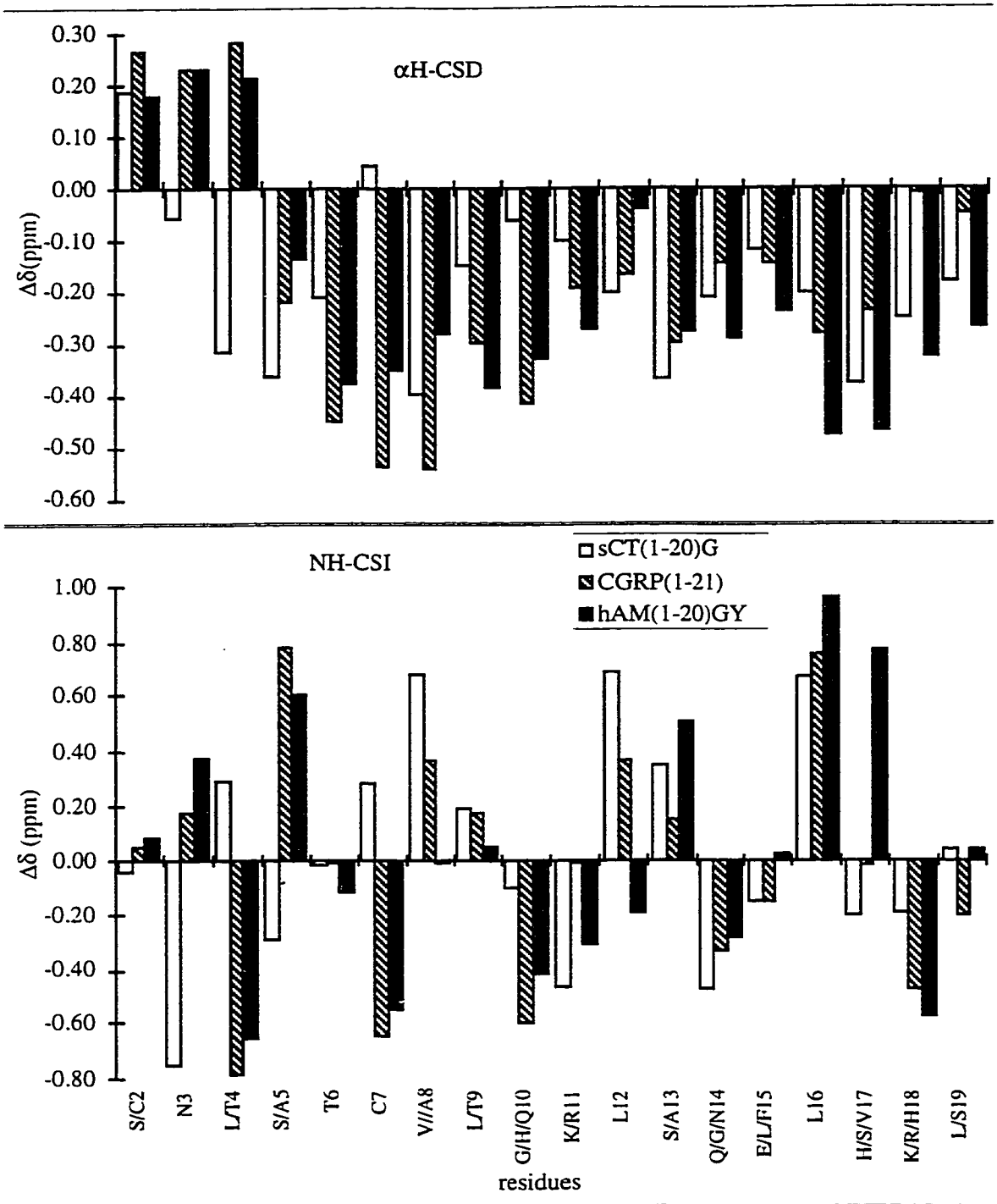

Figure 6.27 αH-CSD and NH-CSD Histograms of sCT(1-20)G, hCGRP(1-21) and hAM(1-20)G in 25% HFIP.

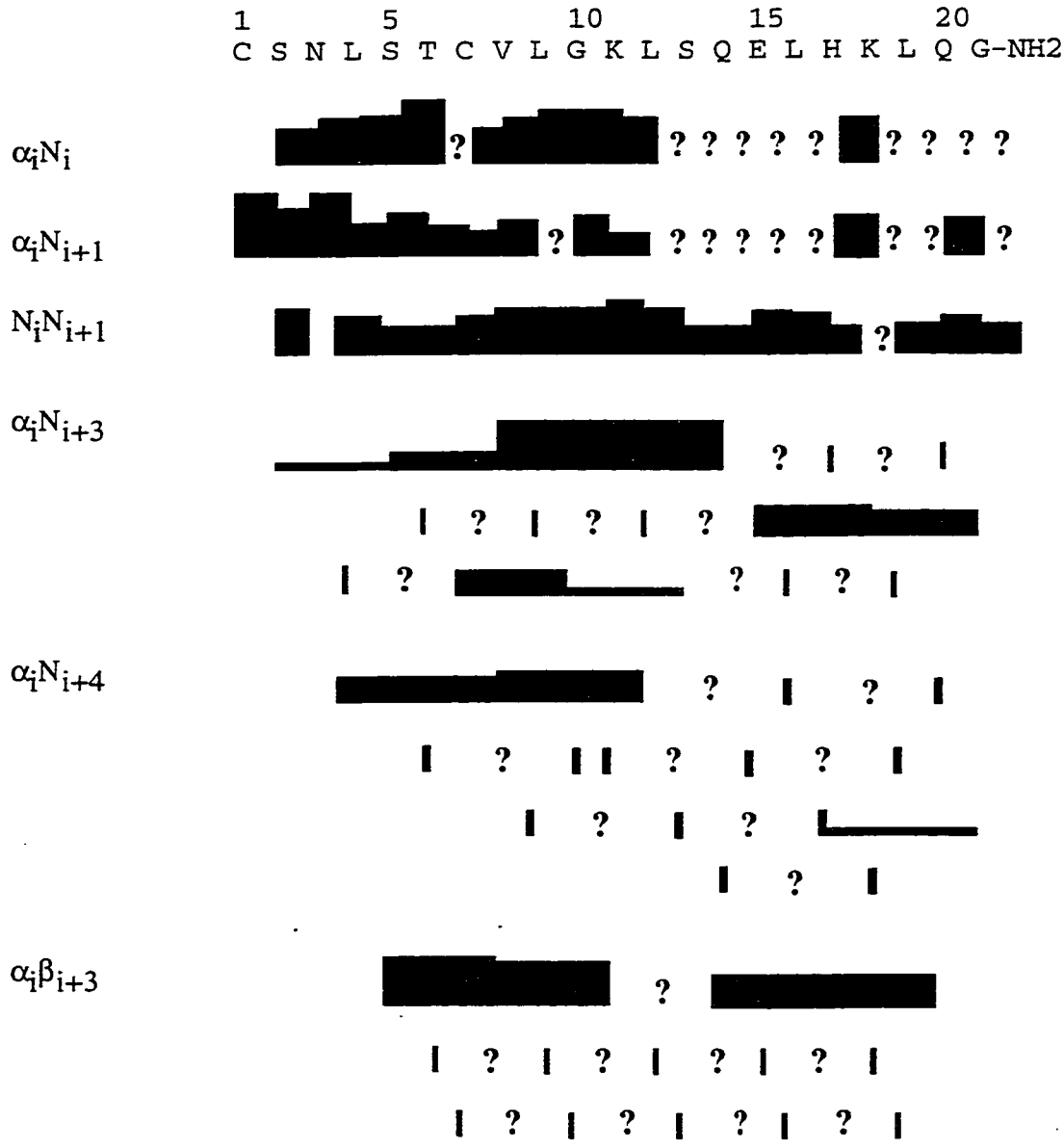

Figure 6.28 Sequential and Medium Range NOEs of sCT(1-20)G in 25% HFIP.

(The thickness of the bar represents the intensity of NOEs observed. The blank, represents no detectable NOEs. The ? represents unknown due to overlap)

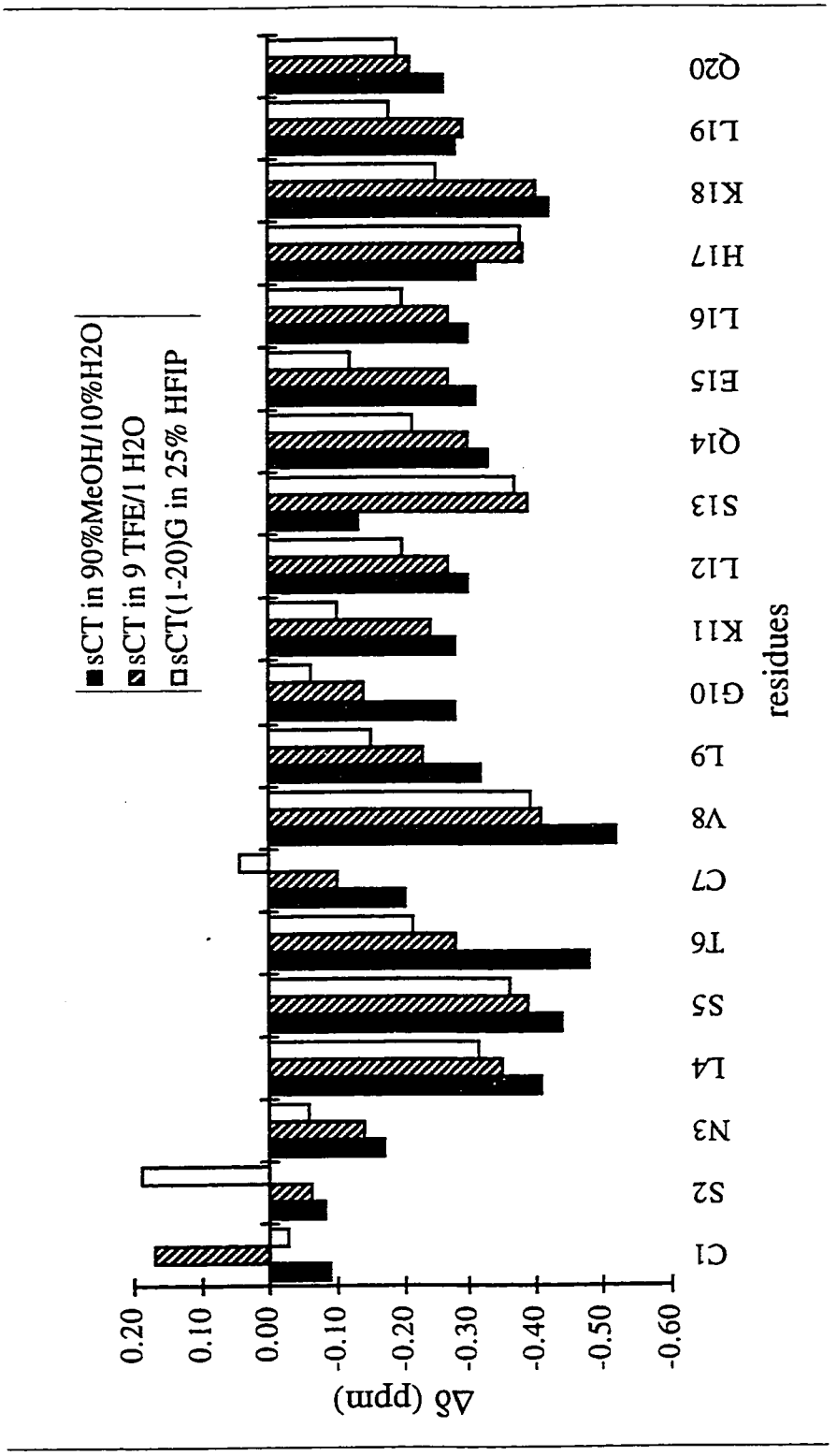

Figure 6.29 αH-CSD Comparisons of sCT in 90% MeOH (data taken from Meadows et al., 1991) or TFE Aqueous (data taken from Meyer et al., 1991) Media and sCT(1-20)G in 25% HFIP.

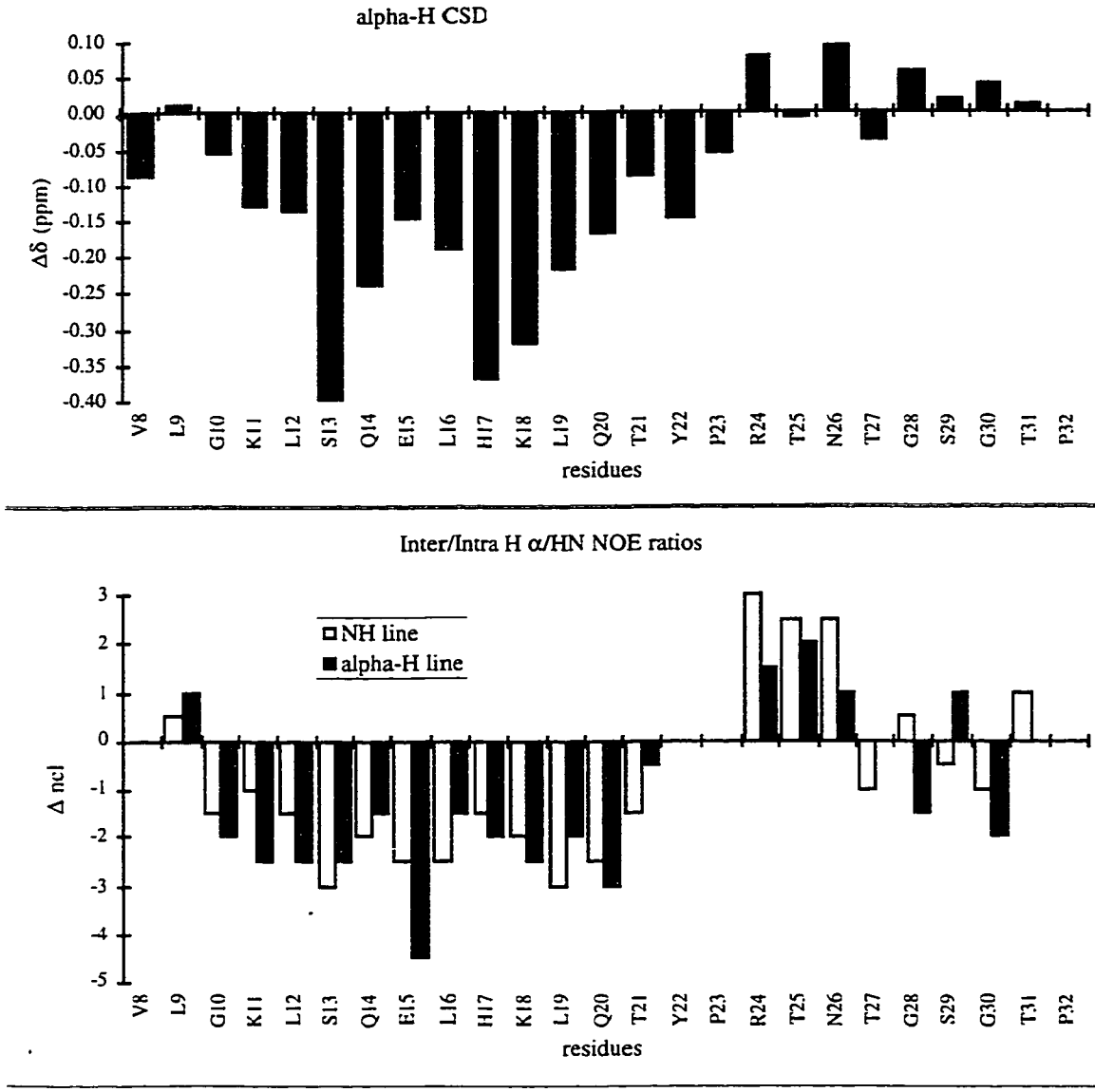

Figure 6.30 αH-CSD and NOE Ratios Histograms of sCT(8-32) in 25% HFIP.

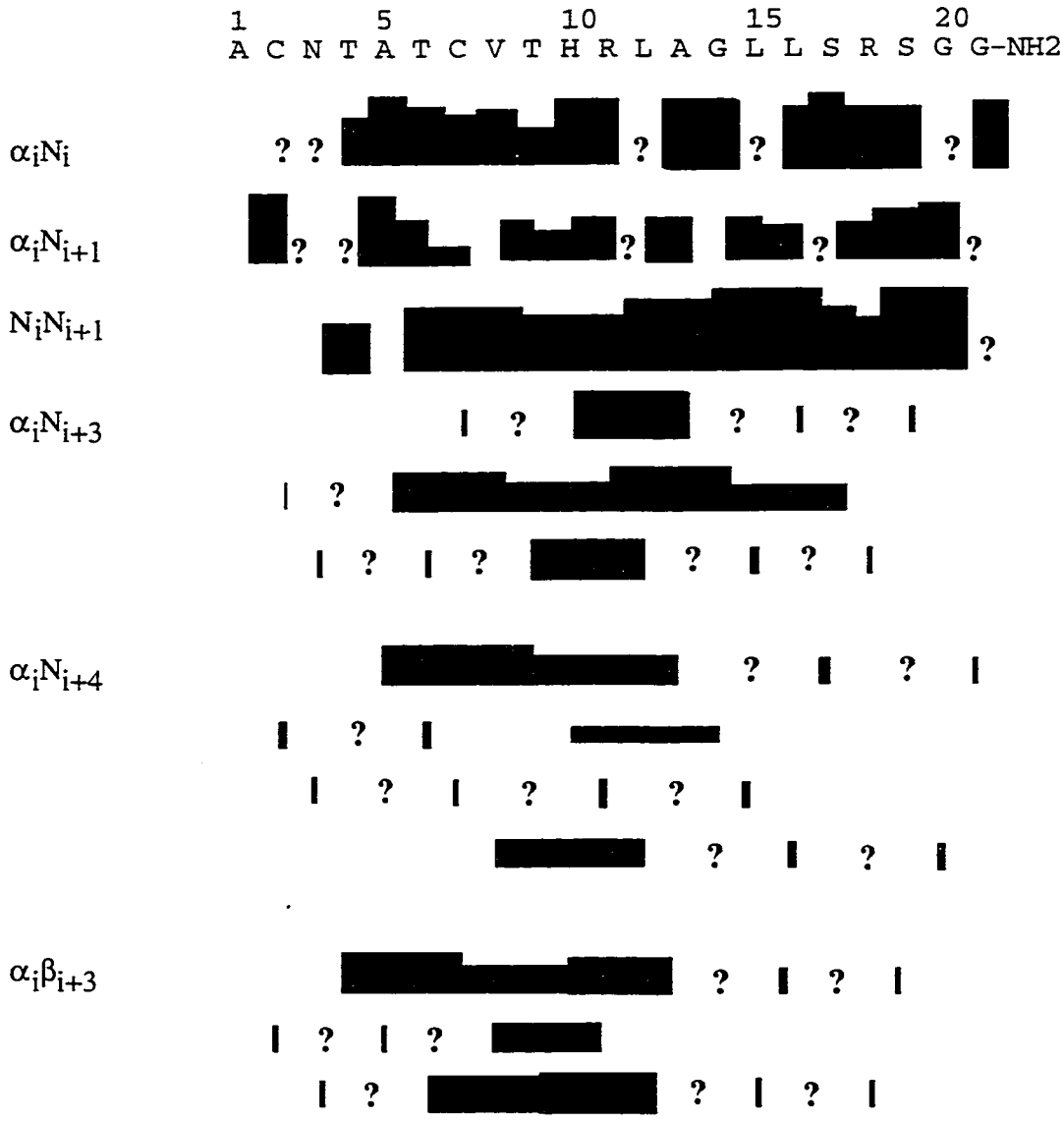

Figure 6.31 Sequential and Medium Range NOEs of CGRP(1-21) in 25% HFIP.
(The thickness of the bar represents the intensity of NOEs observed. The blank, represents no detectable NOEs. The ? represents unknown due to overlap)

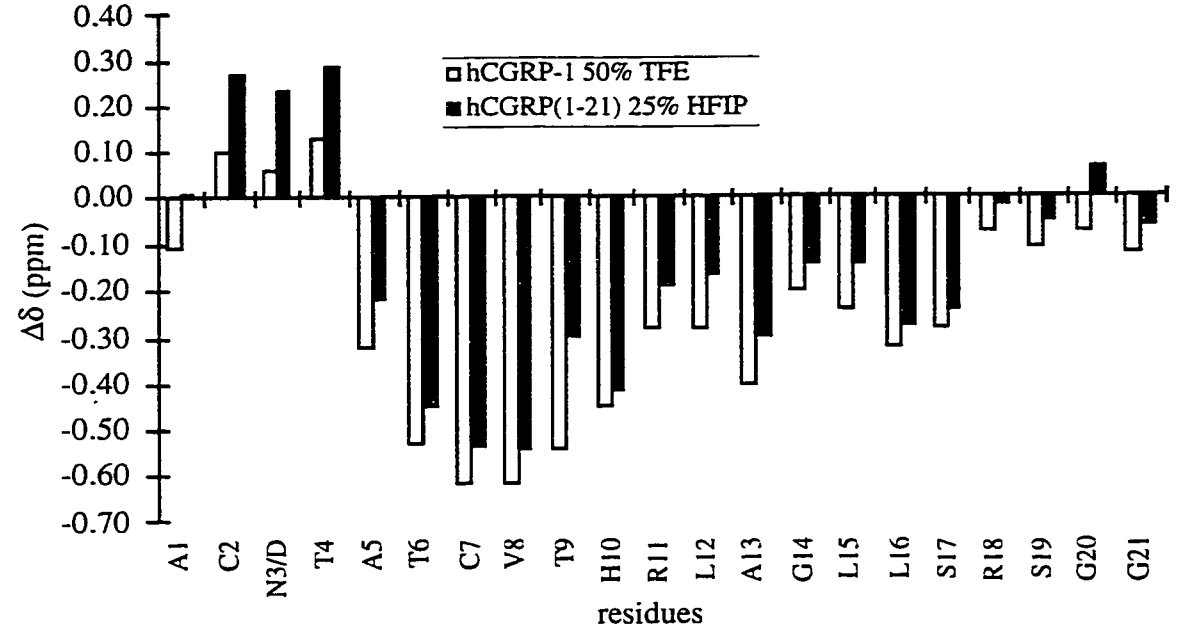

Figure 6.32 αH-CSD Comparisons of hCGRP-1 in 50% TFE (residues 1-21, data taken from Breeze et al., 1991) and hCGRP(1-21) in 25% HFIP.

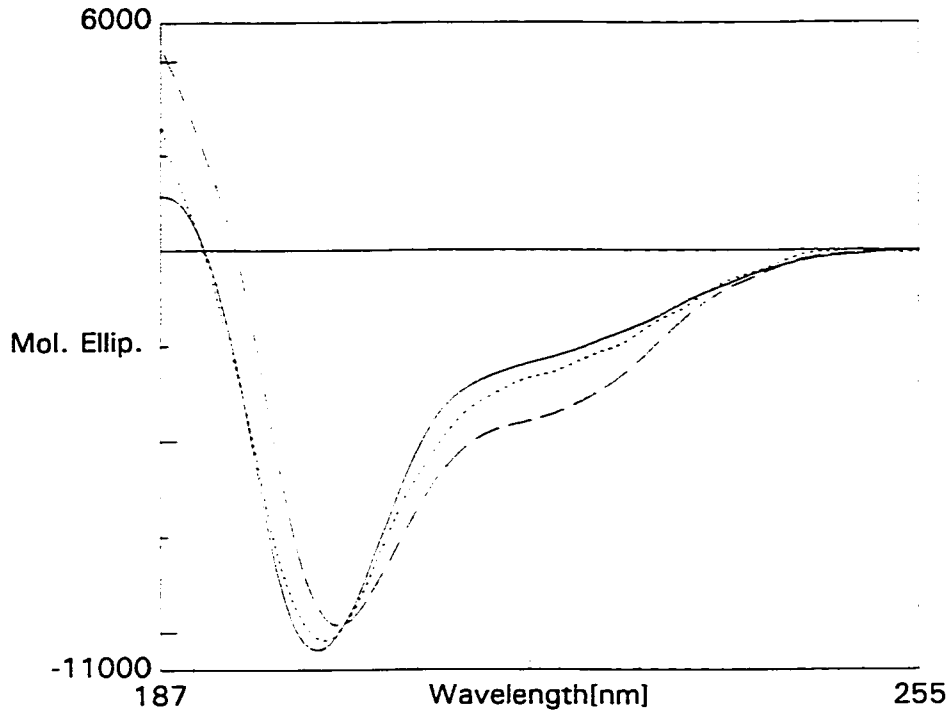

Figure 6.33 CD Comparison of hAM(1-20)GY and hAM/hCGRP Hybrids in Aqueous Buffer (pH ~ 4, 25 °C). (hAM(1-20)GY: solid line; V8-hAM(1-20)GY: dotted line; and V8S9-hAM(1-20)GY: dash line)

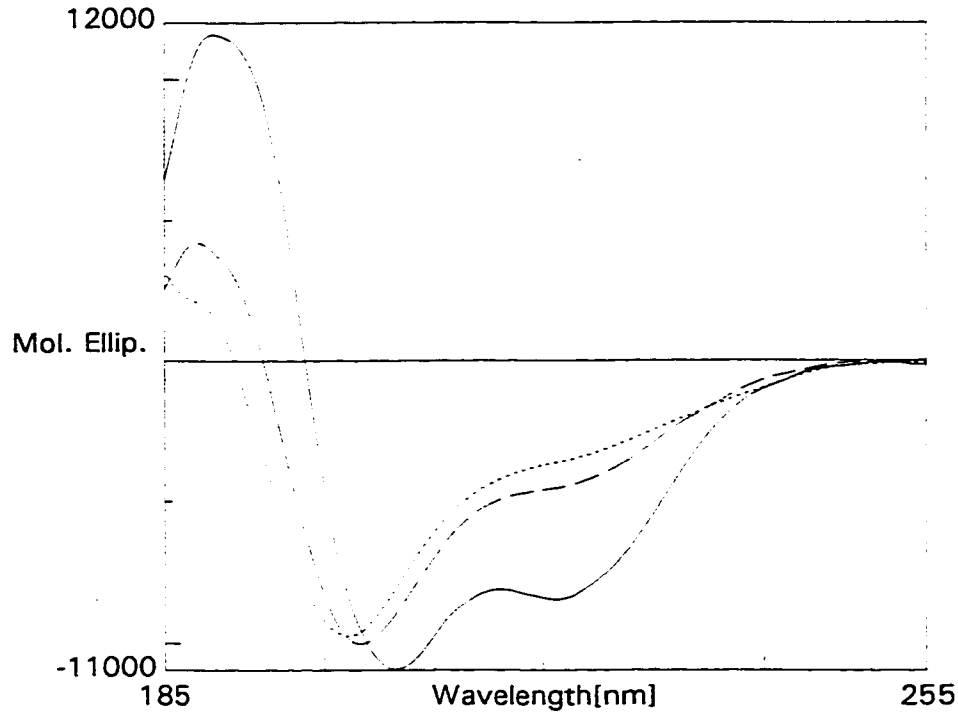

Figure 6.34 Thermal CD Study of V8S9-hAM(1-20)GY in Aqueous Buffer. (dotted line: 66°C; dash line: 24 °C; solid line -1 °C)

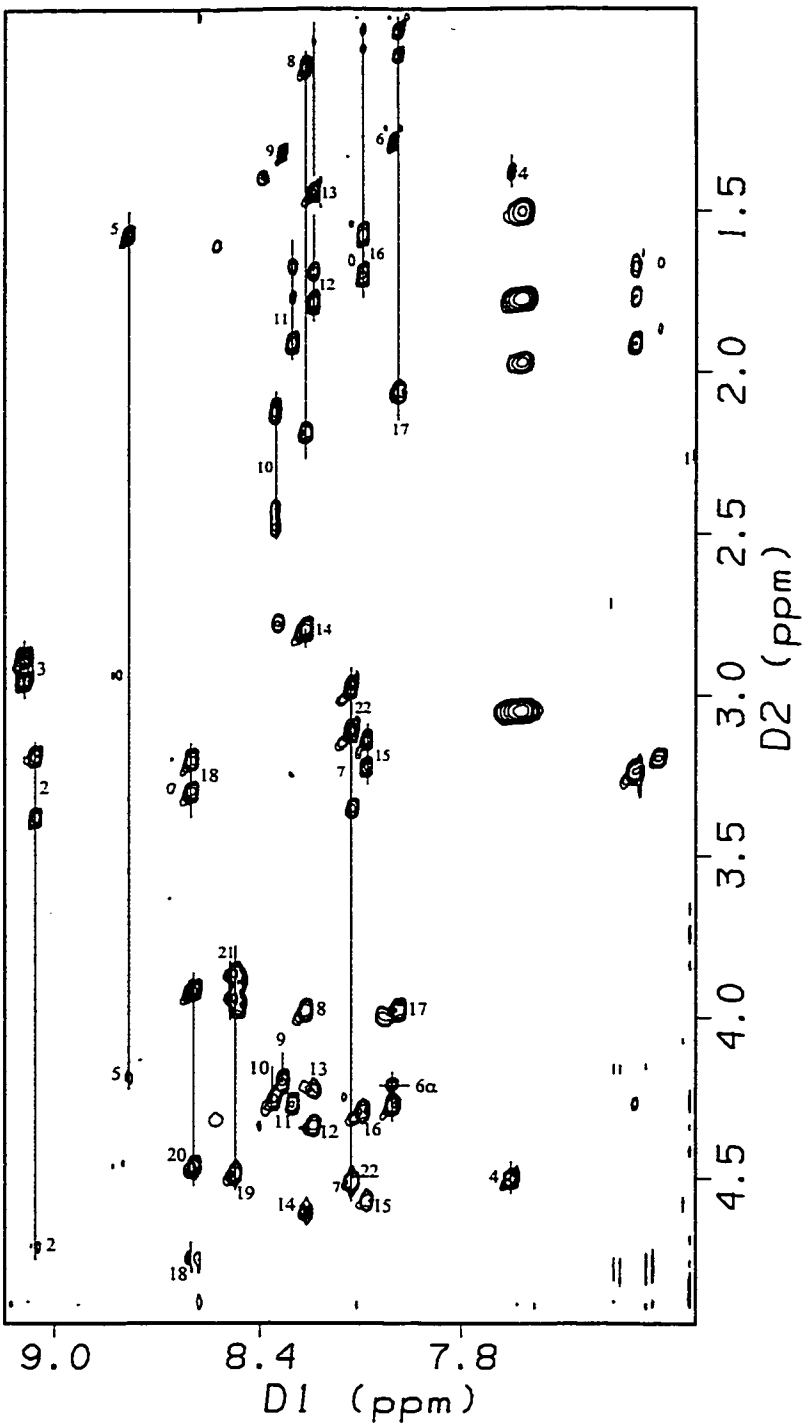

Figure 6.35 N/αβγδ Region of the TOCSY Spectrum of V8-hAM(1-20)GY in Buffer.

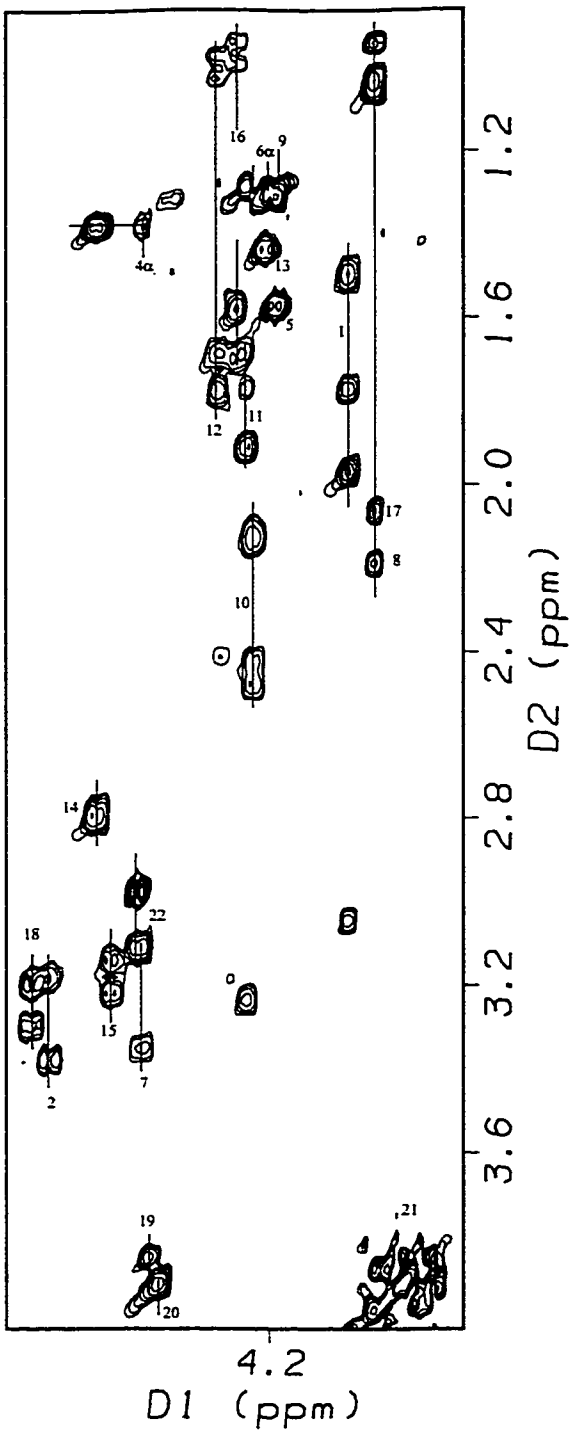

Figure 6.36 α/βγδ Region of the TOCSY Spectrum of V8-hAM(1-20)GY in Buffer.

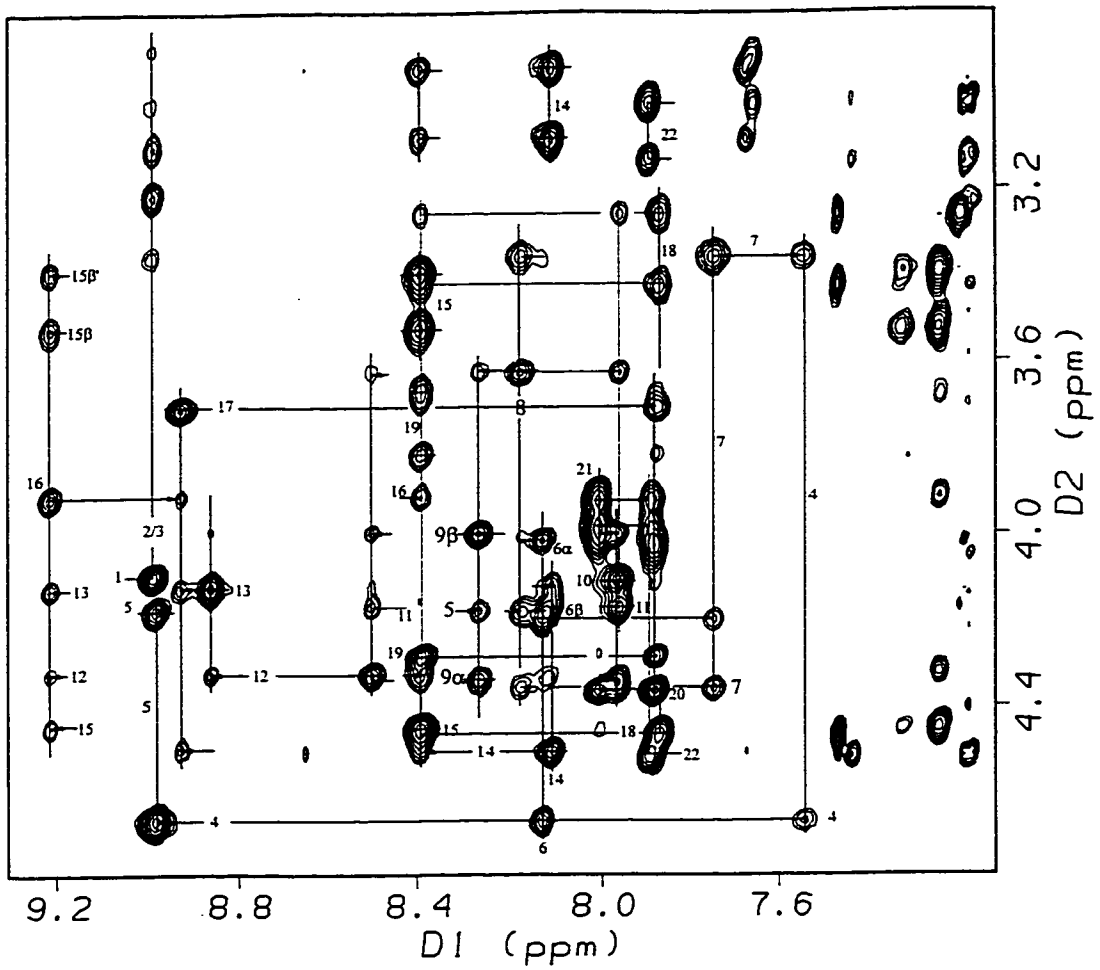

Figure 6.37 αN Region of the NOESY Spectrum of V8-hAM(1-20)GY in 25% HFIP.

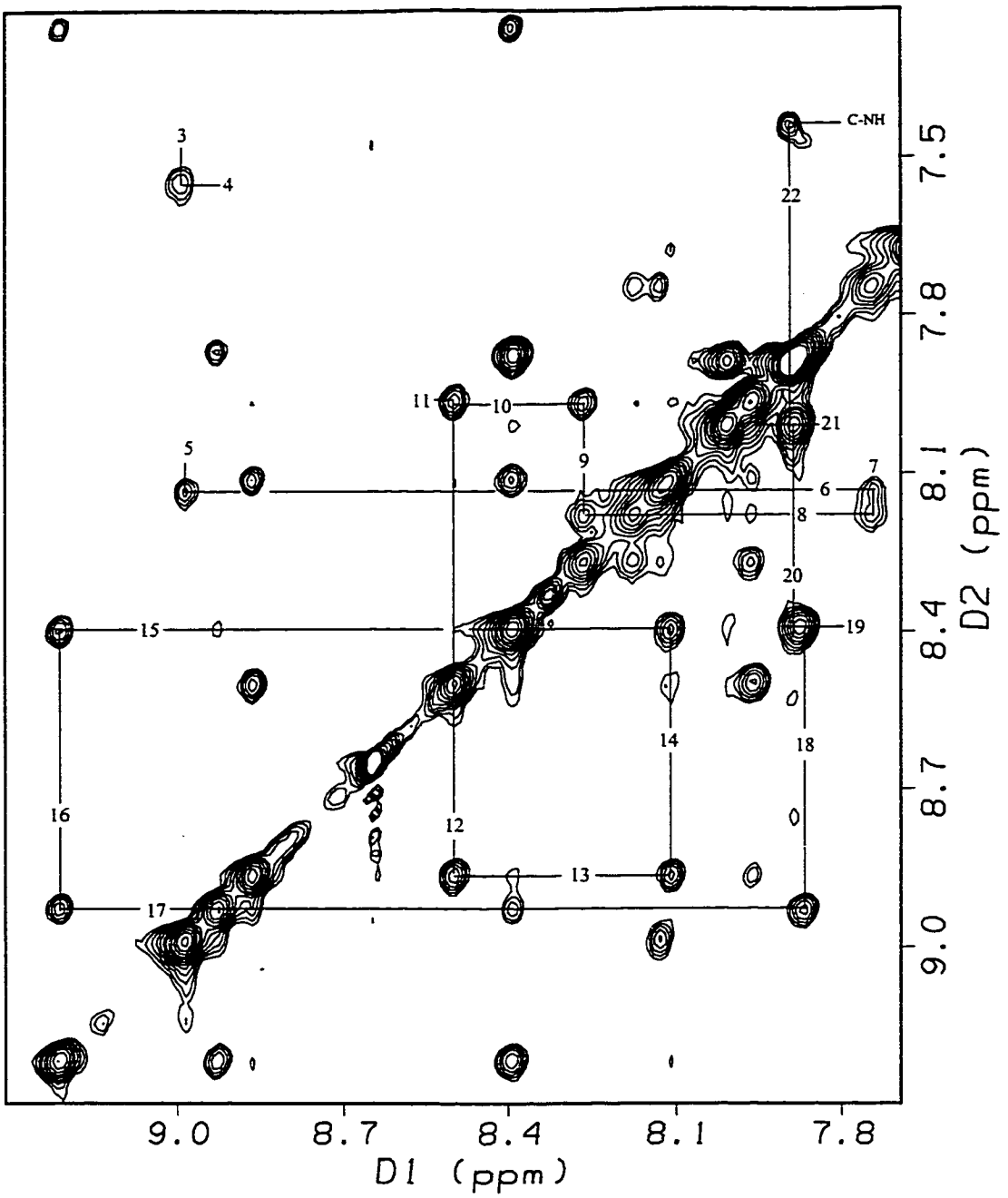

Figure 6.38 NN Region of the NOESY Spectrum of V8-hAM(1-20)GY in 25% HFIP.

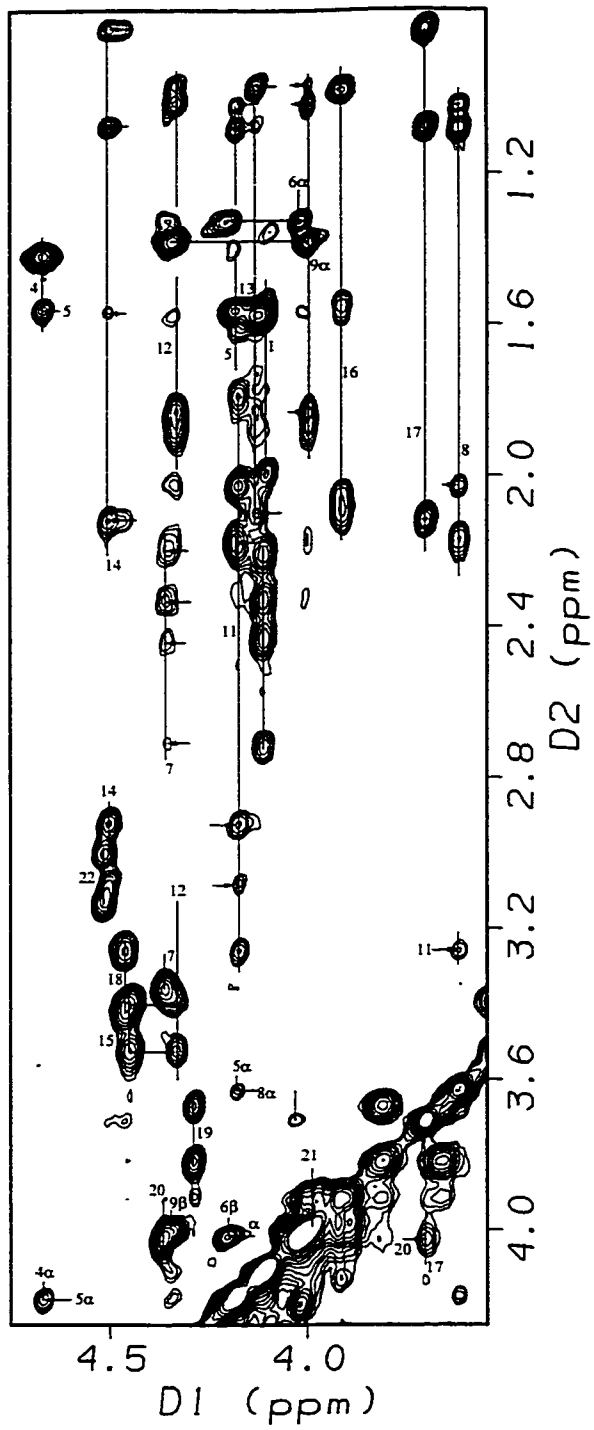

Figure 6.39 α/βγδ Region of the NOESY Spectrum of V8-hAM(1-20)GY in 25% HFIP.

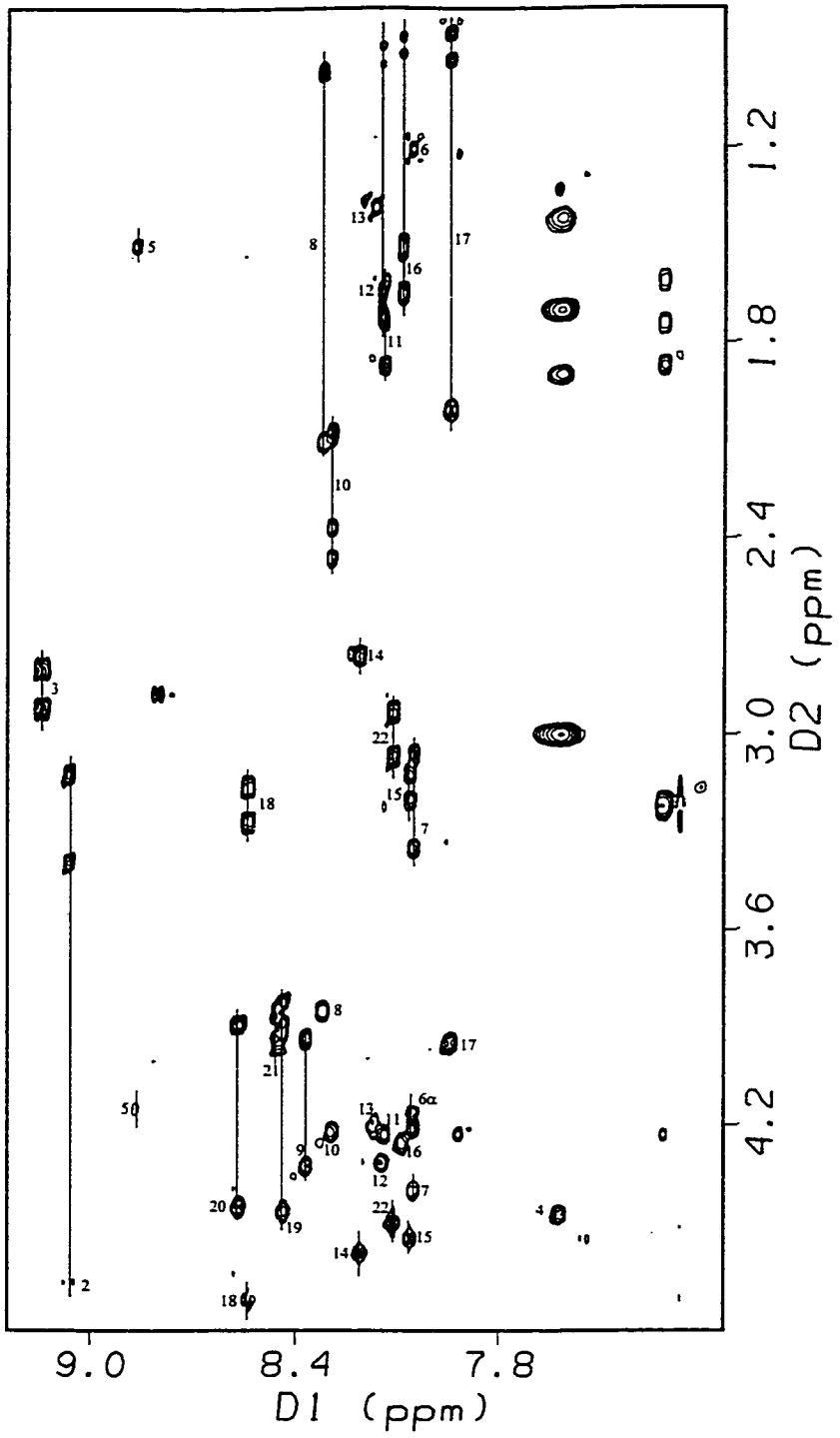

Figure 6.40 N/αβγδ Region of the TOCSY Spectrum of V8S9-hAM(1-20)GY in Buffer. (* indicates impurity peak)

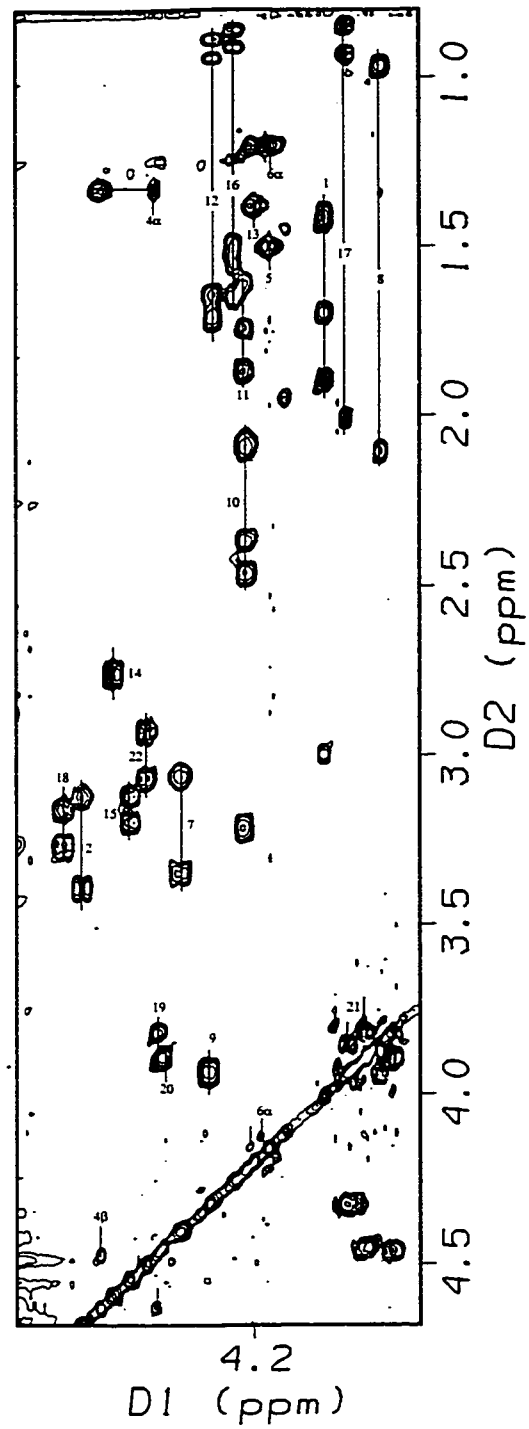

Figure 6.41 α/βγδ Region of the TOCSY Spectrum of V8S9-hAM(1-20)GY in Buffer.

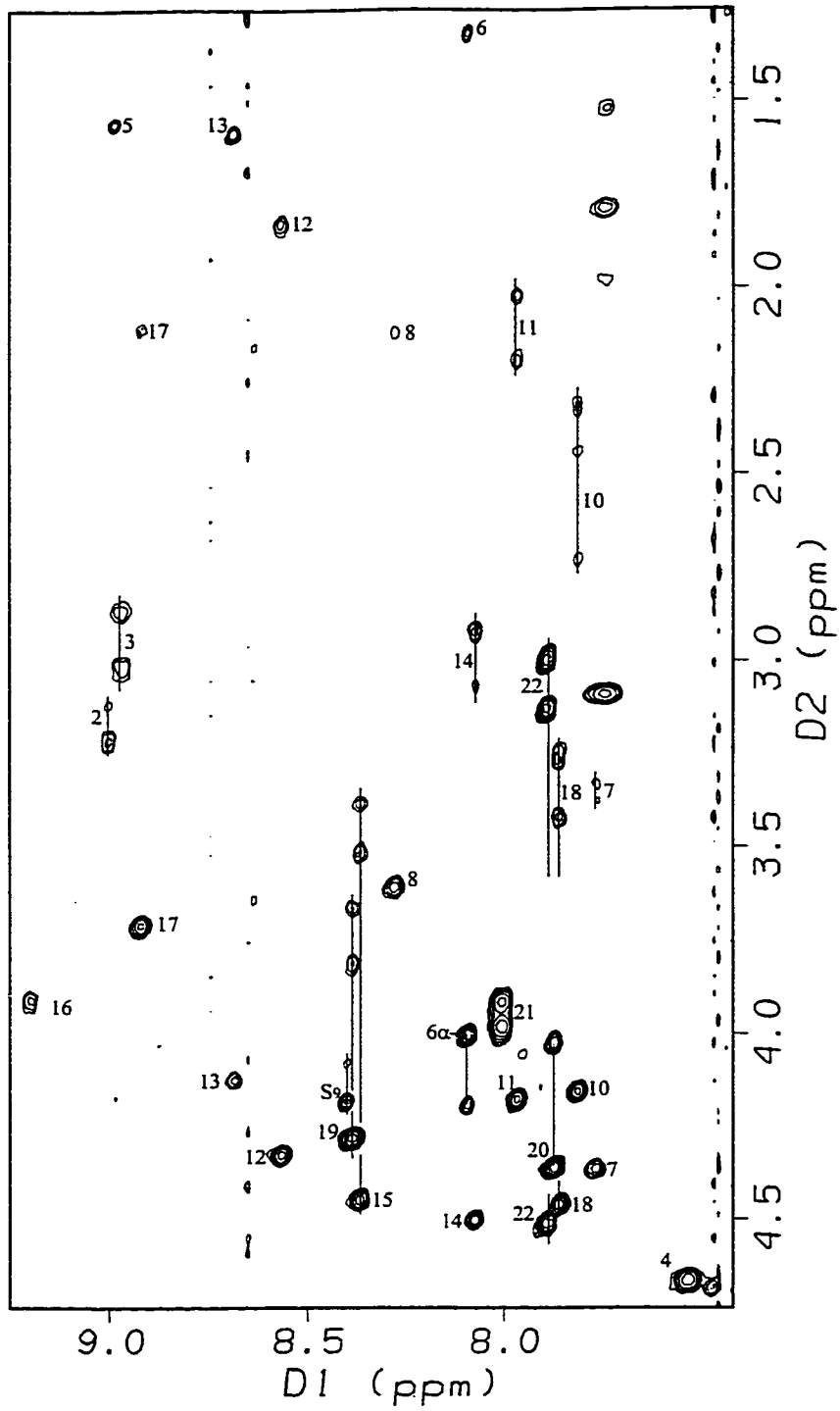

Figure 6.42 N/αβγδ Region of the TOCSY Spectrum of V8S9-hAM(1-20)GY in 25% HFIP.

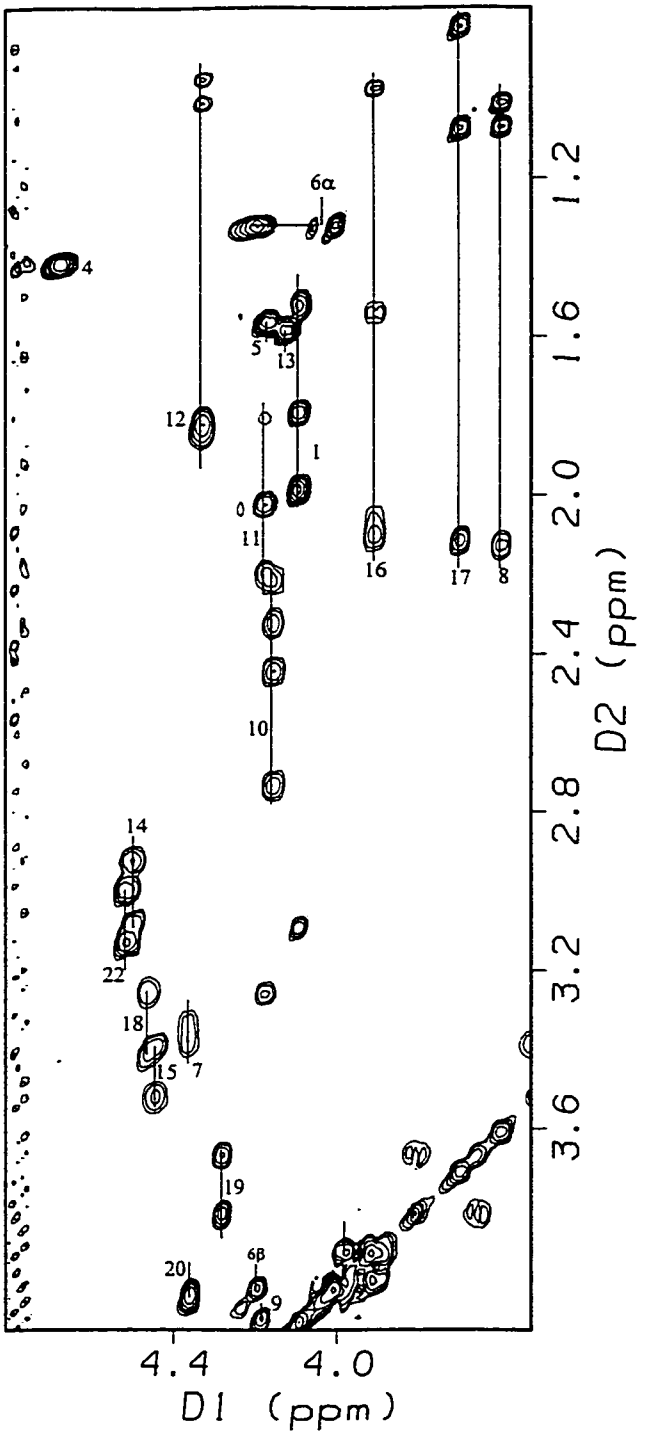

Figure 6.43 α/βγδ Region of the TOCSY Spectrum of V8S9-hAM(1-20)GY in 25% HFIP.

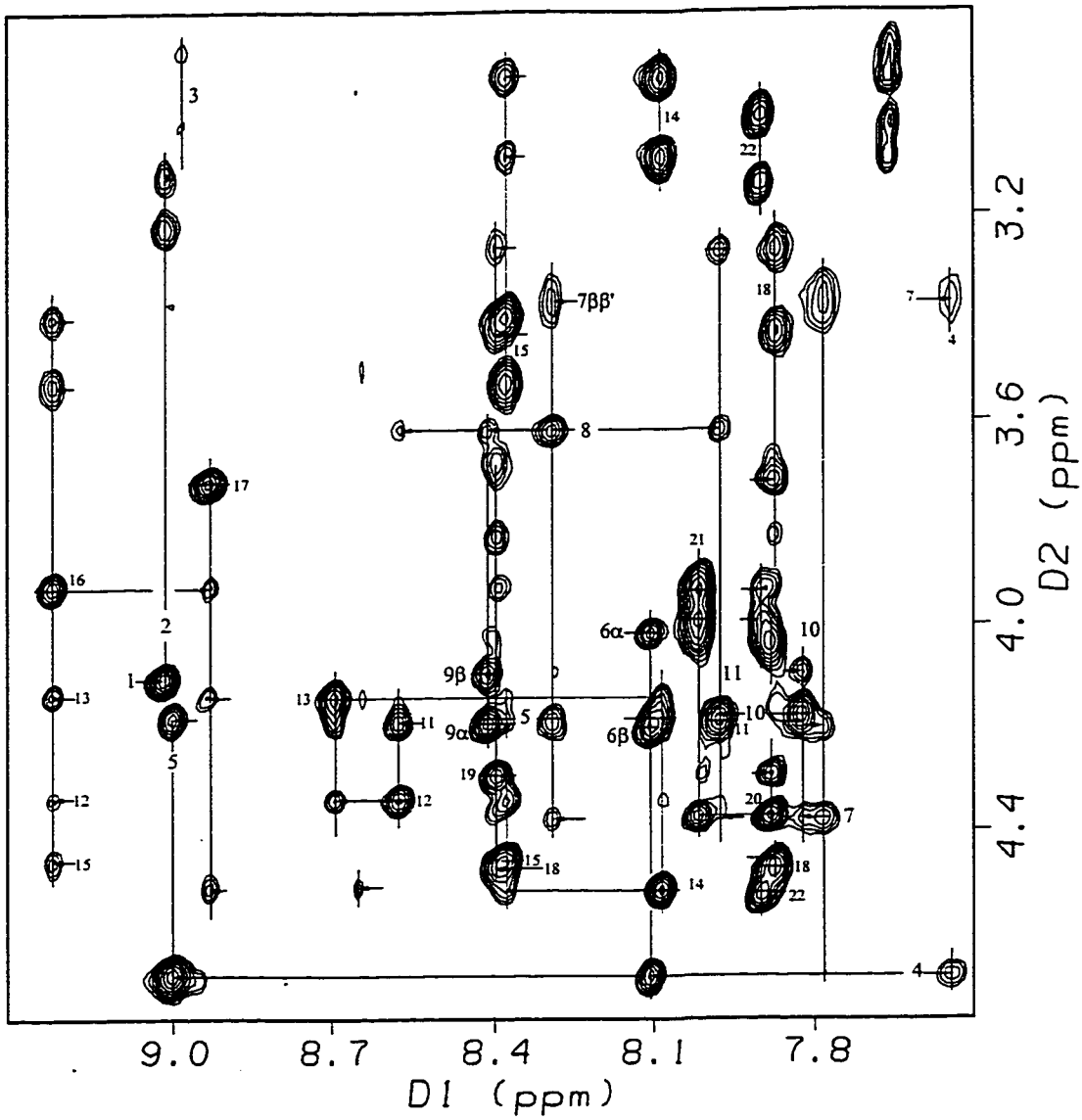

Figure 6.44 αN Region of the NOESY Spectrum of V8S9-hAM(1-20)GY in 25% HFIP.

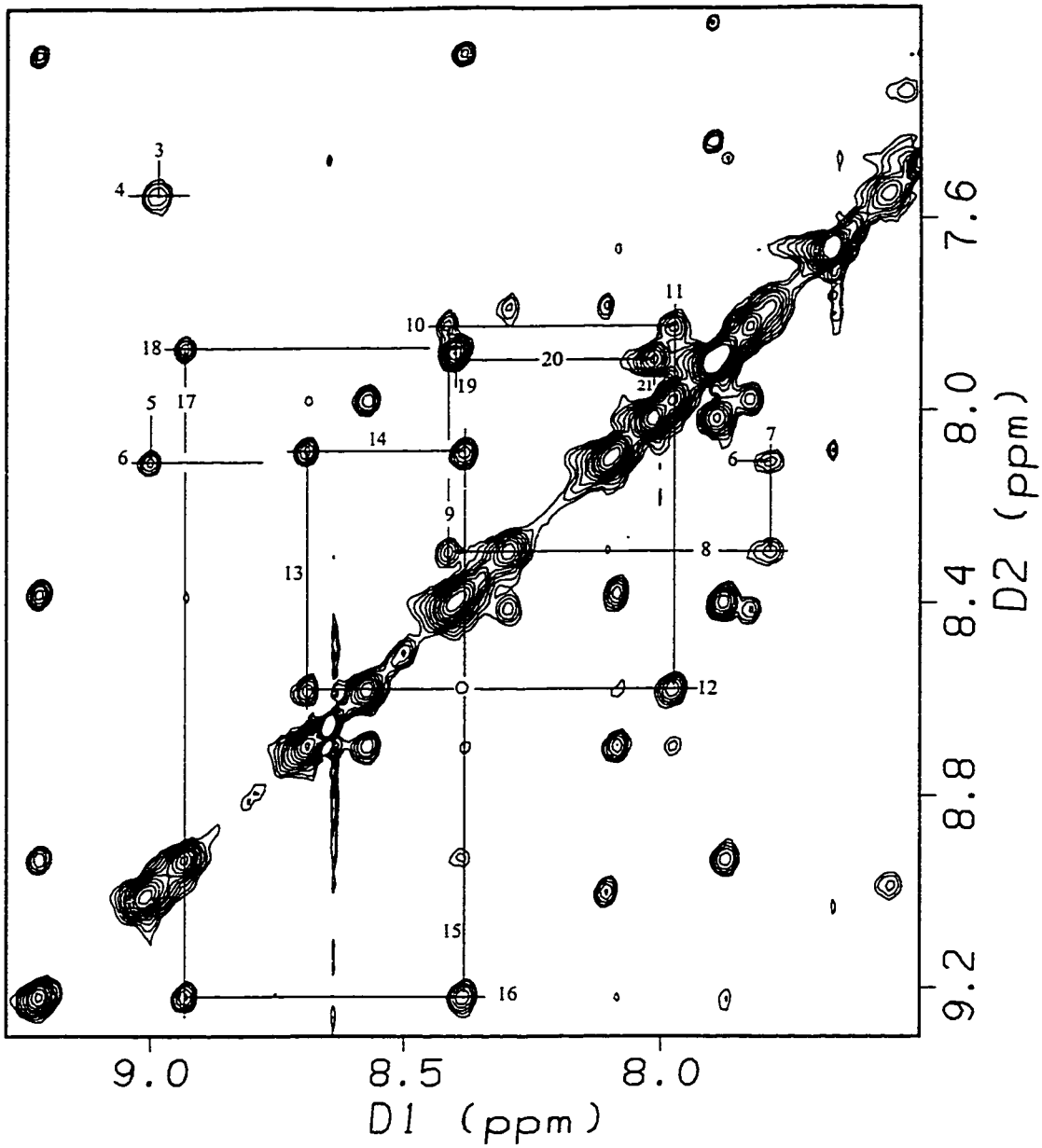

Figure 6.45 NN Region of the NOESY Spectrum of V8S9-hAM(1-20)GY in 25% HFIP

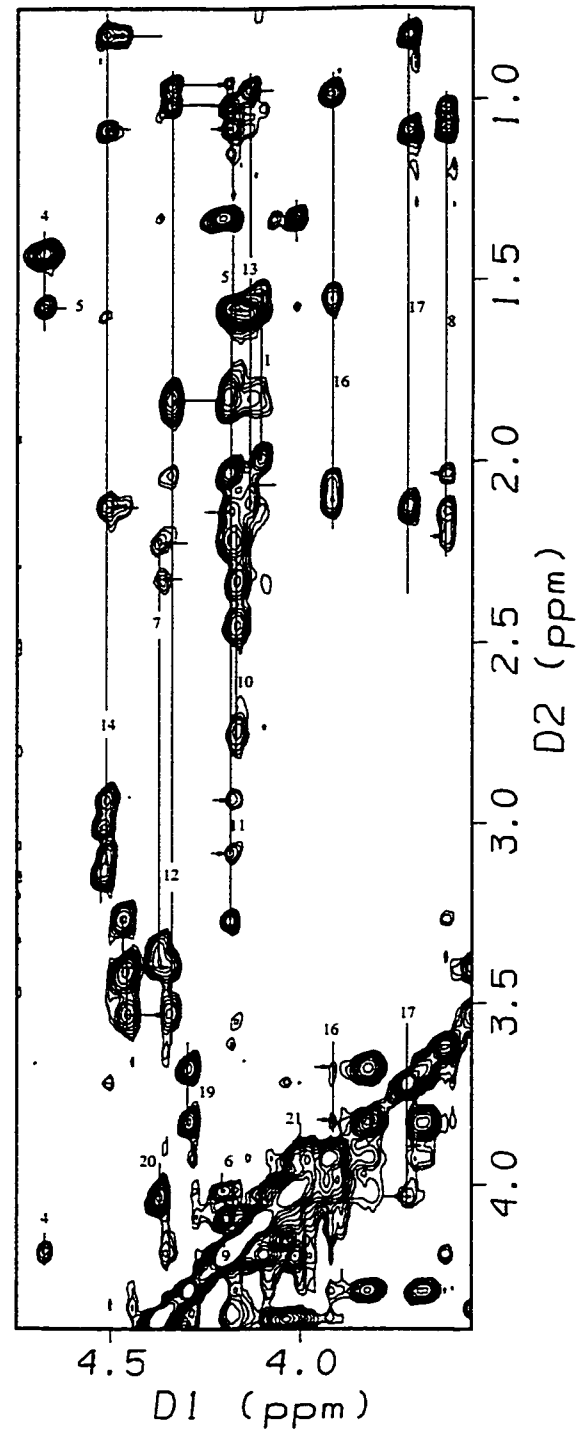

Figure 6.46 α/βγδ Region of the NOESY Spectrum of V8S9-hAM(1-20)GY in 25% HFIP.

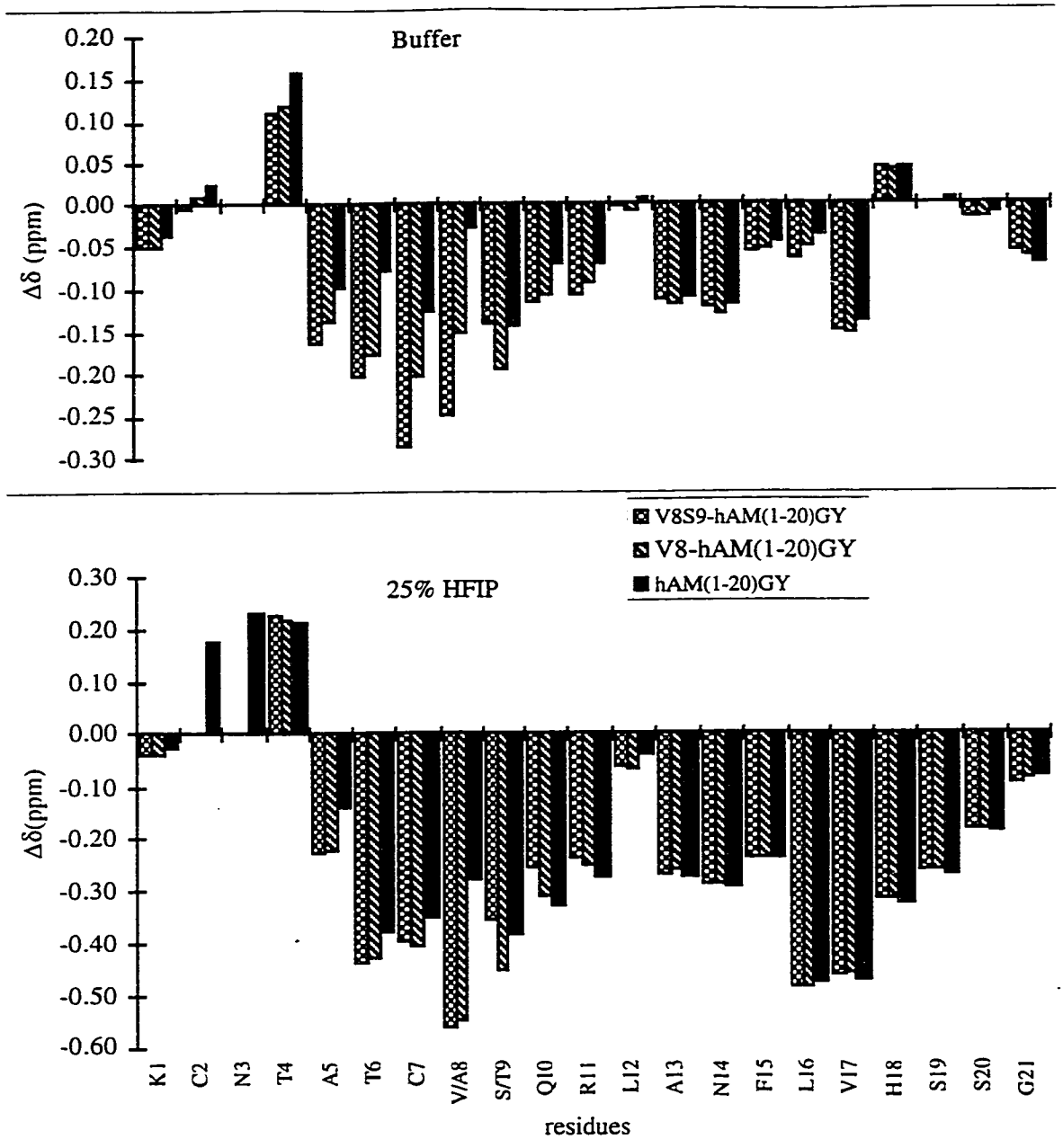

Figure 6.47 αH-CSD Comparisons of V8S9-hAM(1-20)GY, V8-hAM(1-20)GY, and hAM(1-20)GY.

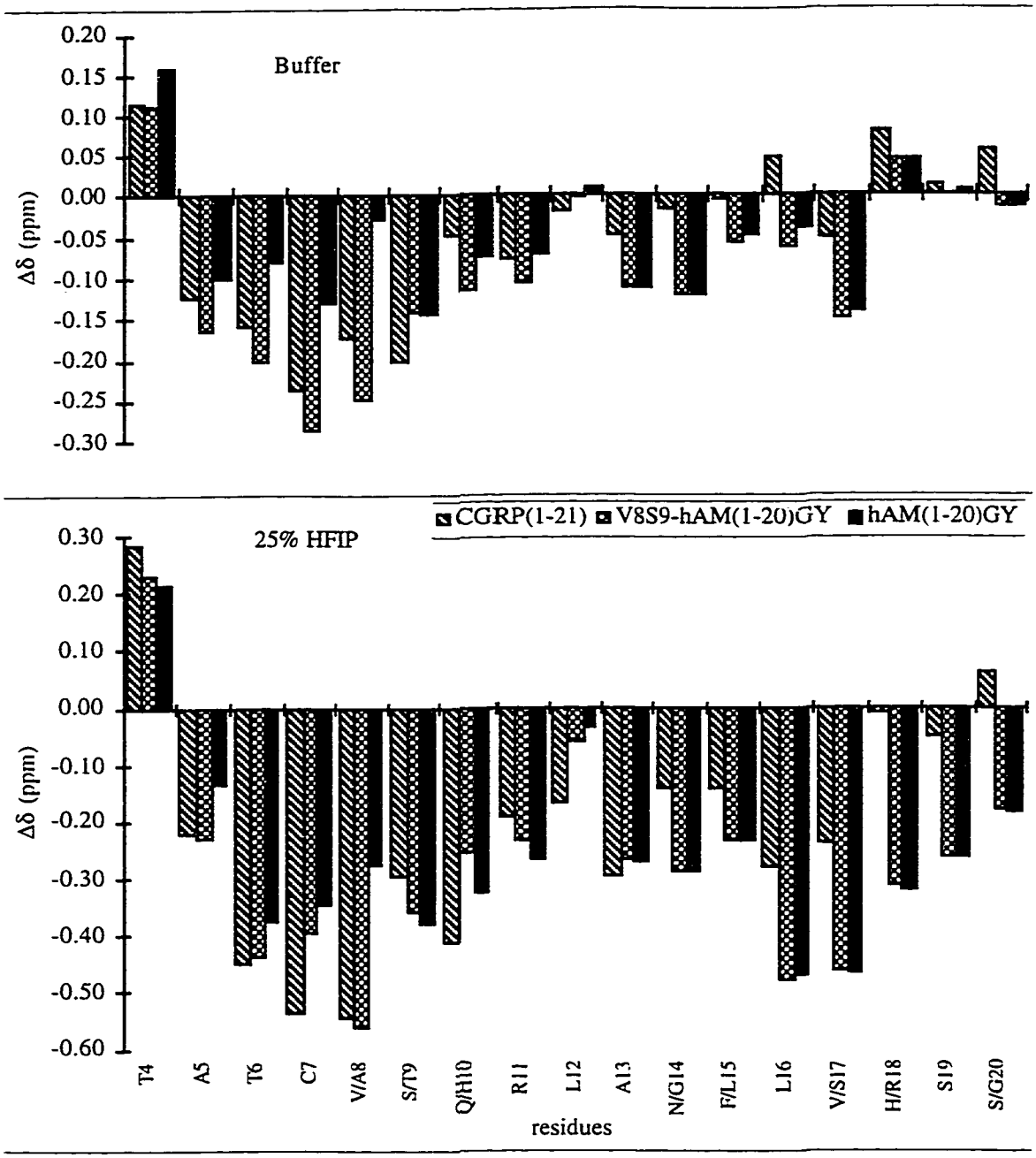

Figure 6.48 αH-CSD Comparisons of hCGRP(1-21), V8S9-hAM(1-20)GY, and hAM(1-20)GY.

References

Andersen, N. H., Neidigh, J., Harris, S. M., Lee, G. M. and Liu Z. (1997a) "Extracting Information from the Temperature Gradients of Polyeptide NH Chemical Shifts: I. The Importance of Conformational Averaging," J. Am. Chem. Soc., 119, 8547-8561.

Andersen, N. H. & Tong, H (1997b) "Empirical Parameterization of a Model for Predicting Peptide Helix/Coil Equilibrium Populations," Protein Science, 6: 1920-1936.

Andersen, N. H., Cort, J., Liu, Z., Sjoberg, S. and Tong, H. (1996a) "Cold Denaturation of Monomeric Peptide Helices," J. Am. Chem. Soc., 118: 10309-10

Andersen, N. H., Liu, Z., and Prickett, K. (1996b) "Efforts Toward Deriving the CD Spectrum of a 3_{10} helix in Aqueous Medium" FEBS Letters 399, 47-52.

Andersen, N. H. et al. (1995a) "A Scheme for Systematic Structural Interpretation of NOE Ratios, Chemical Shifts (and Their Temperature Gradients) for Polypeptide Conformer Mixtures," 36th Experimental NMR Conference, Book of Abstracts, WP134 (Boston).

Andersen, N. H., Lee, G. M., Porubcan, M. A., Hunt, J. T., & Lee, V. G. (1995b) "NMR Structure Elucidation of Endothelin/Apamin Hybrids: Comparisons of Structural Conclusions from Chemical Shift Indices, Local NOE Ratios and NOE-Constrained Simulated Annealing," 36th ENC, poster P133, Book of Abstracts p165.

Andersen, N. H., Harris, S. M., Lee, V. G., Liu, E. C.-K., Moreland, S., and Hunt, J. T. (1995c) Bioorg. and Med. Chem. 3, 113-24.

Andersen, N. H., Cao, B. Rodríguez-Romero, A. and Arreguin, B. (1993) "Hevein: NMR Assignment and Assessment of Solution-State Folding for the Aggutinin-Toxin Motif," Biochem. 32, 1407-22.

Andersen, N. H., Chen, C. Marschner, T. M., Krystek, S. R., and Bassolino, D. A. (1992a) "Conformational Isomerism of Endothelin in Acidic Aqueous Media: A Quantitative NOESY Analysis," Biochem. 31, 1280-95.

Andersen, N. H., Cao, B., & Chen, C. (1992b) "Peptide/Protein Structure Analysis Using the Chemical Shift Index Method: Upfield α-CH Values Reveal Dynamic Helices and α-Sites," BBRC 184(2), 1008-1014.

Andersen, N. H., Lai, X., Hammen, P. K., and Marschner, T. M. (1990) "NMR Applications in biopolymers" Finley et al., Eds. 95-134.

Asakura, T., Taoka, K., Demura, M. and Williamson, M. P. (1995) "The Relationship between Amide Proton Chemical Shifts and Secondary Structure in Proteins," J. Biomol NMR 6, 227-36.

Adler, A. J., Greenfield, N., and Fasman, G. D. (1973) "Circular Dichroism and Optical Rotatory Dispersion of Proteins and Polypeptides," Methods Engymol. 27, 675-735.

Alam A. S. M. T., Moonga, B. S., Bevis, P. J. R., Huang, C. H., Zaidi, M. (1993) "Amylin Inhibits Bone Resorption by a direct Effect on the Mobility of Rat Osteoclsts," Exp. Physiol. 78, 183-96.

Amodeo, P., Antonietta, M., Morelli, C. and Motta, A. (1994) "Multiple Conformations and Proline cis-trans Isomerization in Salmon Calcitonin: A Combined Nuclear Magnetic Resonance, Distance Geometry, and Molecular Mechanics Study," Biochem. 33, 10754-10762.

Amylin Pharmaceuticals (1996) Annual Report.

Ashburn, T. T., & Lansbury, P. T. Jr. (1993) "Interspecies Sequence Variations Affect the Kinetics and Thermodynamics of Amyloid Formation: Peptide Models of Pancreatic Amyloid," JACS 115, 11012-13.

Ashburn, T. T., Auger, M., & Lansbury, P. T. Jr. (1992) "The Structure Basis of Pancreatic Amyloid Formation: Isotope-Edited Spectroscopy in the Solid State," JACS 114, 790-791.

Aue, W. P., Bartholdi, E. and Ernst, R. R. (1976) "Two-dimensional spectroscopy: Application to Nuclear Magnetic Resonance," J. Chem. Phys., 64, 2229-46.

Basus, V. J. (1989) "Proton Nuclear Magnetic Resonance Assignments," Methods in Enzymology, Vol. 177, 132-149.

Bax, A. (1989) "Homonuclear Hartmann-Hahn Experiments," Methods in Enzymology, Vol. 176, 151-168.

Bax, A. and Lerner, L. (1986) "Two-dimensional NMR Spectroscopy," Science, 232, 960-70.

Bax, A. and Subramanian, S. (1986b) J. Magn. Reson., 67, 565.

Bax, A. and Davis, D. G. (1985) J. Magn. Reson., 65, 355.

Bax, A., Griffey, R. H., and Hawkins, B. L. (1983) J. Magn. Reson. 55, 301.

Barlow, D. J. and Thornton, J. M. (1988) "Helix Geometry in Protiens." J. Mol. Biol. 201, 601-619.

Beals, J. M., Haas, E., Krausz, S., Scheraga, H. A. (1991) Biochem. 30, 7680-92.

Bendell, M. R., Pegg, D. T. and Doddrell, D. M. (1983) J. Magn. Reson. 52, 81.

Betsholtz, C., et al. (1993) "Islet Amyloid Polypeptide - Hen or Egg in Type 2 Diabetes Pathogenesis?" Acta Oncologica 32, No. 2, 149-154.

Betsholtz, C., et al. (1990) "The Structure of Cat Islet Amyloid Polypeptide (IAPP) and Identification of Amino Acid Residues of Potential Significance for Islet Amyloid Formation," Diabetes 39, 118-22.

Betsholtz, C., et al. (1989) "Sequence Divergence in a Specific Region of Islet Amyloid Polypeptide (IAPP) Explains Differences in Islet Amyloid Formation Between Species," FEBS Lett, 247, 154-8.

Blanco, F. J., Herranz, J. H., González, C. Jiménez, A. M, Rico, M., Santoro, J. and Nieto, J. L. (1992) "NMR Chemical Shifts: A Tool to Characterize Distortions of Peptide and Protein Helices," JACS, 114, 9676-7.

Blundell, T. L., Barlow, D., Borkakorti, N. and Thornton, J. M. (1983) "Solvent-induced distortions and the curvature of alpha-helices," Nature 306, 281-3.

Bodenhausen, G., Kogler, H., and Ernst, R. R. (1984) "Selection of Coherence-Transfer Pathways in NMR Pulse Experiments," J. Magn. Reson. 58, 370-88.

Borgias, B. A. and James, T., L., (1988) "COMATOSE, A Method for Constrained Refinement of Macromolecular Structure Based on Two-Dimensional Nuclear Overhauser Effect Spectra," J. Magn. Reson. 79: 493-512.

Bothner-By, A., Stephens, R. L. and Lee J. (1984) "Structure Determination of a Tetrasaccharide: Transient Nuclear Overhauser Effcts in the Rotating Frame," J. Am. Chem. Soc. 106, 811-3.

Bradley E. K., Thomason, J. F., Cohen, F. E., Kosen, P. A., Kuntz, I. D. (1990) "Studies of Synthetic Helical Peptides Using Circular Dichroism and Nuclear Magnetic Resonance" J. Mol. Biol. 215, 607-622.

Brain, S. D., wimalawansa, S., MacIntyre, I., Williams, T. J. (1990) "The Demonstration of Vasodilator Activity of Pancreatic Amylin Amide in the Rabbit," Am. J. Pathol. 136, 487-90.

Braun, D., Wider, G. and Wüthrich K. (1994) "Sequence-Corrected ^{15}N "Random Coil" Chemical Shifts," J. Am. Chem. Soc. 116, 8466-9.

Breeze, A. L., Harvey, T. S., Bazzo, R., and Campbell, L. D. (1991) "Solution Structure of Human Calcitonin Gene-Related Peptide by ^{1}H NMR and Distance Geometry with Restrained Moleculare Dynamics," Biochem. 30, 575-582.

Brown, K., Menius, A., Sandefer, E., Edwards, J., James, M. (1994) "The Effects of Amylin on Changes in Plasma Glucose and Gastric Emptying Following an Oral Glucose Load in Conscious Dogs," Diabetes 43, Suppl. 1, 172.

Brooks, B., Bruccoleri, R., Olafson, B., States, D., Swaminathan, S. and Karplus, M. (1983) "CHARMM: A Program for Macromolecular Energy, Minimization and Dynamics Calculations," J. Comp. Chem. Vol. 4, No. 2: 187-217.

Bruch, M. D., Dhingra, M. M., and Gierash, L. M. (1991) Prot. Struct. Func. Gen. 10, 130-9.

Bruix, M., Perello, M., Herranz, J., Rico, M. Nieto, J. L. (1990) "Characterization of Low Populated Peptide Helical Structures in Solution by Means of NMR Proton Conformational Shifts," BBRC Vol. 167, No. 3, 1009-14.

Brushweiler, R., Blackledge, M., and Ernst, R. R. (1991) J. Bio. NMR 1, 3-11.

Brünger A. T. and Nilges M. (1993) "Computational Challenges for Macromolecular Structure Determination by X-ray Crystallography and Solution NMR-Spectroscopy," Quarterly Reviews of Biophysics 26, 1:49-125.

Brünger A. T. (1992) X-PLOR Version 3.1, A System for X-Ray Crystallography and NMR, Yale University press, New Haven, CT.

Brünger A. T. and Karplus M. (1991) "Molecular Dynamics Simulations with Experimental Restrints," Acc. Chem. Res. 24: 54-61.

Brünger A. (1987) X-PLOR. Version 1.0. A System for X-ray Crystallography and NMR. New Haven: Yale Univesity Press.

Bundi, A., Grathwohl, C., Hochmann, J., Keller, R., Wagner, G., & Wüthrich, K. (1975) "Proton NMR of the Protected Tetrapeptides TFA-Gly-Gly-L-X-L-Ala-OCH_3, Where X Stands for One of the 20 Common Amino Acids," J. Magn. Res. 18, 191-198.

Butler, P. C., Chou, J., Carter, W. B., Wang, Y. N. Bu, B. H., Chang, D., Chang, J. K. and Rizza, R. A. (1990) "Effects of Meal Ingestion on Plasma Amylin concentration in NIDDM and Non-Diabetic humans," Diabetes 39, 752-756.

Bystrov, V. F. (1976) Prog. NMR Spectrosc. 10, 41.

Cammers-Goodwin, A., Allen, T. J., Oslick, S. L., McClure, K. F., Lee, J. H., and Kemp, D. S. (1996) "Mechanism of Stabilization of Helical Conformations of Polypeptides by Water Containing Trifluoroethanol," JACS 118, 3082-3090.

Calvin, M., Hermans, J. Jr., and Scheraga, H. A. (1959) "Effect of Deuterium on the Strength of Hydrogen Bonds," J. Am. Chem. Soc. 81, 5048-5050.

Carra, J. H., Anderson, E. A., Privalov, P. L. (1994) Protein Sci. 3, 952-9.

Case, D. A., Dyson J. H. and Wright, P. E. (1994) "Use of Chemical Shifts and Coupling Constants in Nuclear Magnetic Resonance Structural Studies on Peptides and Proteins," Methods in Engymology Vol. 239, 393-416.

Castillo, M. J., Scheen, A. J., and Lefébvre, P. J. (1995) "Amylin Islet Amyloid Polypeptide: Biochemistry, Physiology, Patho-Physiology," Diabete & Metabolisme (Paris) 21, 3-25.

Cefalu, W. T. (1996) "Treatment of Type II Diabetes," Postgraduate Medicine 99, No. 3109-119.

Ciaraldi, T. P., Goldberg, M., Odom, R., Stolpe, M. (1992)"In Vitro Effects of Amylin on Carbohydrate Metabolism in Liver Cells," Diabetes 41, 975-81.

Chen, Y. H., Yang, J. T., and Chau, K. H. (1974) Biochem. 13, 3350-3359.

Chakrabartty, A., Kortemme, T. and Baldwin, R. L. (1994) "Helix Propensities of the Amino Acids Measured in Alanine-based Peptides without Helix-stabilizing Side-chain interactions," Protein Sci. 3:843-52.

Chou, P. Y. and Fasman, G. D. (1974) "Conformational Parameters for Amino Acids in Helical, β-Sheet, and Random Coil Regions Calculated from Proteins," Biochem. Vol 13, No. 2, 211-25.

Clark, A., Charge, S. B. P., Badman, M. K. and Koning, E.J. P. D. (1996) "Islet Amyloid in Type 2 (Non-Insulin-Dependent) Diabetes," APMIS 104, 12-18.

Clark, A., Koning, E. J. P. and Morris, J. F. (1993) "Formation of Islet Amyloid from Islet Amyloid Polypeptide," Biochemical Society Transactions 21, 169-73.

Clayden, N. J. and williams, R. J. P. (1982) J. Magn. Reson. 49, 383.

Clore, M., and Gronenborn, A. (1994) "Structure of Larger Protein, Protein-Ligand and Protein-DNA Complexes by Multidimensional Heteronuclear NMR," Protein Science 3: 372-390.

Clore, G. M. and Gronenborn, A. M. (1993) "NMR of Proteins" CTC Press.

Clore, M. and Gronenborn, A. (1989) "Determination of Three-Dimensional Structures of Proteins and Nucleic Acids in Solution By Nuclear Magnetic Resonance Spectroscopy," Crit. Rev. Biochem. 24:479-563.

Cooper, G. J. S. and Tse, C. A. (1996) "Amylin, Amyloid and Age-Related Disease" Drugs & Aging 9(3), 202-212.

Cooper, G. J. S. (1994) "Amylin Compared with Calcitonin Gene-Related Peptide: Structure, Biology, and Relevance to Metabolic Disease," Endocrine Reviews Vol. 15, No. 2, 163-201.

Cooper, G. J. S., Day, A. J., Willis, A. C., Roberts, A. N., Reid, K. B., and Leighton B. (1989) "Amylin and the Amylin Gene: Structure, Function and Relationship to Islet Amyloid and to Diabetes Mellitus," Biochimica et Biophysica Acta, 1014, 247-58.

Cooper, G. J. S., Leighton, B., Dimitriadis, G. D., Parry-Billings, M., Kowalchuk, J. M., Howland, K., Rothbard, J. B., Willis, A. C., Reid, K. B. (1988) "Amylin Found in Amyloid Deposits in Human Type 2 Diabetes Mellitus May Be a Hormone That Regulates Glycogen Metabolism in Skeletal Muscle," Proc. Natl. Acad. Sci. USA 85(20) 7763-6.

Cooper, G. J. S., Willis, A. C., Clark, A., Turner, R. C., Sim, R. B., and Reid, K. B. (1987) "Purification and Characterization of a Peptide from amyloid-rich Pancreases of Type 2 Diabetic Patients," PNAS, USA 84, 8628-8632.

Constantine, K. L., Mueller, L., Andersen, N. H., Tong, H., Wandler, C. F., Friedrichs, M. S., and Bruccoleri, R. L. (1995) J. Am. Chem. Soc. 117, 10841-10854.

Cornish, J., Callon, K. E., Lin, C. Q., Xiao, C. L., Mulvey, T. B., Coy, D. H., Cooper, G. J., and Reid, I. R. (1998) "Dissociation of the Effects of Amylin on Osteoblast Proliferation and Bone Resorption," Am. J. Physiol. 274(5 Pt 1): E827-33.

Cort J. R. and Andersen N. H. (1997) "Formation of a Molten-Globule-like State of Myoglobin in Aqueous Hexafluoroisopropanol," BBRC 233m 687-691.

Cort J. (1997) "Peptide and Protein Structure in Aqueous Hexafluoroisopropanol: I. Monomeric and Beta-Aggregate Forms of Human Amylin. II. Cold Denaturation of Alpha-Helices." Dissertation.

Cort, J., Liu, Z., Lee, G., Harris, S., Prickett, K., Gaeta, L., and Andersen, N. H. (1994) "β-Structure in Human Amylin and Two Designer β-Peptides: CD and NMR Spectroscopic Comparisons Suggest Soluble β-Oligomers and the Absence of Significant Populations of β-Strand Dimers," Biochem. & Biophys. Res. Comm., 204(3): 10880.

Creighton, T. E. (1993) "Proteins: Structures and Molecular Principles" 2nd Edition. Freeman and company NY.

Croasmun, W. R. and Carlson, R. M. K. (1994) "Tow-Dimensional NMR Spectroscopy: Applications for Chemists and Biochemists" VCH Publishers, Inc.

Dealba, E., Jimenez, M. A., Rico, M., and Nieto, J. L. (1996) "Conformational Investigation of Designed Short Linear Peptides Able to Fold into Beta-hairpin Structures in Aqueous Solution," Folding & Design Vol 1, No. 2, 133-44.

Deems, R. O., Cardinaux, F., Deacon, R. W., et al. (1992) "Amylin or CGRP(8-37) Fragments Reverse Amylin-Induced Inhibition of ^{14}C-Glycogen Accumulation," BBRC 181, 116-20.

Deems, R. O., Deacon, R. W., Young, D. A. (1991) "Amylin Activates Glycogen Phosphorylase and Inactives Glycogen Synthase via a cAMP-Independent Mechanism," BBRC 174, 716-720.

Derome A. E. (1987) "Modern NMR Techniques for Chemistry Research," Pergamon Press.

De Dios, A., Pearson, J. and Oldfield, E. (1993) "Secondary and Tertiary Structural Effects on Protein NMR Chemical Shifts: An ab Initio Approach," Science 260, 1491-6.

Doty, P., and Yang, J. T. (1956) "Polypeptides. VII: Poly-γ-Benzyl-L-Glutamate: The Helix-Coil Transition in Solution," J. Am. Chem. Soc. 78, 498-500.

Draulis, P. J., Clore, G. M., Nilges, M., Jones, T. A., Pettersson, G., Knowles, J., and Gronenborn, A. M. (1989) Biochem. 28, 7241-57.

Driscoll, P. C., Clore, M., Beress, L., and Gronenborn, A. M. (1989) "A Proton Nuclear Magnetic Resonance Study of the Antihypertensive and Antiviral Protein BDS-I from the Sea Anemone Anemonia Sulcata: Sequential and Stereospecific Resonance Assignment and Secondary Structure," Biochem. 28, 2178-87.

Dumont, Y., Fournier, A., St-Pierre, S., and Quirion, R. (1997) "A Potent And Selective CGRP2 Agonist, [Cys(Et)2,7]hCGRP Alpha: Comparison in Prototypical CGRP1 And CGRP2 in Vitro Bioassays," Can. J. Physiol. Pharmacol. 75(6): 671-6.

Dyson, H. J. & Wright, P. E. (1991) Annu. Rev. Biophys. Chem. 20, 519-38.

Dyson, H. J., Rance, M., Houghten, R. A., Wright, P. E. and Lerner, R. A. (1988) "Folding of Immunogenic Peptide Fragments of Proteins in Water Solution. II. The Nascent Helix," J. Mol. Biol. 201, 201-217.

Ernst, P. R., Bodenhausen, G. and Wokaun, a. (1987) "Principles of Nuclear Magnetic Resonance in One and Two Dimensions," clarendon Press, Oxford.

Fischer, J. A., Born, W. (1985) "Novel Peptides from the Calcitonin Gene: Expression, Receptors and Biological Function," Peptides, 6 Suppl 3, 265-71.

Flood, J. F. and Morley, J. E. (1992) "Differential Effects of Amylin on Memory Processing Using Peripheral and Central Routes of Administration," Peptides 13, 577-80.

Forood, B., Feliciano, E. J., and Nambiar, K. P. (1993) Proc. Natl. Acad. Sci. USA 90, 838-42.

Force, T., Bonvertre, J. V., Flannery, M. R., Gorn, A. H., Yamin, M. and Goldring, S. R.,"A Cloned Porcine Renal Calcitonin Receptor Couples to Adenylyl Dyclase and Phospholipase C," Am. J. Physiol. 262, F1110-5.

Fran L. (1996) "Compound Could Help Diabetic Patients Walk Tightrope Between Hyperglycemia, Hypoglycemia," Can. Med. Assoc. J. 154(5), 705-707.

Fresnel, A. (1824) Bull. Soc. Philomat. 9, 150.

Funaloshi, A., Miyasaka, K., Kitani K., Nakamura, S., Fukuda, H. and Fujii, N. (1992) "Stimulatory Effects of Islet Amyloid Polypeptide (Amylin) on Exocrine Pancreas and Gastrin Release in conscious rats," Regul. Pep. 38, 135-43.

Gagné, S. M., Tsuda, S., Li, M. X, Chandra, M., Smillie, L. B., and Sykes, B. D. (1994) "Quantification of the Calcium-induced Secondary Structural Changes in the Regulatory Domain of Troponin-C," Protein Science, 3, 1961-74.

Gans, P. J., Lyu, P. C., Manning, M. C., Woody, R. W. and Kallenbach, N. R. (1991) Biopolymers 31, 1606-1614.

Gronenborn, A. and Clore, M. (1991) "Protein Structure Determination in Solution Using Nuclear Magnetic Resonance Spectroscopy," NIDA-Res-Monogr. 112:78-105.

Griesinger, C., Otting, G., Wüthrich, K., and Ernst, R. R. (1988) "Clean TOCSY for ^{1}H Spin System Identification in Macromolecules," J. Am. Chem. Soc. 110, 7870-2.

Günther H. (1995) "NMR Spectroscopy: Basic Principles, Concepts, and Applications in Chemistry" John Wiley & Sons.

Hagihara, Y., Oobatake, M., Goto, Y. (1994) Protein Sci. 3, 1418-29.

Harris, S. M. (1993) "Solution Conformations of Medium Sized Peptides: A Comparison of the Information Content of CD and NMR Applied to C-Peptide Analogs and Endothelins;" Dissertation.

Heino, P., Oksala, O., Palkama, A., Valo, T., Vihavainen, S., Koskinen, A., and Uusitalo, H. (1998) "Binding of CGRP Analogs and Their Effect on Adenylate Cyclase Activity in Porcine Iris-Ciliary Body," J. Ocul. Pharmacol. Ther. 14(6): 543-54.

Herranz, J., González, C., Ricl, M. Nieto, J., Santoro, J., Jiménez, M. Bruix, M., Neira, J., and Blanco, F. (1992) "Peptide Group Chemical Shift Computation," J. Magn. Reson. Chem. 30, 1012-8.

Hessler, H., Griesinger, C., Kerssebaum, R., Wagner, K., and Ernst, R. R. (1987) "Separation of Cross-Relaxation and J Cross-Peaks in 2D Rotating-Frame NMR Spectroscopy," J. Am. Chem. Soc. 109, 607-9.

Holzwarth, G. and Doty, P. (1965) "The Ultraviolet Circular Dichroism of Polypeptides," JACS 87(2), 218-228.

Howitt, S. G. and Poyner, D. R. (1997) "The Selectivity And Structural Determinants of Peptide Antagonists At The CGRP Receptor Of Rat, L6 myocytes," Br. J. Pharmacol 121(5): 1000-4.

Huang, H. J. S., Young, A. A., Koda, J. E., Tulp, O. L., Johnson, M. J., Cooper, G. J. S. (1992) "Hyperamylinemia, Hyperinsulinemia and Insulin Resistance in Genetically Obese LA/N-cp Rats," Hypertension 19, 1101-9.

Hwang, T. and Shaka, A. J. (1992) "Cross Relaxation without TOCSY: Transverse Rotating-Frame Overhauser Effect Spectroscopy," J. Am. Chem. Soc. 114, 3157-59.

Imperiali, B., Fisher, S. L., Moats, R. A., Prins, T. J. (1992) J. Am. Chem. Soc. 114, 3182.

Johnson, C. W. Jr. (1990) "Protein Secondary Structure and Circular Dichroism: A Practical Guide," Proteins: Structure, Function, and Genetics 7, 205-214.

Jiménez, M., Andreu, D., Blanco, F. J., Nieto, J. L., Herranz, J. & Rico, M. (1993) Eur. J. Biochem. 221, 569-581.

Jiménez, M. A.; Blanco, F. J.; Rico, M.; Santoro, J; Herranz, J. and Nieto, J. (1992) "Periodic Properties of Proton Conformational Shifts in isolated Protein Helices," Eur. J. Biochem. 207, 39-49.

Jiménez, M. A., Nieto, J. L., Herranz, J., Rico, M., & Santoro, J. (1987) "^{1}H NMR and CD evidence of the Folding of the Isolated Ribonuclease 50-61 Fragment," FEB 221, 2. 320-324.

Karle, I. L., Flippen-Anderson, J. L., Gurunath, R. and Balaram, P. (1994) "Facile Transition Between 3_{10}- and alpha-helix: Structures of 8-, 9-, and 10-residue Peptides Containing the -(Leu-Aib-Ala)$_2$-Phe-Aib- Fragment," Protein-Sci. 3(9), 1547-55.

Karle, I. L. and Balaram, P. (1990) "Structural Characteristics of Alpha-Helical Peptide Molecules Containing Aib Residues," Biochem. 29 (29), 6747-56.

Kay, L. E., Marion, D., and Bax A. (1989) "Practical Aspects of 3D Heteronuclear NMR of Proteins," J. Magn. Reson. 84, 72-84.

Kahn, R. C., Vicent, D. and Doria, A. (1996) "Genetics of Non-Insulin-Dependent (Type-II) Diabetes Mellitus," Annu. Rev. Med. 47, 509-31.

Kanatsuka, A., Makino, H., Ohsawa, H., Tokyuama, Y., Yamaguchi, T., Yoshida, S., Adachi, M. (1989) "Secretion of Islet Amyloid Polypeptide in Response to Glucose" FEBS Lett. 259, 199-201.

Kim, P. S. & Baldwin R. L. (1982) "Specific Intermediates in the Folding Reactions of Small Proteins and the Mechanism of Protein Folding," Annu Rev Biochem 51:459-89.

Kitakuni, E., Kuroda, Y., Oobatake, M., Tanaka, T., Nakamura, H. (1994) Protein Sci. 3, 831-7.

Kessler, H. (1982) Angew. Chem. Int. Ed. Engl. 21, 512.

Kirkpatrick, S.; Gelatt, C.; and Vecchi, M. (1983) "Optimization by Simulated Annealing," Science Vol. 220, No.4598: 671-680.

Koda, J. E., Fineman, M., Rink, T. J., Dailey, G. E., Muchmore, D. B., Linarelli, L. G. (1992) "Amylin Concentrations and Glucose Control," Lancet 339, 1179-1180.

Kolterman, O. G., Schwartz, S., Corder., C., Levy, B., Klaff, L., Peterson, J., Gottlieb, A. (1996) "Effect of 14 Days' Subcutaneous Administration of the Human amylin Analogue, Pramlintide (AC137), on an Intravenous Insulin Challenge and

Response to a Standard Liquid Meal in Patients with IDDM," Diabetologia 39, 492-9.

Kolterman, O. G., Gottlieb, A., Moyses, C., and Colburn, W. (1995) "Reduction of Post-Prandial Hyperglycaemia in Subjects with Type 1 Diabetes Mellitus and Other Categories of Glycose Intolerance" Diabetes Care 18, 1179-82.

Kraulis, P. J., Clore, G. M., Nilges, M., Jones, T. A., Pettersson, G., Knowles, J., and Gronenborn, A. M. (1989) Biochem. 28, 7241-57.

Kuroda, Y., Kidokora, S. and Wada, A. (1992) J. Mol. Biol. 223, 1139-53.

Lacassie, E., Delmas, A., Meunier, C., Sy., D. and Trudelie, Y. (1996) "High Thermal Stability and Cold-denaturation of an Artificial Polypeptide," Int. J. Peptide Protein Res. 48, 249-258.

Lee, G. M., Chen, C., Marschner, T. M., and Andersen, N. H. (1994) "Does the Solid-State Structure of Endothelin-1 Provide Insights Concerning the Solution-State Conformational Equilibrium?" FEBS Lett. 355, 140.

Leighton, B., Cooper, G. J. S. (1988) "Pancreatic Amylin and Calcitonin Gene Related Peptide Cause Resistance to Insulin in Skeletal Muscle in Vitro," Nature 335, 632-5.

Li, J., Matsuura, J. E., Waugh, D. J., Adrian, T. E., Abel, P. W., Manning, M. C. and Smith, D. D. (1997) "Structure-Activity Studies on Position 14 of Human Alpha-Calcitonin Gene-Related Peptide," J. Med. Chem. 40(19): 3071-6.

Liu, Z., Cort, J., Andersen, N. H., Janes, S. and Prickett, S. (1997) "Structure and Dynamics of Pramlintide and Amylin as determined by NMR Spectroscopy," 38th Experimental NMR Conference, #P232 (March 1997 Orlando)

Liu, Z., Andersen, N. H, Lumpkin, R. Prickett, K. (1996) "Disulfide Loop Size and Specific Residue Mutation Effects on Helix Formation: An NMR Comparison of Calcitonin, CGRP and Pancreatic Amylin Fragments," 37th Experimental NMR Conference, #WP100 (March 1996 Asilomar).

Liu, Z. and Andersen, N. H (1995) "NMR Quantitaion of the Importance of N-terminal Initiation and C-capping for Stabilizing α Helical Domain," 36th Experimental NMR Conference, P132 (Boston).

Liu, Z., Tong, H, Cort, J., Li, Y, Tomaszewski, J., Chen, C., Cao, B. and Andersen, N. H. (1994) "Chemical Shift (Amide-NH & alpha-H) Temperature Gradients Revisited: Deriving Structural and Dynamics Information for Peptides and Proteins," 35th Experimental NMR Conference, #MP 46 (Asilomar).

Live, D. H., Davis, D. G., Agosta, W.D. and Cowburn, D. (1984) J. Am. Chem. Soc., 106, 1939-43.

Llinás, M. and Klein, M. P. (1975) J. Am. Chem. Soc. 97, 4731-4737.

Lorenzo, A. and Yankner, B. A. (1996) "Amyloid Fibril Toxicity in Alzheimer's Disease and Diabetes," Ann. NY Acad. Sci. 777, 89-95.

Lorenzo, A., Razzaboni, B., Weir, G. C., et al. (1994) "Pancreatic Islet Cell Toxicity of Amylin Associated with Type-2 Diabetes Mellitus," Nature 368,756-60.

Ludvik, B., Kautzky, W. A., Prager, R., Thomaseth, K. and Pacini, G. (1997) "Amylin: History and Overview," Diabet. Med. 14 Suppl 2, S9-13.

Luo, P., Demetrios, T., Subramanian, R. M., Meredith, S. C., and Lynn, D. G. (1994) "Structural and Thermodynamic Characterization of a Bioactive Peptide Model of Apolipoprotein E: Side-Chain Lactam Bridges to Constrain the Conformation," Biochem. 33, 12367-77.

Manning, M. C. and Woody, R. W. (1991) "Theoretical CD Studies of Polypeptide Helices: Examination of Important Electronic and Geometric Factors," Biopolymers 31, 569-586.

Marion, D., Kay, L. E., Sparks, S. W., Torchia, D. A., and Bax, A. (1989) JACS 111, 1515.

Marion, D. & Wüthrich, K. (1983) "Application of Phase Sensitive Two-Dimensional Correlated Spectroscopy (COSY) for Measurements of ^{1}H-^{1}H Spin-Spin Coupling Constants in Proteins," BBRC 113, 967-974.

Markley, J. L., Measows, D. H., and Jardetzky, O. (1967) J. Mol. Biol. 27, 25.

Meadows, R. P., Nikonowicz, E. P., Jones, C. R., Bastian, J. W.and Gorenstein D. G. (1991) "Two-Dimensional NMR and Structure Determination of Salmon Calcitonin in Methanol," Biochem. 30, 1247-54.

Merutka, G., Dyson, J. H., and Wright, P. E. (1995) "'Random Coil' ^{1}H Chemical Shifts Obtained as a Function of Temperature and Trifluoroethanol Concentration for the Peptide Series GGXGG," J. Bio. NMR, 5, 14-24.

Meyer, J-P, Pelton, J. T., Hoflack, J. and Saudek V. (1991) "Solution Structure of Salmon Calcitonin," Biopolymers, Vol. 31, 233-41.

Mihalyi, E.(1968) J. Chem. Eng. Data. 13, 179-182.

Millhauser, G. L. (1995) "Views of Helical Peptides: a Proposal for the Position of 3_{10}-Helix Along the Thermodynamic Folding Pathway," Biochem. 34, 3873-7.

Molina, J. M., Cooper, G.J. S., Leighton, B, Olefsky, J. M. (1990) "Induction of Insulin Resistance in vivo by Amylin and Calcitonin Gene Related Peptide," Diabetes 39: 260-5.

Mosselman, S., Hoppener, J. W., Lips, C. J., Jansz, H. S. (1989) "The Complete Islet Amyloid Polypeptide Precursor Is Encoded by Two Exons," FEBS Lett. 247, 154-8.

Motta, A., Andreotti, G., Amodeo, P., Strazzullo, G., and Castiglione-Morelli, M. A. (1998) "Solution Structure of Human Calcitonin in Membrane-Mimetic Environment: The Role of the Amphipathic Helix Proteins," 32(3): 314-23.

Motta, A., Temussi, P. A., Wünsch, E. and Günter, B. (1991a) "A ^{1}H NMR Study of Human Calcitonin in Solution," Bionchem. 30, 2364-71.

Motta, A., Temussi, P. A., Wünsch, E. and Günter, B. (1991b) "Solution Conformation of Salmon Calcitonin in Sodium Dodecyl Sulfate Micelles as Determined by Two-Dimensional NMR and Distance Geometry Calculations," Bionchem. 30, 10444-50.

Motta, A., Morelli, M. A. C., Goud, N., and Temussi, P. A. (1989) "Sequential ^{1}H NMR Assignment and Secondary Structure Determination of Salmon Calcitonin in Solution," Biochem. 28, 7996-8002.

Muff, R., Born, W., and Fischer, J. A. (1995) "Calcitonin, Calcitonin Gene-Related Peptide, Adrenomedullin and Amylin: Homologous Peptides, Separate Receptors and Overlapping Biological Actions," European J. of Endocrinology 133, 17-20.

Munoz, V, Serrano, L., Jimenez, M. A., Rico, M. (1995) "Structural Analysis of Peptides Encompassing All Alpha-helices of Three α/β Parallel Proteins: Che-Y, Flavodoxin and P21-ras: Implications for α-helix Stability and the Folding of α/β Parallel Proteins," J. Mol. Biol. 7, 247 (4): 648-69.

Neuhaus, D. and Williamson M. (1989) "The Nuclear Overhauser Effect in Structural and Conformational Analysis" VCH Publishers, Inc.

Nelson, J. W., and Kallenbach, N. R. (1989) "Persistence of the alpha-helix stop signal in the S-peptide in trifluoroethanol solutions,"Biochemistry 28, 5256-5261.

Nelson, J. W., and Kallenbach, N. R. (1986) Proteins 1, 211-7.

Nilges, M., Gronenborn, A., Brünger, A. and Clore, G. (1988a) "Determination of Three-Dimensional Structures of Proteins from Interproton Distance Restraints. Application to Crambin, Potato Carboxypeptidase Inhibitor and Barley Serine Proteinase Inhibitor 2," Protein Engineeriubf Vol I: 27-38

Nilges, M., Clore, M., and Gronenborn, M. (1988b) "Determination of Three-Dimensional Structures of Proteins from Interproton Distance Data by Hybrid Distance Geometry-dynamical Simulated Annealing Calculations," FEB Vol. 229, No.2:317-324

Nilges, M., Clore, M, and Gronenborn, M. (1988c) "Determination of Three-Dimensional Structures of Proteins from Interproton Distance Data by Dynamical Simulated Annealing from a Random Array of Atoms," FEB Vol 239, No. 1: 129-136

Nishii, I., Kataoka, M., Tokunaga, F. and Goto, Y. (1994) Biochem. 33, 4903-9.

Nishi, M., Chan, S. J., Nagamatsu, S., Bell, G. I., and Steiner, D. (1989) "Conservation of the Sequence of Islet Amyloid Polypeptide in Five Mammals Is Consistent with Its Putative Role as an Islet Hormone," PNAS, USA 86, 5738-42.

Ogawa, K., Nishimura, S. Uchiyama, S. Kobayashi, K. Kyogoku, Y., Hayashi, M., and Kobayashi, Y. (1998) "Conformation Analysis of Eel Calcitonin--Comparison with the Conformation of Elcatonin," Eur. J. Biochem. 257(2): 331-6.

O'Halloran, D.J., Bloom, S. R. (1991) "Calcitonin Gene Related Peptide: a Major Neuropeptide and the Most Powerful Vasodilator Known," Br. Med. J. 302, 739-740.

Ohsawa, H., Kanatuska, A., Yamaguchi, T., Makino, H., Yoshida, S. (1989) "Islet Amyloid Polypeptide Inhibits Glucose-Stimulated Insulin Secretion from Isolated Rat Pancreatic Islets," BBRC 160, 961-7.

Oldfield, E. (1995) "Chemical Shifts and Three-dimensional Protein Structures," J. Bio. NMR 5, 217-225.

Oosterwijk, C., Hoppener, J. W. M., Hulst, K. L. V. and Lips, C. J. M. (1995) "Pancreatic Islet Amyloid Formation in Patients with Noninsulin-Dependent Diabetes Mellitus," Int. J. Pancreatol. 18, No. 1, 7-14.

Otting, G., Widmer, H., Wagner, G. & Wüthrich, K. (1986) "Origin of t_1 and t_2 Ridges in 2D NMR Spectra and Procedures for Suppression," J. Magn. Res. 66, 187-193.

Ösapay, K. and Case, D. (1994) "Analysis of Proton Chemical Shifts in Regular Secondary Structure of Proteins," J. Bio. NMR 4, 215-30.

Ösapay, G. and Taylor, J. W. (1992) JACS 114, 6966-73.

Ösapay, K. and Case, D. (1991) "A New Analysis of Proton Chemical Shifts in Proteins," JACS 113, 9436-44.

Parrish, J. R., and Blout, E. R. (1972) "The Conformation of Poly-L-alanine in Hexafluoroisopropanol," Biopolymers 11, 1001-1020.

Pastore, A. and Sauder, V. (1990) "The Relationship between Chemical Shift and Secondary Structure in Proteins," J. Magn. Reson. 90, 165-76.

Pauling L. and Corey, R. B. (1951) Proc. Natl. Acad. Sci. USA 37, 205.

Perczel, A., Park, K. and Fasman, G. D. (1992) "Proteins: Structure, Function, Genetics" 13, 57.

Perczel, A. and Fasman, G. D. (1992) "Quantitative Analysis of Cyclic β-turn Models," Protein Science 1, 378-395.

Pfeifer M. A., Halter J. B., Porte D. Jr. (1981) "Insulin Secretion in Diabetes Mellitus," Am. J. Med. 70: 579-88.

Pillay, T. S. and Makgoba (1991) "Molecular Mechanisms of Insulin Resistance," South Africa Medical J. 79, 607-13.

Pieber, T. R., Stein, D. T., Ogawa, A., Alam, Tl, Ohneda, M., McCorkle, K., Chen, L., McGarry, J. D., Unger, R. H. (1993) "Amylin-Insulin Relationships in Insulin Resistance with and without Diabetic Hypperglycemia," Am. J. Physiol. 265, E446-453.

Piotto, M., Saudek, V. and Sklenár V. (1992) "Gradient-Tailored Excitation for Single-Quantum NMR Spectroscopy of Aqueous Solutions," J. Bio NMR 2, 661-665.

Poitout, V. and Robertson, R. P. (1996) "An Integrated View of β-cells dysfunction in Type-II Diabetes," Annu. Rev. Med. 47, 69-83.

Poyner, D. R., Soomets, U., Howitt, S. G., and Langel, U. (1998) "Structural Determinants for Binding to CGRP Receptors Expressed by Human SK-N-MC and Col 29 Cells: Studies with Chimeric and Other Peptides," Br. J. Pharmacol. 124(8): 1659-66.

Pozvek, G., Hilton, J. M., Quiza, M., Houssami, S., and Sexton, P. M. (1997) "Structure/function Relationships of Calcitonin Analogues as Agonists, Antagonists, or Inverse Agonists in a Constitutively Activated Receptor Cell System," Mol. Pharmacol. 51(4): 658-65.

Pratum, T. K., and Moore, B. S. (1993) "Inverse Detection of ^{13}C Multiple-Quantum Coherence for Biosynthetic Studies," J. Magn. Reson. Series B 102, 91-97.

Prasad, B. V., and Balaram, P. (1984) "The Stereochemistry of Peptides Containing Alpha-aminoisobutyric Acid," CRC-Crit-Rev-Biochem. 16 (4) 307-48.

Presta, L. G. & Rose, G. D. (1988) "Helix Signals in Proteins" Science 240, 1632-41.

Prickett K. S., Albrecht, E., Soares, C. J., Lumpkin, R. H., Gaeta, L. S. L., Moore, C. X., Young, A. A., Beeley, N. R. A. and Beaumont, K. (1995) "Design of Receptor Selective Peptides That Antagonize the Actions of Amylin in vivo," The Proceedings of the 14th American Peptide Symposium, Peptides: Chemistry, Structure and Biology, Kaumaya, P.T.P. and Hodges, R.S. (Eds.)

Privalov, P. L. (1990) "Cold Denaturation of Proteins," Crit. Rev. Biochem. & Mol. Biol. 25, 281-305.

Ramachandran, G. N. and Sasisekharan, V. (1968) "Conformation of Polypeptides and Proteins," Adv. Protein Chem. 23, 283

Richardson, J. S. (1981) "The Anatomy and Taxonomy of Protein Structure," Adv. Protein Chem. 34, 167-339.

Rink, T. J., Beaumont, K, Koda, J., & Young, A. (1993) "Structure and Biology of Amylin," TiPS 14, 113-118.

Rose G. D. et al., (1985) Adv. Protein Chem. 37: 1-109.

Sacks, D. B. (1996) "Amylin, a Glucoregulatory Hormone Involved in the Pathogenesis of Diabetes Mellitus?" Clinical Chemistry 42, No. 4, 494-495.

Sacks, D. B. and Mcdonald, J. M.(1996) "The Pathogenesis of Type II Diabetes Mellitus: A Polygenic Disease," Clinical Chemistry 105, No. 2, 149-156.

Saha, S., Waugh, D. J., Zhao, P., Abel, P. W. and Smith, D. D. (1998) "Role of Conformational Constraints of Position 7 of the Disulphide Bridge of H-Alpha-CGRP Derivatives in Their Agonist Versus Antagonist Properties," J. Pept. Res. 52(2): 112-20.

Saldanha, J. & Mahadevan, D. (1991) "Molecular Model-Building of Amylin and α-Calcitonin Gene-Related Polypeptide Hormones Using a Combination of Knowledge Sources," Protein Engineering 4 (5), 539-544.

Sanders, J. K. M. and Hunter, B. K(1993) "Modern NMR Spectroscopy: a Guide for Chemists," Oxford University Press.

Sanke, T., Nanabusa, T., Nakamo, Y., Oki, C., Lkai, K., Nishimura, S., Kondo, M. and Nanjo, K. (1991) "Islet Amyloid Polypeptide (amylin): Levels and Their Responses to Oral Glucose in Type 2 (Non-Insulin-Dependent) Diabetic Patients," Diabetologia 34, 129-32.

Schmitz, O., Nyholm, B., Orskov, L., Gravholt, C. and Moller, N. (1997) "Effects of Amylin and the Amylin Agonist Pramlintide on Glucose Metabolism," Diabet. Med. 14 Suppl 2. P S19-23.

Schurke, P. (1996) Personal communication.

Shalongo, W., Dugad, L. and Stellwagen, E. (1994) J. Am. Chem. Soc. 116, 2500-7.

Silvestre, R. A., Peiró, E., Dégano, P., Miralles, P., Marco, J. (1990) "Inhibitory Effect of Rat Amylin on the Insulin Responses to Glucose and Arginine in the Perfused Rat Pancreas," Regul Pept. 31, 23-31.

Silvestre, R. A., Salas, M., Degano, P., et al. (1993) "Reversal of the Inhibitory Effects of Calcitonin Gene-Related Peptide (CGRP) and Amylin on Insulin Secretion by the 8-37 Fragment of Human CGRP," Biochem. Pharmacol. 45, 2343-7.

Sklenar, V., Piotto, M., Leppik, R., and Saudek, V. (1993) "Gradient-Tailored Water Suppression for ^{1}H-^{15}N HSQC Experiments Optimized to Retain Full Sensitivity," J. Magn. Reson. Series A 102, 241-5.

Smith, L. J., Sutcliffe, M. J., Fedfield, C. and Dobson, M. (1991) "Analysis of Φ and χ_1 Torsion Angles for Hen Lysoayme in Solution from ^{1}H NMR Spin-Spin Coupling Constants," Biochem. 30, 986-996.

Sonnichsen, F. D., Van Eyk, J. E., Hodges, R. S. and Sykes, B. D. (1992) "Effect of Trifluoroethanol on Protein Secondary Structure: An NMR and CD Study Using a Synthetic Actin Peptide," Biochemistry, 31, 8790-8.

Steiner, D. F., Ohagi, S., Nagamatsu, S., Bell, G. I. and Nishi, M. (1991) "Is Islet Amyloid Polypeptide a Significant Factor in Pathogenesis or Pathophysiology of Diabetes?" Diabetes, 40: 305-9.

Szilágyi, L. and Jardetzky, O. (1989) "α-Proton Chemical Shifts and Secondary Structure in Proteins," J. Magn. Reson. 83, 441-449.

Tamburro, A. M., Scatturin, A., Rocchi, R., Marchiori, F., Borin, G., & Scoffone, E. (1968) FEBS Lett. 1, 298-300.

Temussi, P. A., Picone, D., Saviano, G., Amodeo, P., Motta, A. , Tancredi, T., Salvadori, S. and Somatis. R. (1992) "Conformational analysis of an opioid peptide in solvent media that mimic cytoplasm viscosity," Biopolymers 32, 367-72.

Thompson, R. G., Gottlieb, A., Organ, K., Koda, J., Kisicki, J., and Kolterman, O. G. (1997) "Pramlintide: a human amylin analogue reduced postprandial plasma glucose, insulin, and C-peptide concentrations in patients with type 2 diabetes," Diabet. Med. 14(7), 547-55.

Tiffany M. L. and Krimm, S. (1968a) Biopolymers 6, 1379.

Tiffany M. L. and Krimm, S. (1968b) Biopolymers 6, 1767.

Tigelaar, H. L. and Flygare, W. H. (1972) J. Am. Chem. Soc. 94, 343.

Tokuyama, T., Yagui, K.. Yamaguchi, T., Huang, C. I., Kuarmoto, N., Shimada, F., Miyazaki, J., Horie, H., Saito, Y., Makino, H., and Kanatsuka, A. (1997) "Expression of Human Islet Amyloid Polypeptide/Amylin Impairs Insulin Secretion in Mouse Pancreatic Beta Cells," Metabolism 46(9), 1044-51.

Towell III, J. F. and Manning, M. C. (1994) "Analysis of Protein Structure by Circular Dichroism Spectroscopy" Analytical Applications of Circular Dichroism 175-205.

Toniolo, C., Polese, A. Formaggio, F. Crisma, M. and Kamphuis, J. (1996) "Circular Dichroism Spectrum of a Peptide 3_{10} helix," JACS 118, 2744-5.

Turner, R., Hattersley, A., Cook, J., (1992) "Type II Diabetes: Search for Primary Defects," Ann Med 24, 511-6.

US Department of Health and Human Services (1995) Diabetes Statistics, NIH publication No. 96-236.

Vijayakumar, E. K. S., Balaram, P. (1983) "Stereochemistry of Alpha-aminoisobutyric Acid Peptides in Solution: Helical Conformations of Protected Decapeptides with Repeating Aib-L-Ala and Aib-L-Val Sequences," Biopolymers 22, 2133-40.

Waltho, J. P., Merutka, G., Dyson, J. & Wright, P. E. (1993) Biochemistry 32, 6337-6347.

Wang, M. W., Young, A. A., Rink, T. J., et al. (1991) "$^{8-37}$h-CGRP Antagonizes Actions of Amylin on Carbohydrate Metabolism *in vitro* and *in vivo*," FEBS Lett 291, 195-8.

Wang, Z. L., Bennet, W. M., Ghatei, M. A., et at. (1993) "Influence of Islet Amyloid Polypeptide and the 8-37 Fragment of Islet Amyloid Polypeptide on Insulin Release from Perifused Rat Islets," Diabetes 42, 330-5.

Westermark, P., Engstrom, U., Johnson, K. H., Westermark, G. T., Betsholtz, C. (1990) "Islet Amyloid Polypeptide: Pinpointing Amino Acid Residues Linked to Amyloid Fibril Formation," Proc. Natl. Acad. Sci. USA 87, 5036-40.

Wimalawansa, S. J. (1997) "Amylin, Calcitonin Gene-Related Peptide, Calcitonin, and Adrenomedullin: a Peptide Superfamily," Crit. Rev. Neurobiol. 11(2-3), 167-239.

Williamson, M. P. (1990) "Secondary-Structure Dependent Chemical Shifts in Proteins," Biopolymers 29, 1423-1431.

Wishart, D. S., Bigam, C. G., Holm, A., Hodges, R. S. and Sykes, B. D. (1995a) "^{1}H, ^{13}C and ^{15}N Random Coil NMR Chemical Shifts of the Common Amino Acids. I. Investigations of Nearest-neighbor Effects," J. Bio. NMR, 5, 67-81.

Wishart, D. S., Bigam, C. G., Yao, J., Abildgaard, F., Dyson, J. H., Oldfield, E. and Sykes, B. D. (1995b) "^{1}H, ^{13}C and ^{15}N Chemical Shift Referencing in Biomolecular NMR," J. Bio. NMR, 6, 135-140.

Wishart, D. S. and Sykes, B. D. (1994) "Chemical Shifts as a Tool for Structure Determinatioin," Methods in Enzymology, Vol 239, 363-392.

Wishart, D. S., Sykes, B. D. & Richards, F. M. (1992) "The Chemical Shift Index: A Fast and Simple Method for the Assignment of Protein Secondary Structure through NMR Spectroscopy," Biochemistry 31(6), 1647-1651.

Wishart, D. S., Sykes, B. D. & Richards, F. M. (1991) "Relationship between Nuclear Magnetic Resonance Chemical Shift and Protein Secondary Structure," J. Mol. Biol. 222, 311-333.

Woody, R. W. (1994) "Circular Dichroism: Principles and Applications," Nakanishi, K, Berova, N., & Woody, R. W., eds. VCH, New York.

Woody, R. W. (1992) "Circular Dichroism and Conformation of Unordered Polypeptides. Advances in Biophysical Chemistry" JAI Press Inc.

Woody, R. W. (1974) "In Peptides, Polypeptides and Proteins," New York: Wiley, 338-48.

Wright, P. E., Dyson, H. J., and Lerner, R. A. (1988) "Conformation of Peptide Fragments of Proteins in Aqueous Solution: Implications for Initiation of Protein Folding," Biochem 27: 7167-75.

Wüthrich, K. (1986) "NMR of Proteins and Nucleic Acids," John Wiley & Sons.

Yang, J. T., Wu, C. C. and Martinez, H. M. (1986) "Calculation of Protein Conformation from Circular Dichroism" Methods Enzymol. 130, 208-69.

Yki-Järvinen H. (1994) "Pathogenesis of Non-Insulin Dependent Diabetes Mellitus," Lancet 343, 91-5.

Young, A. A., Gedulin, B. and Rink, T. (1996) "Dose-Responses for the Slowing of Gastric Emptying in a Rodent Model by Glucagon-Like Peptide (7-36)NH_2, Amylin, Cholecystokinin, and Other Possibe Regulators of Nutrient Uptake," Metabolism Vol 45, No.1, 1-3.

Young, A. A., Pittner, R., Gedulin, B., Vine, W., and Rink, T. (1995) "Amylin Regulation of Carbohydrate Metabolism" Biochem. Soc. Trans. 23 (2), 325-31.

Young, A. A., Rink, T. S., Vine, W. and Gedulin, B. (1994) Drug Dev. Res. 32: 90-9.

Young, A. A., Cooper, G. J. S., Carlo, P., Rink, T. J. and Wang, M. W. (1993) "Response to Intravenous Injections of Amylin and Glucagon in Fasted, Fed, and Hypoglycemic Rats," Am. J. Physiol. 264m E943-950.

Young, A. A., Gedulin, B., Wolfe-Lopez, D., Greene, H. E., Rink, T. J., Cooper, G. J. S. (1992) "Amylin and Insulin in Rat Soleus Muscle, Dose Responses for Cosecreted Noncompetitive Antagonists," Ann. J. Physiol. 263, E274-E281.

Young, A. A., Cooper, G. J. S., Wang, M. W. (1991) "Amylin Injection Causes Elevated Plasma Lactate and Glucose in the Rat," FEBS Lett. 291, 101-4.

Zagorske, M. G. (1990a) "Improved Frequency Selectivity for Presaturation of H_2O in 2D NMR Spectra of Protiens," J. Magn. res. 86, 400-405.

Zagorske, M. G. (1990b) "How to Obtain Accurate CAMELSPIN or ROESY Spectra with Identical Low-Power Pulses for Both the Preparation and the Mixing Intervals," J. Magn. Reson. 89, 608-14.

Zhou, N. E.; Zhu, B. Y.; Sykes, B. and Hodges, R. (1992) "Relationship between Amide Proton Chemical Shifts and Hydrogen Bonding in Amphipathic α-Helical Peptides," JACS 114, 4320-6.

Zhu, G., Dudley, D. T., and Saltiel, A. R. (1991) "Amylin Incereases Cyclic AMP Formation in L6 Myocytes Through Calcitonin Gene-related Peptide Receptors," BBRC Vol. 177, No. 2, 771-776.

Appendix A

NMR Pulse Programs and Macros

1D Pulse Program with Water Presat Used on Bruker AM500

```
;filename: PRESAT.CBL

ZE
D1 HG O2 S1
LO TO 2 TIMES C
GO=2 DO
EXIT
```

1D Pulse Program Use Decoupler as Transmitter on Bruker AM500

```
;filename: FIDINV.CBL

1 ZE
2 D1 HG O2 S2
  LO TO 3 TIMES C
4 D2 S1 DO PH1
5 P1:D PH1
6 GO=3 PH2
7 EXIT

PH1 = 0 1 2 3
PH2 = R0 R1 R2 R3
```

COSY Pulse Program Used on Bruker AM500

```
;   Filename: COSYPH.AUR
;   COSY 2-D DATA ACQUISITION FOR PHASE-SENSITIVE MODE
;   WITH PURE ABSORPTION/DISPERSION LINESHAPES WITHOUT
;   PHASE-TWIST, AND QUAD DETECTION IN F1,
;   USING TIME-PROPORTIONAL PHASE INCREMENTS (TPPI).
;   MARION & WUETHRICH, BBRC 113, 967 (1983)
;   G.BODENHAUSEN, H.KOGLER, R.R.ERNST, J.MAGN.RES. 58, 370 (1984)

;   REQUIRES NEW 2-D TRANSFORM AND DISPLAY ROUTINES (MC2=W).

1  ZE
2  D1 ;HG O2 S1          ;RELAXATION
   ;LO TO 2 TIMES C
   ;DO
3  P1 PH1                ;90 DEG PREPARATION PULSE
4  D0                    ;EVOLUTION
5  P1 PH2                ;90 DEG MIXING PULSE
6  GO=2 PH3              ;ACQUIRE DATA, LOOP TO 2
7  WR #1                 ;STORE FID
8  IF #1                 ;INCREMENT FILE NUMBER
9  IP1                   ;INCREMENT PHASE PROGRAM PH1 (TPPI)
10 IN=1                  ;INCREMENT D0 AND LOOP TO 1 FOR NEXT EXPERIMENT
   EXIT

;PHASE PROGRAMS FOR AXIAL PEAK (F1=0) SUPPRESSION

PH1=A0 A2 A2 A0 A1 A3 A3 A1
PH2=A0 A2 A0 A2 A1 A3 A1 A3
PH3=R0 R2 R2 R0 R1 R3 R3 R1

;TRANSFORM REQUIRES REDF=N AND REV=Y

;RECOMMEND SI=2*TD  FOR DESIRED RESOLUTION OF J COUPLINGS IN F2. ;THE PHASE
SENSITIVE MATRIX (SI X SI1) WILL HAVE 4 QUADRANTS
;   AND THE RR QUADRANT WILL BE USED FOR DISPLAY AND PLOTTING.
;   EQUAL DIGITAL RES. IN F1 AND F2 REQUIRES SI1=SI, MAX. NE=TD.
;   IT MAY BE DESIRABLE TO USE LESS DIGITAL RES. IN F1, BUT 'SYM'
;   IS NO LONGER POSSIBLE.

;IN=DW (ONE-HALF ITS NORMAL VALUE, E.G.SET ND0=2, SW1=SW/2)

;D1=1-5*T1
;P1=90 DEG
;D0=3E-6
;RD=PW=0
;NS=4 OR 8*N (FULL PHASE CYCLE),  DS=2 OR 4

;TO DEFINE PHASE CORRECTION: SET PW=90 DEG, RD=D1 AND RUN 1-D ;
   SPECTRUM USING SAME SW, SI ETC. PERFORM PHASE CORRECTION IN
;   EP AND EXAMINE PHASE CONSTANTS WITH 'TY'. PERFORM XFB AND PHASE
;   VALUES SHOWN BY 'TY' WILL BE USED FOR F2 DOMAIN, ZERO PHASE
;        CORRECTION IS USED IN F1 DOMAIN.
```

TOCSY (tppi) Pulse Program Used on Bruker AM500

```
;  Filename: HOHAHA.AU
;
;  HOMO-NUCLEAR HARTMAN-HAHN SPIN CORRELATION USING MLEV 17
;
;  Griesinger et al., JACS 110, 7870 (1988).
;  Supplied by Ray Norton October 23, 1990
;  Modified by Bolong Cao

1  ZE
2  D1 ;HG O2 S2
   ;LO TO 2 TIMES C
   D5 S1 DO ;PH1
   (P1 PH1):D
   D0 ;PH4
   (P5 PH4):D
3  (D2 PH3 P1 PH3 D8 PH4 P2 PH4 D8 PH3 P1 PH3):D
   (D2 PH5 P1 PH5 D8 PH6 P2 PH6 D8 PH5 P1 PH5):D (D2 PH5 P1 PH5 D8 PH6 P2
   PH6 D8 PH5 P1 PH5):D (D2 PH3 P1 PH3 D8 PH4 P2 PH4 D8 PH3 P1 PH3):D
   (D2 PH5 P1 PH5 D8 PH6 P2 PH6 D8 PH5 P1 PH5):D (D2 PH5 P1 PH5 D8 PH6 P2
   PH6 D8 PH5 P1 PH5):D (D2 PH3 P1 PH3 D8 PH4 P2 PH4 D8 PH3 P1 PH3):D
   (D2 PH3 P1 PH3 D8 PH4 P2 PH4 D8 PH3 P1 PH3):D (D2 PH5 P1 PH5 D8 PH6 P2
   PH6 D8 PH5 P1 PH5):D (D2 PH3 P1 PH3 D8 PH4 P2 PH4 D8 PH3 P1 PH3):D
   (D2 PH3 P1 PH3 D8 PH4 P2 PH4 D8 PH3 P1 PH3):D (D2 PH5 P1 PH5 D8 PH6 P2
   PH6 D8 PH5 P1 PH5):D (D2 PH3 P1 PH3 D8 PH4 P2 PH4 D8 PH3 P1 PH3):D
   (D2 PH3 P1 PH3 D8 PH4 P2 PH4 D8 PH3 P1 PH3):D (D2 PH5 P1 PH5 D8 PH6 P2
   PH6 D8 PH5 P1 PH5):D (D2 PH5 P1 PH5 D8 PH6 P2 PH6 D8 PH5 P1 PH5):D
   (D2 PH4 P4 PH4):D
   L1 TO 3 TIMES UPR
   (D2 PH4 P5 PH4):D
   GO=2 PH0
   WR #1
   IF #1
   IP1
   IN=1
   EXIT

PH0 = R1 R1 R3 R3 R2 R2 R0 R0
PH1 = 1 1 3 3 2 2 0 0
PH3 = 3 1 3 1 0 2 0 2
PH4 = 0 2 0 2 1 3 1 3
PH5 = 1 3 1 3 2 0 2 0
PH6 = 2 0 2 0 3 1 3 1
```

NOESY (tppi) Pulse Program Used on Bruker AM500

```
;Filename: NOEPHHG.CBL
; HOMONUCLEAR DIPOLAR-CORRELATED 2-D NMR IN PHASE-SENS. (TPPI)
; MODE WITH PRE-SATURATION OF SOLVENT.
; DIPOLAR COUPLING MAY BE DUE TO NOE OR CHEMICAL EXCHANGE.

;  D1 - 90 - D0 - 90 - D9 - 90 - FID

; G.BODENHAUSEN, H.KOGLER, R.R.ERNST, J.MAGN.RES. 58,370 (1984)

; SYMMETRIC MATRIX WITH SHIFTS AND COUPLINGS IN F1, F2
; OFF-DIAGONAL PEAKS CORRELATE SPINS WHICH SHARE A
; DIPOLAR COUPLING.
; ZERO-QUANTUM SCALAR COUPLING CORRELATIONS ARE STRONGLY REDUCED
; BY RANDOM VARIATION OF THE MIXING TIME D9.

1 ZE
2 D1 HG O2 S1     ;RELAXATION, PRE-SAT.
  LO TO 2 TIMES C
3 P1 PH1       ;90 DEG EXCITATION PULSE
4 D0          ;EVOLUTION OF SHIFTS AND COUPLINGS
5 P1 PH2       ;MIXING PULSE, 90 DEG
6 D9          ;MIXING TIME FOR Z-MAGN. EXCHANGE
7 P1 PH3       ;DETECTION PULSE, 90 DEG
8 GO=2 PH4 DO   ;ACQUIRE FID, WITHOUT DEC.
9 WR #1        ;STORE FID
10 IF #1       ;INCREMENT FILE NUMBER
  IP1         ;INCREMENT PHASE PROGRAM PH1 (TPPI METHOD)
11 IN=1        ;INCREMENT D0 AND LOOP FOR NEXT EXPER.
12 EXIT

PH1=A0 A2
PH2=A0 A0 A0 A0 A0 A0 A0 A0
   A2 A2 A2 A2 A2 A2 A2 A2
PH3=A0 A0 A2 A2 A1 A1 A3 A3
PH4=R0 R2 R2 R0 R1 R3 R3 R1
   R2 R0 R0 R2 R3 R1 R1 R3

;PROGRAM REQUESTS FILENAME WITH .SER EXTENSION
;NE DEFINES NUMBER OF FIDS = TD1
;NS = 4, 8 OR 16 (COMPLETE PHASE CYCLE)
;DS = 2 OR 4
;RD=PW=0
;D1 = 1-5*T1
;S3 = MINIMAL DEC. POWER FOR PRE-SATURATION
;P1 = 90 DEG

;D0 = 3E-6 INITIAL DELAY
;IN = DW, ND0=2, MC2=W FOR TPPI MODE  (SEE COSYPH.AU)
;SW1=SW/2

;D9 = MIXING TIME = CA. T1 FOR SMALL MOLECULES (EXTREME
;  NARROWING LIMIT) OR CA. 50-200 MSEC FOR LARGE MOLECULES
;  WITH CROSS-RELAXATION (SPIN-DIFFUSION).
```

```
;V9: CAUSES RANDOM VARIATION OF MAX. +/- V9% FOR D9 TO CANCEL
;  SCALAR CORRELATION EFFECTS. SET V9 TO GIVE CA. 20 MSEC
;  VARIATION TO CANCEL ZERO-QUANTUM COHERENCE BETWEEN SPINS WITH
;  SHIFT DIFFERENCE >50 HZ.

;MC2=W, REV=Y, REDF=N
;TYPICALLY USE TD = SI2, NO ZERO-FILLING IN F2
;          NE = TD/4, ZERO-FILL IN F1, SI1=SI2/2
;MATRIX CAN ONLY BE SYMMETRIZED ABOUT DIAGONAL IF SI2=SI1.

;TO DEFINE PHASE CORRECTION: TAKE FIRST .SER FILE, TRANSFORM (FT)
;  WITH DESIRED WINDOW FUNCTION, AND PHASE CORRECT IN EP SO THAT
;  SPECTRUM HAS PURE NEGATIVE PHASE.
;  EXAMINE CONSTANTS IN PARAMETER DISPLAY OR WITH 'TY'.
;  'XFB' WILL APPLY THESE CONSTANTS IN F2 DOMAIN AND ZERO IN F1.
;  DIAGONAL PEAKS, NEG. NOE, AND CHEM. EXCHANGE WILL BE NEGATIVE,
;  POS. NOE WILL BE POSITIVE, J-CORRELATIONS MAY INTRODUCE
;  MIXED POS/NEG COMPONENTS.
```

Pulse Program to Record NOESY and TOCSY (with water presat) Consecutively Used on Bruker AM500

```
; Filename: PRENOETO.ZHL

;NOESY is collected in inverse mode

1 ZE
2 D3 S2
3 D1 HG O2
 LO TO 3 TIMES C
 D5 S1 DO PH11
 P1:D PH11
 D0
 P1:D PH12
 D5 S2
 D9 HG
 D5 DO S1 PH13
 P1:D PH13
 GO=2 PH14 DO
 WR #1
 IF #1
  IP11
  IN=1
  I0

;Starts TOCSY

11 ZE
12 D5 S2 DO
13 D1 HG O2
 LO TO 13 TIMES C
 D5 S1 DO PH1
 (P1 PH1):D
 D0 PH4
 (P5 PH4):D
14 (D2 PH3 P1 PH3 D8 PH4 P2 PH4 D8 PH3
P1 PH3):D
 (D2 PH5 P1 PH5 D8 PH6 P2 PH6 D8 PH5 P1
PH5):D
 (D2 PH5 P1 PH5 D8 PH6 P2 PH6 D8 PH5 P1
PH5):D
 (D2 PH3 P1 PH3 D8 PH4 P2 PH4 D8 PH3 P1
PH3):D
 (D2 PH5 P1 PH5 D8 PH6 P2 PH6 D8 PH5 P1
PH5):D
 (D2 PH5 P1 PH5 D8 PH6 P2 PH6 D8 PH5 P1
PH5):D
 (D2 PH3 P1 PH3 D8 PH4 P2 PH4 D8 PH3 P1
PH3):D
 (D2 PH3 P1 PH3 D8 PH4 P2 PH4 D8 PH3 P1
PH3):D
 (D2 PH5 P1 PH5 D8 PH6 P2 PH6 D8 PH5 P1
PH5):D
 (D2 PH3 P1 PH3 D8 PH4 P2 PH4 D8 PH3 P1
PH3):D
 (D2 PH3 P1 PH3 D8 PH4 P2 PH4 D8 PH3 P1
PH3):D
 (D2 PH5 P1 PH5 D8 PH6 P2 PH6 D8 PH5 P1
PH5):D
 (D2 PH5 P1 PH5 D8 PH6 P2 PH6 D8 PH5 P1
PH5):D
 (D2 PH4 P4 PH4):D
 L1 TO 14 TIMES UPR
 (D2 PH4 P5 PH4):D
 GO=12 PH0
 WR #2
 IF #2
 IP1
 IN=11
 EXIT

;phase parameter for noesy
PH11=A0 A2
PH12=A0 A0 A0 A0 A0 A0 A0 A0
   A2 A2 A2 A2 A2 A2 A2 A2
PH13=A0 A0 A2 A2 A1 A1 A3 A3
PH14=R0 R2 R2 R0 R1 R3 R3 R1
   R2 R0 R0 R2 R3 R1 R1 R3

;phase parameter for tocsy
PH0 = R0 R0 R2 R2 R1 R1 R3 R3
PH1 = 1 1 3 3 2 2 0 0
PH3 = 3 1 3 1 0 2 0 2
PH4 = 0 2 0 2 1 3 1 3
PH5 = 1 3 1 3 2 0 2 0
PH6 = 2 0 2 0 3 1 3 1
```

ROESY (tppi) with Presat Used on Bruker AM500

```
;ROESY

1  ZE
2  D1
   D5 S1 DO
   D2 PH1
   (P1 PH1):D
   D0 PH2
3  (P2 PH2 D8):D
   LO TO 3 TIMES 7
   D2 PH3
   (P3 PH3):D
   L1 TO 3 TIMES UPR
   GO=2 PH4
   WR #1
   IF #1
   IP1
   IN=1
EXIT

PH1=0 0 1 1 2 2 3 3
PH2=3 3 2 2 1 1 0 0
PH3=1 1 0 0
PH4=R0 R0 R1 R1 R2 R2 R3 R3
```

HMQC Pulse Program Used on Bruker AM500

;Filename HMQCPHD.AUR

```
1 ZE
2 D3 DO S2
  D1 ;HG
  D3 DO S1
  P1:D PH1
  D2
  P12:C4
  P2:T:C4 PH4
  P12:C4
  D0*0.5
  P3:D PH2
  D0*0.5
  P12:C4
  P2:T:C4 PH5
   P12:C4
  D2
  D15
  D12 PH3
4 D15:D PH3
  D12 ADC
   P12:C4:C3   ;GARP DECOUPLING
5 (P11*0.34 PH10 P11*0.61 PH12):T:C4:C3
  (P11*2.86 PH10 P11*2.98 PH12):T:C4:C3
  (P11*0.77 PH10 P11*0.69 PH12):T:C4:C3
  (P11*0.94 PH10 P11*1.02 PH12):T:C4:C3
  (P11*1.49 PH10 P11*2.84 PH12):T:C4:C3
  (P11*0.74 PH10 P11*0.51 PH12):T:C4:C3
  (P11*0.28 PH10 P11*0.81 PH12):T:C4:C3
  (P11*1.33 PH10 P11*1.54 PH12):T:C4:C3
  (P11*2.87 PH10 P11*0.72 PH12):T:C4:C3
  (P11*0.79 PH10 P11*0.86 PH12):T:C4:C3
  (P11*1.09 PH10 P11*1.48 PH12):T:C4:C3
  (P11*2.84 PH10 P11*0.73 PH12):T:C4:C3
  (P11*0.59 PH10):T:C4:C3
  P12:C4:C3
  L1 TO 5 TIMES 2
6 (P11*0.34 PH12 P11*0.61 PH10):T:C4:C3
  (P11*2.86 PH12 P11*2.98 PH10):T:C4:C3
  (P11*0.77 PH12 P11*0.69 PH10):T:C4:C3
  (P11*0.94 PH12 P11*1.02 PH10):T:C4:C3
  (P11*1.49 PH12 P11*2.84 PH10):T:C4:C3
  (P11*0.74 PH12 P11*0.51 PH10):T:C4:C3
  (P11*0.28 PH12 P11*0.81 PH10):T:C4:C3
  (P11*1.33 PH12 P11*1.54 PH10):T:C4:C3
  (P11*2.87 PH12 P11*0.72 PH10):T:C4:C3
  (P11*0.79 PH12 P11*0.86 PH10):T:C4:C3
  (P11*1.09 PH12 P11*1.48 PH10):T:C4:C3
  (P11*2.84 PH12 P11*0.73 PH10):T:C4:C3
  (P11*0.59 PH12):T:C4:C3
  P12:C4:C3
  L2 TO 6 TIMES 2
  L3 TO 5 TIMES UPR
  P12:C4:C3
  D17
  RCYC=2 PH6
  WR #1
  IF #1
  IP4
  IN=1
7 EXIT
  PH10=2
  PH12=0
  PH3=0
  PH1= 0 0; 0 0 2 2 2 2
  PH2= 1 1
  PH4= 0 0
  PH5= 0 2
  PH6= R0 R2; R0 R2 R2 R0 R2 R0
```

Pulse Program for RELAY-HMQC Used on Bruker AM500

```
; Filename: INVRELAY.AUR

1  ZE
2  D3 DO
   D3 S2
   D1 ;HG
   D3 DO S1
3  P1:D PH1
   D2*0.5
   P12:C4
   P4:T:C4 PH7 P3:D PH8
   P12:C4
   D2*0.5
   P12:C4
   P2:T:C4 PH4 P1:D PH9
   P12:C4
   D4*0.5
   P12:C4
   P4:T:C4 PH14
   P12:C4
   D4*0.5
   P12:C4
   P2:T:C4 PH15
   P12:C4
   D0*0.5
   P3:D PH2
   D0*0.5
   P12:C4
   P2:T:C4 PH5
   P12:C4
   D4*0.5
   P12:C4
   P4:T:C4 PH16
   P12:C4
   D4*0.5
   P12:C4
   P2:T:C4 PH17 P1:D PH1
   P12:C4
   D2*0.5
   P12:C4
   P4:T:C4 PH7 P3:D PH8
   P12:C4
   D2*0.5
   D15
   D12 PH3
4  D15:D PH3
   D12 ADC
     P12:C4:C3   ;GARP DECOUPLING
5  (P11*0.34 PH10 P11*0.61 PH12):T:C4:C3
   (P11*2.86 PH10 P11*2.98 PH12):T:C4:C3 (P11*0.77 PH10 P11*0.69 PH12):T:C4:C3 (P11*0.94
   PH10 P11*1.02 PH12):T:C4:C3 (P11*1.49 PH10 P11*2.84 PH12):T:C4:C3 (P11*0.74 PH10
   P11*0.51 PH12):T:C4:C3 (P11*0.28 PH10 P11*0.81 PH12):T:C4:C3 (P11*1.33 PH10 P11*1.54
   PH12):T:C4:C3 (P11*2.87 PH10 P11*0.72 PH12):T:C4:C3 (P11*0.79 PH10 P11*0.86
```

```
   PH12):T:C4:C3 (P11*1.09 PH10 P11*1.48 PH12):T:C4:C3 (P11*2.84 PH10 P11*0.73
   PH12):T:C4:C3 (P11*0.59 PH10):T:C4:C3
   P12:C4:C3
   L1 TO 5 TIMES 2
6  (P11*0.34 PH12 P11*0.61 PH10):T:C4:C3
   (P11*2.86 PH12 P11*2.98 PH10):T:C4:C3 (P11*0.77 PH12 P11*0.69 PH10):T:C4:C3 (P11*0.94
   PH12 P11*1.02 PH10):T:C4:C3 (P11*1.49 PH12 P11*2.84 PH10):T:C4:C3
   (P11*0.74 PH12 P11*0.51 PH10):T:C4:C3 (P11*0.28 PH12 P11*0.81 PH10):T:C4:C3 (P11*1.33
   PH12 P11*1.54 PH10):T:C4:C3 (P11*2.87 PH12 P11*0.72 PH10):T:C4:C3 (P11*0.79 PH12
   P11*0.86 PH10):T:C4:C3 (P11*1.09 PH12 P11*1.48 PH10):T:C4:C3 (P11*2.84 PH12 P11*0.73
   PH10):T:C4:C3 (P11*0.59 PH12):T:C4:C3
   P12:C4:C3
   L2 TO 6 TIMES 2
   L3 TO 5 TIMES UPR
   P12:C4:C3
   D17
   RCYC=2 PH6
   WR #1
   IF #1
   IP4
   IP14
   IP15
   IN=1
7  EXIT
   PH10=2
   PH12=0
   PH3=0
   PH1= 0 0
   PH2= 1 1 3 3
   PH4= 0 2
   PH5= 1 1 1 1 1 1 1 1
            3 3 3 3 3 3 3 3
   PH6= R0 R2
   PH7= 1 1
   PH8= 1 1 3 3
   PH9= 1 1
   PH13= 0 0 0 0 2 2 2 2
   PH14= 1 1
   PH15= 1 1
   PH16= 0 0
   PH17= 0 0
```

Pulse Program for 1D Used on Bruker dmx750 (with Water Suppression Using Water Gate Sequence)

```
;Filename: p3919gp
;avance-version
;1D sequence
;water suppression using 3-9-19 pulse sequence
with gradients
;M. Piotto, V. Saudek & V. Sklenar, J. Biomol.
NMR 2, 661 - 666 (1992)
;V. Sklenar, M. Piotto, R. Leppik $ V. Saudek,
J. Magn. Reson.,
;  Series A 102, 241 -245 (1993)

#include <Avance.incl>
#include <Grad.incl>

1 ze
2 d1 pl1:f1
 p1 ph1
 50u UNBLKGRAD
 p16:gp1
 d16 pl18:f1
 p28*0.231 ph3
 d19*2
 p28*0.692 ph3
 d19*2
 p28*1.462 ph3
 d19*2
 p28*1.462 ph4
 d19*2
 p28*0.692 ph4
 d19*2
 p0*0.231 ph4
 46u
 p16:gp2
 d16
 4u BLKGRAD
 go=2 ph31
 wr #0
exit


ph1=0 2
ph3=0 0 1 1 2 2 3 3
ph4=2 2 3 3 0 0 1 1
ph31=0 2 2 0

;pl1 : f1 channel - power level for pulse
(default)
;pl18: f1 channel - power level for 3-9-19-pulse
(watergate)
;p0 : f1 channel -  90 degree pulse at pl18
;                  use for fine adjustment
;p1 : f1 channel -  90 degree high power pulse
;p16: homospoil/gradient pulse
;p28: f1 channel -  90 degree pulse at pl18
;d1 : relaxation delay; 1-5 * T1
;d8 : mixing time
;d16: delay for homospoil/gradient recovery
;d19: delay for binomial water suppression
;    d19 = (1/(2*d)), d = distance of next null
(in Hz)
;NS: 8 * n
;DS: 4

;use gradient ratio:          gp 1 : gp 2
;                        20 :  20
```

Pulse Program for NOESY without Water Suppression Used on Bruker dmx750

```
;Filename: noesytp
;avance-version
;2D homonuclear correlation via dipolar coupling
;dipolar coupling may be due to noe or chemical exchange.
;phase sensitive using TPPI


#include <Avance.incl>


;;"d0=3u"


1 ze
2 d1
3 p1 ph1
 d0
 p1 ph2
 d8
 p1 ph3
 go=2 ph31
 d1 wr #0 if #0 id0 ip1 zd
 lo to 3 times td1
exit


ph1=0 2
ph2=0 0 0 0 0 0 0 0 2 2 2 2 2 2 2 2
ph3=0 0 2 2 1 1 3 3
ph31=0 2 2 0 1 3 3 1 2 0 0 2 3 1 1 3


;pl1 : f1 channel - power level for pulse (default)
;p1 : f1 channel -  90 degree high power pulse
;d0 : incremented delay (2D)                    [3 usec]
;d1 : relaxation delay; 1-5 * T1
;d8 : mixing time
;in0: 1/(2 * SW) = DW
;nd0: 2
;NS: 8 * n
;DS: 16
;td1: number of experiments
;MC2:  TPPI
```

Pulse Program for NOESY Used on Bruker dmx750 (with Water Suppression Using Water Gate Sequence)

```
;Filename: noesygptp19
;avance-version
;2D homonuclear correlation via dipolar
coupling
;dipolar coupling may be due to noe or
chemical exchange.
;phase sensitive using TPPI
;water suppression using 3-9-19 pulse sequence
with gradients
;M. Piotto, V. Saudek & V. Sklenar, J. Biomol.
NMR 2, 661 - 666 (1992)
;V. Sklenar, M. Piotto, R. Leppik $ V. Saudek,
J. Magn. Reson.,
;  Series A 102, 241 -245 (1993)


#include <Avance.incl>
#include <Grad.incl>


"d0=3u"
"d12=20u"


1 ze
2 d1
3 d12 pl1:f1
 p1 ph1
 d0
 p1 ph2
 d8
 p1 ph3
 d12 pl18:f1
 50u UNBLKGRAD
 p16:gp1
 d16
 p28*0.231 ph4
 d19*2
 p28*0.692 ph4
 d19*2
 p28*1.462 ph4
 d19*2
 p28*1.462 ph5
 d19*2
 p28*0.692 ph5
 d19*2
 p0*0.231 ph5
 46u
 p16:gp2
 d16
 4u BLKGRAD
 go=2 ph31
 d1 wr #0 if #0 id0 ip1 zd
 lo to 3 times td1
exit


ph1=0 2
ph2=0 0 0 0 0 0 0 0 2 2 2 2 2 2 2 2
ph3=0 0 2 2 3 3 1 1
ph4=0
ph5=2
ph31=0 2 2 0 1 3 3 1 2 0 0 2 3 1 1 3


;pl1 : f1 channel - power level for pulse
(default)
;pl18: f1 channel - power level for 3-9-19-pulse
(watergate)
;p0 : f1 channel -  90 degree pulse at pl18
;                  use for fine adjustment
;p1 : f1 channel -  90 degree high power pulse
;p2 : f1 channel - 180 degree high power pulse
;p16: homospoil/gradient pulse
;p28: f1 channel -  90 degree pulse at pl18
;d0 : incremented delay (2D)                  [3
usec]
;d1 : relaxation delay; 1-5 * T1
;d8 : mixing time
;d12: delay for power switching
[20 usec]
;d16: delay for homospoil/gradient recovery
;d19: delay for binomial water suppression
;    d19 = (1/(2*d)), d = distance of next null
(in Hz)
;in0: 1/(2 * SW) = DW
;nd0: 2
;NS: 8 * n
;DS: 16
;td1: number of experiments
;MC2: TPPI

;use gradient ratio:          gp 1 : gp 2
;                        20 :  20
```

Pulse Program for HMQC Used on Bruker dmx750

```
;Filename:hmqctkpwg
;2D H-1/X correlation via heteronuclear zero
and double quantum
;  coherence
;phase sensitive using TPPI
;with decoupling during acquisition


"p2=p1*2"
"d11=30m"
"d12=20u"
"d13=3u"
"d0=3u"

#include <Avance.incl>
#include <Grad.incl>
;be sure next line is commented out for 2D data
#define onedimensional

1 ze
 d11
2 d11
3 d12
 d1
 d12 pl1:f1
 p1 ph1
 d2 pl2:f2
 p3:f2 ph3
 d0
 p2 ph2
 d0
 p3:f2 ph4
 d2
 50u UNBLKGRAD
 p16:gp1
 d16 pl18:f1
 p28*0.231 ph5
 d19*2
 p28*0.692 ph5
 d19*2
 p28*1.462 ph5
 d19*2
 p28*1.462 ph6
 d19*2
 p28*0.692 ph6
 d19*2
 p0*0.231 ph6
 46u
 p16:gp2
 d16
 4u BLKGRAD
 d12 pl12:f2
 go=2 ph31 cpd2:f2
#ifdef onedimensional
 d11 do:f2 wr #0
#endif
#ifndef onedimensional
 d11 do:f2 wr #0 if #0 id0 ip3 zd
 lo to 3 times td1
#endif
exit


ph1=0
ph2=0
ph3=1 3
ph4=1 1 3 3
ph5={0}*4 {1}*4 {2}*4 {3}*4
ph6={2}*4 {3}*4 {0}*4 {1}*4
ph31=0 2 2 0 2 0 0 2
ph29=0


;pl1 : f1 channel - power level for pulse
(default)
;pl2 : f2 channel - power level for pulse
(default)
;pl9 : f1 channel - power level for presaturation
;pl12: f2 channel - power level for CPD/BB
decoupling
;p1 : f1 channel -  90 degree high power pulse
;p2 : f1 channel - 180 degree high power pulse
;p3 : f2 channel -  90 degree high power pulse
;p31:  - 90 degree pulse for decoupling
sequence
;d0 : incremented delay (2D)                [3
usec]
;d1 : relaxation delay; 1-5 * T1
;d2 : 1/(2J)XH
;d11: delay for disk I/O                     [30
msec]
;d12: delay for power switching
[20 usec]
;d13: short delay                           [3 usec]
;in0: 1/(4 * SW(X)) = (1/2) DW(X)
;nd0: 4
;NS: 4 * n
;DS: 16
;td1: number of experiments
;MC2: TPPI
;cpd2: decoupling according to sequence
defined by cpdprg2
```

Pulse Program for 3D NOESY-HMQC Used on Bruker dmx750

```
;Filename:noesyhmqctkp- modified by tkp,
uses f2
;avance-version
;3D sequence with
;  homonuclear correlation via dipolar
coupling
;  dipolar coupling may be due to noe or
chemical exchange.
;  H-1/X correlation via hmqc
;phase sensitive using TPPI (t1)
;phase sensitive using TPPI (t2)
;with decoupling during acquisition
;water suppression using 3-9-19 pulse sequence
with gradients
;V. Sklenar, M. Piotto, R. Leppik $ V. Saudek,
J. Magn. Reson.,
;  Series A 102, 241 -245 (1993)

#include <Avance.incl>
#include <Grad.incl>

"p2=p1*2"
"p4=p3*2"
"d0=3u"
"d10=3u"
"d11=30m"
"d12=20u"
"d13=3u"


1 d11 ze
 d11 pl5:f2
2 d11 do:f2
3 d11*2
4 d1 pl1:f1 pl2:f2
 d12 fq1:f1
 p1 ph1
 d0
 (p4 ph2):f2
 d0
 p1 ph3
 d8
 p1 ph2
 d2 UNBLKGRAD
 (p3 ph5):f2
 d10
 p2 ph2
 d10
 (p3 ph2):f2
 d2
 d12
 p16:gp1
 d16 pl18:f1
 p27*0.231 ph6
 d19*2
 p27*0.692 ph6
 d19*2
 p27*1.462 ph6
 d19*2
 p27*1.462 ph7
 d19*2
 p27*0.692 ph7
 d19*2
 p27*0.231 ph7
 p16:gp2
 d16 pl5:f2
 d12 fq1:f1
 4u BLKGRAD
 go=2 ph31 cpd2:f2
 d11 do:f2 wr #0 if #0 id0 ip1 zd
 lo to 3 times td1
 d11 rd0 ip5
 d11 id10
 lo to 4 times td2
exit

ph1=0 0 2 2
ph2=0
ph3=0 0 0 0 2 2 2 2
ph5=0 2
ph6=0
ph7=2
ph31= 0 2 2 0 2 0 0 2

;pl1 : f1 channel - power level for pulse
(default)
;pl2 : f2 channel - power level for pulse
(default)
;pl5: f2 channel - power level for CPD/BB
decoupling
;pl18: f1 channel - power level for 3-9-19-pulse
(watergate)
;p1 : f1 channel -  90 degree high power pulse
;p2 : f1 channel - 180 degree high power pulse
;p16: homospoil/gradient pulse
;p3: f2 channel -  90 degree high power pulse
;p4: f2 channel - 180 degree high power pulse
;p27: f1 channel -  90 degree pulse at pl18
;d0 : incremented delay (F1 in 3D)
[3 usec]
;d1 : relaxation delay; 1-5 * T1
;d8 : mixing time
;d10: incremented delay (F2 in 3D)
[3 usec]
;d11: delay for disk I/O                    [30
msec]
```

```
;d12: delay for power switching
[20 usec]
;d13: short delay                    [3 usec]
;d15: d19 - p4/2
;d16: delay for homospoil/gradient recovery
;d19: delay for binomial water suppression
;    d19 = (1/(2*d)), d = distance of next null
(in Hz)
;d4: 1/(4J)XH
;d28: d4 - p16 - d16 - d19*3.37 - d13 - 4u"
;d30: (p4 - p2) / 2"
;in0: 1/(4 * SW(H)) = (1/2) DW(H)
;nd0: 4
;in10: 1/(4 * SW(X)) = (1/2) DW(X)
;nd10: 4
;NS: 8 * n
;DS: 32
;td1: number of experiments in F1
;td2: number of experiments in F2
;MC2: TPPI in F1
;MC2: TPPI in F2
;cpd2: decoupling according to sequence
defined by cpdprg3
;pcpd2: f2 channel - 90 degree pulse for
decoupling sequence

;define FQ1LIST (list has to be stored in
"/u/exp/stan/nmr/lists/f1")
;    set on resonance on water signal for noesy-
and inverse-part
;    but center of NH region for detection

;use gradient ratio:   gp 1 : gp 2
;                      20 :  20

;use AQORDER : 3 - 1 - 2
```

Macros for 2D (tppi) Data Transformation

t2:

```
cl
bld 2263 2 2048 2048 0
mat 2263 write
def phase0 -23.9
def phase1 88.7
def input zhl2263.dat
def nrows 1024
def datsiz 2048
set 1
qsb 1900 60 .7
stb 2
for row 1 &nrows
rn &input
bc 0.05
mwb 2
csl 61   {only for data from dmx750}
ft       {rft if data was from am500}
ph
red
sto 0 &row
ty row=&row $
next
ty done
end
```

t1:

```
mat 2242 write
loa 0 1
mul 0.5
sto 0 1
def pivot 122
def phase0 14.9
def phase1 -38.5
def ncol 1024
set 1
qsb 512 60 .7
stb 2
for col 1 &ncol
loa &col 0
zf 2048
mwb 2
rft
ph
red
sto &col 0
ty &col $
next
ty well done
end
```

Macro for Baseline Correction (Cubic Spline):

```
mat 2241 write
def iwidth 0
for row 1 1024
loa 0 &row
bas z
bas a 10
bas a 25
bas a 50
bas a 75
bas a 121
bas a 146
bas a 164
bas a 180
bas a 226
bas a 238
bas a 250
bas a 282
bas a 305
bas a 318
bas a 336
bas a 350
bas a 450
bas a 490
csp
ty &row $
sto 0 &row
next
end
```

Macro for 3D (tppi) Data Transformation:

(pulse program used to collect the 3D NOESY-HMQC writes ^{1}H first, then ^{15}N)

dmx23.mac:

```
cl
bld 2264 3 1024 256 64
0
mat 2264 write
def phase0 -17.7
def phase1 60.4
def input zhl2264.dat
def ntiers 62
def nrows 256
def datype 1
set 1
stb 2
for tier 1 &ntiers
for row 1 &nrows
rn &input
def datsiz 1024
bc 0.05
mwb 2
csl 70 (shift left)
ft
ph
red
sto 0 &row &tier
ty row=&row
tier=&tier $
next
next
ty done
end
```

dmx13.mac:

```
def phase0 118.7
def phase1 -224.0
def ncols 1024
def ntiers 62
for tier 1 &ntiers
for col 1 &ncols
loa &col 0 &tier
def datsiz 256
bc 0.5
lpf
zf 512
sb 256 90
rft
ph
red
def datsiz 256
sto &col 0 &tier
ty col=&col tier=&tier
next
next
ty done
end
```

dmx33.mac

```
def phase0 -6.0
def phase1 0.0
def ncols 1024
def rows 256
for col 1 &ncols
for row 1 &rows
loa &col &row 0
def datsiz 62
bc 0.5
lpl 62 10 10 63 128
lpf
sb 128 90
rft
ph
red
def datsiz 64
sto &col &row 0
ty row=&row col=&col
next
next
ty done
end
```

Appendix B

Final Constraints Tables and Molecular Dynamic Protocols

Final Set of Constraints of Pramlintide in 35% HFIP

For Major Conformer: Capped Helix

The constraints were mainly extracted from [15]N-NOESYHMQC(2264.mat), NOESY(2255.mat) recorded on 750MHz spectrometer. Some of the constraints were taken from NOESY(2132.mat) recorded on 500Mhz NMR, and 4α,β/N5-7 from c21Y NOESY (2239.mat) in 16%TFE.

Distance Constraints--Categories 1

```
remarks  pram1b_CH.tbl last modified by ZHL on 7/24/97

set echo=false end
set wrnlev=0 end

remarks                                                        lowr uppr
remarks                                                         (-)  (+)

remarks: aiNi+1
assign (resid  3 and name HA )(resid  4 and name HN ) 3.05 0.30 0.45
assign (resid  4 and name HA )(resid  5 and name HN ) 2.70 0.35 0.40
assign (resid  5 and name HA )(resid  6 and name HN ) 3.00 0.20 0.60
assign (resid  7 and name HA )(resid  8 and name HN ) 3.45 0.25 0.25
assign (resid  8 and name HA )(resid  9 and name HN ) 3.55 0.25 0.25
assign (resid  9 and name HA )(resid 10 and name HN ) 3.40 0.40 0.40
assign (resid 11 and name HA )(resid 12 and name HN ) 3.30 0.40 0.50
assign (resid 12 and name HA )(resid 13 and name HN ) 3.55 0.25 0.25
assign (resid 13 and name HA )(resid 14 and name HN ) 3.40 0.25 0.40
assign (resid 14 and name HA )(resid 15 and name HN ) 3.70 0.30 0.30
assign (resid 15 and name HA )(resid 16 and name HN ) 3.70 0.30 0.30
assign (resid 16 and name HA )(resid 17 and name HN ) 3.55 0.25 0.25
assign (resid 17 and name HA )(resid 18 and name HN ) 3.55 0.25 0.25
assign (resid 18 and name HA )(resid 19 and name HN ) 3.15 0.25 0.30
assign (resid 21 and name HA )(resid 22 and name HN ) 2.95 0.25 0.30
assign (resid 22 and name HA )(resid 23 and name HN ) 2.80 0.35 0.35

remarks: aiNi+2
assign (resid  4 and name HA )(resid  6 and name HN ) 3.80 0.40 0.50
assign (resid  5 and name HA )(resid  7 and name HN ) 3.20 0.25 6.00
assign (resid  7 and name HA )(resid  9 and name HN ) 4.15 0.25 6.00
assign (resid  9 and name HA )(resid 11 and name HN ) 4.00 0.25 5.00
assign (resid 10 and name HA )(resid 12 and name HN ) 3.70 0.70 0.75
assign (resid 12 and name HA )(resid 14 and name HN ) 4.20 0.40 6.00
assign (resid 13 and name HA )(resid 15 and name HN ) 4.00 0.20 0.45
assign (resid 15 and name HA )(resid 17 and name HN ) 4.00 0.40 6.00
assign (resid 16 and name HA )(resid 18 and name HN ) 4.40 0.60 6.00
assign (resid 17 and name HA )(resid 19 and name HN ) 4.20 0.40 0.40
assign (resid 18 and name HA )(resid 20 and name HN ) 4.25 0.40 6.00
assign (resid 21 and name HA )(resid 23 and name HN ) 3.85 0.40 0.60

remarks: aiNi+3
assign (resid  2 and name HA )(resid  5 and name HN ) 4.15 0.35 6.00
assign (resid  3 and name HA )(resid  6 and name HN ) 4.15 0.35 6.00
assign (resid  4 and name HA )(resid  7 and name HN ) 4.20 0.50 6.00
assign (resid  5 and name HA )(resid  8 and name HN ) 3.30 0.20 0.70
```

```
assign (resid   7 and name HA  )(resid  10 and name HN  ) 3.75 0.30 0.25
assign (resid   8 and name HA  )(resid  11 and name HN  ) 3.80 0.80 0.60
assign (resid   9 and name HA  )(resid  12 and name HN  ) 3.10 0.40 0.50
assign (resid  11 and name HA  )(resid  14 and name HN  ) 3.20 0.40 0.40
assign (resid  12 and name HA  )(resid  15 and name HN  ) 3.45 0.35 0.35
assign (resid  13 and name HA  )(resid  16 and name HN  ) 3.45 0.35 0.25
assign (resid  14 and name HA  )(resid  17 and name HN  ) 3.55 0.35 0.25
assign (resid  15 and name HA  )(resid  18 and name HN  ) 3.70 0.35 0.60
assign (resid  16 and name HA  )(resid  19 and name HN  ) 3.55 0.30 0.25
assign (resid  19 and name HA  )(resid  22 and name HN  ) 4.20 0.50 6.00
assign (resid  20 and name HA  )(resid  23 and name HN  ) 4.30 0.60 6.00
assign (resid  21 and name HA  )(resid  24 and name HN  ) 3.70 0.30 6.00
assign (resid  27 and name HA  )(resid  30 and name HN  ) 3.70 0.25 6.00
assign (resid  29 and name HA  )(resid  32 and name HN  ) 3.90 0.40 0.40
assign (resid  31 and name HA  )(resid  34 and name HN  ) 3.60 0.40 0.35

remarks: aiNi+4
assign (resid   2 and name HA  )(resid   6 and name HN  ) 4.15 0.20 9.00
assign (resid   3 and name HA  )(resid   7 and name HN  ) 3.60 0.20 9.00
assign (resid   5 and name HA  )(resid   9 and name HN  ) 3.75 0.35 0.45
assign (resid   9 and name HA  )(resid  13 and name HN  ) 3.70 0.30 0.60
assign (resid  15 and name HA  )(resid  19 and name HN  ) 3.70 0.30 0.60

remarks: particularly large intraresidue constraints
assign (resid  31 and name HA  )(resid  31 and name HN  ) 2.30 0.25 0.20

remarks biai
assign (resid  14 and name HB1 )(resid  14 and name HA  ) 2.95 0.15 0.20
assign (resid  14 and name HB2 )(resid  14 and name HA  ) 2.45 0.25 0.25

remarks: NiNi+1
assign (resid   3 and name HN  )(resid   4 and name HN  ) 2.50 0.25 0.30
assign (resid   3 and name HN  )(resid   4 and name HN  ) 2.50 0.40 0.40
assign (resid   4 and name HN  )(resid   5 and name HN  ) 4.50 0.50 1.20
assign (resid   5 and name HN  )(resid   6 and name HN  ) 2.80 0.30 0.25
assign (resid   6 and name HN  )(resid   7 and name HN  ) 2.70 0.15 0.30
assign (resid   7 and name HN  )(resid   8 and name HN  ) 2.80 0.35 0.35
assign (resid   9 and name HN  )(resid  10 and name HN  ) 2.70 0.15 0.20
assign (resid  10 and name HN  )(resid  11 and name HN  ) 2.70 0.20 0.25
assign (resid  12 and name HN  )(resid  13 and name HN  ) 2.55 0.20 0.30
assign (resid  13 and name HN  )(resid  14 and name HN  ) 2.70 0.35 0.30
assign (resid  14 and name HN  )(resid  15 and name HN  ) 2.70 0.35 0.30
assign (resid  15 and name HN  )(resid  16 and name HN  ) 2.55 0.20 0.30
assign (resid  16 and name HN  )(resid  17 and name HN  ) 2.65 0.20 0.20
assign (resid  17 and name HN  )(resid  18 and name HN  ) 2.70 0.15 0.15
assign (resid  18 and name HN  )(resid  19 and name HN  ) 2.70 0.15 0.15
!assign (resid  19 and name HN  )(resid  20 and name HN  ) 2.80 0.15 0.25
assign (resid  30 and name HN  )(resid  31 and name HN  ) 2.80 0.35 0.35

remarks: biNi
assign (resid   4 and name HB  )(resid   4 and name HN  ) 3.30 0.30 0.30
assign (resid  13 and name HB* )(resid  13 and name HN  ) 2.35 0.15 0.50
!assign (resid  14 and name HB* )(resid  14 and name HN  ) 2.15 0.25 0.50
assign (resid  20 and name HB* )(resid  20 and name HN  ) 3.35 0.35 0.25
assign (resid  23 and name HB* )(resid  23 and name HN  ) 2.70 0.25 0.25
!assign (resid  23 and name HBu )(resid  23 and name HN  ) 2.50 0.30 0.30
```

```
!assign (resid  23 and  name HBd )(resid  23 and  name HN  ) 3.25 0.30 0.35

remarks:  biNi+1
assign (resid   1 and  name HB* )(resid   2 and  name HN  ) 2.90 0.20 0.40
assign (resid   3 and  name HB* )(resid   4 and  name HN  ) 3.20 0.25 0.25
assign (resid   4 and  name HB   )(resid   5 and  name HN  ) 3.00 0.30 0.35
assign (resid   5 and  name HB* )(resid   6 and  name HN  ) 2.90 0.20 0.50
assign (resid   8 and  name HB* )(resid   9 and  name HN  ) 2.70 0.25 0.45
assign (resid  10 and  name HB* )(resid  11 and  name HN  ) 2.90 0.25 0.50
assign (resid  11 and  name HB* )(resid  12 and  name HN  ) 2.95 0.20 0.45
assign (resid  12 and  name HB* )(resid  13 and  name HN  ) 2.50 0.25 0.45
assign (resid  15 and  name HB* )(resid  16 and  name HN  ) 2.70 0.15 0.45
assign (resid  16 and  name HB* )(resid  17 and  name HN  ) 2.80 0.40 0.40
assign (resid  17 and  name HB   )(resid  18 and  name HN  ) 2.70 0.15 0.25
assign (resid  31 and  name HB* )(resid  32 and  name HN  ) 4.05 0.45 0.85
assign (resid  34 and  name HB* )(resid  35 and  name HN  ) 3.65 0.30 0.60

remarks:  biNi+2
assign (resid   4 and  name HB   )(resid   6 and  name HN  ) 3.10 0.20 0.45
assign (resid   4 and  name HB   )(resid   6 and  name HN  ) 3.00 0.25 0.25

remarks:  aibi+3
assign (resid   4 and  name HA   )(resid   7 and  name HB* ) 4.20 0.45 5.70
assign (resid   6 and  name HA   )(resid   9 and  name HB   ) 3.20 0.45 0.40
assign (resid   7 and  name HA   )(resid  10 and  name HB* ) 3.05 0.35 0.70
assign (resid   9 and  name HA   )(resid  12 and  name HB* ) 2.80 0.40 0.40
assign (resid  11 and  name HA   )(resid  14 and  name HB1 ) 2.80 0.65 0.45
assign (resid  12 and  name HA   )(resid  15 and  name HB* ) 3.05 0.35 0.50
assign (resid  13 and  name HA   )(resid  16 and  name HB* ) 2.95 0.35 0.35
assign (resid  14 and  name HA   )(resid  17 and  name HB   ) 3.05 0.35 0.30
assign (resid  15 and  name HA   )(resid  18 and  name HB* ) 3.10 0.45 0.45
assign (resid  16 and  name HA   )(resid  19 and  name HB* ) 3.20 0.45 0.60
assign (resid  16 and  name HA   )(resid  19 and  name HB2 ) 3.50 0.40 0.60
assign (resid  31 and  name HA   )(resid  34 and  name HB* ) 3.60 0.30 0.85

remarks:  DiNi,i+1,...
assign (resid  12 and  name HD* )(resid  13 and  name HN  ) 3.70 0.30 1.00

remarks:special constraints involving Val17 side chain
assign (resid  17 and  name HG1* )(resid  17 and  name HN  ) 3.50 0.30 0.85
assign (resid  17 and  name HG2* )(resid  17 and  name HN  ) 2.80 0.30 0.30

remarks:  Proline related
assign (resid  28 and  name HD1 )(resid  27 and  name HA  ) 2.55 0.35 0.35
assign (resid  28 and  name HD2 )(resid  27 and  name HA  ) 2.50 0.45 0.35
assign (resid  28 and  name HA   )(resid  29 and  name HD* ) 2.55 0.30 0.45

set echo=false end
set wrnlev=5 end
```

Distance Constraints--Categories 2

remarks pram2b_CH.tbl last modified by ZHL on 7/24/97

set echo=false end
set wrnlev=0 end

```
remarks                                                                    lowr uppr
remarks                                                                    (-)  (+)

remarks: aiNi+1
assign (resid   2 and name HA  )(resid   3 and name HN  ) 2.10 0.30 0.35
assign (resid   6 and name HA  )(resid   7 and name HN  ) 2.90 0.10 0.45
assign (resid  19 and name HA  )(resid  20 and name HN  ) 3.15 0.20 0.20
assign (resid  20 and name HA  )(resid  21 and name HN  ) 2.75 0.50 0.20
assign (resid  25 and name HA  )(resid  26 and name HN  ) 2.15 0.25 0.30
assign (resid  26 and name HA  )(resid  27 and name HN  ) 2.10 0.20 0.35
assign (resid  31 and name HA  )(resid  32 and name HN  ) 2.60 0.15 0.25
assign (resid  36 and name HA  )(resid  37 and name HN  ) 2.35 0.20 0.25

remarks: aiNi+2
assign (resid   2 and name HA  )(resid   4 and name HN  ) 3.70 0.30 0.30
assign (resid   3 and name HA  )(resid   5 and name HN  ) 4.15 0.20 6.00
assign (resid  14 and name HA  )(resid  16 and name HN  ) 4.40 0.40 6.00
assign (resid  19 and name HA  )(resid  21 and name HN  ) 4.25 0.20 6.00
assign (resid  20 and name HA  )(resid  22 and name HN  ) 3.90 0.75 0.40
assign (resid  22 and name HA  )(resid  24 and name HN  ) 3.45 0.25 0.25
assign (resid  24 and name HA* )(resid  26 and name HN  ) 4.10 0.20 6.00
assign (resid  25 and name HA  )(resid  27 and name HN  ) 4.00 0.35 6.00
assign (resid  29 and name HA  )(resid  31 and name HN  ) 3.85 0.35 0.40
assign (resid  34 and name HA  )(resid  36 and name HN  ) 3.85 0.40 0.40
assign (resid  30 and name HA  )(resid  32 and name HN  ) 3.70 0.30 0.50
assign (resid  32 and name HA  )(resid  34 and name HN  ) 4.30 0.40 0.60
assign (resid  33 and name HA* )(resid  35 and name HN  ) 3.70 0.30 6.00

remarks: aiNi+3
assign (resid  18 and name HA  )(resid  21 and name HN  ) 4.25 0.40 6.00
assign (resid  23 and name HA  )(resid  26 and name HN  ) 4.10 0.25 6.00
assign (resid  24 and name HA* )(resid  27 and name HN  ) 4.05 0.25 6.00

remarks: aiNi+4
assign (resid   7 and name HA  )(resid  11 and name HN  ) 4.00 0.20 5.00
assign (resid  11 and name HA  )(resid  15 and name HN  ) 4.00 0.30 0.50
assign (resid  12 and name HA  )(resid  16 and name HN  ) 3.85 0.25 0.25
assign (resid  13 and name HA  )(resid  17 and name HN  ) 3.70 0.30 0.35
assign (resid  14 and name HA  )(resid  18 and name HN  ) 5.00 1.00 4.90
assign (resid  16 and name HA  )(resid  20 and name HN  ) 3.70 0.30 0.60
assign (resid  17 and name HA  )(resid  21 and name HN  ) 4.30 0.40 5.50
assign (resid  18 and name HA  )(resid  22 and name HN  ) 4.10 0.25 9.00
!assign (resid  19 and name HA  )(resid  23 and name HN  ) 4.00 0.40 0.40
assign (resid  20 and name HA  )(resid  24 and name HN  ) 4.20 0.25 9.00
assign (resid  22 and name HA  )(resid  26 and name HN  ) 4.10 0.20 9.00
assign (resid  23 and name HA  )(resid  27 and name HN  ) 4.05 0.20 9.00
assign (resid  26 and name HA  )(resid  30 and name HN  ) 4.05 0.20 9.00
assign (resid  28 and name HA  )(resid  32 and name HN  ) 4.15 0.20 9.00
assign (resid  29 and name HA  )(resid  33 and name HN  ) 4.05 0.20 9.00
```

```
assign (resid  30 and  name HA  )(resid  34 and  name HN  ) 4.00 0.20 9.00
assign (resid  32 and  name HA  )(resid  36 and  name HN  ) 3.90 0.20 9.00
assign (resid  33 and  name HA* )(resid  37 and  name HN  ) 4.00 0.20 9.00

remarks: particularly large intraresidue constraints
assign (resid  22 and  name HA  )(resid  22 and  name HN  ) 2.30 0.25 0.30
assign (resid  26 and  name HB  )(resid  26 and  name HA  ) 3.00 0.30 0.40

remarks: H-bonding
assign (resid   8 and  name  O  )(resid  12 and name  HN  ) 1.96 0.25 0.25
assign (resid   8 and  name  O  )(resid  12 and name  N   ) 2.95 0.30 0.30
assign (resid   9 and  name  O  )(resid  13 and name  HN  ) 1.86 0.15 0.15
assign (resid   9 and  name  O  )(resid  13 and name  N   ) 2.88 0.10 0.15
assign (resid  10 and  name  O  )(resid  14 and name  HN  ) 1.96 0.25 0.25
assign (resid  10 and  name  O  )(resid  14 and name  N   ) 2.95 0.30 0.30
assign (resid  12 and  name  O  )(resid  16 and name  HN  ) 1.86 0.15 0.15
assign (resid  12 and  name  O  )(resid  16 and name  N   ) 2.88 0.10 0.15
assign (resid  13 and  name  O  )(resid  17 and name  HN  ) 1.86 0.15 0.15
assign (resid  13 and  name  O  )(resid  17 and name  N   ) 2.88 0.10 0.15

remarks biai
assign (resid   7 and  name HB1 )(resid   7 and  name HA  ) 2.95 0.15 0.20
assign (resid   7 and  name HB2 )(resid   7 and  name HA  ) 2.45 0.25 0.25
assign (resid  18 and  name HB1 )(resid  18 and  name HA  ) 2.45 0.25 0.25
assign (resid  18 and  name HB2 )(resid  18 and  name HA  ) 2.95 0.15 0.20

remarks: NiNi+1
assign (resid   3 and  name HN  )(resid   4 and  name HN  ) 2.50 0.40 0.40
assign (resid  19 and  name HN  )(resid  20 and  name HN  ) 2.75 0.15 0.40
assign (resid  31 and  name HN  )(resid  32 and  name HN  ) 2.85 0.20 0.25
assign (resid  32 and  name HN  )(resid  33 and  name HN  ) 2.90 0.25 0.70

remarks: NiNi+2
assign (resid  13 and  name HN  )(resid  15 and  name HN  ) 4.40 0.40 0.40
assign (resid  14 and  name HN  )(resid  16 and  name HN  ) 4.30 0.30 0.30
assign (resid  15 and  name HN  )(resid  17 and  name HN  ) 3.90 0.30 0.35

remarks: biNi
assign (resid   7 and  name HB1 )(resid   7 and  name HN  ) 2.55 0.25 0.25
assign (resid   7 and  name HB2 )(resid   7 and  name HN  ) 2.55 0.20 0.45
assign (resid   8 and  name HB* )(resid   8 and  name HN  ) 2.50 0.20 0.45
assign (resid   9 and  name HB  )(resid   9 and  name HN  ) 2.70 0.15 0.20
assign (resid  10 and  name HB* )(resid  10 and  name HN  ) 2.55 0.15 0.45
assign (resid  11 and  name HB* )(resid  11 and  name HN  ) 2.70 0.25 0.40
assign (resid  14 and  name HB1 )(resid  14 and  name HN  ) 2.60 0.35 0.35
assign (resid  14 and  name HB2 )(resid  14 and  name HN  ) 2.05 0.15 0.35
assign (resid  16 and  name HB* )(resid  16 and  name HN  ) 2.45 0.45 0.45
assign (resid  18 and  name HB2 )(resid  18 and  name HN  ) 2.50 0.35 0.30
assign (resid  18 and  name HB1 )(resid  18 and  name HN  ) 3.10 0.45 0.60
assign (resid  19 and  name HB1 )(resid  19 and  name HN  ) 2.70 0.45 0.25
assign (resid  19 and  name HB2 )(resid  19 and  name HN  ) 2.70 0.30 0.45
assign (resid  32 and  name HB  )(resid  32 and  name HN  ) 2.55 0.20 0.20
assign (resid  35 and  name HB* )(resid  35 and  name HN  ) 2.55 0.20 0.35
assign (resid  37 and  name HB* )(resid  37 and  name HN  ) 2.70 0.15 0.50
```

```
remarks: biNi+1
assign (resid   2 and name HB* )(resid   3 and name HN  ) 2.45 0.25 0.45
assign (resid   6 and name HB  )(resid   7 and name HN  ) 2.95 0.30 0.30
assign (resid   9 and name HB  )(resid  10 and name HN  ) 3.00 0.20 0.20
!assign (resid  12 and name HB* )(resid  13 and name HN  ) 2.45 0.15 0.45
assign (resid  13 and name HB* )(resid  14 and name HN  ) 2.45 0.15 0.45
assign (resid  14 and name HB1 )(resid  15 and name HN  ) 2.85 0.35 0.35
assign (resid  14 and name HB2 )(resid  15 and name HN  ) 3.50 0.45 0.50
assign (resid  19 and name HB1 )(resid  20 and name HN  ) 3.10 0.45 0.25
assign (resid  19 and name HB2 )(resid  20 and name HN  ) 3.30 0.35 0.55
assign (resid  20 and name HB* )(resid  21 and name HN  ) 3.50 0.45 0.45
assign (resid  23 and name HB* )(resid  24 and name HN  ) 3.75 0.35 0.70
!assign (resid  23 and name HBu )(resid  24 and name HN  )3.50 0.45 0.50
!assign (resid  23 and name HBd )(resid  24 and name HN  )4.00 0.60 0.60
assign (resid  25 and name HB* )(resid  26 and name HN  ) 2.90 0.30 0.55
assign (resid  26 and name HB  )(resid  27 and name HN  ) 2.90 0.20 0.55
assign (resid  29 and name HB* )(resid  30 and name HN  ) 3.20 0.30 0.50

remarks: biNi+2,+3....

assign (resid   4 and name HB  )(resid   6 and name HN  ) 3.10 0.20 0.45
assign (resid   4 and name HB  )(resid   6 and name HN  ) 3.00 0.25 0.25
assign (resid   4 and name HB  )(resid   6 and name HN  ) 3.00 0.25 0.25

!assign (resid   2 and name HB* )(resid   4 and name HN  ) 3.60 0.40 0.60
!assign (resid  21 and name HBd )(resid  23 and name HN  ) 4.00 0.30 6.00
assign (resid  22 and name HB1 )(resid  24 and name HN  ) 4.00 0.40 6.00
assign (resid  22 and name HB2 )(resid  24 and name HN  ) 4.00 0.40 6.00
!assign (resid  31 and name HBu )(resid  33 and name HN  ) 4.00 0.30 6.00
assign (resid  32 and name HB  )(resid  34 and name HN  ) 4.00 0.35 6.00
!assign (resid  34 and name HBu )(resid  36 and name HN  ) 4.00 0.30 6.00
assign (resid  35 and name HB1 )(resid  37 and name HN  ) 4.00 0.40 6.00
assign (resid  35 and name HB2 )(resid  37 and name HN  ) 4.00 0.40 6.00


assign (resid   4 and name HB  )(resid   7 and name HN  ) 3.80 0.80 1.00
assign (resid   8 and name HB* )(resid  11 and name HN  ) 4.20 0.70 1.05

assign (resid   2 and name HB* )(resid   8 and name HN  ) 3.80 0.45 0.45


remarks: aibi+3
assign (resid  10 and name HA  )(resid  13 and name HB* ) 3.30 0.65 0.65
assign (resid  11 and name HA  )(resid  14 and name HB2 ) 2.90 0.30 0.65
assign (resid  12 and name HA  )(resid  15 and name HB1 ) 3.05 0.45 0.30
assign (resid  18 and name HA  )(resid  21 and name HB* ) 4.00 0.40 6.00
assign (resid  19 and name HA  )(resid  22 and name HB1 ) 4.00 0.65 6.00
assign (resid  19 and name HA  )(resid  22 and name HB2 ) 4.00 0.35 6.00
assign (resid  20 and name HA  )(resid  23 and name HB* ) 4.40 0.70 1.20
assign (resid  29 and name HA  )(resid  32 and name HB  ) 3.40 0.45 0.65

remarks: GiNi from 3D
!assign (resid  10 and name HGu )(resid  10 and name HN  ) 4.10 0.50 0.50
!assign (resid  10 and name HGd )(resid  10 and name HN  ) 3.00 0.30 0.35
assign (resid  26 and name HG11 )(resid  26 and name HN  ) 2.80 0.30 0.20
assign (resid  26 and name HG12 )(resid  26 and name HN  ) 2.90 0.15 0.50
```

```
assign (resid  32 and  name HG* )(resid  32 and  name HN  ) 2.80 0.25 0.90
assign (resid  36 and  name HG2* )(resid  36 and  name HN  ) 3.15 0.30 0.60

remarks: GiNi+1.....
assign (resid   1 and  name HG* )(resid   2 and  name HN  ) 3.70 0.35 0.60
assign (resid   9 and  name HG2* )(resid  10 and  name HN  ) 4.00 0.35 0.65
assign (resid  26 and  name HG2* )(resid  27 and  name HN  ) 2.70 0.30 0.45
!assign (resid  26 and  name HG1u )(resid  27 and  name HN  ) 3.85 0.25 0.25
!assign (resid  26 and  name HG1d )(resid  27 and  name HN  ) 2.50 0.15 0.15
assign (resid  30 and  name HG2* )(resid  31 and  name HN  ) 3.85 0.30 0.80
assign (resid  36 and  name HG2* )(resid  37 and  name HN  ) 3.85 0.30 0.75

assign (resid   4 and  name HG2* )(resid   6 and  name HN  ) 3.40 0.40 0.80
assign (resid   6 and  name HG2* )(resid   8 and  name HN  ) 5.00 1.00 4.90
assign (resid  30 and  name HG2* )(resid  32 and  name HN  ) 4.30 0.80 5.00

assign (resid   9 and  name HG2* )(resid  12 and  name HN  ) 4.30 0.50 1.00
assign (resid  30 and  name HG2* )(resid  33 and  name HN  ) 5.00 1.00 5.00

assign (resid   9 and  name HG2* )(resid  13 and  name HN  ) 4.10 0.50 0.60
assign (resid  30 and  name HG2* )(resid  34 and  name HN  ) 5.00 1.00 5.00

remarks: DiNi,i+1,...
assign (resid  16 and  name HD* )(resid  16 and  name HN  ) 3.15 0.20 0.90
assign (resid  16 and  name HD* )(resid  17 and  name HN  ) 4.00 0.40 1.10

remarks: Proline related
assign (resid  25 and  name HA  )(resid  25 and  name HB1  ) 2.45 0.25 0.25
!assign (resid  25 and  name HA  )(resid  25 and  name HGu  ) 2.60 0.30 0.30
!assign (resid  25 and  name HA  )(resid  25 and  name HDd  ) 3.90 0.45 0.75
!assign (resid  25 and  name HDu  )(resid  25 and  name HB1  ) 3.20 0.50 0.45
!assign (resid  25 and  name HDd  )(resid  25 and  name HB1  ) 3.60 0.60 0.60
assign (resid  25 and  name HD* )(resid  25 and  name HB1  ) 3.25 0.35 0.80
!assign (resid  25 and  name HDu  )(resid  25 and  name HGu  ) 3.05 0.30 0.30
!assign (resid  25 and  name HDd  )(resid  25 and  name HGu  ) 2.90 0.40 0.30
assign (resid  28 and  name HA  )(resid  28 and  name HB1  ) 2.45 0.25 0.25
assign (resid  28 and  name HA  )(resid  28 and  name HB2  ) 2.75 0.30 0.35
!assign (resid  28 and  name HA  )(resid  28 and  name HGd  ) 3.05 0.30 0.30
assign (resid  28 and  name HB1  )(resid  28 and  name HD*  ) 3.40 0.45 0.75
!assign (resid  28 and  name HB1  )(resid  28 and  name HDd  ) 3.40 0.40 0.50
assign (resid  28 and  name HD* )(resid  28 and  name HB2  ) 3.00 0.40 0.65
!assign (resid  28 and  name HDu  )(resid  28 and  name HB2  ) 2.90 0.40 0.45
!assign (resid  28 and  name HDd  )(resid  28 and  name HB2  ) 3.60 0.60 0.60
assign (resid  28 and  name HD* )(resid  28 and  name HB2  ) 3.05 0.30 0.80
assign (resid  28 and  name HD* )(resid  27 and  name HB* ) 3.00 0.40 0.50
!assign (resid  28 and  name HDu  )(resid  27 and  name HBd  ) 3.25 0.30 0.70
!assign (resid  28 and  name HDu  )(resid  27 and  name HBu  ) 3.25 0.30 0.40
assign (resid  28 and  name HD1  )(resid  27 and  name HD*  ) 3.15 0.30 1.25
!assign (resid  28 and  name HDd  )(resid  27 and  name HBd  ) 3.40 0.40 0.80
!assign (resid  28 and  name HB1  )(resid  29 and  name HDd  ) 3.05 0.30 0.30
!assign (resid  28 and  name HB2  )(resid  29 and  name HDd  ) 3.15 0.30 0.35
assign (resid  28 and  name HA  )(resid  29 and  name HD*  ) 2.70 0.40 0.55
!!assign (resid  28 and  name HA  )(resid  29 and  name HDu  ) 2.60 0.35 0.30
!assign (resid  28 and  name HA  )(resid  29 and  name HDd  ) 2.80 0.40 0.35
assign (resid  29 and  name HA  )(resid  29 and  name HB1  ) 2.45 0.25 0.25
assign (resid  29 and  name HD1  )(resid  29 and  name HB1  ) 3.25 0.35 0.65
```

```
assign (resid  29 and name HD2 )(resid  29 and name HB1  ) 3.25 0.35 0.40
assign (resid  29 and name HA  )(resid  30 and name HG2* ) 3.90 0.40 1.25
assign (resid  29 and name HA  )(resid  32 and name HG*  ) 3.70 0.40 1.35
!assign (resid  29 and name HA  )(resid  32 and name HGd* ) 3.70 0.40 1.05

remarks: other(aiXj)
assign (resid   5 and name HA  )(resid   2 and name HB*  ) 4.20 0.50 0.85
assign (resid   8 and name HA  )(resid   2 and name HB*  ) 3.70 0.50 1.15
assign (resid   8 and name HA  )(resid  11 and name HD*  ) 3.15 0.30 0.50
assign (resid   9 and name HA  )(resid  12 and name HD*  ) 3.65 0.45 0.80
assign (resid  12 and name HA  )(resid  12 and name HD*  ) 3.10 0.50 0.60
assign (resid  12 and name HA  )(resid  15 and name HD*  ) 3.45 0.50 0.75
assign (resid  13 and name HA  )(resid  12 and name HD*  ) 3.65 0.60 1.05
!assign (resid  13 and name HA  )(resid  16 and name HDu* ) 2.75 0.30 0.50
!assign (resid  21 and name HA  )(resid  22 and name HBu  ) 3.40 0.40 0.70

remarks: side chain to N
assign (resid  15 and name HD*  )(resid  16 and name HN  ) 3.70 0.65 0.55
assign (resid  15 and name HD*  )(resid  15 and name HN  ) 3.95 0.85 0.90

remarks: special constraints involving Val17 side chain
assign (resid  17 and name HG1* )(resid  16 and name HN  ) 4.10 0.25 9.90
assign (resid  17 and name HG1* )(resid  18 and name HN  ) 3.55 0.25 0.65
assign (resid  17 and name HG2* )(resid  18 and name HN  ) 3.65 0.25 1.20
assign (resid  17 and name HG2* )(resid  18 and name HA  ) 5.00 1.00 4.90
assign (resid  17 and name HG2* )(resid  18 and name HE1  ) 4.70 0.60 4.00
assign (resid  17 and name HG1* )(resid  21 and name HD22 ) 4.10 0.30 1.60
assign (resid  17 and name HG1* )(resid  21 and name HD21 ) 4.10 0.45 1.00
assign (resid  17 and name HA  )(resid  17 and name HB  ) 3.05 0.10 0.15

remarks: 'reversed' in loop
assign (resid   7 and name HB2 )(resid   4 and name HN  ) 3.30 0.50 0.45
assign (resid   7 and name HB1 )(resid   4 and name HN  ) 3.30 0.30 0.75

remarks: disulfides
assign (resid   2 and name SG  )(resid   7 and name SG  ) 2.02 0.06 0.05
assign (resid   2 and name SG  )(resid   7 and name CB  ) 3.05 0.25 0.42
assign (resid   7 and name SG  )(resid   2 and name CB  ) 3.05 0.25 0.42
assign (resid   2 and name CB  )(resid   7 and name CB  ) 3.94 0.70 0.45


set echo=false end
set wrnlev=5 end
```

Distance Constraints--Categories 3

```
remarks  pram3b_CH.tbl last modified by ZHL on 7/24/97

set echo=false end
set wrnlev=0 end

remarks                                                                    lowr uppr
remarks                                                                    (-)  (+)

remarks: aiNi+1
assign (resid   1 and name HA  )(resid   2 and name HN  ) 2.70 0.20 0.25
assign (resid  23 and name HA  )(resid  24 and name HN  ) 2.70 0.30 0.35
assign (resid  29 and name HA  )(resid  30 and name HN  ) 2.60 0.25 0.50
assign (resid  34 and name HA  )(resid  35 and name HN  ) 2.60 0.15 0.45
assign (resid  35 and name HA  )(resid  36 and name HN  ) 2.25 0.20 0.40

remarks: aiNi+2
assign (resid  28 and name HA  )(resid  30 and name HN  ) 4.15 0.50 0.50
assign (resid  31 and name HA  )(resid  33 and name HN  ) 4.00 0.20 6.00
assign (resid  35 and name HA  )(resid  37 and name HN  ) 4.00 0.20 6.00

remarks: aiNi+3
assign (resid  28 and name HA  )(resid  31 and name HN  ) 4.20 0.25 6.00
assign (resid  30 and name HA  )(resid  33 and name HN  ) 4.00 0.35 6.00
assign (resid  32 and name HA  )(resid  35 and name HN  ) 4.15 0.25 6.00
assign (resid  33 and name HA* )(resid  36 and name HN  ) 3.90 0.25 6.00
assign (resid  34 and name HA  )(resid  37 and name HN  ) 4.00 0.25 6.00

remarks: aiNi+4
assign (resid   6 and name HA  )(resid  10 and name HN  ) 3.55 0.55 0.80
assign (resid  19 and name HA  )(resid  23 and name HN  ) 4.10 0.40 6.00

remarks: particularly large intraresidue constraints
assign (resid   4 and name HA  )(resid   8 and name HN  ) 4.10 0.40 1.60
assign (resid   5 and name HA  )(resid   5 and name HN  ) 2.35 0.25 0.35
assign (resid  16 and name HA  )(resid  16 and name HN  ) 2.50 0.20 0.20
assign (resid  17 and name HA  )(resid  17 and name HN  ) 2.45 0.20 0.23
assign (resid  30 and name HA  )(resid  30 and name HN  ) 2.35 0.25 0.20
assign (resid  34 and name HA  )(resid  34 and name HN  ) 2.45 0.25 0.23


assign (resid  12 and name HA  )(resid  12 and name HD1* ) 3.10 0.50 0.60
assign (resid  12 and name HA  )(resid  12 and name HD2* ) 3.30 0.40 0.80

remarks: particularly large intraresidue constraints
!blue
assign (resid   4 and name HA  )(resid   4 and name HN  ) 2.40 0.25 0.40
!red
!assign (resid   4 and name HA  )(resid   4 and name HN  ) 2.90 0.25 0.25

remarks biai
assign (resid   3 and name HB1 )(resid   3 and name HA  ) 2.95 0.15 0.20
assign (resid   3 and name HB2 )(resid   3 and name HA  ) 2.45 0.25 0.25
assign (resid  12 and name HB1 )(resid  12 and name HA  ) 2.95 0.15 0.20
assign (resid  12 and name HB2 )(resid  12 and name HA  ) 2.45 0.25 0.25
```

```
assign (resid  15 and  name HB1  )(resid  15 and  name HA   ) 2.95 0.15 0.20
assign (resid  15 and  name HB2  )(resid  15 and  name HA   ) 2.45 0.25 0.25
assign (resid  19 and  name HB2  )(resid  19 and  name HA   ) 2.45 0.25 0.25
assign (resid  19 and  name HB1  )(resid  19 and  name HA   ) 2.95 0.15 0.20
assign (resid  21 and  name HB2  )(resid  21 and  name HA   ) 2.95 0.15 0.20
assign (resid  21 and  name HB1  )(resid  21 and  name HA   ) 2.45 0.25 0.25
assign (resid  23 and  name HB1  )(resid  23 and  name HA   ) 2.95 0.15 0.20
assign (resid  23 and  name HB2  )(resid  23 and  name HA   ) 2.45 0.25 0.25

remarks biNi
assign (resid   2 and  name HB*  )(resid   2 and  name HN   ) 2.80 0.20 0.55
assign (resid   3 and  name HB2  )(resid   3 and  name HN   ) 2.80 0.35 0.35
assign (resid   3 and  name HB1  )(resid   3 and  name HN   ) 2.55 0.35 0.30
assign (resid   5 and  name HB*  )(resid   5 and  name HN   ) 2.50 0.20 0.50
assign (resid   6 and  name HB   )(resid   6 and  name HN   ) 3.00 0.40 0.40
assign (resid  12 and  name HB2  )(resid  12 and  name HN   ) 2.55 0.15 0.45
assign (resid  12 and  name HB1  )(resid  12 and  name HN   ) 2.20 0.20 0.45
assign (resid  15 and  name HB2  )(resid  15 and  name HN   ) 2.65 0.35 0.20
assign (resid  15 and  name HB1  )(resid  15 and  name HN   ) 2.80 0.30 0.35
assign (resid  21 and  name HB*  )(resid  21 and  name HN   ) 3.15 0.30 0.55
assign (resid  26 and  name HB   )(resid  26 and  name HN   ) 2.50 0.25 0.50
assign (resid  31 and  name HB*  )(resid  31 and  name HN   ) 2.70 0.20 0.50
assign (resid  36 and  name HB   )(resid  36 and  name HN   ) 2.70 0.20 0.40

remarks biNi+1
assign (resid   3 and  name HB2  )(resid   4 and  name HN   ) 3.70 0.20 6.00
assign (resid   3 and  name HB1  )(resid   4 and  name HN   ) 3.15 0.35 0.40
assign (resid   7 and  name HB1  )(resid   8 and  name HN   ) 2.70 0.30 0.30
assign (resid   7 and  name HB2  )(resid   8 and  name HN   ) 2.80 0.15 0.60
assign (resid  12 and  name HB2  )(resid  13 and  name HN   ) 3.00 0.35 0.60
assign (resid  12 and  name HB1  )(resid  13 and  name HN   ) 2.40 0.30 0.25
assign (resid  15 and  name HB2  )(resid  16 and  name HN   ) 3.20 0.50 0.70
assign (resid  15 and  name HB1  )(resid  16 and  name HN   ) 2.60 0.30 0.50
assign (resid  18 and  name HB2  )(resid  19 and  name HN   ) 2.75 0.35 0.30
assign (resid  18 and  name HB1  )(resid  19 and  name HN   ) 3.35 0.40 0.50
assign (resid  22 and  name HB*  )(resid  23 and  name HN   ) 3.35 0.30 0.80
assign (resid  32 and  name HB   )(resid  33 and  name HN   ) 2.95 0.25 0.95
assign (resid  35 and  name HB*  )(resid  36 and  name HN   ) 3.30 0.50 0.80
assign (resid  36 and  name HB   )(resid  37 and  name HN   ) 3.20 0.25 0.45

remarks biNi+2,...
assign (resid   2 and  name HB*  )(resid   4 and  name HN   ) 3.60 0.65 0.60
assign (resid   3 and  name HB2  )(resid   5 and  name HN   ) 4.00 0.30 6.00
assign (resid   8 and  name HB*  )(resid  10 and  name HN   ) 4.00 0.30 1.00
assign (resid  12 and  name HB1  )(resid  14 and  name HN   ) 4.00 0.30 6.00
assign (resid  12 and  name HB2  )(resid  14 and  name HN   ) 4.00 0.30 6.00
assign (resid  14 and  name HB1  )(resid  16 and  name HN   ) 4.00 0.30 6.00
assign (resid  14 and  name HB2  )(resid  16 and  name HN   ) 4.00 0.30 6.00
assign (resid  15 and  name HB1  )(resid  17 and  name HN   ) 4.00 0.30 6.00
assign (resid  15 and  name HB2  )(resid  17 and  name HN   ) 4.00 0.30 6.00
assign (resid  16 and  name HB1  )(resid  18 and  name HN   ) 4.00 0.30 6.00
assign (resid  16 and  name HB2  )(resid  18 and  name HN   ) 4.00 0.30 6.00
assign (resid  17 and  name HB   )(resid  19 and  name HN   ) 4.00 0.30 6.00
assign (resid  20 and  name HB*  )(resid  22 and  name HN   ) 4.15 0.65 0.65
assign (resid  30 and  name HB   )(resid  32 and  name HN   ) 3.70 0.30 0.55
```

```
assign (resid    8 and  name HB*  )(resid   12 and  name HN   ) 3.80 0.40 1.25

remarks GiNi,+1,
assign (resid    4 and  name HG2* )(resid    4 and  name HN   ) 3.30 0.50 0.95
assign (resid    6 and  name HG2* )(resid    6 and  name HN   ) 3.25 0.30 0.90
assign (resid    9 and  name HG2* )(resid    9 and  name HN   ) 3.40 0.30 0.90
assign (resid   10 and  name HG*  )(resid   10 and  name HN   ) 3.15 0.25 0.90
assign (resid   27 and  name HG   )(resid   27 and  name HN   ) 2.30 0.15 0.55
assign (resid   30 and  name HG*  )(resid   30 and  name HN   ) 3.30 0.30 0.80

assign (resid    4 and  name HG2* )(resid    5 and  name HN   ) 3.55 0.50 0.95
assign (resid    6 and  name HG2* )(resid    7 and  name HN   ) 3.90 0.55 0.60

remarks: DiNi,i+1,...
assign (resid   16 and  name HD*  )(resid   13 and  name HN   ) 4.15 0.45 1.15

remarks:  NiNi+1
assign (resid   21 and  name HN   )(resid   22 and  name HN   ) 2.60 0.25 0.45
assign (resid   23 and  name HN   )(resid   24 and  name HN   ) 2.70 0.25 0.50
assign (resid   33 and  name HN   )(resid   34 and  name HN   ) 2.70 0.35 0.30
assign (resid   34 and  name HN   )(resid   35 and  name HN   ) 2.60 0.25 0.35
assign (resid   35 and  name HN   )(resid   36 and  name HN   ) 2.70 0.25 0.80

remarks: side chain to N
assign (resid   21 and  name HD21 )(resid   20 and  name HN   ) 3.40 0.25 0.60

remarks:aibi+3
assign (resid    9 and  name HA   )(resid   12 and  name HB1  ) 3.40 0.65 0.60
assign (resid    9 and  name HA   )(resid   12 and  name HB2  ) 2.80 0.45 0.40
assign (resid   17 and  name HA   )(resid   20 and  name HB*  ) 3.65 0.85 0.50
assign (resid   32 and  name HA   )(resid   35 and  name HB*  ) 4.00 0.70 1.20

remarks: Proline related
assign (resid   25 and  name HD*  )(resid  24 and  name HN   ) 3.25 0.40 0.60
assign (resid   25 and  name HD1  )(resid  24 and  name HA1  ) 2.90 0.45 0.50
assign (resid   25 and  name HD2  )(resid  24 and  name HA1  ) 2.70 0.60 0.40
assign (resid   25 and  name HD1  )(resid  24 and  name HA2  ) 2.90 0.40 0.60
assign (resid   25 and  name HD2  )(resid  24 and  name HA2  ) 2.80 0.40 0.60
assign (resid   28 and  name HD2  )(resid  27 and  name HD*  ) 3.45 0.60 1.30
assign (resid   28 and  name HG1  )(resid   27 and  name HA   ) 3.40 0.45 0.70
assign (resid   28 and  name HG2  )(resid   27 and  name HA   ) 3.40 0.45 0.95

remarks: reversed( from 3D)
assign (resid   13 and  name HB*  )(resid   12 and  name HN   ) 3.65 0.35 1.20
assign (resid   16 and  name HB*  )(resid   15 and  name HN   ) 4.20 0.40 0.80
!assign (resid   16 and  name HBu  )(resid   15 and  name HN   ) 4.20 .40 0.40

remarks: other(aiXj)
assign (resid    1 and  name HA   )(resid    2 and  name HB*  ) 3.80 0.60 1.40
assign (resid    4 and  name HA   )(resid    5 and  name HA   ) 3.90 0.60 0.75
assign (resid    4 and  name HA   )(resid    5 and  name HB*  ) 3.45 0.60 1.10
assign (resid    6 and  name HB   )(resid    2 and  name HB*  ) 4.20 0.50 0.70
assign (resid    7 and  name HA   )(resid    6 and  name HG2* ) 3.90 0.60 1.40
assign (resid    7 and  name HA   )(resid   10 and  name HG1  ) 3.60 0.40 0.70
assign (resid    7 and  name HA   )(resid   10 and  name HG2  ) 3.60 0.40 0.80
assign (resid    8 and  name HA   )(resid   11 and  name HE   ) 3.70 0.40 0.40
```

```
assign (resid   9 and name HA  )(resid  12 and name HD2* ) 3.50 0.50 0.40
assign (resid   9 and name HA  )(resid  12 and name HD1* ) 3.90 0.40 0.85
assign (resid  12 and name HA  )(resid  16 and name HD*  ) 3.40 0.40 0.80
assign (resid  13 and name HA  )(resid  12 and name HD2* ) 3.60 0.40 1.20
assign (resid  13 and name HA  )(resid  16 and name HD*  ) 3.15 0.30 0.80
assign (resid  14 and name HA  )(resid  13 and name HB*  ) 3.40 0.40 0.75
assign (resid  14 and name HA  )(resid  18 and name HE1  ) 3.80 0.45 1.00
assign (resid  14 and name HA  )(resid  18 and name HD2  ) 3.60 0.35 1.20
assign (resid  17 and name HA  )(resid  18 and name HA   ) 3.45 0.40 1.20
assign (resid  19 and name HA  )(resid  20 and name HA   ) 3.60 0.40 1.40
assign (resid  21 and name HA  )(resid  22 and name HB*  ) 3.50 0.45 0.85
assign (resid  23 and name HA  )(resid  18 and name HB2  ) 3.70 0.50 1.00
assign (resid  23 and name HA  )(resid  18 and name HB1  ) 4.10 0.40 6.00
assign (resid  26 and name HA  )(resid  27 and name HB*  ) 3.25 0.30 1.00


remarks:other
assign (resid   4 and name HB   )(resid   7 and name HB*  ) 4.20 0.40 0.60
assign (resid   6 and name HG2* )(resid   9 and name HB   ) 3.60 0.40 1.20

remarks: special constraints involving Val17 side chain
assign (resid  17 and name HG2*  )(resid  13 and name HA   ) 3.35 0.55 1.05
assign (resid  17 and name HG1*  )(resid  14 and name HA   ) 3.45 0.50 1.30
assign (resid  17 and name HG2*  )(resid  14 and name HA   ) 3.00 0.45 0.90
assign (resid  17 and name HG2*  )(resid  16 and name HN   ) 3.70 0.55 1.05
assign (resid  17 and name HG1*  )(resid  18 and name HA   ) 3.25 0.40 0.95
assign (resid  17 and name HG1*  )(resid  18 and name HE1  ) 4.00 0.45 1.10
assign (resid  17 and name HG1*  )(resid  18 and name HD2  ) 4.05 0.65 1.20
assign (resid  17 and name HG2*  )(resid  18 and name HD2  ) 4.80 0.70 2.00
assign (resid  17 and name HG2*  )(resid  21 and name HD22) 4.30 0.35 5.00
assign (resid  17 and name HG2*  )(resid  21 and name HD21) 4.30 0.35 5.00

remarks: 'reversed' in loop
assign (resid   7 and name HB2  )(resid   4 and name HN   ) 3.30 0.50 0.40
assign (resid   7 and name HB1  )(resid   4 and name HN   ) 3.30 0.30 0.70

remarks: side chain to N
assign (resid  21 and name HD21 )(resid  18 and name HN   ) 3.40 0.25 1.50

set echo=false end
set wrnlev=5 end
```

Distance Constraints--Categories 4

```
remarks  pram4b_CH.tbl last modified by ZHL on 7/24/97

set echo=false end
set wrnlev=0 end

remarks                                                                    lowr  uppr
remarks                                                                    (-)   (+)

remarks biNi+1,+2,...
assign (resid   5 and  name HB*  )(resid  10 and  name HN  ) 4.20 0.30 1.20

remarks giNi,+5
assign (resid  30 and  name HG2* )(resid  35 and  name HN  ) 4.20 0.50 1.60

remarks:reversed
assign (resid   4 and  name HG2* )(resid   3 and  name HN  ) 3.75 0.45 1.10
assign (resid   9 and  name HG2* )(resid   8 and  name HN  ) 4.20 0.40 2.40

remarks:aibi+3
assign (resid  27 and  name HA   )(resid  30 and  name HB  ) 3.80 0.40 1.00


remarks: Proline related
assign (resid  25 and  name HA   )(resid  26 and  name HB  ) 3.25 0.30 0.50

remarks: other(aiXj)
assign (resid   5 and  name HA   )(resid   4 and  name HG2* ) 3.40 0.40 1.80
assign (resid  12 and  name HA   )(resid   8 and  name HB*  ) 3.90 0.40 1.65
assign (resid  12 and  name HA   )(resid  13 and  name HB*  ) 3.60 0.40 1.30
assign (resid  26 and  name HA   )(resid  23 and  name HN  ) 4.00 0.40 0.40


set echo=false end
set wrnlev=5 end
```

Dihedral Angle Constraints:

```
remarks title: pram124.dih
remarks values based on aqueous buffer soln NH line coupling consts.

set echo=false end

 assign ( resid 2 and name c )
      ( resid 3 and name n )
     ( resid 3 and name ca )
     ( resid 3 and name c ) 200.0 -120.0 25.0 2

 assign ( resid 4 and name c )
      ( resid 5 and name n )
     ( resid 5 and name ca )
     ( resid 5 and name c ) 200.0 -20.0 30.0 2


 assign ( resid 6 and name c )
      ( resid 7 and name n )
     ( resid 7 and name ca )
     ( resid 7 and name c ) 25.0 -65.0 20.0 2


scale=$kcdi
end
```

3rd Stage XPLOR Protocol

```
remarks: file name -- prmt3stg_CH.com

evaluate ($first = 1)
evaluate ($last = 40)
evaluate ($pdbfilein = "c")
evaluate ($pdbfileout = "CH")
evaluate ($psfilein = "pram.psf")
evaluate ($psfileout = "test")
evaluate ($constraintscat1 = "pram1b_CH.tbl")
evaluate ($constraintscat2 = "pram2b_CH.tbl")
evaluate ($constraintscat3 = "pram3b_CH.tbl")
evaluate ($constraintscat4 = "pram4b_CH.tbl")
evaluate ($constraintsdih = "pram124.dih")
evaluate ($squareconstant = 0.8)
@prmt_3rdstage.inp
{@loopout.com}
@phipsi_test.com
```

```
 remarks: prmt_3rdstage.inp last modification on 7/25/97 by zhl
remarks:apt3stg.inp (apamer stage3 refinement)From 3ap1ref.inp 9/95 ; Also used as
remarks:is for refinement of apamer structures after during prochiral analysis
remarks:can be setup for daisy chain introduces the Lennard Jones potential in
remarks:the last refinement for testing potential prochirals.
remarks:
parameter
@parallhsa.pro
nbfix s s 462 13.6 462 13.6
end

evaluate ( $currenti = $first )
evaluate ( $lasti  = $last )
evaluate ( $sqcon = $squareconstant )

while ($lasti GE $currenti) loop main
  evaluate ( $pdb1 = $pdbfilein + encode($currenti) + ".pdb" )
  evaluate ( $pdb2 = $pdbfileout + encode($currenti) + ".pdb" )
  evaluate ( $psf2 = $psfileout +".psf" )
  structure reset end
  structure @@$psfilein end       {psf file}
  coordinates init end
  coordinates @@$pdb1             {pdb file}

evaluate ($knoe  = 10.0)
evaluate ($asym  = 0.35)     { if the specific structure has been previously }
                        { refined to all noe.tbl entries, $asym can be  }
                         { set at 0.6                                    }
evaluate ($kcdi  = 0.1)
flags
 exclude elec dihe
end
noe
 reset
```

```
  nrestraints = 1200
  ceiling = 100

class cat1 @@$constraintscat1     { contains key sequential noes, typically }
  averaging  cat1 r-6
  potential  cat1 soft
  scale      cat1 $knoe
  sqoffset   cat1 0.0
  sqconstant cat1 $sqcon
  sqexponent cat1 2
  soexponent cat1 1
  asymptote  cat1 $asym
  rswitch    cat1 0.8

class cat2 @@$constraintscat2     { other intra- and sequential noe  }
  averaging  cat2 r-6
  potential  cat2 soft
  scale      cat2 $knoe
  sqoffset   cat2 0.0
  sqconstant cat2 $sqcon
  sqexponent cat2 2
  soexponent cat2 1
  asymptote  cat2 $asym
  rswitch    cat2 0.7

class cat3 @@$constraintscat3
  averaging  cat3 r-6
  potential  cat3 soft
  scale      cat3 $knoe
  sqoffset   cat3 0.0
  sqconstant cat3 $sqcon
  sqexponent cat3 2
  soexponent cat3 1
  asymptote  cat3 $asym
  rswitch    cat3 0.6

class cat4 @@$constraintscat4
  averaging  cat4 r-6
  potential  cat4 soft
  scale      cat4 $knoe
  sqoffset   cat4 0.0
  sqconstant cat4 $sqcon
  sqexponent cat4 2
  soexponent cat4 1
  asymptote  cat4 $asym
  rswitch    cat4 0.4

end
@@$constraintsdih                 { tables of torsion constraints}
evaluate ($rcon = 0.002)
parameters
  nbonds
    wmin =  0.01
    cutnb =  4.5
    tolerance 0.3
    repel=   1.0
```

```
   rexp   = 2
   irex   = 2
   rcon=$rcon
  end
end
flags exclude noe cdih end
mini powell nstep=100 drop= 10 end        {for patched but un-minimized      }
                                  {structures this also introduces    }
                                  { SS bonds                          }
flags include noe cdih end
vector do (mass  =  10.0) (all)
vector do (fbeta = 100.0) (all)
evaluate  ($bath  = 1000.01)
constraints interaction (all) (all)
  weights
    angles    0.4
    impropers 0.1
  end
end
shake
  reference = parameter bonds (all) (all)
  tolerance = 1.0e-2
end
set seed=4068119 end
vector do (vx=maxwell(600)) (all)        {in some structures, noe deviations }
vector do (vy=maxwell(600)) (all)        {are lower and Enoe is insufficient }
vector do (vz=maxwell(600)) (all)         {to warm system                    }
while ( $kcdi < 0.6 ) loop stg1
evaluate ( $kcdi = min(0.6, $kcdi + 0.1))

noe
  potential cat1 square
  potential cat2 square
  potential cat3 square
  potential cat4 square
  scale     cat1 30
  scale     cat2 30
  scale     cat3 15
  scale     cat4  1
end

dynamics verlet
     nstep=100              { as in previous non-cyclic example this     }
     timestep=0.001         { dynamics course enforces the torsion       }
     iasvel=current         { constraints while knoe is at a modest level}
     tcoupling=true
     tbath=$bath
     nprint=50
     iprfrq=100
     ntrfr=0
end
end loop stg1

evaluate ( $kcdi=0.25 )
noe
  potential cat4 soft
```

```
  scale cat1 80
  scale cat2 30
  scale cat3 30
  scale cat4 2
end

dynamics  verlet
      nstep=2000
      timestep=0.002
      iasvel=maxwell
      firsttemperature = $bath
      tcoupling = true
      tbath = $bath
      ntrfr = 999999999
      nprint=50
     iprfrq=100
end

evaluate ($kcdi=0.05)
while ($rcon  < 0.6) loop stg2
   evaluate ($asym  = min(0.6, $asym  + 0.05))
   noe asymp all $asym  end
   evaluate ($kcdi  = min(0.25, $kcdi  + 0.05))
   evaluate ($rcon  = min(0.60001, $rcon  * 1.4))
   parameters
    nbonds repel 0.9 rcon $rcon  end
   end
   dynamics  verlet
      nstep=100
      timestep=0.002
     iasvel=current
      tcoupling = true
      tbath = $bath
      nprint=50
     iprfrq=100
      ntrfr = 0
   end
end loop stg2

noe
  scale cat1 70
  scale cat2 40
  scale cat3 20
  scale cat4 1
end
parameters
  nbonds
    repel 0.8
    rconst 4
    wmin 1.5
  end
end
energy end
if ($grad > 100) then
  mini powell nstep=25 drop=50 end
end if
```

```
evaluate ($kcdi=0.15)
while ($bath  gt 600) loop stage2
 dynamics  verlet
    nstep=60
    timestep=0.002 {ps}
    iasvel=current
    tcoupling = true
    tbath = $bath
    nprint=30 iprfrq = 30
    ntrfrq = 0
 end
 evaluate ($bath  = $bath  - 50)
end loop stage2

noe
 scale cat1 55
 scale cat2 30
 scale cat3 20
 scale cat4 0.4
end
parameters
 nbonds
   repel 0.8
   rconst 4
   wmin 1.5
 end
end
energy end
if ($grad > 100) then
 mini powell nstep=25 drop=50 end
end if
evaluate ($kcdi=0.15)
while ($bath  gt 350) loop stage2
 dynamics  verlet
    nstep=60
    timestep=0.002 {ps}
    iasvel=current
    tcoupling = true
    tbath = $bath
    nprint=30 iprfrq = 30
    ntrfrq = 0
 end
 evaluate ($bath  = $bath  - 50)
end loop stage2

noe
 scale cat1 50
 scale cat2 18
 scale cat3 10
 scale cat4 0.1
 evaluate ($asym=0.4)
end
parameters
 nbonds
   repel 0.8
   rconst 4
```

```
    wmin 1.5
  end
end
energy end
if ($grad > 100) then
  mini powell nstep=25 drop=50 end
end if
evaluate ($kcdi=0.15)
parameters                {Lennard-Jones Potential Parameters}
   nbonds
     wmin   =  1.50
     cutnb  =  8.5
     tolerence 0.5
     ctofnb =  7.50
     ctonnb =  6.50
     repel  =  0.0
     vswitch
   end
end
while ($bath  gt 250) loop stage2lj
  dynamics  verlet
     nstep=60
     timestep=0.002 {ps}
     iasvel=current
     tcoupling = true
     tbath = $bath
     nprint=30 iprfrq = 30
     ntrfrq = 0
  end
  evaluate ($bath  = $bath  - 25)
end loop stage2lj

shake reset end
constraints interaction (all) (all)
  weights
    angles    1.0
    impropers 1.0
  end
end

evaluate($kcdi=0.08)
noe
scale cat1 40
scale cat2 14
scale cat3 8
scale cat4 0.0
end
mini powell nstep=500 drop = 10.0
end
   write coor output=$pdb2 end
print threshold=0.15 noe
evaluate ($currenti = $currenti + 1)
end loop main
write structure  output=$psf2 end
```

VITA

Zhihong Liu

In 1989, immediately after receiving Bachelor of Science in Chemistry from Peking University, China, Zhihong Liu pursued graduate education at Bowling Green State University, Ohio, where she received Master of Science in Biochemistry in 1991. Then, she entered Ph.D. program in Department of Chemistry at the University of Washington, Seattle, Washington in October, 1991. In August 1997, she started working at Chemical Design, Inc.-- later, a Member of Oxford Molecular Group Inc., as a customer support scientist. She defended her thesis and received Ph.D. in May, 1999 from bioorganic/biophysics program at University of Washington.

PUBLICATIONS

"Spectroscopic Characterization of a Potent Soluble Analog of Human Pancreatic Amylin and Comparisons with Natural Systems," N. H. Andersen, J. R. Cort, G. M. Lee, Z. Liu, Biochem. In press.

"Extracting Information from the Temperature Gradients of Polypeptide NH Chemical Shifts: I. The Importance of Conformational Averaging," N. H. Andersen, J. W. Neidigh, S. M. Harris, G. M. Lee and Z. Liu, J. Am. Chem. Soc., 119, 8547-8561(1997).

"Efforts Toward Deriving the CD Spectrum of a 3_{10} -Helix in Aqueous Medium," N. Andersen, Z. Liu and K. Prickett, FEBS LETTERS 399: 47-52 (1996).

"Cold Denaturation of Monomeric Peptide Helices," N. Andersen, J. Cort, Z. Liu, S. Sjoberg and H. Tong, J. Am. Chem. Soc., 118: 10309-10 (1996).

"β-Structure in Human Amylin and Two Designer β-Peptides: CD and NMR Spectroscopic Comparisons Suggest Soluble β-Oligomers and the Absence of Significant Populations of β-Strand Dimers," J. Cort, Z. Liu, G. Lee, S. Harris, K. Prickett, L. Gaeta, and N. H. Andersen, Biochem. & Biophys. Res. Comm., 204(3): 10880 (1994).

"Nucleic Acid Photoproduct quantum Yields in Defined Sequence DNA Oligonucliotides Analyzed in Terms of Conformational Effects," R. W. Midden, Z. Liu, J. Ma, M. Willems, and K. Bougall, Photochem. Photobiol., 59S, 43S (1994).